マイクロフィルム用資料

Technical Memorandum
of PWRI No.3920

PROCEEDINGS OF THE 19TH U.S. -JAPAN BRIGE ENGINEERING WORKSHOP

October 27,28 and 29, 2003

PUBLIC WORKS RESEARCH INSTITUTE
Independent Administrative Institutions

1-6, Minamihara, Tsukuba-shi, Ibaraki-ken, 305-8516 Japan

Opinions, findings, conclusions and recommendations expressed in the papers contained in this publication are those of the author(s).

Copyright © (2003) by P.W.R.I.

All rights reserved. No part of this book may be reproduced by any means, nor transmitted, nor translated into a machine language without the written permission of the Chief Executive of P.W.R.I.

この報告書は、独立行政法人土木研究所理事長の承認を得て刊行したものである。したがって、本報告書の全部又は一部の転載、複製は、独立行政法人土木研究所理事長の文書による承認を得ずしてこれを行ってはならない。

Technical Memorandum
of PWRI No.3920

PROCEEDINGS OF THE 19TH U.S. -JAPAN BRIGE ENGINEERING WORKSHOP

By

Editors: Masahiro Ishida
Masahiro Shirato

Synopsis:

The proceeding documents the results of the 19th U.S. – Japan Bridge Engineering Workshop which was held at Tukuba, Japan, on October 27, 28, and 29, 2003, as apart of the activities of the Panel on Wind and Seismic Effects, UJNR. The Workshop was organized by Task Committee G "Transportation Systems" (U.S. side chairman: Dr.P.Yen, FHWA, Japan side chairman: Dr. H. Sato, PWRI) of the Panel.

Key Words: Bridge, Construction, Material, Design, Maintenance, Seismic, UJNR

PREFACE

The 19th US – Japan Bridge Engineering Workshop is a continuation of a series of technical interchanges between the Untied States and Japan on all topics related to bridge engineering. This series of workshops has been conducted under the auspices of Task Committee "G" of the US – Japan Panel on Wind and Seismic Effects, which is one of the 16 panels making up the United States – Japan Cooperative Program in Natural Resources (UJNR). The previous workshops are indicated below.

1st	February 20-23, 1984	Tsukuba Science City, *Japan*
2nd	August 19-20, 1985	San Francisco, California, *United States*
3rd	May 8-9, 1987	Tsukuba Science City, *Japan*
4th	May 11-12, 1988	San Diego, *United States*
5th	May 9-10, 1989	Tsukuba Science City, *Japan*
6th	May 7-8, 1990	Lake Tahoe, Nevada, *United States*
7th	May 8-9, 1991	Tsukuba Science City, *Japan*
8th	May 11-12, 1992	Chicago, Illinois, *United States*
9th	May 10-11, 1993	Tsukuba Science City, *Japan*
10th	May 10-11, 1994	Lake Tahoe, Nevada, *United States*
11th	May 30-31, 1995	Tsukuba Science City, *Japan*
12th	October 29-30, 1996	Buffalo, New York, *United States*
13th	October 2-3, 1997	Tsukuba Science City, *Japan*
14th	November 3-4, 1998	Pittsburgh, Pennsylvania, *United States*
15th	November 9-10, 1999	Tsukuba Science City, *Japan*
16th	October 2-4, 2000	South Lake Tahoe, Nevada, *United States*
17th	November 12-14, 2001	Tsukuba Science City, *Japan*
18th	October 22-24, 2002	St. Louis, Missouri, *United States*
19th	October 27-29, 2003	Tsukuba Science City, *Japan*

The steering committee for the 19th US-Japan Bridge Engineering Workshop consisted of Phil Yen, Hiroshi Sato, David Sanders, and Jiro Fukui. The principal funding for the workshop was provided by PWRI.

The workshop was held in the NILIM, Tsukuba. The participants of the Workshop reached the total of 61 persons (45 persons from Japan side and 16 from the U.S. side). The main topics of this

workshop were 1) Advancing Technology in Seismic Engineering and 2) Innovative Technology on Extending Bridge Service Lives, there were 40 presentations (23 papers from Japan side and 17 from the U.S. side).

The study tour was held in three locations: The construction site of the connection bridge for New Kita-Kyushu Airport which will be opened on manmade island on the sea; Wakato-Ohashi Bridge, the first cable stayed bridge in Japan; Kanmon-Kyo Bridge, the second cable stayed bridge in Japan; Kintai-Kyo Bridge, old timber bridge; Shimanami-Kaido, one of Honshu-Shikoku bridge routes, including Tatara-Ohashi bridge (the longest cable stayed bridge in the world) and Kurushima-Kaikyo-Ohashi bridge (three continuous suspension bridges); Bridges over Sumida-river in Tokyo

Editors: Masahiro Ishida, Senior Research Engineer, PWRI
Masahiro Shirato Research Engineer, PWRI

ACKNOWLEDGEMENTS

There are many people that have assisted in the organizing 19th US-Japan Bridge Engineering Workshop and Study Tour. Dr. Phillip Yen is the Chairman of US side. Dr. David Sanders is responsible for organizing US delegations. Fukuoka Prefectural Government, City of Iwakuni, Japan Highway Public Corporation and Honshu Shikoku Bridge Authorities arranged the study tour.

TABLE OF CONTENTS

PREFACE

WORKSHOP PROGRAM 1

PAPERS 9

Breakout Session 11

- Maintenance

The Present Situation of Road Installations of Tokyo Metropolitan Government and New Maintenance Management 13
Sentaro Takagi

Long Term Bridge Monitoring to Support Bridge Technology Innovations 19
Steven B. Chase

-Seismic

Detailed Investigation of PC Cable-stayed Bridge Damaged in the 1999 Taiwan Earthquake 27
Kenji KOSA, Kenji TASAKI

Rocking Motion of a Bridge Foundation Platform 41
W. Phillip Yen, Kornel Kerenyi

Construction and Material 51

Construction of Nagisa Bridge -Hybrid System of Cable-stayed PC Bridge and Steel Suspension Bridge- 53
Yuzuru SATO, Shinichi SASAKI , Katsutoshi MOROHASHI, Nobumasa SUZUKI

Performance Evaluation of Shear Links and Orthotropic Bridge Deck Panels for the San Francisco-Oakland Bay Bridge 61
Chia-Ming UANG, Frieder SEIBLE, Cole MCDANIEL, Chung-Che CHOU

An Experimental Study on Slip Strength of HSFG Bolted Joints Treated with High-Friction Inorganic Zine-Rich Paint 75

Yohei KOIKE, Keiji TERAO

Extending Service Life of Timber Bridges with Preservatives 81
James P. WACKER, Douglas M. CRAWFORD

The Design and Construction of the Chitose Bridge 91
Mitsugu ISHIDA, Yoshinori NAGAI, Kenji FUJITANI, Yasunari NAKANO

Static and Fatigue Behavior of the Connections of Aluminum Decks to Steel Girders 105
Ichiro OKURA, Nobuyasu HAGISAWA, Osamu OKADA, Shingo YAMAGUCHI

Fatigue Tests of Open Grid Steel Decks under Running Wheel Loads 117
Jun MURAKOSHI, Minoru TAKAHASHI, Noriyasu ARIMA, Toru FUJIWARA

Maintenance 1 129
Mitigation of Corrosion in Concrete Bridges 131
Paul Virmani, John M. Hooks,

Corrosion of 30 Years Old Weathering Steel Bridges 139
Kenji IKEDA, Takashi SATO, Kazunori WATANABE, Shizuo KATO,
Toshiya SUGAWARA

Federal Highway Administration Bridge Research and Technology Deployment Initiatives 149
Ian M. FRIEDLAND, Edgar P. SMALL

Field Tests of RC Deck Slabs Deterioration Assessment System by Digital Images 161
Shinya OKADA, Kenji IKEDA , Kazunori WATANABE, Hiroshi KOIDE,
Masakazu UEKITA

Florida's Approach to Bridge Preservation 175
Ivan R. Lasa, Rodney G. Powers

Nondestructive Inspection of the Suspender Ropes in a Suspension Bridge 189
Hiroaki HOASHI, Takeshi SUGIMOTO

Maintenance 2 ····· 201

Anti-subsidence Measure Using King-post Cables against Subsidence in A PC Box Girder with Central Hinge ····· 203
Takeshi SUZUKI, Shigeru MATSUMOTO, Kousuke WAKATSUKI, Hideki MANABE

Assessing Bridge Performance - When, What, How ····· 213
Richard Land, Ganapathy Murugesh, Madhwesh Raghavendrachar

Experimental Studies on Retrofit by Partially Encased Concrete to the Steel I-Girder subjected to Buckling Deformation ····· 229
Kenji HAYASHI, Shoji ONO, Shun-ichi NAKAMURA

U.S.A.'s Experience Using Fiber Reinforced Polymer (FRP) Composite Bridge Decks to Extend Bridge Service Life ····· 237
Jerome S. O'CONNOR, John M. HOOKS

Fatigue Life Extension of Damaged RC Slabs by Strengthening with Carbon Fiber Sheets Attaching Method ····· 249
Nobuhiro HISABE, Masasumi OKADA, Daisuke MIYAMA, Shigeyuki MATSUI, Hiroshi ONISHI, Akira KOBAYASHI, Hideaki FUKAGAWA, Yousuke MIMOTO

Preservation of Existing Bridges in Kentucky Using Advanced Composites ····· 259
Issam HARIK, Tong ZHAO, Ching Chiaw CHOO

Seismic 1 ····· 269

Enforcing Methods of Existing Old Bridges on Soft Ground For a Very Large Earthquake (In-Cap Method) ····· 271
Yukitake SHIOI, Mamoru AOYAGI, Tsutomu OOYA, Koji KATO, Hisashi FUKUDA

Comparative Design of a Bridge in New Jersey using the NCHRP 472 Comprehensive Specification for the Seismic Design of Bridges and the 1998 LRFD ····· 281
Harry A. Capers Jr.

Experimental Study on Liquefaction-induced Earth Pressure on Bridge Abutment ····· 295
Masuo KONDOH, Keiichi TAMURA

Static and Dynamic Behavior of Flared-Column Bents ·····303
Suhas S. CHANDANE, David H. SANDERS, M. "Saiid "SAIIDI, Saad EL-AZAZY

Structural Response Characteristics in Consideration of Directional Uncertainty of Earthquake Ground Motion ·····317
Hideaki NISHIDA , Shigeki Unjoh

Seismic 2 ·····327
The Effect of Abutments as Displacement Limiting Measure on Seismic Performance of Bridges ·····329
Taku MIKAMI, Shigeki UNJOH, Masuo KONDOH

Blue Ribbon Panel Recommendations for Bridge and Tunnel Security ·····337
James D. Cooper, Michael C. Smith, Steven L. Ernst

Ultimate Shear Strength of Pile Caps ·····355
Masahiro SHIRATO, Jiro FUKUI, Naoki MASUI, Kenji KOSA

A Sloping Surface Roller Bearing and its lateral Stiffness Measurement ·····369
George C. Lee, Zach Liang

·····379
Design and Construction Highway Piers with Interlocking Hoops in Japan
Kazuyuki MIZUGUCHI, Norimasa HIGASHIDA, Koji OSADA, Gaku OHASHI

Seismic 3 ·····387
A Study on Site-Specific Strong Ground Motion for Seismic Retrofit Design of the Hanshin Expressway Long-Span Bridges in Osaka Bay Area ·····389
Tsutomu NISHIOKA, Toshihiko NAGANUMA, Hidesada KANAJI, Takao KAGAWA

Seismic Retrofit of the Poplar Street Bridge ·····403
Mark R. Capron

Seismic Verification of Long-span Bridge of Honshu-Shikoku Bridges ·····411
Chihiro KAWATOH, Koji KAWAGUCHI

Seismic Design and Retrofit of Bridges on Missouri's Earthquake Priority Routes ·····421
Shyam Gupta, Bryan A. Hartnagel

Seismic 4 ·····435

Seismic Retrofit Strategy using Damage Control Design Concept and the Response Reduction Effect for a Long-span Truss Bridge ·····437
Hidesada KANAJI, Masahiko KITAZAWA, Naoto SUZUKI

Research Opportunities using the U.S. George E. Brown, Jr. Network for Earthquake Engineering Simulation (NEES) ·····449
Joy M. PAUSCHKE

Experimental Study on the Repair Effect of RC Piers Damaged by Earthquakes ·····461
Kazunori WATANABE, Akira HATAYAMA, Norimitsu KISHI, Tadashi HASEGAWA

APPENDIX
JAPAN PARTICIPANTS ·····469

US PARTICIPANTS ·····479

STUDY TOUR GUIDES ·····487

Proceedings of the 19th US-Japan Bridge Engineering Workshop

UJNR Panel on Wind and Seismic Effects

WORKSHOP PROGRAMS

19th U.S.-JAPAN BRIDGE ENGINEERING WORKSHOP
PROGRAM SCHEDULE

October 27, 28 and 29, 2003
At the PWRI, Tsukuba, Japan

First day, October 27 (Monday)

9:15-9:45 **Session 1: Opening Session (Conference Hall)**

Co-Chairs: J. Fukui, D. Sanders

Welcome Remarks: Tadahiko Sakamoto (Chif Exective, PWRI)

Remarks: Phillip Yen (Chairman for the U.S. Side)

Remarks: Hiroshi Sato (Chairman for the Japan Side)

9:45-10:05 **Coffee Break**

10:05-11:45 **Session 2: Seismic 1 (Conference Hall)**

(100 min.) co-Chairs: S. Unjoh & J. Cooper

1. Y. Shioi	Enforcing Methods of Existing Old Bridges on Soft Ground For a Very Large Earthquake (In-Cap Method)
2. H.A. Capers Jr.	Comparative Design of a Bridge in New Jersey using the NCHRP 472 Comprehensive Specification for the Seismic Design of Bridges and the 1998 LRFD
3. M. Kondoh	Experimental Study on Liquefaction-induced Earth Pressure on Bridge Abutment
4. D. Sanders	Static and Dynamic Behavior of Flared-Column Bents
5. H. Nishida	Structural Response Characteristics in Consideration of Directional Uncertainty of Earthquake Ground Motion

11:45-12:00 **Photograph** (Entrance of PWRI Main Building)

12:00-1:15 **Lunch Break**

13:15-15:15 **Session 3: Maintenance 1 (Conference Hall)**

(120 min.) co-Chairs: S. Nakatani & I. Harik

1.	J. Hooks	Mitigation of Corrosion in Concrete Bridges
2.	K. Ikeda	Corrosion of 30 Years Old Weathering Steel Bridges
3.	I. Friedland	Federal Highway Administration Bridge Research and Technology Deployment Initiatives
4.	S. Okada	Field Tests of RC Deck Slabs Deterioration Assessment System by Digital Images
5.	I. R. Lasa	Florida's Approach to Bridge Preservation
6.	T. Sugimoto	Nondestructive Inspection of the Suspender Ropes in a Suspension Bridge

15:15-15:45 **Coffee Break**

15:45-17:25 **Session 4: Seismic 2 (Conference Hall)**

(100 min.) co-Chairs: H. Kanaji & R. Land

1.	T. Mikami	The Effect of Abutments as Displacement Limiting Measure on Seismic Performance of Bridges
2.	J. D. Cooper	Blue Ribbon Panel Recommendations for Bridge and Tunnel Security
3.	M. Shirato	Ultimate Shear Strength of Pile Caps
4.	G. C. Lee	A Sloping Surface Roller Bearing and its lateral Stiffness Measurement
5.	K. Osada	Design and Construction Highway Piers with interlocking Hoops in Japan

19:00

Reception hosted by Chief Executive of PWRI at Hotel Okura

Second day, October 28 (Tuesday)

9:15-9:20 Opening

9:20-10:40 **Session 5: Seismic 3 (Conference Hall)**

(80 min.) co-Chairs: M. Ishida & G. Lee

1.	T. Nishioka	A Study on Site-Specific Strong Ground Motion for Seismic Retrofit Design of the Hanshin Expressway Long-Span Bridges in Osaka Bay Area
2.	M. R. Capron	Seismic Retrofit of the Poplar Street Bridge
3.	C. Kawatoh	Seismic Verification of Long-span Bridge of Honshu-Shikoku Bridges
4.	S. Gupta	Seismic Design and Retrofit of Bridges on Missouri's Earthquake Priority Routes

10:40-11:00 **Coffee Break**

11:00-12:00 **Session 6: Seismic 4 (Conference Hall)**

(60 min.) co-Chairs: M. Shirato & S. Gupta

1.	H. Kanaji	Seismic Retrofit Strategy using Damage Control Design Concept and the Response Reduction Effect for a Long-span Truss Bridge
2.	J. M. Pauschke	Research Opportunities using the U.S. George E. Brown, Jr. Network for Earthquake Engineering Simulation (NEES)
3.	K. Watanabe	Experimental Study on the Repair Effect of RC Piers Damaged by Earthquakes

12:00-13:15 **Lunch Break**

13:15-15:15 **Session 7: Maintenance 2 (Conference Hall)**

(120 min.) co-Chairs: J. Murakoshi & I. Friedland

1.	T. Suzuki	Anti-subsidence Measure Using King-post Cables against Subsidence in A PC Box Girder with Central Hinge

	2. R. Land	Assessing Bridge Performance – When, What, How
	3. S. Ono	Experimental Studies on Retrofit by Partially Encased Concrete to the Steel I-Girder subjected to Buckling Deformation
	4. J. S. O'Connor	U.S.A.'s Experience Using Fiber Reinforced Polymer (FRP) Composite Bridge Decks to Extend Bridge Service Life
	5. H. Fukagawa	Fatigue Life Extension of Damaged RC Slabs by Strengthening with Carbon Fiber Sheets Attaching Method
	6. I. Harik	Preservation of Existing Bridges in Kentucky Using Advanced Composites

15:15-15:45 **Coffee Break**

15:45-17:25 **Breakout Session:**

(100 min.) **- Maintenance (Conference Hall)**

co-Chairs: H. Kawano & S. Chase

Presentations for relating topics:

- Y. Fujisaki: The Present Situation of Road Installations of Tokyo Metropolitan Government and New Maintenance Management
- S. Chase: Long Term Bridge Monitoring to Support Bridge Technology Innovations

- Seismic (Room 725)

co-Chairs: K. Tamura & P. Yen

Presentations for relating topics:

- K. Kosa: Detailed Investigation of PC Cable-stayed Bridge Damaged in the 1999 Taiwan Earthquake
- P. Yen: Rocking Motion of a Bridge Foundation Platform

19:00

Reception hosted by the U.S. delegation

Third day, October 29 (Wednesday)

9:15-9:20 Opening

9:20-11:40 **Session 8: Construction and Material (Conference Hall)**

(140 min.) co-Chairs: K. Ikeda & M. Capron

1.	N. Suzuki	Construction of Nagisa Bridge –Hybrid System of Cable-stayed PC Bridge and Steel Suspension Bridge–
2.	Chia-Ming Uang	Performance Evaluation of Shear Links and Orthotropic Bridge Deck Panels for the San Francisco-Oakland Bay Bridge
3.	Y. Koike	An Experimental Study on Slip Strength of HSFG Bolted Joints Treated with High-Friction Inorganic Zine-Rich Paint
4.	J. P. Wacker	Extending Service Life of Timber Bridges with Preservatives
5.	K. Fujitani	The Design and Construction of the Chitose Bridge
6.	I. Okura	Static and Fatigue Behavior of the Connections of Aluminum Decks to Steel Girders
7.	J. Murakoshi	Fatigue Tests of Open Grid Steel Decks under Running Wheel Loads

11:40-12:00 **Session 9: Closing Session (Conference Hall)**

Co-Chairs: H. Sato, P. Yen

Settlement of Resolution

Remarks: Phillip Yen (Chairman for the U.S. Side)

Steve Chase (U.S. Side)

Closing Remarks: Hiroshi Sato (Chairman for the Japan Side)

12:00-13:30 **Lunch Break**

13:30- **Group A** Meeting of the governmental members (Room 730)

Group B Short study tour

Proceedings of the 19th US-Japan Bridge Engineering Workshop

UJNR Panel on Wind and Seismic Effects

TECHICAL PAPERS

19th US-Japan Bridge Engineering Workshop

Breakout Sessions

Maintenance

co-Chairs:

H. Kawano & S. Chase

The Present Situation of Road Installations of Tokyo Metropolitan Government and New Maintenance Management

S. Takagi

Long Term Bridge Monitoring to Support Bridge Technology Innovations

S. Chase

Seismic

co-Chairs:

K. Tamura & P. Yen

Detailed Investigation of PC Cable-stayed Bridge Damaged in the 1999 Taiwan Earthquake

K. Kosa

Rocking Motion of a Bridge Foundation Platform

P. Yen

The present situation of road installations of Tokyo metropolitan government and new maintenance management.

Tokyo Metropolitan Government
Bureau of Construction
Road and street administration Division
Assistant manager
Sentaro Takagi

SUMMARY

Bureau of Construction manages road installations built in large quantities by Tokyo Olympics holding before and after. As for the these road installations, it was designed economy to the first. Therefore many of institutions do not have enough durability performance, and there is the institution which cannot satisfy the life that I assumed at first. Now Bureau of Construction does not have the source of revenue that these update many road installations which deteriorated. Therefore we investigated a deterioration cause of road installations and did the result with growing life of providing equipment by reference. We decided the deterioration time of an institution by the deterioration cause that we investigated. In late years a countermeasure lengthening economic life is developed a lot, and there are the results. In the same institution, priority sequence decision of measures was possible, but the comparison of a different institution was difficulty. Therefore we tried a priority sequence judgment of an institution by assets evaluation of value of an institution.
I call this calculation method "Tokyo Metropolitan Government road asset management". Terminal decision does new calculation method by trial and error.

1. INTRODUCTION

The road which Bureau of Construction manages, the number of route is 283. Length of road, 2,245km, an area of road are 38,031,015 m^2. When road compares it with time of the Tokyo Olympics, it is 1.17 times by total extension, and total area is 1.95 times. Same as increasing road, road installations such as a bridge or a tunnel increase. Now, as for the management road installations, there are many institutions built to the high economic growth period which assumes the Tokyo Olympics an opportunity. I planned road as the first aim, and we designed reduction of construction cost (initial cost) in those days. As a result, uneasiness is left in durability performance partly, and there are the road installations that long-term safety and ease of use are anxious about. In road installations, a bridge is important greatly. Now Bureau of Construction manages 1,225 places road

bridge.

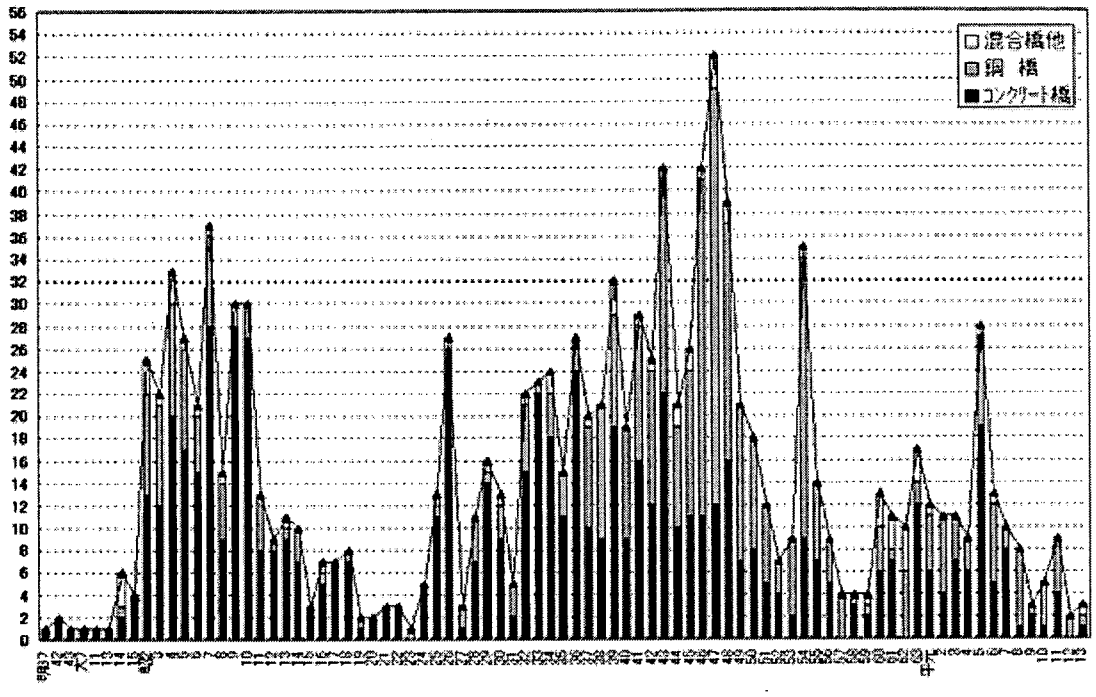


Figure – 1 Number of according to Construction year management bridges

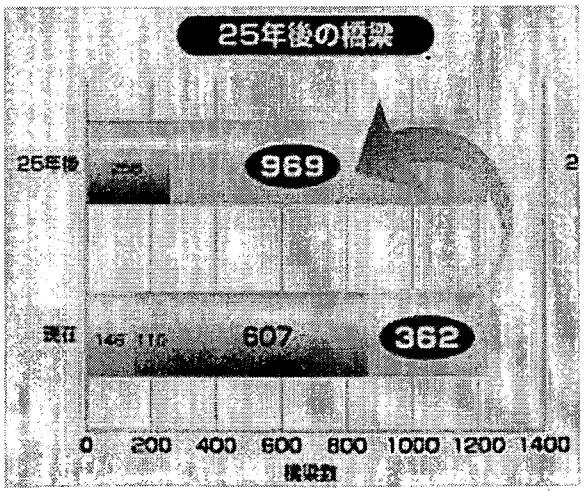


Figure-2 Change of management bridge after 25 years

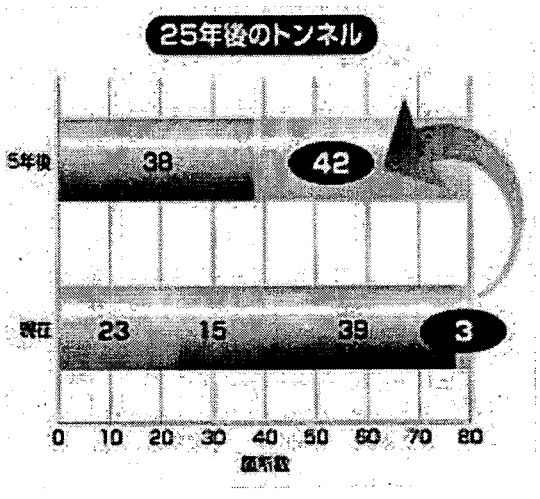


Figure-3 Change of management tunnel after 25 years

Now, as for those bridge, 362 places of the whole pass more than 50 years. However, 25 years later, 969 places become obsolete and become percentage of 79.1%. In addition, Bureau of Construction manages 80 places of tunnels. It is three places, and the superannuation tunnel which it passed through after construction more than 50 years is a

ratio of 3.8%. However, 25 years later, 42 places become obsolete, and the ratio becomes 52.5%.Many road installations managing become obsolete rapidly.
The financial situation of Tokyo metropolitan government turns worse year by year.
According to the financial prospective income and expenditure of Tokyo metropolitan

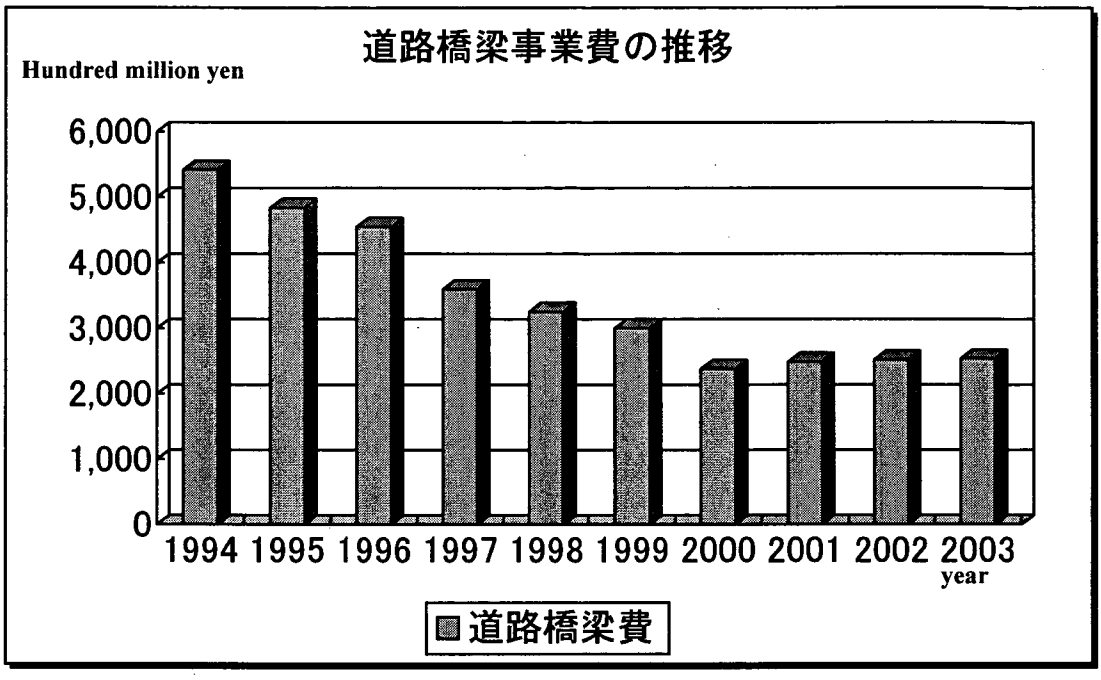


Figure-4 Change of Tokyo metropolitan government road budget

government of 2003, it predicts lack in source of revenue of 2006 with 3,500-3,700 hundred million yen every year from 2004. When this situation continues, a source of revenue to rebuild old road installations becomes insufficient. A budget about maintenance management of road is in inverse proportion with increase of management scale and decreases, and the maintenance management that is need is the present conditions that it is not possible for. The dilapidation advances to road installations unless a necessary budget is worth maintenance management, and road is closed to traffic. In New York City of the 20th century and other many foreign countries, there are many similar examples.

2. REBUILDING AND INCREASE OF DURABILITY OF MANAGEMENT BRIDGE

For example, as for Bridge that the length that Bureau of Construction manages is more than 40 meters, as for the steel bridge older than 50 years old and Prestressed concrete bridge (PC bridge) and Reinforced concrete bridge older than 60 years old, it is it with 45 places. About 2,144 hundred million yen is necessary to rebuild all these. A period of completion is about 20 when it calculates the number of years that is need to rebuild it from total expense used for rebuilding of management bridge till now. It did this steel

product corrosion survey by supersonic wave. The data number which it used for corrosion calculation by this investigation is 1,424 streetlights and 38 road sign column. The corrosion rate of steel product calculated these by the following expressions.

Corrosion rate = (nominal rating stock thickness - measurement minimum stock thickness) / (the investigation date - establishment date)

It shows it about the column progress the number of years and a change of corrosion rate that it investigated this time. When corrosion rate of steel product compares it with galvanizing processing in the case of painting processing, around 10 times are big painting processing. From findings, galvanizing processing is more superior in rust prevention ability than painting processing. In addition, in structure of the foundation outskirts of Streetlight and Road-sign pillar, it compared most concrete and other corrosion rate.

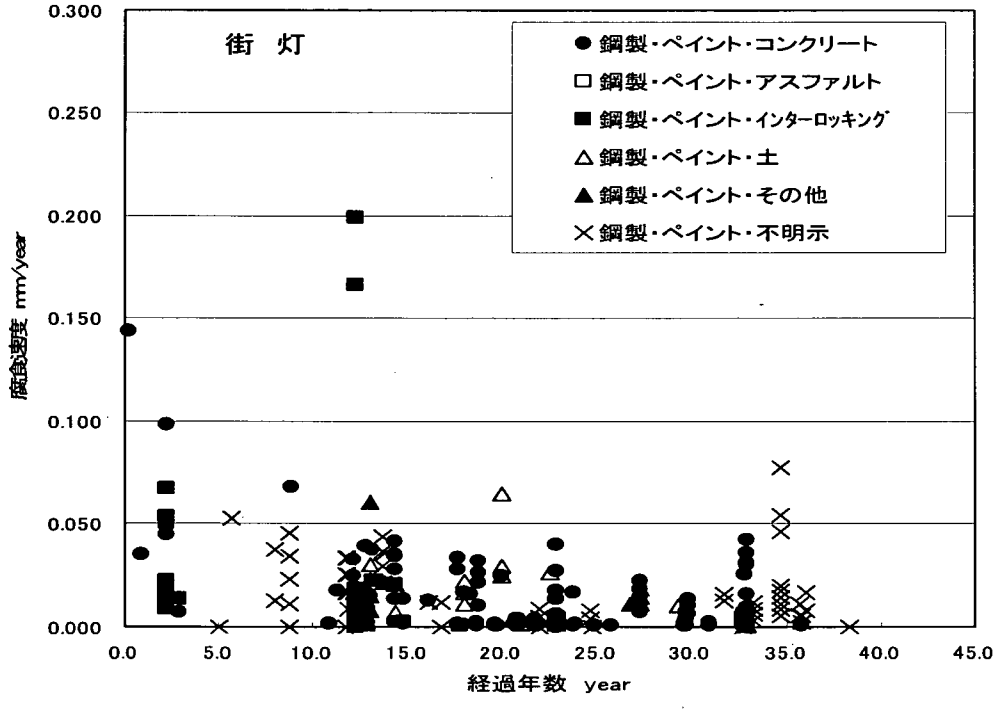


Figure – 5 Corrosion rate of Steel-pipe column (in the case of painting)

Corrosion rate of concrete foundation is 0.05mm / year. Corrosion rate of interlocking block foundation is 0.2mm / year. The corrosion rate when steel product contacted with soil was 0.06mm / year. It writes down a reason of a difference of corrosion rate next.

Because it is superior in watertight ness ability, concrete foundation does not have water retention ability. Soil and an interlocking block base have water retention ability. These water retention ability has a long drying time of rain-water of the steel product outskirts. As for the base of steel product with water retention ability, it is it with big corrosion rate by being the environment that resembled water surface neighborhood. In addition, there is the peculiar example that corrosion rate is big in concrete foundation in this investigation

data, but it is thought with a cause by excretion wastewater of dogs. It explains the effect which investigated corrosion rate according to materials. When aluminum and stainless steel compare it with steel product, corrosion rate is very small with 0.001mm / year. In addition, average corrosion rate of the steel product which it painted is 0.007mm / year. In the case of steel product of galvanizing processing, it is 0.003mm / year and it is 0.001mm / year in the case of aluminum and stainless steel. Corrosion rate of steel materials in Tokyo metropolitan government, it is it with 0.1mm / year when it judges corrosion rate for reference in this findings and return such as "corporate judicial person / steel product club" or "foundation / coast development technology center". This corrosion rate is the set point which thought about security enough. It carries out a periodic inspection of steel product once in 5.

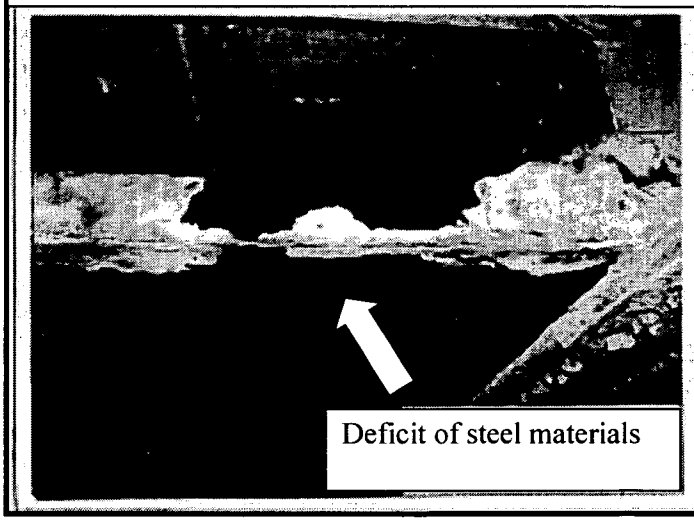
Therefore it set relation of thickness of board of a management standard and thickness of board of a limit.

"Management reference value" = "limit" + "5 *0.1 mm" / age = "limit" +0.5 mm

The deterioration of concrete investigated the situation of concrete structure of Tokyo metropolitan government.

The deterioration of concrete investigated an inner wall of a tunnel built in a beach district.

Figure – 6 Corrosion example of Road bridge



The damage of a concrete inner wall deteriorates by salt of seawater. Reinforcement corrodes by the salt which penetrated and expands. As for the deterioration of reinforced concrete construction, corrosion of reinforcement is the biggest as the damage. It is important that reinforced concrete construction and prestressed concrete structure prevent corrosion of reinforcement. Concrete is alkalinity.

Concrete becomes neutral from alkalinity by outside air. If concrete becomes neutral, internal reinforcement is easy to come to corrode. It investigated deterioration by salt and deterioration by outside air.

Deterioration of steel product has fatigue damage. Fatigue of steel product occurs a lot in weld. We investigate a cause of fatigue of steel product and the measures.

Our investigation is according to structure and is according to materials, and it is environment distinction. We are to elucidate a deterioration cause and deterioration speed of road installations by the next year.

3. NEW MAINTENANCE MANAGEMENT (T.M.G. ROAD ASSET MANAGEMENT)

A decision of the time extending life of road installations is deterioration speed and life.
Next of decision of the measures time is decision of anti-institution measure priority sequence. The decision of priority sequence was done till now by every institution. It judged the priority sequence to be it in deterioration degree or soundness. It was hard to understand the conventional priority sequence decision method in a judgment every institution. New priority sequence decision is the method how assets evaluation of value makes road installations. Assets evaluation of value does an institution, and a private enterprise is decided with improvement contents and order of an institution on grounds in assets value. Bureau of Construction thinks about the method how assets evaluation of value makes road installations same as private enterprise. When lack in source of revenue continues, a budget to rebuild an institution becomes insufficient. Lack of expense to rebuild becomes a big problem in safety and the durability of road installations. Lack in source of revenue takes a traffic function of people. An effective application of a source of revenue is introduction of the road asset management. Bureau of Construction introduces the road asset management early and gets a desirable traffic function. The road asset management switches it to preventive type maintenance management. Introduction of the road asset management is an action of new Tokyo metropolitan government.
The Metropolitan citizens expect it in a policy of new Bureau of Construction.

Key word ; corrosion rate, deterioration, improvement of the durability, maintenance management of a preventive type, asset management:

Long Term Bridge Monitoring to Support Bridge Technology Innovations

Steven B. Chase[1]

Abstract

The state of the practice of bridge inspection and bridge management in the United States is briefly discussed. This practice has many limitations. The most significant limitation is that the data collected is based solely upon visual inspection, augmented with limited mechanical methods such as hammer sounding or prying. Visual inspection is highly variable, subjective and inherently unable to detect invisible deterioration, damage or distress. There are many types of damage and deterioration that need to be detected and measured that are beyond the capabilities of visual inspection. Bridge performance also needs to be measured. The FHWA and many others have conducted research and development in technologies that can help meet these needs. Several examples illustrating the application of this technology for the long term monitoring of bridges are described. While the summary is not comprehensive it demonstrates that technology exists to meet the needs identified. Future directions and further application of bridge monitoring technology are also briefly discussed.

Introduction

In the United States as of 2002, XX% of the US bridges were structurally deficient or functionally obsolete, as reported by the Federal Highway Administration (FHWA). This assessment of the structural and functional condition of the nation's highway bridges is based upon data reported to the FHWA by bridge owners across the country and maintained by FHWA in the National Bridge Inventory (NBI) database. Bridge owners have been reporting this data to FHWA since 1972 when FHWA established the National Bridge Inspection Program. The National Bridge Inspection Program was established in response to the collapse of the "Silver" Bridge in 1967 and the program focuses on the safety of highway bridges. The bridge inspection program requires that qualified inspectors inspect highway bridges at least once every two years and that the results are reported to the FHWA. This data is used to report the condition of the nation's highway bridges to Congress every two years and to administer the Highway Bridge Replacement and Rehabilitation Program (HBRRP). Last year the HBRRP provided more than $3.5 billion to replace or rehabilitate deficient bridges.

Background and Need

The type of data collected and reported for the National Bridge Inspection Program is adequate for managing and administering a national program aimed at eliminating deficient bridges but it is inadequate for some other purposes. The data is not detailed enough to support bridge maintenance programs. The NBI does not record the condition of paint systems, joints or provide information on local damage or deterioration. The data

[1]Dr. Eng., Technical Director for Bridge Research and Development, U.S. Federal Highway Administration

is too general, subjective and qualitative to be used to develop plans and estimates for repair or rehabilitation work. For example, the NBI records condition data for the entire supersructure of the bridge with a subjective rating ranging from excellent to failed as a integer from 9 to 0. In response to these limitations, many states augment the NBI by collecting additional information or use a different, more refined, approach to collection and recording of bridge condition data. The more refined approach characterizes a bridge as a collection of elements, such as girders and piers, and records quantitative condition data on each element. Standardized elements have been defined for highway bridges and automated methods are used to translate the element level data into the NBI data required by the FHWA.

Although the element level inspections provide more detailed and useful information for network level bridge management, especially at the state and local level, the information collected is still very limited in several respects. The most significant limitation is that the data collected is based solely upon visual inspection, augmented with limited mechanical methods such as hammer sounding or prying. Visual inspection is highly variable. The FHWA's Nondestructive Evaluation Validation Center recently completed the first comprehensive and quantitative study of the reliability of visual inspection and the NBI condition rating system. The results of that study indicate that a range of condition ratings of 3 or 4 numerical values can be expected routinely with different inspectors reporting results for same bridge in the same condition. This variability is in addition to the inherent limitation of visual inspection to fail to detect invisible deterioration, damage or distress. There are many types of damage and deterioration that need to be detected and measured in order to determine if a bridge is safe or if repairs are required. Many of these are difficult or impossible to detect visually unless the damage or deterioration is severe. For example, it is not possible to look at a bridge and determine if it has been overloaded or if it has settled unless the damage is so severe as to cause the lines of the bridge to change. Frozen bearings, corrosion and fatigue damage can exist with no visible indications. Routine visits by bridge inspectors also do not collect information on the operational performance of bridges such as congestion, accident history or fatigue of structural members.

The implementations of customer driven quality improvement programs or asset management supported by true engineering economic analysis are immediately hindered by the lack of necessary information. We currently guess at average daily traffic values. We do not know the size, number and weight of the trucks our bridges carry. The actual stresses, strains, deflections and displacements the bridges experience are unknown. There is a need to more accurately quantify the operational performance of highway bridges. The performance measures, which are most immediate to the traveling public, are concerned with congestion, accidents, and service. These same performance measures can help to quantify the value of bridge as assets in terms of user costs and benefits. These need to be measured. It is a basic tenet of modern management theory and practice that if you can't measure it you can't manage it.

This same information is also needed to implement true life cycle cost analysis or performance based specifications. FHWA, like all federal agencies in the United States, is directed by

executive order to consider life cycle cost for major projects. However, the life cycle of bridges has not been defined. The deterioration rates of different materials, structural systems in different environments of loading and climate have not been measured. There is a specific need to integrate quantitative performance measures into the management systems for the highway infrastructure. Some of the measurement and detection needs currently not met by our standard practice of visual inspections are tabulated below.

Damage	Detection	Operation	Service
Impact Overload Scour Seismic Fatigue Settlement Movement Lack of Movement	Corrosion Fatigue Water absorption Loss of prestress force Unintended structural behavior	Traffic counts Weight of trucks Maximum stress Stress cycles Deflection Displacement	Congestion Accidents Reduced traffic capacity Performance measures

These measurement and detection needs exist at many levels and can serve many purposes.

Summary of recent research to respond to this need

The FHWA and others have conducted research and development in technologies that can help meet these needs. Several examples illustrating the application of this technology to monitor and measure bridges are described in this article. This summary is not comprehensive. It is intended to demonstrate that technology exists to meet the needs identified and to stimulate interest in application and further development of innovative technologies to monitor the long term performance of bridges.

Global health monitoring has evolved to the point where a number of large systems have been implemented on large bridges in many parts of the world. One such system has been installed and is operating on the Commodore Barry Bridge over the Delaware River in Pennsylvania. Although promising, the full potential of this technology has not been realized or defined and significant issues remain to be researched. The information technology component is one such issue. In spite of these limitations, the information these types of systems already provide has proven to be very useful to the owners of the bridges where they have been installed. One example of the type of information these systems provide is the detection and quantification of unexpected bending of tension elements due to differential solar radiation exposure

Non-intrusive load capacity measurement is a pressing need. Substandard load capacity is the single most frequent reason for a bridge to be classified as structurally deficient in the United States. One technology, which the FHWA has adapted to meet this need, is a laser measurement system for bridge load testing. The system uses a computer-controlled mirror to aim an invisible, eye safe, infrared laser beam at a point on the bridge. The laser measures the

range to the point on the bridge and reports the three-dimensional spherical coordinates of that point, relative to the local origin set by the laser system. The system can repeat this measurement at different points on the bridge hundreds of times in a few minutes. The system has a measurement range of about 30 meters and an accuracy, resolution and repeatability of a fraction of a millimeter. The system does not require special targets and works well on ordinary steel, concrete and timber surfaces. Using this system it is possible to rapidly measure the three dimensional deflection response of a bridge to a heavy truck. The system can also be used to rapidly and quantitatively measure if any part of the bridge has moved since the last time the bridge was scanned, with an accuracy, precision and repeatability of a fraction of a millimeter. This system is also capable of early detection of subsidence or loss of prestress. This example demonstrates that long-term monitoring does not always require a dedicated and permanently installed monitoring system for each bridge.

The detection and measurement of fatigue and vulnerability to fracture continue to be a pressing need for the hundreds of thousands of steel bridge in the nation. The National Bridge Inspection Program was initiated in 1971 in response to a bridge failure caused by a brittle fracture. The brittle fracture of a welded plate girder resulted in complete bridge failure in Milwaukee, Wisconsin in December 2001 demonstrates that this vulnerability still exists. This bridge had been visually inspected a few weeks prior to the failure and there was no visual indication of the impending failure. Subsequent forensic analysis has confirmed vulnerability to sudden brittle fracture due to welding practices and details that produced high residual stress and triaxial restraint. Visual inspection alone is not capable of detecting or quantifying these conditions.

Although fatigue was not a contributing factor to the brittle fracture in Milwaukee, it continues to be a major problem on aging steel bridges. The measurement and characterization of the random, variable amplitude cyclic stress that brides are subjected to is an essential measure need. Technology has been developed to help manage fatigue. Numerous examples of portable, battery powered, data acquisition systems now exist. These systems offer very high dynamic range, very low noise and adaptive digital spread spectrum radio network telemetry capabilities. Using this technology it is possible to rapidly instrument a bridge at fatigue prone or critical details and measure what happens under traffic and wind loading.

The wireless network technology can quantify the fatigue-loading regime at a fatigue prone detail but it cannot measure if a fatigue crack is growing under that load. These cracks do not grow continuously but advance in microscopic steps. The advance of the crack front is accompanied by release of potential energy that produce ultrasonic stress waves. This is similar in concept to the release of energy associated with an earthquake but on a microscopic scale. The stress waves can be detected using special sensors tuned for this purpose. The method is call acoustic emission (AE) and it has been used for many years in the energy and process industries. However, prior AE instruments were not practical for long term monitoring of fatigue cracks on highway bridges. The lack of electrical power on most bridges, the difficulty in accessing the details on the bridge, the very high background noise environment, and perhaps most importantly, the random loadings with rare high load events

driving crack extension all worked against successful application of AE on bridges. A new battery powered, eight channel AE instrument specifically designed for the bridge monitoring need was developed in cooperation with the FHWA's NDE Validation Center. This system can also telemetry information via modem or radio link.

While the two prior systems are very useful, they are expensive (10's of $K), and they are still limited by battery power to relatively short term monitoring. A totally passive and inexpensive fatigue measurement sensor has also been developed to meet the need for very long duration fatigue measurement. This sensor is attached to the bridge and strains along with the bridge. The sensor is based upon a special passive strain amplification design and two, pre-cracked, coupons with integral analog crack length gages. The two coupons are fabricated with materials that have different crack growth properties. These manufactured fatigue cracks grow in response to the random variable amplitude strains on the bridge. By periodically measuring the crack lengths in the two coupons with a special reader, the effective number of cycles at a predetermined stress range can be quantified. This sensor can be likened to a fatigue odometer. Using this technology, it is possible to measure how the fatigue life of a highway bridge is being consumed.

Another example of new technology applied to help collect essential performance information is the development of a smart bridge bearing. Non-operating bearings, and the tremendous stresses that result, are a common factor in bridge failures. They are also a very common maintenance requirement. In addition, the distribution of live and dead loads to the bearings through the structural systems of the bridges is a possible diagnostic and damage detection capability that this technology will enable. If there is a significant change in stiffness of a structural member due to fracture, impact or other reason, it is likely that the distribution of the loads to the bearings will change. A smart bearing could "feel" the damage in the bridge. The enabling technologies are sophisticated but the concept is simple. The intelligence for the bearing is provided by multi-axis fiber optic strain sensors, capable of measuring both vertical and shear strains, that have been integrated into a composite panel. The panel can be integrated into the bearing. The panel could be laminated between the neoprene bearing pads commonly used on highway bridges and can measure the vertical and lateral forces transmitted from/to the bridge.

There are an almost unlimited number of possible applications for sensing and measurement technologies for highway bridges. The technology does not need to be expensive and sophisticated. Another example concerns a wing wall that was moving due to excessive hydrostatic pressure. Remedial measures were taken and the owner wanted to monitor the movement of the wall relative to the abutment. The environment is severe and an inexpensive but reliable sensor was needed. The NDE Validation Center conceived, designed, built and installed an inexpensive displacement sensor in a few weeks. The sensor has been monitoring the wall for three years and has proven that the remedial measures were effective. Over the years FHWA has developed a versatile modular instrumentation concept that facilitates rapid prototyping and deployment of specialized sensing applications. This lends itself to specialized

and critical component monitoring where unique features or requirements can be readily accommodated.

An illustration of this versatility is another application on a fracture critical hanger on a pin and hanger detail. The hanger is being monitored using the same modular system that was used to monitor the wing wall. The sensors in use are welded resistive foil strain gages. The hanger is supposed to freely rotate about the pin as the bridge expands and contracts due to temperature changes. The hanger transfers vertical load and is designed as a tension element. If the pin and hanger interface corrodes, a very common occurrence, the friction between the pin and hanger can cause significant bending in the hanger. In addition, the sudden slippage of the pin hanger interface can result in tremendous dynamic stress. The fatigue and possible fracture consequences of this phenomenon were not considered in the design of these details. The response of the hanger was measured during a load test. In addition to bending in the expected direction, unexpectedly transverse bending of the hanger was also measured. Detection and measurement of unintended structural behavior is a major benefit of this type of monitoring.

Steel bridges are not the only bridges vulnerable to sudden failure and collapse. A number of prestressed concrete bridges have collapsed due to undetected corrosion of tendons. One recent example was the collapse of a pedestrian bridge in the summer of 2000 after only seven years of service. The failure was caused by corrosion and failure of the high strength steel tendons that helped support the bridge. The localized corrosion of the tendons was attributed to calcium chloride unexpectedly found its way into the grout used to fill in holes created during the fabrication of the precast girders. The source of the calcium chloride is still unknown but undetected corrosion of prestressing steel has led to the failure of a number of bridges.

When such a wire breaks there is a sudden and significant release of potential energy. Such wire breaks generate stress waves which propagate outward from the structure and which can be detected by sensors, such as accelerometers. By analyzing the arrival times of the signals, it is not only possible to detect the wire breaks but to also locate where the break occurred. The method is similar to a network of seismometers to locate and quantify earthquakes. Such systems are commercially available and are installed on a number of bridges.

Detecting wire breaks is certainly useful, but a potentially more useful technology is the detection and quantification of corrosion before failure occurs. The most common cause of corrosion in highway bridges is the salt placed on the bridges to keep the bridge open during winter storms. The corrosion of structural steel is usually visible. However, the corrosion of reinforcing and prestressing steel in concrete structures is not visible until significant damage has occurred. A new device, developed in cooperation with the FHWA, is an embeddable corrosion sensor. The sensor is designed to be placed inside of concrete structures and to measure corrosion rate, concrete conductivity and chloride ion concentration. The instrument is small and eventually will be powered and interrogated by wireless radio frequency methods. If the size and cost can be reduced, hundreds or thousands of these sensors could be economically embedded in a bridge to provide quantitative information about the state of corrosion well before severe damage has occurred.

Future direction

This paper has documented that much of the technology to monitor bridges is already available. This technology can provide the quantitative and objective information necessary to move beyond our current subjectively based bridge management systems. There is a need to evolve to a more quantitatively driven management approach. This need has been identified and emphasized by the United States National Academies of Science and Engineering.

The Academies have held several workshops where stakeholders from the public, private and academic communities have been bought together to identify the most pressing and highest priority research needs for dealing with an aging highway infrastructure. The result is a National Infrastructure Renewal Research Agenda. The need for reliable and timely data and information is recognized as critical to the efficient management of the nation's highways. The agenda also identifies the need for much improved decision support tools as well as to integrate probabilistic life-cycle analysis into infrastructure management. The need to value infrastructure assets and quantify the benefits of the system is also specifically mentioned. Quantitative, relevant and useful measures of performance are emphasized. Long term bridge monitoring addresses all of these needs.

The safety assurance of highway structures for extreme events would also be greatly enhanced by short and long term monitoring and measurement of the loading and structural response during extreme events. As already demonstrated, assessment and management of bridges and other structures demand the quantitative measurements provided by the monitoring of structures. It is not possible to develop enhanced specifications without long-term observation and quantitative measurement of structural behavior and deterioration. Finally, the basic information necessary to support the automation of design, construction and maintenance, identified as a national priority for infrastructure research and development must be provided by sensing and measurement technology.

For all of the reasons outlined, the Federal Highway Administration is proposing to begin a Long Term Bridge Performance Program. This program would be modeled after the Long Term Pavement Performance Program. The program will include detailed inspections and periodic evaluations conducted on a representative sample (in the thousands) of bridges to monitor and measure their performance over an extended period of time (at least 20 years). It is anticipated that the resulting database will provide high quality, quantitative, performance data for highway bridges to support improved designs, improved predictive models, and better bridge management systems. A second component of this long-term bridge performance program will be a subset of instrumented bridges (in the hundreds) that can provide continuous long-term structural bridge performance data. The third component of the program will include detailed forensic autopsies of several hundred bridges each year (out of the several thousand bridges that are decommissioned each year). These forensic autopsies could also be conducted for bridges that fail unexpectedly. The intent is to collect valuable performance data on

corrosion, overloads, alkali-silicate reaction, and all other deterioration processes from these bridges.

The long-term bridge performance program will be designed to accommodate and develop both general trend information, and information specific to a variety of bridge types, locations, and environmental exposures.

Closure

To summarize, long term bridge monitoring can provide quantitative data for network and bridge level management. This could contribute to a much greater level of reliability and utility of data necessary for asset management. Bridge safety, especially during extreme events, is enhanced by measurement and monitoring of critical bridge components. Enhanced safety, reliability and efficient maintenance can result from improved incident detection and assessment. Global bridge health and performance assessment in support of asset management and enhanced specifications must be, and arguably can only be, accomplished using quantitative measurement methods. Subjective assessment simply is not adequate to meet these needs.

Detailed Investigation of PC Cable-stayed Bridge Damaged in the 1999 Taiwan Earthquake

Kenji KOSA[1] and Kenji TASAKI [2]

ABSTRACT

Among the bridges damaged in the 1999 Chi-Chi earthquake in Taiwan, the Ji-Ji-Da Bridge (cable-stayed) suffered problematic damage which is unacceptable in terms of seismic design of this type of bridge. For example, plastic hinges were produced not only at the pier bottom but also in the main pylon and the main girder, and one diagonal cable pulled out from the anchorage section. The damage mechanism of this bridge was analyzed using a frame model, with the incorporation of field measurement results and detailed drawings obtained from bridge administrators in Taiwan. It was found that that the cause of cable pullout was the insufficient anchoring strength.

1. INTRODUCTION

Tremendous damage was caused in the central region of Taiwan in the Chi-Chi Earthquake that occurred in Sept. 1999 with a magnitude of M=7.3. Many bridges fell or suffered a crucial damage in the area along the Chelungph Fault that runs north to south near the hypocenter shown in Fig. 1. Among the damaged bridges, the cable-stayed Ji-Ji-Da Bridge which was under construction at the time suffered a problematic damage that needs discussion in terms of seismic design. For example, damage occurred not only to the bottom of the pier but also to the main pylon and the main girder, in addition to the pullout of a diagonal cable from the anchorage section. In view of the importance of the damage, various investigations, such as linear dynamic analysis and strength check, have been carried out nationally and internationally, including ours [1)-3)]. Our previous investigation was not fully successful in identifying the cause of damage of this bridge, partly because the analysis was performed based on limited information.

To pursue the problem, the authors once again visited the damage site in Taiwan in November 2002 to conduct a field survey and to see the progress of retrofit. At that time, we had a chance to talk with bridge administrators in Taiwan and could get detailed drawings of the bridge. Using the information thus obtained and the results of micro-vibration measurement taken at the bridge site, a detailed investigation was conducted on the damage mechanism of this bridge. This paper presents the results of this investigation.

---

1) Professor of Civil Engineering, Kyushu Institute of Technology, Kitakyushu, Japan
2) Senior Engineer, Structural Engineering Division, Nippon Engineering Consultants Co., Ltd. (Currently in the doctoral program at Kyushu Institute of Technology)

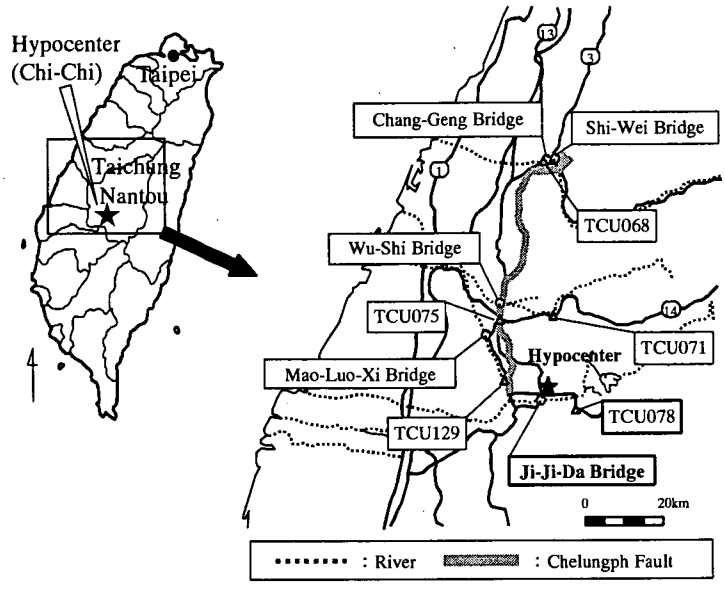


Fig. 1 Bridges surveyed and measuring locations of strong motion

2. STRUCTURE OF THE BRIDGE AND OUTLINE OF DAMAGE

The Ji-Ji-Da Bridge is a PC cable-stayed bridge with two spans which is located at about 3 km away from the hypocenter at Chi-Chi. At the time of the earthquake, this bridge was under construction and four panels of precast members on one side at the connection area of the main pylon and the main girder were not yet built, as shown in Fig. 2.

The main girder of this bridge consists of arc-curved one box girder with two cells. The girder height is 2.75 m, the girder width is 24.0 m and the span length is @120 x 2 = 240 m. The main pylon is an RC column, 58 m in height, having a deformed diamond shaped cross section with a hollow, measuring 3.0 m x 4.0-6.0m, as shown in Figs. 3 and 4. The cables are arranged in two rows. In one row, 17 cables are arranged on each side of the main pylon. The pier below the main pylon is an oval-shaped RC column measuring 6.0 x 6.3 m, as seen in Fig. 5. The Foundation below the main pylon is the cast-in-place pile type (ϕ 1500). The concrete strength (σ ck) is 34.3 N/mm^2 for all of the main girder, the main pylon, and the pier.

The damage was widespread extending over the main girder, the main pylon, the pier, as well as the cable, as shown in Fig. 2. For example, the cover concrete fell from the faces of the perpendicular direction at the bottom of the main pylon, and the ends of the main girder detached from each adjoining girder and swayed to the perpendicular direction. Also, the cover concrete was separated and the main reinforcement buckled in the main girder on the south side at the rigid connection section with the main pylon. From these damages, it is considered that a large seismic force acted in both the axial direction and the perpendicular direction of the bridge.

As to the cables, one cable on the south side, the 11th from the top, was pulled out from the anchorage section of the main pylon. Many sockets were also pulled out from the anchorage section. This means that large tension was caused to the diagonal cables during the earthquake. On the other hand, according to our first field measurement immediately after the earthquake, the span length before the earthquake, 120 m, did not changed virtually after the earthquake.

In view of the fact that (a) a fault was not found in the vicinity of the bridge and (b) the seismic waveform obtained at TCU078 (to be explained later) did not show any waveform like a directivity pulse even though its location is close to the Chelungph Fault, it is considered that the damage occurred to this bridge was primarily caused by the seismic motion during the earthquake.

As to the progress of retrofit as of November 2002, Ji-Ji-Da Bridge was already open for service, but the pullout cable was still left as it was and a bent support was still in place. However, the bottom of the main pylon had been repaired with concrete jacketing and the bottom of the pier with steel jacketing.

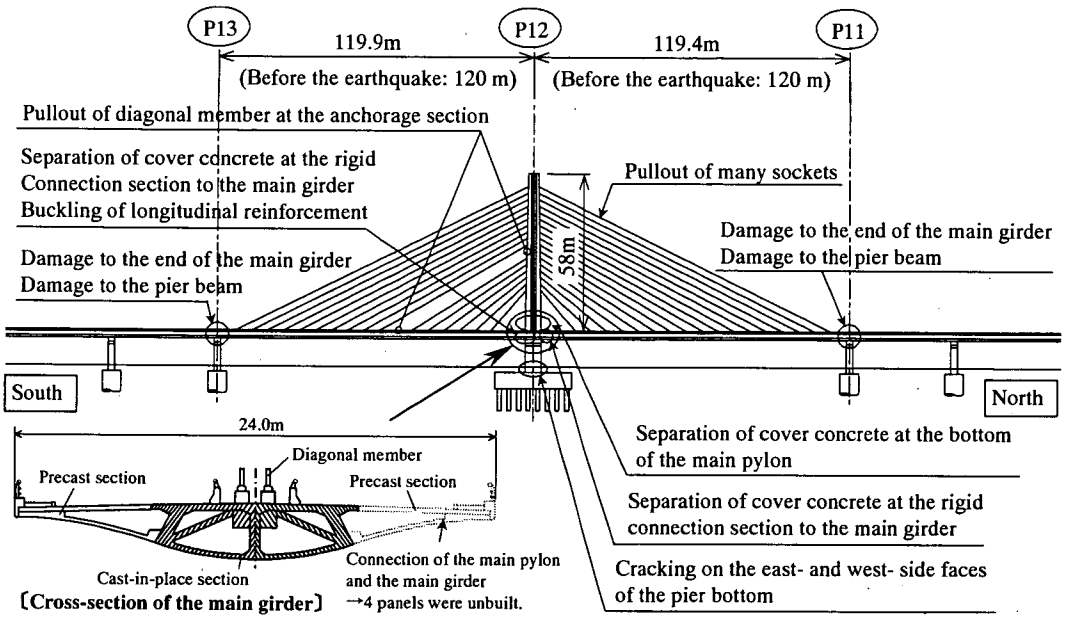


Fig. 2 Damage to the Ji-Ji-Da Bridge and measurement results

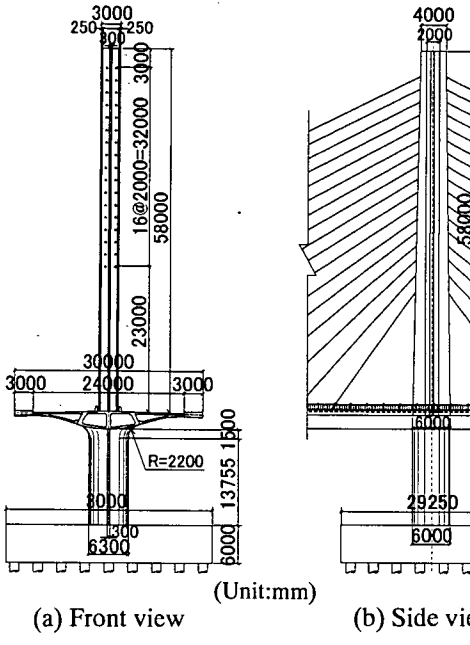


Fig. 3 Structure of the main pylon

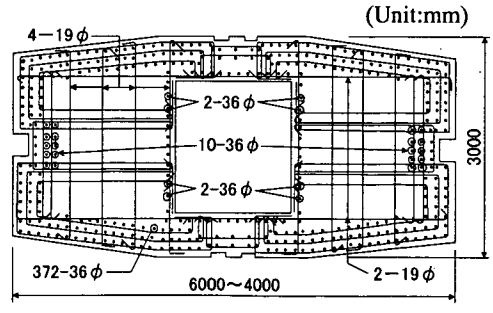


Fig. 4 Cross section of the main pylon

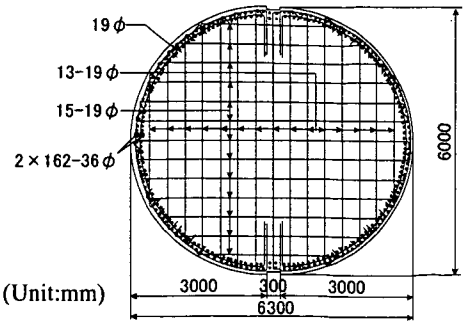


Fig. 5 Cross section of the pier at the main pylon

3. SEISMIC RESPONSE ANALYSIS

3.1 Analysis Model

The main span (@120 x 2 = 240 m) of the Ji-Ji-Da Bridge shown in Fig. 2 was modeled as the 3D frame model, as shown in Fig. 6, and a nonlinear time history response analysis was performed using this model. The sectional constants of the main girder, the main pylon, and the pier shown in Table 1 were determined based on the detailed drawings of the reinforcement arrangement. The bending moment-curvature relationships (M-ϕ)of the main pylon and the pier were calculated by considering the level of the axial force when the dead load is working. In the frame model, the main girder was modeled by the elastic beam elements, the main pylon and the pier by the elasto-plastic beam elements, and the diagonal cables by the linear truss elements having the stiffness only in the axial direction. As to the rigid connection section of the main pylon and the main girder, rigid elements were placed as shown in Fig. 6. The mass of the cables was divided into two and each was added to each joint on the main pylon and the main girder at the end of the elements. As to the boundary conditions, the only conditions fixed were the bearing conditions in the vertical and perpendicular directions of the piers (Pier 11 and Pier 13).

(1) Modeling of the main girder

As said earlier, four panels of precast members on one side of the main girder were unbuilt at the time of the earthquake. In the analysis model, this effect was taken into account in the flexural rigidity of the main girder. As shown in Fig. 7, the 6.0-m section which is equal to the width in the axial direction at the bottom of the pylon was modeled as the rigid members, and the two 0.68-m sections were modeled as the elastic beam elements in consideration of the incompleteness of the cross section.

Table 1 Constants of the cross-section

Cross section	Geometrical moment of inertia (m^4)			Yield bending moment (MN・m)		Yield curvature (1/m)		Sectional area (m^2)
	Ix	Iy	Iz	Myox	Myoy	ϕyox	ϕyoy	A
Main girder (built section)	-	15.10	1579.67	-	-	-	-	15.732
Main girder (unbuilt section)	-	14.71	450.97	-	-	-	-	12.571
Top of the main pylon	9.51	11.26	-	89.50	133.43	7.942E-4	4.077E-4	8.905
Bottom of the main pylon	13.13	53.74	-	180.31	324.16	9.319E-4	4.479E-4	14.120
Pier	86.26	79.54	-	426.72	415.12	4.546E-4	4.771E-4	30.074
Average of the cables	-	-	-	-	-	-	-	0.0092
[Definitions of the structural axes] X axis: axial direction, Y axis: perpendicular direction, Z axis: vertical direction								

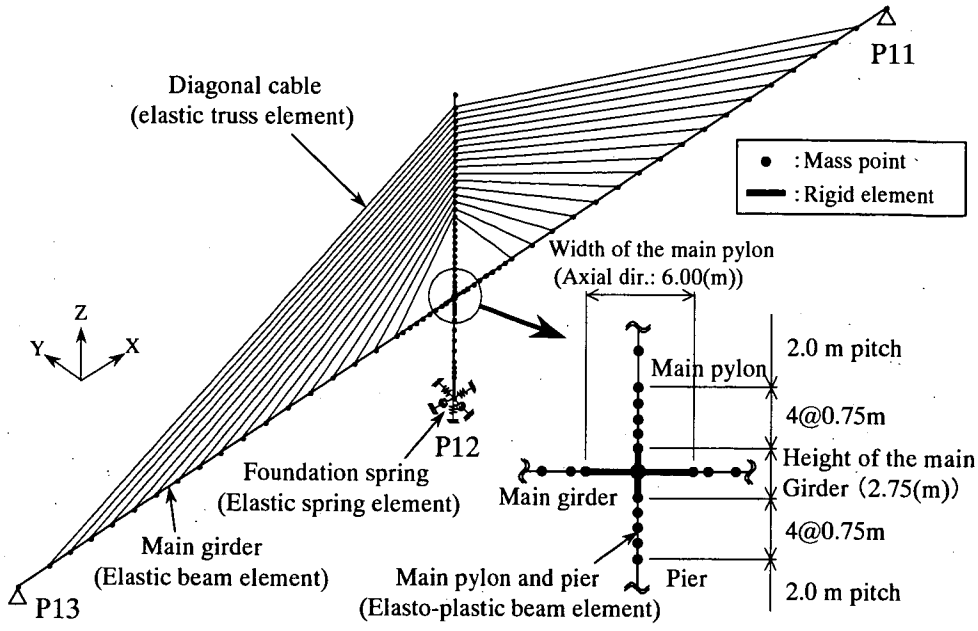


Fig. 6 Frame model for analysis

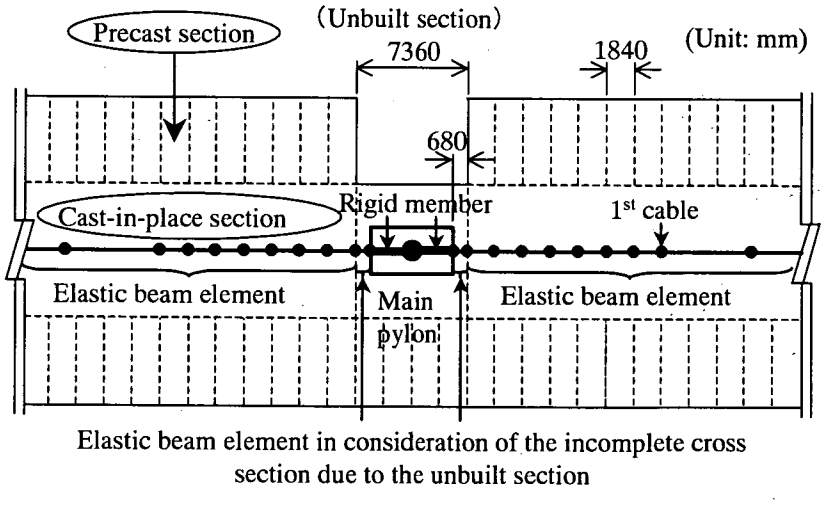


Fig. 7 Modeling of the rigid connection section of the main girder and the main pylon (Plan view)

(2) Modeling of the main pylon, pier, and foundation

The nonlinear characteristics of the bending in the elasto-plastic beam elements of the main pylon and the pier were modeled by the Takeda Model (the rigidity decrease ratio: $\gamma = 0.4$) which has a bending moment-curvature relationship of the trilinear type that takes cracking into account, in accordance with the Specifications for Highway Bridges - Seismic Design (hereafter referred to as the Bridge Specifications) [4]. As to the foundation, the collective spring constants in the horizontal, vertical, and rotating directions were calculated in accordance with the Bridge Specifications, and then a virtual rigid member was installed up to the position where the coupled term of the horizontal direction and the rotating direction becomes zero, at the bottom of which a foundation spring was installed.

3.2 Analysis Method

The axial stress acting at the bottom of the main pylon of this bridge is 7.35 N/mm^2 when the dead load is working. This is a very high axial force, about 7 times as high as that of an ordinary RC pier. Accordingly, the bending action caused by the horizontal displacement of the main pylon, the so-called P-Δ effect, was taken into account in the time history response analysis. To take the geometric non-linearity into account, the local coordinate system of each member was renewed at each analysis step, and the conversion matrix between the entire coordinate system and the local coordinate system was reevaluated at each analysis step.

On the other hand, the β value (0.25) of the Newmark method was used for the numerical integration in the time history response analysis and the interval of the integration time was made to Δt = 1/1000 seconds. In addition to the time-based damping of each nonlinear member, the viscosity damping constant was employed, which is 2 % for the main girder, main pylon, and pier, 20 % for the foundation, and 0% for the rigid members, and Rayleigh damping was employed for the entire system.

3.3 Input Seismic Motion

In Taiwan, a total of 631 strong motion measuring locations are being operated by the Central Weather Bureau (CWB) and many strong motion records were taken during the Chi-Chi Earthquake. The measuring location closest to the Ji-Ji-Da Bridge which could take a record during the earthquake was TCU078. It is located at 7.34 km from the bridge and 5.96 km from the hypocenter. Because the bridge is located on the same ground with TCU078 in terms of the fault as seen in Fig. 8, it is considered that the seismic motion acted on the bridge was closer to that recorded at TCU078. As the bridge lies north to south, the E-W component was installed as the perpendicular direction of the bridge and the N-S component as the axial direction, and the waveforms of the two directions were input simultaneously.

The N-S component and the E-W component of the original waveform taken at TCU078 are shown in Fig. 9 (a) and (b), respectively. The maximum acceleration at this location was 302.4 gal for the N-S component and 439.6 gal for the E-W component. From these waveforms and the direction of the fault in Fig. 8, it is known that the seismic motion of the E-W component was dominant at the bridge location. However, when these waveforms were used for analysis, the obtained results were quite different from the actual damage observed, with a small response at the main pylon and the main girder (to be explained in Section 3.4 below).

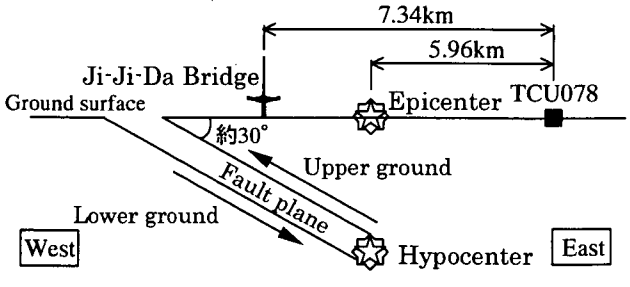
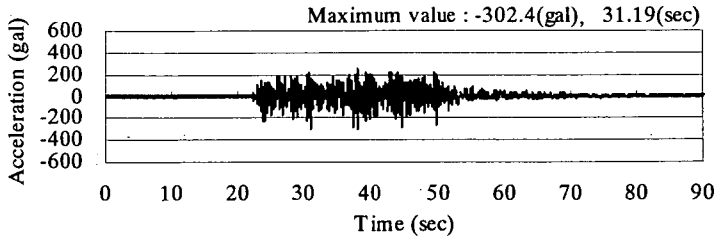
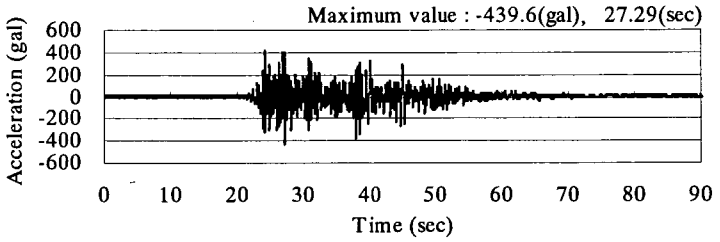


Fig. 8 Relative locations of the bridge and the strong motion measurement point (TCU078)



(a)TCU078 (N-S)



(b)TCU078 (E-W)

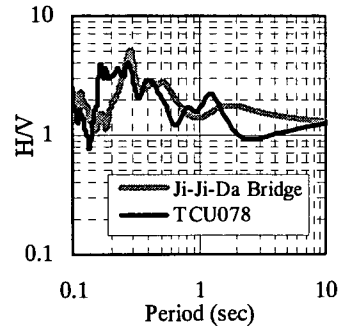
Fig. 9 Input seismic waveform (TCU078 - original waveform)

In the meantime, according to the contour figure on the maximum acceleration in the Taichung region which was prepared by the National Center for Research in Earthquake Engineering (NCREE) in Taiwan based on a number of strong motion records during the earthquake, the estimated maximum acceleration value at the ground surface where the Ji-Ji-Da Bridge is located was 400 gal for the N-S component and 600 gal for the E-W component [5]. This means that approximately 35% larger maximum acceleration as compared with theU078 was caused in both directions.

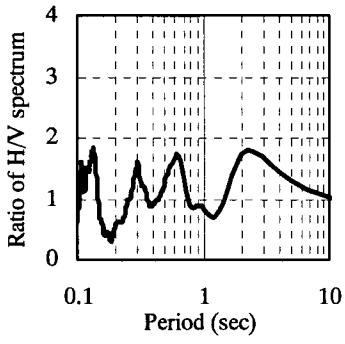
Hence, to find an adequate input seismic motion for the current analysis, the authors paid attention to a good correlation between the H/V spectrum (the ratio of spectrums of the horizontal component and the vertical component) which was obtained through our ground micro-vibration measurements during the visit in November 2002 and the H/V of the seismic motion during the earthquake [6]. And then, the H/V spectrums at the bridge location and TCU078 were compared to estimate the seismic motion at the bridge. Figure 10 (a) shows the H/V spectrums at the bridge and TCU078. Figure 10 (b) shows the ratio of the H/V derived by dividing the H/V of the bridge by the H/V of the TCU078. With regard to the H/V of the bridge, a clear peak is seen around 0.3 seconds.

From the thickness of the surface layer at this location, 15 m, found from geological data, the velocity of shear elastic waves (Vs) is estimated to be 200 m/s and the ground type is Type II. Although a good correlation is seen between the H/V spectrums of the two locations, there is a zone where the H/V at the bridge is 1.8 times larger than that at TCU078 around a period of 2 seconds and others Hence, only the amplitude of the Fourier spectrum at TCU078 was corrected using the ratio of the H/V spectrum shown in Fig. 10 (b). And then, the waveforms of the seismic motion at the bridge was estimated using this correction, which is shown in Fig. 11. In this figure, (a) and (b) respectively show the acceleration component in the N-S and E-W directions.

The maximum acceleration at the Ji-Ji-Da Bridge which was estimated by the above process was about 50% larger in the N-S component and about 30 % larger in the E-W component as compared with those at TCU078. These are approximately equal to the maximum acceleration values estimated by the NCREE.

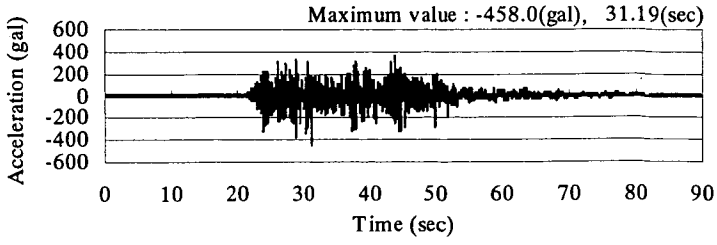


(a) H/V spectrum

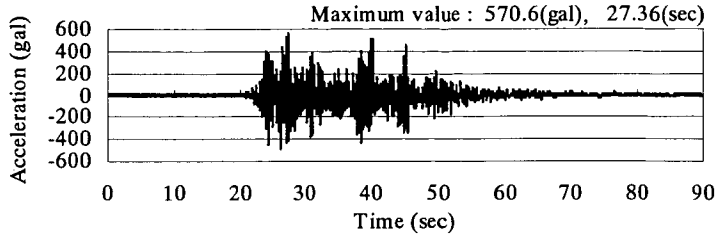


(b) H/V spectrum

Fig. 10 Measurement results of micro-vibration of the ground



(a) TCU078 - corrected (N-S)



(b) TCU078 - corrected (E-W)

Fig. 11 Input seismic waveform (TCU078 - corrected waveform)

3.4 Results of Analysis

3.4.1 Maximum response at the main girder, main pylon and pier

Figure 12 shows the response history (bending moment vs. curvature relationship) of the perpendicular direction at the bottom of the main pylon when the TCU078 original waveforms were input. According to this figure, the maximum response bending moment at the bottom of the main pylon does not reach the yield bending moment. However, according to our field observation immediately after the earthquake, the main reinforcement in the perpendicular direction buckled and the cover concrete fell at the bottom of the pylon, which is the evidence that this area reached the nonlinear range by exceeding the yield point. This means that if the TCU078 original waveforms are input, the actual damage occurred cannot be reproduced.

From the above results, it is considered that the seismic motion acted at the bridge area was probably much stronger than that given by the TCU078 original waveforms. Hence, we then used the seismic motion having approximately the same scale of maximum acceleration with that estimated by the NCREE as the input waveforms (Corrected TCU078) which are shown in Fig. 11. Figure 13 shows the response history in the axial and perpendicular directions taken at the top of the main pylon when the corrected TCU078 was input. It is seen in this figure that the maximum response displacements in the axial and perpendicular directions at the top of the main pylon are 0.14 m and 0.66 m, respectively, which means that the response in the perpendicular direction is predominant.

Table 2 shows the maximum response at the end of the main girder, the bottom of the main pylon, and the bottom of the pier where damage actually occurred during the earthquake. Shown in the table are the maximum compressive stress due to bending and the maximum compressive stress due to axial force which are obtained from the maximum

bending moment and the initial axial force. With regard to the response at the main girder, it is seen in the table that the main girder with an unbuilt section is larger in both the maximum compressive stress due to bending and the maximum compressive stress due to axial force than the main girder without an unbuilt section. The main girder without an unbuilt section here means the section on the main girder which is located next to the unbuilt section and has the largest moment among sections on the main girder because of its location closest to the main pylon. The maximum compressive stress in the axial direction of the unbuilt section of the main girder exceeds the design strength of the concrete, σck = 34.3 N/mm^2, only by the bending moment. As to the perpendicular direction, the maximum compressive stress exceeds the design strength of the concrete if the maximum compressive stress due to axial force is combined. From this, it is known that the stress acting on the cross section of the main girder of the unbuilt section is in excess of the design strength of the concrete, and that there is the possibility that a severe damage such as the fracture of concrete or the buckling of main reinforcement are caused if a seismic wave like the current case occurs.

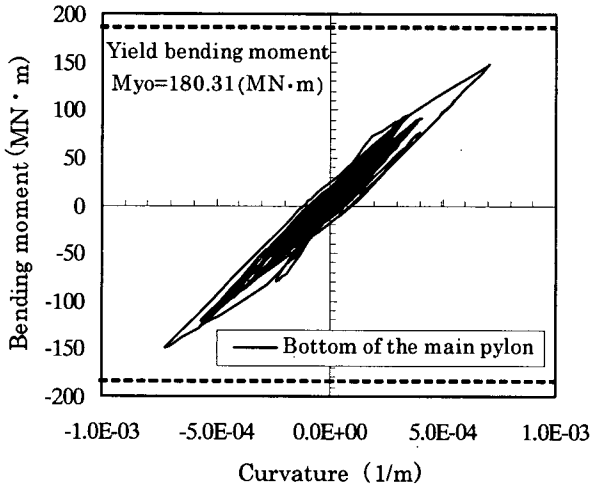


Fig. 12 Response hysteresis at the bottom of the main pylon (perpendicular direction) (Results of the input of the TCU078 original waveform)

Table 2 Maximum response

Position	Maximum bending moment		Maximum compressive stress due to bending		Maximum curvature		Maximum axial compressive force	Maximum compressive stress due to axial force
	Axial direction	Perpendicular direction	Axial direction	Perpendicular direction	Axial direction	Perpendicular direction		
	MN・m	MN・m	N/mm^2	N/mm^2	1/m	1/m	MN	N/mm^2
Main girder (built section)	193.02	428.67	22.14	15.97	-	-	94.15	5.98
Main girder (unbuilt section)	213.30	450.08	41.65	32.11	-	-	98.04	7.80
Bottom of the main pylon	234.98	198.55	21.84	35.64	2.68E-4	2.53E-3	103.79	7.35
Bottom of the pier	512.81	472.86	26.59	23.97	1.99E-3	1.07E-3	131.48	4.37
Design strength of concrete: σck = 34.3 (N/mm^2)								

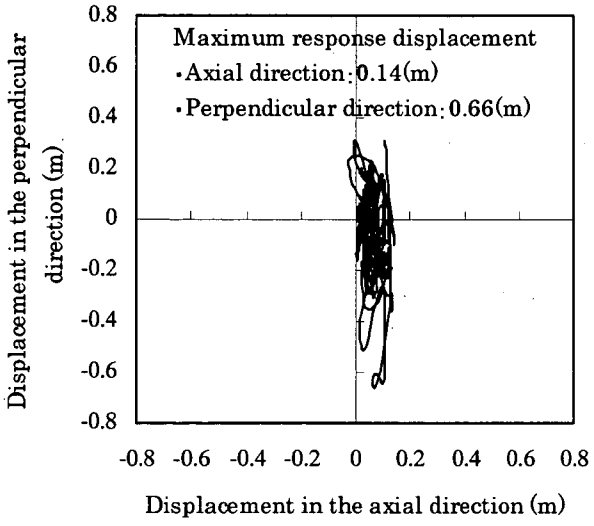


Fig. 13 Response-displacement hysteresis at the top of the main pylon

Figure 14 shows the response history (bending moment vs. curvature relationship) in the perpendicular direction at the bottom of the main pylon and the bottom of the pier. According to the analysis results, the maximum response plasticity ratio, μmax, at the pier bottom and the pylon bottom was 2.35 and 2.12, respectively, both reaching the yield strength. As to the pier bottom, this ratio is relatively in good agreement with the actual damage at the pier bottom where bending cracks occurred in the section up to 4 m from the bottom but cover concrete was not separated from the pier. As to the pylon bottom, however, the cover concrete fell from the east side face of the pylon bottom and hence it is presumed that the actual linear response was larger than the analytical results, although a relatively good agreement is seen between the analytical results and the tendency of the damage.

One of the reasons for this is the effect of the high axial force that is working on the main pylon. According to past researches on the nonlinear response of RC members having high axial force, it is known that the deformation capacity decreases because the horizontal displacement accompanies a large additional bending [7]. The axial stress working on the bottom of the pylon is 7.35 N/mm^2 under the dead load as shown in Table 2, which is approximately 7 times as high as the axial stress working on ordinary RC piers. Although the additional bending due to the horizontal displacement of the main pylon was duly considered in the analysis by the geometrical nonlinearity, a decrease in the strength due to the additional bending was not considered in the nonlinear history model of the pylon bottom, which may resulted in the underestimation of the axial stress than the actual response.

The reason that damage occurred not only at the pier bottom but also at the pylon bottom is probably due to the effect of high level modes of the main pylon. Primary modes in the perpendicular direction derived from the analysis of eigenvalues are shown in Fig. 15. In addition to the primary mode, the 5th mode and the 9th mode are predominant. As seen from the distribution of the maximum bending moment in the perpendicular direction of the main pylon and the pier shown in Fig. 16, the distribution of bending moment at the time of the maximum response at the pylon bottom differs from that at the pier bottom by the effect of high level modes.

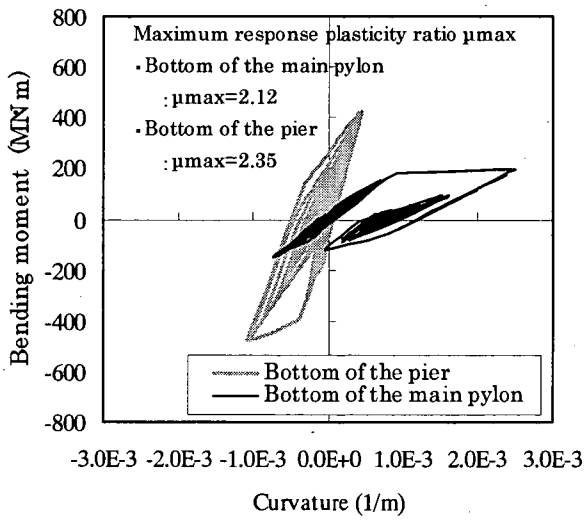
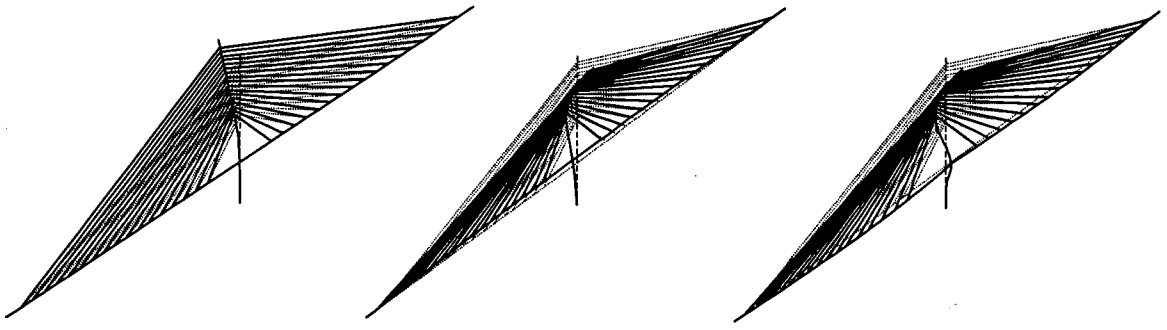


Fig. 14 Response hysteresis at the bottom of the main pylon and at the bottom of the pier



(a) The 1st mode (T=2.080sec) (b) The 5th mode (T=0.637sec) (c) The 9th mode (T=0.230sec)

Fig. 15 Predominant mode in the direction perpendicular to the bridge axis

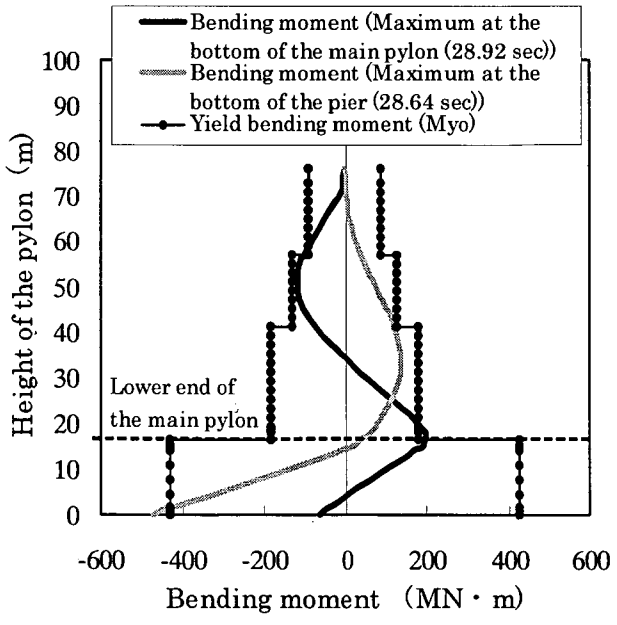


Fig. 16 Flexural strength at the main pylon and the pier and the distribution of bending moment

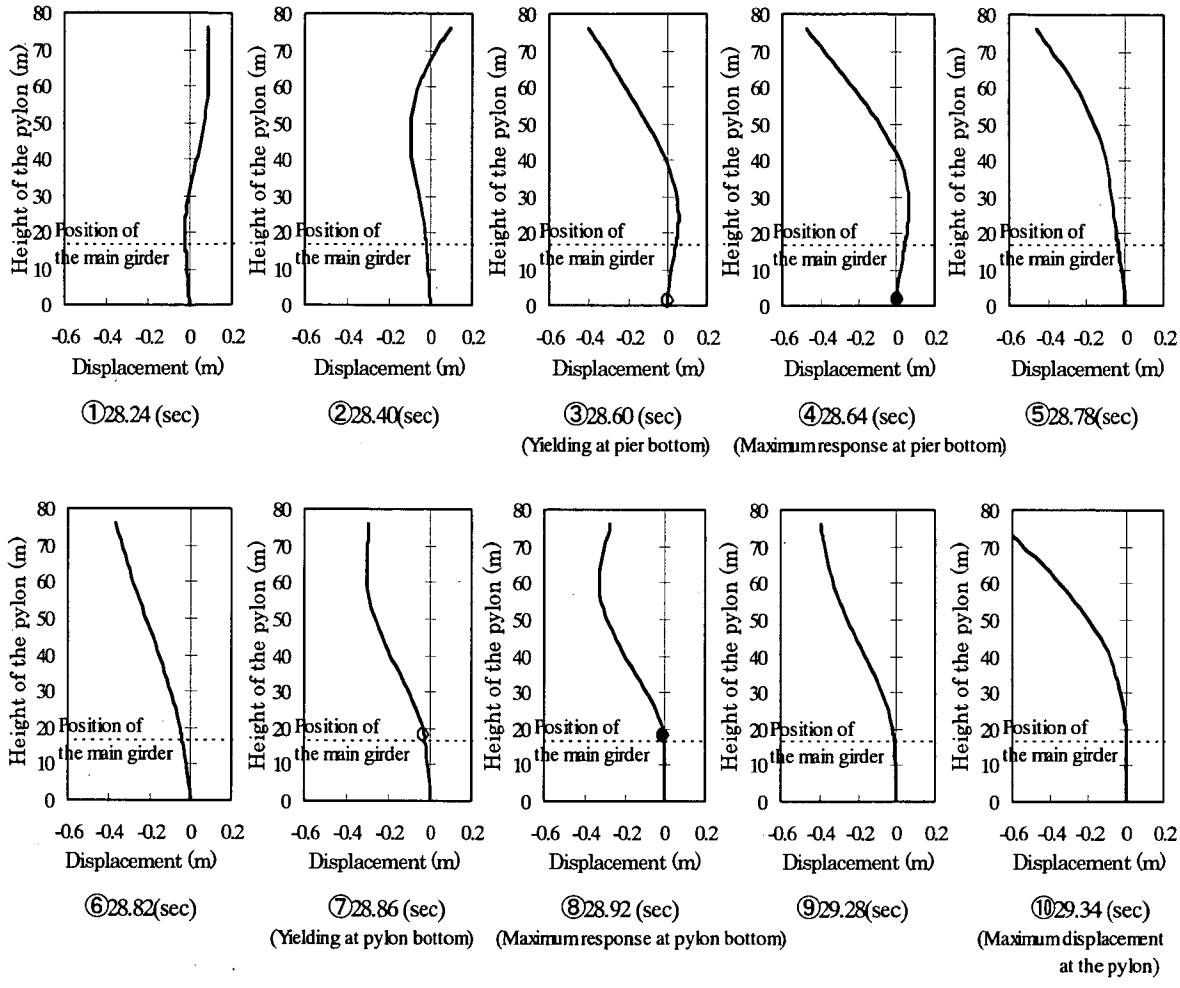


Fig. 17 Development of displacement at the main pylon and the pier

Here, to grasp the effect of the high level modes, developments of deformation at the main pylon was tracked at each time step. The deformations of the pylon seen around the time of 28.2 - 29.3 seconds which are the time of the maximum response of the pylon are shown in Fig. 17.

At ① 28.24-②28.40 seconds, the responses of the pylon bottom and the pier bottom were still elastic, but they were already showing the deformation of high level modes. At around ③28.60-④28.64 seconds, the pier bottom reached yielding by the 5th mode deformation, and immediately after that the maximum response was obtained. At this time, the pylon bottom did not yet reach yielding. At ⑤28.78-⑥28.82 seconds, the pier bottom exhibited the deformation of the primary mode in the nonlinear range. Then at ⑦ 28.86-⑧28.92 seconds, the pylon bottom reached yielding by the deformation of the 9th mode, and immediately after that the maximum response was obtained. At ⑨29.28-⑩ 29.34 seconds, both the main pylon and the pier was in the nonlinear state, at which the deformation of the primary mode was predominant and the top of the pylon reached the maximum displacement.

As seen, the pier bottom failed by the deformation of the 5th mode and the pylon bottom by that of the 9th mode, and then the nonlinear response advanced.

3.4.2 Tension force of diagonal cables

Fig. 18 shows the distribution of the maximum tension force of the diagonal cables. The initial tension, the maximum tension, and the tensile stress of the cables, numbering from 1 to 34, are shown in the figure. The difference between the maximum tension and the initial tension is the fluctuating tension associating with the seismic response. As this is a cable-stayed bridge, cables are pulled from the main pylon towards the both sides. Hence, the initial tension becomes larger as the anchorage position becomes distant from the pylon because of the effect of the cable weight and the anchoring angle. Also, as the pylon and the main girder are rigidly connected, the initial tension of cables located near the pylon is small relatively. At the time of the earthquake, construction of this bridge was almost over leaving a part of the precast section of the main girder and the deck construction. And, it is considered that an initial tension of 486 N/mm^2 on average, which is approximately 26% of the tensile strength, was introduced to the cables at the time of construction. The cross section of the cable consists of PC steel multi-strand wires having diameters of ϕ 12.7 mm, 15.2 mm, and 7 mm, and the tensile strength is 1,860 N/mm^2 which is equivalent to SWPR7B.

The largest maximum stress of the cables was 720 N/mm^2 which was taken around the pullout 11th cable. But, this value is about 40% smaller compared with the design tensile strength of the cable, which is 1,860 N/mm^2. With this maximum stress value, it seems structurally impossible for the cables to be pulled out from the anchorage section.

However, when we had a talk with the bridge administrators in Taiwan in November 2002, they told us that the cable anchorage section had actually been constructed at the strength about 30% of the design tensile strength due to some construction reasons. In our analysis, the maximum tensile stress of the cables was derived as about 40% of the design tensile strength. If the actual strength of the cable anchorage was about 30% of the design tensile strength as the Taiwan administrators say, it can be said that there was the possibility that all the cables except the 14th through 21st might have been pulled out from the anchorage section. From these results, it is said that the cause of the cable pullout was the insufficient strength of cable anchorage.

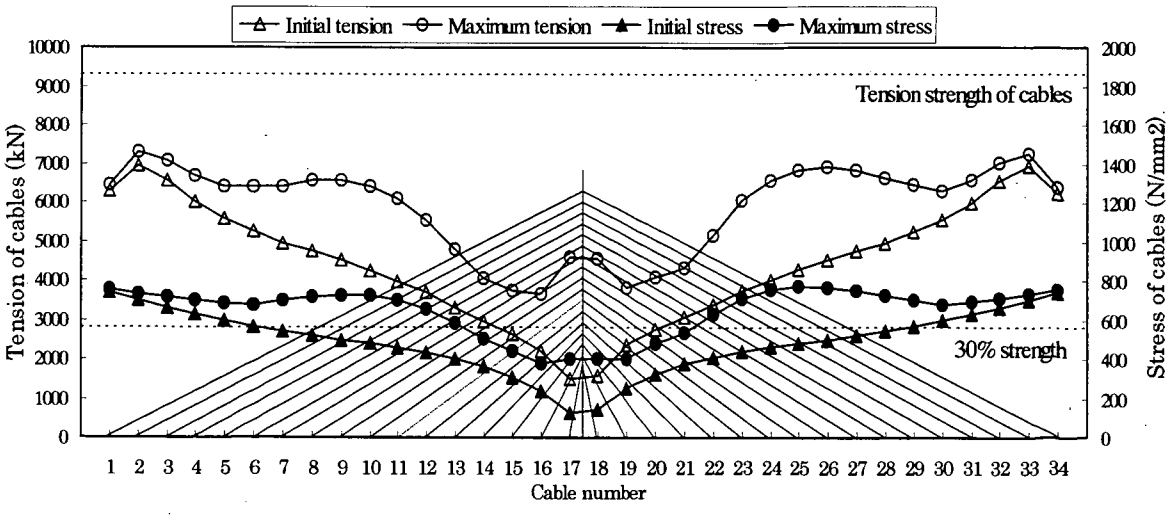


Fig. 18 Distribution of the maximum tension of the diagonal cables

4. CONCLUSIONS

The following conclusions were drawn from the seismic response analysis conducted on the cable-stayed Ji-Ji-Da Bridge damaged in the 1999 Chi-Chi Earthquake. The detailed drawings of the bridge obtained from bridge administrators in Taiwan were a great help in this analysis.

(1) The responses of the main pylon and the pier were predominant in the perpendicular direction when the seismic waves of the two directions were input simultaneously.

(2) The stress acting on the unbuilt section of the bridge was in excess of the design strength due to the bending moment and the axial force. Therefore, if a large seismic wave like that seen in the current earthquake occurs, it is possible that serious damage such as the fracture of the concrete or the buckling of the main reinforcement is caused.

(3) With regard to the cause of damage to the perpendicular direction of the main pylon, it was found from the nonlinear time history response analysis that the pier bottom reached yielding by the predominance of the 5th deformation mode and the pylon bottom reached yielding by the predominance of the 9th deformation mode, and then the nonlinear response advanced.

(4) It was clarified that the cause of cable pullout at this bridge was probably the insufficient anchoring strength at the time of construction.

REFERENCES

1) Kyushu Institute of Technology: *A Survey Report on Bridge Damage in the 1999 Chi-Chi Earthquake*, April 2000.

2) JSCE Working Committee on Seismic Engineering of the JSCE: *A Research Report on the Development of Seismic Design Method Based on Ultimate Bearing Capacity*, pp.567-576, March 2001.

3) Gregory L. Fenves, Charles B. Chadwell, and Stephen A. Mahin: "Near-Source Earthquake Effects on a Cable-stayed Bridge", 3rd International Workshop on Performance-based Seismic Design and Retrofit of Transportation Facilities, pp.137-148, July 2002.

4) Road Association of Japan: Specifications for Highway Bridges and Commentary, V – Seismic Design, March 2002.

5) National Center for Research in Earthquake Engineering (NCREE) : *A survey Report on Bridge Damage in Sept. 21 Chi-Chi Earthquake*, NCREE-99-052, 1999.

6) Nakamura, Y. and Ueno, M.: "An Estimation of the Subsurface Ground Characteristics Utilizing Vertical Component and Horizontal Component of the Ground Surface Motion", Proceedings of the 7th Earthquake Engineering Symposium of the JSCE, pp.265-270, 1986.

7) Adachi, Y., Unjoh, S., Nagaya, K., and Hayashi, M.: "Experimental Study on the Deformation Capacity of High Strength RC Members under High Axial Forces", Proceedings of the Japan Concrete Institute, Vol. 21, No. 3, 1999.

Rocking Motion of a Bridge Foundation Platform

W. Phillip Yen, Ph.D., P.E. *, Kornel Kerenyi, Ph.D., **

* Research Structural Engineer, Seismic Hazard Mitigation (HRDI-07), Federal Highway Administration, 6300 Georgetown Pike, McLean, Virginia 22101; PH (202) 493-3056; FAX (202) 493-3442; email: wen-huei.yen@fhwa.dot.gov

** Hydraulic Research Engineer, GKY and Associates, Inc., 5411-E Backlick Road, Springfield, Virginia 22151; PH (703) 642-5080; FAX (703) 642-5367; email: kornel.kerenyi@fhwa.dot.gov

Abstract

The goal of this research is to test the response of an oscillating foundation platform, which is positioned on soil and submerged by water. The oscillating platform is modeled as a linear spring-damper-mass oscillator with two perpendicular degrees of freedom. The platform is mounted so it can rotate around the directions corresponding to its main bending axis. A specially designed flume, which is 3000 mm long and 400 mm wide, allows for the investigation of different soil conditions and various flow depths. The oscillating platform is mounted elastically on a structure over the test section of the flume. Three synchronous linear drive motors apply the dynamic loads. Complex plane representation of the dynamic moments is used to identify the nonlinear fluid and soil moments. Additional goals are to detect the nonlinear fluid and soil coupling moments.

Introduction

This study will investigate how bridge foundations, such as spread footings, interact with soil and water during an earthquake. These interactions can occur at bridge foundations constructed under water (such as in a creek, a river or even a bay area) as well as at foundations constructed within the groundwater table. While an earthquake vibrates bridge foundations, the foundation might be exposed to a bi-directional rocking motion. When the rocking motion becomes significant, water can alternatively be sucked into gaps and pressed out of gaps that occur as the foundation rocks up and down. The effects of the interactions

between the water and foundations can become significant and affect the bridge stability if the rocking motion is significant. Current design code for earthquake resistance does not consider these effects. This preliminary study will use a small-scale multi-hazard dynamic testing model to simulate these effects.

The experimental set-up is designed to study the fluid-soil structure interaction of a rigid foundation platform modeled as a two degree of freedom (2-DOF) oscillator using a forced oscillation experiment. The linear 2-DOF oscillator acts as a reference system to investigate the nonlinear behavior of the system when it interacts with fluid and soil. The identification concept to determine the fluid and soil moments and to analyze the coupling effects based on a forced oscillation test are similar used to model fluid dynamic damping and stiffness.
Kerenyi and Yen (2002) use forced oscillation tests to determine fluid and soil coefficients. The tests were conducted in a flume having a recess for different soil conditions. Billeter and Staubli (2000) investigated a multiple mode vibration test on a vertical plate. They use force coefficients and phase angle to compute fluid dynamic damping and mass. Staubli (1983) and Deniz (1997) used forced oscillation tests in a tow-tank to determine force coefficients and phase angle to describe the fluid dynamic system. Kerenyi and Staubli (2000) analyze the stability of a prism oscillating with two degrees of freedom in cross flow. Phase angle relationship is used to determine if the body is exited or damped.

Experimental Set-Up

The experimental set-up consists of two major subsystems: a flume to simulate various flow and riverbed conditions and the shaking device to apply different dynamic loadings.

Flume

The flume consists of a 1300 mm long inlet and a 2000 mm straight channel (Figure 1). The upstream flow conditioning is achieved using filter mats, a honeycomb flow straightener, and a carefully designed trumpet-shaped inlet. The flume is designed to have a uniform flow distribution over the width and to have fully developed turbulent flow (following Prandtl's velocity distribution) at the test section. The recess at the test section is 400 mm x 300 mm (length x width) and 80 mm deep, and can be filled with sand particles of various sizes. The roughness of the fixed bed upstream of the recess can be varied according to the sand particles used in the recess. A 25 l/s pump provides the flume with water, which is stored under the flume in a water tank. A flow meter measures the discharge and an ultra sonic flow depth meter determines the flow depth. A laser distance meter, which is mounted on a portal robot, can scan scour holes during test runs. The flow velocity is measured with an electro magnetic velocity probe.

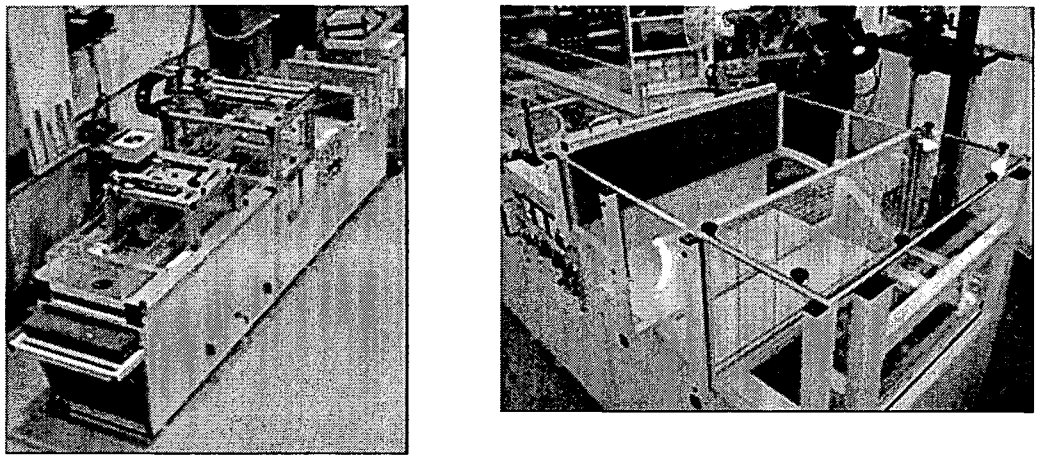


Figure 1. Test flume and trumpet shaped inlet

Shaking Device

The shaking device is mounted above the flume on a rigid frame at the test section. Three synchronous linear drive motors apply dynamic forces up to 10 Hz. Three lasers provide the feedback signal for the linear drive motors. The driving signals have to be superposed to achieve the rocking movement (Figure 2).

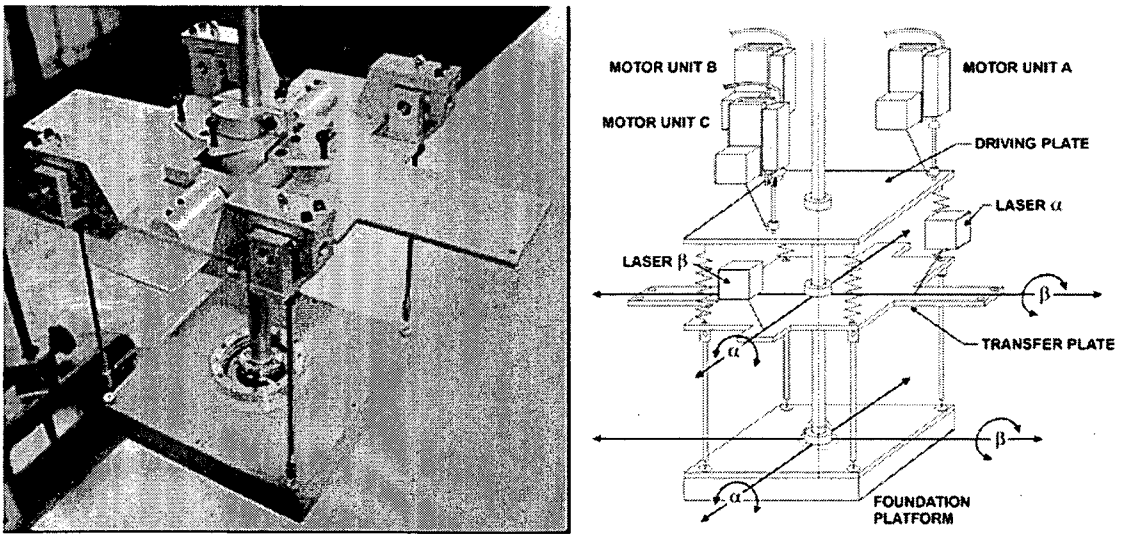


Figure 2: Shaking device

Band limited random noise can be used to simulate earthquake loading. The platform is mounted so it can rotate around the directions corresponding to its main bending axis. The foundation platform is linked to a transfer plate using four thin columns. The transfer plate is elastically mounted to the diver system. Using different coil springs for the elastical support can vary the natural frequency. The mechanical (structural) subsystem represents a linear

spring-damper-mass oscillator with two perpendicular degrees of freedom, which is lightly damped to study a significant peak resonant response. The damping ratio is determined by the Half-Power (Band-Width) method. The angular response displacement is measured with a laser distance meter and the angular response acceleration with accelerometers. The angular response velocity is determined by integrating the angular response acceleration. Four load cells measure the applied dynamic loading.

Mathematical Background

The objective of this research, how the equilibrium of forces change by adding fluid and soil to the oscillating foundation platform to determine the non-linear behavior of the additional stiffness and damping coefficients (Figure 3).

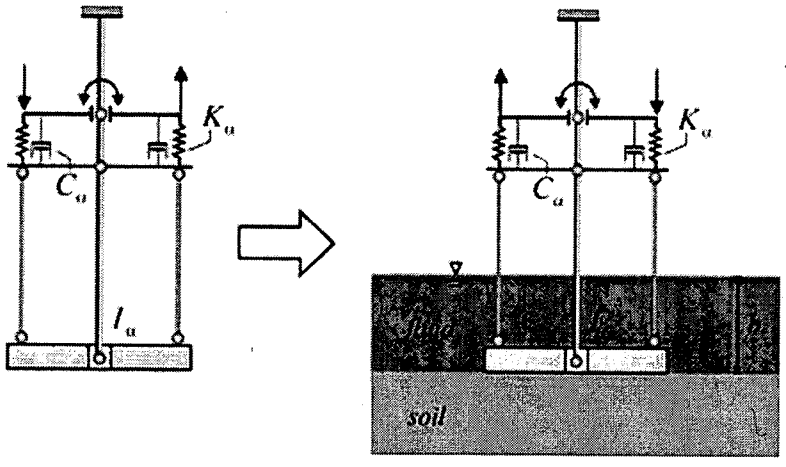


Figure 3: Fluid-soil spring-damper system

Identification Procedure

The identification procedure is based on the idea of a forced oscillation experiments used to determine fluid and soil dynamic stiffness and damping. Additional damping and stiffness coefficients can model the fluid dynamic and the soil subsystem (equation 1), which are functions of several parameters (e.g., amplitude and frequency). The mechanical subsystem has no coupling coefficients, because the degrees of freedom are orthogonal.

$$\mathbf{I}\begin{pmatrix}\ddot{\alpha}(t)\\ \ddot{\beta}(t)\end{pmatrix}+\mathbf{C}\begin{pmatrix}\dot{\alpha}(t)\\ \dot{\beta}(t)\end{pmatrix}+\mathbf{K}\begin{pmatrix}\alpha(t)\\ \beta(t)\end{pmatrix}+\begin{pmatrix}\overline{C}_{\alpha} & \overline{C}_{\alpha,\beta}\\ \overline{C}_{\beta,\alpha} & \overline{C}_{\beta}\end{pmatrix}\begin{pmatrix}\dot{\alpha}(t)\\ \dot{\beta}(t)\end{pmatrix}+\begin{pmatrix}\overline{K}_{\alpha} & \overline{K}_{\alpha,\beta}\\ \overline{K}_{\beta,\alpha} & \overline{K}_{\beta}\end{pmatrix}\begin{pmatrix}\alpha(t)\\ \beta(t)\end{pmatrix}=\begin{pmatrix}M_{\alpha,o}\exp(\mathrm{i}\,\overline{\omega}_{\alpha}t)\\ M_{\beta,o}\exp(\mathrm{i}\,\overline{\omega}_{\beta}t)\end{pmatrix} \quad (1)$$

where

$$\mathbf{I}=\begin{pmatrix}I_{\alpha} & 0\\ 0 & I_{\beta}\end{pmatrix},\ \mathbf{C}=\begin{pmatrix}C_{\alpha} & 0\\ 0 & C_{\beta}\end{pmatrix},\ \mathbf{K}=\begin{pmatrix}K_{\alpha} & 0\\ 0 & K_{\beta}\end{pmatrix}. \quad (2)$$

For the tests described here only the exciting frequencies ω_α, ω_β and the amplitudes α_o, β_o will be varied, by keeping the soil conditions and the flow depth h constant.
The identification concept is based on the balance of moments acting on the linear mass two degree of freedom (2-DOF) oscillator (Figure 4) under steady state harmonic condition whereby the total response for both coordinates is:

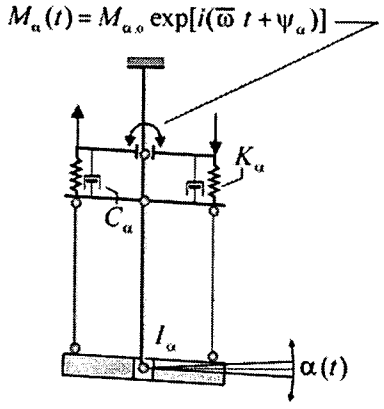


Figure 4: Linear 2-DOF system showing the α-coordinate

$$\alpha(t) = \alpha_o \exp(i\overline{\omega} t) \quad \text{and} \quad \beta(t) = \beta_o \exp[i(\overline{\omega} t + \varphi)] \tag{3}$$

Moment equilibrium requires that the sum of the inertial $M_{I,i}(t)$, damping $M_{D,i}(t)$ and stiffness moments $M_{S,i}(t)$ for $i = \alpha, \beta$ are equal the applied load

$$\begin{aligned} M_\alpha(t) &= M_{\alpha,o} \exp[i(\overline{\omega}\, t + \psi_\alpha)] \\ M_\beta(t) &= M_{\beta,o} \exp[i(\overline{\omega}\, t + \psi_\beta)] \end{aligned} \tag{4}$$

Using equation (3), these moments are:

$$\begin{aligned} M_{I\alpha} &= I_\alpha \ddot{\alpha}(t) = -I_\alpha \overline{\omega}^2 \alpha_o \exp(i\overline{\omega} t) \\ M_{I\beta} &= I_\beta \ddot{\beta}(t) = -I_\beta \overline{\omega}^2 \beta_o \exp[i(\overline{\omega} t + \varphi)] \end{aligned} \tag{5}$$

$$\begin{aligned} M_{D\alpha} &= C_\alpha \dot{\alpha}(t) = i K_\alpha \overline{\omega}\, \alpha_o \exp(i\overline{\omega} t) \\ M_{D\beta} &= C_\beta \dot{\beta}(t) = i C_\beta \overline{\omega}\, \beta_o \exp[i(\overline{\omega} t + \varphi)] \end{aligned} \tag{6}$$

$$\begin{aligned} M_{S\alpha} &= K_\alpha \alpha(t) = K_\alpha \alpha_o \exp(i\overline{\omega} t) \\ M_{S\beta} &= K_\beta \beta(t) = K_\beta \beta_o \exp[i(\overline{\omega} t + \varphi)] \end{aligned} \tag{7}$$

along with the applied loading, are shown as vectors in the complex plane (Figure 5) also shown is the closed polygon of moments required for equilibrium in accordance with equation (8)

$$M_{I,i}(t) + M_{D,i}(t) + M_{S,i}(t) = M_i(t) \quad \text{for } i = \alpha, \beta \tag{8}$$

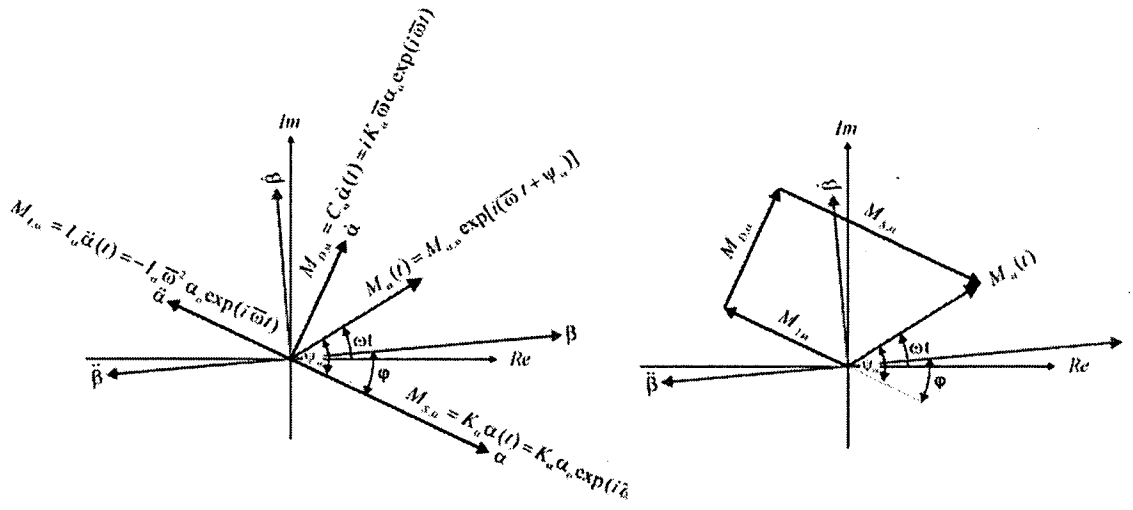


Figure 5: Steady state harmonic moments using viscous damping in a complex plane representation and closed moment polygon representation (moments are plotted only for the α-coordinate

Inertial, damping, and spring moments as given in equation (5-7) are in phase with the angular acceleration, velocity, and displacement motions, respectively.
If the 2-DOF linear mass oscillator interacts with flow and soil additional damping and stiffness moments are required for equilibrium. These additional moments also include fluid and soil-coupling moments as the 2-DOF system interacts with fluid and soil (Figure 6 and 7). These moments are frequency and amplitude dependent. To identify

$$\overline{C}_\alpha, \overline{C}_\beta, \overline{K}_\alpha, \overline{K}_\beta \tag{9}$$

one degree of freedom has to be blocked, as indicated in figure 6, where the β-coordinate is blocked. In this case the additional fluid and soil moments by substituting equation (3) are

$$\overline{M}_{S,\alpha}(t) = \overline{K}_\alpha(\alpha_o, \overline{\omega})\alpha(t) = \overline{K}_\alpha(\alpha_o, \overline{\omega})\alpha_o \tag{10}$$

$$\overline{M}_{D,\alpha}(t) = \overline{C}_\alpha(\alpha_o, \overline{\omega})\dot{\alpha}(t) = i\,\overline{C}_\alpha(\alpha_o, \overline{\omega})\,\overline{\omega}\,\alpha_o \tag{11}$$

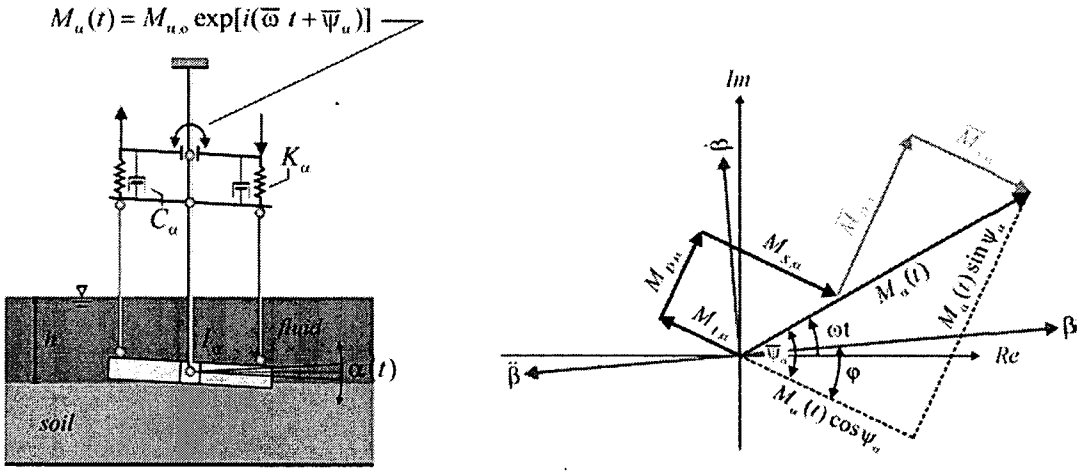


Figure 6.: 2-DOF system interacting with fluid and soil and closed polygon representation including additional damping and stiffness moments for the α-coordinate

To determine these additional moments cross power spectrum is used to compute the phase angle ψ_α between body response angular displacement amplitude α_o and applied dynamic moment amplitude $M_{\alpha,o}$. The moments can be expressed by equilibrating the dynamic moment components

$$\bar{M}_{S,\alpha} = M_\alpha(t)\cos\bar{\psi}_\alpha - M_{S,\alpha} - M_{I,\alpha} \tag{12}$$

$$\bar{M}_{D,\alpha} = M_\alpha(t)\sin\bar{\psi}_\alpha - M_{D,\alpha} \tag{13}$$

Substituting equations (5) to (7) and equations (10) and (11) into equation (12) and (13), one obtains the fluid-soil coefficient functions for the α-coordinate

$$\bar{K}_\alpha(\alpha_o, \bar{\omega}) = \frac{M_{\alpha,o}(t)\cos\bar{\psi}_\alpha - K_\alpha\alpha_o - I_\alpha\bar{\omega}^2\alpha_o}{\alpha_o} \tag{14}$$

$$\bar{C}_\alpha(\alpha_o, \bar{\omega}) = \frac{M_{\alpha,o}(t)\sin\bar{\psi}_\alpha - C_\alpha\bar{\omega}\alpha_o}{\bar{\omega}\alpha_o} \tag{15}$$

To identify the coupling coefficients

$$\bar{C}_{\alpha.\beta}, \bar{C}_{\beta,\alpha}, \bar{K}_{\alpha,\beta}, \bar{K}_{\beta,\alpha} \tag{16}$$

the 2-DOF oscillator is exited in both directions. As indicated in figure 7 for the α-coordinate additional fluid-soil coupling damping and stiffness moments are required for equilibrium.

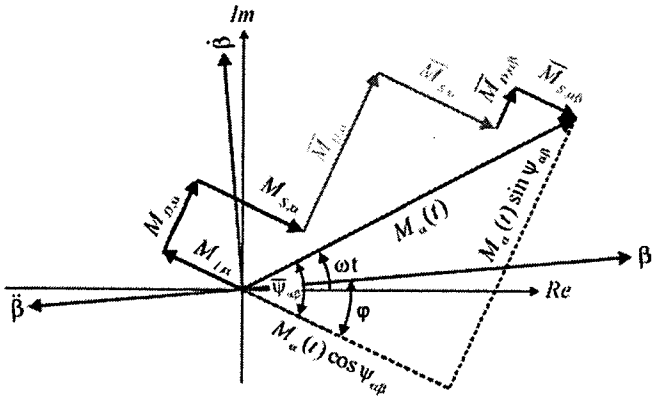


Figure 7.: Complex plane representation of the 2-DOF system interacting with fluid and soil to determine the additional coupling moments for the α-coordinate

Again cross power spectrum is used to compute the phase angle $\psi_{\alpha\beta}$ between body response angular displacement amplitude α_o and applied dynamic moment amplitude $M_{\alpha,o}$ and to determine the phase angle between response angular displacement amplitude α_o and β_o. The moments can be expressed by equilibrating the dynamic moment components (for the α-coordinate)

$$\overline{M}_{S,\alpha\beta} = M_\alpha(t)\cos\overline{\psi}_{\alpha\beta} - M_{S,\alpha} - M_{I,\alpha} - \overline{M}_{S,\alpha}\,, \tag{17}$$

$$\overline{M}_{D,\alpha} = M_\alpha(t)\sin\overline{\psi}_{\alpha\beta} - M_{D,\alpha} - \overline{M}_{D,\alpha}\,. \tag{18}$$

using the fluid and soil moments derived in equation (12 and 13). Coordinate transformation leads to

$$\overline{K}_{\alpha\beta}\beta(t) = \overline{M}_{D,\alpha\beta}\sin\varphi + \overline{M}_{S,\alpha\beta}\cos\varphi\,, \tag{19}$$

$$\overline{C}_{\alpha\beta}\dot{\beta}(t) = \overline{M}_{D,\alpha\beta}\cos\varphi - \overline{M}_{S,\alpha\beta}\sin\varphi\,. \tag{20}$$

Substituting equation (3) into equation (19) and (20) one obtains the coupling coefficients for the (α-coordinate):

$$\overline{K}_{\alpha\beta}(\beta_o,\overline{\omega}) = \frac{\overline{M}_{D,\alpha\beta}\sin\varphi + \overline{M}_{S,\alpha\beta}\cos\varphi}{\beta_o} \tag{21}$$

$$\overline{C}_{\alpha\beta}(\beta_o,\overline{\omega}) = \frac{\overline{M}_{D,\alpha\beta}\cos\varphi - \overline{M}_{S,\alpha\beta}\sin\varphi}{\overline{\omega}\beta_o}\,. \tag{22}$$

References

Deniz S., Staubli T., (1997), Oscillating Rectangular and Octagonal Profiles: Interaction of Leading- and Trailing-Edge Vortex Formation, Journal of Fluids and Structures, Vol. 11, p. 3-31.

Billeter P., Staubli T., (2000), Flow-Induced Multiple Mode Vibrations of Gates with Submerged Discharge, Journal of Fluids and Structures, Vol. 14, p. 323-338.

Kerenyi K., Staubli T., (2000), Stability Analysis of an Oscillating Rectangular Profile in Cross-Flow, Proceedings of the 7th International Conference on Flow-Induced Vibration-FIV2000, Lucerne, Switzerland, p. 131-140.

Kerenyi K., Yen P. W., (2002), Multi Hazard Dynamic Testing for Bridge Piers, Proceedings of the 18th US-Japan Bridge Engineering Workshop, St Luis, Missouri, p. 77-82.

Staubli, T., (1983), Investigation of Oscillating Forces on a Vibrating Cylinder in Cross-Flow, Doctoral Dissertation, ETH Zuerich, Switzerland.

19th US-Japan Bridge Engineering Workshop

Construction and Material

co-Chairs:
K. Ikeda & M. Capron

Construction of Nagisa Bridge –Hybrid System of Cable-stayed PC Bridge and Steel Suspension Bridge–
N. Suzuki

Performance Evaluation of Shear Links and Orthotropic Bridge Deck Panels for the San Francisco-Oakland Bay Bridge
Chia-Ming Uang

An Experimental Study on Slip Strength of HSFG Bolted Joints Treated with High-Friction Inorganic Zine-Rich Paint
Y. Koike

Extending Service Life of Timber Bridges with Preservatives
J. P. Wacker

The Design and Construction of the Chitose Bridge
K. Fujitani

Static and Fatigue Behavior of the Connections of Aluminum Decks to Steel Girders
I. Okura

Fatigue Tests of Open Grid Steel Decks under Running Wheel Loads
J. Murakoshi

CONSTRUCTION OF NAGISA BRIDGE
HYBRID SYSTEM OF CABLE-STAYED PC BRIDGE AND STEEL SUSPENSION BRIDGE

Yuzuru Sato[1]
Shinichi Sasaki[2]
Katsutoshi Morohashi[3]
Nobumasa Suzuki[4]

Abstract

Nagisa Bridge, a single span footbridge, was recently completed in Aomori prefecture, Japan. The structure of this bridge is a hybrid structure of cable-stayed prestressed concrete bridge and steel suspension bridge. It is the first application as this structure type of bridge in the world. Concrete girders near pylons are supported by stay cables. Steel girders are supported by suspension cables in the central part of the span. This is new type system for prestressed concrete bridges with longer span and has many structural features compared with ordinary cable-stayed bridge and suspension bridge. This paper reports a brief overview of construction of Nagisa Bridge with this hybrid system.

1. Introduction

Nagisa Bridge, a single span footbridge recently constructed over the Nakamura river mouth in Aomori prefecture, Japan, is the first hybrid system bridge in the world that is a compound structure of cable-stayed prestressed concrete (PC) bridge and steel suspension bridge (**Photo 1**). PC girders are used for the stay cable sections near pylons. And steel girders are used for the suspended cable section in the central part of the span. There are two bridges which adopted a similar combination of cable-stayed system and cable-suspended system. These are Saint-Ilpize bridge in France [1] and Sidi M'Cid Bridge in Algeria [2]. Both bridges, however, have steel decks only. Nagisa Bridge is the first application of a hybrid system with a combination of PC girder and steel girder.

About the design of Nagisa Bridge, some requirements had to be satisfied. These were to eliminate piers in the river and to design the bridge which would be perceived as a landmark of this area. In consideration of these conditions, the hybrid system which can be made having long span and characteristic appearance was selected. This paper reports a brief overview of construction of Nagisa Bridge with the new hybrid system, including field tests conducted prior to the opening of the bridge.

---

1. Nishi Agriculture, Forestry, and Fisheries Office / Nishi Fisheries Infrastructure Office, Aomori Prefecture Japan
2. 3. 4. P.S.Mitsubishi Construction Co., Ltd

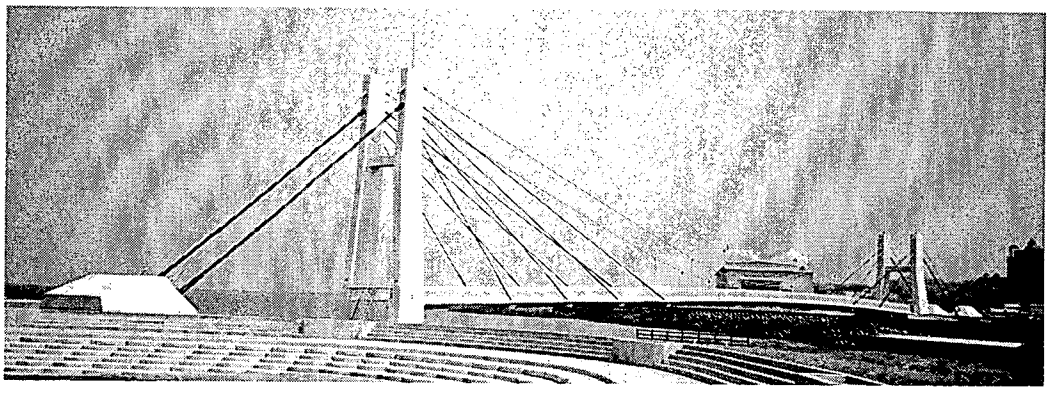


Photo 1 Nagisa Bridge

2. Hybrid System Bridge Features

The hybrid system bridge has many structural features compared with ordinary cable-stayed bridge and suspension bridge. **Fig.1** shows concepts of the hybrid system bridge and ordinary cable supported bridges. In comparison with cable-stayed bridge, this system has better buckling stability and is applicable for longer span, because the axial force occurring in the girder can be reduced by decreasing the number of stay cables. Cable erection can be easier and cable vibration problems can be solved due to shorter stay cables. The height of pylons can be lowered by reducing the number of stay cables. In comparison with suspension bridge, this system has better aerodynamic stability, because the stay cables restrain the deformation of the girder. It is achieved to lessen the tension force occurring in the main cables, because the stay cables support more weight. And anchorage lateral force can be reduced.

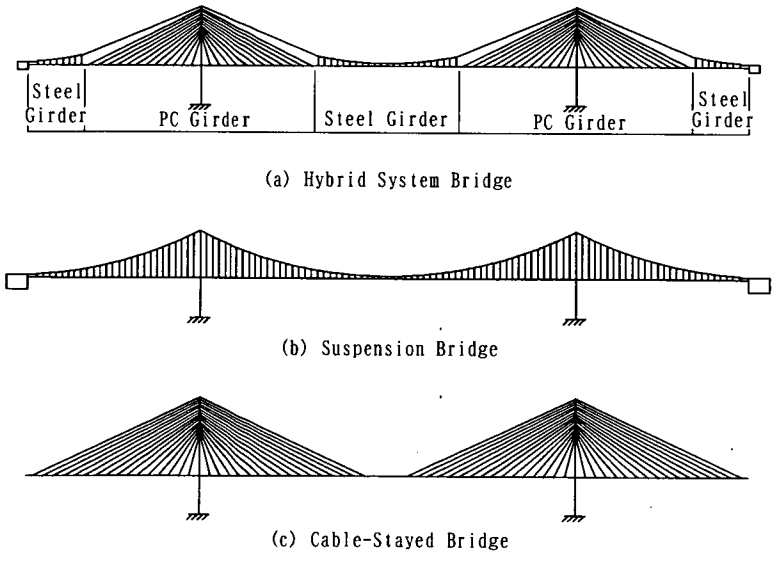


Fig.1 Concepts of Cable Supported Bride

3. Overview of the bridge

A general view of the bridge is shown in **Fig.2**. Nagisa Bridge is a single span bridge with span of 110.15 m. The main girder is a height of 0.7 m and a width of 7.0 m (effective width of 4.0 m). There are 2 pylons, and those heights are 20.0 m and 12.1 m respectively. A symbolic appearance was emphasized by making pylon height and cable arrangement asymmetrical. The pylons are composite structures of concrete members and steel shell members.

The main materials used in the bridge are shown in **Table 1**. PC strands and PC bars were used internally in the longitudinal direction. The stay cables were double rustproof cables with a anti-corrosive oil coating and a polyethylene resin covering. For suspension cables, galvanized locked coil ropes with good durability were adopted.

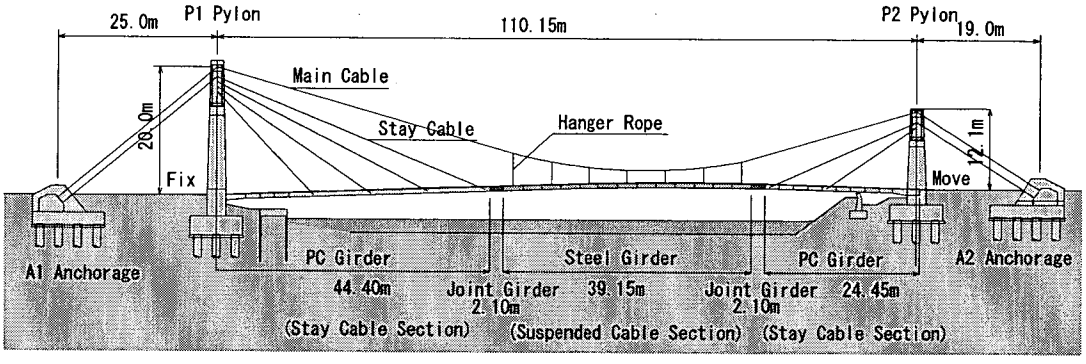


Fig.2 General view

Table 1 Main materials

Concrete	Plyon : F_{ck} = 40 N/mm^2
	Anchorage : F_{ck} = 40 N/mm^2
	Main girder : F_{ck} = 50 N/mm^2
Steel Plate	SM400A. SM490YB
PC Strand	1S19.3, 1S28.6
PC Bar	φ23, φ32
Reinforcing Bar	SD345
Stay Cable	SEEE / F-PH
Suspension Cable	Locked coil rope φ80
	Hanger rope ST1570

4. Construction

4.1 Overview of Construction

Due to the environment and construction conditions at the bridge site, the bridge was constructed using a precast segmental method with a 450-ton crawler crane. The construction steps are shown in

Fig.3. On the first step, the pylons and the anchorages for the suspension cables and the back stay cables were constructed. On the second step, cantilever erection of concrete segments was performed, and the stay cables were installed every four segments. On the third step, the suspension cables were placed and steel girders were erected. On the last step, concrete was placed around the steel shell members anchoring the stay cables on the pylons, and pavement was placed on the girder.

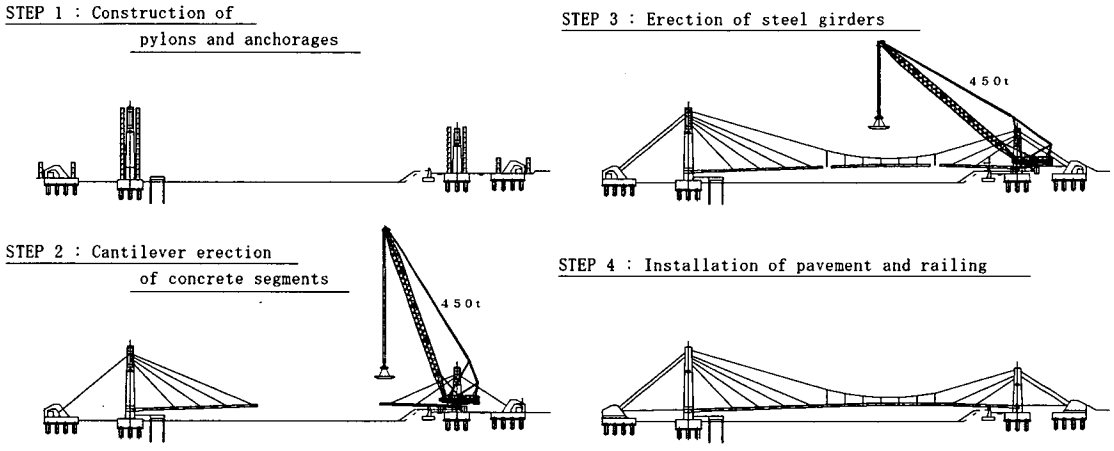
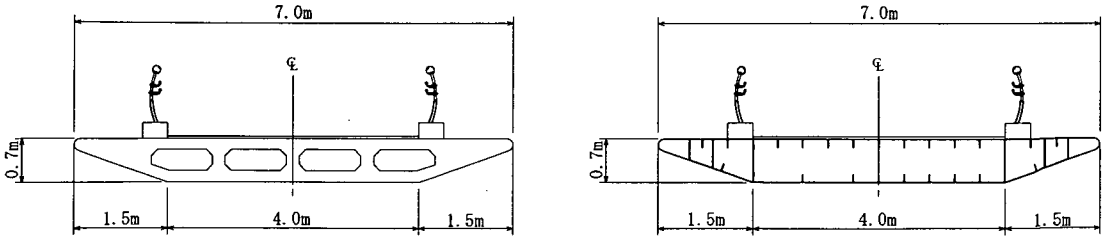


Fig.3 Construction step

4.2 Fabrication of Main Girders

Fig.4 shows sections of the main PC girder and the main steel girders. The section was designed in consideration of wind stability, durability, and reduction in self-weight. Concrete segment fabrication was done using the long line match-cast method in the factory (**Photo 2**). The length of each segment was 2.25 m, and its weight was about 220 kN. Steel segments were fabricated in the factory, with a length of 3.0 m and a weight of 70 kN.

It was very important for the jointing segment to transfer the stress between the PC girder and the steel girder smoothly. The jointing segment comprised of a combination of a concrete member and a steel member (**Fig.5**). The steel member was fabricated first, and filled with self-compacting concrete. The concrete member was fabricated using the match-cast method, and finally prestressing was introduced in order to control crack width caused by the restraint on the concrete at early age.



(a)PC girder section (b)Steel girder section

Fig.4 Main girder section

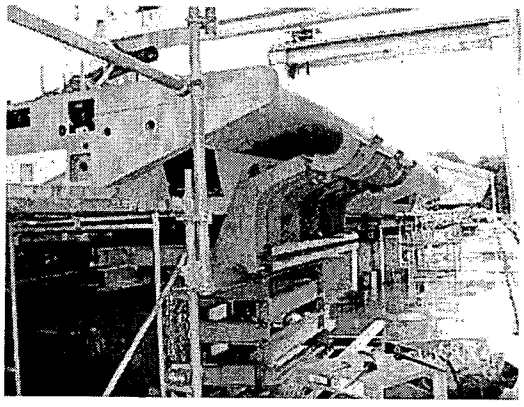


Photo 2 Fabrication of concrete segments

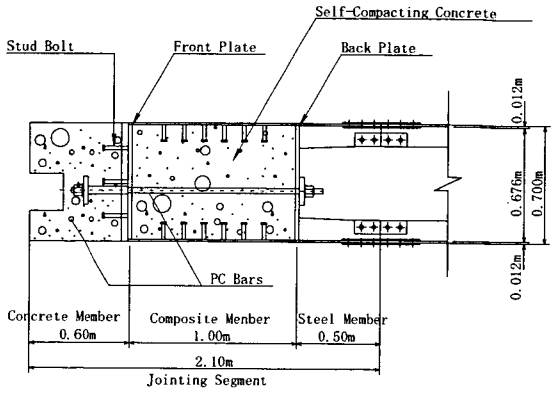


Fig.5 Jointing segment

4.3 Construction of Pylons and Anchorages

The main bodies of pylons are reinforced concrete structures. In order to make the pylon more compact, steel members were adopted to anchor the stay cables to the pylon (**Fig.6**). After the concrete section for 2/3 of the pylon was constructed, steel shell members were placed on top of it (**Photo 3**). After the cantilever erection of the concrete girders and the erection of the steel girders had completed, concrete was placed around the steel shell members to create an integrated unit.

The anchorages have very dense bar arrangement. Therefore, self-compacting concrete with a slump flow of 65 cm was used. Concrete volume was 175 m^3 for the left anchorage and 162 m^3 for the right one.

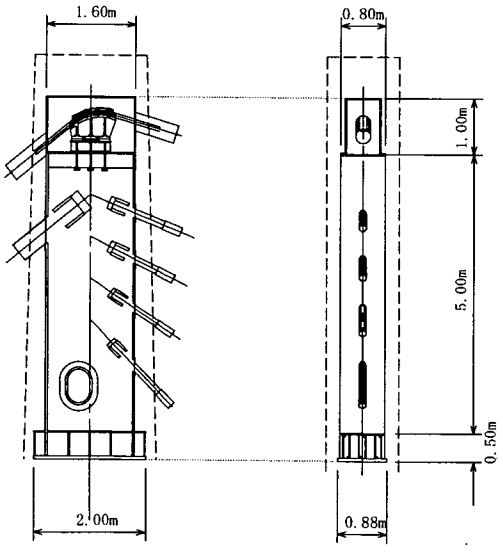


Fig.6 Steel shell member of P1

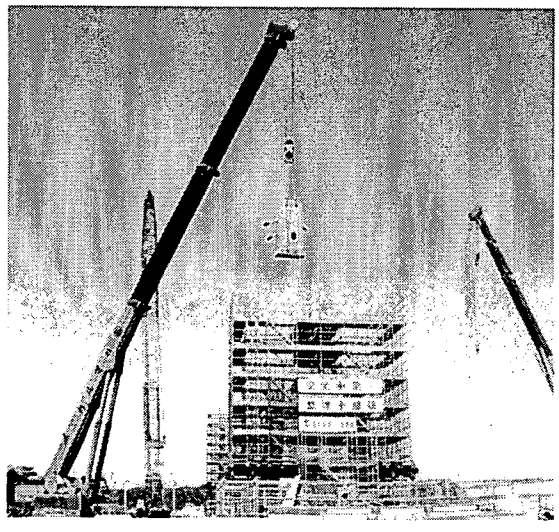


Photo 3 Steel shell member of P2

4.4 Erection of Concrete Segments

Cantilever erection of concrete segments was performed by using a 450-ton crane without any false work and scaffolding in the river (**Photo 4**). Cantilever erection was made by tensioning the inner PC bars at each segment. The stay cables, which were fabricated in a factory, were installed every four segments (anchorage span of 9 m).

4.5 Erection of Steel Girders

When the erection of the concrete segments and the jointing segments were completed, the suspension cables were placed from A1 anchorage to A2 anchorage through the saddles on top of the pylons using a winch and a crane. The steel girder segments were hung on the hanger lopes using a 450-ton crane (**Photo 5**). Connection of each steel segments and connection of the jointing segments and steel segments was conducted, after all of the steel segments were suspended.

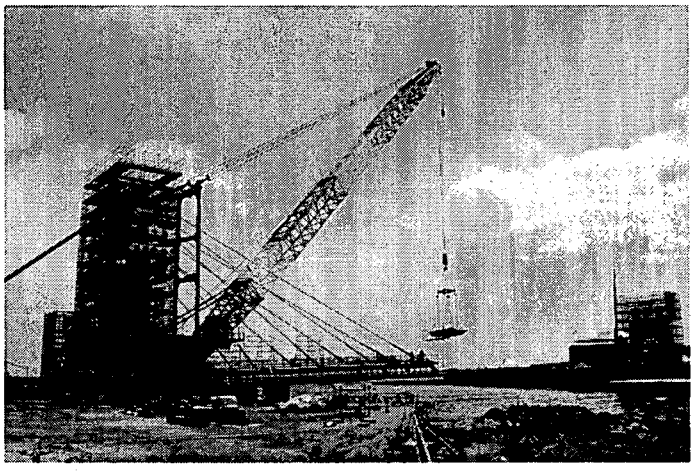


Photo 4 Erection of concrete segments

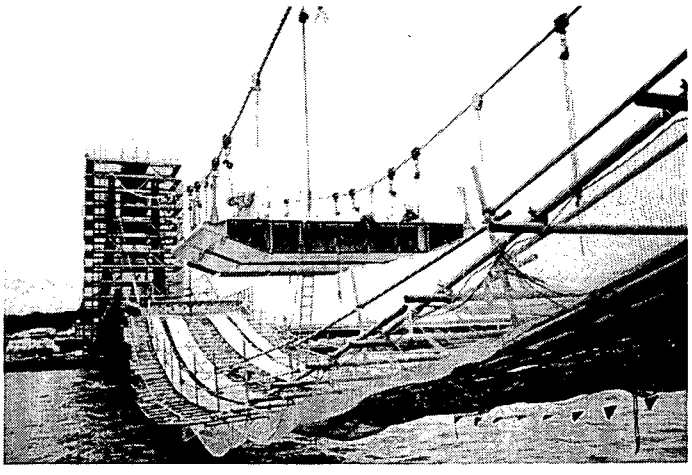


Photo 5 Erection of steel girders

5. Field Test

Prior to the opening of Nagisa Bridge, the field loading tests were conducted in order to verify the performance of the bridge system and the validity of the analysis method. Two loaded vehicles, each weight of 42 kN, were used for the tests (**Photo 6**). **Fig.7** shows the mid-span deformation measured when loaded in the center of the span, including the results of the finite deformation analysis with the 2 dimensional model. The test results did not indicate a complicated performance, even if different bridge systems, cable-stayed PC bridge and steel suspension bridge, were combined. The measured values are lower than the analytical values a little, but the trend is very similar.

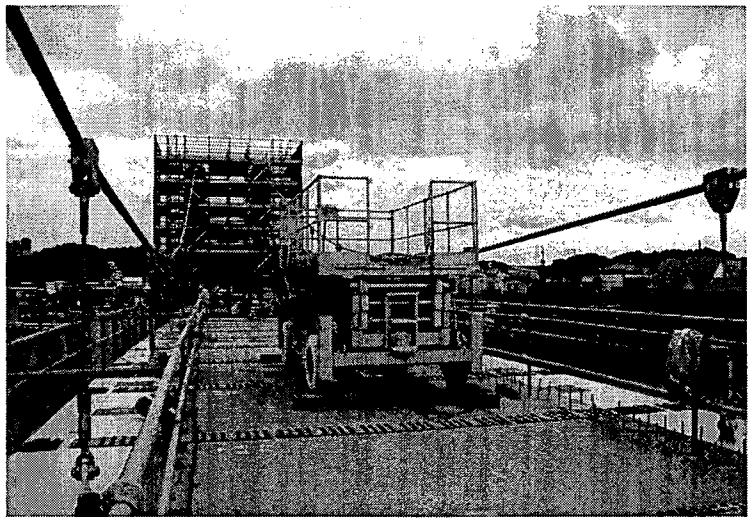


Photo 6 Field test

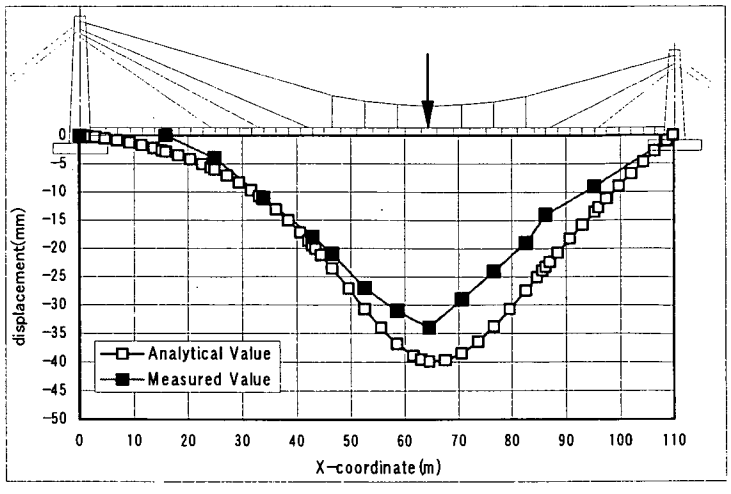


Fig.7 Results of measurement of deformation

6. Conclusions

Nagisa Bridge was the first challenge as a compound bridge of cable-stayed prestressed concrete bridge and steel suspension bridge. Therefore there were many problems to deal with during design, material selection, and execution. Nagisa Bridge, however, was completed in December 2002. And the bridge was opened for pedestrians in July 2003.

It is clear that the hybrid system bridge of cable-stayed PC bridge and steel suspension bridge has many features and is competitive in comparison with ordinary cable supported bridges. The successful completion of Nagisa Bridge demonstrated the superior feature of the hybrid system. And the behavior of such bridges with the hybrid system was verified by conducting field loading tests. It is expected that the adoption of the hybrid system for longer span bridge will increase in the future.

References

[1] Marcel PRADE : "PONTS et VIADUCS au XIXe SIECLE.", ERRANCE, BRISSAUD, 1988, pp.112-113

[2] Macro PETRANGELI, Marcello PETRANGELI : Rehabilitation of Sidi N'Cid Suspension Bridge, Algeria , Structural Engineering International , Vol.10, No.4, 2000, pp.254-258

[3] Y.SATO, K.NOGUCHI, K.SUZUKI, K.MOROHASHI, S.NAKAI : Design and Construction of Nagisa Bridge, Journal of Prestressed Concrete, Japan, Vol.45, No.3, May 2003, pp.22-27

[4] Y.SATO, S.SASAKI, K.MOROHASHI, N.SUZUKI : Construction and Field Tests of Nagisa Bridge –Hybrid System of Cable-Stayed PC Bridge and Steel Suspension Bridge– , Bridge and Foundation Engineering, Vol.37, No.7, 2003, pp.2-9

PERFORMANCE EVALUATION OF SHEAR LINKS AND ORTHOTROPIC BRIDGE DECK PANELS FOR THE SAN FRANCISCO-OAKLAND BAY BRIDGE

Chia-Ming UANG[1], Frieder SEIBLE[1], Cole MCDANIEL[2], and Chung-Che CHOU[3]

Abstract

This paper presents results from testing and the associated analytical studies of steel shear links and orthotropic bridge decks to support the design of the new East Span for the San Francisco-Oakland Bay Bridge. Cyclic testing of full-scale built-up links showed that the specimens were able to reach an inelastic rotation more than twice that would be produced from a 1,500-year Safety Evaluation Earthquake event. Nevertheless, brittle fracture occurred before the inelastic design rotation capacity as specified in the AISC Seismic Provisions was developed. Based on a parametric study, a modification to the welding details was proposed, which proved to be effective in preventing this type of fracture in a subsequent testing program. Monotonic testing of two reduced-scale orthotropic bridge deck panels, one stiffened with closed ribs and another one with open ribs, also showed that these specimens could develop a compression capacity greater than that would be produced by the design earthquake. The post-buckling behavior was associated with the buckling direction and the type of ribs.

1. INTORDUCTION

The East Span of the new San Francisco-Oakland Bay Bridge (SFOBB), designed by the joint venture of T.Y. Lin International and Moffatt & Nichol [6], is a 565-m long single tower steel self-anchored suspension bridge with a main span of 385 m (Figure 1). The tower of the bridge consists of four steel shafts interconnected in the transverse and longitudinal directions by replaceable steel shear links (Figure 2). The suspension cable loops around the west bent and anchors to the bridge deck at the east bent; floor beams are spaced at 5 m inside the box girders. These box girders (Figure 3), a key component of the load-resisting system, balance the cable tension forces in compression. Three different types of longitudinal ribs (troughs, structural tees, and flat plates) are used to stiffen the girder plates such that the yield strength of the girder section can be developed. The tower shafts and box girders are designed to remain elastic under the Safety Evaluation Earthquake (SEE) with a return period of 1,500 years, while the shear links are designed to deform inelastically to protect the tower shafts from damage.

Large-size testing of steel components was conducted at the University of California, San Diego to support the design of SFOBB. The testing program was composed of two parts. First, full-scale tests of two built-up wide-flange shear links were conducted to evaluate the force and deformation characteristics under cyclic loading. Second, monotonic tests were conducted on two reduced-scale orthotropic decks that simulated a portion of the top and bottom decks of the main span box girders to assess the ultimate compressive strength and post-buckling behavior.

[1] Department of Structural Engineering, University of California San Diego, La Jolla, CA 92093, USA

[2] Washington State University, Department of Civil and Environmental Engineering, Pullman, WA 99163, USA

[3] Department of Civil Engineering, National Chiao Tung University, Hsinchu 300, Taiwan

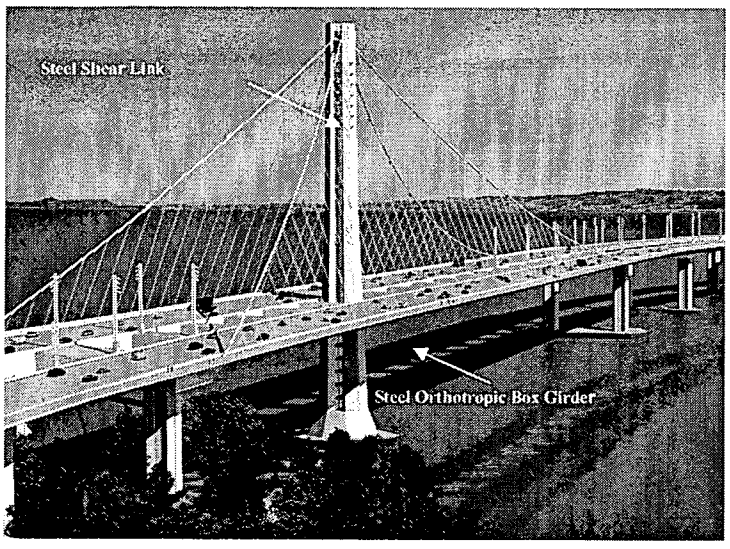


Figure 1 New SFOBB East Main Span

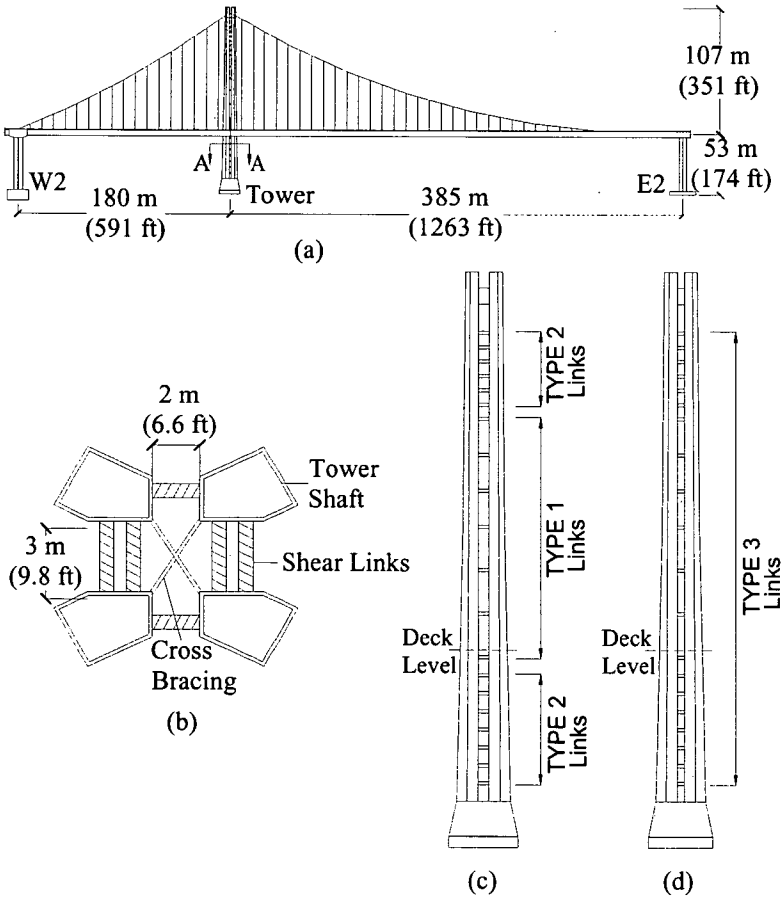


Figure 2 Tower Cross Section and Elevations: (a) Main Span Elevation; (b) Section A-A; (c) Transverse Tower Elevation; (d) Longitudinal Tower Elevation

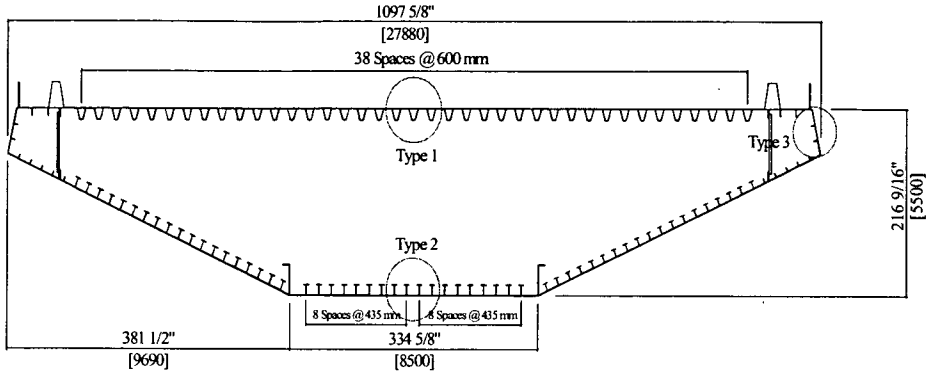


Figure 3 Main Span Girder Cross Section

2. SHEAR LINK STUDY

The objectives of this test program were: (1) to evaluate the cyclic force and deformation characteristics of the full-scale built-up links, and (2) to evaluate the cyclic overstrength of the links, which is needed for capacity design of the towers and the link connections to towers.

2.1 Test Specimens

Two full-scale shear link specimens were tested; one transverse link, TYPE 1, and one longitudinal link, TYPE 3 (see Figure 2). The shear links were built-up steel wide-flange sections with a shear "deformable region" in the center and a "connection region" on either side. Figure 4 shows the details of the Type 1 specimen. The connection region was defined as the portion outside the deformable region. The cross section dimensions were the same for both link types except for a variation in flange width (the flange width for Type 2 link was 475 mm). The plates for the shear link deformable regions were A709 Grade 50 steel with an additional requirement that the actual yield strength, as obtained from tensile coupon tests, not exceed 379 MPa. This upper limit, included in the specifications for the new SFOBB, was introduced by the designers to ensure that the ultimate shear force in the links did not exceed the design capacity of the connection regions. Both tensile and Charpy V-Notch (CVN) tests for the steel plates in the deformable region were conducted. The measured material characteristics are summarized in Table 1. The connection regions were made of A709 Grade HPS70W High Performance Steel. A490 high strength bolts, 30 mm in diameter, were used to splice the shear link flanges and webs to the columns.

Table 1 Link Specimen Material Test Results

(a) Tensile Coupon Test Results

Plate	Yield Strength (MPa)	Tensile Strength (MPa)	Elong. Based on 203 mm gage length (%)
Web	354	497	25
Flange	366	532	27

(b) Charpy V-Notch test Results

Coupon	CVN (Joules)	Average (Joules)
Flange at -22 °C	8 26 34	23
Web at -12 °C	27 34 33	31

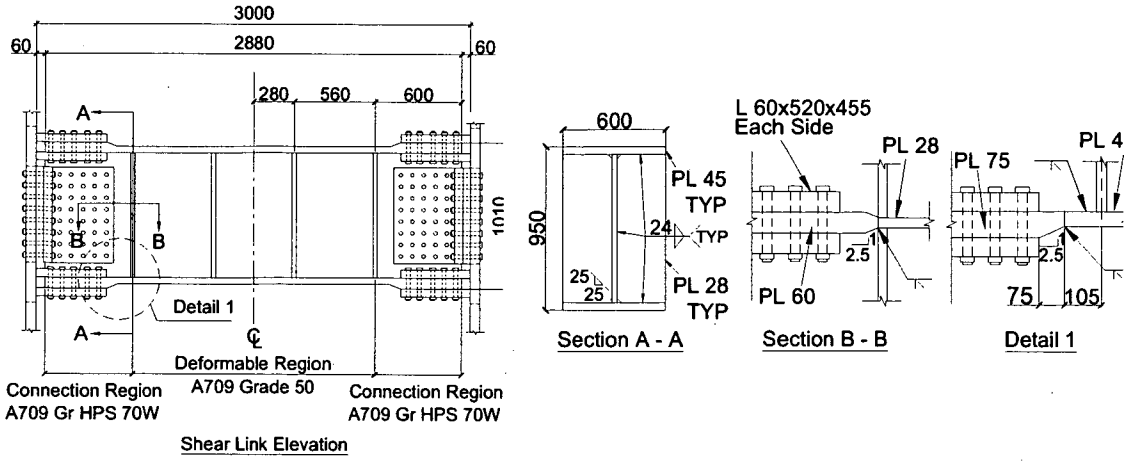


Figure 4 Link Geometry and Details (Type 1)

The links were designed in accordance with the AISC Seismic Provisions [1]. The length, e, of both links was less than $1.6M_p/V_p$, where V_p is the nominal shear strength, M_p is the nominal plastic flexural strength. Therefore, shear behavior is expected to dominate the response. To delay the onset of local buckling in the web, the designer provided intermediate stiffeners in the web such that the spacing was not more than $30t_w-d/5$, where t_w is the web thickness and d is the beam depth. According to the AISC Seismic Provisions, links thus designed would provide an inelastic design rotation capacity (γ_p) of 0.08 radian. Based on nonlinear time-history analyses with the SEE event as the input ground motions, the designer predicted that the maximum inelastic rotation demand for the TYPE 1 and TYPE 3 links were only 0.01~0.02 radian and 0.03~0.04 radian, respectively.

The test specimens were fabricated by a commercial fabricator. The fabrication sequence was similar for both links. Once the plates were cut and prepped, the connection regions and deformable region of the flange plates were spliced together by complete joint penetration (CJP) groove welds. The same procedure was carried out for the web plate. Next, the flanges and web were welded together by CJP welds. Transverse stiffeners were then fillet welded to both sides of the web. All the shear link CJP groove welds were performed by the flux-cored arc welding process with E91T-1 electrodes for the Grade 70 material and E71T-1 for the Grade 50 material. The specified minimum CVN toughness for the welding electrodes was 34 J at –30 °C.

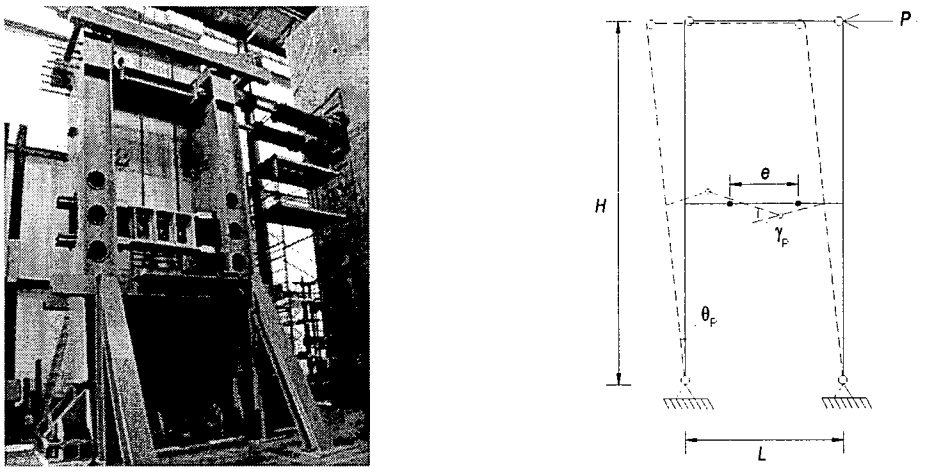
2.2 Test Setup

The test setup was designed such that a large shear force demand can be applied to the full-scale specimens. Figure 5 shows that the setup included two pin-based columns, a shear link specimen, an upper pinned strut, and a lateral restraint system.

2.3 Loading Sequence

The testing was conducted in a displacement controlled mode. A prescribed quasi-static cyclic loading sequence was imposed laterally to the top of the test setup. The loading sequence was a variation of that proposed for testing link-to-column connections [1]. The loading protocol was followed until the inelastic rotation of the link exceeded that predicted from time history analyses by the designer. From then on, a single cycle at each deformation amplitude was imposed to the test specimen until the specimen failed. Such a modification was justified from results of time-history analysis, which indicated that the AISC loading protocol would unrealistically impose a very large cumulative

inelastic deformation demand to the link specimens. Figure 6 shows the loading sequence that was imposed to the test specimens.



(a) Overall View (b) Test Setup Geometry

Figure 5 Shear Link Test Setup

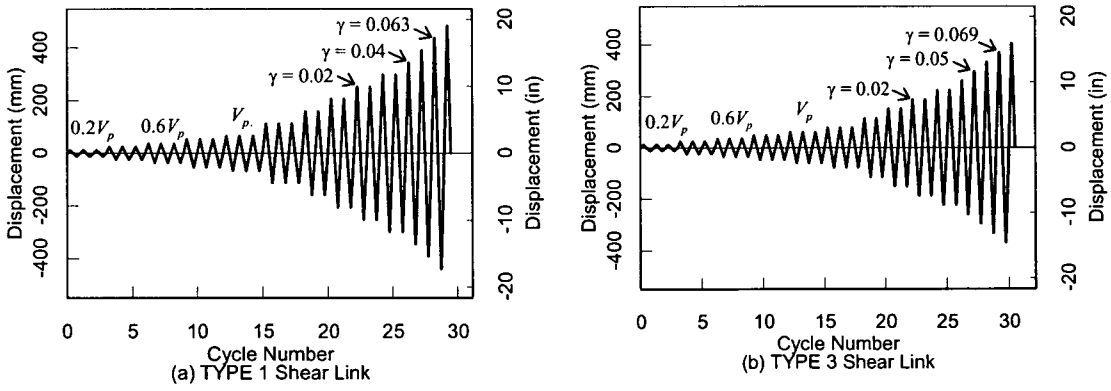


Figure 6 Link Loading Sequence

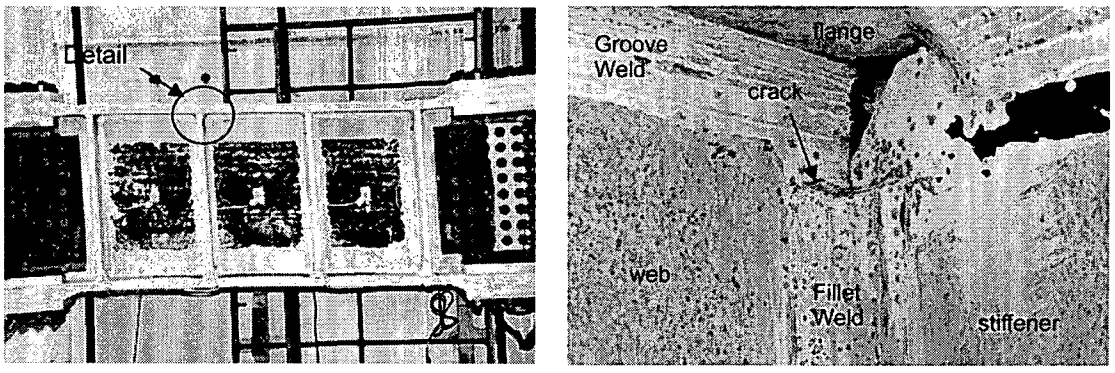
2.4 Test Results

The behavior of the two specimens was similar. Minor flaking of the mill scale in the link web was visually identifiable in the early stage of testing. The first occurrence of slipping of the bolted flange splices, which was accompanied by a loud noise as the splice plates slid past the flanges, was observed during the first cycle when the imposed lateral displacement (Δ) was 66 mm. As the lateral displacement was increased, the splices continued to slip in both the push and pull directions. At 345 mm, cracks were visually observed at the ends of the vertical fillet welds connecting the intermediate stiffeners to the link web [see Figure 7(b)]. The cracks continued to propagate into the link web as the lateral displacement was increased. As the deformation was increased further, brittle fracture of the link web occurred [see Figure 8(a)]. A close-up at the crack initiation location is shown in Figure 9. A similar failure mode was also observed in the TYPE 3

link [see Figure 8(b)].

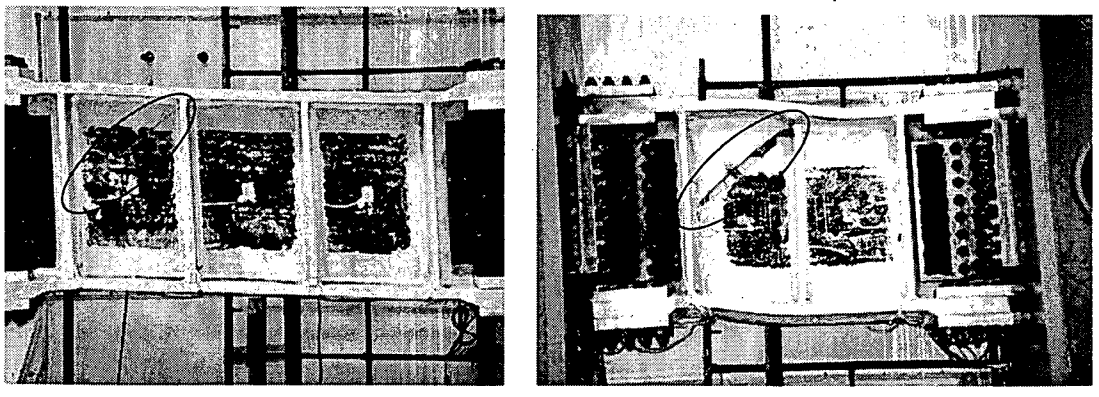
The link shear versus average shear deformation relationships of the deformable region are shown in Figure 10. Excluding the last incomplete cycle, the inelastic rotation reached 0.06 and 0.066 radians for the TYPE 1 and TYPE 3 links, respectively. The shear deformation in the connection regions was low, with the response remaining in the elastic range throughout the test.

The overstrength factor developed in each of the two test specimens was calculated by dividing the maximum shear strength by the plastic shear strength, which was based on the measured yield strength of the web material. The corresponding overstrength factors are 1.83 and 1.94, indicating that the value (1.25) recommended by the AISC Seismic Provisions for capacity design is non-conservative by a large margin.



(a) Deformed Configuration (b) Crack at End of Stiffener/Web Fillet Weld

Figure 7 TYPE 1 Link at Δ = 345 mm



(a) Type 1 Specimen (b) Type 3 Specimen

Figure 8 Brittle Fracture of Link Specimens

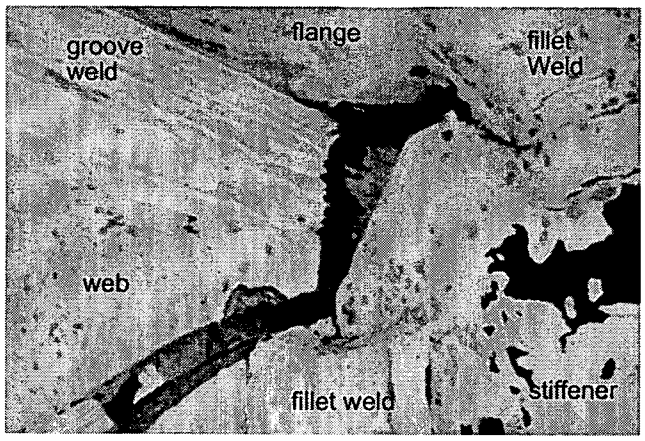
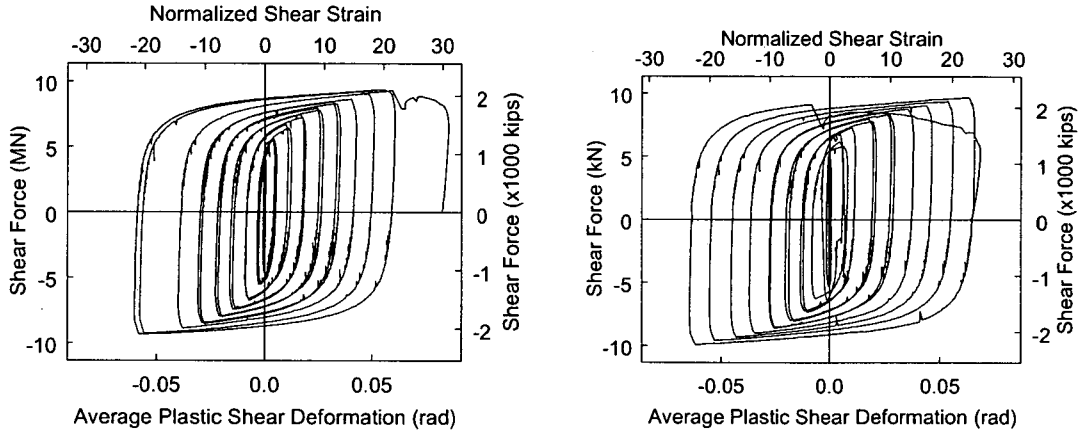


Figure 9 Close-up of Crack Initiation Location (Link Type 1)



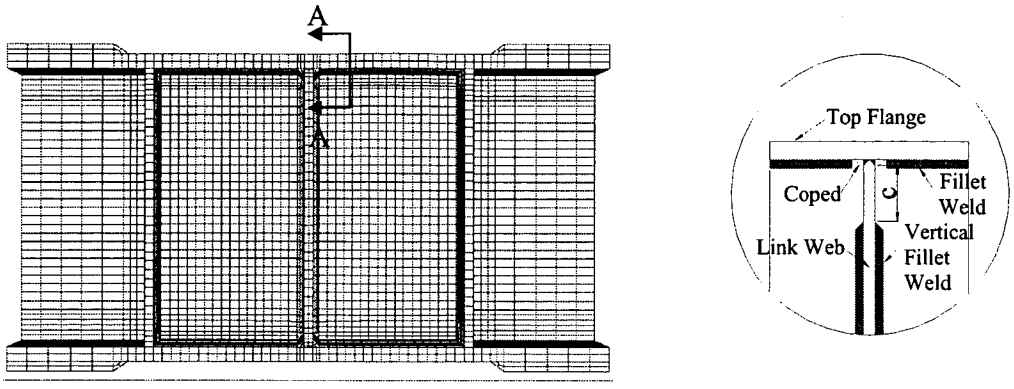
(a) Type 1 Specimen

(b) Type 3 Specimen

Figure 10 Link Shear Force versus Inelastic Rotation Relationships

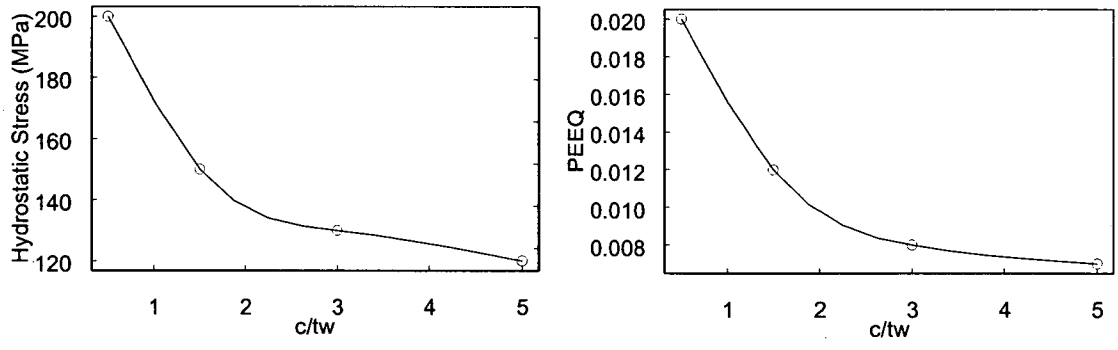
2.5 Crack Prevention Measures

The brittle fracture failure mode that occurred in such large-size built-up links had not been reported previously. The cracks in the two full-scale link specimens occurred at the ends of vertical welds of the intermediate stiffeners, near the highly restrained location where the flange-to-web groove weld, and the vertical and horizontal fillet welds of the stiffeners met (Figure 9). To mitigate the potential for crack initiation at the end of the fillet weld, one option is to terminate the welds further from the web-flange-stiffener intersection. The effectiveness of this scheme was explored by a series of 3-D finite element analysis using the model similar to that shown in Figure 11(a); the nonlinear finite element analysis computer program ABAQUS [4] was used for this purpose [5]. By varying the distance (c) from the end of vertical fillet welds to the near toe of the web-to-flange [Figure 11(b)], the results showed that the hydrostatic stress and the effective plastic strain were reduced significantly when c was increased to about 5 times the web thickness (see Figure 12). This recommendation, which was adopted for the fabrication of links for SFOBB, was demonstrated later to be effective to avoid brittle fracture in another test program conducted at the University of Nevada, Reno [3].



(a) Elevation (b) Detail A

Figure 11 Finite Element Model



(a) Hydrostatic Stress (b) Equivalent Plastic Strain

Figure 12 Link Finite Element Analysis Results

3 ORTHOTROPIC BRIDGE DECK STUDY

The objective of this test program was to evaluate the ultimate compressive strength and post-buckling behavior of the longitudinally stiffened panels for the box girders. Unlike the cyclic testing of links that are expected to yield and dissipate energy during a major seismic event, monotonic testing was conducted on two reduced-scale stiffened panel models because the box girders are expected to remain elastic during an SEE event.

3.1 Test Specimens

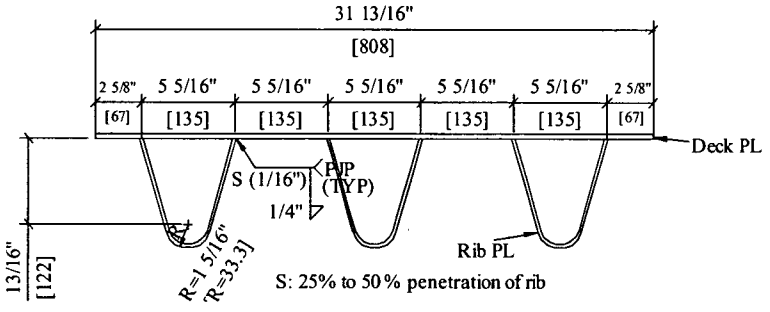
Portions of the top and bottom decks of a box girder (Figure 3) were investigated in this study. Since floor beams are spaced at 5 m on center inside the box girder, each deck can buckle longitudinally in an S shape. To study the buckling behavior of the stiffened panels in both positive and negative bending directions, it was decided that each specimen include two spans. Reduced-scale models were tested due to the high force demand for testing. Figure 13 shows the cross sections of both specimens. Specimen 1, with a scale factor of 0.45, was composed of three closed ribs and a top deck plate; Specimen 2, with a scale factor of 0.48, was made up of a bottom deck plate and four T-shaped ribs.

The specimens were specified to be non-fracture critical member with ASTM A709 Grade 345 steel. Tensile material properties as obtained from the certified mill test reports

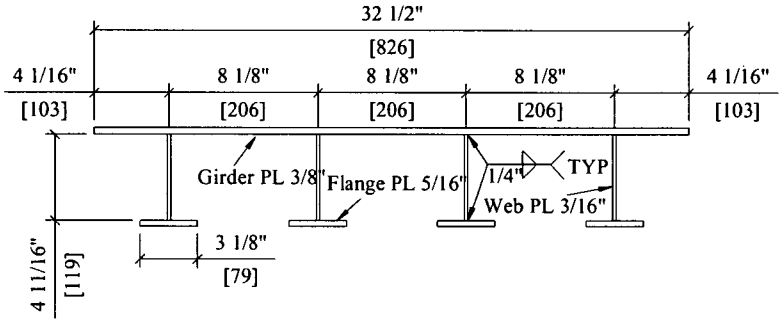
are summarized in Table 2.

3.2 Test Setup

The test setup, shown in Figure 14, was composed of a horizontal loading beam, pin devices at both top and bottom ends, a specimen, and a concrete support. A lateral support connected by a diaphragm plate at the mid-height of the specimen was designed to simulate the lateral restraint provided by the floor beam.



(a) Specimen 1

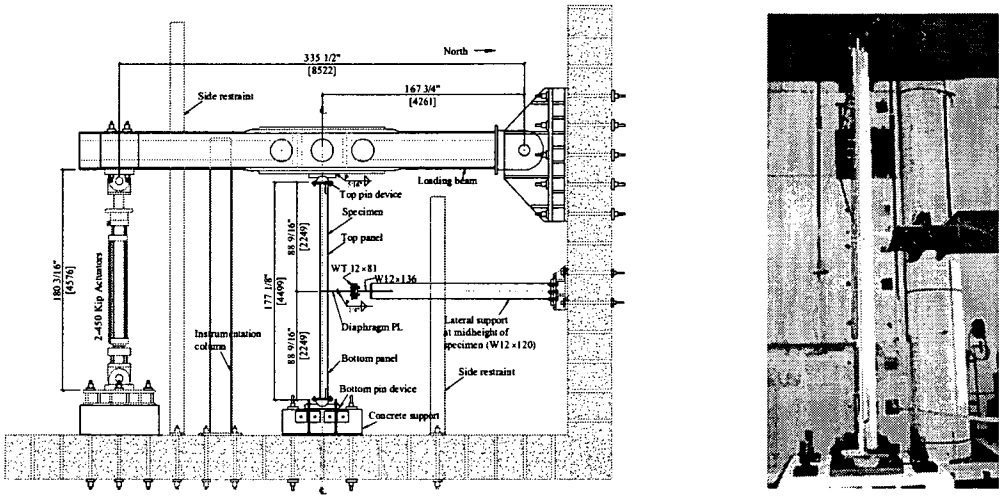


(b) Specimen 2

Figure 13 Cross Section of Orthotropic Bridge Deck Specimens

Table 2 L Deck Specimen Material Properties

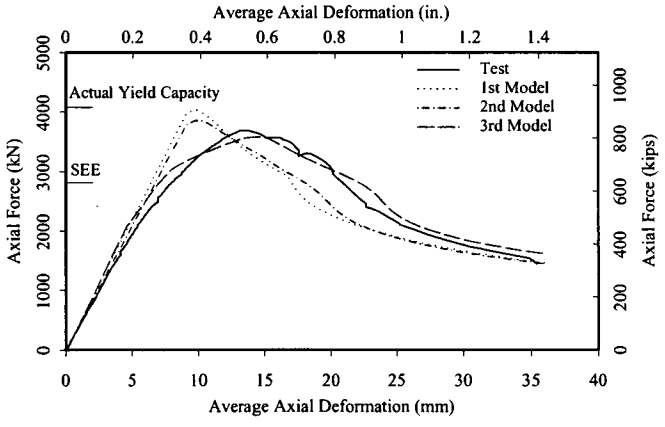
Specimen No.	Plate		Thickness mm (in.)	Yield Strength (MPa)	Tensile Strength (MPa)	Elong. Based on 203-mm gage length (%)
1	Girder Plate		6	372	510	20
	Rib Plate		5	427	579	20
2	Girder Plate		10	427	534	24
	Rib	Web Plate	5	427	579	20
		Flange Plate	8	476	573	21



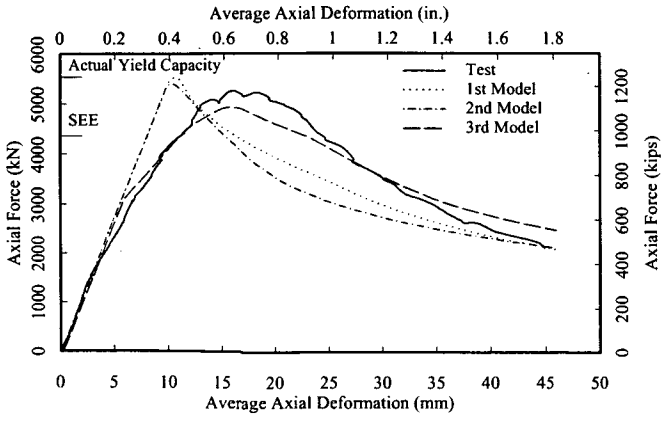
(a) Schematic

(b) Elevation

Figure 14 Bridge Deck Test Setup



(a) Specimen 1



(b) Specimen 2

Figure 15 Applied Load versus Axial Deformation Relationships (Deck Specimens)

A quasi-static, monotonic loading was applied to the specimen by using two 2000-kN actuators at one end of the loading beam. The testing was conducted in a displacement-controlled mode with axial deformation, Δ, of the specimen as the controlling variable.

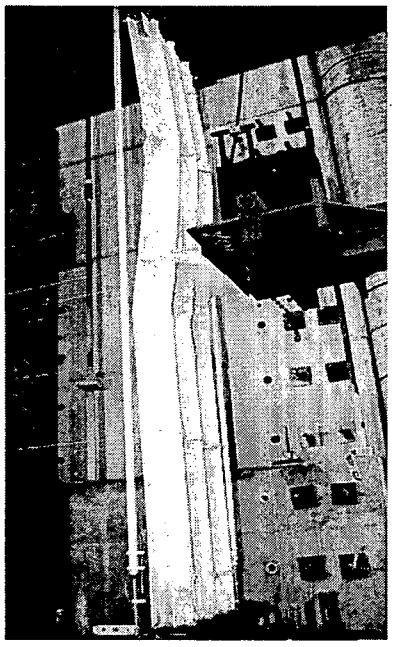
3.3 Test Results

The applied load versus axial deformation relationship of Specimen 1 is shown in Figure 15(a), in which both the yield capacity based on the actual yield strength and the seismic demand produced by an SEE event are marked. As the load was gradually applied, the maximum strength of the specimen was reached at Δ = 14 mm. The upper panel buckled in one direction and the lower panel buckled in the other direction as shown in Figure 16(a). As the imposed axial deformation was increased further, local buckling of the deck plate across the width of the upper panel was observed, which then triggered rib buckling; the symmetric bulging buckling configuration of the ribs shown in Figure 16(b) was compatible in deformation with the buckling pattern of the deck plate. Figure 16(c) shows the buckling of the ribs that occurred near the upper end of the lower panel; note that the deck plate did not buckle. This buckling configuration is different from that shown in Figure 16(b) for the upper panel. The difference was primarily caused by the direction of bending after the maximum strength of the specimen was reached.

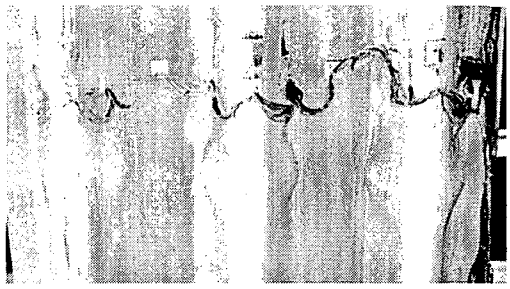
The applied load versus axial deformation relationship of Specimen 2 is shown in Figure 15(b), in which the SEE demand and actual yield capacity are also marked. The peak compression force was reached at Δ = 17 mm, with the specimen buckled in reverse curvature as shown in Figure 17(a). Torsional buckling of the T-shaped ribs was observed in the lower panel of the specimen [see Figure 17(c)], but torsional buckling of the ribs was not observed in the upper panel [see Figure 17(b)]. Twisting of the specimen at the lower panel was also observed at the later stage of testing. It was due to the loss of torsional rigidity of the section after the T-shaped ribs experienced torsional buckling. No torsional buckling of the T-shaped ribs and twisting of the section was observed in the upper panel, but local buckling of the deck plate was observed between the intersection points of the web and girder plates.

3.4 Finite Element Analysis

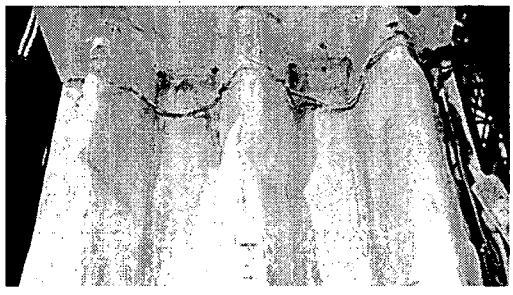
Specimens 1 and 2 were modeled using the nonlinear finite element computer program ABAQUS [4] with the four-node doubly curved thin shell element S4R. Because the initial geometric imperfections and residual stresses have pronounced influences on the ultimate strength and post-buckling behavior of the stiffened panel, these two effects were considered in the study [2]. The measured geometric imperfection of each specimen was introduced by applying a uniform pressure perpendicular to the deck plate to mimic the deformed pattern and magnitude between the middle and end of the specimen. Three models were considered for each test specimen. Without considering the effects of both geometric imperfections and residual stresses, the first model shows that the actual yield capacity of the specimen could be reached (see Figure 15) before strength degradation due to buckling. By considering only the initial geometric imperfections in the second model, the ultimate strength and elastic stiffness were slightly lower than that of the first model, but were higher than the test results. When the both effects were considered, the third model predicted response well the ultimate strength and the post-buckling behavior. The analysis also showed that the buckling modes can be simulated when the effects of geometric imperfections and residual stresses were considered (see Figure 18).



(a) Overall View

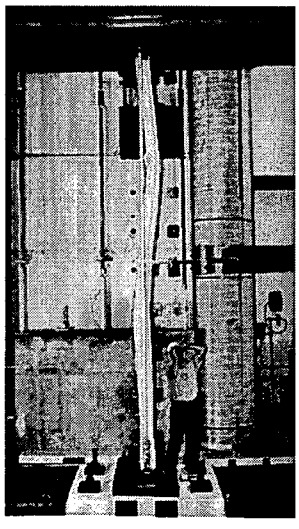


(b) Upper Panel

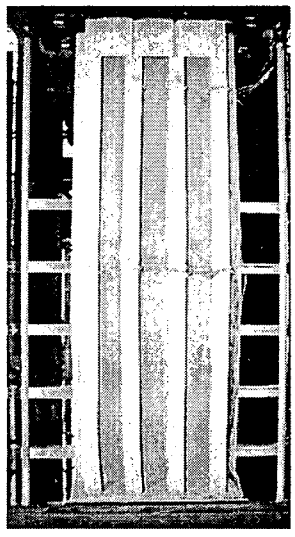


(c) Lower Panel

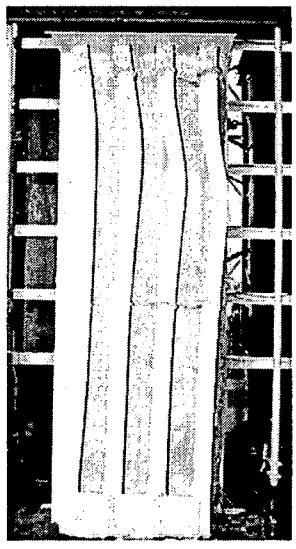
Figure 16 Deformed Configurations after Testing (Deck Specimen 1)



(a) Overall View

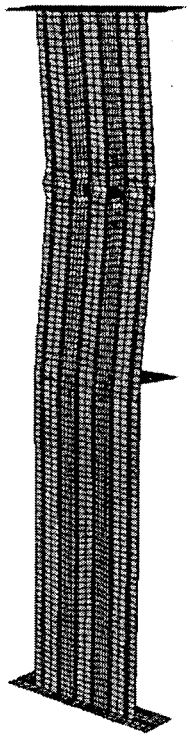


(b) Upper Panel

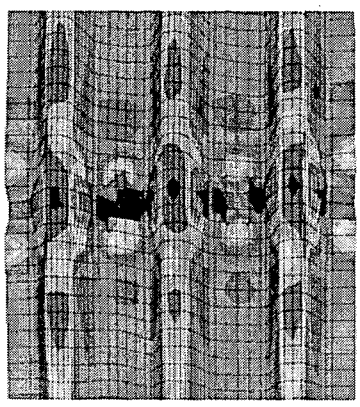


(c) Lower Panel

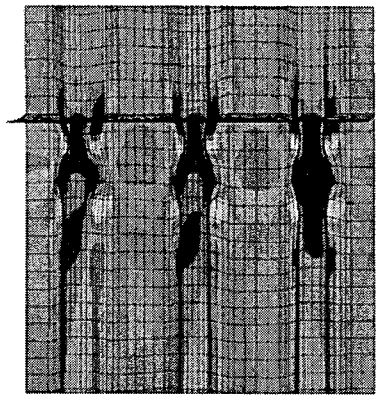
Figure 17 Deformed Configurations after Testing (Deck Specimen 2)



(a) Overall View



(b) Upper Panel



(c) Lower Panel

Figure 18 Predicted Deformed Configurations (Deck Specimen 1)

4 CONCLUSIONS

Large-size testing of steel components was conducted at the University of California, San Diego to support the design of the new East Span of the San Francisco-Oakland Bay Bridge. The testing program was composed of two parts. First, full-scale tests of two built-up wide-flange shear links were conducted to evaluate the force and deformation characteristics as well as the cyclic overstrength factor. Cyclic testing showed that both link specimens were able to reach an inelastic rotation greater than twice that would be produced by a Safety Evaluation Earthquake event. Nevertheless, the inelastic rotation capacity did not reach that specified in the AISC Seismic Provisions due to brittle fracture of the link web, which initiated from a highly restrained region where several welds met. A parametric study using a nonlinear finite element analysis program suggested that offsetting the stiffener-to-web fillet welds from the flanges by at least 5 times the web thickness would reduce the deformation demand in these susceptible areas. This recommendation proved to be beneficial in preventing brittle fracture in another testing program conducted later at the University of Nevada, Reno. The test results also showed that, for capacity design, the overstrength factor (1.25) as specified in the AISC Seismic Provisions is significantly lower than that measured (1.83 to1.94) and is, thus, non-conservative for the links tested.

The ultimate axial capacities of two reduced-scale, orthotropic bridge deck specimens were evaluated from monotonic loading. The full width of the girder plate in

both specimens, stiffened longitudinally by the rib plates, reached yield before local buckling of the plate occurred. Both specimens reached a compression capacity greater than that would be produced by a Safety Evaluation Earthquake event. After the ultimate strength was reached, the strength degradation of the first specimen, which was stiffened with closed ribs, was due to global buckling, local buckling of the lower-panel ribs and the upper-panel girder plate. For the second specimen, which was stiffened with open ribs, the strength degradation was initiated by torsional buckling of the lower-panel ribs, followed by the twisting of the lower panel and local buckling of the upper-panel girder plate. It was also found from numerical simulation that the residual stresses have a more influence on the ultimate strength and post-buckling behavior than the geometric imperfections.

ACKNOWLEDGEMENTS

This research project was sponsored by the California Department of Transportation (Caltrans). Dr. Wenyi-Long served as the Project Contact. Dr. Marwan Nader and Mr. Laurent Rus of T.Y. Lin International provided information and guidance for the design and fabrication of the specimens.

REFERENCES

[1] AISC, *Seismic Provisions for Structural Steel Buildings*, American Institute of Steel Construction, Chicago, IL, 1997.

[2] Chou, C. C., Uang, C. M., and Seible, F., "Compression testing of orthotropic steel deck for the new San Francisco-Oakland bay self-anchored suspension bridge." *Rep. No. SSRP-2002/12*, Department of Structural Engineering, University of California, San Diego, La Jolla, CA, 2003.

[3] Dusicka, P., Itani, A., and Buckle, I. G., "Cyclic Behavior of Shear Links and Tower Shaft Assembly of San Francisco-Oakland Bay Bridge Tower," *Report No. CCEER 02-6*, Civil Engineering Department, University of Nevada, Reno, 2002.

[4] HKS, *ABAQUS User's Manual Version 6.2,* Hibbitt, Karlsson, & Sorensen, Inc., Pawtucket, RI, 2001.

[5] McDaniel, C. C., Uang, C. M., and Seible, F., "Cyclic Testing of Built-up Steel Shear Links for the New Bay Bridge." *Journal of Structural Engineering*, Vol. 129, No. 6, pp. 801-809, 2003.

[6] Tang, M., Manzanarez, R., Nader, M., Abbas, S., and Baker, G., "Replacing the East Bay Bridge." *Civil Engineering*, ASCE, Vol. 70, No. 10, pp. 38-43, 2000.

An Experimental Study on Slip Strength of HSFG Bolted Joints Treated with High-Friction Inorganic Zinc-Rich Paint

Yohei Koike* and Keiji Terao*

ABSTRACT

Recently for the purpose of cost reduction in construction, rationalization of high-strength friction grip bolted joints in plate girder bridges is encouraged. As a method of the rationalization, it is proposed to increase the design slip factor specified as 0.4 in the Japanese Specifications for Highway Bridges (JSHB)[1]. Since it is relatively small compared with other countries and the increase of the factor leads directly to the reduction of the number of bolts, high-friction inorganic zinc-rich paint having high slip factor over 0.7 was developed through tensile tests in this study.

1. INTRODUCTION

In recent years, in accordance with the enlargement of cross-sections by adoption of bridges with greater girder spacing, the number of HSFG bolts has been increased, and the size of splices has been expanded. To reduce the number of bolts, it is proposed to increase the design slip factor specified as 0.4 in JSHB. While the shift of the design method from allowable stress design method to performance based design method, the increase of slip factor is expected to contribute to rationalization of bolted joint. As shown in Table 1, although various values are already specified according to the conditions of the friction surfaces in the design criteria of other countries, slip factor specified in the JSHB is uniformly 0.4, and the value in Japan is relatively small compared with one of other countries. On the other hand, increase of slip factor is expectable with the development of the paint technique in recent years.

With these backgrounds, many tensile tests using specimens with inorganic zinc-rich paint were carried out, and the conventional zinc-rich paint was improved and new high- friction paint has been developed. This paint has the same functions, such as the corrosion protection performance and the working performance, as that of conventional one.

2. EXPERIMENT PROCEDURE

As shown in Fig. 1, a tensile specimen has the bolt arrangement of one-line two-rows, and was designed so that the base plates and the splices did not yield before load reached slip strength. The grade of the steel material is SM490Y and M22(F10T) was used for high-strength bolts. Inorganic zinc-rich paint was applied to the friction surfaces after shot-blasting. A painting scene is shown in Photo 1.

* Yokogawa Bridge Corp. Research Laboratory
No.27,Yamano-cho,Funabashi-shi,Chiba-ken,273-0026,Japan

Table 1 International comparison of slip factor

slip factor	the treatment or the condition of the friction surface	slip factor	the treatment or the condition of the friction surface
●Eurocode[2] (1997)		●AASHTO[3] (1994)	
0.50	shot-blasting or grid-blasting	0.33	the surface with clean mill scale
0.50	zinc based metal spray guaranteed the slip factor 0.5 at least after shot-blasting or grid-blasting	0.50	class A coating after blasting
0.30	the surface removed loose scale after cleaned by wire brushing or flame cleaning	0.50	blasting
0.20	none	0.40	class B coating after blasting
		0.40	the rough surface with galvanization
●ISO[4] (1997)		●SIA[5] (1979)	
0.33	the surface with clean mill scale	0.30	the surface with clean mill scale
0.40	the surface removed mill scale and loose scale and after exposure outdoors	0.50	sand-blasting or flame cleaning
0.50	shot-blasting or grid-blasting	0.40～0.50*	zinc based metal coating after sand-blasting
0.50	inorganic zinc-rich painting with thickness under 60 micrometer	0.30～0.45*	zinc based organic coating after sand-blasting
0.35	organic zinc-rich painting with thickness under 60 micrometer	0.35	the rough surface with galvanization
0.40	blasting on the galvanized surface with thickness over 50 micrometer	The value of * is depened on the process of the painting	
●BS[6] (1982)		●DIN[7] (1990)	
0.45	the surface removed mill scale and loose scale and after exposure outdoors	0.50	shot-blasting or grid-blasting
0.50	shot-blasting or grid-blasting	0.50	flame cleaning twice
0.35	inorganic zinc-rich painting	0.50	alkali silica zinc powder painting
●the Japanese Specifications for Highway Bridges[1] (2002)			
0.40	the rough surface removed mill scale		
0.40	thick inorganic zinc-rich painting		

As shown in Table 2, experiments are 32 cases in total, and the main parameters are paint composition, film thickness and surface roughness. In consideration of the dispersion, three specimens were tested in each case.

High-strength bolts were fastened by 60% of bolt tension specified in JSHB at first, and then tightened by 100 % (= 225.5kN). The tension in the fixed side was increased by 10% so that a slip might not occur.

In consideration of the relaxation of high-strength bolts, the experiments were carried out more than seven days after bolts were tightened. The displacement between base plates and the axial force of bolts in case 23-32 were measured, and

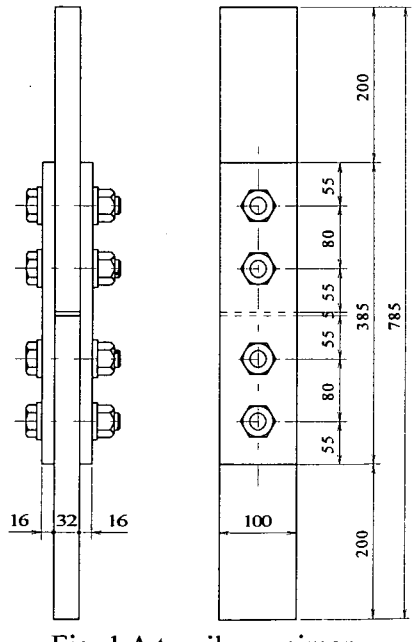


Fig. 1 A tensile specimen

load was increased linearly until a major slip occurred. An experiment setup is shown in Photo 2.

Table 2 Experiment cases

case	target base plate film thickness (μ m)	target splice film thickness (μ m)	target surface roughness (μ mRz)	curing period	main parameters
1 - 4	20	75	80	2 weeks indoors	pigment
5 - 7	20	75	80	2 weeks indoors	zinc particle size
8 - 11	20	75	80	2 weeks indoors	resin material
12 - 15	20,75	75	80,100	2 weeks indoors	zinc particle size surface roughness film thickness
16 - 17	75	75	80	2 weeks indoors	mix proportion
18 - 22	75	75	80	2 weeks indoors	pigment
23 - 32	75	75	80	7 weeks indoors	hardened pigment

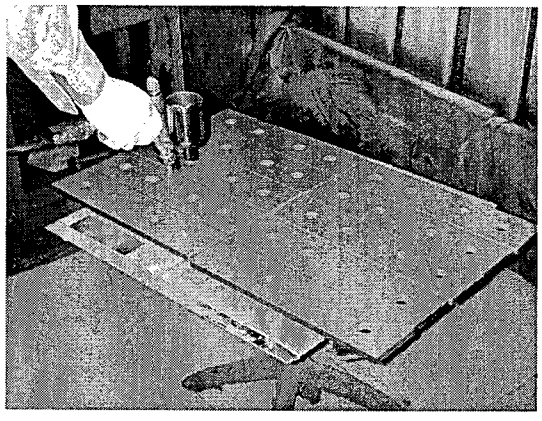


Photo 1 View of painting

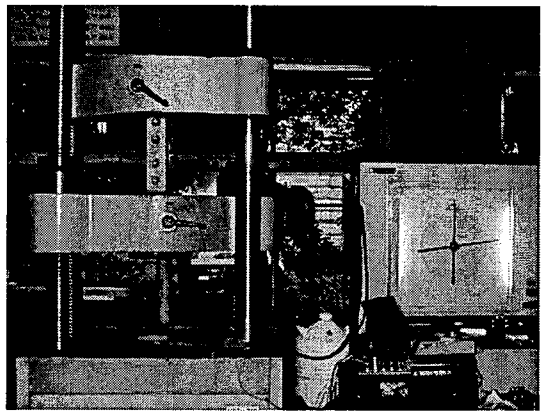


Photo 2 View of experiment

3. EXPERIMENT RESULTS

An experiment result is shown in Fig. 2. The slip factor was calculated using equation (1) as shown below.

$$\mu = \frac{P_{slip}}{m \cdot n \cdot N} \tag{1}$$

μ :slip factor
P_{slip} :major slip load
m :the number of bolts (=2)
n :the number of friction surfaces (=2)
N :initial bolt tension (=225.5kN)

A slip factor was not significantly influenced by zinc particle size or resin material, and was improved greatly by hardened pigment. This result is expected to originate that the shear capacity between coating films increased. The slip factor of case 29 was the maximum and the average was 0.783.

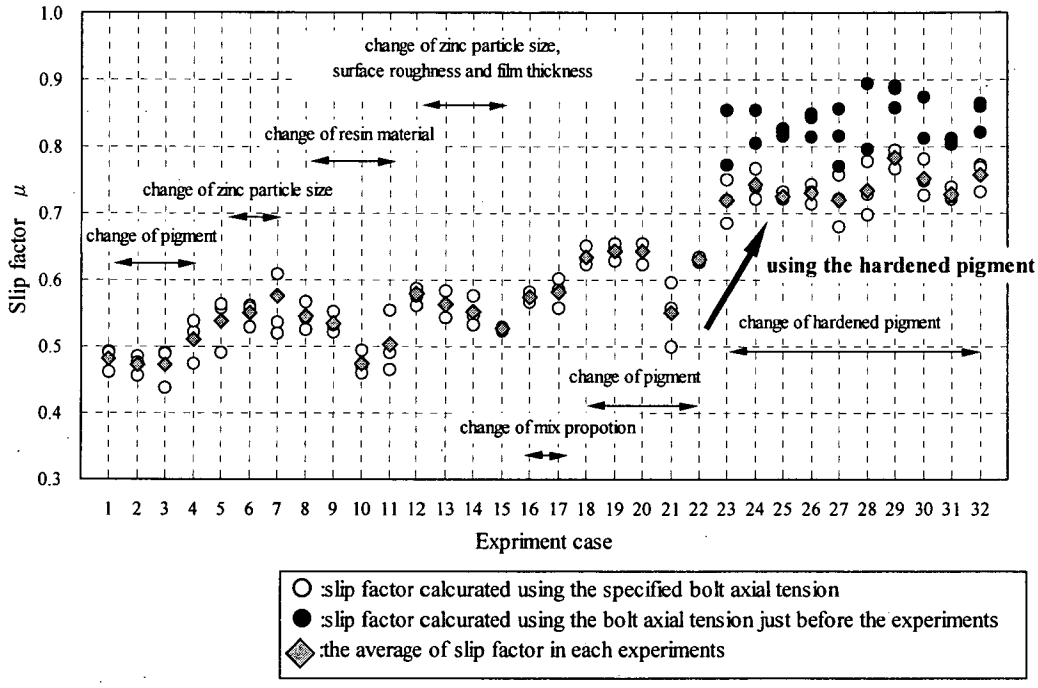


Fig. 2 Result of experiments

4.APPLICATION OF HIGH-FRICTION PAINT

Since the allowable force per high-strength bolt can be improved by increasing slip factor, it becomes possible to reduce the number of high-strength bolts and the size of splices when this developed paint is applied to actual bridges. The tentative calculation was performed in order to investigate how bolt joints can be rationalized by using this paint. The example bridge is the simple composite bridge with 4 main I-section girders shown in Fig. 3.

Although the maximum slip factor was approximately 0.8 according to the experiment results, the tentative calculation was done by setting the slip factor to 0.7 by taking safety into consideration.

The calculation result of the number of high-strength bolts is shown in Table 3 and Fig. 4, and of the weight of splices and the painting area is shown in Table 4. As compared with the conventional design, the number of high-strength bolts can be reduced by about 40% by increasing the design slip factor to 0.7. Furthermore, the size of splices becomes smaller, the painting area and weight of splices can also be reduced by about 40%. Therefore, not

only the amount of painting in factories becomes smaller, but work efficiency in field is also improved. These values are almost decreased in proportion to the increment of slip factor.

5.CONCLUSIONS

Based on the results, the main conclusions are drawn as follows:

(1) High-friction inorganic zinc-rich paint having high slip factor over 0.7 was developed thorough tensile tests.

(2) In order to increase slip factor, use of hardened pigment was most effective.

(3) The number of high-strength bolts, painting area, and weight of splices can be reduced by about 40% by increasing the design slip factor to 0.7 as a result of tentative calculation.

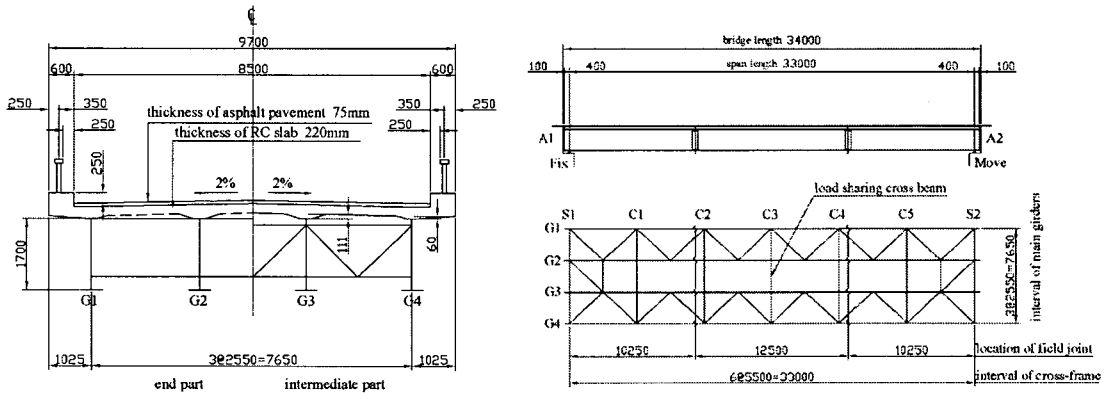


Fig. 3 General dimensions of the example bridge

Table 3 Calculation results of the number of bolts required

case	(A)	(B)
the design slip factor	0.4	0.7 (1.75)
the allowable force of high-strength bolt (kN)	96	168
the design bending moment (kN·m)	3213	
the design shear force (kN)	411	
the number of bolts in upper flange	12	8
the number of bolts in web	48	32
the number of bolts in lower flange	36	18
the total number of bolts	96	58 (1/1.66)

* The value in a parenthesis is a ratio to (A) of (B)

*The value in the table is the quantity per one joint of G1 girder.

*The allowable force is the value per two friction surfaces

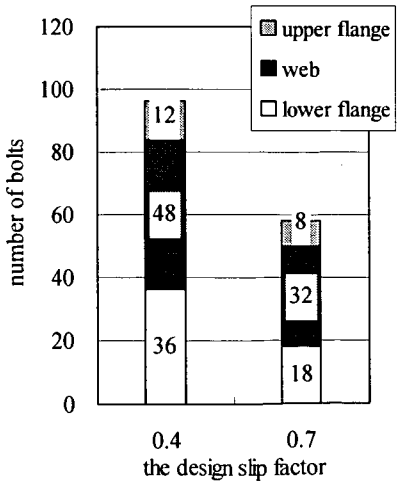
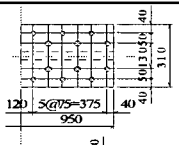
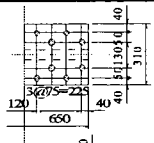
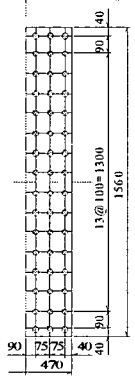
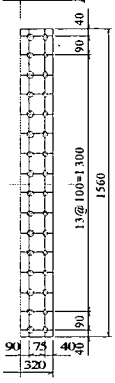
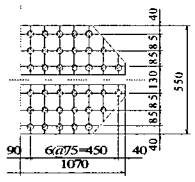
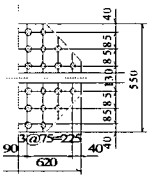


Fig. 4 The number of bolts in each member

Table 4 Calculation results of weight of splices and painting area

case		(A)	(B)
the design slip factor		0.4	0.7 (1.75)
the layout of bolts	upper flange		
	web		
	lower flange		
the weight of splices (kg)		326.3	204.0 (1/1.60)
the painting area (m^2)		6.26	4.04 (1/1.55)

* The value in a parenthesis is a ratio to (A) of (B)

*The value in the table is the quantity per one joint of G1 girder.

6.FUTURE RESEARCH

Since only small tensile coupon tests were carried out in this study, the experiments for girder models are being scheduled.

REFERENCES

1) Japan Road Association (2002), The Japanese Specifications for Highway Bridges
2) prENV1993-1:(Eurocode3:Design of steel structures-Part 1:General rules and rules for buildings).
3) AASHTO:Standard Specifications for Highway Bridges, 1994.
4) ISO:ISO 10721-1, Steel structures-Part 1:Materials and design, 1997.
5) SSEA:SIA 161, Steel Structures, 1979.
6) BSI:BS5400, Part 3, Code of practice for design of steel bridges, 1982.
7) DIN:DIN 18800 Teil 1, Stahlbauten;Bemessung und Konstruction, 1990.11.

EXTENDING SERVICE LIFE OF TIMBER BRIDGES WITH PRESERVATIVES

James P. WACKER[1] and Douglas M. CRAWFORD[2]

Abstract

Treated timber bridges have been widely used for railroad and highway bridges throughout the United States during the 20th century. However, improvements in preservative technology are needed as a result of changing environmental views and public perceptions concerning the use of preservative treated wood in aquatic environments. Within the past 15 years, three national programs have been established to advance technologies related to timber transportation structures. A key design aspect for timber highway bridges is the selection of preservative treatment to improve durability while minimizing potential environmental impacts. This paper summarizes timber bridge preservation technology in the United States, including pressure treatment preservatives, field treatments, and remedial techniques.

Introduction

The versatility and durability of preservative-treated timber make it an important engineering material for bridge construction (AITC 1973). Wood has several properties that make it well-suited for bridge construction, including a high strength to weight ratio, energy-absorbing capabilities, and ability to carry short-term overloads. Timber bridges can typically be constructed by low-skilled labor in nearly all weather conditions and are not adversely affected by de-icing chemicals. In addition, wood is a renewable natural resource that uses substantially less energy in manufacture when compared to other bridge materials.

The misconception that wood provides a short service life has plagued timber as a construction material (Ritter 1992). Although most species of wood are susceptible to deterioration under specific conditions, the durability of wood substantially improves when the wood is protected from moisture and/or pressure-treated with preservatives. Designers of covered timber bridges in early America incorporated roof structure details that extended bridge service life to more than 80 years. The key benefit of the bridge roofs was to keep the main structural (untreated) members dry and eliminate their susceptibility to decay and insect attack. Today, modern wood preservatives are used in lieu of bridge roofs to extend the service life of timber bridges. However, in the past decade, the covered bridge design approach is again becoming an increasingly popular option in the United States, despite its higher initial costs.

The use of chemicals for preservation of timber bridges began in the United States around 1870 when railroad bridge ties were treated with creosote, an oil-based preservative (Webb

[1] Professional Engineer, United States Department of Agriculture, Forest Service, Forest Products Laboratory, Madison, Wisconsin, USA.
[2] Forest Products Technologist, United States Department of Agriculture, Forest Service, Forest Products Laboratory, Madison, Wisconsin, USA.

1976). By the 1920s, creosote had become the treatment of choice for the railroad industry; it was introduced for highway bridges shortly thereafter. Pentachlorophenol (Penta) is another oil-based preservative that has been widely used for timber bridges since the 1940s. Changing environmental views, stricter Federal and State regulations, and public perceptions related to the use of preservative treatment chemicals for highway bridges have reduced viable treatment options for bridge designers and emphasized the need to develop more environmentally friendly preservatives for timber bridge applications. This paper summarizes timber bridge preservation technology in the United States, including preservative treatment options, field treatments, and remedial techniques to extend service life.

U.S. Timber Bridges

The United States has approximately 32,400 timber bridges according to the National Bridge Inventory (NBI), a comprehensive database maintained by the Federal Highway Administration (FHWA) that includes bridge inspection data for nearly 591,000 highway bridges that span at least 6 m (20 ft) (FHWA 2002). An estimated 6,000 timber bridges, in addition to those recorded by the NBI, are located on Federal government lands and/or span less than 6 m. A large majority of these timber bridges are located on secondary highways in rural America. Timber beam bridges are the predominant superstructure type, simply supported with a typical span range from 5 to 20 m (16 to 65 ft).

National Programs for Wood In Transportation

Within the past 15 years, three national programs have been initiated by the U.S. Congress with the common goal of increasing the utilization and efficiency of timber as a structural material in transportation structures. The Wood in Transportation Program administered by the Department of Agriculture, Forest Service (FS) was established by the Enhancing Rural America Act of 1989 and placed a strong emphasis on the development of innovative bridge designs along with the utilization of non-traditional wood species for bridges (USDA 2003). The Federal Highway Administration's (FHWA) Timber Bridge Program was established by the Intermodal Surface Transportation Efficiency Act (ISTEA) of 1991 and placed a strong emphasis on conventional bridge designs accepted by the American Association of State Highway and Transportation Officials (AASHTO) *Standard Specifications for Highway Bridges* (AASHTO 2002). Both national programs funded demonstration bridge projects (up to 50% Forest Service and 80% FHWA) with grants awarded to State and local governments. In addition, each national program had research components that were merged into a joint FS/FHWA research program in 1991 within the following main research areas:

- System development and design
- Preservatives
- Inspection and rehabilitation
- Lumber properties
- Alternative transportation system structures
- Technology and information transfer

The goal of this joint research program is to advance technologies related to timber bridges and to increase utilization of timber in bridge and other transportation structures. A comprehensive review of the National Wood in Transportation Program (Duwadi and

others 2000) and the joint FS/FHWA research program for wood transportation structures (Ritter and Duwadi 1998, FHWA 1998) are available.

Several research projects have addressed preservative-related issues applicable to bridges (Table 1). The three main study areas include field treatments, environmental considerations, and improved preservatives and treatments methods. Field treatments include both surface and internal methods. Surface treatment (liquid) preservatives are typically applied by brushing, spraying, or soaking methods to prevent decay where untreated wood has been exposed by field cuts and borings or by damage during construction. Internal treatment preservatives are typically inserted into pre-bored holes in timber components and then diffuse into the surrounding wood to arrest internal decay. Environmental considerations include monitoring preservative retention levels in the bridge members and the surrounding soil and water for potential impacts to aquatic life. Improved preservatives involve the development and efficacy testing of new and alternative preservatives that are more environmentally acceptable.

Table 1. Preservative-related research projects and available publications resulting from joint Forest Service/Federal Highway Administration research program

Study area	Project title	Available reports[a]
Field treatments	Development of a comprehensive manual on field treating with wood preservatives	Cassens and others 1995
	Evaluation of various wood preservatives and fumigants as remedial treatments for bridges	DeGroot and others 2000 Morrell and others 1996
Environmental considerations	Evaluation of environmental effects of creosote, penta, and CCA-treated timber bridges	Brooks 2000
	Environmental impact of a treated boardwalk	Lebow and others 2000
	Minimizing environmental impacts of treated wood	Lebow and Tippie 2001
Improved preservatives and treatment methods	Accelerated testing of new preservatives	DeGroot and Evans 1998 DeGroot and others 1998
	Moisture protection for timber members	Blankenhorn and others 1999
	Efficacy of copper naphthenate preservative	St. John and others 1998 Niemi and others 1998

[a] Complete citations are listed after the text.

In 1998, the Transportation Equity Act for the 21st Century (TEA-21) established the National Historic Covered Bridge Preservation Program (NHCBP). Administered by the FHWA, the NHCBP provides funding for (1) preservation, rehabilitation, and restoration of the Nation's historic covered bridges and (2) research and technology transfer. Recognizing a need, the FHWA initiated a study to develop guidelines that identify suitable wood preservatives and fumigants to preserve and protect these historic structures, while meeting the requirements of the Secretary of Interior's Standards for the Treatment of Historic Structures. Further information about the NHCBP program is available (FHWA 2003).

Pressure Treatment Preservatives

Wood preservatives are broadly classified as either oil-based or water-based, based on the chemical composition of the preservative and the carrier used during the pressure treating process (Lebow and Makel 1995). Table 2 summarizes wood preservatives commercially available and applied with pressure-treatment methods for timber bridges. Some key preservative characteristics important to timber bridge applications are chemical composition, surface cleanliness, migration potential, odor, and environmental status.

Table 2—Summary of wood preservatives applied by pressure-treatment methods for timber bridges in the United States

Common name	Chemical composition	Surface cleanliness	Migration potential	Odor	Environmental status[a]
		Oil-based Preservatives			
Creosote	polycyclic aromatic hydrocarbons (PAHs)	oily residues	tends to exude, or bleed	strong	restricted use pesticide
Penta	pentachlorophenol (light oil carrier)	relatively clean	saltwater leachability	light	restricted use pesticide
Copper naphthenate	naphthenic acids, copper salts	relatively clean	leach resistant	light	unclassified pesticide
		Water-based Preservatives			
CCA[c]	hexavalent chromium, copper, arsenic	clean	leach resistant	none	restricted use pesticide
ACZA[b]	Ammonia, copper, zinc, arsenic	clean	leach resistant	none	restricted use pesticide
ACQ[b]	copper, quaternary ammonium compounds	clean	leach resistant	none	restricted use pesticide
CC[b]	copper oxide, citric acid	clean	leach resistant	none	restricted use pesticide
CDDC	copper ethanolamine, sodium dimethyldithiocarbamate	clean	leach resistant	none	restricted use pesticide
Borates	sodium octa-, sodium tetra-, sodium penta-borate	clean	highly leachable	none	unclassified pesticide

[a] Based on current regulations of U.S. Environmental Protection Agency. "Restricted use pesticides" does not ban the use of treated wood, but requires certified applicators trained in proper and safe handling techniques. "Unclassified" does not require certified applicators and are commercially available.
[b] Waterborne preservatives using ammonium solutions are typically used to achieve good penetration in difficult-to-treat species.
[c] Beginning in 2004, the use of CCA wood preservative in the United States will be restricted to industrial and commercial uses (such as bridges) and not permitted for residential applications.

Timber bridges can provide over 35 years of low maintenance service life provided they are properly preservative-treated using modern techniques. The selection and use of preservatives for U.S. timber bridges is becoming more complicated as a result of changing environmental views, stricter Federal and State regulations, and public perceptions. Bridge design standards and specifications (AASHTO 2002) currently

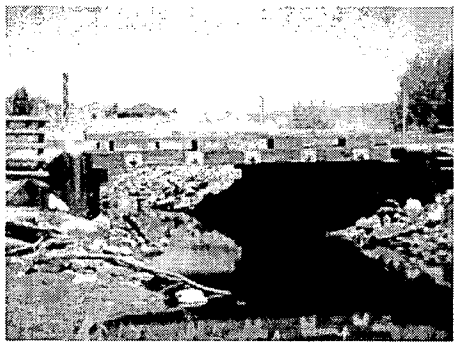


Figure 1—Stress-laminated deck bridge treated with copper naphthenate preservatives.

require bridge timbers to be pressure-treated with a wood preservative approved for use by the American Wood Preservers' Association (AWPA 2002) industry standards. In addition, oil-type preservatives are highly recommended for bridge structures primarily because of their moisture-barrier properties over an extended service life. Oil-type preservatives typically exhibit an oily surface that acts to retard moisture movement in and out of timber bridge members. This "water repellency" characteristic helps to minimize in-service checking, which can potentially provide avenues for moisture and decay to penetrate the preservative protective shell produced during pressure treatment. However, environmental concerns have been raised as a result of excessive oil-type preservative exudation, or bleeding, at several creosote-treated bridges (Wacker and others 2003). Many bridge designers are specifying water-based preservatives for non-structural bridge components such as pedestrian walkways and railings. Another growing trend is the utilization of untreated, naturally durable wood species, despite their comparatively higher cost.

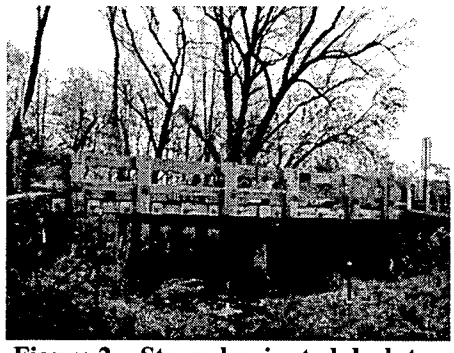


Figure 2—Stress-laminated deck treated with ACQ preservatives.

New interest has been focused on copper naphthenate (Fig. 1), an oil-based preservative that has been widely used for treating power transmission poles in the United States for many years, as an attractive alternative for timber bridges due to its relatively clean surface and resistance to exudation, or bleeding, in service. Waterborne preservatives are generally not recommended for structural members of timber bridges, due to their tendency for large

surface checks, especially with large glued-laminated timber members. However, an increasing number of timber bridges are being pressure-treated with water-based preservatives because of their surface cleanliness and low migration potential. Effective water repellent additives are being considered for several water-based preservatives, which is advantageous for timber bridge applications. Potential concerns about oil-type preservative migration can be greatly reduced by following Best Management Practices (BMPs) for the use of treated wood in aquatic environments (WWPI 1996) and AWPA Standard M20-00 (AWPA 2000).

New wood preservatives are currently being developed that will potentially produce less environmental concerns and have improved surface cleanliness, water-repellent characteristics, and low corrosive properties when in contact with metal fasteners (Crawford and DeGroot 1996). If these new preservatives achieve approval from AWPA, they have the potential to be ideal alternatives for new timber bridges.

All preservative chemicals must be evaluated and approved by the U.S. Environmental Protection Agency (EPA) and registered for use as a preservative for wood. Most preservatives are registered as "restricted use pesticides," which does not ban the use of treated wood but requires certified applicators trained in proper and safe handling techniques (EPA 2003). Copper naphthenate (oil-based) and borates (water-based) are two exceptions that are unclassified; they are commonly available to consumers through local suppliers. New environmental regulations, placing additional restrictions on the use of CCA wood preservatives, have led to increased interest in the use and development of more environmentally benign preservatives. Beginning in 2004, new EPA voluntary restrictions on residential uses of CCA could significantly reduce its availability for timber bridges. Several new water-based preservatives, which do not contain arsenic and chromium, are being introduced as treatment alternatives for timber bridges (Figure 2). However, these new water-based preservative options may have accelerated corrosive interaction with metal fasteners and need further evaluations.

Field Treatments and Remedial Techniques

Field treatment methods for timber bridge components are vital to preventing deterioration from insects and decay. Field treatment methods involve moisture protection methods and field preservatives. Moisture protection methods aim to keep the main structural members dry enough to prevent decay deterioration by adding a roof structure (as in historic covered bridges) or by using a waterproof membrane beneath an asphalt concrete wearing surface. In addition, various design details can be utilized that reduce moisture accumulation in timber bridge components (Kropf 1996, Blankenhorn and others 1999). Other field treatment methods involve the application of liquid preservatives by brushing, spraying, or soaking methods to prevent decay where untreated wood has been exposed by field cuts, boring, or damage during construction and by deep checks, which may develop when large timber members dry in service.

Remedial treatments are especially important in arresting decay already present in timber bridge components, as with historic covered bridges and older timber trestle railroad

bridges. To arrest decay in existing timber bridge components, liquid or grease-type preservative treatments are typically inserted into pre-bored holes that surround the decayed zone. Remedial treatments can be reapplied at periodic intervals in the same holes used for initial treatment, but these holes should always be plugged with newly treated wood dowels.

Field treatments and remedial treatments in conjunction with routine inspection are key factors in preventing and/or limiting deterioration and can significantly extend the service life of timber bridges. More details on preventive field treatments and remedial techniques can be found in Ritter (1992, ch. 14) and Eslyn and Clark (1979).

Concluding Remarks

Shifting environmental views, stricter Federal and State regulations, and public perceptions concerning the use of treated wood for highway bridges in the United States have emphasized the need to develop more environmentally friendly preservative chemicals. As part of three National Wood in Transportation Programs within the past 15 years, significant research has been conducted to address preservative treatment issues related to timber bridge applications. The technological advancements related to wood preservatives, along with ongoing research efforts, should help to provide more designer options, improve bridge performance, and extend the service life of timber highway bridges.

References

AASHTO. 2002. Standard specifications for highway bridges, 17th edition. Washington, DC: American association of state highway and transportation officials.

AITC. 1973. Modern timber highway bridges—A state of the art report. Englewood, CO: American Institute of Timber construction. 79 p.

AWPA. 2000. Standard M20-00. Guidelines for minimizing oil-type wood preservative migration. Granbury, TX: American Wood Preservers' Association.

Blankenhorn, P.R.; Bukowski, S.; Kainz, J.A.; Ritter, M.A. 1999. Moisture protection for timber members. Pp. 240–248 in Walford, G.B.; Gaunt D.J. (Eds.) In: Proceedings, Pacific Timber Engineering Conference Vol.2, 14–18 March 1999, Rotorua, New Zealand. New Zealand Forest Research Institute, Forest Research Bulletin No. 212.

Brooks, K.M. 2000. Assessment of the environmental effects associated with wood bridges treated with creosote, pentachlorophenol, and chromated copper arsenate. Res. Pap. FPL-RP-587. Madison, WI: U. S. Department of Agriculture, Forest Service, Forest Products Laboratory. 100 p.

Cassens, D.L.; Johnson, B.R.; Feist, W.C.; DeGroot, R.C. 1995. Selection and use of preservative-treated wood. Madison, WI: Forest Products Society, Publication No. 7299. 104 p.

Crawford, D.M.; DeGroot, R.C. 1996. Evaluation of new creosote formulations. In: Proceedings, National Conference on Wood Transportation Structures. Ritter, M.A., S. R. Duwadi, P.D.H. Lee (Eds.). Gen. Tech. Rep. FPL-GTR-94.Madison, WI: U.S. Department of Agriculture, Forest Service, Forest Products Laboratory. 494 p.

DeGroot, R.C.; Evans, J.W. 1998. Patterns of long-term performance—how well are they predicted from accelerated tests and should evaluations consider parameters other than averages? In: Proceedings, 29th Annual IRG Meeting, Maastricht, The Netherlands, June 14–19, 1998. Stockholm, Sweden: International Research Group.

DeGroot, R.C; Evans, J.W.; Forsyth, P.G.; Freitag, C.M.; Morell, J.J. 1998. Soil-contact decay tests using small blocks—procedural analysis. Res. Pap. FPL-RP-571. Madison, WI: U.S. Department of Agriculture, Forest Service, Forest Products Laboratory. 7 p.

DeGroot, R.C.; Felton, C.C.; Crawford, D.M. 2000. Distribution of borates around point source injections in wood members exposed outside. Res. Note FPL-RN-0275. Madison, WI: U.S. Department of Agriculture, Forest Service, Forest Products Laboratory. 5 p.

Duwadi, S.R.; Ritter, M.A.; Cesa, E. 2000. Wood in transportation: an overview. Transportation Research Record 1696, Paper No. 5B0105 Vol. 1: 310-315.Washington, DC: Transportation Research Board. National Research Council.

EPA. 2003. Consumer safety information sheets for pressure- treated wood. Washington, DC: U.S. Environmental Protection Agency.

Eslyn, W. E.; Clark, J. W. 1979. Wood bridges: decay inspection and control. Agric.Handbk. 557. Washington DC: U.S. Department of Agriculture, 32 p.

FHWA. 1998. Timber bridge related research summary. www.tfhrc.gov/structur/struc98/ch4set.htm. McLean, VA: Federal Highway Administration, Turner–Fairbanks Highway Research Center.

FHWA. 2002. The National Bridge Inventory Program. www.fhwa.dot.gov/bridge/nbi.htm. Washington DC: Federal Highway Administration.

FHWA. 2003. The National Historic Covered Bridge Program. www.fhwa.dot.gov/bridge/covered.htm. Washington DC: Federal Highway Administration.

Kropf, F.W. 1996. Durability and detail design— the result of 15 years of systematic improvements. In: Proceedings, National Conference on Wood Transportation Structures. Ritter, M.A., S. R. Duwadi, P.D.H. Lee (Eds.), p 321–327. Gen. Tech. Rep. FPL-GTR-94. Madison, WI: U.S. Department of Agriculture, Forest Service, Forest Products Laboratory. 494 p.

Lebow, S.T.; Makel, W.J. 1995. Selection and use of preservative treated wood in forest service recreational structures. TEO1A35. San Dimas, CA: U.S. Department of Agriculture, Forest Service, San Dimas Technology and Development Center.12 p.

Lebow, S.T., Lebow, P.L.; Foster, D.O. 2000. Environmental impact of preservative-treated wood in a wetland boardwalk. Res. Pap. FPL-RP-582. Madison, WI: U.S. Department of Agriculture, Forest Service, Forest Products Laboratory. 126 p.

Lebow, S.T.; Tippie, M.; 2001. Guide for minimizing the effect of preservative-treated wood on sensitive environments. Gen. Tech Rep. FPL-GTR-122. Madison, WI: US Department of Agriculture, Forest Service, Forest Products Laboratory. 18 p.

Morrell, J.J.; Love, C.S.; Freitag, C.M. 1996. Integrated remedial protection of wood in bridges. In: Proceedings, National Conference on Wood Transportation Structures. Ritter, M.A., S. R. Duwadi, P.D.H. Lee (Eds.), p. 445-454. Gen. Tech. Rep. FPL-GTR-94. Madison, WI: U.S. Department of Agriculture, Forest Service, Forest Products Laboratory. 494 p.

Niemi, B.; St. John, W.; Woodward, B.; DeGroot, R.; McGinnis, G.; 1998. Development of naphthenic acid fractionation with supercritical fluid extraction for use in wood decay testing. In: Proceedings, 94th annual meeting of American Wood Preservers' Association, 17–19 May, 1998, Scottsdale, AZ. p. 165–177.

Ritter, M.A. 1992. Timber bridges—design, construction, inspection, and maintenance. Engineering Management Series EM7700-8. Washington, DC: U.S. Department of Agriculture, Forest Service. 944 p.

Ritter, M.A.; Duwadi, S.R.; 1998. Research accomplishments for wood transportation structures based on a national research needs assessment. Gen. Tech. Rep. FPL-GTR-105. Madison, WI: U.S. Department of Agriculture, Forest Service, Forest Products Laboratory. 30 p.

St. John, W.P.; Rughani, J.; Green, S.A.; McGinnis, G.D. 1998. Analysis and characterization of naphthenic acids by gas chromatography–electron impact mass spectrometry of tert.-butyldimethylsilyl derivatives. J. Chromatog. A 807: 241–251.

USDA. 2003. National Wood in Transportation Information Center program.. www.fs.fed.us/na/wit. Morgantown, WV: U.S. Department of Agriculture, Forest Service, State and Private Forestry, Northeastern Area.

Wacker, J.P.; Crawford, D.M.; Eriksson, M.O. 2003. Creosote retention levels of timber highway superstructures in Michigan's lower peninsula. Res. Note FPL-RN-289. Madison, WI: U.S. Department of Agriculture, Forest Service, Forest Products Laboratory. 17 p.

Webb. D.A. 1976 Environmental considerations on creosote: A step in the right direction. Pittsburg, PA: Koppers Company, Inc.

WWPI. 1996. Best management practices for the use of treated wood in aquatic environments. Vancouver, WA: Western Wood Preservers' Institute. 35 p.

The Design and Construction of the Chitose Bridge

Mitsugu Ishida : Manager of Bridge Department, Public Works Division, Public Works Bureau of Osaka City Government

Yoshinori Nagai : Chief of Bridge Department, Public Works Division, Public Works Bureau of Osaka City Government

Kenji Fujitani : Staff of Bridge Department, Public Works Division, Public Works Bureau of Osaka City Government

Yasunari Nakano : Staff of Eastern District Public Works Station, Administration Division, Public Works Bureau of Osaka City Government

ABSTRACT

The Chitose Bridge was constructed over the Taisho Inner-Port in Osaka City as shown in Fig.1 and was opened to traffic in April 2003.

In the Taisho Inner-Port, there was so much traffic of vessels to influence the structural specifications of the bridge over the sea and to restrict occupation of waters in the extended period under construction. From such conditions, the Chitose Bridgewas designed as a 2-span continuous un-symmetrical braced rib arch, which is the main bridge over the sea (Photo. 1). And it was erected by large block erection method with floating cranes (FC) after marine transportation.

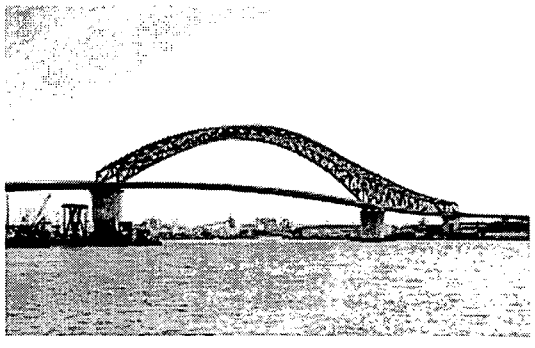


Photo. 1 Grandview of the Chitose Bridge

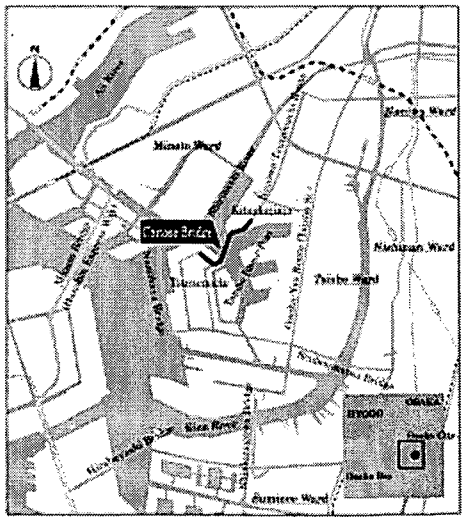


Fig. 1 Map around the Chitose Bridge

I. PLAN AND DESIGN AT THE CHITOSE BRIDGE

1. Plan for Bridge

1.1. Porpose of Enterprise

It was difficult to form a road traffic network in Taisho Ward, which was surrounded by the Kizu river and the Shirinashi river and had the Taisho Inner-Port as shown in Fig.1.

With a background of technological development of bridge construction in recent years, great bridges were constructed to this area such as the Senbonmatsu Bridge, a continuous box girder type with spiral access viaducts, the Sinkizugawa Bridge, a balanced Nielsen-Lohse arch type, Namihaya Bridge, a continuous curved box girder type and so on. However, on the Osaka-Yao route, called the Taisho St. and the main route in Taisho Ward, heavy traffic came out as the road network service had developed around this area.

Therefore, the Chitose Bridge, over the Taisho Inner-Port, was planned to improve the Naniwa-Tsurumachi route as the bypass of the Taisho St. and so to make ease traffic congestion there. And this route was to form a loop with the Taisho St. so as to contribute the development of traffic in the water front area.

1.2. Span Length and Clearance to Passage of Vessels

When planning construction of a bridge at this point of the Taisho Inner-Port, it was necessary to consider the vessels sailing to this area on a plan of the Osaka Port.

Two types of ship were dealt with. One was 1,000GT freighter, which was the biggest type among sailing vessels of here. The other was 200GT freighter, which was standard type of sailing frequently.

The height of under clearance was determined so that the aforementioned vessels could sail under this bridge at nearly highest high water (OP+1.9m) with overhead clearance of 2m. As to 1,000GT vessel (24.2m tall) it was OP+28.64m high. And as to 200GT vessel (19.2m tall) it was OP+23.64m high. ("OP" is the standard mean sea level of Osaka Bay.)

The width of passage for 1,000GT vessels was defined as 165m, from twice of the ship length (81.0m). And the one for 200GT vessels was defined as 230m by the field survey so that vessels could be free to sail. The main span of this bridge was determined 260m long as some of clearance was added to the passage width.

1.3. Selection of Bridge Type

As the Chitose Bridge was to be located far above from the passage condition, the access viaducts were needed as shown in Fig.2. It was not desirable in an economical and structural view that the farther its pavement was located above, the longer access viaducts were. So in order that the girder height was to be kept small, the main span, which was

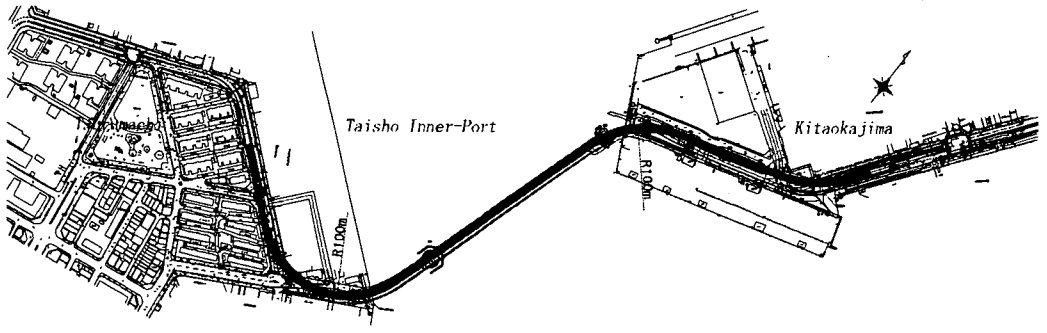
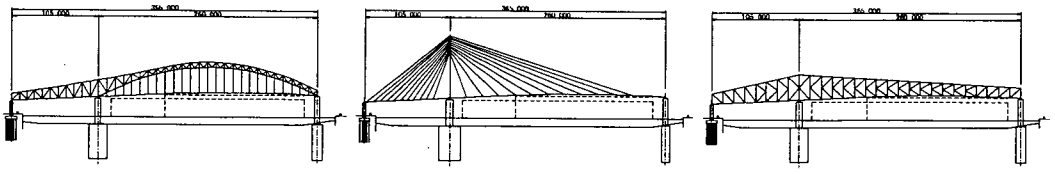


Fig. 2 Plan of the Chitose Bridge

265m from the passage condition, should be made continuity with the next spans. However, as shown in Fig. 2, the side spans were curved. Especially, the north span was curved through although the south side span had some straight part continuously from the main span. Many of curved bridges have problems of torsion. So, as the main bridge over the sea, the main span was made a two-span continuous bridge with the north side span with less effect of torsion.

Truss type was selected as the bridge type of the side span with curved part because of its high torsional rigidity. And arch type was selected as the type of main span because it could connect to the side truss by adoption of braced-rib and it was to be built of less steel than truss type.

As to foundation type, steel pipe sheet pile well foundations were selected, which can also serve as the temporary coffering facilities on chuting the footing and can occupy the small area of waters under construction. And RC piers were selected as substructure.



(a) Arch Bridge Type (b) Cable-Stayed Bridge Type (c) Truss Bridge Type

Fig. 3 Types of Bridge in the Comparison

1.4. Structural Section Form

This bridge has narrow width of only 14m to its span of 260m. Therefore, the horizontal rigidity was considered in addition to the vertical rigidity. Parallel rib form and basket handle rib form, which are shown in Fig. 4, were compared by the analysis. Generally, basket handle rib form has higher horizontal rigidity

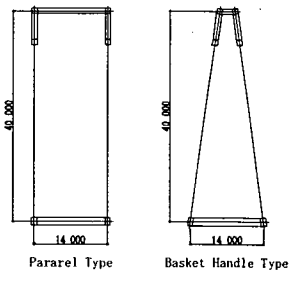


Fig. 4 Type of Arch Section Form

with arch effect than parallel rib form. But as shown in Table 2, basket handle form had more horizontal displacement in the case of this bridge. For, this bridge was so narrow that the arch effect didn't work enough but the horizontal rigidity around its arch crown was decreased. And so the parallel rib form was selected.

Table 2 Displacements at the middle of arch span in each form

		Arch Rib		Stiffning Girder	
		Prarel	Basket Handle	Prarel	Basket Handle
Horizontal Displacement (mm)	to Dead Load	-6.5	-2.8	-3.5	0.0
	to Live Load	-4.1	-3.1	-1.8	0.8
	to Wind Load	577.6	920.0	392.2	479.0
Virtical Displacement (mm)	to Dead Load	-393.1	-400.5	-421.6	-430.9
	to Live Load	-87.1	-91.1	-102.4	-107.2
	to Wind Load	102.8	9.0	101.9	69.0

2. Design

2.1. Structure Specification and Design Condition

The general view of the Chitose Bridge is shown in Fig. 5, and a design conditions are shown in Table 3.

The road specification of the Chitose Bridge was No.4 type, Class 2 as it was to be situated in a metropolitan area and its traffic flow was estimated at 7,000 vehicles per a day.

This bridge alignment was to be with curves of R=100m near the both sides of Taisho Inner-Port to access the existing roads as shown in Fig. 2.

Table 3 Design Conditions of the Chitose Bridge

Road Specification	No.4 type, Class 2
Design Speed	40km/h
Class of Bridge	First Class Bridges
Bridge Type	2-Span Continuous Braced Rib Arch type
Length and Span	364.9293m = 259.9293 m + 105m
Width	7.0m of Roadway, 3.0m of Walkway
Alinement	R = 100m- ∞
Profile	Maximum of 5.5%
Crossing Slope	2% of Roadway, 2% of Walkway
Floor Slab	Steel Deck Plate
Pavement	80mm of Roadway, 30mm of Walkway
Live load	TT-43
Main Steels	SM570,SM490Y,SM400,SS400,PWS
Coating (full shop)	External : Fluorocarbon Resin Coating (Blue) Internal : Tar-Epoxy Resin Coating
Steel Weight	4,487t

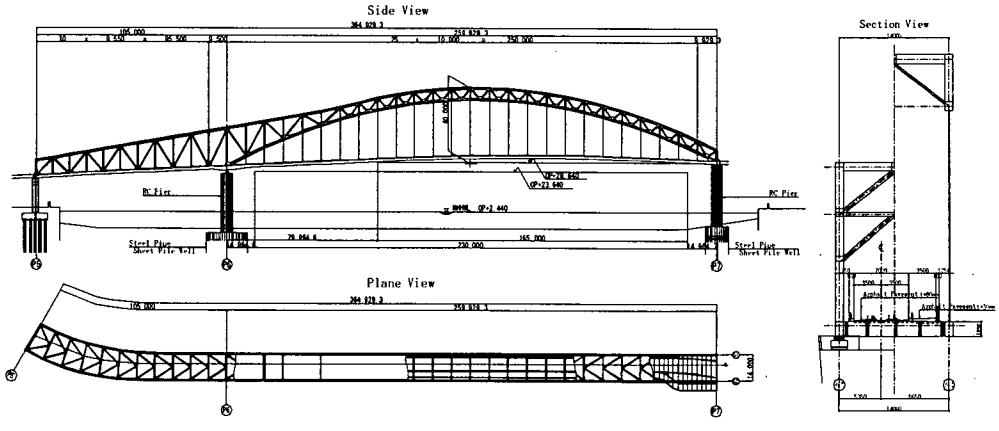


Fig.5 General View of the Main Bridge over the Sea

2.2. Section Designing

Design section forces were calculated by solid frame analysis to evaluate the influence of the torsion in the curve in the side span and so on.

In addition to the entire system to the dead and live loads and the temporary system by each construction step, the states of erection blocks which was to fluctuate on the marine transportation and to be lifted by FC were analyzed for designing of the temporary facilities and construction management.

2.3. FEM Analysis of Middle Fulcrum Part

The P6 middle fulcrum part was a complicated structure which had a jointed corner part between the arch rib lower cord member and the stiffening girder and also gathered a vertical member and deck plate. Therefore, its local stress condition was checked by FEM analysis.

The stress contour is shown in Fig.6. According to the result of the analysis, most of the stress between the arch rib lower chord member and the stiffening girder transmitted through their web and there was no more local stress concentration particularly than the previous assumption. The validity of this structure could be confirmed. And it was found that he stress by the axial force of the diagonal member was distributed over the area within 20-degrees range from the girder.

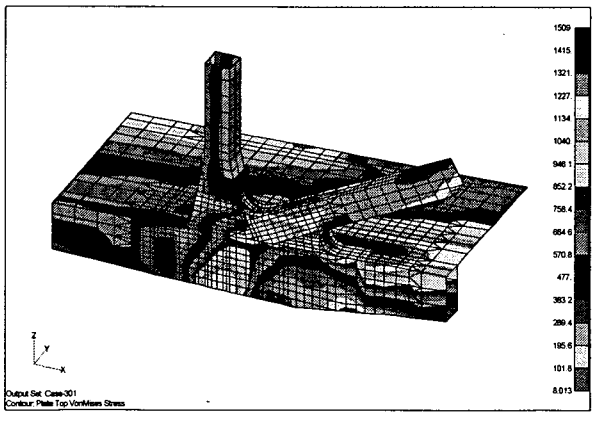


Fig. 6 FEM Analysis of Middle Fulcrum Part (Stress Contour)

2.4. Seismic Design

2.4.1. Outline of Dynamic Response Analysis

The time history non-linear dynamic response analysis was done to verify earthquake-proof against the great earthquakes which hardly occur during the use period. As the entry earthquake wave, it used the standard corrugation for the time history dynamic response analysis prescribed in "SPECIFICATION FOR HIGHWAYBRIDGE" and the corrugation, as shown in Fig. 7, in the neighborhood of the position of this bridge out of the assumed corrugation for design of civil engineering structure in the Osaka City area.

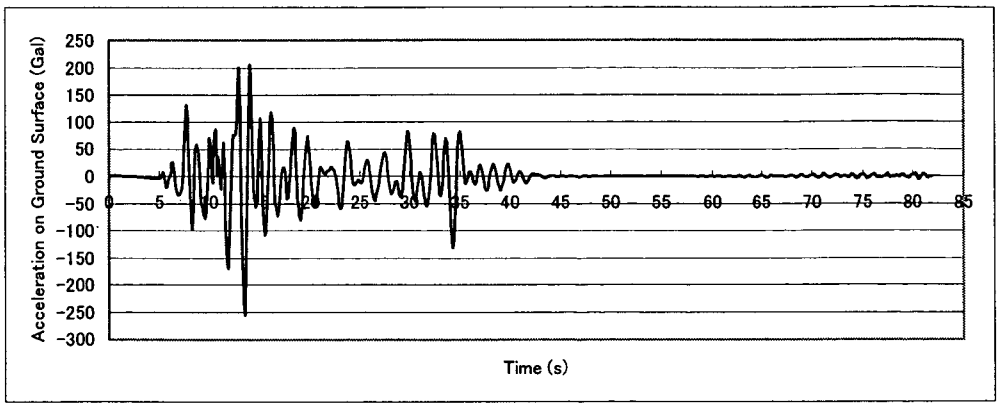


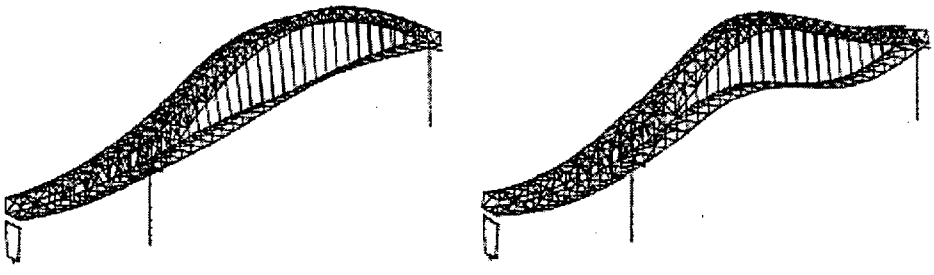
Fig. 7 Assumed Corrugation for Design of Civil Engineering Structure in the Osaka City Area (4s-35e)

2.4.2. Analysis Result

As a result of the eigenvalue computation, the 1st mode was the horizontal opposite phase vibration that the arch ribs and the girders displaced to the opposite in the horizontal direction at the natural period of 1.97 seconds, which is pretty long. The 2nd mode was the opposite symmetrical vertical vibration that the main span displaced to the vertical direction. The mode figure is shown in Fig. 8.

To the earthquake to the direction of the bridge axis, the superstructure response was eased because of extension of the natural period by the plastic-ization of a substructure however the girder end much moved.

To the earthquake to the crossing direction to the bridge axis, the large axial couple reactions of 5,855tf occurred on the fixed bearings. They were 2.2 times of the reactions of the fixed bearings by the earthquake to the direction of bridge axis. Generally, fixed bearings restrict a rotation in the horizontal plane which accompanies a deflection to the crossing direction to the bridge axis, and because bridges like arch type are with long span



(a) 1st Mode : Natural Period of 1.97 s

Horizontal Opposite Phase Vibration of Arch Rib and Girders

(b) 2nd Mode : Natural Period of 1.44 s

Opposite Symmetrical Vertical Vibration

Fig. 8 Results of Eigenvalue Anakysis

and have only two bearings in a support line, large axial couple reactions often occur. In the case of this bridge, by improved type of rubber bearing, the axial reactions were reduced.

2.4.3. Improvement of Fixed Bearing to Large Force

The clearance between the upper shoe and the side block that was about 3mm in usual was widened 20mm in the both side as shown in the Fig. 9, so that the horizontal rotation was to be ease so that the couple reactions could reduce to 2,651tf as much as reactions on the earthquake to the direction of the bridge axis. To add to the side blocks, flex bars were installed which worked to the firm loads but deformed plastically to great earthquake forces.

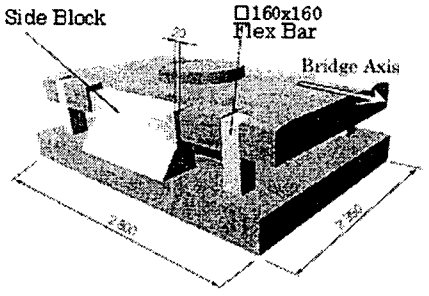


Fig. 9 Improved Fixed Rubber Bearing

2.5. Analysis of Ultimate State

2.5.1. Purpose and Outline

As this bridge is an un-symmetrical braced-rib-arch bridge of a special bridge form, elasto-plastic finite displacement analysis of structural buckling was made to grasp the behavior to its ultimate state and to confirm the safety of its ultimate strength to the design loads.

2.5.2. Cases of Loading

The cases of loading were as the followings. And "α", the loading parameter, was increased gradually.

- Case-1 α (D +Ps +L)
- Case-2 α (D +Ps +W)

where D : dead load, Ps : The pre-tension of the hanger cables, L: live load, W : wind load,
α : loading parameter (magnification to the design load)

2.5.3. Analysis Result

The deformation mode at the ultimate state at each case, and the loading parameter α - displacement relation are shown in Fig. 10.

1) Case-1

- At α=1.9, an upper cord member near the arch rib crown part yielded.
- At α=2.2, as more of upper cord members yielded, the arch rib began structural

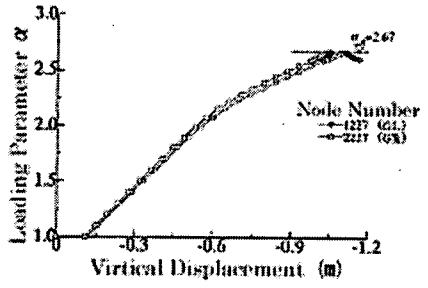
- buckling, and the non-linear behavior of the entire structure was seen noticeably.
- At $\alpha = \alpha_u = 2.67$, the lower chord members near the middle fulcrum buckled and the entire structure resulted in the ultimate state.
- Supposing that the load parameter was required more than $\alpha_{req} = 1.7$ of the safety factor of steels, the structure was safe enough where $\alpha_u > \alpha_{req}$.

1) Case-2

- At $\alpha = 1.7$, the upper cord member on the truss part near the middle fulcrum on the side of the windward yielded over the full section by tension and the non-linear behavior of the entire structure was seen noticeably.
- At $\alpha = \alpha_u = 2.23$, the lower chord member near the arch crown on the side of the windward yielded over full section and the entire structure resulted in instability and the ultimate state.
- Supposing that the load parameter was required more than $\alpha_{req} = 1.7/1.25 = 1.36$ of the safety factor of steels under wind loading, the structure was safe enough where $\alpha_u > \alpha_{req}$.



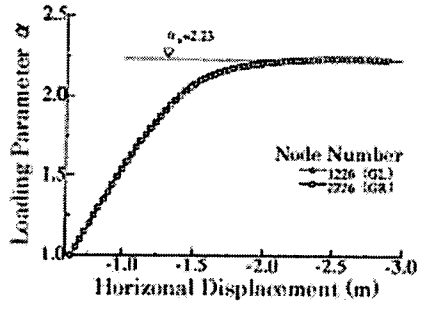
(a) Deformation at the Ultimate State (Case-1)



(b) α - Vertical Displacement Relation (Case-1)



(c) Deformation at the Ultimate State (Case-2)



(d) α - Horizontal Displacement Relation (Case-2)

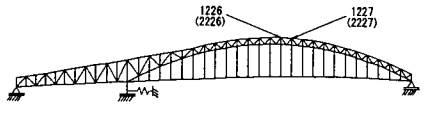


Fig.10 Results of Buckling Proof Analysis

II. The Large Block Erection of Main Bridge over the Sea

1. Outline of Construction

As the Taisho Inner-Port, which was the erection point of the Chitose Bridge, had much traffic of vessels, it was difficult to occupy this area in the extended period when its superstructure was erected. Therefore it was erected by large block erection method with FC having assembled the arch block and the truss block in the different yard.

The arch block was set on a 16,000t-DB (a deck barge: 16,000t DW) with a 3,700t-FC

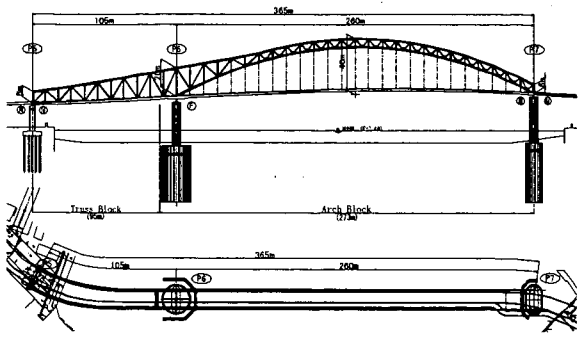


Fig. 11 Erection Blocks

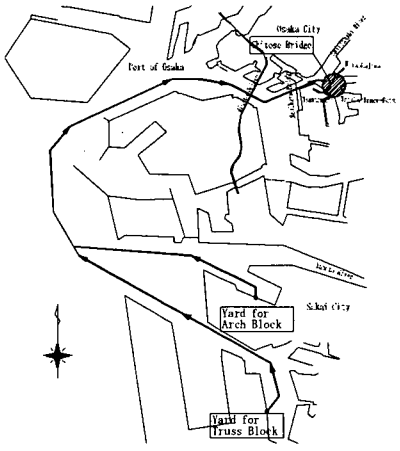


Fig. 12 Transportation Route Map

(FC: lifting Load of 3,700t) and 2,200t-FC (FC: lifting Lad of 2,200t) at the wharf of the assembly yard on October 30th in 2002. The arch block on the DB and the FCs were transported to Taisho Inner-Port on a different day of November 1st to 3rd, for it was not desirable for the large fleets to navigate in Taisho Inner-Port at once in the view to the safe passage of the other vessels. Then the arch block was set on November 4th.

Two weeks after, the truss block was transported on a 7,000t-DB and set on November 17th with the same 2,200t-FC that had been used at the arch block erection. It was joined to the arch block by moment joint method.

2. Block Assembly in the Yard

It was necessary that each assembly yard was so large as to assemble a grand block and had a wharf. Members were assembled into a block with track crane or crawler crane in the stressless condition by bents.

The appearances of blocks in the assembly yard are shown in Photo. 2 and Photo. 3. And the assembly process of arch block is shown in Fig. 13.

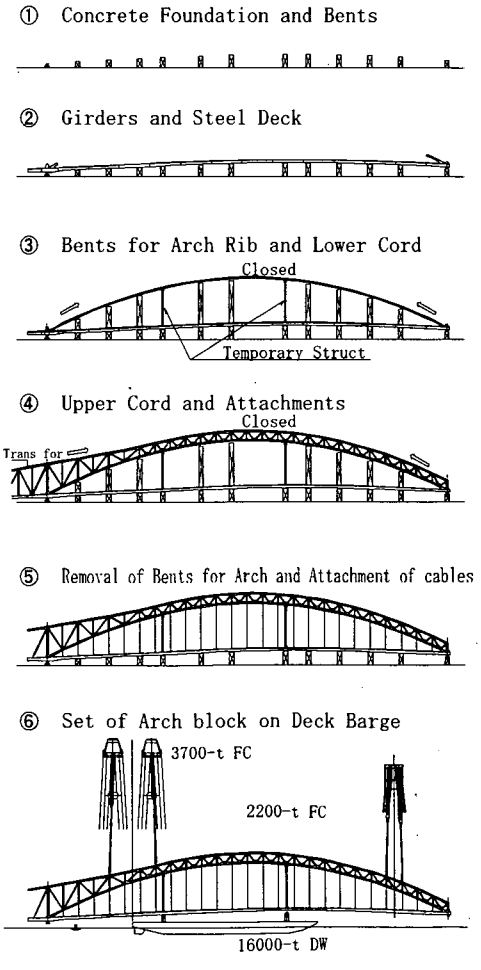


Fig. 13 Assembly Process in Yard

2.1. Yard Bents and their Foundations

The bent which was used for the assembly of the arch block designed considering not only reactions in usual erection with truck crane but added reactions by girders bending on lifting the block and horizontal forces by sway of lifted block and so on.

And, according to the soil bearing power test in the yard, concrete spread foundations of bent were made.

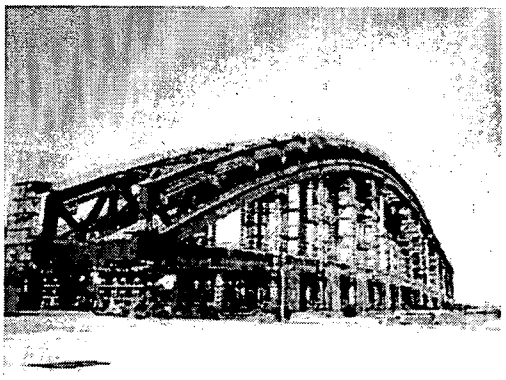


Photo.2 Assembly of Arch Block in the Yard

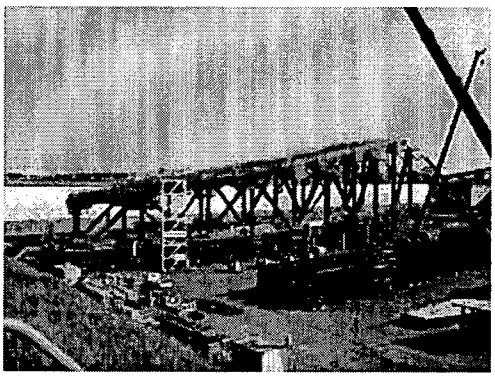


Photo.3 Assembly of Truss Block in the Yard

2.2. Precision Management of the joint

Because the arch block and the truss block were to be joined by moment joint method, especially high precision about the connections between the blocks was required.

Therefore it was the inspection of the precision about the connections that first one panel of the truss block was assembled with the arch block and then it was transferred from the arch yard to the truss yard.

3. Marine Transportation of Blocks

Each block was transported from the yard via outer harbor to Taisho Inner-Port as shown in Fig.12.

3.1. Transportation height

The large blocks on the deck barges had to pass under the Minato Bridge and the Namihaya Bridge as shown in Fig. 12. The arch rise of the Chitose Bridge was keeped low

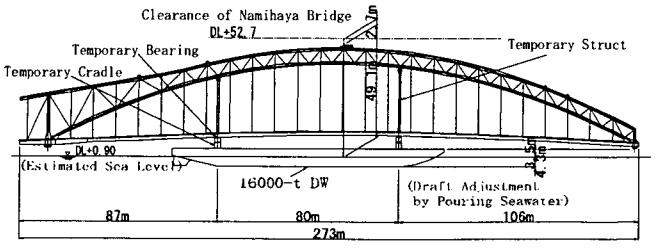


Fig. 14 Arch Block on the Deck Barge

to be 40m by the clearance under the Namihaya Bridge at transportation in design as shown in Fig. 14. So the height of the arch block was to be managed strictly also at actual transportation. Based on the estimated sea level in Osaka Port of the time that the arch block was to be pass under the Namihaya Bridge, the height on transportation was adjusted the draft of barge by pouring 7,213t of seawater inside.

3.2. Temporary Facilities for Transportation

As shown in Fig. 14, the center of gravity at transportation of the arch block was high position and the front and the rear of the arch block was much projected from the supports.

Table 4 Condition about Marine Transportation

Significant Wave	1.50m
Highest Wave	2.90m
Wave Period	6.1-9.3 seconds
Route	from the Sakai Port to the Port of Osaka
Season	2002 10-November
Deck Barge	120m*34.0m*7.8m
Freight	3,900 t of Bridge Block

Therefore, and the stability analysis was implemented considering fluctuation by waves and winds at transportation. The condition of the wave to have used for stability analysis was set as shown in Table 4 by NKKK (Nippon Kaiji Kentei Kyoukai) based on the conditions in transportation. And, temporary structures in transportation were designed as the following based on this analysis.

Temporary struts were installed in the assembly yard to keep the shape of arch rib and to transmit the weight of the arch rib to the temporary support. At the temporary supports, temporary cradles are installed on the deck to transmit the reaction of temporary struts and the weight of the stiffening girders considering the deflection of projecting parts for its weight. And the deck barge was reinforced insides at the temporary supports.

Because the deflection shape of the stiffening girders changed on lifting of block with the FC or by the fluctuation at transportation, bearing shoes which could follow the deflection was set on the temporary supports.

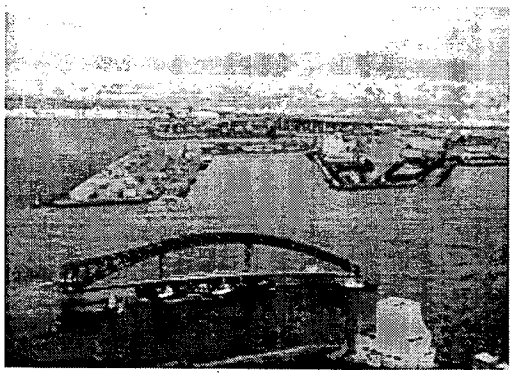


Photo.4 Marine Transportation

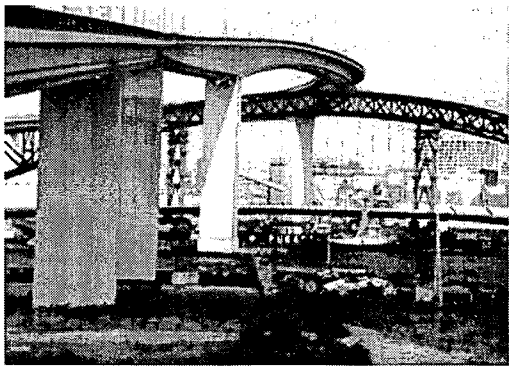


Photo.5 Passage under the Namihaya Bridge

4. Large Block Erection

Each block was lifted by FC twice, to set on the DB at the assembly yard, and to set at the erection site. As the arch block was lifted tandem by 3,700t-FC and 2,200t-FC, which coordinated the winching speed each other. When lifting the truss block, its curved part inclined to unbalance the loads at each hook. So, it was lifted carefully by 2,200t-FC which could control the winching load the each hook. And it was jointed to the arch block with lifted with FC.

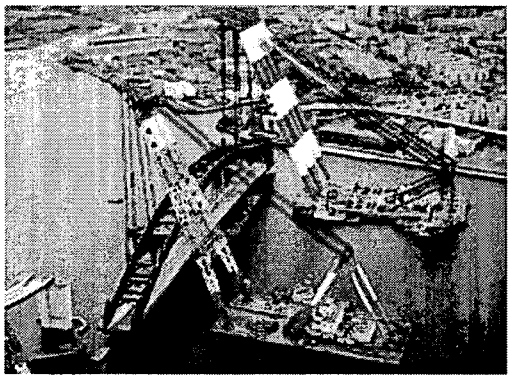


Photo. 6 Erection of Arch Block

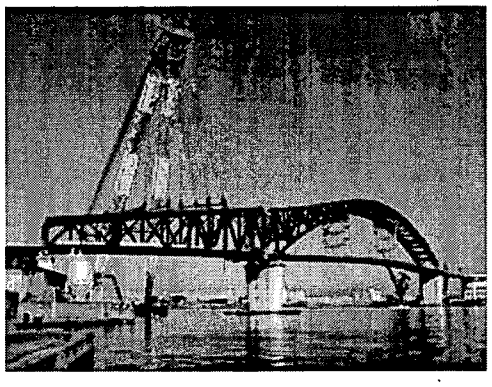


Photo.7 Erection of Truss Block and Moment Joint

4.1. Lifting of Arch Block

The wires were winched under the control that the load of each hook was increased or decreased 10% of the full by the step having been calculated by previous frame analysis. The outline of load control is shown in Table 5.

And on lifting the block, FC was controlled at any time on the check of the position of the block by transits

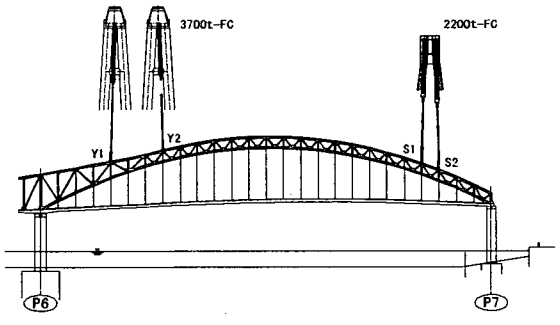


Fig. 15 Lifting of the Arch Block

Table 5 Summary of Winching Load Management (tf)

	10 %		50 %		100 %	
	Measured Value	Analysis Value	Measured Value	Analysis Value	Measured Value	Analysis Value
Y1-L	60	*60*	305	*302*	595	*603*
Y1-R	50	*62*	290	*310*	600	*619*
Y2-L	70	*60*	300	*302*	650	*604*
Y2-R	60	*62*	310	*300*	610	*620*
Subtotal	240	*245*	1195	*1223*	2455	*2446*
S1-L	35	*33*	165	*164*	320	*328*
S1-R	35	*34*	170	*170*	330	*341*
S2-L	35	*33*	165	*164*	320	*328*
S2-R	35	*34*	170	*170*	330	*341*
Subtotal	140	*134*	670	*669*	1300	*1338*
TOTAL	380	*378*	1865	*1892*	3755	*3784*

4.2. Moment Joint

By moment joint method, the truss block was joined to the arch block so that the dead load, previous to setting the truss block, could be borne by the

entire system of the continuous structure. In the case of the Chitose Bridge, the truss block was joined to the arch block with lifted with the 2,200-t lift FC with some of overhead clearance of P5 pier and it was subsequently jacked down so that a section moment was forced to be introduced.

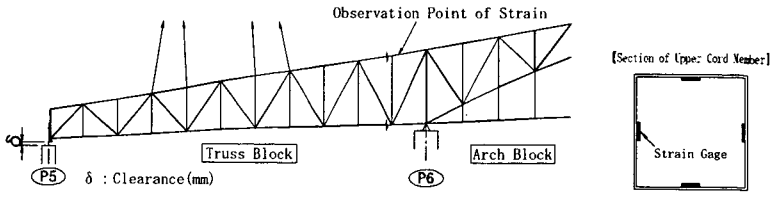


Fig. 16 Moment Joint

The working error of the clearance was to influence the introduced moment because the blocks had high structural rigidity. Therefore the introduction of moment had been simulated by the frame analysis, and defined the allowable range. The measurements of the clearance at bolts tightening of the joint met the allowable range as shown in Table 6. And strain gages were put on the inside of the upper cords near the bolt joints and the sectional forces was checked while the truss block was jacked down as shown in Table 7.

Table 6 Clearance δ at P5 (mm)

	Measured Value	Analysis Value	Allowable Range
GL	140	188	75～248
GR	175	211	98～271

Table 7 Increment of Sectional Forces of Upper Cord Member

		Measured Value	Analysis Value
At FC Load Released	Axial Force	122 (tf)	157 (tf)
	Bending Moment	28 (tf·m)	21 (tf·m)
At P5 Jacked Down	Axial Force	119 (tf)	127 (tf)
	Bending Moment	2 (tf·m)	2 (tf·m)

CONCLUSION

The Chitose Bridge was designed as 2-span continuous braced rib arch bridge, which was rarely seen, by various knowledge and analyses about bridge planning and designing. And under the condition of the inner port that had much traffic, the large block erection could be implemented with bridge construction technologies and managements.

The opening of this bridge is expected to lead the facilitation of the road traffic, the activation of the water front area the improvement of the user-friendliness by the operation of city buses and so on.

The Chitose Bridge, which has an elegant shape in vivid blue, is expected to feel familiar for a long time together with the nearby bridges, the Minato Bridge and the Namihaya Bridge as a symbolic landmark.

Finally we authors express our sincere appreciation to all the partners for their assistances and advices to go ahead of this enterprise.

REFERENCES

1) Takei, Yokota, Yubisui, Aketa, Kanazawa, Miyagawa: BRIDGE AND FOUDATION

ENGINEERING, Planning and Design of Chitose Bridge, March 2003
2) Kawashima, Doi, Mochida, Shibahara, Miyake, Kuwabara: BRIDGE AND FOUDATION ENGINEERING, Erection of Chitose Bridge, September 2003

STATIC AND FATIGUE BEHAVIOR OF THE CONNECTIONS OF ALUMINUM DECKS TO STEEL GIRDERS

Ichiro Okura[1], Nobuyasu Hagisawa[2], Osamu Okada[3] and Shingo Yamaguchi[4]

ABSTRACT

A connection of aluminum decks to steel girders is developed. Specimens of a simple beam type and of an overhang type are provided for statically loading and fatigue tests. The aluminum beam of hollow section is joined to the top flange of steel girders, using stud shear connectors of steel and non-shrinkable mortar. A concentrated load is applied at the span center for the simple beam type specimens, and at the beam end for the overhang type ones. The statically loading tests show that the connection developed is a rigid one. The fatigue tests demonstrate that the connection has sufficient durability, although some shear connectors experience fatigue cracks.

Keywords: aluminum deck, steel girder, static and fatigue behavior, shear connector, non-shrinkable mortar

1. INTRODUCTION

In Japan, the amendment of the design vehicle load from 196 kN to 245 kN in 1994 urges concrete decks and girders of existing bridges to be reinforced. To cope with this issue, an idea of reducing the weight of the roadway by replacing concrete decks with aluminum ones was put forward. Then an aluminum deck was fabricated by the friction stir welding, and its fatigue behavior was investigated. This was presented at the 17th Japan-US Bridge Engineering Workshop[1)].

Since then, as shown in Fig. 1, an aluminum deck was adopted for the sidewalk to widen the roadway of the Shin-Kakogawa bridge in Hyogo prefecture. The aluminum deck used is about 4 m in width and about 400 m in length.

To put aluminum decks to practical application to roadway bridges, the connections of the aluminum decks to steel girders have to be developed. In this research, a connection is proposed, and its static and fatigue behavior is investigated by statically loading and fatigue tests.

[1]Associate Professor, Osaka University, Department of Civil Engineering, 2-1 Yamadaoka, Suita, Osaka 565-0871, Japan
[2]Manager, Nippon Light Metal Co., Ltd., R & D Center, 1-34-1 Kambara, Ihara, Shizuoka 421-3291, Japan
[3]Graduate Student, Osaka University, Department of Civil Engineering, 2-1 Yamadaoka, Suita, Osaka 565-0871, Japan
[4]Director, Sumikei Nikkei Engineering Co., Ltd., 2-35-13 Kamedo, Kohto-ku, Tokyo 136-0071, Japan

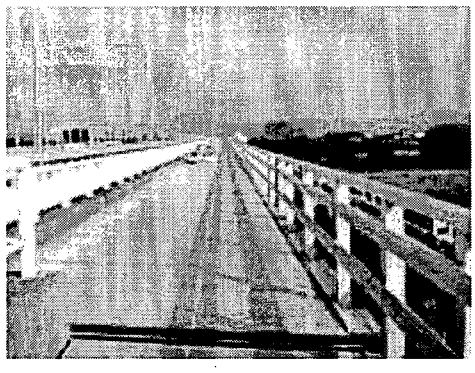


Figure 1. Aluminum deck of the Shin-kakogawa bridge

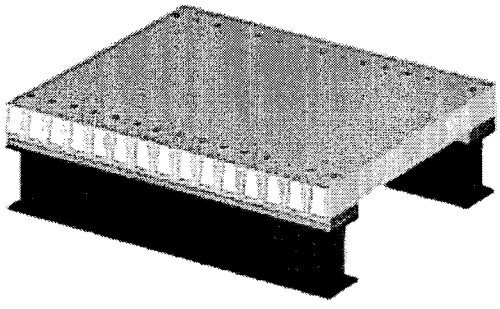


Figure 2. Aluminum deck on steel girders

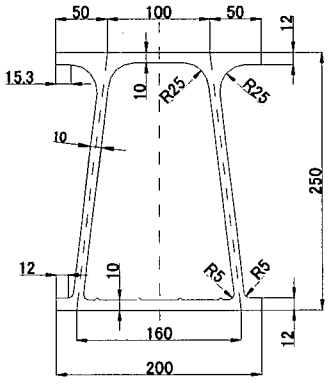
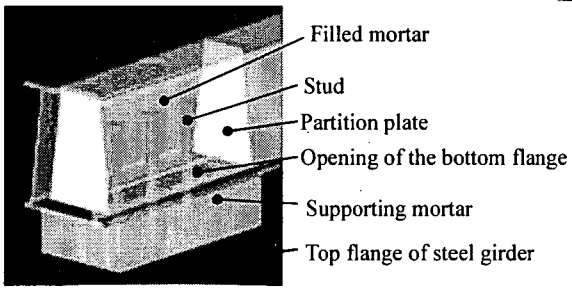


Figure 3. Dimensions of extrusion



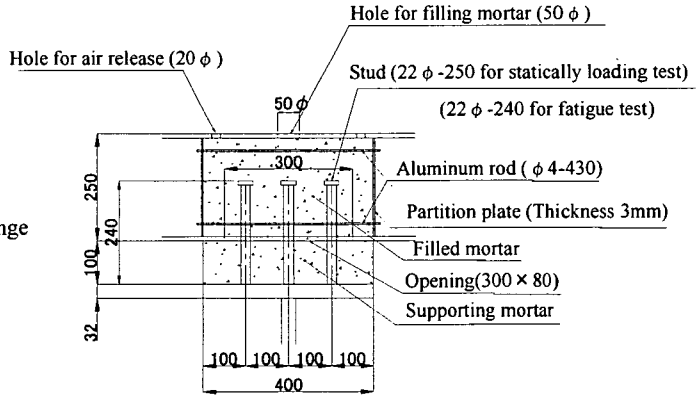


Figure 4. Connection of aluminum deck to steel girder

2. TEST SPECIMENS

Figure 2 shows a general view of an aluminum deck on steel girders. The aluminum deck consists of the extrusions connected parallel. The longitudinal direction of the extrusions spans between steel girders. Only one extrusion is enough to understand the static and fatigue behavior in the bridge-transverse direction of the connections of the aluminum deck to the steel girders.

Figure 3 presents the cross section of the extrusions used for the specimens. The aluminum alloy of the extrusions is A6N01-T5. Its mechanical properties are given in Table 1(a). The aluminum lot is different between the statically loading and fatigue tests.

As shown in Fig 4, three steel stud shear connectors of 22 mm in diameter were welded to the top flange of the steel girder in one row in the bridge-transverse direction. A formwork was laid surrounding the studs to leave the supporting mortar between the top flange of the steel girder and the bottom flange of the aluminum extrusion. The studs were inserted inside the extrusion through a rectangular cutting on the bottom flange. The non-shrinkable mortar was filled through the hole on the top flange of the extrusion. The two aluminum plates which were tied with three aluminum rods were installed inside the extrusion to prevent the mortar from running out. The mechanical properties of the studs and the mortar used are listed in Tables 1(b) and (c), respectively.

The supporting mortar is necessary to absorb the camber of the steel girders, which is created when existing concrete slabs are replaced by aluminum decks. Besides it prevents the electric corrosion of aluminum, since it avoids the direct contact of the aluminum extrusions with the steel girders.

A simple beam type specimen and an overhang type one are shown in Fig. 5. The former models the decks between steel girders, and the latter does the overhang decks.

3. STATICALLY LOADING TESTS

3.1 Simple Beam Type Specimen

3.1.1 Outline of test

As shown in Fig. 6, the load was applied at the span center of the aluminum beam. The base plates of the connections were fixed to the test floor with high strength steel bars. The vertical deflection at the span center and the strains on the lower surface of the bottom flange and the upper surface of the top flange as well as the strains on the sides of the supporting mortar and the strains on the studs were measured. The strain gauges were glued on the studs before the mortar was filled.

First the load was increased to 294 kN and unloaded. Second it was increased to 618 kN, which is the capacity of the loading machine, without failure. The load was again increased to 618 kN, and the test was terminated.

3.1.2 Relation between load and deflection

Figure 7 presents the relation between the load and the vertical deflection at the span center. The load is taken on the vertical axis, and the vertical deflection is done on the horizontal axis. The thick solid line represents the FEM results for the fixed conditions at both the ends of the beam of 2m in length, and the thick broken line does for the simply

Table 1. Mechanical properties

(a) A6N01S-T5 alloy

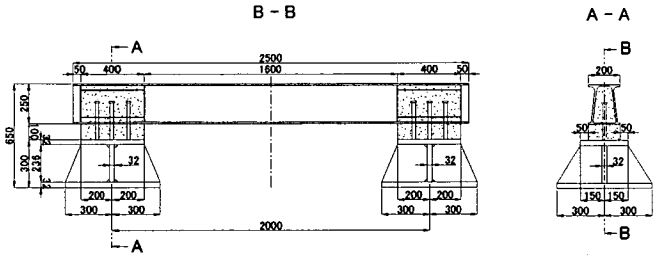
Tests	Tensile strength (MPa)	0.2% proof stress (MPa)	Elongation (%)	Young's modulus (GPa)	Poisson's ratio
Statically loading	325	299	16.6	71.5	0.32
Fatigue	308	289	16.0	71.0	0.31

(b) Steel studs

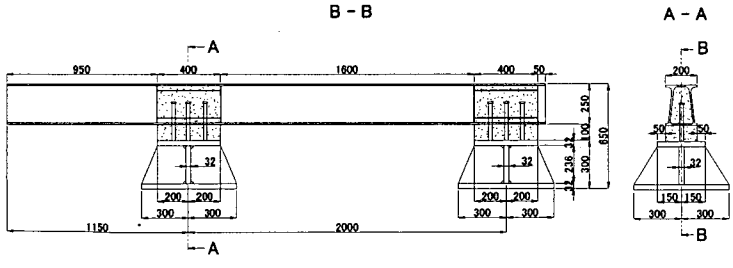
Tests	Statically loading	Fatigue
Yield stress (MPa)	283	296
Tensile strength (MPa)	443	469
Elongation (%)	26	27

(c) Mortar

Tests	Statically loading	Fatigue
Material age (day)	100	187
Compression strength (MPa)	77.4	78.1
Young's modulus (GPa)	29.4	28.9
Poisson's ratio	0.213	0.204



(a) Simple beam type



(b) Overhang type

Figure 5. Specimens

supported conditions.

For the first loading to 294 kN, the residual deflection is almost zero. The curve for the second loading to 618 kN is not on the unloading curve, leaving a residual deflection. Since the curves for the first and second loadings have almost the same slope as that of the thick solid line, the degree of the connection of the aluminum extrusion to the steel girder is near the fixed conditions at both the ends.

3.1.3 Relation between load and strains of stud shear connectors

Figure 8 shows the relation between the load and the strains of the stud shear connectors. The strains are an average of the two strain gauges which are glued symmetrically about the axis of the studs. The tensile force is produced in the central and outside studs, and the compressive force is done in the inside stud. The compressive force of the inside stud decreases at the load 300 kN. While the increase in strain of the outside stud stops above the load 520 kN, the strain of the central stud increases. Accordingly the share of the load shifts from the outside stud to the central and inside ones.

3.1.4 Relation between load and strains on the sides of supporting mortar

Figure 9 shows the relation between the load and the strains in the vertical direction on the sides of the supporting mortar. The compressive strain is created only at the strain gauge C1. The rate of increase in the strain of the strain gauge C1 decreases over the load 300 kN, and the stain decreases around the load 500 kN. This is the reason the strain is released due to cracking of the supporting mortar around the strain gauge C1.

The tensile force of the studs and the compressive one at the edge of the supporting mortar develop a moment, which makes the connection rigid.

Figure 10 shows the appearance of the cracks on the side of the supporting mortar after the loading to 618 kN. Since the width of the cracks is too small to see, the cracks are exaggerated by a marker.

3.2 Overhang Type Specimen

3.2.1 Outline of test

As shown in Fig. 11, the load was applied at the point 1 m away from the middle of the north connection. The vertical deflection just under the loading point and the strains on the lower surface of the bottom flange and on the upper surface of the top flange of the aluminum beam as well as the strains on the sides of the supporting mortar and the strains on the stud shear connectors were measured.

Cyclic loadings were repeated 5 times with a gradual increase at each loading. The maximum loads were 98 kN, 138 kN and 178 kN at the first, second and third loadings, respectively. At the load 334 kN in the fourth loading, the edge on the loading side of the supporting mortar of the north connection was crushed. At the load 326 kN in the fifth loading, a crack started at the edge of the air-release hole of the top flange on the loading side of the aluminum extrusion. Then the statically loading test was terminated.

3.2.2 Relation between load and deflection

Figure 12 presents the relation between the load and the vertical deflection just under the load. The test results are the values for the forth loading. The thick solid line is the FEM

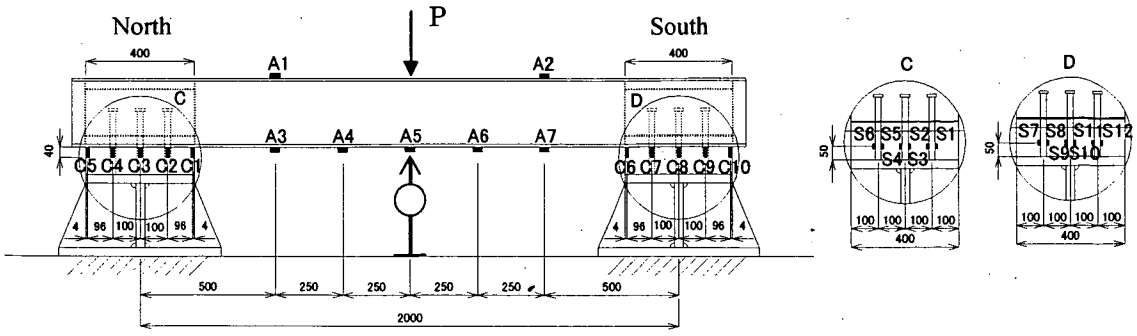


Figure 6. Loading point and measuring points of deflection and strains in simple beam type specimen

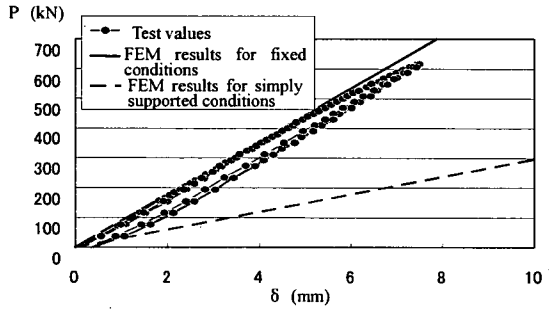


Figure7. Relation between load and deflection at span center

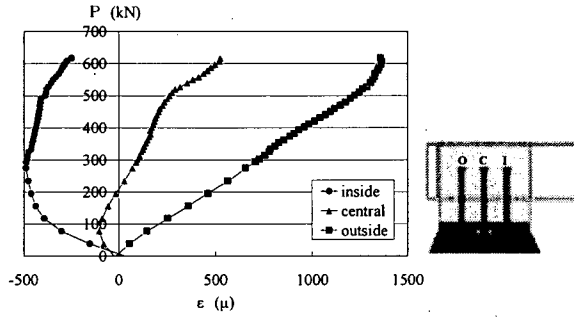


Figure8. Relation between load and strains of studs [North connection]

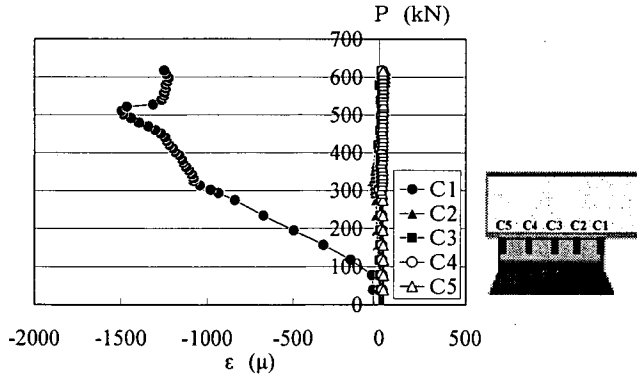


Figure9. Relation between load and strains on the side of supporting mortar [North connection]

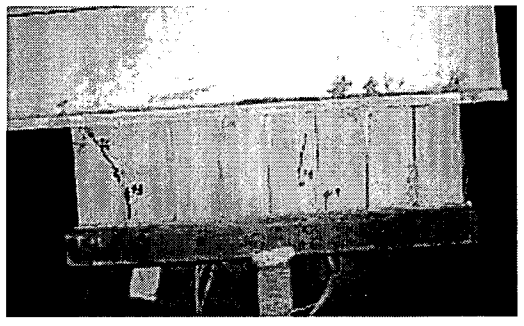


Figure10. Appearance of cracks of supporting mortar of simple beam type specimen [North connection, Back side]

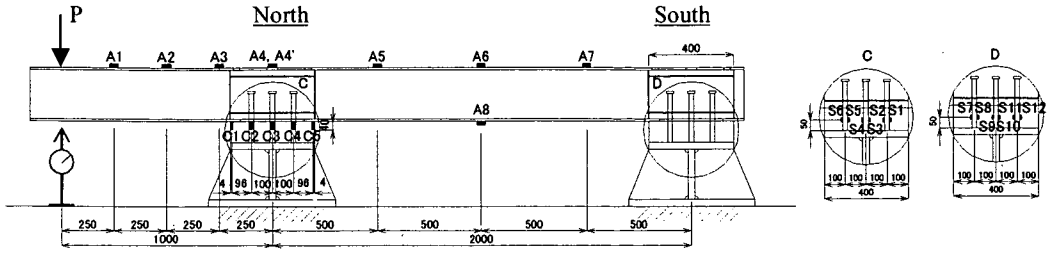


Figure 11. Loading point and measuring points of deflection and strains in overhang type specimen

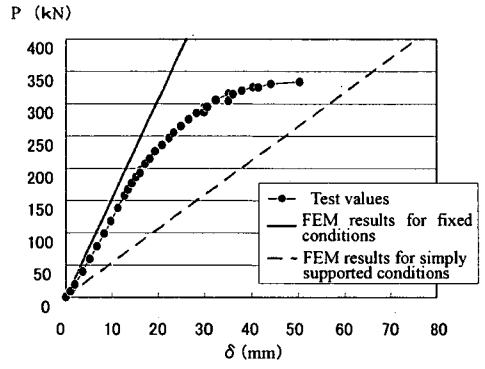


Figure 12. Relation between load and deflection

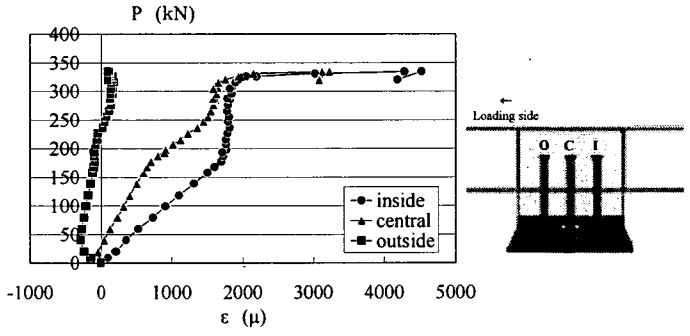


Figure13. Relation between load and strains of studs [North connection]

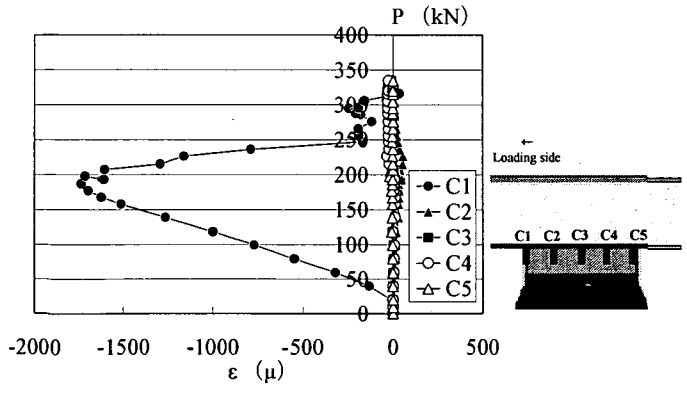


Figure14. Relation between load and strains on the side of supporting mortar [North connection]

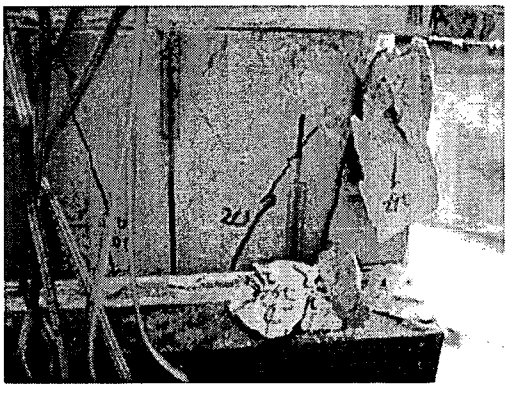


Figure15. Crushing of supporting mortar in overhang type specimen[North connection, Back side]

results for the cantilever beam of 1 m in length, and the thick broken line is those for the overhang beam of 1 m in length with the simple beam of 2 m in length. The test values vary linearly until 207 kN. The test values are closer to the FEM results for the cantilever beam than those for the overhang beam. From this, as in the simple beam type specimen, the connection of the overhang type specimen is also rigid.

3.2.3 Relation between load and strains of stud shear connectors

Figure 13 shows the relation between the load and the strains of the stud shear connectors. The strains are the axial strains, that is, the average strain mentioned in Subsection 3.1.3. The tensile force is developed in the central and inside studs. In the outside stud, the force is compressive until 220 kN, and after that, it is tensile. While the increase in strain of the inside stud stops at the load 177 kN, the strain of the central stud increases. As in the simple beam type specimen, the force shifts from the inside stud to the central and outside ones.

3.2.4 Relation between load and strains of supporting mortar

Figure 14 shows the relation between the load and the vertical strains on the sides of the supporting mortar. The compressive strain is developed only at the strain gage C1. The values of the strain gage C1 decreases at the load 190 kN, since the strain of the supporting mortar around the strain gauge is released due to cracking.

As in the simple beam type specimen, the tensile force of the studs and the compressive force at the edge of the supporting mortar develop a moment, which makes the connection rigid.

Figure 15 shows the appearance of crushing of the supporting mortar after the loading to 334 kN.

4. FATIGUE TEST

4.1 Simple Beam Type Specimen

4.1.1 Outline of test

For the specimen with the same dimensions as the simple beam type specimen in the statically loading test, the load of the upper limit 245 kN and the lower limit 24.5 kN was repeated at the span center with the frequency of 1 Hz. Expecting that the fatigue strength of the outside stud will be the grade E in the Japanese Fatigue Design Guideline[2], the range of the load was determined for the stud to break at 5×10^5 cycles. In the middle of the fatigue test, the repeated load was stopped, followed by the statically loading test to measure the deflection at the span center and the strains of the studs, and to observe the fatigue cracks of the studs and the cracks of the supporting mortar. The locations of the strain gauges glued to the studs were the same as in the statically loading test.

4.1.2 Relation between deflection and number of cycles

Figure 16 shows the relation between the deflection at the span center and the number of cycles. On the vertical axis, the deflection at the upper load 245 kN is taken, and on the horizontal axis, the number of cycles is done. In the figure, the horizontal line represents

the deflection given by the FEM for the beam of 2 m in length with both the ends fixed.

The deflection at the first loading was identical to the FEM value. The deflection suddenly increased at 5.7×10^5 cycles and 7.95×10^5 cycles, since the outside studs of the south and north connections broke at these numbers of cycles, respectively. The deflection increased moderately from 7.95×10^5 cycles to 2.59×10^6 cycles. After 2.59×10^6 cycles, the deflection did not vary.

4.1.3 Fatigue cracks of studs

Table 2 summarizes the fatigue cracks initiated in the studs. At 5.7×10^5 cycles, the axial strain of the outside stud of the south connection suddenly dropped to zero, followed by failure of the stud. At that time, the deflection of the beam increased rapidly and the hair-like cracks of the supporting mortar grew.

Similarly, at 7.95×10^5 cycles, the axial strain of the outside stud of the north connection dropped to zero, the stud broke, and the cracks of the supporting mortar propagated. The initiation of the fatigue cracks of the studs made the strain of other undamaged studs increase. This is because instead of the cracked studs, the undamaged studs take over the pulling force.

After 7.95×10^5 cycles, the initiation of cracks of the supporting mortar diminished. At 1.12×10^6 cycles and 2.85×10^6 cycles, fatigue cracks were initiated in the central studs of the north and south connections, respectively. Since the strain gauges showed a certain degree of strain, these studs did not break. After 1.12×10^6 cycles, the crack initiation was not detected in the supporting mortar. The fatigue test was not terminated until 3.19×10^6 cycles. Even if fatigue cracks are induced in the studs, the durability of the connections is high.

4.1.4 Fatigue strength of studs

The range of the axial stress of the studs is calculated, using the axial strain by the following equation:

$$\Delta\sigma_m = E\Delta\varepsilon_m \tag{1}$$

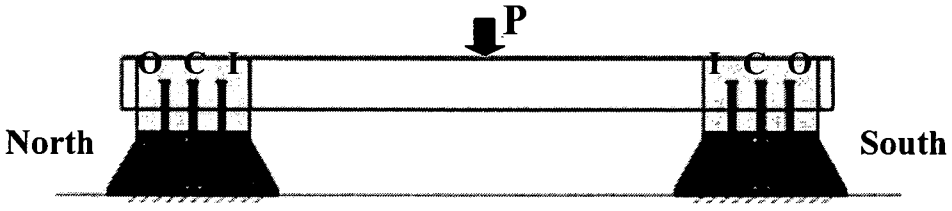
where E = Young's modulus of the studs (=206 GPa)

$\Delta\varepsilon_m$ = range of axial strain of the studs

Figure 17 shows the range of axial stress of the studs and the number of cycles when the studs broke due to fatigue cracking. The range of axial stress of the studs is taken on the vertical axis, and the number of cycles is done on the horizontal axis. The design S-N curves specified in the Japanese Fatigue Guideline[2] are also presented in the figure. The

Table 2. Summary of fatigue cracks of studs

Cycles	Connections	
	North	South
0.57×10^6	———	Failure of outside stud
0.795×10^6	Failure of outside stud	———
1.12×10^6	Initiation of crack in central stud	———
2.85×10^6	———	Initiation of crack in central stud
3.19×10^6	Fatigue test terminated	



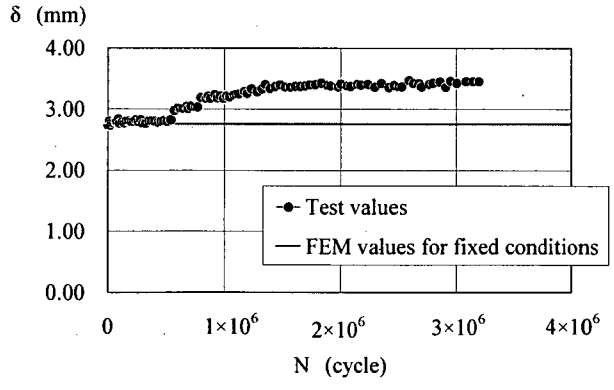


Figure 16. Relation between deflection at span center and number of cycles

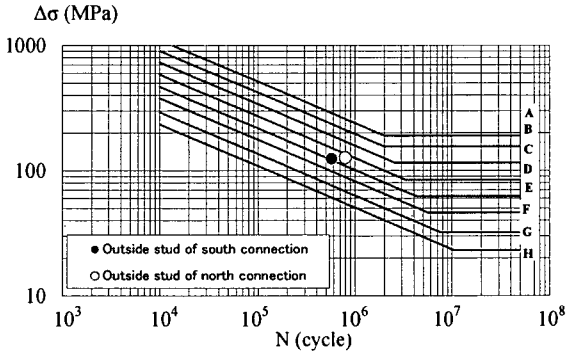


Figure 17. S-N relation of studs



Figure 18. Fatigue crack initiated at the air-release hole of the top flange of the aluminum beam

fatigue strength of the studs used in the connections is compatible with the grade E, as was predicted.

4.2 Overhang Type Specimen

For the specimen with the same dimensions as the overhang type specimen in the statically loading test, the repeated load of the upper limit 98 kN and the lower limit 9.8 kN was given at the point 1 m away from the middle of the north connection with the frequency of 1 Hz. Since it was revealed that in the fatigue test of the simple beam type specimen, the fatigue strength of the studs was the grade E in the Japanese Fatigue Guideline[2], for the overhang type specimen, the range of the load was determined for the inside stud to break at 5×10^5 cycles in the grade E.

At 1.2×10^5 cycles, as shown in Fig. 18, a fatigue crack was initiated at one edge of the air-release hole of the top flange of the aluminum beam on the loading side in the north connection, and at 1.43×10^5 cycles, a fatigue was produced at another edge of the hole. At 1.88×10^5 cycles, the fatigue cracks propagated to both the edges of the top flange. At 1.89×10^5 cycles, when the load was statically loaded to measure the deflection and the strains, the top flange of the aluminum beam broke at the load 94 kN.

To avoid the cracks at the air-release hole, it is required to move the location of the hole or to change the shape of the hole to an ellipse.

5. CONCLUSIONS

In this research, the connection of aluminum decks to steel girders was proposed, and the static and fatigue behavior of the connection was investigated. The main results are as follows:

(1) The proposed connection of aluminum decks to steel girders is a rigid one. The compressive force is developed at the edge on the loading side of the supporting mortar, and the tensile force is induced in the central stud and the one far from the loading side. These two forces develop a moment, which makes the connection rigid.
(2) The static strength of the connection is governed by crush of the supporting mortar.
(3) The fatigue strength of the connection is governed by that of the studs. The fatigue strength of the studs is the grade E in the Japanese Fatigue Guideline. Even if the stud far from the loading side has fatigue failure, the durability of the connection does not decrease, since the tensile force shifts to other studs.
(4) In the fatigue test of the overhang type specimen, fatigue cracks are initiated at the air-release hole on the top flange of the aluminum beam. It is required to move the location of the hole or to change the shape of the hole to an ellipse.

REFERENCES

1) I. Okura, N. Hagisawa, M. Naruo and H. Toda: Fatigue behavior of aluminum deck fabricated by friction stir welding, 17th Japan-US Bridge Engineering Workshop, Tsukuba, Japan, pp.153-166, November, 2001.
2) Japanese Society of Steel Construction: Guideline for Fatigue Design of Steel Structures, Gihodo Shuppan Co., Ltd., Tokyo, 1993. (in Japanese)

Fatigue Tests of Open Grid Steel Decks under Running Wheel Loads

Jun Murakoshi[1], Minoru Takahashi[2], Noriyasu Arima[3], Toru Fujiwara[4]

ABSTRACT

To ensure aerodynamic stability for super-long-span suspension bridges, a two-box girder type with open grid steel deck has been proposed based on the wind tunnel tests. In Japan, however, there have never been actual cases of application of open grid steel decks to traffic lanes which is exposed to traffic load. Fatigue tests of full-scale models of open grid decks with different structural details were conducted using Wheel Running Machine in order to investigate the fatigue behavior and the fatigue resistance. Using the test results, estimation of the fatigue life under traffic load was carried out by applying the cumulative damage rule.

1. INTRODUCTION

One of the most important subjects in designing long-span bridges is to ensure aerodynamic stability. The deck with open gratings is advantageous in terms of aerodynamic stability and cost reduction of such long-span bridges. The application of open grid steel decks to super-long span bridges with span length of more than 2,000m has been studied for the purposes of reducing the weight of superstructures and ensuring aerodynamic stability. Based on the results of the wind tunnel studies and analytical studies, it is found that a two-box girder type with open gratings (see Figure 1) is one of the possible stiffening girders for super-long -span brdiges. In another advantageous aspect of open gratings, they are also expected to be useful for ordinary bridges from the viewpoint of reducing snow-removal work in snowy areas.

In Japan, however, there have been few cases of application of open grid steel decks to traffic lanes of bridges, though they have been partially applied to truss-stiffened suspension bridges as aerodynamic countermeasure; i.e. to the shoulders and the center strip where no vehicles run. Several tests regarding the safety of driving vehicles and the fatigue durability were conducted. This paper describes the results of the fatigue tests for open grid steel decks tested using Wheel Running Machine.

2. FATIGUE TEST PROGRAM

2.1 Test Specimens

Figure 2 shows open grid steel deck investigated in this study, which is a two-layer

1 Team Leader, Bridge Structure Team, Public Works Research Institute
2 Researcher, ditto
3 Researcher, ditto
4 Director, Engineering Development Division, Long-span Bridge Engineering Center, Honshu-Shikoku Bridge Authority

structure consisting of surface members (main bar and cross bar) and their supporting stringers. The surface members are connected with stringers by HS-bolts. It enables easy replacement of the surface members directly exposed to traffic load. Figure 3 shows the structural details of a full-scale specimen (Model AR). The surface members are supported by 17 stringers (130mm spacing) which were designed to be grid structure supported by three cross girders. These stringers are penetrated by two I-shape cross beams at the span center and connected by fillet welding.

Table 1 shows the structural details of surface members of test specimens. Model A has a 75mm square grid structure consisting of main bars and cross bars. Model B has a structure using 6mm x 6mm square screw bars which is connected by pressure welding. This Model has been widely used as the members of the drain covers of roadside. Model C has a grid structure of about 50mm x 100mm consisting of the flat bars diagonally placed in longitudinal direction considering high stability of driving vehicles and motor cycles at high speed. Model AR is a modified version of Model A, which increases the rigidity of the main bars. Except Model B, it was confirmed that Model A, C and AR satisfy the fricition requirements between wheels and deck surface at high speed driving based on the results of driving tests. These main and cross bars of surface members were designed as continuous beams supported at the grid points.

2.2 Test Method

Wheel running machine (WRM) of the PWRI shown in Figure 4 and Photo.1 was used for the fatigue tests. Load was applied by moving a 500mm-wide steel wheel back and forth for a distance of ± 1.5m on a track made of loading blocks (500mm x 200mm) placed continuously in a line on the specimens. The frequency of cyclic loading is about 0.8 Hz (the rotation speed of the flywheel is about 25 rotation/min). A steel plate (thickness 12mm x width 560mm x length 4,500mm) is placed on the surface of a piece of plywood (thickness 6mm) laid on the loading blocks for cushioning. The steel wheel runs on the steel plate. A 3.2mm-thick steel plate and a 20mm-thick rubber sheet were also placed under the loading blocks. The combination of two steel plates, a rubber sheets, and plywood give the effect of distributing the contact pressure of the loading blocks as equally as possible.

Step-up loading pattern in which the wheel load increases with a constant number of cycles was applied to each specimen. Loading started with wheel load of 100kN, which was smaller than the design live load of 140kN(including an impact coefficient of 0.4), and increased by 20kN for every 40,000cycles, suspending the wheel load running for each 20,000 cycles to measure static responses of the deck.

3. TEST RESULTS

3.1 Cycles to cracking

Figure 5 shows the numbers of cycles to cracking occurred at specimens. The solid lines indicates loading step(wheel load vs. number of cycles). The tests finished when cracks propagated to some extent. In all the models except Model B, cracks occurred in the surface members at a small number of cycles(the surface members of Model B did

not have cracks). At 250,000 to 300,000 cycles, in all the models except Model A(the test finished at about 240,000 cycles), cracks occurred at stringers. Figure 6 shows the displacement for each Model at the center span of the center stringer. The broken line shows the displacement calculated by grid analysis without taking the rigidity of the surface members into account. Though measured displacement become a little larger than calculated value, there is not so much difference until the end of the test, which indicates the deck systems keep load carrying capacities.

3.2 Damage Condition

(1) Surface Members

Figure 7 shows the crack distribution on the half panel of each Model observed after the test. The solid symbols in the figure correspond to the damage conditions that the main bars and/or the cross bars were fractured, and the open symbols indicate that they are cracked although cracks did not reach the stages of fracturing. Figure 8 shows relation between the number of cracks (at 1/4 loading area) at the surface members and the number of cycles. Evaluating the fatigue resistance of each model based on the occurrence frequencies of the crack, it can be listed in descending order as follows: Model B > Model C > Model AR> Model A.

The cracks of Model A and Model AR were roughly distributed in a line in the direction perpendicular to the bridge axis. The locations of the damages closely matched those of the boundaries of the loading blocks with a size of 500mm x 200mm, presumably because the wheel loading via the loading blocks caused relatively high concentrated load around the boundaries. Regarding Model B, no crack was observed in the surface members until the end of the tests (about 360,000cycles at wheel load 280kN). The major reasons are considered as follows: (1)The pressure-welding of the grid point resulted in the high fatigue resistance compared with the fillet welding of the other models. (2)The main bar spacing is small compared with that of the other models so the local stress is smal. In Model C, the number of the cracks of the surface members at the end of the tests was small next to Model B. The main and cross bars of the diagonal grids are connected at an angle of 45° in the londitudinal direction of the bridge axis, and the flexural rigidity in this direction is higher than those of the other models for the tire pressure, resulting in a high wheel load distribution effect.

(2) Stringers

Figure 9 shows an example of the crack occurred at stringers. All the cracks occurred at the welded connections between stringers and cross beams. All the cracks were produced in the upper or lower portions on the stringer sides. The damages are concentrated in the areas directly under the wheel load.

4. ESTIMATION OF FATIGUE LIFE

Rough estimation of fatigue life under traffic load was carried out for Model AR by applying the cumulative damage rule to the fatigue test results. Using axle-weight distribution data (see Figure 10) of large vehicles measured on National Highway Route

357 (Ariake, Tokyo in 1984), the equivalent wheel load Peq (root-mean-cube value) was 33kN. The average number of axles was 2.6axles/vehicle. Figure 11 shows relationship between fatigue life and daily traffic volume of large vehicles calculated from Peq and the average number of axles per vehicle. As described before, about 300,000cycles at the test corresponds to the time when cracks occurred at about 5 grid points of the surface members and that when the first crack initiated at the connection of the stringer. The cycle at the end of the test has no specific meaning, but as shown in Figure 6, at least at that time the deck had its sufficient load carrying capacity. In the range of 2,000 to 3,000 (vehicles/day/lane), the number of years at the time of reaching 300,000cycles was about 20years and 40-60years at the completion of the test. Since the surface members are replaceable structures, they can be maintained by replacing them. On the other hand, the supporting stringers, which is difficult to be replaced, need to be improved for fatigue resistance. This estimation was made under conservative assumptions. Further accurate calculation need to be carried out.

In this study we investigated application of the open gratings to the passing lanes of super-long-span bridges(see Figure 1), therefore nearside lanes are made of orthotropic steel decks. Under heavy traffic conditions, One of practical measures is considered to limit the driving of truck traffic on the open grid steel decks as is sometimes done on suspension bridges abroad.

5. SUMMARY

Wheel running tests of full-scale models of open grid decks with different structural details were carried out to investigate the fatigue durability. Regarding surface members, Models C and Model AR had relatively high fatigue durability among the models which were confirmed to satisfy the requirements for the safety of traveling vehicles by driving tests. Regarding the supporting stringers, the cracks occurred at the welded connections between the stringers and the cross beams. The connection detail needs to be investigated from the point of view of fatigue resistance for practical use. And based on the test results, the fatigue life under traffic load was estimated for Model AR.

ACKNOWLEDGEMENTS

Fatigue tests were conducted as a part of the joint research program on aerodynamic and economic deck systems of super-long-span bridges between the PWRI (the former PWRI until 2000) and the Honshu-Shikoku Bridge Authority from FY2000 to FY2002. The authors wish to all participants in the joint research program for their work.

REFERENCES

1) Bridge and Offshore Engineering Association, "Fiscal 1997 Research Report on Super-Long Span Suspension Bridges with Open Grid Steel Deck", Mar. 1998 (in Japanese)

2) Public Works Research Institute et al., "Cooperative Research Report on the Safety of Traveling Vehicles of Open Gratings (No. 1)", Cooperative Research Report of PWRI, No.231, Aug. 1999(in Japanese)
3) Nakatani, Uchida, Nishikawa et al., "Tests on the Fatigue Durability of Higway Bridge Decks", Technical Memorandum of NILIM, No. 28, Mar. 2002 (in Japanese)
4) Fujiwara, Iwasaki and Tanaka, "Study on Design Live Load in the Ultimate-Strength Design Method", Technical Memorandum of PWRI, No.2539, Jan. 1988 (in Japanese)
5) Murakoshi, Takahashi, Tokuhashi, Suzuki, Kishi, "A Study on Fatigue Durability of Open Gridge Steel Deck under Running Wheel Loading", Journal of Structural Engineering, Vol.49A, Mar. 2003 (in Japanese)

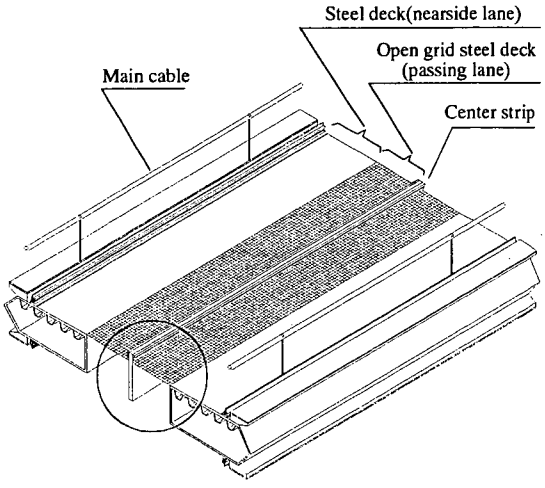


Figure 1 Two-box girder with open grid steel deck

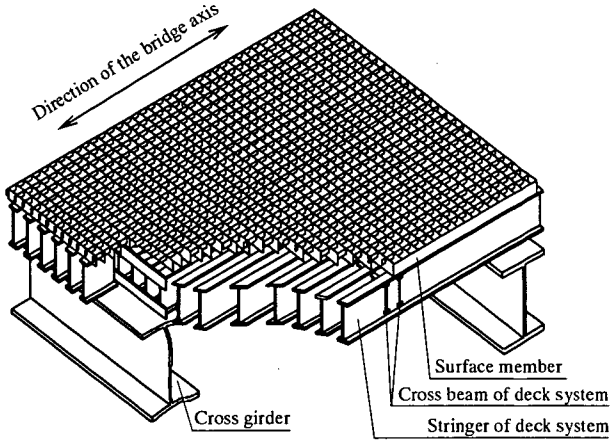


Figure 2 Structure of open grid steel deck investigated

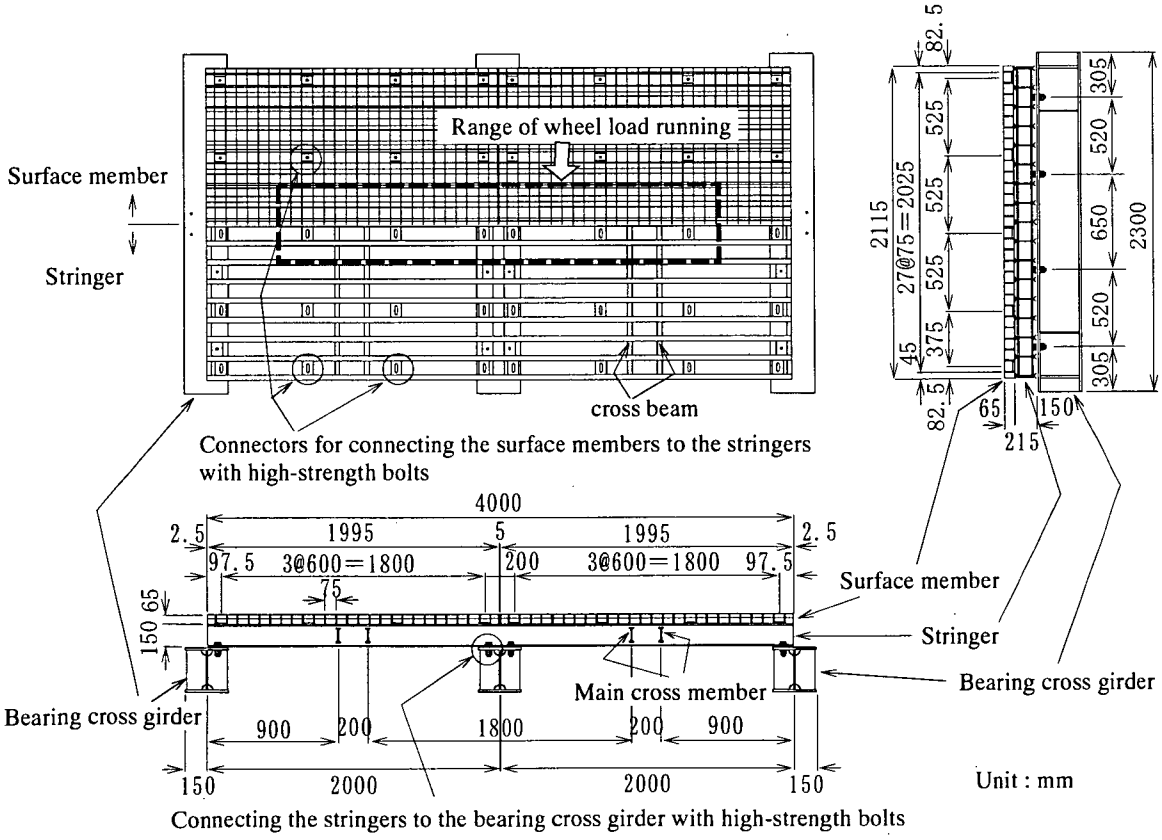
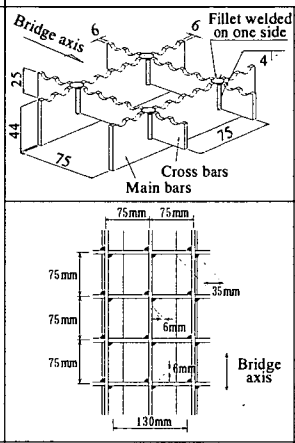
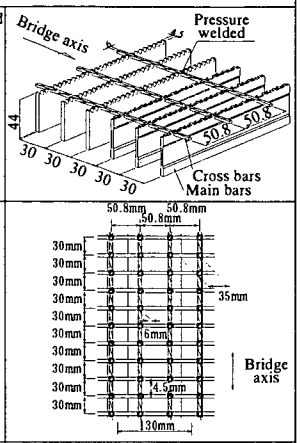
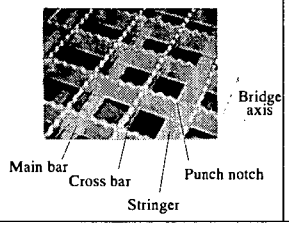
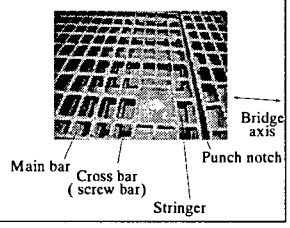
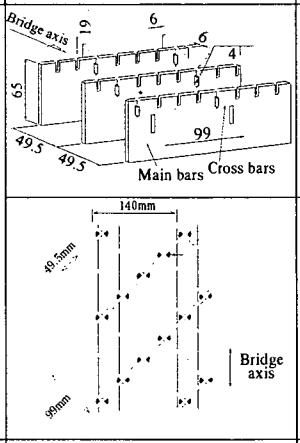
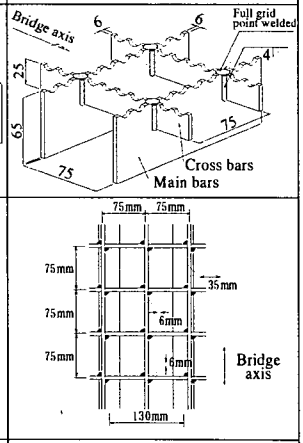
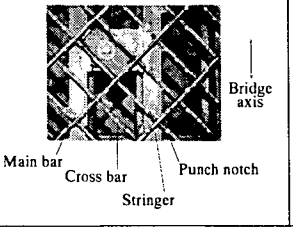
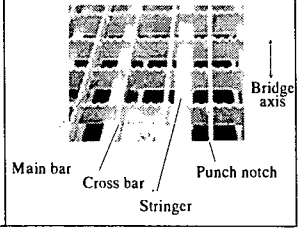


Figure 3 Dimensions of the test specimen

Table 1 Structural details of surface members

Model Name		Model A	Model B
Characteristics	Surface member	Main bar :FB44× 6 Cross bar:FB25× 6	Main bar :FB44× 4.5 Cross bar:SB6× 6
		Main bars are cut out at the grid points and fillet welded with cross bars on one side.	The grid points of flat bars are pressure-welded with screw bars.
	Structural girders	Stringer :I-150× 35× 35× 4.8 Cross beam:I-105× 30× 35× 4	
Structural drawing			
Photograph			

Model Name		Model C	Model AR
Characteristics	Surface member	Main bar :FB65× 6 Cross bar:FB19× 6	Main bar :FB65× 6 Cross bar:FB25× 6
		Main bars are cut out at the grid points and fillet welded with cross bars on one side.	Main bars are cut out at the grid points and fillet welded with cross bars on one side.
	Structural girders	Stringer :I-150× 35× 50× 5 Cross beam:I-105× 30× 35× 4	Stringer :I-150× 35× 35× 4.8 Cross beam:I-105× 30× 35× 4
Structural drawing			
Photograph			

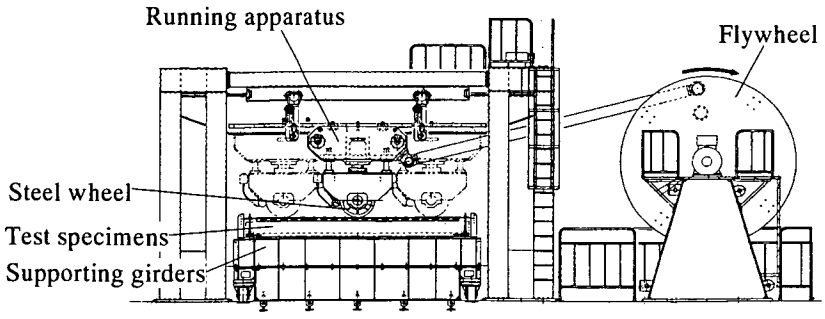


Figure 4 Outline of the wheel load running machine(WRM)

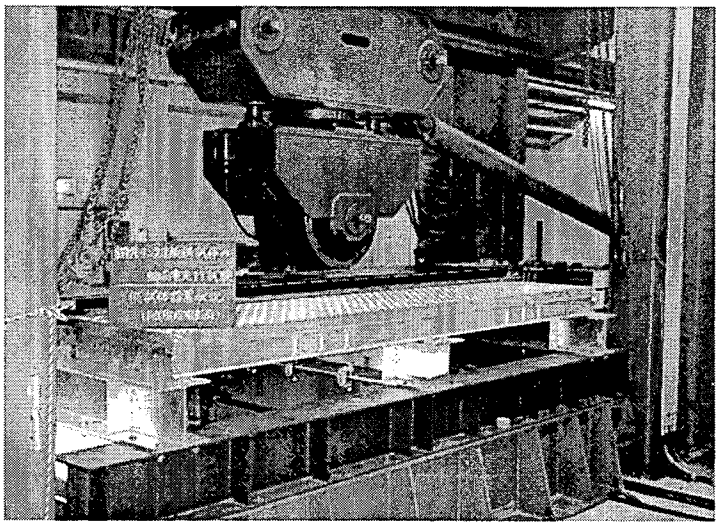


Photo. 1 Test setup

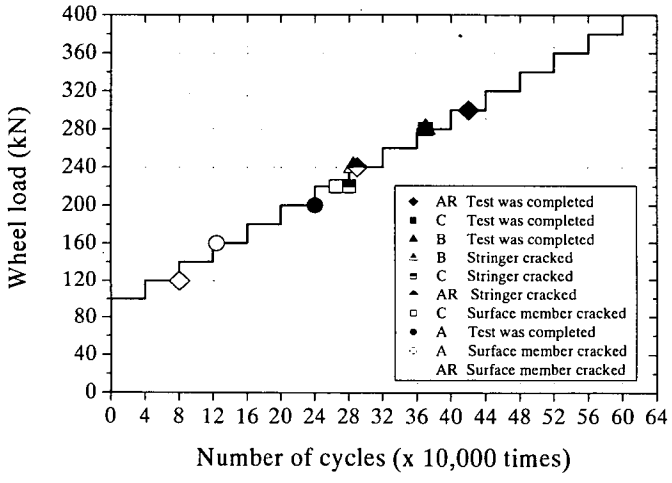


Figure 5 Results of the wheel load running tests of Models A, B, C and AR

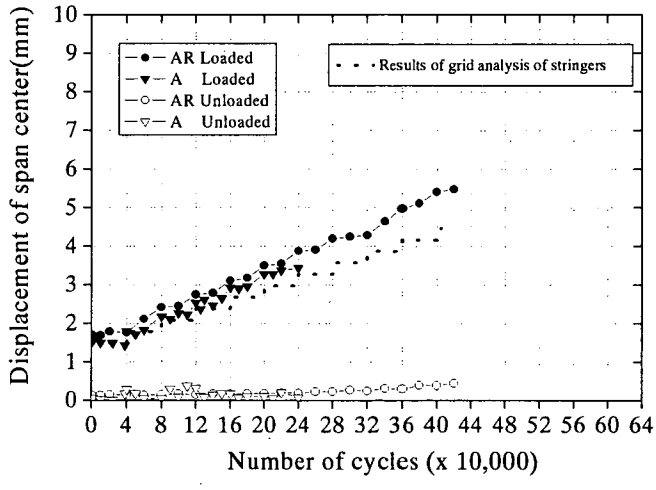


Figure 6 Displacement of the center stringer at span center

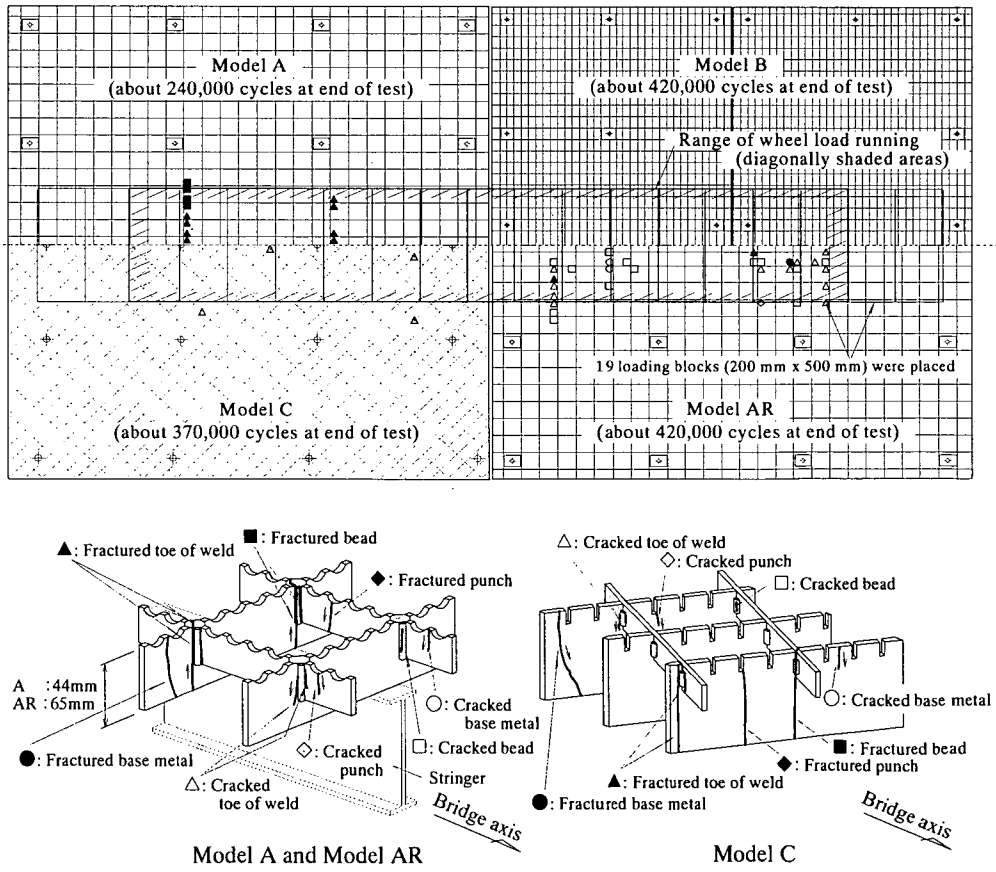


Figure 7 Crack distribution of the surface members (at end of tests)

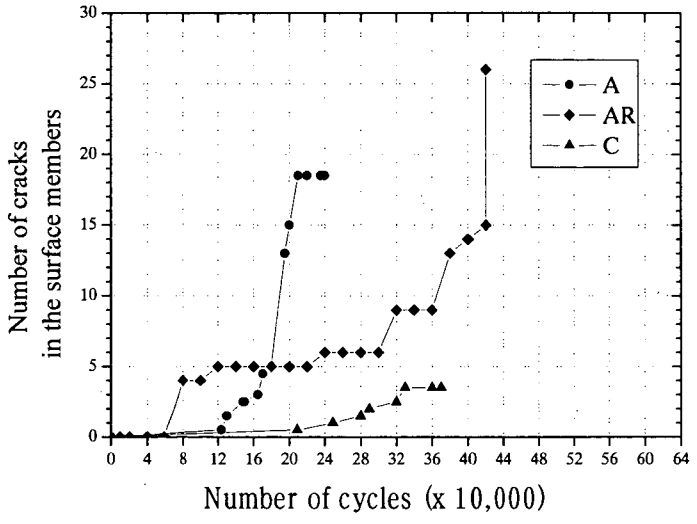


Figure 8 Relationship between the number of cracks in the surface members and the number of cycles

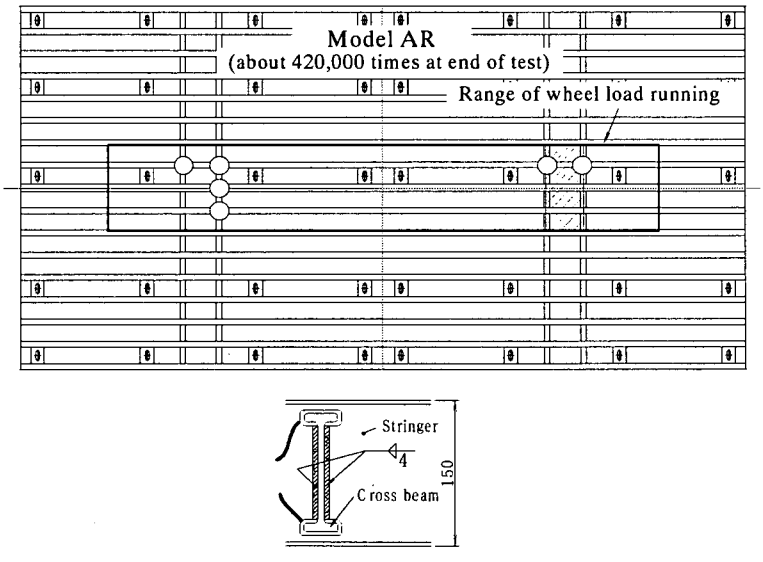


Figure 9 Crack distribution the stringer of Model AR (At end of test)

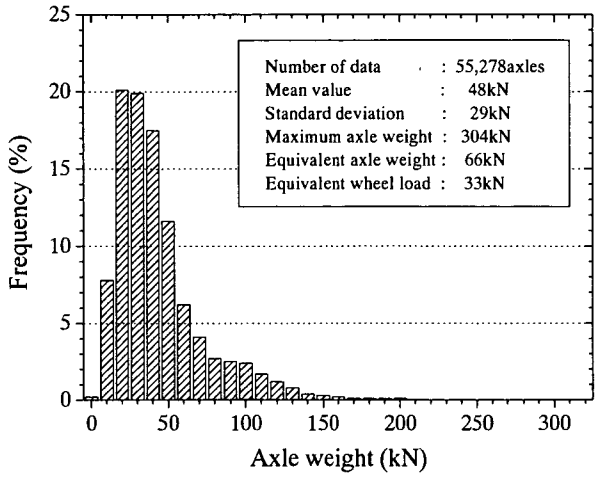


Figure 10 Axle weight distribution of large vehicles

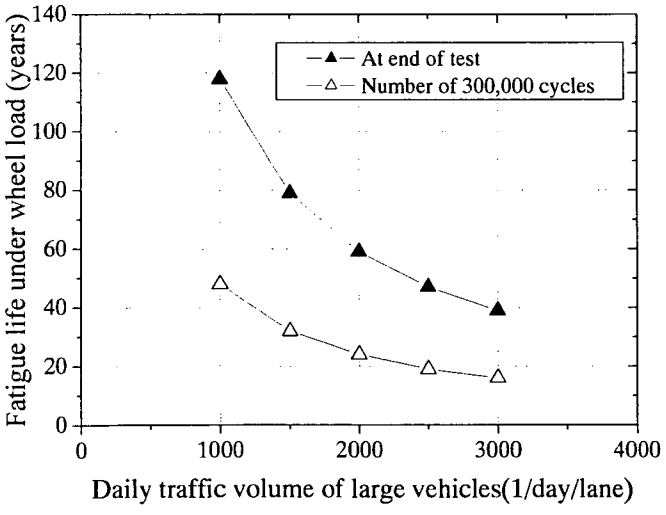


Figure 11 Converted number of years with respect to equivalent converted axle weight

19th US-Japan Bridge Engineering Workshop

Maintenance 1

co-Chairs:
S. Nakatani & I. Harik

Mitigation of Corrosion in Concrete Bridges
J. Hooks

Corrosion of 30 Years Old Weathering Steel Bridges
K. Ikeda

Federal Highway Administration Bridge Research and Technology Deployment Initiatives
I. Friedland

Field Tests of RC Deck Slabs Deterioration Assessment System by Digital Images
S. Okada

Florida's Approach to Bridge Preservation
I. R. Lasa

Nondestructive Inspection of the Suspender Ropes in a Suspension Bridge
T. Sugimoto

MITIGATION OF CORROSION IN CONCRETE BRIDGES

Paul Virmani, Federal Highway Administration, McLean, VA
John M. Hooks, Federal Highway Administration, McLean, VA

Background

The deterioration of various concrete bridge components built in the past with black steel reinforcement is one of the most common, most damaging and most costly problems facing bridge owners in the United States. The major cause of concrete deterioration (cracking, delamination, and spalling), is the corrosion of embedded black steel reinforcing bars as a result of chloride ions (permeating through the concrete cover) in combination with moisture and oxygen. The average black steel reinforced concrete (R/C) bridge deck, in a snow belt State, showed spalling in about 7-10 years. Although prestressed concrete (PS/C) bridge members are generally cast with good control of mix designs and curing regimes, they are still vulnerable to corrosion (of the pretensioned, uncoated strands) similar to that of the black steel in reinforced concrete, albeit after a longer period of service. Since PS/C members rely on the tensile strength of the strands to resist loads, loss of a few strands per member could be catastrophic. Even small corrosion pits cause fracture of a strand, as compared to non-prestressed concrete reinforcing that will literally rust away without breaking.

For post-tensioned concrete (PT/C) bridge members (both external and internal prestressing), the voids in grouted ducts and/or excessive bleed water (in certain grout mix designs), in addition to chloride/water entering the rough breached ducts or faulty joints at anchorage locations, will corrode the uncoated strands. The underlying difficulty is that there are no reliable, rapid and cost-effective non-destructive methods to assure owners that completed PT/C structures have met the construction specifications. One of the major inspection concerns is whether the ducts in PT/C members have been completely filled with grout and whether there is a uniform coverage over the prestressing steel.



Figure 1. Corroded Strands

Many times, it has been found invariably that the ducts have large voided sections and were only

filled partially with grout. In addition, it is very difficult to assess the condition of anchorage areas. Past research has identified that excessive bleed water in certain commercial grouts corroded the strands in a very short time, and that in due time under load, these corroded strands can break prematurely. Since PS/C members rely on the tensile strength of the strand to resist loads, loss of a few strands in members could be catastrophic. Even small pits lead to fracture of a strand, as compared to R/C concrete where the reinforcing will literally rust away (if preventative measures are not taken) without breaking.

This paper summarizes the status of various corrosion protection systems in use for construction and rehabilitation with advantages, limitations, issues and concerns for their use to provide cost effective solutions in controlling corrosion in concrete bridges in the United States.

Corrosion of Bridges in the United States

Corrosion of reinforcing bars and prestressing tendons is one of the most significant and unremitting factors in the process of deterioration of bridges. Of approximately 478,336 bridges (not including tunnels and culverts) in the United States, about 78, 609 bridges are rated structurally deficient. Corrosion is the underlying cause of many of these bridges being rated deficient and many more bridges are showing signs of imminently serious corrosion. In combination with water and oxygen, the main ingredient for corrosion is chloride ions from applications of deicing salts in the snow belt region or marine exposure of concrete bridge members. Chloride ions eventually penetrate the concrete cover, react with embedded reinforcement to form expansive corrosion products, causeing concrete to crack with eventual concrete spalling due to debonding of concrete accelerated by traffic induced vibrations.



Figure 1. Corrosion Damage to Concrete Bridge Pier

While there is a downward trend in the percentage of structurally deficient bridges, the costs to replace aging bridges increased by 12 percent over a recent 5 year period. In addition, there has

been a significant increase in the required maintenance of the aging bridges. Although the vast majority of the approximately 108,000 prestressed concrete bridges have been built since 1960, many of these bridges will require maintenance in the next 10 to 30 years. Therefore, significant maintenance, repair, rehabilitation, and replacement activities for the nation's highway bridge infrastructure are foreseen over the next few decades before current construction practices begin to reverse the trend.

A recent study has determined that the total cost of corrosion in the United States alone is approximately $276 billion/year. This figure represents about 3.1 percent of the Gross National Product (GNP) based on 1998 figures. The dollar impact of corrosion on highway bridges is considerable. The annual direct cost of corrosion for highway bridges is estimated to be $6.43 billion to $10.15 billion, consisting of $3.79 billion to replace structurally deficient bridges over the next 10 years, $1.07 billion to $2.93 billion for maintenance and cost of capital for concrete bridge decks, $1.07 billion to $2.93 billion for maintenance and cost of capital for concrete substructures and superstructures (minus decks), and $0.50 billion for the maintenance painting cost for steel bridges. This gives us an average annual cost of corrosion of $8.29 billion. Life-cycle analysis estimates indirect costs to the user due to traffic delays and lost productivity at more than 10 times the direct cost of corrosion. In addition, it was estimated that employing "best maintenance practices" versus "average practices" could save 46 percent of the annual corrosion cost of a bridge deck reinforced with black steel bars, or $2,000 per bridge per year.

Following is a synopsis of various corrosion protection systems for construction of new concrete bridges and rehabilitation of existing salt-contaminated bridge members.

Corrosion Protection Systems for Construction of Concrete Bridges

Epoxy Coated Reinforcing Bars (ECR)

Epoxy coating for reinforcing bars is a barrier system, developed by FHWA in 1974, for the purpose of preventing chloride ions from reaching the surface of the black steel bars. To date, ECR has been used in approximately 100,000 structures including 20,000 highway bridges. Total accumulated usage of ECR is about 4.5 million tons and there are 35 coating plants in North America.

At this time, all States (except Florida) use this system extensively. In general, epoxy coated reinforcing bars have shown excellent performance in bridge decks. Excessive defects, bare area and holidays will compromise ECR's good performance. Experience indicates that prefabrication of bars should be done first and then the coating applied- better performance will result due to avoidance of bending stresses in the coating. ECR top bar mats should not be coupled with a large uncoated cathode, such as a black steel bottom bar mat to avoid macro-cell corrosion currents. ECR reinforcing used in situations involving excessive moisture, salt and high temperatures, marine exposure, highly permeable concrete, cracks, etc. are prone to premature failure. In these situations, a reduction in adhesion of epoxy to reinforcing bars has been

observed in concrete with or without chloride ions. Long-term corrosion performance of ECRs in concrete cannot be guaranteed on the basis of increased adhesion evaluated by available laboratory screening tests. Accelerated laboratory tests for adhesion (cathodic disbondment, hot water immersion in varying pH and salt) are not the best indicators for ECR performance in concrete.

Epoxy coated reinforcing bars have proven to be a cost-effective corrosion protection system for bridge decks, especially when both the top and bottom mats are coated. The premium cost of epoxy coated steel versus uncoated black steel is about 20%. However, the total cost increase on a typical bridge structure is in the range of 1 to 2%. In the United States, the estimated potential savings in bridge deck costs due to ECR use (with projected twice the corrosion-free service life for bridge decks already constructed with ECR instead of black steel) is in the $5 to $10 billion range.

Solid Stainless Steel Reinforcing Bars

Solid stainless steel reinforcing bars experience corrosion rates of up to 100 times less than black steel and show excellent performance in laboratory in both accelerated corrosion tests and long-term performance in concrete specimens. No macro-cell current can be detected between a stainless anode and a black steel cathode in a salt contaminated reinforced concrete slab. The 316 grade of stainless steel exhibits better performance than the 304 grade steel. The high cost of solid stainless steel bars - around $2 to $3 per pound compared to 15 cents/pound for black steel – can be prohibitive because total structure costs may increase by up to15 to 20 percent versus a structure reinforced with black steel. The process of fabricating bar deformations by welding wire on smooth reinforcing bars has reduced the price by 20 percent. Evaluation of this process is underway compared to normal rolled down stainless reinforcing bar in conventional steel mills, but the supplier of this product from the United Kingdom is currently out of business. Structures reinforced with solid stainless steel reinforcing bars can be expected to provide a maintenance-free service life of greater than 75 years. In the US, there are a few states, namely Virginia, Oregon, New Jersey, Michigan and Montana, using solid stainless steel reinforcing bars on an experimental basis. The high costs for this system can be justified for strategic bridges due to lost man-hours caused by detours and environmental concerns with high traffic density. A good example is the bridge crossing the Middle Fork of the Flathead River on US Route 2 near Essex, Montana. One end of the bridge terminates in Glacier National Park and the other at Flathead National Forest. Heavy snow, frequent salt applications and freeze-thaw cycles result in a harsh environment and any closure of the bridge involves a detour of 300 miles.

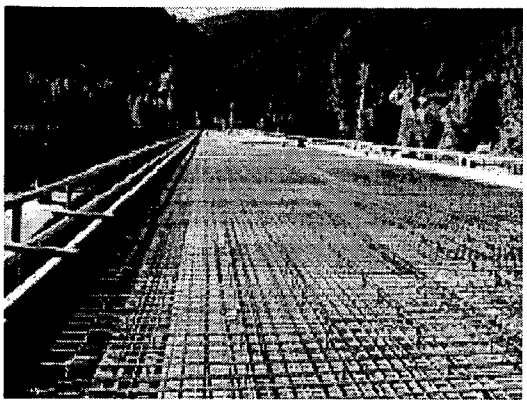


Figure 2 a. US Route 2 with Stainless Steel Bars

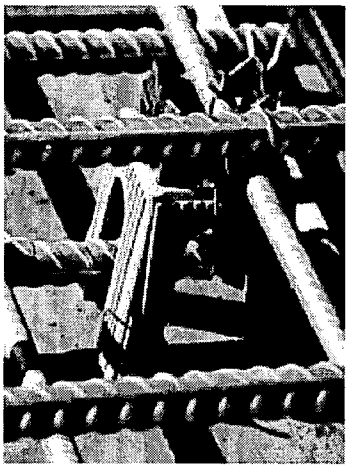


Figure 2 b. Stainless Bars & Chairs

Stainless-clad Reinforcing bars

A promising alternative to the high cost of solid stainless steel reinforcing bars is bars with a stainless steel cladding on the surface. The estimated production cost of 60-75 cents per pound compare very favorably to the $2 to $3 per pound for solid stainless steel bars and is just four times the cost of black steel (resulting in a total structure cost increase of about 5 percent). Stainless-clad reinforcing bars have exhibited excellent performance in accelerated laboratory tests. Issues related to fabrication include: protection of bare cut ends - welding a stainless steel cap on the cut end or stainless metal spray is under evaluation; and deformation and bendability at present may not be as good as that of solids bars. The long-term physical properties and performance of the core steel and the cladding is a concern in the two currently competing processes for manufacturing clad bars – Nuovinox and plasma coated. About 10 to12 field installations are planned by various states in the United States. Early results of laboratory testing indicate a bright future if the price can be held at the present level.

Corrosion Inhibitors

Corrosion inhibitors, generally mixed in with the water during concrete mixing, present an alternative to epoxy coated reinforcing bars at roughly comparable costs. Performance of inhibitors has been shown to be variable due to varying chemical composition - some are better than others. Basic inhibitor types include anodic, cathodic and mixed (or organic). At this time, calcium nitrite is the only corrosion inhibitor that has shown promise to combat corrosion. Equal amounts of nitrite ions are required in the concrete to counteract the corrosion caused by same amount of chloride ions. For good performance, expected chloride ions at reinforcing bar level for the total design service life should not exceed available nitrite ions. With time, nitrite ions redistribute towards the bottom of concrete slab and eventually can leach out after long-term

service exposure. Corrosion inhibitors are more commonly used in prestressed concrete members due to non-use of coated strands. Corrosion inhibitors are not considered effective for rehabilitation of salt-contaminated structures because there is no efficient system capable of delivering the inhibitor ions to the reinforcing bar level thru hardened concrete. In a marine environment (continuous high salt, moisture and temperature), the use of corrosion inhibitors in conjunction with epoxy coated reinforcing bars is recommended as an effective corrosion protection system.

High Performance Concrete

High quality ("High Performance") concrete is the primary corrosion protection system for any concrete structure or element. It is the first defense against intrusion of chloride ions and also to provide high alkalinity for a passive environment for the reinforcement. High quality concrete should have a low w/c ratio, low permeability, be crack-free and provide adequate cover over the reinforcing bars. Most bridge owners in the US employ proven additives such as fly ash, silica fume, polymers, epoxies, or latex modifiers to reduce concrete permeability. These admixtures should be used in optimal amounts so as to not reduce the pH of the hardened concrete. The majority of states are now developing and specifying high performance concrete mix designs and procedures for use in the field to construct bridges with fewer members or slender design at low cost as well as for basic corrosion protection. In one current example of high quality concrete as a protection system, the State of Florida mostly relies on the use high quality concrete with good cover alone for corrosion protection of their bridges located in a marine environment. At present, corrosion inhibitors, stainless steel and clad reinforcing bar, etc. are being used experimentally on a few projects. The Florida Department of Transportation has experienced premature corrosion with ECR in marine environments and they do not use ECR while they continue to evaluate corrosion resistant reinforcing alloys that would perform better than ECR.

Rehabilitation Systems for Concrete Bridges

Cathodic Protection (CP)

In the past several decades the FHWA has developed a number of impressed-current, cathodic protection (CP) systems for concrete bridges and approximately five hundred bridges in the United States are currently protected by CP systems – the State of Missouri alone has installed CP on about 200 bridges. The FHWA initially developed a conductive polymer anode for slotted and mounded CP systems. Currently, titanium mesh anode covered with an overlay is a standard impressed CP system for horizontal surfaces, (e.g., bridge decks). The cost of CP installations is reasonable at $6 to 8 per square foot ($0.56 to $0.75 per square meter) of concrete surface but CP systems are being used more in parking garages than on the bridges.

Impressed current CP systems require maintenance of rectifiers and other electrical circuits for them to function. If an impressed-current CP system is not properly functioning and polarizing the steel adequately, the structure is not protected and corrosion can continue. Maintenance is a

significant problem for impressed CP systems. The FHWA has now developed tow maintenance-free galvanic CP systems for substructure bridge members and the states of Florida and Oregon are leaders in developing and installing galvanic CP technology for their bridges. Three galvanic anode systems, zinc-hydrogel, zinc-Indium-Aluminum alloy, and zinc alone or with humetants are in use today for inland vertical and upside bridge members away from the water. Galvanic CP systems have broader appeal to the State DOT's with their limited personnel resources and minimal maintenance requirements. For PS/C, tendon to concrete bond is only reduced slightly for charge transfer equal to 160 years of CP. For PS/C, hydrogen embrittlement is not an issue when polarization is maintained below -0.90v (SCE) and there is a methodology available for qualifying PS/S members for CP. Normally, galvanic anodes are a more suitable choice for PS/C in avoiding accidental hydrogen embrittlement of high strength steel strands because they deliver low currents at low voltages.

Electrochemical Chloride Extraction (ECE)

Another method of protecting concrete elements from chloride induced corrosion is to move the chloride ions away from the location of the reinforcing steel. This can be done via a procedure known as electrochemical chloride extraction, which in principle is simply an accelerated cathodic protection process. The reinforcing steel in the concrete bridge member (pier column, deck, etc.) is the cathode; a temporary anode is anchored to the outer surface of concrete in an electrolytic solution and a current (0.1 to 0.2 amps per square foot of concrete surface) is applied from a direct current power source. This current is 100-200 times higher than that for cathodic protection and the process is applicable to reinforced concrete only. The procedure takes approximately 4 weeks. The chloride ions move outwards and sodium ions inwards toward the reinforcing bars to eliminate corrosion. In general, the concrete surface is either coated with sealers (substructure) or overlaid with concrete (decks) after chloride removal to inhibit the penetration of future chloride ions.

This technology was tested for more than 25 years ago by FHWA at Kansas DOT and Battelle Institute. A number of states have now used this technology and the costs are reasonable. No maintenance is required after completion of the process. The costs of ECE are comparable to use of a CP system, but long-term performance of the process in protecting the concrete member treated with ECE is not yet well known. More research is underway to define criterion for process completion with some assurance of desired corrosion-free service life.

Conventional Methods - Overlays, Sealers and Patching

The majority of bridge owners still prefer and depend on conventional methods over electrical methods such as cathodic protection and electro-chemical chloride extraction process. Low permeability concrete overlays have been shown to extend the life of bridges by 15-30 years. Latex-modified concrete, silica-fume concrete, low water - cement ratio concrete and polymer concrete are the most commonly used overlays to slow down the future ingress of chloride ions. This rehabilitation methodology requires no maintenance after installation, but corrosion continues since chloride still resides at the reinforcement level. After overlay installation, the

corrosion rate somewhat decreases with passage of time due to drying of concrete at reinforcing bar level and the lesser availability of future ingress of chloride ions. The cost of a low permeability overlay at $5 to $10 per square foot ($0.46 to $0.93 per square meter) is reasonable, but it does not stop the corrosion process completely.

Conclusions

Corrosion is an inescapable process, since all processed construction materials eventually revert back to their natural form. The FHWA has made much progress in the area of new bridge construction for the last 25 years. The corrosion protection systems that are in use today are performing satisfactorily. More needs to be done in developing corrosion resistant reinforcements and other corrosion protection systems such as corrosion inhibitors and more durable concrete mix designs. Since all materials will eventually degrade, in the future we have to find ways to rehabilitate the so-called corrosion-resistant bridges of today with improved cost-effective methods and technologies. At present, there are 250,000 bridges, which contain black steel and will need rehabilitation in the future. The present challenge is to make CP, chloride removal, and other processes cost-effective for bridge owners to use. Corrosion engineers and scientists will always play major roles in the development of corrosion-resistant materials for more durable new bridges as well as to find more cost-effective methodologies for extending the life of existing bridges.

Corrosion of 30 Years Old Weathering Steel Bridges

Kenji Ikeda[1], Takashi Sato[2], Kazunori Watanabe[3], Shizuo Kato[4], Toshiya Sugawara[5]

1.Abstruct

Atmospheric corrosion-resistant steel is unique in forming a tight and stable rust layer on its surface, which acts as a protective film that retards the corrosion of steel. Once stable rust forms, no coating is needed for many years, thereby reducing maintenance costs. However, on some bridges with such steel, stable rust has failed to form and the base metal has become corroded; as a result, the specification has been changed to painting. There are also cases where serious corrosion has required a bridge to be reconstructed. It is necessary to fully understand corrosion conditions through inspections or investigations and to conduct proper maintenance such as by removing and minimizing the causes of corrosion. Hokkaido Development Bureau is developing a technique for evaluating the deterioration of bridges built with weathering steel. The evaluation method is suited to the severe natural environment of Hokkaido. In 2003, this development program started with corrosion investigations on a corrosion-resistant bridge on Muroran Shindo (National Highway 36). This paper explores the extent of corrosion and factors of corrosion progress by comparing investigation results obtained in 2003 with those of 1987.

2.Introduction

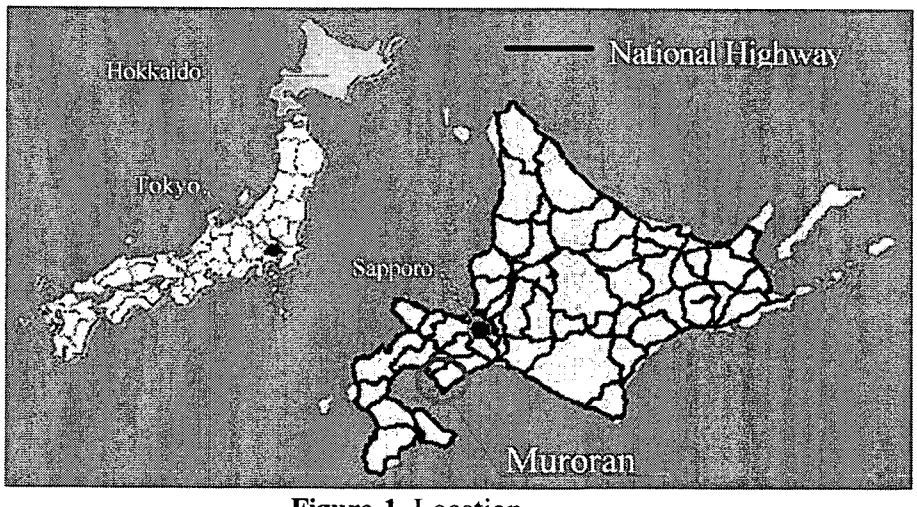


Figure 1. Location

Muroran Shindo in Muroran City is a section of National Highway 36. The section extends for 8.3 km and is used as a bypass to relieve traffic congestion in the city. Its construction began in 1970 and was completed in 1980.

The highway runs over eight bridges, which were built using about 7,800 tons of corrosion-resistant steel (Table 1). The bridges (Figure 1) are 0.5 to 3 km from the shoreline and are affected by windborne sea salt. In addition, the formation of stable rust is considered to be hindered by smoke from the factories found in this area, the largest industrial district in Hokkaido. The Weather Coat rust-stabilizing system was adopted for bridges toward reducing maintenance costs and preventing rust-containing water from splashing by promoting the formation of stable rust at an early stage.

1) Structures Division, Civil Engineering Research Institute of Hokkaido, Independent Administrative Institution.
2) Structure Dept., Docon Co., Ltd.

Table 1 Overview of corrosion-resistant steel bridges

Bridge Name	Span #	Type of Bridge	Span Length	Completion
Washibetu Pedestrian	2	Box Girder	23.6+14.5	1974
Hinode OB	2	Box Girder	22.4+31.2	1975
Wanishi OB(1)	2	Box Girder	2×52.0	1977
Wanishi OB(2)	2	Box Girder	2×52.0	1977
Wanishi OB(3)	3	Open Girder	30.5+39.5+30.5	1977
Nakamachi OB(1)	3	Open Girder	30.5×25.0	1976
Nakamachi OB(2)	3	Open Girder	30.5×25.0	1976
Nakamachi OB(3)	3	Open Girder	30.5×25.0	1976
Nakamachi OB(4)	3	Open Girder	30.5×25.0	1976
Nakamachi OB(5)	3	Open Girder	30.5×25.0	1976
Nakamachi OB(6)	3	Open Girder	30.5×25.0	1976
Nakamachi OB(7)	3	Open Girder	30.5×23.2	1976
Nakamachi OB(8)	3	Open Girder	30.5×25.0	1976
Nakamachi OB(9)	3	Open Girder	30.5×25.0	1976
Nakamachi OB(10)	3	Open Girder	30.5×25.0	1976
Nakamachi OB(11)	3	Open Girder	30.5×25.0	1976
Mizunoe OB(1)	3	Open Girder	23.0+34.0+23.0	1978
Mizunoe OB(2)	3	Open Girder	3×26.5	1978
Mizunoe OB(3)	3	Open Girder	3×26.5	1978
Mizunoe OB(4)	3	Open Girder	3×26.5	1978
Mizunoe OB(5)	3	Open Girder	3×26.5	1978
Mizunoe OB(6)	2	Box Girder	53.65+43.05	1978
Mizunoe OB(7)	1	Open Girder	36.9	1978
Mizunoe OB(8)	1	Open Girder	36.9	1978
Mizunoe OB(9)	2	Box Girder	38.8+36.25	1978
Misaki OB(1)	2	Open Girder	2×35.0	1976
Misaki OB(2)	2	Open Girder	2×35.0	1976
Misaki Ramp(1)	2	Open Girder	33.0+23.0	1973
Misaki Ramp(2)	2	Open Girder	2×23.12	1973
Misaki Ramp(3)	3	Open Girder	3×23.12	1973
Misaki Ramp(4)	3	Open Girder	3×23.12	1973
Misaki Ramp(5)	2	Open Girder	2×23.12	1973
Misaki Ramp(6)	2	Open Girder	2×23.12	1973
Misaki Ramp(7)	3	Open Girder	3×23.12	1973
Misaki Ramp(8)	3	Open Girder	3×23.12	1973
Misaki Ramp(9)	2	Open Girder	2×23.12	1973
Bokoi OB(1)	2	Open Girder	22.0+28.0	1977
Bokoi OB(2)	2	Open Girder	2×35.0	1977
Bokoi OB(3)	3	Box Girder	40.0+50.0+40.0	1977
Bokoi OB(4)	2	Open Girder	28.0+22.0	1977

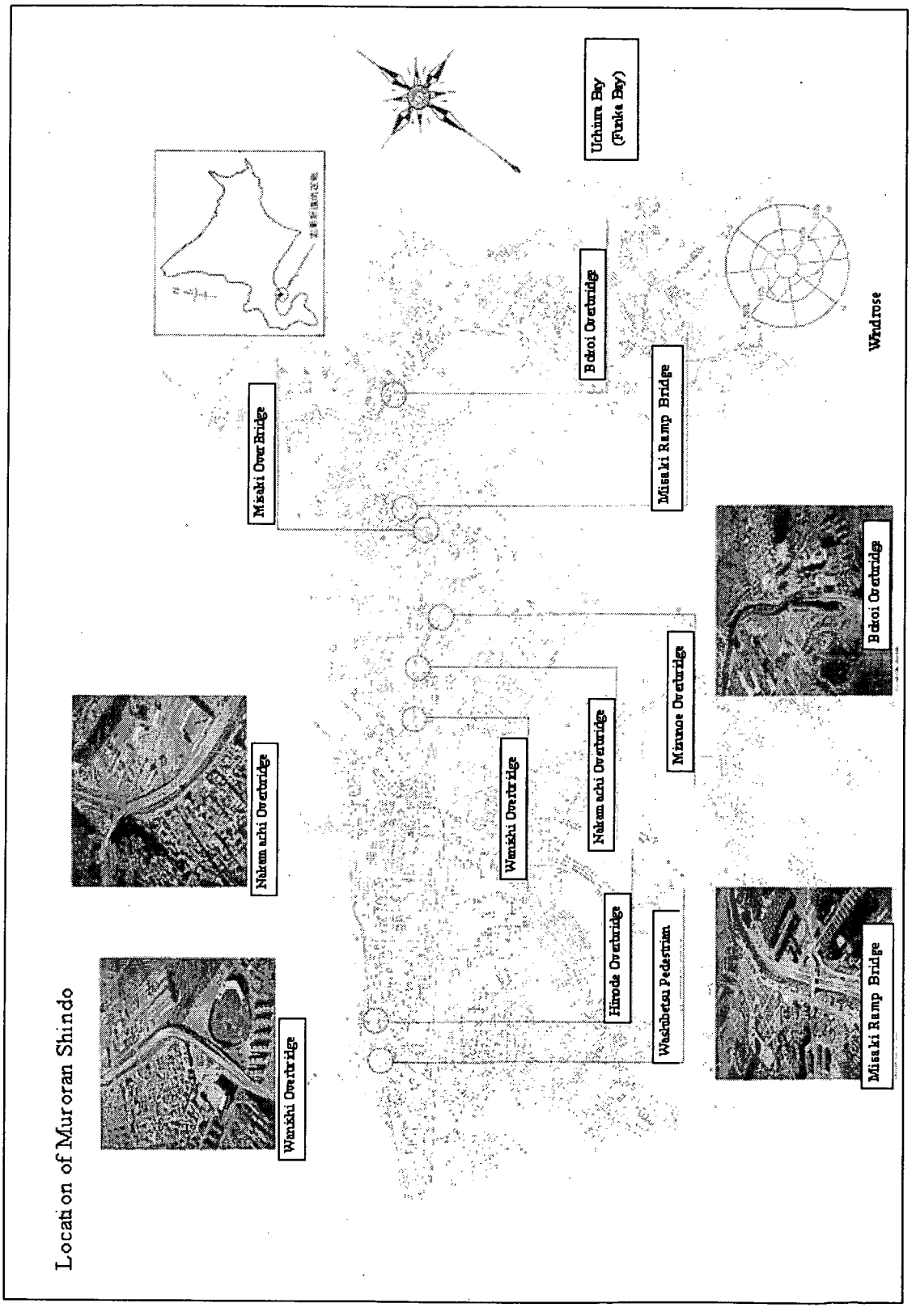


Figure 2 Sites of corrosion-resistant steel bridges on the Muroran Shindo

2. Investigations on corrosion-resistant steel bridges on Muroran Shindo

To identify the condition of surface rust on the bridges, investigations were made at predetermined fixed points.

(1) Examination of appearance

Surface rust condition was observed and color tone was examined by photograph.

(2) Examination of film thickness

Total thickness of film (thickness of Prepalen acrylic coating + rust thickness) was measured to investigate the corrosion progress.

(3) RST measurement (ion permeation resistance)

Ion permeation resistance was measured to investigate the progress of steel-corrosion protection afforded by rust film and rust-stabilization film.

(4) Measurement of salt deposition

Salinity on the steel surface was measured using electrical conductivity, to investigate the influence of salinity.

3. Investigation Results

3.1 Hinode Overbridge

The observation location in this study was on the A1 abutment (Hinode A1) and the outer side of the main girder on the A2 abutment section (Hinode A2). Both locations were chosen as observation points at the beginning of construction. The results, along with the results of previous film thickness investigations, are shown in Figure 3.

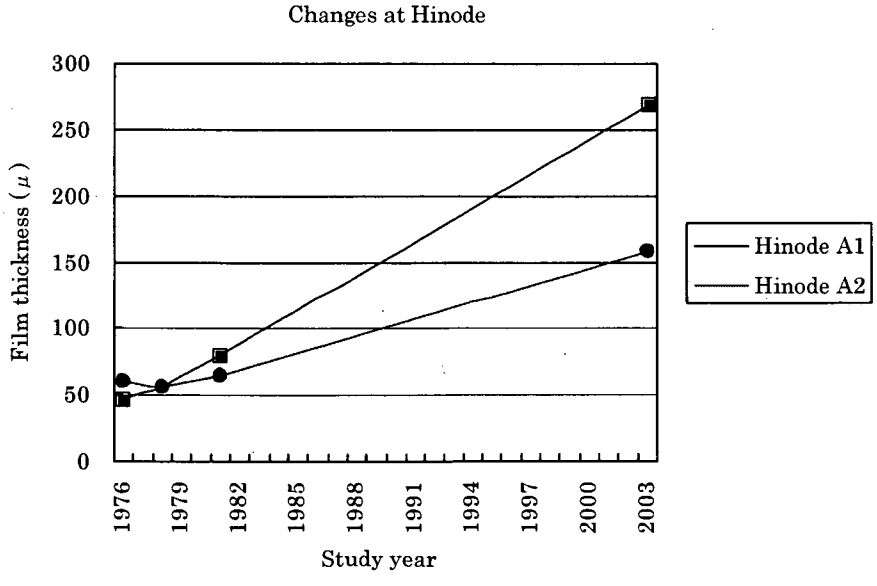


Figure 3 Temporal changes in film thickness

Investigations at A2 found a thickness increase of 6.5 μ/year from 1976 through 1981, and 8.6 μ/year after 1981. Investigations at A1 found increases of 0.8 to 4.3 μ/year. Our study found thickness of 158 μ at A1 and 268 μ at A2. This is probably due to the bridge's proximity to the frontage road and the low clearance (Figure 4). Use of

anti-icing agents began to increase from the 1980s, and we suggest that anti-icing agents were spattered on the overbridge by passing cars. Investigations on salt deposition were made in 2001 and 2003. Deposition was 562 mg/cm^2 in 2001 and 620 mg/cm^2 in 2003, i.e., salt deposition increased. It is judged that surface rust has not yet reached a stable state.

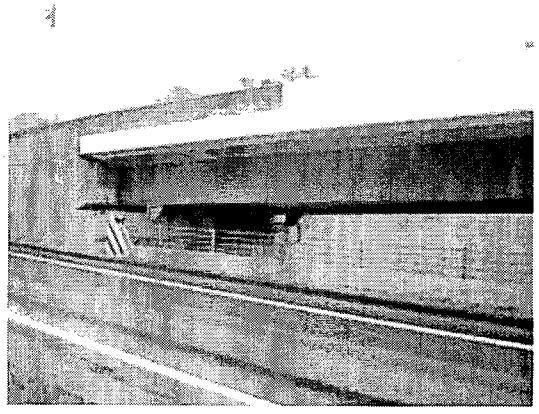


Figure 4(a) Hinode A1

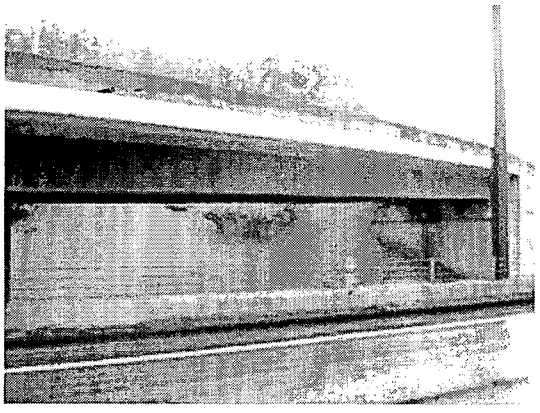
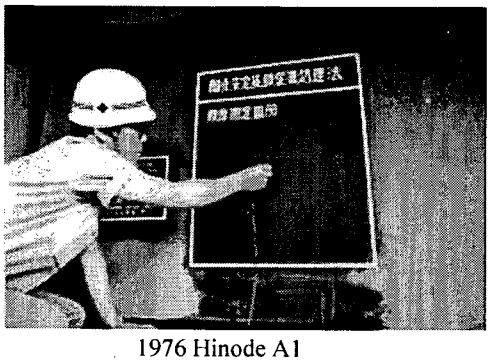
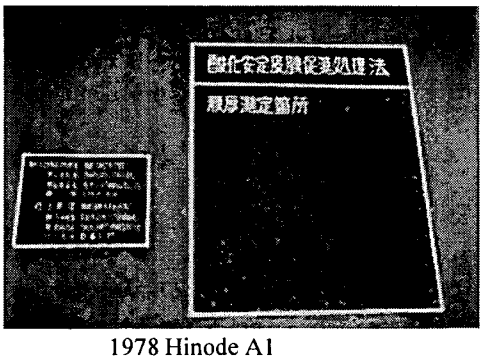


Figure 4(b) Hinode A2

Figure 5 shows temporal changes in appearance.



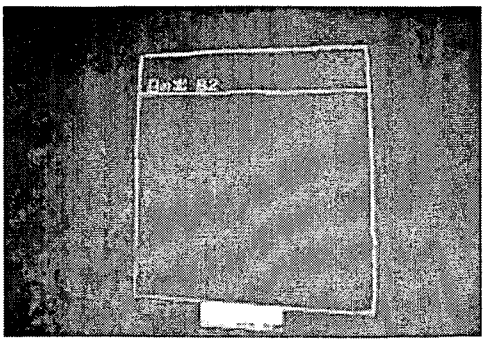
1976 Hinode A1



1978 Hinode A1

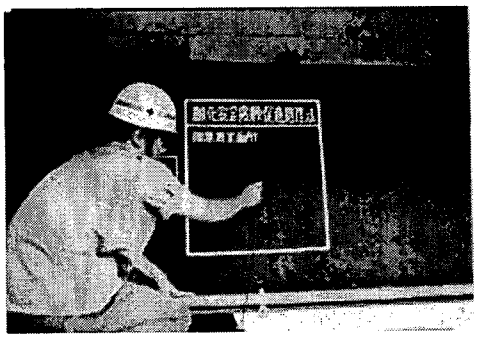


1981 Hinode A1



2003 Hinode A1

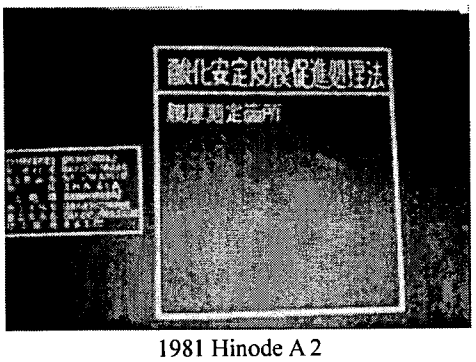
Figure 5(a) Appearances of Hinode A1



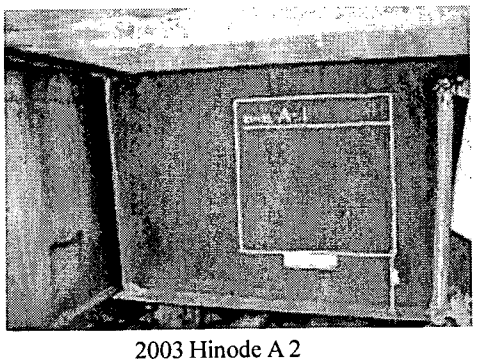
1976 Hinode A 2



1978 Hinode A 2



1981 Hinode A 2



2003 Hinode A 2

Figure 5(b) Appearances of Hinode A2

Figure 6 shows the corrosion characteristics of Hinode Overbridge. Figure 6(a) shows corrosion at the girder end section that resulted from water leakage from the expansion joint. This corrosion seems to be progressing. Figure 6(b) shows layer-by-layer rust exfoliation on the upper surface of the main girder bottom flange. Corrosion is probably progressing due to deposits such as salt-containing dust on the upper surface of the flange.

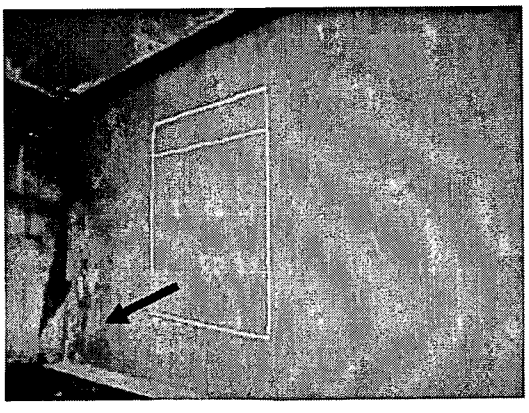


Figure 6(a) Corrosion at the girder end section

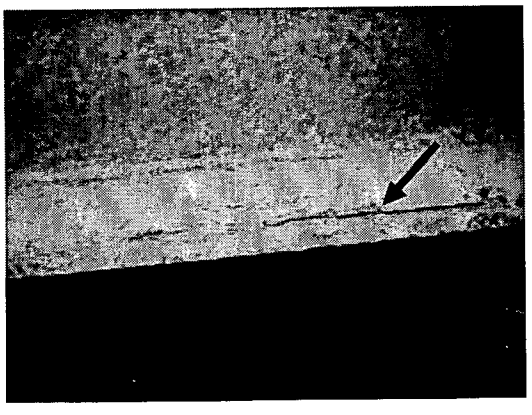


Figure 6(b) Layer-by-layer rust exfoliation on the flange upper surface

3.2 Wanishi Overbridge

Figure 7 shows temporal changes in film thickness at this bridge. The film thickness investigation found that the film thickness has been gradually increasing. The thickness increase was 3.1 μ/year between 1978 and 1981. Since 1981, the thickness increase has stabilized at 1.4 μ/year. The surface condition is favorable. Compared to the other bridges studied, the salt deposition was small, which is favorable for corrosion-resistant steel. Figure 8 shows the temporal changes in appearance.

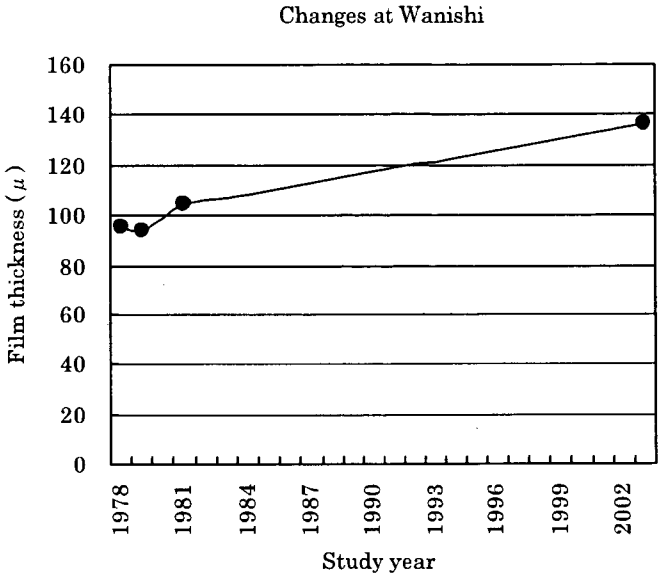


Figure 7 Temporal changes in film thickness at Wanishi Overbridge

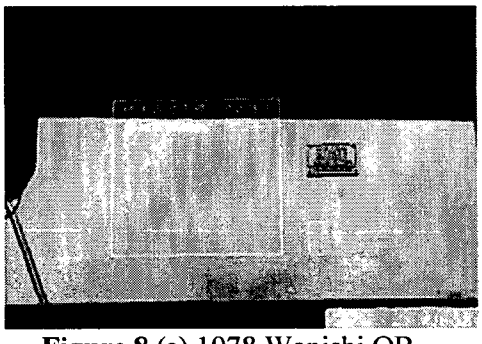


Figure 8 (a) 1978 Wanishi OB



Figure 8 (b) 1979 Wanishi OB

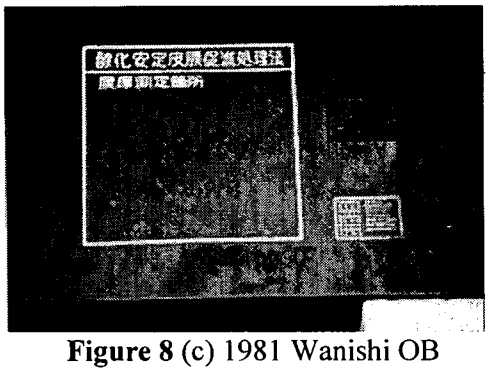


Figure 8 (c) 1981 Wanishi OB



Figure 8 (d) 2003 Wanishi OB

Figure 8 Temporal changes in appearance of Wanishi Overbridge

3.3 Misaki Overbridge

Figure 9 shows the temporal changes in film thickness at this bridge. The investigation from 1975 to 1982 found the thickness to fluctuate around the value of 60 μ. Since 1982, the thickness increase has been 5 μ/year. At the surface, stabilizer remains at some parts and rust is present at other parts. This suggests that stable rust is still being formed. Corrosion here is characterized by marked corrosion resulting from water leakage from the expansion joint, as with the other bridges.

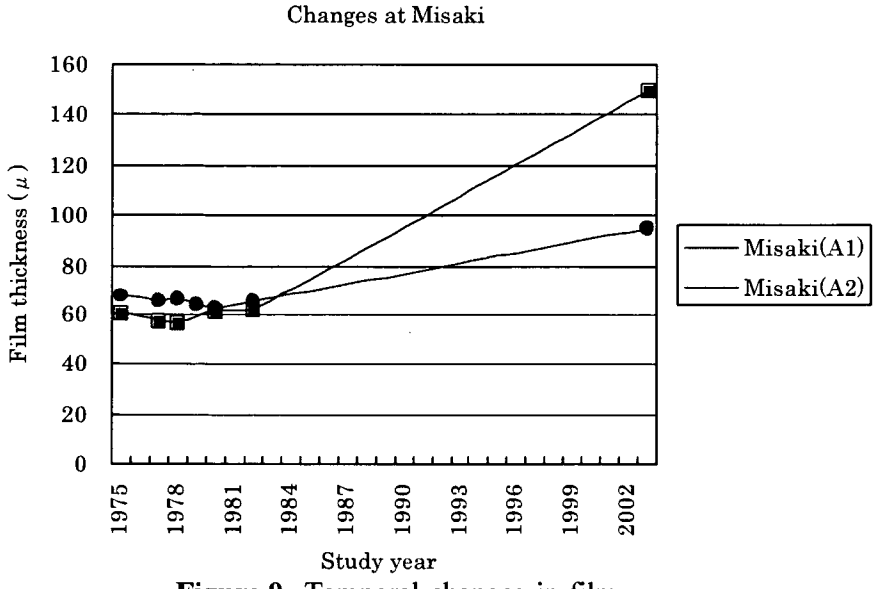


Figure 9 Temporal changes in film thickness at Misaki Overbridge

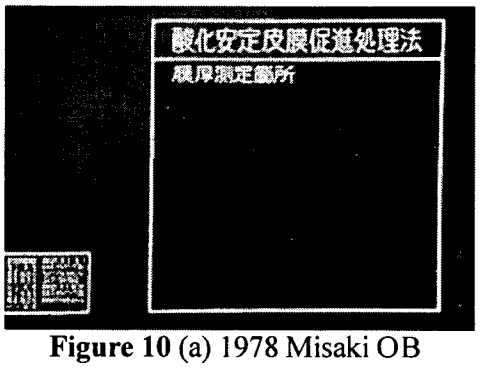


Figure 10 (a) 1978 Misaki OB

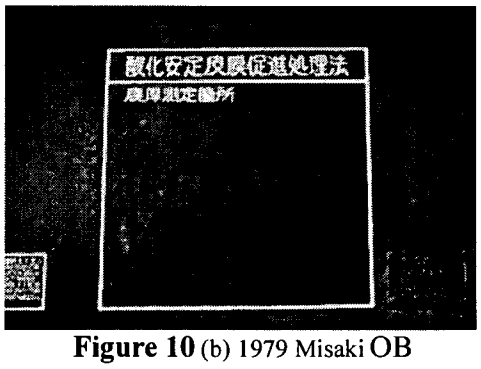


Figure 10 (b) 1979 Misaki OB



Figure 10 (c) 1982 Misaki OB

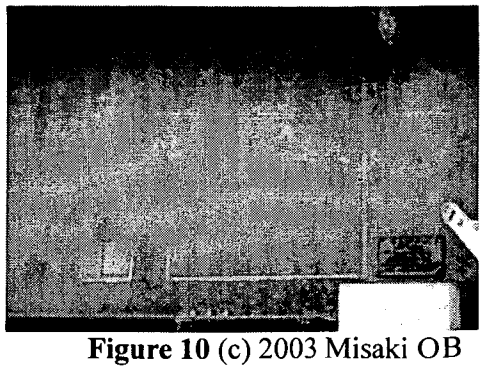


Figure 10 (c) 2003 Misaki OB

Figure 10 Temporal changes in appearance of Misaki Overbridge

3.4 Bokoi Overbridge

Figure 11 shows the temporal changes in film thickness at this bridge. The investigation from 1975 to 1982 found that the film thickness fluctuated between 80 and 90 μ (0.4 μ/year). Since 1982 the film thickness increase has been 2.4 μ/year. Stable rust seems to have formed on the surface, but it does not seem thick enough to serve as a protective film. Corrosion is characterized by marked corrosion resulting from water leakage from the expansion joint, as with the other bridges.

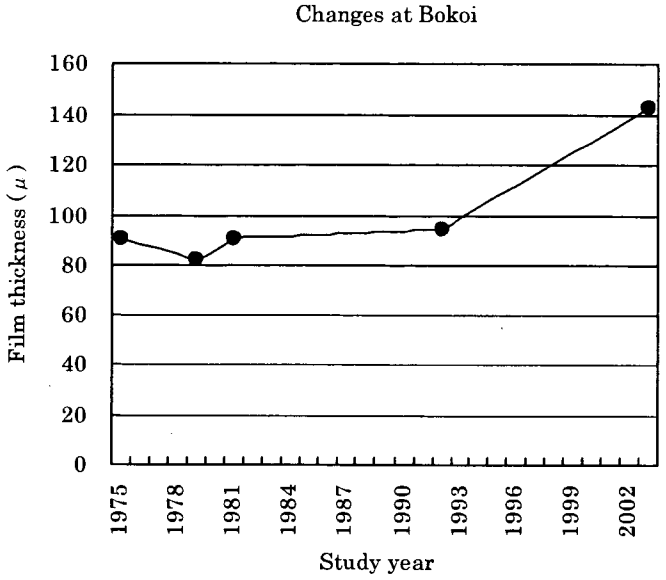


Figure 11 Temporal changes in film thickness at Bokoi Overbridge

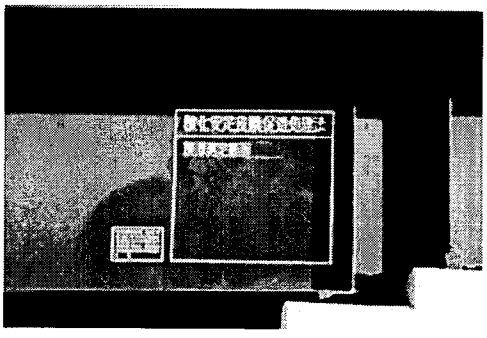


Figure 12 (a) 1979 Bokoi OB

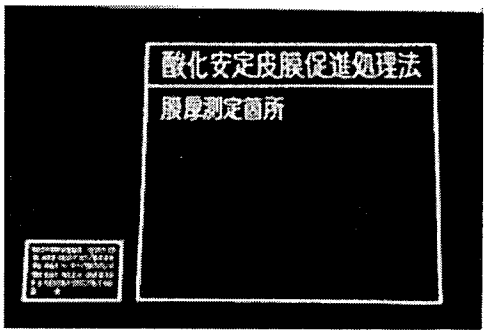


Figure 12(b) 1981 Bokoi OB

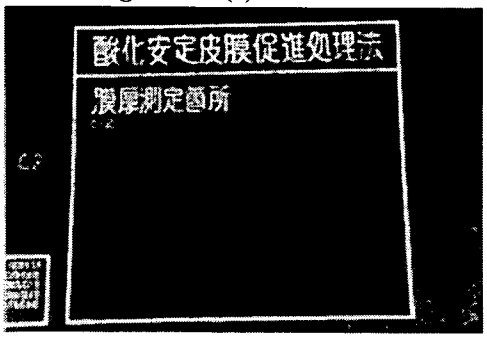


Figure 12 (c) 1985 Bokoi OB

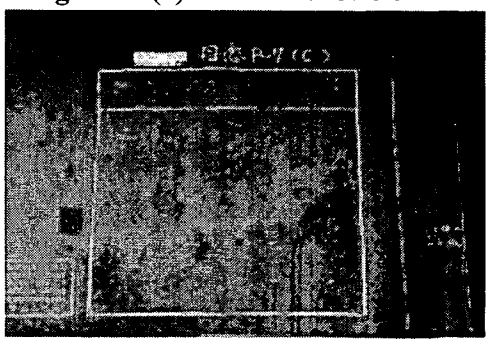


Figure 12 (d) 2003 Bokoi OB

Figure 12 Temporal changes in appearance of Bokai Overbridge

4 Summary

1) The investigations on appearance and film thickness conducted at fixed points on the four bridges found the following.

- o As a whole, the surface rust was basically in a condition to act favorably as a protective film. However, corrosion progressed due to water leakage from the expansion joint and the deck. Some portions of steel members were observed to have corroded away.
- o Given the trends of film thickness increase, a protective film of stable rust is considered to be in the process of forming.
- o In some places other than fixed points, serious corrosion was seen at the sections connected in situ. This is probably because rainwater or runoff flowed out and collected at the connected sections, which generated wetness, and because dirt and dust were easily deposited around bolts and connection plates.

2) It is necessary to take measures against water leakage from the expansion joint and deck.

3) The investigations on appearance and film thickness did not show significant corrosion. However, it is necessary to make further investigations (at span mid-section, cross beam, etc.) in order to evaluate the overall condition of a bridge, as the investigations in this study were carried out at fixed points for the purpose of continuous observation.

4) The film thickness of surface rust tended to increase. It is necessary to evaluate whether surface rust will perform well as a protective film. Investigations are also necessary to see whether film thickness will show further increase.

5) Based on these findings, we are planning to do sampling on existing bridges, and to develop a soundness evaluation method for atmospheric corrosion-resistant bridges through measurements of surface condition, rust thickness, plate thickness, deposition salinity, roughness of rust and others.

FEDERAL HIGHWAY ADMINISTRATION BRIDGE RESEARCH AND TECHNOLOGY DEPLOYMENT INITIATIVES

Ian M. FRIEDLAND, P.E.[1] and Edgar P. SMALL, Ph.D[2]

ABSTRACT

The Federal Highway Administration (FHWA) has long-standing technology programs and continues to support both short-term and long-term research needs. In the area of bridge engineering, FHWA's current bridge research and technology research and deployment thrusts include: (1) accelerated repair and construction, (2) bridge and tunnel security, (3) bridge system preservation (management, inspection, maintenance and rehabilitation), and (4) load and resistance factor design (LRFD) implementation. The FHWA is also currently developing a more formal structure for stakeholder involvement in research agenda-setting and monitoring, and in the delivery and deployment of new technologies to the bridge engineering community. This paper provides an overview of the FHWA's current bridge technology focus areas and describes a proposed approach for involvement of bridge engineering stakeholders in a formalized research and technology deployment process.

INTRODUCTION

The Federal Highway Administration (FHWA) has a long history of promoting highway technology and facilitating the construction of the network of roads and bridges within the United States. The focus on new highway construction peaked in the mid-1960s, during the development of the Interstate Highway System. With the Interstate System substantially complete, the focus of the FHWA shifted from new construction to one which has an increased emphasis on broader and more diverse U.S. highway transportation needs, in order to enhance user mobility and interstate commerce, ensure safety to the traveling public, and promote efficiency and intermodal connectivity within the system. The current focus also has FHWA providing technology solutions to its State and industry partners, which are intended to provide support in solving short-term problems, and laying the groundwork for the development of new technologies for use by the U.S. highway industry in the longer term.

In the United States, highways accommodate 90% of all personal travel and more than 80% of freight, and are thus critical for both personal mobility and commerce. Demands on the system increase annually and traffic volume growth has been dramatic both for passenger vehicles and freight. Meanwhile, the highway system infrastructure, including bridges, earth retaining structures, and tunnels, continue to age and deteriorate.

[1] Bridge Technology Engineer, Federal Highway Administration, Washington, DC
[2] Structural Engineer, Federal Highway Administration, Washington, DC

Bridges comprising the U.S. highway system are, on average, more than 40 years old. The majority of these structures were designed with a theoretical 50-year design life and yet are assumed to have essentially an infinite life. Although these structures continue to age, demands on their use continually increase. Today, more than 25% of the inventory of nearly 600,000 highway structures contained within the National Bridge Inventory (i.e., more than 150,000 bridges with a length in excess of 20 ft) is classified as structurally or functionally deficient and in need of repair, rehabilitation or reconstruction. Sufficient funds are not available to address the current level of needs; meanwhile, we are faced with a rapidly growing increase in the number of structures requiring work and in the complexity of work required to provide the level of service required of these highway structures.

In order to meet the challenge of improving our highway bridge network in the face of increased demands, continued deterioration, and constrained funding, things must be done differently. Bridge owners must work smarter and more efficiently in their maintenance and reconstruction programs. They will, however, need technological solutions to assist in this effort, and both short- and long-term research and development efforts are required to provide these technology solutions. In the short-term, there are many recently developed technologies and innovations that can be put into practice to enhance system performance. Longer-term, higher-risk, and potentially higher-payoff research is also required to complement these short-term efforts, in order to provide the breakthrough technologies that will be needed to support the challenges of the future.

The FHWA has historically partnered with the American Association of State Highway and Transportation Officials (AASHTO), State transportation agencies, the Transportation Research Board (TRB) and its National Cooperative Highway Research Program (NCHRP), and private industry and academia in research and technology programs. These partnerships will be enhanced as FHWA continues its leading role in sponsoring, conducting, and guiding research and technology efforts to improve and sustain the Nation's highway infrastructure.

In this regard, several critical needs and priority focus areas have been identified by the FHWA for highway bridges. Among these for the short term are:

- Accelerated Repair and Construction Technologies – In order to decrease the impact on the traveling public, accelerated repair and construction technologies and approaches are required. Bridges must be repaired or replaced in less time and with less cost, in order to decrease the impact on the traveling public and maximize the use of limited available funds.

- Bridge and Tunnel Security – Vulnerabilities within the inventory of structures must be identified and mitigated to ensure adequate levels of highway system performance following the occurrence of natural or manmade extreme events.

- Bridge System Preservation – As noted above, the inventory of existing structures is aging, and limited funds are available for rehabilitation and replacement. In order to "get ahead of the deterioration curve," smart preservation strategies must be employed in order to prevent structures from becoming deficient, and decision support systems must be effectively implemented to assist decision makers in optimizing the expenditure of limited funds.

- Implementation of Load and Resistance Factor Design – Previous bridge design codes and load rating procedures only minimally considered structural safety and reliability in an explicit manner. Current design philosophies feature the use of limit states, multiple load and resistance factors, and a semi-probabilistic determination of a structure's reliability. The Load and Resistance Factor Design (LRFD) approach has been adopted by AASHTO for the design of new bridges, and AASHTO has indicated its intent to standardize on LRFD design nationwide by 2007. Efforts are underway by FHWA to facilitate and assist bridge owning agencies to effectively implement the LRFD philosophy.

Each of these priority areas are discussed in further detail below. The most critical aspect of ensuring success in the deployment of these technologies, however, is to ensure adequate stakeholder involvement at every stage in the research identification, conduct, and deployment process. As a result, FHWA has proposed an enhanced mechanism for improving stakeholder involvement in FHWA research and technology activities, which is also described below.

RESEARCH PRIORITY AREAS

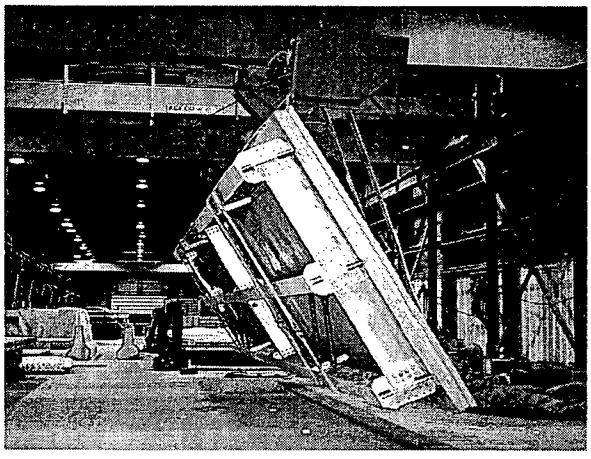
Accelerated Repair and Construction Technologies

The need for accelerated repair and construction is clearly evident when considering urban environments. Traffic growth in cities throughout the country has reached levels so significant that mobility disruptions occur any time that activities are initiated. It becomes difficult to close lanes to repair a structure without causing extremely large traffic disruptions, even in the late evening hours or overnight. Rapid repair techniques are required to strengthen a structure within a shortened time-frame in order to minimize traffic disruption and the associated impacts on mobility and commerce. These techniques should also minimize the potential for future interventions by improving long-term performance. Consider that, today, a new segment of highway typically takes years to construct – sometimes as many as 10 years for a 10 mile stretch of pavement with 5 bridges on it; why can't this be decreased to 1 year or even 6 months using innovative design, contracting, and construction approaches?

It is for this reason that the current FHWA "mantra" is to "get in, get out, and stay out." A number of studies have been performed in recent years intended to address the needs of accelerated repair and construction. This has culminated in a focused program supported both

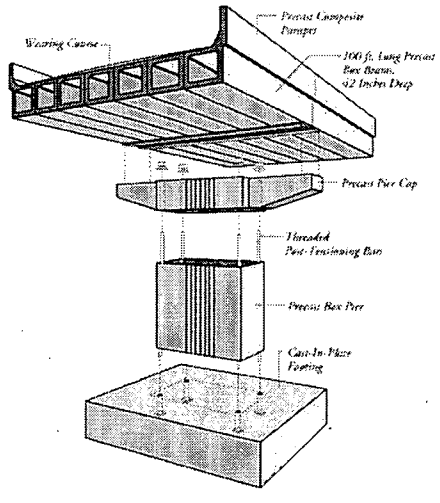
by FHWA and AASHTO in accelerated repair and construction. From a bridge technology standpoint, much of the current effort is on the appropriate application of high performance materials, smart foundation construction technologies, and prefabricated bridge components and systems.

High performance materials typically include high performance concrete (HPC), high performance steel (HPS), and fiber reinforced polymer (FRP) composites. High performance does not necessarily mean, nor does it necessarily exclude, properties that relate to high strength; high performance does, however, include properties that relate to significantly improved constructability, durability, and resistance to environmental and vehicular degradation.



HPC and HPS members and structures can be made lighter and possibly simpler than those comprised of conventional concretes and steels, thereby easing construction and facilitating rapid application. These advanced structural materials can also be engineered to eliminate problems with the traditional materials; e.g., with increased density or lower permeability which reduces chloride intrusion, or with improved weldability and increased fracture toughness. HPC members can be constructed with rapid-curing properties, allowing structures to be opened to traffic more quickly, thereby minimizing the impact on the traveling public.

FRP composites, which are used extensively in aerospace and military structural applications, are making inroads into the civil and bridge engineering infrastructure. In its FRP composite research program, FHWA seeks to advance the technology for new construction, rehabilitation and preservation, and strengthening of the existing structural inventory. FRP composite bridge decks and structural members are typically much lighter, and can be preassembled to facilitate construction. The use of the FRP materials for repair and strengthening of structural concrete members is increasing and, when properly designed and applied, can be effective and efficient.



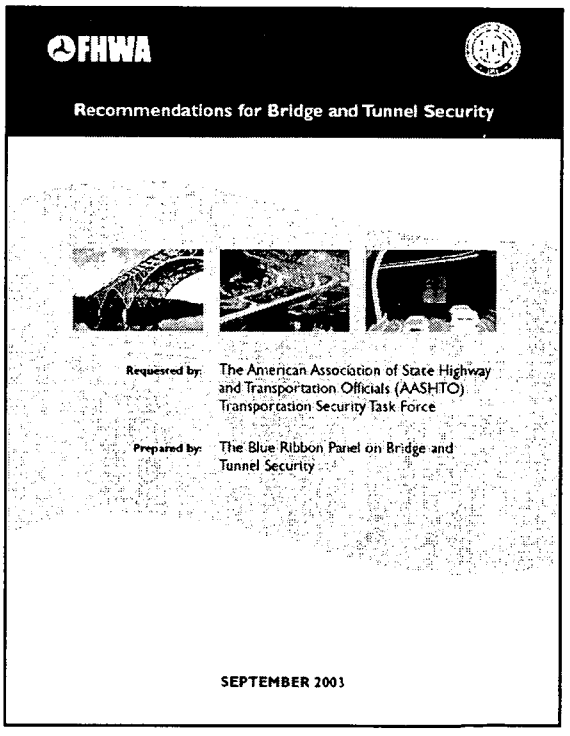
For a growing number of States, the use of

prefabricated bridge elements and systems is also helping to achieve reduced traffic and environmental impacts, enhanced safety, improved bridge constructibility, and accelerated project completion. Prefabricated bridge elements, which range from bent caps to deck panels, and superstructure and substructure systems, are manufactured under controlled conditions and brought to the construction site ready to install. Prefabricated elements are particularly useful in situations where traditional cast-in-place construction would have to be sophisticated and expensive; e.g., at long water crossings or complex interchanges. Prefabrication also facilitates construction in urban settings, where work space is limited. Safety is improved and traffic impacts are lessened because some of the construction is moved from the roadway to a remote site, minimizing the need for lane closures, detours, and use of narrow lanes.

Bridge and Tunnel Security

For bridge engineers, protecting bridges and other structures used to mean guarding against such processes as fatigue, scour, and earthquakes. The events which occurred on September 11, 2001, changed all that as engineers are now also faced with the challenge of how to protect structures from potential terrorist attack. Bridge and tunnel engineers throughout the United States are being asked to assess the vulnerability of their structures, and to provide solutions to reduce this vulnerability. To equip engineers to answer these new and complex questions, FHWA has launched a number of structural security initiatives.

Among these is a workshop developed in cooperation with the U.S. Army Engineer Research and Development Center (ERDC). For the past 35 years, the ERDC has carried out structural vulnerability research and development work, which has included numerous full-scale explosive tests on bridges and tunnels, the analysis of complex structural data, and developing appropriate computer design and analysis tools. FHWA and the ERDC have created an ongoing workshop series intended to train FHWA, State, and private sector engineers on topics which range from bridge and tunnel vulnerability to explosive attack, structural response to blast-induced loadings, and vulnerability predictive tools and mitigation methods.



The FHWA has also been working in partnership with AASHTO under the flag of the FHWA/AASHTO Blue Ribbon Panel on

Bridge and Tunnel Security. The panel is developing short- and long-term strategies for increasing the security of critical bridges and tunnels, including implementing design and retrofit techniques, and is identifying current and future research needs. Opportunities exist for research to better understand blast loading and the effectiveness of retrofit techniques, the development of enhanced risk analysis procedures, introduction and use of information technologies to mitigate and prevent damage due to terrorist activities, and other areas to reduce the threat and the exposure. The results of this effort will be used to establish a roadmap for prudent, cost-effective measures to make our transportation system more secure.

The report of the Blue Ribbon Panel was recently completed, and has been posted on the FHWA web site at http://www.fhwa.dot.gov/bridge/security/brp.pdf

Bridge System Preservation

With an aging bridge population, appropriate decisions must be made regarding when and what type of maintenance is required for a large number of bridges; and whether rehabilitation or replacement is a more appropriate strategy for other bridges. In order to address this need, rigorous decision support systems are required and more detailed and detailed bridge inspection information is required. The FHWA has been performing research in these areas for a number of years and, through this effort, many new applications have been developed and implemented. Research continues to be conducted in order to enhance current bridge management system decision support systems and to develop and implement inspection technologies that provide improved characterization of structural damage.

Improved bridge and tunnel inspection technologies are being developed via the Non-Destructive Evaluation Validation Center (NDEVC), which is located at the FHWA's Turner Fairbanks Highway Research Center. With more accurate, non-contact and non-destructive inspection techniques, damage can be characterized at earlier stages so that life- and performance-preserving corrective actions can be taken. Among recent techniques for quantitative, non-subjective non-destructive evaluation of bridges which have been developed through the NDEVC are:

- Ultrasonic systems which send waves into the material to detect cracks;
- Eddy current testing which creates a magnetic field that opposes the magnetic field of the original material – locations of cracks will appear where the created impedance diverge;
- Bridge acoustic emission Local Area Monitoring, which can be used to track known defects, whether corrective measures are working, and to monitor structural integrity of welds and connection points;



- Laser measurement technologies to track the deformation of material under stress;
- Ground-penetrating radar is being tested for application in bridge deck inspections to identify areas of delamination; and
- Active thermographic crack detection which detects changes in temperature when heat is applied to a material – these temperature changes are a result of cracks which allow the escape of heat.

A number of other activities are also underway at FHWA to support bridge system preservation strategies. Research to develop technologies which provide relatively simple repairs for deteriorated or cracked concrete or steel members has been an ongoing program for many years. Improvement of and support for bridge management systems and approaches is an important part of the FHWA bridge program.

To support the bridge system preservation initiative, FHWA and AASHTO jointly sponsored an international scanning tour in the spring of 2003. The FHWA/AASHTO Panel on Bridge System Preservation and Maintenance, which was comprised of ten members representing AASHTO, FHWA, State transportation agencies, the National Association of County Engineers, and academia, traveled to the African and European continents and met with highway agency representatives, and bridge management and inspection technology practitioners and researchers, from South Africa, Switzerland, Germany, France, Denmark, Sweden, Finland, Norway, England, and Wales. Specific topics of interest addressed during the scanning tour included:

- Organizational, policy and administrative issues including: relationship among agencies (national, local); organization of their bridge activities (design, construction, operation, inspection); inventory ownership and management; inventory characteristics (number, type, materials, span lengths); and inspection type, frequency, and rigor;

- Status of their Bridge Management Systems (BMS) including: economic modeling and forecasting; deterioration modeling; and information technology (databases, architecture, input, and updating);

- Inspection issues and practices including: typical practices; innovative methods; use of non-destructive evaluation (NDE) technologies; use of load testing; design for inspection (e.g., accessibility) and "smart" bridges; and

- Operations issues and practices including: permit vehicles; load rating and load posting; indicators of performance and their relationship to design, maintenance, repair, and enforcement.

A number of important policy and operational issues that could have a significant impact on U.S. bridge management practices were identified during the scanning tour, and will be further evaluated and discussed with appropriate U.S. bridge owning and operating agencies.

Included in these are: setting a rational bridge inspection frequency based on bridge type and consequence risk; defining minimum bridge inspector qualifications and training; development of integrated highway structure management approaches which include bridges, tunnels, free-standing retaining walls, sign and light structures, etc.; and, application and use of appropriate waterproofing systems for bridge deck protection.

The AASHTO/FHWA Panel is currently preparing a draft report documenting the findings of the Scanning Tour, which should be ready for dissemination and technology implementation by AASHTO and the FHWA near the end of 2003.

Implementation of Load and Resistance Factor Design

The bridge engineering profession is currently moving to the Load and Resistance Factor Design (LRFD) philosophy. The AASHTO LRFD Bridge Design Specifications employ state-of-the-art analysis and design methodologies, and make use of load and resistance factors based on the known variability of applied loads and material properties. The load and resistance factors contained in these specifications are calibrated from statistics obtained from the inventory of existing bridges, and are intended to provide a uniform level of safety. Bridges designed with the LRFD Specifications should therefore lead to a higher level of serviceability and maintainability.



As LRFD will positively impact the safety, reliability, and serviceability of newly designed bridges, AASHTO has set a transition date of October 2007 by which time all new bridges must be designed with the LRFD Specifications. The FHWA has therefore developed a strategic plan to assist and facilitate State transitioning to LRFD by the 2007 target date. This strategic plan includes:

- Identifying past, current, and future LRFD implementation plans of States;
- Identifying and deploying a showcase of successful LRFD implementation approaches by States which have completed their transitioning;
- Developing a model implementation plan and guidelines that can be used by States to identify and prioritize items to be accomplished for successful LRFD implementation; and to make decisions, set priorities, determine actions, and review performance on a regular basis;
- Providing hands-on implementation and transition planning assistance that assists a State in initiating its detailed implementation planning process;
- Developing two comprehensive design examples – one each for a steel and concrete bridge;

- Deploying technical LRFD design training to States;
- Developing detailed, hands-on courses, to be delivered by the FHWA's National Highway Institute;
- Compiling and maintaining a comprehensive list of LRFD resources (books, software, courses, etc.); and
- Supporting LRFD research.

A wealth of information supporting LRFD transition activities can be found on the AASHTO LRFD website at http://lrfd.aashtoware.org

STAKEHOLDER INVOLVEMENT IN FHWA RESEARCH AND TECHNOLOGY

Stakeholder involvement is critical to the success of both the short- and long-term research and technology deployment efforts undertaken by the FHWA. Past efforts to involve stakeholders in bridge research and technology programs has been somewhat ad hoc in nature, although there have been fairly high levels of involvement over time. Current efforts within FHWA are focused on the creation of a more structured and proactive mechanism to ensure adequate stakeholder involvement in research agenda setting, research progress and output monitoring, metrics for measuring success, and in the effective deployment of new technologies.

FHWA's research and technology stakeholder model assumes the following characteristics: that involvement is strategic rather than tactical; long-range rather than immediate; continuous rather than periodic; provides a process that is open, visible, and transparent; and is representative of broad range of stakeholders and needs. We are looking to involve recognized leaders in bridge research and technology deployment, provide an equal voice for all participants, ensure proactive participation in the process, and for stakeholders to provide additional insights on issues of a technical, operational, political, user constraint, and cost basis.

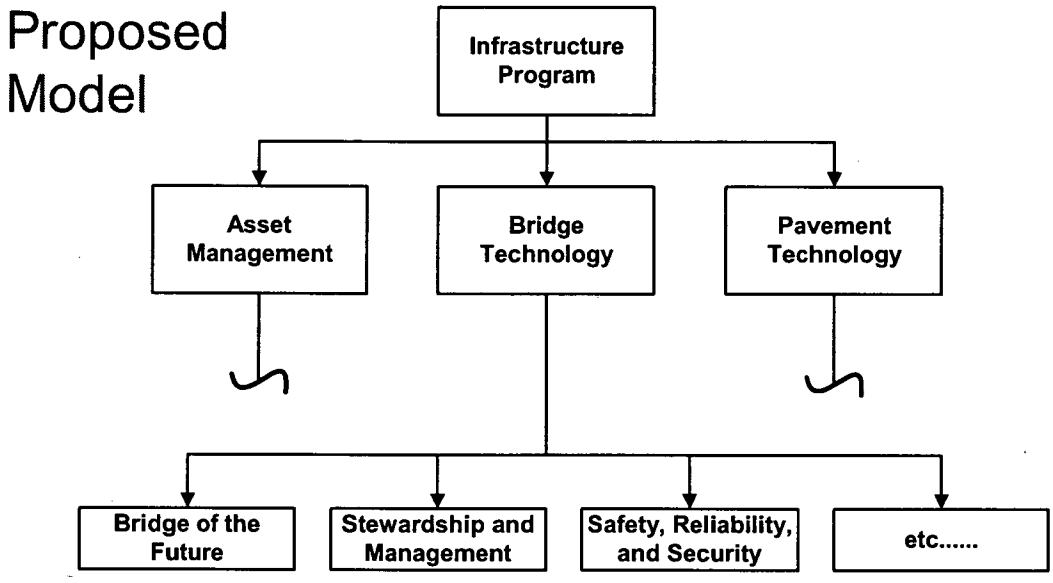
FHWA envisions the role of stakeholders in its research and technology programs as:

- Providing focus and direction for the program via a peer review process;
- Identifying needs and gaps, opportunities, and innovations;
- Setting priorities;
- Evaluating quality and value; and
- Identifying champions to assist in new technology deployment.

However, this is an evolving stakeholder involvement model and process, and there are still a large number of unresolved issues and concerns which must be addressed before the process is finalized. Among these are:

- The level and source of funding necessary to support research and technology activities, stakeholder involvement, and FHWA staff time;
- The amount of time and level of effort which will be required of stakeholders and FHWA staff;
- The size, representation, and rotation rules for stakeholder committees; and
- Whether this stakeholder structure is operated by FHWA, TRB, AASHTO, or another organization to ensure independence and effective interaction.

The FHWA is currently encouraging the bridge engineering stakeholder communities to share their thoughts regarding our proposed stakeholder involvement model.



CONCLUSION

The need for a focused highway bridge and tunnel research and technology program cannot be understated. With significantly escalating demands and reduced resources, "business as usual" is not sustainable. The FHWA has a number of high priority bridge engineering technology development and deployment areas, of which four are briefly described herein: (1) accelerated repair and construction, (2) bridge and tunnel security, (3) bridge system preservation, and (4) implementation of load and resistance factor design.

The drivers for these bridge technology programs are the needs of the bridge engineering stakeholder community. It is recognized that all of these programs require a high level of stakeholder involvement, which can provide input on the broad range of research and technology deployment activities. Among the areas for inclusion of stakeholders are: policy

and agenda setting, project scoping, merit review, research evaluation, and deployment and implementation.

Field Tests of RC Deck Slabs Deterioration Assessment System by Digital Images

Shinya Okada[1] , Kenji Ikeda [2], Kazunori Watanabe [3]
Hiroshi Koide[4], Masakazu Uekita[5]

1. Abstract

Currently, there is a strong call for development of a bridge management and maintenance system that extends the service life of bridges in a rational and effective manner. In this study, we focused on deterioration of concrete slab of steel bridges due to cracking, the damage to which is exacerbated by increases in heavy vehicle traffic and by the application of anti-freezing agent. For this study, we developed the "RC Deck Slab Deterioration Assessment System" (hereinafter *the System*), which fully utilizes digital image processing technology. Our five development objectives were: 1) elimination of scaffolding used for inspection and its associated cost; 2) reduction of time expended for field inspection; 3) quantification of and normalization of deterioration assessment results; 4) improvement of tractability of changes resulting from the passage of time since the completion of the bridge, and 5) use of digital information.

This paper reports on the System's applicability to bridges in service and its cost effectiveness.

2. Evaluation of applicability

Conventionally, detailed inspection on cracking of concrete slab have been made directly with the naked eye: an inspector positioned on scaffolding performs a close-range visual examination to measure lengths and widths of cracks and to judge degree of deterioration. Diagrams of the crack patterns are then made. With the System, images of the lower surface of deck slab are recorded by digital camera from a distance, a diagram of the cracking is generated from the images, and the level of deterioration of the deck slab is assessed.

In this study we report on surveys conducted with the System on some bridges in service. These surveys were carried out to evaluate the System's accuracy of assess

[1,2,3] Structures Section, Civil Engineering Research Institute of Hokkaido, Independent Administrative Institution
[4] 4th System Division, Nikon Systems Inc.
[5] Disaster Management Dept., Docon Co., Ltd.

-ment. This study compares examples of the System's deterioration assessments with those of conventional detailed close-range direct visual inspections capable of attaining a high level of accuracy. Direct visual inspection was made using the scaffolding set up to re-paint the bridge. The comparisons were made on following items:

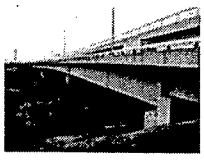
1) Accuracy of assessments of deterioration due to cracking
2) Work efficiency in terms of the total time required for both fieldwork and lab work

The bridges in our survey were chosen from those that tend to have damage to deck slab: urban viaducts exposed to heavy traffic, and mountain bridges subjected to heavy application of anti-freezing chemicals.

3. Outline of subject bridges

Viaduct A lies on a section of National Highway 5, which forms a part of Sapporo Shindo, an arterial of the city of Sapporo (population 1.8 million). Some parts of Viaduct A have been repaired for cracking of the deck slab. Bridge B is built on National Highway 274 in Sapporo. The section of National Highway 274 where Bridge B is located is also a part of Sapporo Shindo. Bridges on Sapporo Shindo near Bridge B have undergone replacement of deck slab concrete. Bridge C is on the scenic National Highway 230 in a mountainous area within the Sapporo city limits. Despite its suburban location, Bridge C has heavy traffic. The peak season for tourism brings heavy congestion.

Table 1 Surveyed Bridges

Name	Bridge type	Year of completion (year)	Age (years)	Length (m)	Span lengths (m)	Traffic volume (vehicles / day)	Interval of main girders (m)	Slab height (m)
Viaduct A	 Continuous steel girder bridge with non-composite slab	1971	32	429	4@32.8 ~9@33.0	43,407	3.4	0.22
Bridge B	 Steel composite girder bridge	1979	24	548	43.059 +43.070,other	59,190	2.8	0.21
Bridge C	 Continuous steel girder bridge with non-composite slab	1969	34	48	2@23.65	23,397	3.4	0.19

4. Deterioration Assessment via the System

4-1 Assessment criteria for deck slab deterioration

As the deterioration assessment criteria for the System, we used "Repair and Rehabilitation of RC Deck Slab of Road Bridges" (Apr. 1976, Monthly Report of Civil Engineering Research Institute, Hokkaido Development Bureau). This is one set of assessment criteria used with detailed close-range direct visual inspections. Deterioration level is classified by quantitatively evaluating crack opening width, crack spacing and crack index. The nine categories of deterioration are: no cracks (level 0); early stages (levels 1 and 2); intermediate stages (levels 3 and 4); terminal stages (levels 5 and 6); and failure (levels 7 and 8). Table 2 outlines each deterioration level.

Level		Condition of cracks			
		Cross cracking	Spacing L(m)	Cracking index p(m/m2)	Notes
	(0)	No	-	-	No cracking
Early Stage	(1)	No	L≧LG	0.5≧p	Scattered parallel cracks.
	(2)	No	LG>L≧0.5	2.0>p>0.5	Scattered parallel cracks. Generation of free lime and slurry.
Medium Stage	(3)	Yes	LG>L≧0.5	3.0>p≧2.0	Generation of cross cracks in two directions.
	(4)	Yes	0.5>L≧0.3	5.0>p≧3.0	Linking of cracks generating an alligator crack.
Terminal Stage	(5)	Yes	RP≧L	5.0≧p	Alligator cracks. Crack spacing becomes small.
	(6)	Yes	RP≧L	5.0≧p	Alligator cracks. Small scale spalls occur.
Breakdown	(7)	Yes	RP≧L	5.0≧p	Alligator cracks. Spalling occurs. (Delamination about to occur.)
	(8)	Yes	RP≧L	5.0≧p	Delamination of concrete.

Crack width: equal to or over 0.1 mm, LG: interval of main girders, RP: reinforcement pitch

Table 2 Criteria for Deterioration Assessment

4-2 Assessment of deterioration

Following are the results of the System's assessment of deck slab deterioration. The panels in our survey were located on and near the intermediate supports, where damage tends to occur.

4-2-1 Viaduct A

One of slab panels of Viaduct A was evaluated with the System. First, we traced the cracks from digtal images of the panel. The automatically calculated cumulative length of the cracks was 58.5m. Based on the spacing between cracks and crack index, the panel was evaluated to have a deterioration level of 4.

<Assessment by the System> Deterioration level 4

Following is the System's computer output.

Panel No.	Deterioration level	Crack width (mm)	Crack spacing (m)	Crack index (m/m²)	Cumulative crack length (m)	Spalling area (m²)
Panels 19 - 22	4	0.1	0.363773	3.183892	58.456254	0

<Calculated from the System's output>

Interval of main girders: LG = 3.40 m

Interval of diaphragm: B = 5.40 m

Slab area: $A = 3.40 \times 5.40 = 18.36\ m^2$

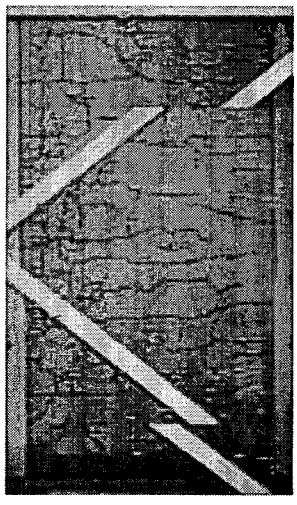
Crack spacing: L = 0.36 m

Cumulative crack length: $\sum L = 58.45m$

Crack index: $p = 58.45 / 18.36 = 3.18\ (m/m^2)$

<Assessment results>

Following is the deterioration level determined by manually consulting Table 2 with the above values calculated from the System output.



Cross cracks

Crack spacing: $0.3\ m \leq L < 0.5\ m$

Crack index: $3.0\ m/m^2 \leq p < 5.0\ m/m^2$

Deterioration level: 4 --- This assessment result conformed to the assessment produced by the System automatically.

4-2-2 Bridge B

Two slab panels of Bridge B were evaluated for their slab deterioration using the System. Example 1 has a cumulative crack length of 9.12 m, which was calculated automatically. Based on the spacing between cracks and the crack index, the panel was judged to have a deterioration level of 2.

Example 1

<Assessment by the System> Deterioration level 2

Following is the System's computer output.

Panel No.	Deterioration level	Crack width (mm)	Crack spacing (m)	Crack index (m/m²)	Cumulative crack length (m)	Spalling area (m²)
Panel 2	2	0.1	1.623063	0.638485	9.117565	0

<Calculated from the System's output>

Interval of main girders: LG = 2.80 m

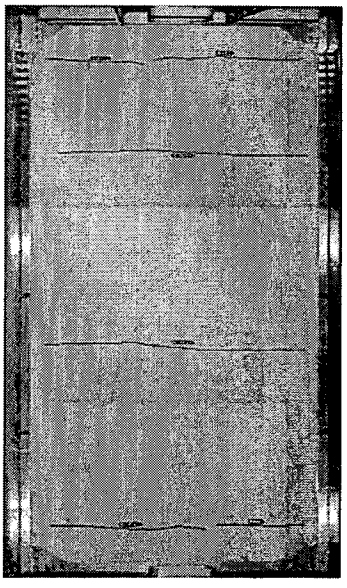
Interval of diaphragm: B = 5.10 m

Slab area: A = 2.80 × 5.10 = 14.28 m^2

Crack spacing: L = 1.62 m

Cumulative crack length: $\sum$ L = 9.12 m

Crack index: p = 9.12 / 14.28 = 0.64 (m/m^2)



<Assessment results>

Following is the deterioration level determined by manually consulting Table 2 with the above values calculated from the System output.

Parallel cracks

Crack spacing: 0.5 m ≤ L < LG

Crack index: 0.5 m/m^2 ≤ p < 2.0 m/m^2

Deterioration level: 2 --- This assessment result conformed to the assessment produced by the System automatically.

Example 2

<Assessment by the System> Deterioration level 4

Following is the System's computer output.

Panel No.	Deterioration level	Crack width (mm)	Crack spacing (m)	Crack index (m/m²)	Cumulative crack length (m)	Spalling area (m²)
Panel 4	4	0.1	0.435554	3.478134	49.667758	0

<Calculated from the System's output>

Interval of main girders: LG = 2.80 m

Interval of diaphragm: B = 5.10 m

Slab area: A = 2.80 × 5.10 = 14.28 m^2

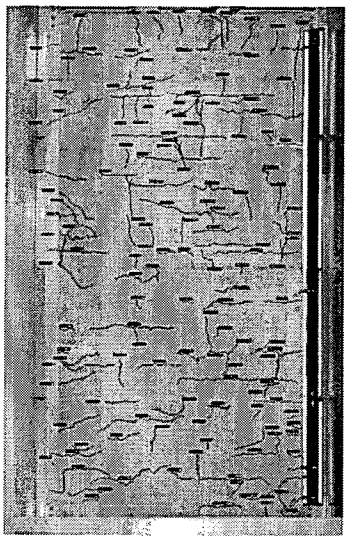
Crack spacing: L = 0.44 m

Cumulative crack length: $\sum$ L = 49.67 m

Crack index: p = 49.67 / 14.28 = 3.48 (m/m^2)

<Assessment results>

Following is the deterioration level determined by manually consulting Table 2 with the above values calculated from the System output.



Cross cracks

Crack spacing: 0.3 m ≤ L < 0.5 m

Crack index: 3.0 m/m^2 ≤ p< 5.0 m/m^2

Deterioration level: 4 --- This assessment result conformed to the assessment produced by the System automatically.

4-2-3 Bridge C

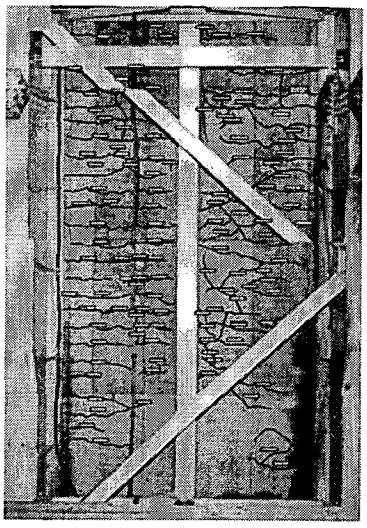
One panel of deck slab of Bridge C was examined with the System for slab deterioration. After the cracks were traced, the cumulative crack length was calculated automatically to be 52.88 m. Based on the spacing between cracks and crack index, the panel was judged to have a deterioration level of 4.

<Assessment by the System> Deterioration level 4

Following is the System's computer output.

Panel No.	Deterioration level	Crack width (mm)	Crack spacing (m)	Crack index (m/m²)	Cumulative crack length (m)	Spalling area (m²)
12~15	4	0.1	0.435319	2.800588	52.875098	0

<Calculated from the System's output>
Interval of main girders: LG = 3.20 m
Interval of diaphragm: B = 5.90 m
Slab area: A = 3.20 × 5.90 = 18.88 m^2
Crack spacing: L = 0.44 m
Cumulative crack length: $\sum$ L = 52.88 m
Crack index: p = 52.88 / 18.88 = 2.80 (m/m^2)
<Assessment result>
Following is the deterioration level determined by manually consulting Table 2 with the above values calculated from the System output.



Cross cracks
Crack spacing: 0.3 m ≤ L < 0.5 m → Deterioration level 4
Crack index: 2.0 m/m^2 ≤ p< 3.0 m/m^2 → Deterioration level 3
Selecting lower evaluation level: Deterioration level: 4 --- This assessment result conformed to the assessment produced by the System automatically.

5. Deterioration assessment via close-range direct visual inspection

An inspector performed a detailed, close-range, naked-eye inspection at Viaduct A, where scaffolding installed for re-painting was available.

5-1 Procedure for direct visual inspection

When a detailed direct visual inspection from a short distance is carried out, most of the work time is expended at the bridge site. Figure 2 gives the flow and contents of direct visual inspection.

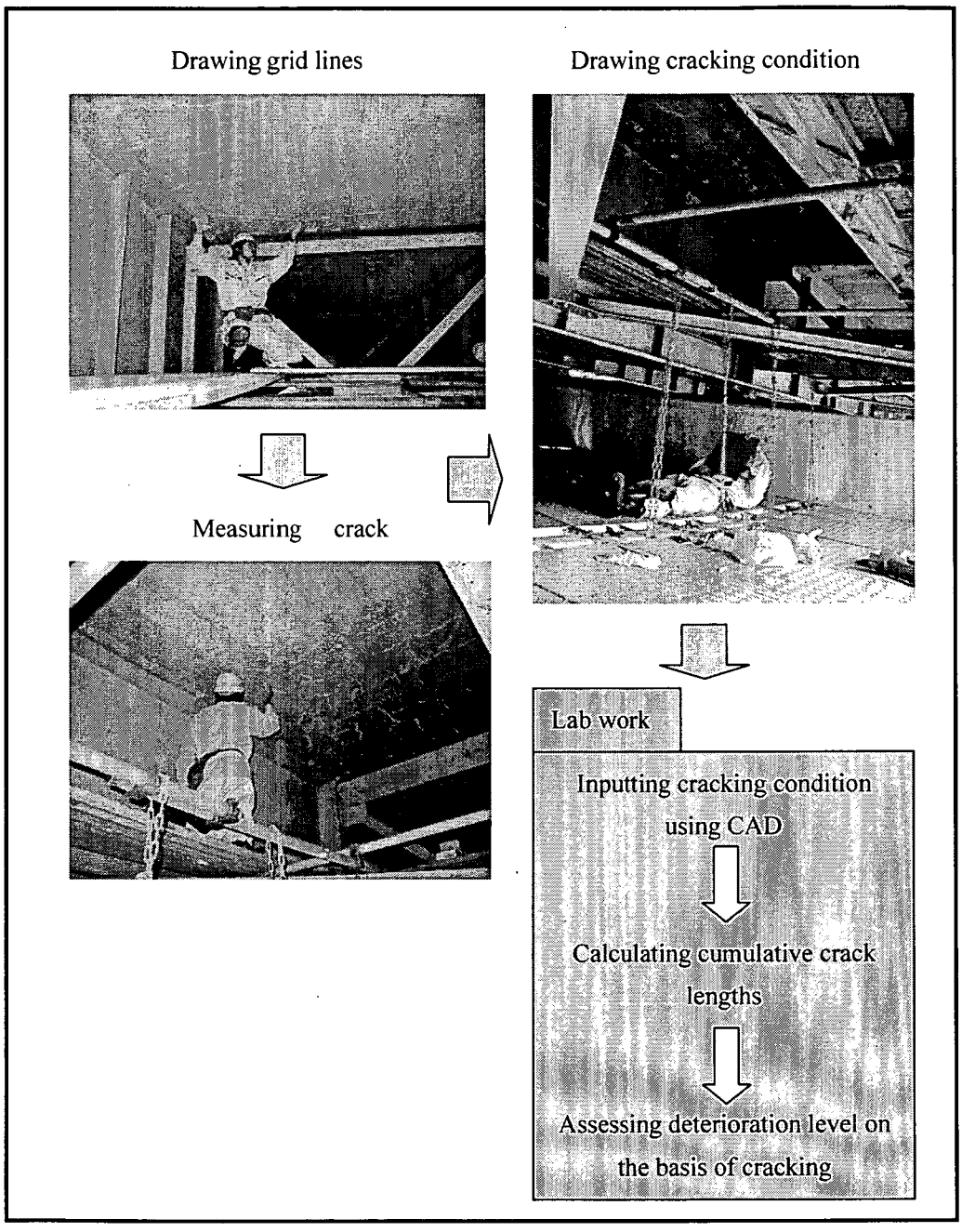


Figure 1 Work Flowchart of Close-range Direct Visual Inspection

5-2 Results of deterioration level assessment

By measuring the crack lengths on the diagram made by the inspector, cracks of widths exceeding 0.1 mm had a cumulative length of 75.04 m. Based on crack spacing and crack index, the panel was judged to have a deterioration level of 4. The assessment results and a photograph of the observed deck follow (Figure 2).

<Assessment results>

Following is the deterioration level determined by manually consulting Table 2 with the above values calculated from the System output.

Interval of main girders: LG = 3.40 m

Interval of diaphragm: B = 5.40 m

Slab area: A = 3.40 × 5.40 = 18.36 m^2

Cracks in two directions

Crack spacing: L = 0.3 m: 0.3 m ≤ L < 0.5 m

Cumulative crack length: $\sum$ L = 75.04 m

Crack index: p = 75.04 / 18.36 = 4.09 (m/m^2): 3.0 m/m^2 ≤ p< 5.0 m/m^2

→ Deterioration level: 4

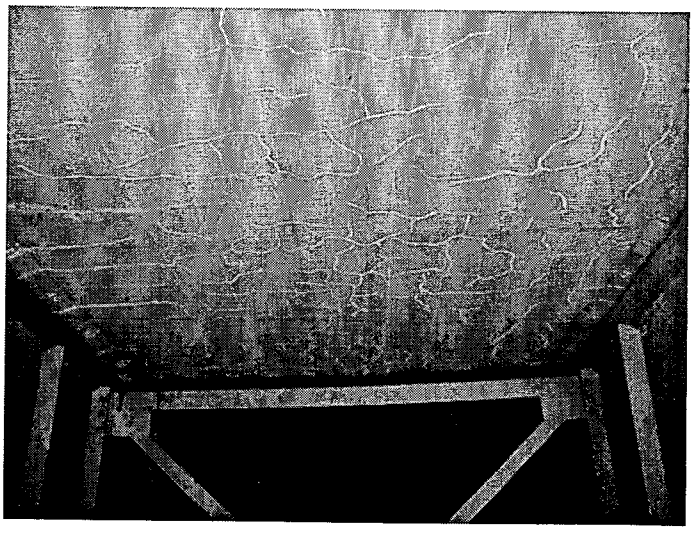


Figure 2 Photograph of the deck panel

6. Verification by Comparison

6-1 Accuracy of deterioration level assessments of cracking

Figure 3 shows the crack diagrams produced from close-range direct visual inspection and those produced by the System. As indicated in Section 5, the cumulative crack length determined by direct visual inspection was 75.0 m, while that measured by the System was 58.5 m, where the short side of the rectangle of the angular fields is set at 2.0 m. The System had a recognition accuracy equal to 78% of that of direct visual inspection. The recognition accuracy of the System was low for cracks 0.1 mm in width. The reason is that the electronic flash made cracks on the deck slab less recognizable because the strong light eliminates shadows of cracks. Lateral bracing may have hidden some cracks during photographing. However, both results had a deterioration level of 4.

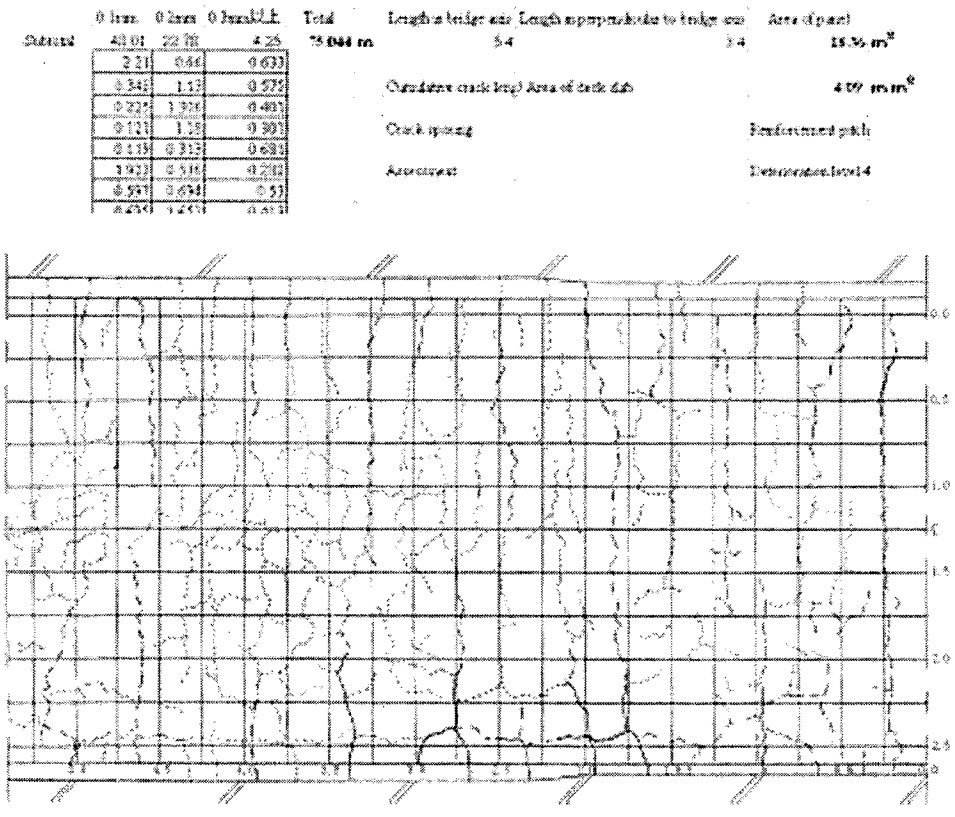


Figure 3 Crack Diagram Produced by Close-Range Direct Visual Inspection

Panel No.	Deterioration level	Crack width (mm)	Crack spacing (m)	Crack index (m/㎡)	Cumulative crack length (m)	Spalling area (㎡)
Panels 19 - 22	4	0.1	0.363773	3.183892	58.456254	0

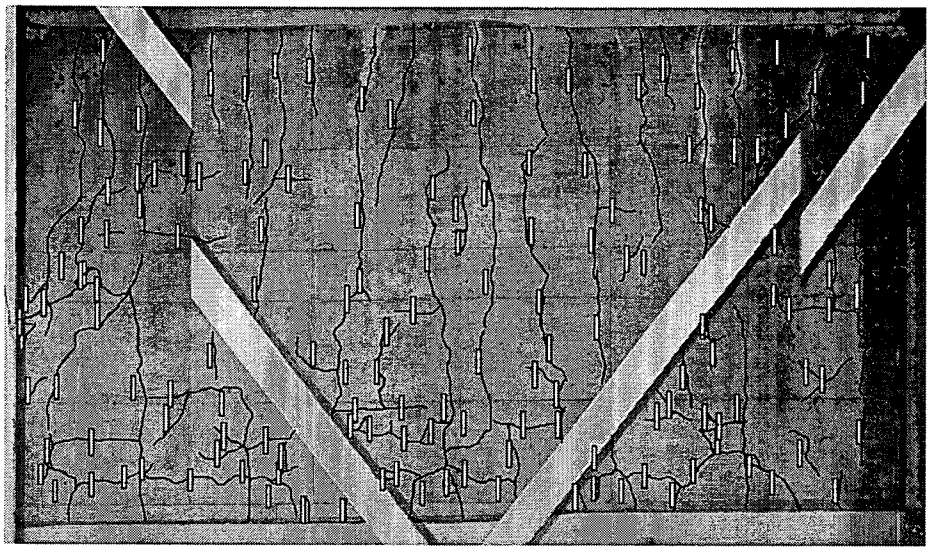


Figure 4　Crack Diagram Produced by the System

6-2　Work efficiency in terms of time

The following procedure is used for the System To assess deterioration level of deck slab. The example of time taken is assuming a deck slab of deterioration level 4.

1) The deck slab is photographed at the bridge site with digital camera, a process which takes less than
5 minutes per panel.

2) In the lab, the digital image is processed, taking about 45 minutes per panel. Cracks in the panel are traced, taking about 10 minutes per panel.

3) The deterioration level of the panel is assessed from the traced cracks, requiring only a few seconds per panel.

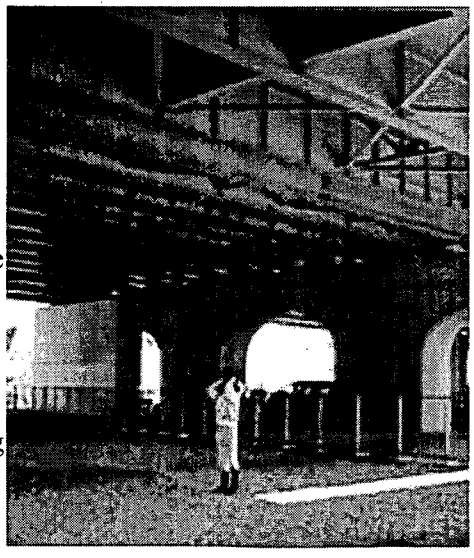


Figure 4.　Photographing the

The total time to assess one panel is about one hour.

As shown in Table 3, direct visual inspection requires about 5 hours to assess the deterioration level of one panel. To do the same work, the System takes only one hour,

one-fifth (1/5) of that of the conventional method.

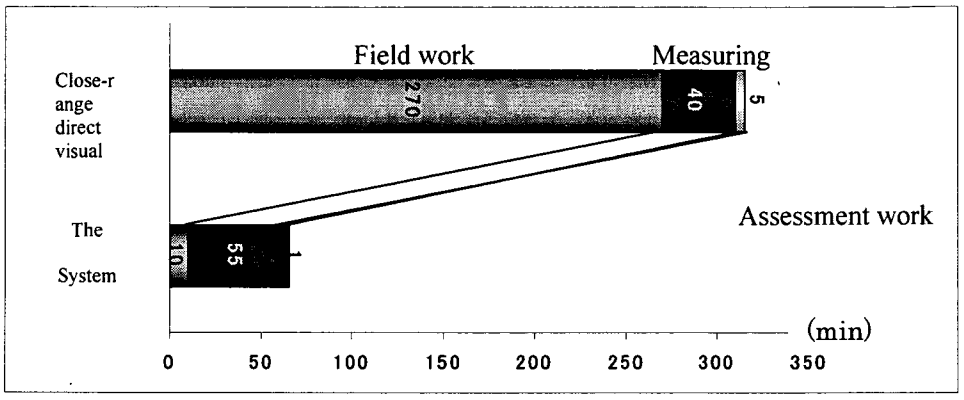


Figure 5. Comparison of Total Time

Table 3 Details of Work Hours

Close-range direct visual inspection	Field work (min.)		Measuring (person)		Assessment work (min)
Fieldwork	90	×	3	=	270.00
Measuring cracks	40	×	1	=	40.00
Assessment	5	×	1	=	5.00
					315.00

The System	Time (min.)		No. of operator (person)		Total time (min.)
Fieldwork	5	×	2	=	10.00
Measuring cracks	55	×	1	=	55.00
Assessment	1	×	1	=	1.00
					66.00

7. Conclusion

We used the System to make surveys to assess the deterioration level of bridges in service. The assessment results of the System and conventional close-range direct visual inspection agreed closely, a fact which verifies the applicability of the System. The effectiveness of the System was confirmed for the use of deterioration level assessment of deck slab cracking.

Also, the comparison of the close-range direct visual inspection and the System revealed following:

(1) Deterioration assessment of cracking

- Recognition ratio of the System was 78 % of that of the conventional inspection method. However, the location information of cracks is much more accurate than manually produced drawings because the cracks are traced from digital image.
- Recognition ratio of cracks can be improved through some additional effort during photography.
- Assessment of deterioration levels by both the conventional inspection method and the System agreed closely.

(2) Work efficiency in terms of time

- The System requires much less time for fieldwork at the bridge site. Total time is reduced to one-fifth of that of conventional visual inspection. This improvement translates into a great reduction in survey cost.
- The System does not require scaffolding to be set up. This also contributes to cost reduction.

From the survey of bridges in service, we confirmed the cost effectiveness and economic advantages of "RC Deck Slab Deterioration Assessment System" over the conventional method. We are planning to develop a manual on photographing deck slab so that the System will be extensively used, and we are aiming to further refine the System.

References

(1) H. Koide et al., "Development of algorithm for crack recognition on concrete structures," presented at the Academic Lectures Meeting on the 55th Conference of Japan Society of Civil Engineers.

(2) M. Togawa et al., "Verification of correlation between field angle and identifiable crack width on digital image," presented at the Academic Lectures Meeting on the 55th Conference of Japan Society of Civil Engineers.

(3) Y. Sasaki et al., "Development of deck slab deterioration judging system by the digital image," presented at the 55th Conference of Japan Society of Civil Engineers.

(4) "Maintenance Control of Concrete Standard Specification, 2002"Japan Society of Civil Engineers.

(5) K.Watanabe et al., "Development of RC deck slab deterioration judging system by the digital image," presented at the 18th US-Japan Bridge Engineering Workshop.

(6) S. Sasaki et al., "Development of RC deck slab deterioration assessment system by the digital image," presented at the 25th International Symposium of Japan Concrete Institute.

(7) M. Uekita et al., "Verification of RC deck slab deterioration assessment system by the digital image," presented at the 58th Conference of Japan Society of Civil Engineers.

Florida's Approach to Bridge Preservation

Ivan R. Lasa[1] and Rodney G. Powers[2]

Abstract

Corrosion of reinforcing steel in concrete bridges is a problem of major concern for entities responsible for the maintenance and safe operation of such structures. In the state of Florida in the United States, millions of dollars are spent yearly in the rehabilitation of structures due to corrosion deterioration. In this regard, the Florida Department of Transportation has adopted effective design and materials standards to delay corrosion development and has developed effective corrosion mitigation systems for older bridges where corrosion has already initiated. On older structures where corrosion has been identified as the source of deterioration, cathodic protection is used to stop the damaging corrosion effect as it is recognized that standard repairs provide only a short term solution.

This paper describes the newest materials and the design criteria used for corrosion prevention as well as various cathodic protection systems used on different structures in Florida.

Introduction

Reinforcing steel in concrete is considered the major cause of deterioration on reinforced concrete bridges in the United States. It has been reported that billions of dollars may be required to correct the corrosion damage to bridges and associated liabilities (1) that accompany this deterioration in the United States alone. On bridges, this corrosion deterioration is typically concentrated either in the substructure or the superstructure although depending on the climate and geographical location, corrosion may be present on both.

In the state of Florida, corrosion is typically concentrated on the substructure of the bridges due to their proximity to corrosive marine environments. Experience as well as research has made it very clear that standard rehabilitation methods such as patching or application of pneumatic concrete are not adequate remedial actions as these are only

[1] *Corrosion Mitigation and Rehabilitation Technologist, Florida Department of Transportation, 5007 NE 39th Avenue, Gainesville, FL, US*

[2] *State Corrosion Technologist, Florida Department of Transportation, 5007 NE 39th Avenue, Gainesville, FL, US*

performed as quick repairs and do not provide the long term rehabilitation needed. Furthermore, often the corrosion activity develops at higher rates due to the changed characteristics of the repaired areas. Other standard repairs such as pile jacketing or encapsulation, aggravate the condition of the structure by hiding on-going corrosion deterioration from visual detection, thus new damage is likely to be undetected or underestimated[2]. This is of major concern due to the possible severe structural consequences (Figure 1).



Figure 1: Spalling and rebar cross-sectional loss on a bridge piling due to corrosion.

Typically, in chloride contaminated concretes, the passive steel surrounding a corroding area develops potentials that, although considered corrosion potentials (more negative than -0.350v – ASTM C876), are cathodic to the potential of the corroding area. As a result, active corrosion does not take place around the spall. In fact, the rebar at the corroding spot prevents or slows down the initiation of corrosion in the surrounding concrete. When the concrete is repaired, the new deteriorating effect of localized patching or jacketing as previously mentioned, makes the steel passive and its potential becomes less negative. The new passive potential in the repaired area now becomes cathodic to the formerly passive surrounding zones and active corrosion promptly develops in the surrounding zones leading to a "ring" or "halo" damage effect around the patch. Results of a federally (US-FHWA) funded project conducted on one of these highly contaminated bridges and on which several repair materials were evaluated, concluded that new corrosion damage was produced on repairs using all types of repair materials in less than 4.5 years [3]. The new deterioration occurred not in the repaired area, but on the original concrete adjacent to the repair.

After over twenty years of evaluation of the corrosion behavior on marine structures and vast experimentation with new materials for corrosion prevention and corrosion control, the Florida Department of Transportation (FDOT) has developed design criteria that provides an estimated corrosion free service life on these structures of over 75 years. These estimates are based primarily on chloride diffusion coefficients of the concrete and the depth of concrete cover over the reinforcement. For older structures where corrosion has already developed, the Department considers that cathodic protection is the only means to properly rehabilitate these structures and significantly increase their service life. Cathodic protection has been installed on over sixty bridge structures statewide with very successful results. The experience acquired has improved the process of matching systems to site conditions, allowed for the consideration of short and long term economic factors, and advanced the monitoring techniques of these cathodic protection systems. This paper describes the approach and criteria developed for new construction as well as some of the most implemented cathodic protection systems for marine structures.

Discussion

Corrosion Prevention

Corrosion prevention criteria have been implemented as part of the general structures design guidelines for the state. These criteria are mostly directed toward the long term durability of the structures and have been established as an independent design parameter that needs to be incorporated into the general structural design norms. All structures owned by the Florida Department of Transportation are designed following these guidelines.

Table 1: Corrosion Classification of Soils and Water for Substructures

A.	Slightly Aggressive: when all of the following conditions exist: 1) PH greater than 6.6 2) Resistivity greater than 3,000 ohm-cm 3) Sulfates less than 150 ppm 4) Chlorides less than 500 ppm
B.	Moderately Aggressive: This classification must be used at all sites not meeting requirements for either Slightly Aggressive or Extremely Aggressive Environments.
C.	Extremely Aggressive: when any of the following conditions exists. 1) For concrete structures: pH less than 5.0 2) For steel structures: pH less than 6.0 3) Resistivity less than 500 ohm-cm 4) Sulfates greater than 1,500 ppm 5) Chlorides greater than 2,000 ppm

The first task under the criteria is the identification of the potential for development of corrosion activity at the site where the structure is going to be built. The task consists of measuring the chloride and sulfate content, the pH, and the electrical resistivity of the water and/or soil at the site. Three corrosion classifications have been established based on these measurements: a) Slightly Aggressive b) Moderately Aggressive c) Extremely Aggressive. Requirements for a site to meet any of the classifications are based on all of the above mentioned measurements (see Table 1). Specific test procedures for the measurement of each of the above mentioned parameters have also been established.

Based on the final classification of the site, established guidelines are incorporated into the final design. This process ensures that appropriate corrosion prevention methods are used in the design.

Different parameters are given for the corrosion classification of substructures and superstructures based on the conditions that are particularly applicable to each. The parameters for the superstructure include, in addition to the above, the distance from the site to other high corrosive atmospheric environments such as pulp and fertilizer plants, or other similar industries (Table 2). Also, if the new structure is replacing an existing one, evaluation

Table 2: Corrosion Classification for Superstructures

A.	Slightly Aggressive; Any superstructure situated in an environment that is not classified either Moderate or Extremely Aggressive
B.	Moderately Aggressive; Any superstructure located within 0.76 km (2,500 ft) of any coal burning industrial facility, pulpwood plant, fertilizer plant or any other similar industry where, in the opinion of the District Materials Engineer, a potential environmental corrosion condition exists, or any other specific conditions and/or locations described.
C.	Extremely Aggressive; Any superstructure situated in an area such that a combination of environmental factors indicate that significant corrosion potential exists, or with specific conditions and/or locations described.

of the chloride contamination of the old structure is allowed to determine the final classification for the new superstructure.

For structures at sites classified as extremely aggressive, the cast-in-place concrete requirements include (in addition to standard good construction practices); a) a minimum rebar cover ranging from 76 to 114 mm (3 to 4.5 in), depending on type of component, b) the use of high performance concretes containing flyash, calcium nitrite and/or microsilica ,

Table 3: Structural Concrete Class for Specific Uses (Structures Design Guidelines) *

CONCRETE LOCATION AND USAGE	ENVIRONMENTAL CLASSIFICATION		
	Slightly Aggressive	Moderately Aggressive	Extremely Aggressive
Superstructure	*Concrete Class*	Concrete Class	Concrete Class
Cast-in-Place (Other Than Bridge Decks)	Class II	Class IV	Class IV
Cast-in-Place Bridge Decks (Including Diaphragms)	Class II (Bridge Deck)	Class IV	Class IV
Approach Slabs	Class II (Bridge Deck)	Class II (Bridge Deck)	Class II (Bridge Deck)
Precast or Prestressed Components	Class III, IV, V, or VI	Class IV, V, or VI	Class IV, V, or VI
Substructure			
Cast-in-Place (Other Than Bridge Seals)	Class II	Class IV	Class IV or V
Retaining Walls	Class II or III	Class IV	Class IV
Cast-in-Place Seals	Class III (Seal)	Class III (Seal)	Class III (Seal)
Precast or Prestressed (Other Than Piling)	Class III, IV, V, or VI	Class IV, V, or VI	Class IV, V, or VI
Cast-In-Place Columns Located Directly in the Splash Zone	Class II	Class IV	Class V
Piling	Class V Special	Class V Special	Class V Special
Drilled Shafts	Class IV (Drilled Shaft)	Class IV (Drilled Shaft)	Class IV (Drilled Shaft)

* *See Table 4 for description of the various concrete mixes.*

c) a minimum elevation of the superstructure of 3.6 m (12 ft) from the water level. For structures located in slightly or moderately aggressive classifications, the requirements for the cast-in-place concretes include: a) a minimum rebar cover ranging from 76 to 102 mm (3 to 4 in), depending on type of component, b) the requirement for high performance concrete is retained, but the use of the corrosion inhibitor is relaxed.

For precast bridge pilings under all environment classifications, a high performance concrete containing microsilica with a minimum concrete cover of 76 mm (3 in) is required.

Several high performance concretes have been developed for different uses (Table 3). The properties of these concretes have been enhanced to provide higher structural capacities as well as extended durability. Because the major cause of corrosion in Florida is the exposure to the marine environment, the enhanced durability mostly consists of a higher resistance to chloride penetration. The compressive strength of these concretes range from 38 MPa (5,500 psi) to 59 MPa (8,500 psi). The water cement ratio is kept in the range of 0.37 to 0.41 for aggressive corrosion environments and 0.41 to 0.49 for slightly and moderately aggressive sites (Table 4).

Table 4: Characteristics of Several Concrete Classes

	Class of Concrete	Compressive Strength MPa (psi)	Water-Cement Ratio	Min. Total Cement kg/m^3 (lb/yd^3)	Target Slump mm (in)	Max. Chloride kg/m^3 (lb/yd^3)
Standard Concretes	II (Standard)	23 (3,400)	0.49	335 (564)	75 (3)	0.20 (0.34)
	II (Bridge Deck)	31 (4,500)	0.44	365 (611)	75 (3)	0.20 (0.34)
	III (Standard)	35 (5,000)	0.44	365 (611)	75 (3)	0.20 (0.34)
	III (Seal)	21 (3,000)	0.52	365 (611)	200 (8)	0.20 (0.34)
	IV (Drilled Shaft)	28 (4,000)	0.41	390 (658)	200 (8)	0.20 (0.34)
High Performance Concretes	IV (Standard)	38 (5,500)	0.41	390 (658)	75 (3)	0.20 (0.34)
	V (Special)	41 (6,000)	0.37	445 (752)	75 (3)	0.20 (0.34)
	V (Standard)	45 (6,500)	0.37	445 (752)	75 (3)	0.20 (0.34)
	VI	59 (8,500)	0.37	445 (752)	75 (3)	0.20 (0.34)

These design criteria have been in place for over fifteen years with yearly updates as materials and technology improve. Several of the older structures built under these guidelines have been evaluated and found still in a corrosion free stage.

Corrosion Control

For structures built under previous or no specific durability design guidelines, the preservation approach relies on providing adequate corrosion control such that the structure will not become structurally deficient due to corrosion damage. For most older structures,

when rehabilitation is sought, extensive corrosion damage already exists although a few (based on available budget) are provided with corrosion control as preventive maintenance. Typically, a structural analysis of the damage is performed and the corrosion control measures are implemented incorporating the necessary structural repairs such as rebar replacement and concrete restoration.

Cathodic protection is the only effective, long term corrosion control method recognized by the Florida Department of Transportation at this time. The technique of cathodic protection is based on electrically polarizing the most anodic areas present on a metallic corrosion cell (rebar) to a potential that is cathodic in relation to an anode specifically placed on or about the structure. Typically, this anode is placed externally to the structure but in some cases, anodes embedded in the concrete are also used (for CP of reinforced concrete structures). Standard NACE (National Association of Corrosion Engineers) norms based on the measurements of the potential of the rebars are used to determine the effectiveness of the cathodic protection being applied without visually inspecting the rebar for corrosion [4]. These standards are used by FDOT to monitor and evaluate the performance and ensure adequate protection.

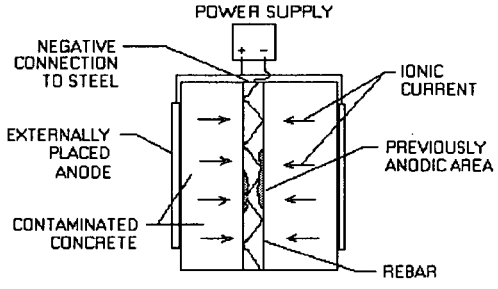


Figure 2: Protection mechanism of impressed current cathodic protection on reinforcing steel.

The Florida Department of Transportation has a rather vast history in the development and evaluation of cathodic protection anodes and anode systems for reinforced concrete. Several of these systems have become a standard corrosion control measure for reinforced concrete structures and are discussed below. The cathodic protection systems to be discussed include galvanic (sacrificial) anode as well as impressed current systems. The galvanic systems use a metal higher in energy than the steel to provide the cathodic protection current while the impressed current types use an external power source to produce the current.

The impressed current systems consist of: 1) titanium mesh anode cast into structural concrete, 2) titanium mesh anode embedded in gunite, and, 3) titanium mesh anode cast into pile jackets. The galvanic anode systems include: 1) zinc mesh anode cast into pile jackets and, 2) sprayed zinc anodes.

The system components will be briefly described in the following subsections. Most of the systems have already been previously reported [5] and are commercially available.

Titanium Mesh Anode Embedded in Gunite

The titanium anode is an expanded catalyzed titanium wire mesh with an external coating of mixed metal oxides. These anodes are capable of current outputs of up to 37.8 mA/m^2 (3.44 mA/ft^2) of protected concrete without adversely affecting the manufacturer's specified service life of 75 years. The anode mesh is typically installed on the structure by attaching the mesh directly to the existing concrete surface at the areas to be protected using plastic fasteners (Figure 3). The mesh is provided in 1.2 m (4 ft) wide rolls which can be spliced to larger widths by resistance welding two mesh panels to a strip of flat titanium bar. A strip of the flexible titanium bar also extends outside the protected area for connection to the wires originating at the rectifier. Following installation on the existing concrete, the anode is embedded in gunite at a depth of 5.1 cm (2 in).

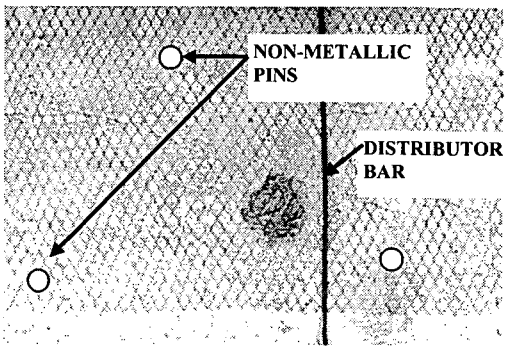


Figure 3: Titanium mesh anode installed over existing concrete surface. Mesh is then encapsulated in gunite or concrete.

The first system of this type evaluated by FDOT was installed in 1988 on a bridge pier at the Howard Frankland Bridge in Tampa, Florida. The pier is comprised of three square footer type pile caps, three rectangular columns, and two struts (Figure 4). The bottom portion of the footers come in direct contact with the tidal waters during the periods of high tide while columns and struts are frequently wetted by the splash activity. Although the system was designed as a single circuit system, reference electrodes were provided for each pier component (footers, columns, and struts) such that potentials could be monitored individually for each zone. This system was designed by the anode manufacturer who additionally provided quality control during construction.

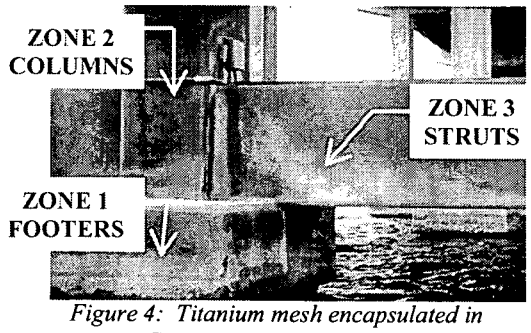


Figure 4: Titanium mesh encapsulated in gunite. Connection wires are routed outside the Gunite and directed in conduit to a rectifier.

After installation, the system was energized using the E Log I criterion (NACE Criterion) which determined the amount of current needed for cathodic protection. Voltage potential data gathered during the entire evaluation period indicated satisfactory cathodic protection levels even though after the first six months, the gunite placed at the elevation in direct contact with the water, partially delaminated from the original concrete surface. The delamination was attributed to the physical properties of the gunite material which could not provide a good bond to the existing concrete surface in moisture saturated conditions. It was determined

however, that even though partial delamination of the gunite occurred, protection current was being discharged through the salt water and the reinforcement potentials maintained cathodic protection values. The delamination problem was corrected for later installations by identifying a more suitable gunite material. After 14 years of service, the system is still in operation and no further corrosion has been detected.

Routine testing of this cathodic protection system includes depolarization tests which typically produce average polarization decays ranging from 132 to 214 mV. At this time, this type of system is recommended for bridge components (typically mass concrete components) not in direct contact with tidal waters. Similar systems were installed on the substructures of the Banana River Bridge in 1996 and the Sebastian Inlet Bridge in 2002, both located on the East coast of Florida.

Titanium Mesh Anode Cast Into Structural Concrete

The anode used for this system is the catalyzed expanded titanium mesh anode identical to that described in the previous section. This system is typically used on bridge mass concrete components which require structural rehabilitation due to degradation related to inadequate reinforcement, settlement, and/or corrosion of the original rebar. This system combines structural rehabilitation with corrosion control. Installation of the system requires the removal of all existing delaminated concrete and cleaning of the remaining concrete surface and exposed reinforcing steel. If present, remaining cracks in sound concrete are filled with mortar grout and the catalyzed titanium mesh anode is installed over the concrete surface similar to the gunite encapsulation system. Reinforcing steel encasement is then placed around the component being rehabilitated as dictated by the required structural repair (Figure 5). Forms for the new structural jacket are placed and the concrete is cast around the deteriorated component encapsulating the anode and the new steel. Electrical isolation between the existing and the new reinforcing steel is maintained such that the two steel systems may be energized at different current levels since the older steel will exhibit a higher level of corrosion activity due to its' surrounding concrete.

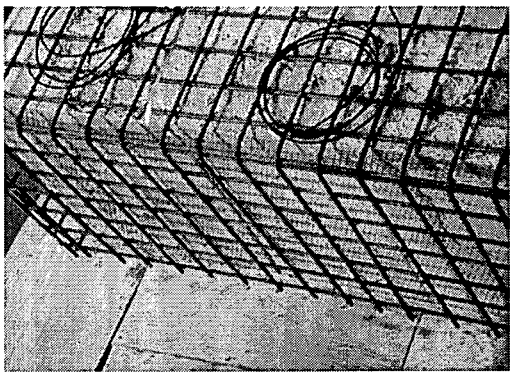


Figure 5: Titanium mesh anode installed over original concrete to be encapsulated in structural concrete.

The first of these systems was installed at Verle Allen Pope Bridge in Crescent Beach, Florida. The system was installed on eight pier footers which had experienced structural deterioration as a result of inadequate reinforcement volume. The resulting cracks allowed the intrusion of salt water into the concrete which consequently produced severe reinforcement corrosion and subsequent concrete spalling. The system design provided one constant-current/constant-voltage rectifier per pier (two footers). Connection wires to the steel were

provided such that new and existing steel could be energized separately. Only the existing steel was energized initially, while the corrosion level on the new steel was periodically monitored for connection to the system when needed.

When installation was completed, the system was energized by FDOT personnel using the E Log I criterion and performance was closely monitored. Reflective cracking in the newly placed concrete developed soon after the repairs were completed allowing salt water intrusion to the new reinforcement. After three years the footer was replaced due to structural concerns, the cathodic protection system maintained the reinforcing steel in a corrosion free condition even at the locations where the cracks intersected the rebar. This was verified by visual inspection of the reinforcement when the footer was demolished for replacement and the rebars extracted.

Following the success on this bridge, this system was incorporated to repairs on other bridges of similar configuration. On these bridges, the system was combined with structural repairs requiring structural jackets with post-tensioning. In all cases, the system has proven very effective in controlling corrosion.

Impressed Current CP Pile Jacket System

This system is specifically designed for corrosion control on bridge piles. Similar to the previously discussed systems, it is of the impressed current type and requires an external power supply to provide the cathodic protection current. The anode utilized by this system is the expanded titanium mesh anode which, in this case, is mechanically suspended on the inside face of a standard fiberglass stay-in-place form (Figure 6). The anode is positioned such that it will be located equidistant from the pile and the jacket form.

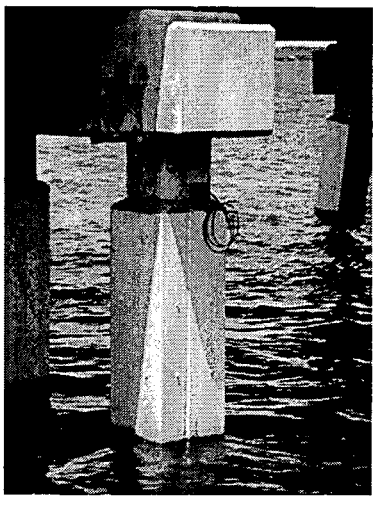


Figure 6: Titanium mesh pile jacket installed at splash zone elevation. The anode is pre-installed in the fiberglass form then placed around the pile and filled with mortar/concrete.

The concept was developed by the Florida Department of Transportation and the first system was installed on forty-four piles at the Ribault River Bridge in Jacksonville, Florida. On this project the jackets were 1.2 m (4 ft) tall and were vertically centered at high tide elevation. The system included four rectifiers installed at different locations along the length of the bridge with the ability to provide individual current output adjustment to each pile bent. Installation of the jackets consisted of removing all delaminated concrete and cleaning the remaining concrete surface and exposed steel of all marine growth or debris. Because the jackets were later filled with mortar, no concrete restoration was required. The anode jackets were installed and filled as specified, and a

conduit-wiring system was installed to provide the steel and anode connections from every pile to the rectifiers.

The system was energized using the E Log I criterion on four bents, and the -850 mV criterion on the remaining portions[6]. Effective cathodic protection was achieved as demonstrated by periodic potential depolarization tests, which indicate an average minimum polarization of 150 mV on each bent. This system was later installed on other bridges and likewise exhibited excellent performance. This system has become one of the FDOT standard bridge pile rehabilitation methods and today it has been used to provide corrosion control on over 500 piles statewide.

Sacrificial Cathodic Protection Pile Jacket

Similar to the impressed current pile jacket described above, this sacrificial anode cathodic protection system was developed jointly by the Florida Department of Transportation and a manufacturer of zinc products [1] to provide corrosion protection to bridge pilings where concrete restoration due to corrosion deterioration is required. The system protects the submerged portion of the piling, the splash area, and the area immediately above. The system consists of a standard pile jacket provided with an internally placed expanded zinc mesh anode, an additional bulk zinc anode installed at an elevation of 0.6 m (2 ft) below low tide, and a connection to the reinforcement (Figure 7). The bulk anode is used to minimize current demand on the zinc mesh anode by the reinforcement in submerged portion of the pile. If necessary, sprayed zinc can be applied to the areas above the jacket to control any corrosion activity at this elevation. The jacket is a two piece, stay-in place fiberglass form provided with the expanded zinc mesh anode pre-installed on the inside face of the form. Being of the sacrificial type, this system does not require an external power source and the anode is connected directly to the reinforcement to establish the cathodic protection circuit.

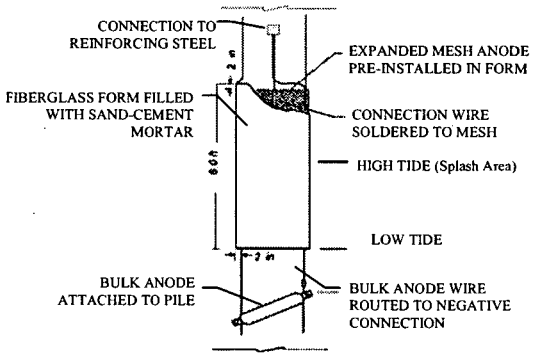


Figure 7: Schematic of sacrificial cathodic protection pile jacket with submerged bulk anode.

Installation consists of removing all delaminated concrete from the pile and clean-up of the remaining concrete as well as the exposed steel. The jacket is then placed around the pile from low water elevation upward providing a 5.1 cm (2 in) annular space between the pile surface and the fiberglass form. The bulk anode is installed below water level at the

---

[1] *Alltrista Zinc Products, Greenville, Tennessee, USA*
U.S. Patent No. 5,714,045 – Feb. 1998

specified elevation and the connection cable is routed upward inside the jacket to the anode steel connection location. The jacket is then mortar filled and the zinc mesh and bulk zinc anodes are connected to the reinforcing steel. The filling material is a portland cement-sand grout with a minimum cement content of 558 kg/m^3 (940 lb/yd^3) of grout although, concrete is sometimes used for structural applications.

Initial field evaluation was conducted by providing two standard reinforcement, pre-cast concrete piles at the Broward River Bridge in Jacksonville, Florida with the system. The piles were provided with instrumentation to measure system current and the voltage potential of the reinforcing steel. The NACE 100 mV polarization and polarization decay criterion was used to evaluate the cathodic protection performance. A polarization decay test conducted on each pile after 400 days of operation. At that time, the measured potential indicated an average polarization of 140 mV.

The cost of this system compares favorably with the cost of standard (No-CP) pile jackets when considering the added benefits of the corrosion control anode. When compared to impressed current systems, this system has the advantage of requiring only minimal monitoring and maintenance since external power supplies are not required. It is also expected that the minimum effective service life of the system will be 45 years based on the consumption rate of the anodes. This system is commercially available for various pile sizes.

At this time this system is also considered another standard rehabilitation method for bridge pilings in direct contact with salt water and has been installed on several bridges protecting over 900 piles.

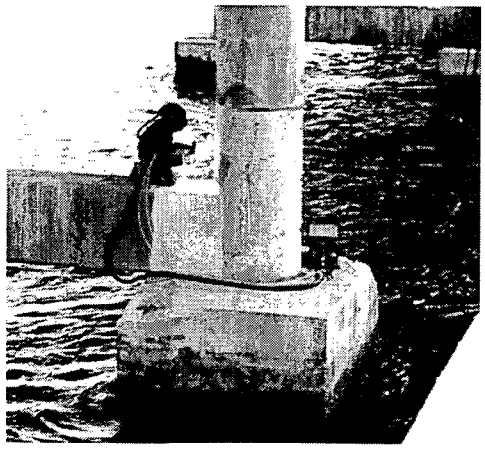


Figure 8: Arc-sprayed zinc applied to the concrete surface to produce the cathodic protection current.

Arc-Sprayed Zinc Anode System

This system is of the sacrificial anode group and it also uses zinc as the anode to provide the cathodic protection current. The potential of the zinc anode is around -1.1 volts while the potential of corroding steel is typically around -0.450 volts ($Cu/CuSO_4$). The installation consists of removing all the deteriorated concrete from the structure and sandblasting clean the surrounding concrete surface and exposed steel. The zinc is applied over the concrete surface as well as the exposed reinforcement. Spraying over the reinforcement provides the electrical connection between the zinc and the steel. In this manner, the zinc directly protects the exposed steel while the steel within the concrete receives cathodic protection current through the concrete itself (Figures 8-9).

The application process for the zinc anode is made similar to that of spray painting. A hand held gun creates an electric arc between two direct current charged zinc wires fed through the gun. The zinc melts at this point and is sprayed onto the concrete surface by an air nozzle provided at the gun. The zinc coating is applied to a thickness ranging from 0.4 to 0.5 mm (15 to 20 mils). The typical zinc to concrete bond strength is around 1,034 kPa (150 psi). This system has the ability of functioning as a sacrificial or impressed current system (no direct contact to the steel if used as impressed current), although the FDOT has only used it in sacrificial mode.

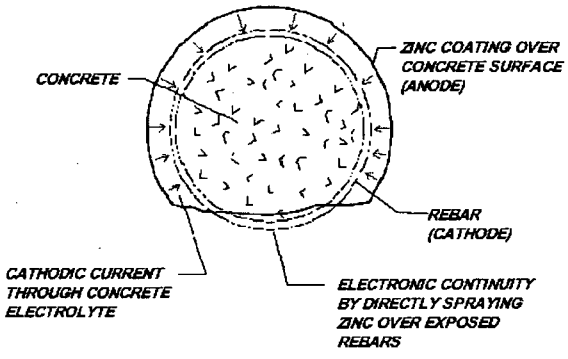


Figure 9: Current transfer mechanism of the arc-sprayed zinc system.

Initial evaluation of this system was conducted on five circular columns at the Niles Channel Bridge in the Florida Keys in 1989. The columns were 0.9 m (3 ft) in diameter and were built using epoxy-coated rebar. All of the columns exhibited advanced stages of corrosion development with significant spalling. Three of the columns were metalized and further visually evaluated and sound tested periodically to observe any corrosion progression. The other two columns were instrumented prior to metalizing such that current flow and polarization could be measured. Polarization measurements in excess of 100 mV were observed at all elevations within the metalized area on both instrumented columns. After five years, only one of the exposed bars in one of the columns exhibited some degree of corrosion progression.

The estimated service life of the anode is between five to eight years in severe environments, at which time re-metalizing is required. This system is recommended for applications not in direct contact with the water since this accelerates the consumption rate of the anode, and significantly decreases the anode service life. Additional evaluation has been performed on structures containing standard (uncoated) rebar. At this time FDOT has used this system ten bridges comprising over 32,500 m^2 (350,000 ft^2) of metalized concrete. In typical applications, the sprayed zinc anode has prevented further corrosion deterioration for more than five years on 95% of the protected components provided with this approach. In a few instances, premature consumption of the zinc was observed resulting from frequent direct exposure to salt water. Direct exposure to the water generates accelerated atmospheric corrosion of the zinc which combined with the cathodic protection consumption, rapidly depletes the zinc.

Conclusions

a. It is clear that for new construction in extremely corrosive environments, a proactive approach to prevent corrosion development provides a long term economic advantage. However, to obtain this advantage, it is necessary to correctly identify the environment prior to the design phase such that the proactive investment on higher quality materials and design practices are adequately used.

b. After more than 15 years of implementing corrosion prevention measures on new bridge structures in aggressive corrosion environments, the Florida Department of Transportation recognizes the effectiveness of these measures based on actual experience. It is recognized that the use of denser concretes significantly reduces the amount of chloride penetration, therefore delaying the onset of corrosion.

c. The Department also recognizes that the use of standard repairs in chloride contaminated concretes are only temporary remedies as new deterioration soon develops on the old concrete adjacent to new repair.

d. Because of the previous, only cathodic protection is recognized as an effective means of producing long term rehabilitation of chloride contaminated concrete structures in marine environments. Successful results have been achieved with sacrificial as well as with impressed current cathodic protection systems. Some of these systems have been in place for over 16 years and no significant corrosion has reappeared on the protected components.

References

(1) G.H. Koch, P. Virmani, J.H. Payer, "Corrosion Costs and Preventive Strategies in the United States", FHWA Report No. FHWA RD-01-156 and FHWA RD-01-157, Supplement to Materials Performance Magazine, July 2002.

(2) W.H.Hartt, M.Rapa, "Condition Assessment of Jackets Upon Pilings for Florida Bridge Substructures", Florida Atlantic University, Final Report for Project WPI 0510803, April 13, 1998.

(3) W.T. Scannell, "Evaluation of Experimental Corrosion Control Repair Strategies on Bridge Substructure Components", FDOT Interim Report, May, 2003.

(4) NACE International, "Standard Recommended Practice RP0290", 2000

(5) I.R. Lasa, R.G. Powers, R.J. Kessler, "Practical Application of Cathodic Protection Systems for Reinforcing Steel Substructures in Marine Environment", Paper presented at the International Seminar and Workshop on the Repair and Rehabilitation of Reinforced Concrete Structures, May, 1997, Maracaibo, Venezuela

(6) Martin B.L., Firlotte C.A. "Protecting Substructures in Marine Environments," NACE, Materials Performance Journal, volume 34, 1995.

Nondestructive Inspection of the Suspender Ropes in a Suspension Bridge

Hiroaki HOASHI[1], Takeshi SUGIMOTO[2]

Abstract

Two suspender ropes at Innoshima Bridge which elapsed 16 years after completion were removed and inspected to verify the state of interior corrosion. As the result, corrosion was found to be progressing inside the suspenders comparing with its surface, and the circumstances associated with the corrosion could be elucidated.

Thus, Honshu-Shikoku Bridge Authority undertook to develop the technology of non-destructive inspection of suspenders in order to perform future maintenance management rationally. From the results of examinations, it has been ascertained that the non-destructive inspection using the main flux method can verify the state of corrosion of the interior part of suspenders with sufficient precision.

1. INTRODUCTION

Innoshima Bridge is the first opened suspension bridge in the Honshu-Shikoku Bridges (1983). The suspender ropes of this bridge are center-fit-rope-core (CFRC) type, which is widely adopted in suspension bridges worldwide. The rope of this type hangs the saddle to a main cable, and is used.

Conventionally, external visual inspection has been relied upon to evaluate the soundness of the suspender ropes since no other effective method is available. Visual inspection of the Innoshima Bridge's suspender ropes, conducted in 1997, revealed rust on the external surfaces of the suspender ropes, and rusty water oozing from the rope surfaces near the sockets. In 1999, two suspender ropes were removed from the bridge, and disassembled and inspected for internal corrosion. Local corrosion was identified inside the ropes though not serious enough to have an adverse influence on the rope strength. The inspection results showed that the locations of internal corrosion did not correlate with the external appearance of the ropes, and that internal corrosion cannot be detected by external visual inspection alone.

Under these circumstances, we developed a nondestructive inspection technique that uses an electromagnetic method (main flux method) to identify internal corrosion of suspender ropes from the exterior.

This report describes the results of inspection after disassembly of 16-year-old suspender ropes of the Innoshima Bridge, and the development of the nondestructive inspection technique for suspender ropes, and the results of an investigation of the bridge by the developed nondestructive inspection technique.

1) Manager of Bridge maintenance Division, Maintenance Department, HSBA, Japan
2) Bridge maintenance Division Maintenance Department, HSBA, Japan

2. INSPECTION AFTER DISASSEMBLY

2.1 DETAIL OF INSPECTED ROPES AFTER DISASSEMBLY

Suspender ropes from the Innoshima Bridge are CFRC cables with 54 mm in diameter. **Fig 1** shows a cross-section of the rope. The rope is composed of galvanized steel wires and painted on its outer surface as specified in **Table 1**.

From the 400 locations (100 panel points) subjected to close visual inspection in 1998, the approximate center of the center span was selected as the rope sampling point, for the reason that external corrosion was severe there and that suspender ropes in the center are shorter (approximately 14 m in length) and easy to replace. Two suspender ropes were removed from this point (**see Fig 2**).

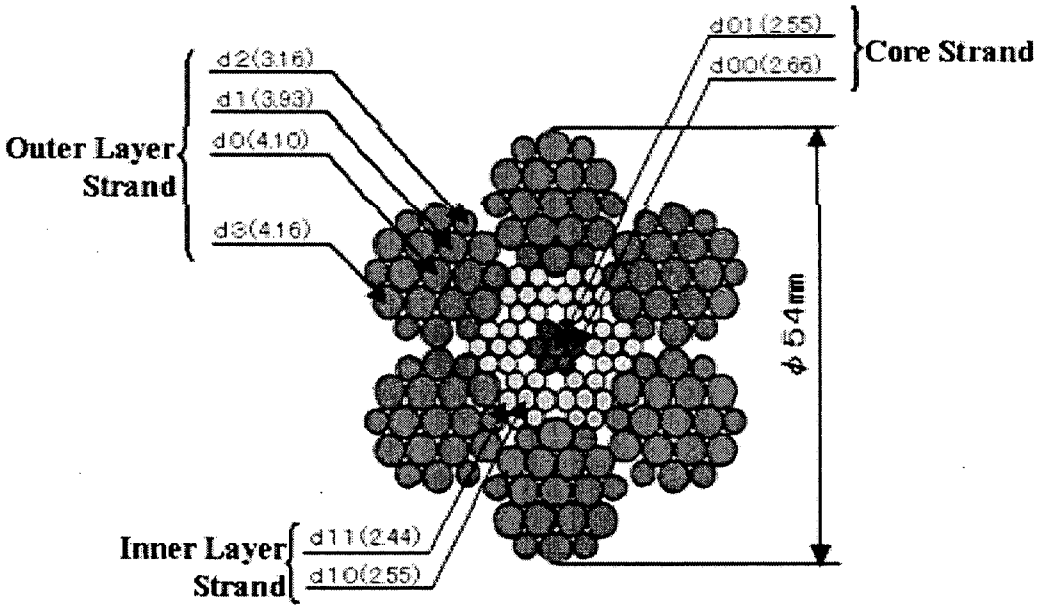


Fig 1 Cross Section of Suspender Rope

Table 1 Painting Specifications for Suspender Rope

Position of painted rope	Surface treatment	1st coat	2nd coat	3rd coat	4th coat	5th coat	Total dry coat thickness
1A - 3P (Brush-painted)	Cleaning	Chloroplane rubber calcium plumbate primer 35 μ (180g/m²)	Chloroplane rubber calcium plumbate primer 35 μ (180g/m²)	Chloroplane rubber calcium plumbate primer 35 μ (180g/m²)	Chloroplane rubbe paint (Base coat) 35 μ (160g/m²)	Chloroplane rubber paint (Surface coat) 25 μ (130g/m²)	165 μ
3P - 4A (Dipping-painted)		Thick-coating epoxy resin (Base coat) 130 μ (280g/m²)	Chloroplane rubber paint (Surface coat) 35 μ (150g/m²)	–	–	–	

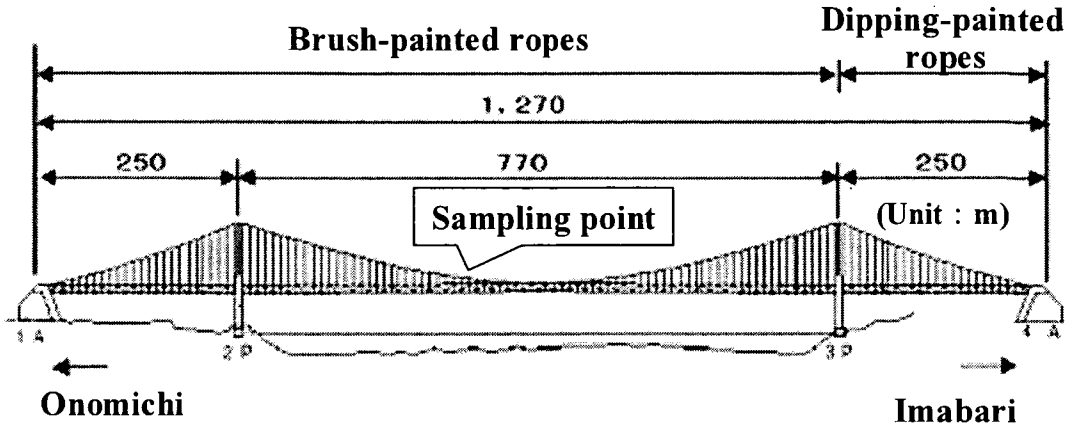


Fig 2 Sampling Point of Suspender (Innoshima Bridge)

2.2 TEST ITEMS

Table 2 shows the test items conducted after disassembly. The primary objectives of these tests are as follows:

① Determination of the internal corrosion status of the suspender ropes
② Determination of the suspender rope strengths
③ Identification of corrosion products in the case of the presence of corrosion

Table 2 Laboratory Test Items after Disassembly

	Test item		Qty.	Application
1)	Visual inspection of rope before and after paint removal		2 ropes	Entire length (Paint removed : one rope)
2)	Visual inspection of strands (Inspection after disassembly)		1 rope	One of two removed ropes
3)	Rope test	Tensile test	3 times	One of two removed ropes was divided into three parts.
4)	Wire test	・Measurement of wire diameter and difference in wire diameter ・Tensile test ・Torsion test ・Winding test ・Zinc-deposit measuring test	27 wires for each	After visual inspection of strands, three sample wires were taken from each of corroded, intact and cable band portion of outer layer, inner layer, and core strands.
5)	Microscopic inspection of cross section		36 test pieces	Nine test pieces were prepared from each of corroded, intact, cable band portion of rope, and new rope.
6)	Qualitative and quantitative analyses of corrosion products		5 times	Corroded portion of outer layer, inner layer, and core strands Intact and cable band portion of inner layer strands

2.3 RESULTS OF INSPECTION AFTER DISASSEMBLY

(1) External visual inspection of ropes before and after removal of paint

The appearance of each suspender rope removed from the bridge was visually inspected before and after removal of the paint. The results of the inspection showed the following:

① Corrosion was found at many surface areas of the rope near the sockets.
② The rope surface under paint film remained intact (free of corrosion).

(2) Visual inspection of strands

Each removed suspender rope (14 m in length) was divided into 16 sections, and each section was disassembled into strands to inspect the interior of the rope visually. Rust was observed in the range shown in **Fig 3**. Close inspection revealed the following:

① The rope sections near the sockets remained intact though corrosion in these sections had been anticipated from overseas reports on corrosion.

② The core and inner strands corroded along the entire circumferential surfaces as shown in **Photo 1**.

③ Although the exterior side of each outer layer strand that has been protected by paint remained intact, corrosion was present on the interior side that had been in contact with the inner layer strands.

④ The strands of the cable band portion remained intact since the rope was entirely caulked.

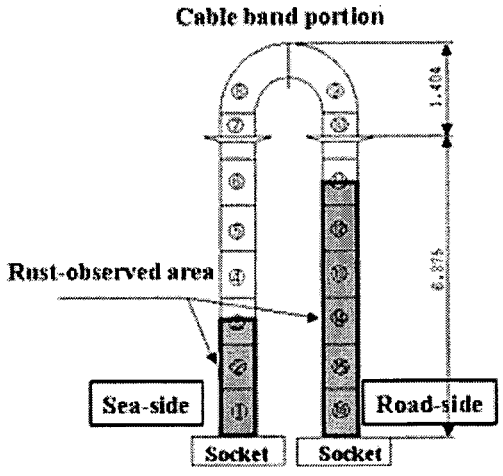


Fig 3 Development Picture of Suspender Rope

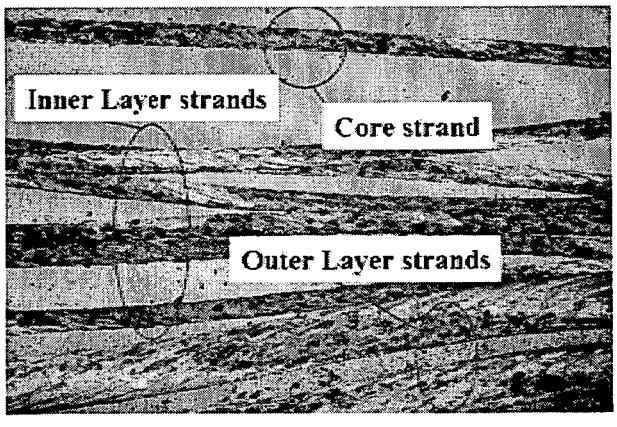


Photo 1 Corrosion of Each Strand

(3) Rope test

Table 3 shows the tensile test results of suspender ropes. The breaking load was far higher than the minimum breaking load (1,942 kN), and not lower than the average breaking load (2,246 kN) measured at the time of the rope's manufacture. That was, no drop in tensile strength was confirmed. However, initial wire-breaking noise was heard immediately before rope breakage, in the non-corroded strand, which was the cable band portion, and corroded strand was heard earlier.

Investigation of rope wires broken in the tensile test showed that the wires in the non-corroded cable band portion were broken uniformly at their approximate centers, while those in the rope sections with corrosion were broken at various locations.

Table 3 Tensile Test Result of Rope

	Length (mm)	Breaking load (kN)	Elongation (mm)	Elongation percentage (%)	Load for initial breaking noise(kN)
Sea-side	3, 330	2, 220	215. 3	6. 5	1, 608
Cable band portion	3, 330	2, 273	258. 3	7. 8	2, 256
Road-side	3, 330	2, 249	222. 7	6. 7	2, 010

Note) "Load for initial breaking noise" refers to the load at which wire breaking noise is heard for the first time during tensile test.

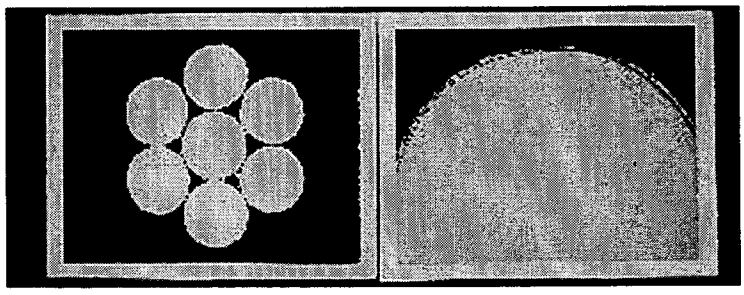
(4) Wire tests

To be subjected to the wire tests, d3 wires were sampled from an outer layer strand, d11 wires from an inner layer strand, and d01 wires from the core strand, in each of intact, cable band, and corroded sections of suspender ropes. All wires sampled from the strands in intact and cable band sections remained virtually unchanged in tensile strength. However, the tensile strength of wires from the inner layer and core strands in the corroded section had decreased below the standard value. And also, corroded wires had dropped in ductility.

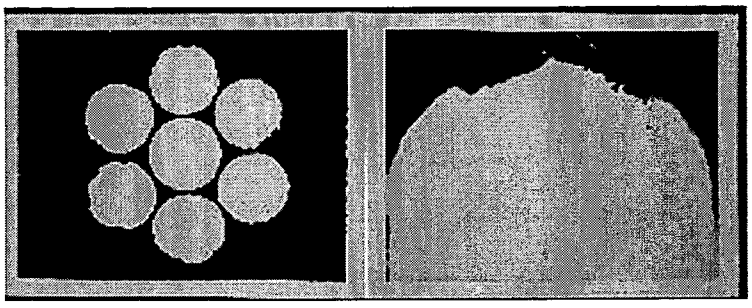
(5) Microscopic inspection of cross-section

The cross-section of each suspender rope was microscopically observed to determine the corrosion status. **Photo 2** shows the cross-sections of intact and corroded core strand sections.

The plating on the intact core strand section is partly reduced in thickness, presumably due to friction between strands when they were twisted to form the rope. The corroded core strand cross-section shows the occurrence of corrosion on the exterior side (in contact with the surrounding inner layer strands).



(a) Intact Core Strand Portion



(b) Corroded Core Strand Portion

Photo 2 Microscopic Photograph of Cross Section

(6) Qualitative and quantitative analyses of corrosion products

Corrosion products were qualitatively and quantitatively analyzed using electron probe microanalysis (EPMA) and X-ray diffract meter (XDM) techniques. Specimens were prepared by scraping the surfaces of the outer layer, inner layer and core strands of corroded sections, and the inner layer strands of intact and cable band sections. **Table 4** and **Table 5** show the analytical results.

The EPMA and XDM analyses revealed the following:

① The residual zinc amount in terms of zinc-to-iron weight ratio determined in the EPMA, was greater in the following order: intact section > cable band section > outer layer strand in corroded section > inner layer strand in corroded section > core strand in corroded section.

② The specimens taken from the inner layer strands in intact and cable band sections contained large quantities of $Zn_5(CO_3)_2(OH)_6$ (basic zinc carbonate). Due to a protective fixed film of zinc compound formed on the surface, corrosion had progressed extremely slowly on these strands.

③ A large quantity of Fe_3O_4 (magnetite) was contained in the corrosion products of iron. This phenomenon, corrosion had progressed in an oxygen-lean environment, implies that cell of light and shade of oxygen is one of the major causes of the corrosion.

④ Sodium was detected on the outer layer strand in corroded sections; this implied that salts flying in the air had entered the rope.

Table 4 Result of EPMA (Electron Probe Micro-Analysis)

		Corroded portion (Outer)	Corroded portion (Inner)	Corroded portion (Core)	Intact portion (Inner)	Cable band portion (Inner)
○	Carbon (C)	8. 433	1. 440	1. 195	2. 764	3. 895
△	Oxygen (O)	21. 559	25. 394	24. 550	25. 262	25. 601
	Sodium (Na)	1. 736	–	–	–	–
△	Magnesium (Mg)	0. 157	0. 120	0. 184	–	0. 390
△	Aluminum (Al)	0. 191	–	–	0. 366	0. 627
○	Silicon (Si)	0. 476	0. 180	0. 194	0. 930	3. 876
○	Sulfur (S)	0. 379	0. 209	0. 190	1. 034	
△	Chlorine (Cl)	0. 925	0. 320	0. 105	0. 479	0. 367
	Potassium (K)	0. 148	0. 054	–	0. 127	0. 125
△	Calcium (Ca)	0. 725	0. 340	0. 212	0. 179	0. 818
△	Titanium (Ti)	0. 878	0. 494	0. 149	0. 531	0. 231
○	Manganese (Mn)	0. 291	0. 380	0. 385	–	–
	Iron (Fe)	30. 069	39. 248	43. 008	0. 242	0. 786
	Zinc (Zn)	33. 086	31. 820	29. 828	68. 086	62. 009
△	Lead (Pb)	0. 947	–	–	–	1. 068

Note) Weight percentage values (%) are given.
○ denotes elements contained in both paint and wire; △ denotes elements contained in paint only.

Table 5 Result of XDM (X-ray Diffract Meter) Analysis

Sampling portion	Detected crystal structure	Remark
Corroded portion (Outer Layer strand)	ZnO Fe_3O_4 α-FeOOH $Zn(OH)_2$ γ-FeOOH	① through ⑦ show the status of corrosion progressing in galvanized steel wire. ①Zn ②$Zn_5(CO_3)_2(OH)_6$ ③$Zn(OH)_2$ ④ZnO ⑤γ-FeOOH ⑥α-FeOOH ⑦Fe_3O_4 · "?" indicates that detection quantity is too small to definitely identify the crystal structure. · Zn in the intact and cable band portions presumably came from the zinc scraped off from galvanized steel wire when sample was taken. · Crystal structures are listed in the order of detection quantity.
Corroded portion (Inner Layer strand)	ZnO Fe_3O_4 α-FeOOH $Zn(OH)_2$ γ-FeOOH	
Corroded portion (Core strand)	ZnO Fe_3O_4 α-FeOOH $Zn(OH)_2$ γ-FeOOH	
Intact portion (Inner Layer strand)	Zn $Zn_5(CO_3)_2(OH)_6$ SiO_2? TiO_2? α-$K_2S_2O_7$?	
Cable band portion (Inner Layer strand)	Zn $Zn_5(CO_3)_2(OH)_6$ α-$K_2S_2O_7$? SiO_2? TiO_2?	

3. NONDESTRUCTIVE INSPECTION METHOD

Table 6 shows typical nondestructive inspection methods applicable to steel ropes, etc. The main flux method was adopted for nondestructive inspection of the Innoshima Bridge's suspender ropes since it can quantitatively evaluate the extent of corrosion in the ropes.

Table 6 Typical Non-destructive Inspection Methods

Inspection method		Characteristics	Wire breakage measurement	Corrosion measurement
Visual inspection		Assesses surface conditions only	△~○	△
Electromagnetic method	Magnetic flux leakage method	Measures local defects, such as fatigue-caused wire breakage	◎	△
	Main flux method	Measures change in cross sectional area caused by abrasion or corrosion	△~○	◎
Electromagnetic ultrasonic method		Produces elastic waves in the axial direction of rope by non-contact method, to check for reflection surface and elastic-wave attenuation	△~○	△~○
Acoustic emission method		Detects energy emission resulting from wire breakage	◎	×

Note) ◎: Certainly Possible, ○: Possible, △: Difficult, ×: Impossible

3.1 Inspection Using the Main Flux Method

The applicability of the main flux method was investigated in 1999. Consequently, the main flux method is applicable to nondestructive inspection of suspender ropes, though it provides a large measurement error at positions near ferromagnetic bodies, such as a rope anchorage zone. With the aim of reducing measurement error, solenoid type magnetizing coils were incorporated in the main flux method to improve the magnetizing capability and compensate factors that give influence to magnetic flux. This modified main flux method was used for the inspection conducted in 2000. The modified method provides four times higher magnetizing capability than the conventional method, and has substantially reduced measurement error so that it is practically usable to examine the corrosion of a suspender ropes. However, the measuring apparatus used for the inspection in 2000 is designed for measurement at the fixed points of suspender ropes, and not applicable for examining the entire length of rope. Therefore, it was not possible to locate the most severely corroded point. This measuring apparatus was improved to enable continuous examination of the entire length of rope, and the Innoshima Bridge's suspender ropes were inspected to evaluate the extent of corrosion in 2001.

3.2 Fixed-point Measurement and Continuous Measurement by the Main Flux Method

When a wire rope is strongly magnetized in the longitudinal direction, magnetic flux (the number of magnetic lines of force passing through a unit cross-sectional area) flows in the rope (**see Fig 4**). The main flux method is a nondestructive inspection technique based on the principle that the magnetic flux is proportional to a unit cross-sectional area. There are two types of main flux methods: fixed-point measurement method and continuous measurement method. The former method compares the magnetic flux in

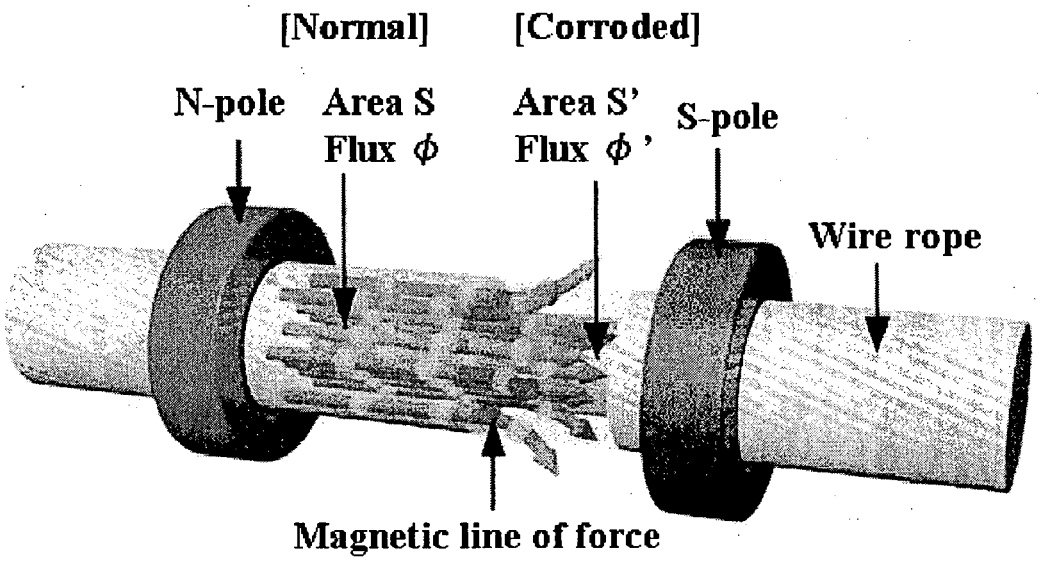


Fig 4 Principle of Main Flux Method

the approach-to-saturation region of an intact section with that of a corroded section to evaluate the extent of corrosion. The continuous-measurement method measures magnetic-flux variation at a certain magnetic field intensity. This method can locate defects along an entire length of rope and evaluate the degree of change in cross-sectional area.

3.3 Continuous Measurement Test by Main Flux Method in Laboratory

Prior to on-site inspection, laboratory testing was carried out using the continuous-measurement main flux method to evaluate changes in magnetic flux and magnetic field intensity. The measuring apparatus was moved along a 35.5-diameter rope with artificially created defects (four different patterns of changes in cross-sectional area at intervals of approximately 300 mm) to measure changes in magnetic flux and field intensity. **Fig 5** shows the results. The measured change of magnetic flux resembles the change in cross-sectional area caused by the artificial defects. The magnetic field intensity also changes at each artificial defect. These results indicate that the continuous-measurement of main flux method is effective in evaluating the extent of corrosion in suspender ropes.

The same test in laboratory was conducted on polyethylene-covered ropes, which are widely used as cables for cable-stayed bridges. The test yielded similar results without any influence on a cover and proved, proving that the continuous-measurement of main flux method was also applicable for evaluating the extent of corrosion in PE covered ropes.

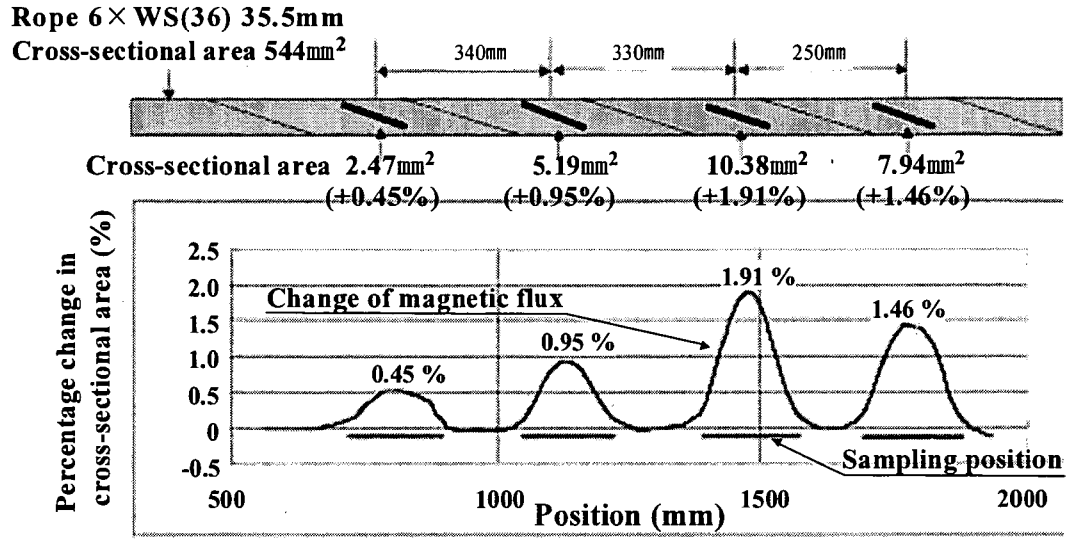


Fig 5 Result of Continuous Measurement Test by Main Flux Method in Laboratory

4. ON-SITE MEASUREMENT

Twelve suspender ropes (approximately 70 m in each length) near the main tower of the Innoshima Bridge were measured. The suspender ropes of this bridge are either brush-painted or dipping-painted. To compare the internal corrosion status between brush-painted and dipping-painted ropes, each six target ropes was selected, from the brush-painted and dipping-painted zones.

4.1 Paint Film on Suspender Ropes

Prior to the on-site measurement by the nondestructive inspection, the paint film status on the target suspender ropes was visually inspected. The inspection revealed the following:

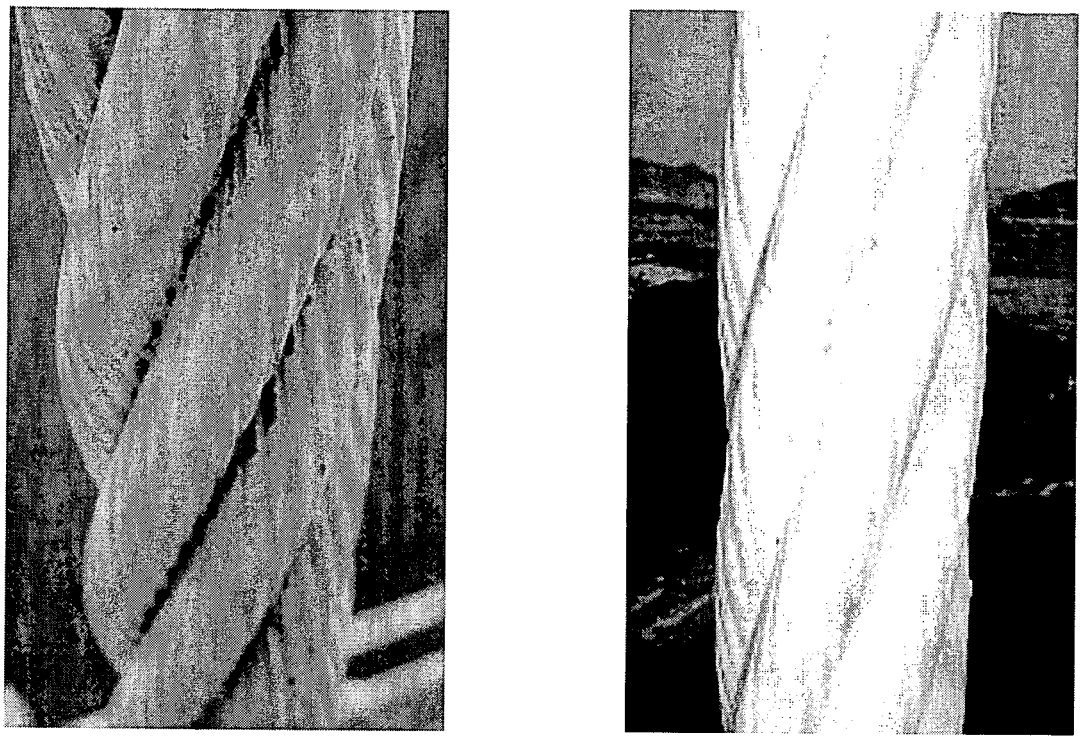
(1) Brush-painted ropes (**Photo 3(a)**)

① There were areas in which the surface coat and base coat have almost completely been lost.

② In the grooves between strands, there were areas with multiple holes, with paint film completely lost.

(2) Dipping-painted ropes (**Photo 3(b)**)

① Paint film remained in larger areas, and there were fewer quantities of holes in the grooves than on brush-painted ropes.



(a) Brush-Painted **(b) Dipping-Painted**

Photo.3 Status of Paint

4.2 Measurement Results

To evaluate the extent of corrosion, the magnetic flux in each suspender rope measured by the continuous-measurement was compared with the average magnetic flux (standard value) measured suspender ropes which had been replaced in 1999. **Fig 6** shows the results.

(1) Brush-painted ropes

① Cross-sectional area reduction was detected at two to five positions in each rope.

② The maximum decrease percentage in cross-sectional area was approximately 1.5%.

③ No positional trend could be identified regarding reduction of cross-sectional area.

④ There was no correlation between external appearance and cross-sectional area reduction of rope.

(2) Dipping-painted ropes

① Reduction of cross-sectional area was detected in the entire upper section of each rope.

② The maximum decrease percentage in cross-sectional area was approximately 2%.

③ There was no correlation between external appearance and cross-sectional area reduction of rope.

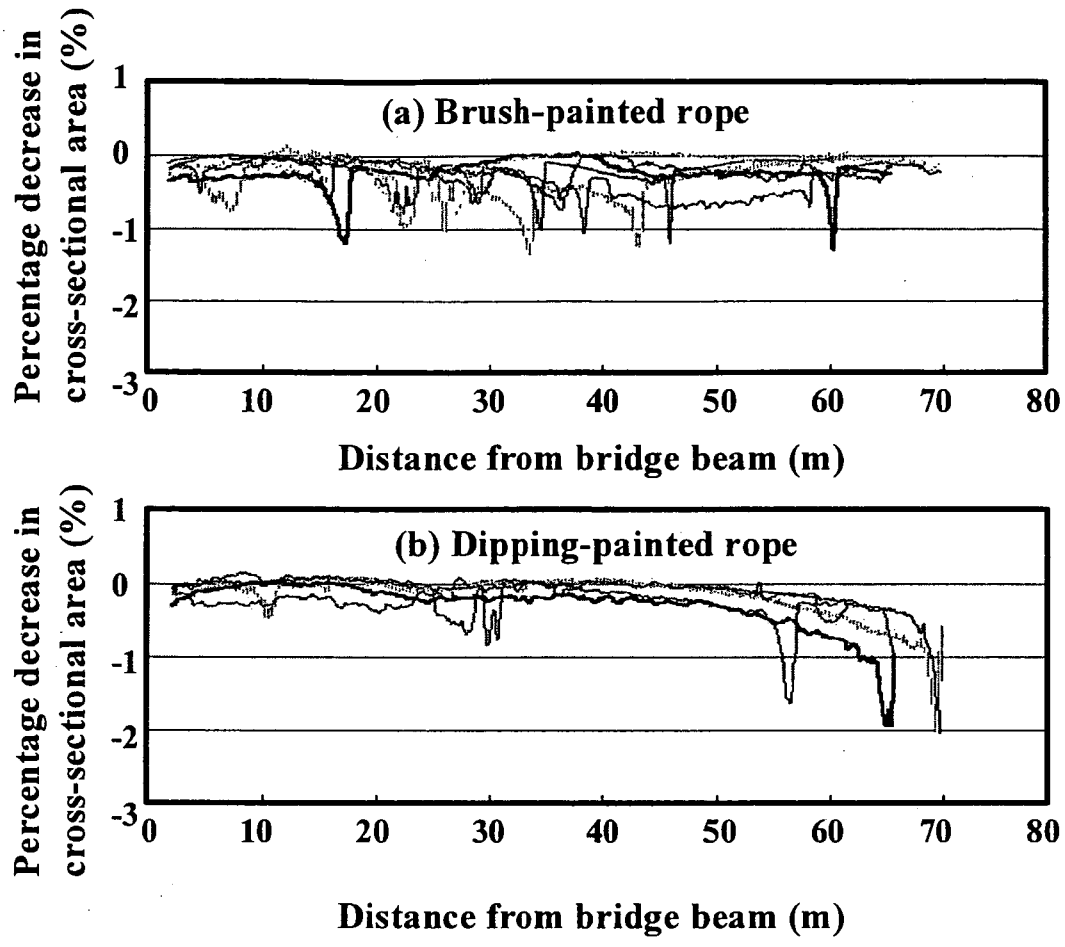


Fig 6 Result of Non-destructive Inspection

5. SUMMARY

Disassembly and inspection of suspender ropes of the Innoshima Bridge showed the occurrence of corrosion in unspecified areas inside the ropes. No correlation could be found between external appearance and internal corrosion and this indicated that the internal corrosion of ropes couldn't be detected by external visual inspection alone.

At present, the corrosion has not progressed to reduction of the safety of the bridge by the impairment of rope strength yet. However, quantitative evaluation of the internal corrosion status of suspender ropes is essential to the rational maintenance of them, and we are sure that the developed nondestructive inspection technique will be effective on management of suspender rope.

Now, Honshu-Shikoku Bridge Authority is investigating the corrosion mechanism of suspender ropes and studies for a long-life of them. And Honshu-Shikoku Bridge Authority aims at the establishment of the maintenance method of suspender rope by using this nondestructive inspection technique together.

19th US-Japan Bridge Engineering Workshop

Maintenance 2

co-Chairs:
J. Murakoshi & I. Friedland

Anti-subsidence Measure Using King-post Cables against Subsidence in A PC Box Girder with Central Hinge
T. Suzuki

Assessing Bridge Performance – When, What, How
R. Land

Experimental Studies on Retrofit by Partially Encased Concrete to the Steel I-Girder subjected to Buckling Deformation
S. Ono

U.S.A.'s Experience Using Fiber Reinforced Polymer (FRP) Composite Bridge Decks to Extend Bridge Service Life
J. S. O'Connor

Fatigue Life Extension of Damaged RC Slabs by Strengthening with Carbon Fiber Sheets Attaching Method
H. Fukagawa

Preservation of Existing Bridges in Kentucky Using Advanced Composites
I. Harik

Anti-subsidence Measure Using King-post Cables against Subsidence in A PC Box Girder with Central Hinge

Takeshi SUZUKI[1)], Shigeru MATSUMOTO[2)], Kousuke WAKATSUKI[3)], Hideki MANABE[4)]

Abstract: Four dyvidag bridges with hinge on the Hanshin Expressway Network were found subsiding in the central hinge region. Displacement was most significant in the Kireuriwari Viaduct of the Osaka Matsubara Route which exhibited a subsidence of more than 30 cm from the initial level. Anti-subsidence measure was investigated as a part of the major repair work on this route in fiscal 2003. Through comparative studies between a composite truss, external cables installed inside the box girder and other proposals, a king post cable structure was chosen because of its advantages in terms of local and structural conditions of the bridge. This method was to install new struts to the underside of the main girder and lay external cables eccentrically. This report covers detailed design of the king post cable reinforcement technique.

Keywords: continuous three-span PC rigid frame bridge with hinge, sag, king post cables, ASR, major repair work, soundness evaluation, maintenance plan

1. Introduction

The Kireuriwari Viaduct is a continuous three-span prestressed concrete (PC) rigid frame bridge with hinge completed in 1979. Photo.1 shows the whole view of this 154 m long bridge. This type of structure was used in many bridges built in 1960s to 1980s, being considered favorable for long bridges with not so high piers. In such structures with hinge dead load bending moment in a

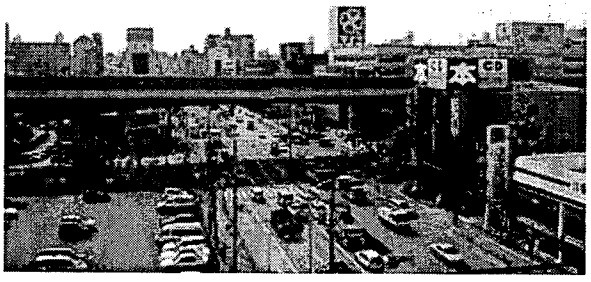


Photo.1 View of the entire Kireuriwari Viaduct

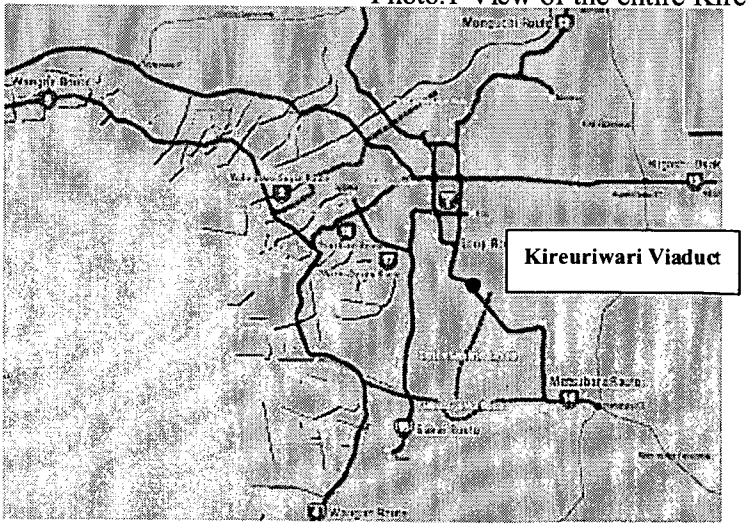


Fig.1 Hanshin expressway network

completed structural system, horizontal seismic force is distributed to each pier, and there is no redundant force due to temperature change and drying shrinkage which usually occurs in ordinary continuous rigid frame bridge. However, many of them have been changed into continuous girders since hinge shoes required frequent maintenance and, in some of them, sagging or angle-bending was beyond design levels, causing problems with driving comfort and water drainage from bridge decks.

The Kireuriwari Viaduct experienced the same problems, with a sag in the central hinge region found in 1985, after five years from the start of service in March 1980. Although overlay of 70 mm was applied in 1986 and again in 1993 in order to sustain serviceability, continued observation and examination suggested a possibility of further decline in its structural performance. The amount of sag already reached a considerable degree and was expected to further increase. Dynamic characteristics of the concrete indicated deterioration due to alkali-silica reaction (ASR). Since combined effects of creep in the concrete, ASR and other factors were suggested, it was decided to restore serviceability and prevent or even correct the sag using the king post cable reinforcement technique. This report covers the detailed design of this reinforcement.

2. Current condition of the existing bridge

2.1 General

Table.1 and Fig. 2 show specifications and general views of the bridge which passes over the Uriwari intersection in Hirano-ku, Osaka. Since this site was a major intersection of two national roads (#309 and #479) with a daily traffic inflow of about 76,000 vehicles, the construction must be carried out under many restrictions including assured visibility for vehicles on the streets, compliance with clearance limits and limited space available for the work.

Table.1 Specifications of the bridge

Structure	continuous 3-span prestressed concrete rigid frame twin main girder bridge with hinge
Bridge length	154.0 m (span lengths: 44.450 + 65.000 + 44.450 m)
Width	0.400 + 8.700 + 0.800 + 8.700 + 0.400 = 19.000 m
Live load	B live load (TL-20 at construction)
Gradient	incline: 1.167%; crossfall: 2.0% (upward gradient)
Bearings	8 roller bearings, 162 tf (overall)
Central hinged shoes	4 Gelenk shoes + 2 horizontal rubber bearings (overall)
Concrete strength	superstructure: 40 N/mm^2; substructure: 24 N/mm^2
Prestressing steel	internal cable: SBPR 930/1180 (dia. 26 mm; existing) external cable: SWPR7BL 19S15.2

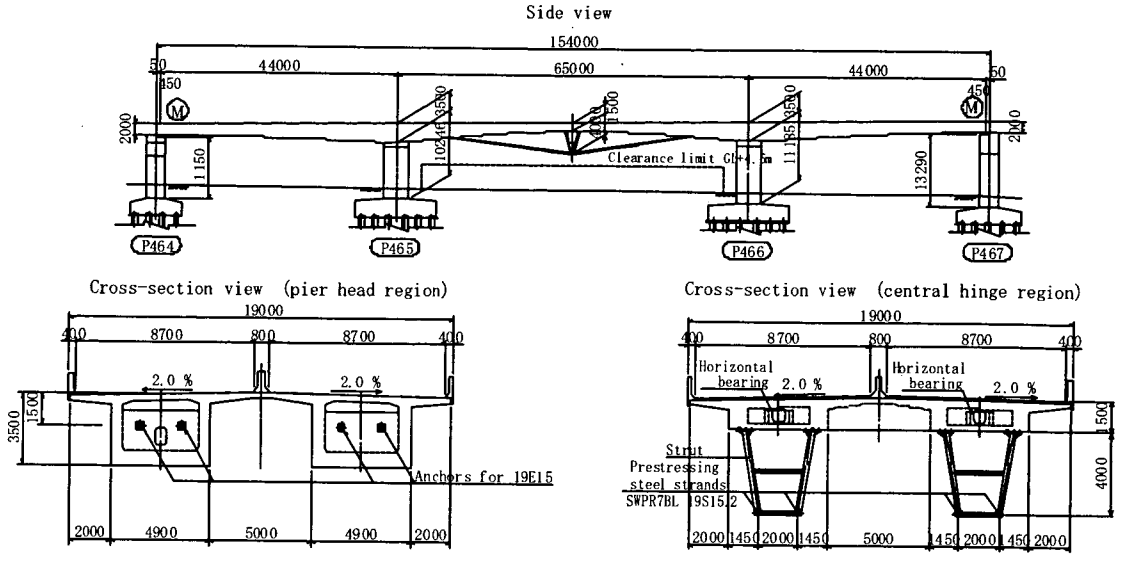


Fig. 2 General structural views of the Kireuriwari Viaduct

2.2 Changes in the bridge from the completion

(1) Sag in the main girder

Figure.3 shows the amounts of sag in the main girder. The bridge began to bend sharply at around 10 m from the center of the span, with minor displacement in the side spans. The overlays for serviceability recovery in 1986 and 1993 caused deflections of 4 mm and 7

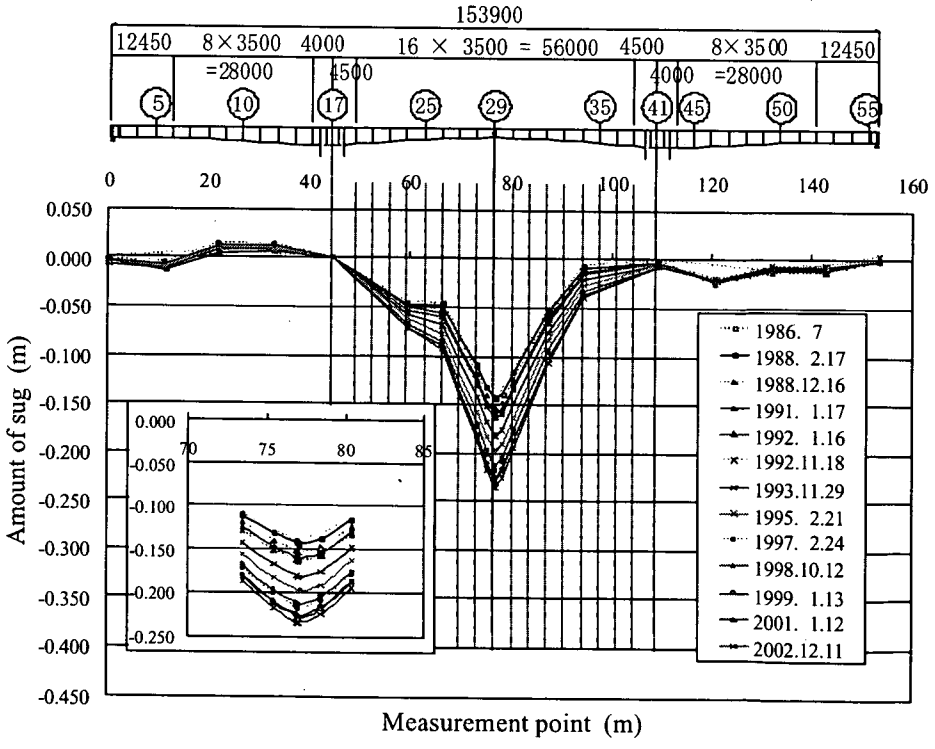


Fig. 3 Measurement results: cumulative amounts of sag (the inbound lane)

mm, respectively, in the central hinge region. None of the piers exhibited major subsidence. Cumulative amount of sag in the central hinge region measured in December 2002 was 236 mm from the design longitudinal alignment. On the other hand, according to the records, this bridge was given an additional elevation of 85.4 mm at construction. Therefore, the actual cumulative amount of sag reached 321 mm. Although there was some influence of temperature variations between measurements, recent data revealed that the rate of sagging was increasing by about 2 mm to 9 mm each year.

(2) Concrete properties

Table.2 shows the results of investigation on concrete properties. Although the design characteristic strength was 40 N/mm^2, actual compressive strength ranged from 28.0 N/mm^2 to 45.5 N/mm^2, suggesting lack of strength partially. Static modulus of elasticity was 60% to 80% of a design level of 3.5×10^4 N/mm^2. Chemical tests and petrographic examinations revealed potential deleteriousness, indicating ASR as one of the possible causes of sagging.

Table.2 Investigation results: properties of the concrete

Year of test	Sampling location	Compressive strength (N/mm^2)	Static modulus of elasticity ($\times10^4$ N/mm^2)	Expansion (1×10^{-6})
1987	Diaphragm	36.4--42.2	2.07--2.54	Mortar-bar: 327 (26W) Chemical: potentially deleterious
1988	Diaphragm	28.0--44.8	1.88--2.72	325--414
1991	Diaphragm	--	--	153--295
1992	Diaphragm	38.4--45.5	2.45--2.55	--
2000	Web	29.7--30.6	2.13--2.34	JCI-DD2: 270 (13W) Canadian Std: 830 (28-day)

(3) Cracking

Cracking of the major part of the bridge was slight. However, alligator cracking occurred in the pier head regions, cross beams and other massive regions. Cracks in the slabs were found along the prestressing steel. In 1988, diagonal cracks were found in the central span at around one fourth the span length from each end. Cracking was significant in the outer webs which were exposed to environmental variations. Investigations were carried out to determine cracking behavior and influence of torsion, resulting in a reinforcement using the steel plate bonding technique in 1993.

3. Detailed design of the king post cable reinforcement

3.1 General

Figure.4 shows the overview of the detailed reinforcement design which consists of the following major items.

(1) Detailed design of the king post cable reinforcement
(2) Concrete property investigation for the main girder
(3) Measurements during prestressing, and existing bridge loading tests
(4) Soundness evaluation, and future deformation estimation
(5) Medium-range monitoring plans

As steps (2) to (5) are still under examination, this report mainly covers step (1).

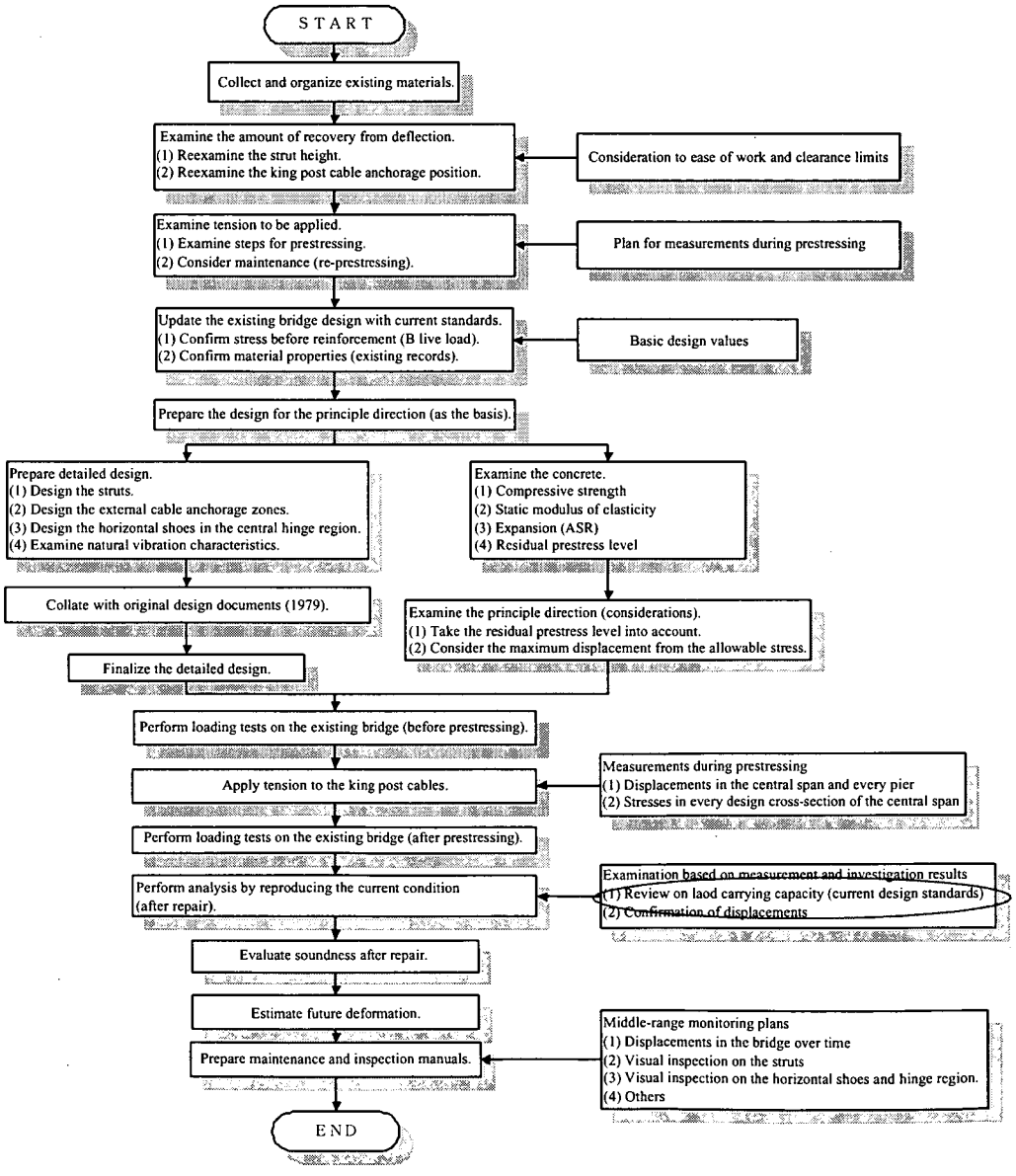


Fig. 4 Flowchart

3.2 Reinforcement in the principal direction

In order to design a continuous rigid frame box girder having the external cables laid with large eccentricities, the elastic plane analysis was used with the king post cables taken into account as members resisting the axial force only. The positions of the king post cables were determined to allow the largest possible eccentricities for optimum recovering effects. Anchoring position was set to 1.5 m from the upper slab where the existing transverse prestressing cables in the pier head region were not interfered with. Struts height were 4.0 m and was placed under the main girder, assuring good visibility for vehicles on the streets and complying with clearance limits.

Tension to be applied to the king post cables was set to initial tensile force σ_{pi} = 1200 N/mm^2 (pi = 3,162 kN/cable), taking stress variations due to live load and temperature changes into account.

Modulus of elasticity of the main girder concrete was obtained from trial mixing results reported during construction. The recorded value was about 2.5×10^4 N/mm^2, which was almost 70% of the original design value (3.5×10^4 N/mm^2). However, since the mix was actually used in the existing bridge, the figure was used as a design value for the current reinforcement.

Figure. 5 shows combined stress under dead load. The current reinforcement was found favorable in terms of stress, with compressive stress due to bending in the central span decreased to around 2.0 to 6.0 N/mm^2. A sag correction of 47 mm was estimated in the central hinge region.

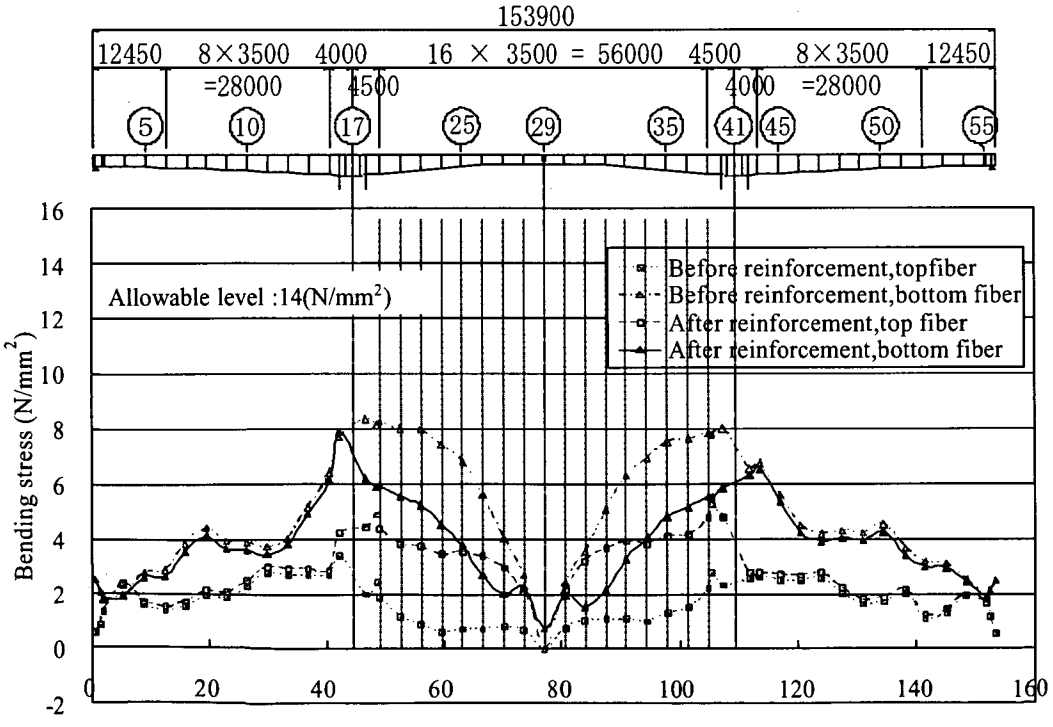


Fig. 5 Combined stress under dead load

3.3 Details

(1) Struts

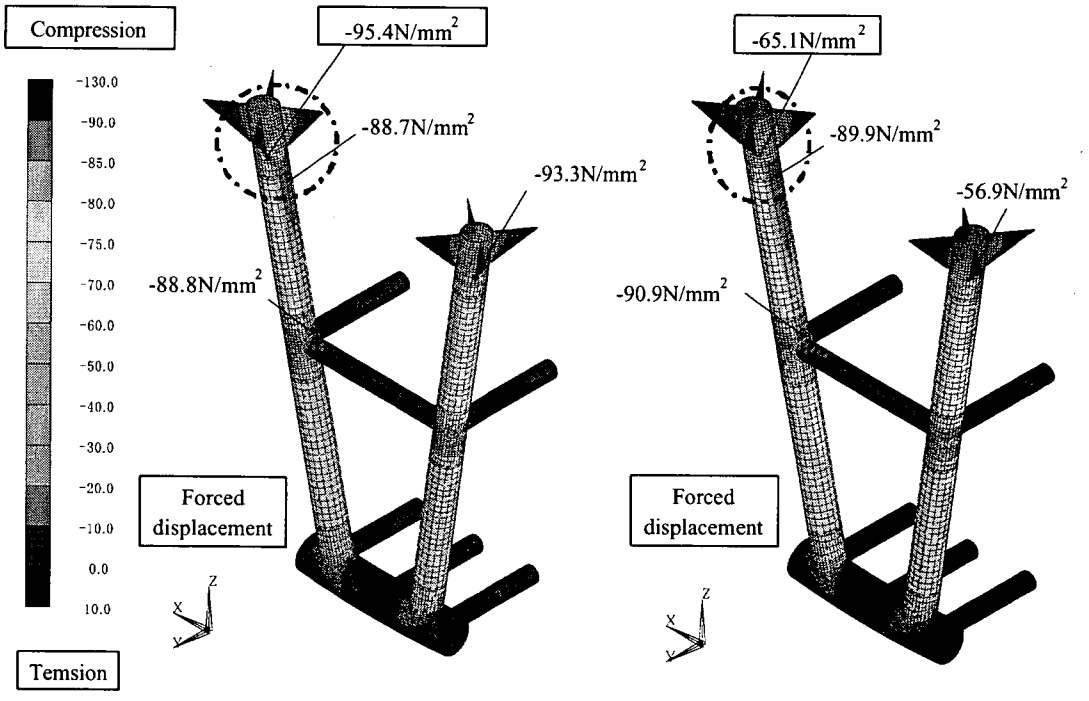
Struts and saddles were designed to have a simple and light-weight structure, using simplex steel pipes for the struts and duplex steel pipes filled with shrinkage-compensating mortar for the saddles[5]. Struts had ribs at their roots, with the pipes filled with shrinkage-compensating mortar for the height of the ribs in order to prevent stress from concentrating at the tips of the ribs.

Members were designed using the three dimensional (3D) frame analysis, and local stress was examined using the 3D FEM analysis. Since the struts were crossing over the hinge, relative displacements between the two sides were measured at site and included in the design.

Figure .6shows the 3D FEM analysis results under design load, with relative displacements taken into account. As shown in the case without filling (left) and the case with filling (right), minor principal stress at the tips of the ribs was improved by filling with mortar from -95.4 N/mm^2 to -65.1 N/mm^2, or to 68%, indicating successful dispersion of stress.

Although stress amplitude under live load was only 2.0% of that under full design load by the overall frame analysis, full penetration weld joints were adopted for the steel pipes for assured safety against fatigue in the struts.

Safety against buckling in the struts was verified by a buckling ratio of 13.5 in the primary buckling mode.



Without shrinkage-compensating motar filling With shrinkage-compensating motar filling

Fig. 6 3D FEM analysis on the struts

(2) Horizontal rubber bearings in the central hinge region, and reinforcement of the existing cross beams

The hinge in the existing bridge consisted of Gelenk shoes which transferred shear force only and did not transfer bending or axial force. When the current reinforcement was simulated without modifying the existing hinge, the bottoms of the existing piers could not bear the specified stress due to the prestressing and temperature change. In order to allow axial force to be transferred to the central hinge region, horizontal rubber bearings were installed. Steel shoe seats were used for ease of work.

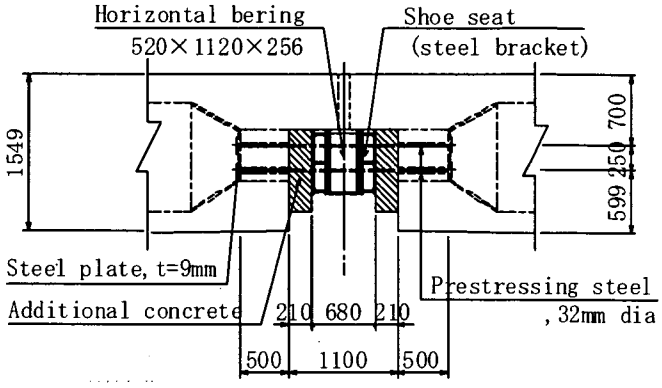


Fig. 7 Details of the central hinge region (side view)

Axial force acting on these horizontal bearings was about 6350 kN/shoe under design load (temperature change and variation), suggesting that the existing cross beams were insufficient to obtain adequate flexural and punching shear capacities. Therefore, they were reinforced with additional concrete and bonded steel plates as shown in Fig. 7.

(3) King post cable anchorage zones

The king post cables were anchored to the existing pier head regions. Anchors and deviators were installed by placing additional concrete. The thickness of the additional concrete was set to 0.75 m for the front of the anchorage zones due to the layout of anchor components and, across the pier head region, 0.6 m for the deviation zones in order to maintain cable angle settings.

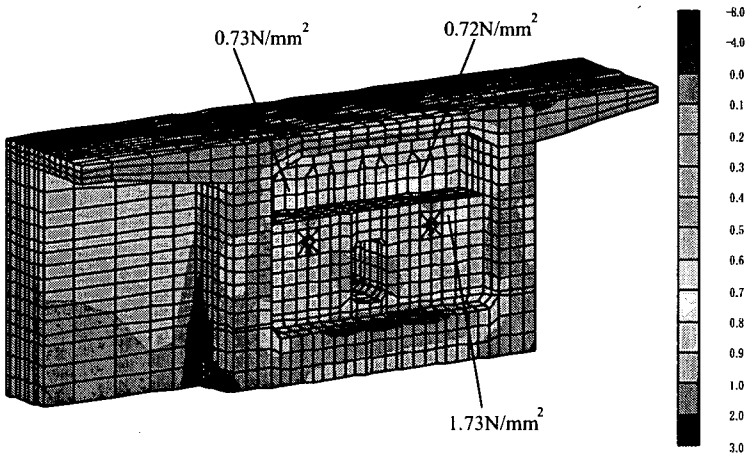


Fig. 8 3D FEM analysis results on the king post cable deviation zone

Local stress of this region was investigated by the 3D FEM analysis. Major principal stress was σ_{max} = 1.73 N/mm^2 in the vicinity of the anchors, exhibiting no deleterious tensile stress. Reinforcing bars were added to cope with the tension. Figure. 8 shows the 3D FEM analysis results on the king post cable deviation zones.

(4) Natural vibration characteristics

In an externally prestressed structure, structural vibration due to travelling vehicles and other factors is amplified by the resonance with external cables when the frequency of the free length of the cables is close to the lowest order deflection frequency of the main girder. Therefore, in order to confirm vibration characteristics after the reinforcement and the validity of the vibration controller spacings, natural vibration was analyzed using a plane

frame model, taking shear stiffness due to the tension in the king post cables into account. As shown in Fig. 9, the frequency of the external cables (f_c) was larger than five times the frequency of the main girder (f_h) ($5f_h < f_c$), suggesting that no deleterious vibration accompanied by resonance would occur[6]. It was decided to install vibration controllers at spacings of less than 10 [7] to increase safety against resonance which was already assured by the analysis results even without them.

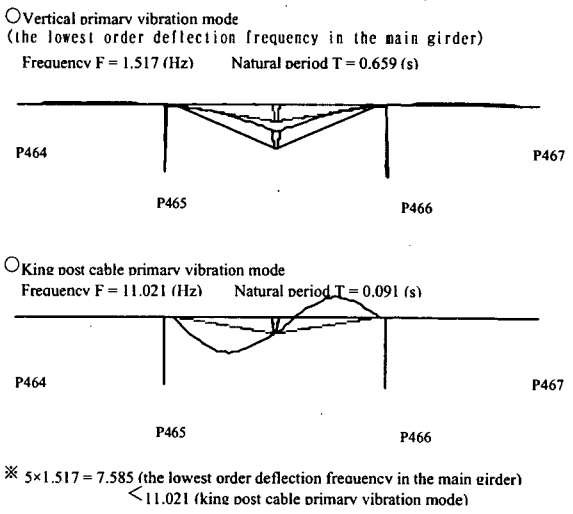


Fig. 9 Natural vibration analysis results

4. Conclusion

Reinforcement using king post cables was examined to prevent or correct sag in the central hinge region of a rigid frame box girder. There were following findings through its detailed design.

(1) Updating of the existing bridge design with current standards: When B live load was applied, tensile stress under minimum design load exceeded a specified level partly on the central span top fiber before the reinforcement but was controlled within a satisfactory range in every cross-section after the reinforcement.

(2) Combined stress: Every cross-section was fully prestressed after the reinforcement, with a minimum compressive stress in the bottom fiber around the central hinge region and a margin of 2.0 N/mm^2 from an allowable level in tensile stress. The amount of recovery from sag was 47 mm at the central hinge region, suggesting that proper layout and tension were selected for the king post cables.

(3) Design of the struts: Stress concentration was reduced analytically to about 68% by filling steel pipes at their roots with shrinkage-compensating mortar. This point will be confirmed during the measurements on the existing bridge.

(4) Relative displacement across the central hinge: There was a vertical displacement of 0.96 mm between the two sides. Although safety was confirmed during the designing of the struts with a forced displacement of 5 mm, future maintenance should include inspection of the Gelenk shoes which transfer shear force in order to evaluate their wear over time.

(5) The additional concrete reinforcement on the cross beams in the central hinge region which was required for installing the horizontal rubber bearings resulted in a slight increase in dead load but also provided an intermediate for a plane contact between a steel shoe seat and the existing cross beam, eliminating the concern over the installation accuracy of the horizontal rubber bearings..

(6) Natural vibration characteristics: Safety against resonance was assured after the reinforcement even without vibration controllers.

5. Future examinations

5.1 Design verification based on the property investigation results

The current detailed design is a basis established based on the property values from previous investigations. Further investigations are under way at present for collecting property data, and measurements are planned to obtain residual prestress data which are not sufficient at this moment. Design verification will be carried out using these additional data which will represent the condition of the existing bridge more accurately.

5.2 Measurement plans for the existing bridge

Previous data was insufficient to identify the major factors of the sag occurring in the central hinge region. Since the current reinforcement technique has not been proven by actual applications, it is necessary to confirm if the existing bridge behaves as calculated in the design. Following measurements are planned for both design verification and future maintenance.

(1) Displacement in major members and stress in the main girder cross-section will be measured during prestressing so that tension in the king post cables will be controlled at real time.
(2) Static loading tests will be performed before and after prestressing in order to verify effect of the current reinforcement and behavior caused by live load.
(3) Follow-up investigations will be carried out to confirm preventive effect against sagging and establish proper maintenance plans, so that soundness after the reinforcement will be evaluated and basic data required for preparing maintenance manuals will be collected.

Reference

1) Assistant Manager, Survey and Design Division, Osaka Business and Maintenance Department, Hanshin Expressway Public Corporation
2) Assistant Manager, Survey and Design Division, Kobe Business and Maintenance Department, Hanshin Expressway Public Corporation
3) Survey and Design Division, Osaka Business and Maintenance Department, Hanshin Expressway Public Corporation
4) Manager ,Technical development Department, Osaka Branch, Fuji P.S. Corporation, Pr.Eng.
5) Shinozaki, et al.: Study on fatigue durability of deviation zone members in an externally prestressed truss bridge having large eccentricities, Proc. of JCI, Vol. 24, No. 2, pp. 595--600, 2000
6) Expressway Technology Center: Design manual for PC bridges using external cables, pp. 51--52, August 1996
7) Japan Prestressed Concrete Engineering Association: External cable structures, precast concrete design and construction standards (proposal), pp. 72--73, March 1996
8) Matsumoto, et al.: Evaluation of natural vibration characteristics of the Torisaki River Park Bridge, Proc. of JSCE, pp. 1163--1164, 2002
9) Sakai: Repair on the Misasagi Bridge, Bridge and Foundation Engineering, August 1983
10) Hashiba, et al.: Study on time dependent displacement in a PC rigid frame bridge having hinge, Proc. of JSCE, No. 478/V-21, November 1993
11)Sakamoto, et al.: Soundness evaluation and reinforcement plan for the Jintsugawa Bridge, Bridge and Foundation Engineering, pp. 27--31, April 2003

ASSESSING BRIDGE PERFORMANCE – WHEN, WHAT, HOW

Richard Land[1], Ganapathy Murugesh[2] and Madhwesh Raghavendrachar[3]

Abstract

This paper outlines the value of assessing bridge performance of major bridges that incorporate innovative design procedures, structure types, construction methods, and new materials. Such innovative procedures, methods and materials help enhance long-term durability, increase expected bridge life, and help decrease the cost and impact of construction. When to consider a health monitoring system, what should be measured, and how various aspects of a structure are measured are described using the new Benicia Martinez Bridge in California as a case study. A brief overview of the instrumentation plan for this bridge is presented. The information collected will be used to periodically evaluate the performance of the bridge and to validate/enhance current design practice.

1.0 Introduction

With new innovative materials, new methods of construction, and complex analysis methods, bridge designers continue to challenge standard practices with longer spans and more sophisticated designs. When incorporating new state-of-the art/state-of-the-practice developments into the design of bridges, particularly large important bridges, designers should consider establishing a way to assess the actual long term performance. Although all the analyses may indicate successful performance, in some cases, it is prudent to monitor specific aspects of performance and hence validate design assumptions. This assessment of performance is also called "health monitoring."

Health monitoring can be used to assess the deterioration of a bridge due to service conditions over its service life, or to assess bridge performance subsequent to unforeseen loading conditions. Health monitoring can help bridge owners to: plan and design effective retrofit strategies; program long term maintenance; reduce life cycle costs through preventive maintenance; and, evaluate bridge integrity immediately after rare events such as floods, earthquakes, vehicle/vessel collisions, etc. Health monitoring can lead to a better understanding of bridge behavior, better analysis and design approaches and improved construction methods. When to employ some means of continuously and systematically assessing performance of particular bridge structures needs to consider several factors. Once it is deemed important to establish a health monitoring system, careful consideration must be given to exactly what should be monitored, how the data will

[1] State Bridge Engineer, California Department of Transportation
[2] Senior Bridge Engineer/Contract Manager-Benicia Martinez Bridge Project, California Department of Transportation
[3] Senior Bridge Engineer/Reinforced Concrete Committee Chair, California Department of Transportation

be collected and how the data will be used.

2.0 When To Consider Health Monitoring

For typical overcrossing, undercrossing and interchange bridges, regular bi-annual inspections by trained engineers is usually adequate to assess the health of these "ordinary" structures. But on "non-typical" structures with high replacement costs and significant impacts if damaged, regular physical inspections are not enough. Large toll bridges, bridges deemed critical and important to the public, and other structures that incorporate unique design features or specialized construction methods or materials, such as segmental construction or lightweight concrete need to be monitored. Cable-stayed bridges, suspension bridges, scour-critical bridges, and critical structures in high seismic areas are examples of structures where additional health monitoring may make sense.

One example of such a structure is the new high level Benicia Martinez bridge, (Fig. 1) across the Carquinez Strait that connects the cities of Benicia and Martinez in California. In addition to relieving the current traffic congestion, this structure has significant seismic importance, as it is part of the State of California lifeline route system. This structure is designed using Caltrans' "Important Bridge" seismic design criteria and needs to be serviceable within hours of a major seismic event. A significant portion of this structure is designed to be constructed segmentally using sand lightweight concrete and has maximum spans of approximately 200 meters. The 25 meter wide superstructure is being designed as a single cell box with large overhangs accommodating light rail loading. Several factors that were instrumental in initiating the health monitoring of this $600 million bridge include: a) high seismic demands, b) long spans subject to excessive deflections, c) use of sand lightweight concrete with lower modulus of elasticity, and, d) a cast-in-place balanced cantilever segmental construction method that results in significant creep and shrinkage. Listed below is a more detailed summary of these and other factors considered:

2.1 Seismic Importance

The site for the new Benicia Martinez bridge is located 3 miles west of the potentially active Green valley (M=6.75) fault. The new Benicia Martinez Bridge is on a "Seismic Lifeline Route". The bridge is designed to remain operable shortly after a major seismic event. The unique topography of this site, with the rockline dipping at steep 70-degree angles at both ends of the bridge, has required varying column lengths along the length of the bridge. The seismic design has been a challenge. Replacement of this structure would take several years of significant effort and considerable cost. It is of paramount importance to monitor the seismic behavior of this structure during a seismic event to help quickly assess the bridge's condition and evaluate short and long-term safety concerns and

recovery strategies.

2.2 Sand lightweight concrete

The new bridge is designed with long spans to minimize the number of columns in the bay. This reduces the substructure cost, which comprises a significant fraction of the total outlay. However the long spans increase the seismic demands on each supporting pier. In an effort to reduce the seismic demands and the sizes of substructure elements, sand lightweight concrete (LWC) has been selected as the material of choice for the superstructure as it gives a 20% weight reduction.

Historical data from structures constructed with LWC indicate problems and the need for proper use of LWC parameters. The modulus of elasticity for LWC is significantly lower than normal weight concrete. This increases the concern for long-term deflections due to the long spans on this structure. For this structure lightweight aggregates from different vendors have been subject to short-term tests to prequalify aggregates to meet minimum modulus requirements. Short-term tests using several lightweight aggregates have indicated the need for high strength concrete mixes to obtain the design values for the modulus of elasticity. With a limited national database on long span LWC structures to compare and learn from, it is essential to instrument and monitor the short and long term behavior of this bridge.

2.3 Creep and Shrinkage

It is well recognized that creep and shrinkage play a vital role in the redistribution of internal forces like bending moment, shear, and prestressing. The actual characterization of system change due to creep and shrinkage in bridge structures has been limited, especially in the LWC long span bridges. Lightweight aggregates have significant creep and shrinkage characteristics. Several assumptions and analytical models have been used to predict the creep and shrinkage behavior of this bridge. Monitoring actual behavior of the structure can validate these analytical assumptions. Health monitoring can aid in tracking these complex time dependency effects.

2.4 Type of Construction

The new Benicia Martinez bay crossing is over 2.5 kilometers long. The bridge stands over 30m above the mean water level and spans across a busy navigational channel. Therefore, the cast in place balanced cantilever segmental erection technique has been chosen as the method of construction. This type of construction involves sequential stressing of segments across each span. The concrete is stressed at the relatively young

age approximately 2-4 days from the time of casting. The modulus of elasticity of concrete is very low at this time resulting in significant creep. In addition, as the balanced cantilever operation progresses, stressing operations of subsequent segments result in a complex creep phenomenon.

2.5 Unique Features

The 200m longest span of this bridge puts it among the top few long-span structures built using this method of construction. The 25m wide superstructure is designed as a single cell box with 6m overhangs on either side. The superstructure is designed to carry 5 lanes of highway traffic plus a light rail load on the overhang. The maximum depth of the superstructure is about 11.5m. The superstructure is transversely prestressed with supporting ribs and an edge beam. Hollow columns with confined corner elements have been designed at several piers. All of the above nonstandard features further substantiate the need for health monitoring of this structure.

2.6 Near Midspan Hinges

A result of the balanced cantilever construction is the provision for near midspan span hinges. Deep steel box beams have been used at these hinges to transfer large static and dynamic loads. The hinges have posed significant design issues with respect to the transfer of forces. These deflection and load concerns add to the need for monitoring the behavior of this structure.

3.0 Health Monitoring – What to Monitor

Once a bridge owner determines the necessity for more definite methods to assess performance of a particular structure over the life of that structure, the focus must then be placed on exactly what needs to be monitored. The goals of a particular health monitoring program must be clear.

For the Benicia Martinez bridge it was established during the design phase that ongoing monitoring and instrumentation would be useful both in understanding and assessing the condition of the bridge throughout its life and in evaluating the unique features of this bridge for future bridge designs in California and elsewhere. While the safety of the bridge under quasi-static loading is well established by design methods, the service performance over time and the details of the response of the structure to seismic forces are less precisely known. Listed below are some of the goals of the health monitoring instrumentation program for this bridge:

a. Monitor and assess bridge deflections, rotations and concrete strains of the mainspan superstructure over time. Assessment will be made by calibrating and modifying the design computer model for the bridge for the actual material properties, temperature distribution, tendon forces, deflections, strains and environmental conditions. This "best fit model" will then be studied to understand how creep, shrinkage and consequent moment distribution have affected the bridge response. This understanding will be used to make the best possible rational assessment of the present condition and to forecast the future condition of the bridge.
b. Monitor the seismic behavior of the structure during a seismic event with the help of downfield and freefield sensors installed in the ground and at several locations on the bridge.
c. Monitor and assess the post-tensioning in the bridge over its service life. This is accomplished by monitoring the relaxation of representative tendons and by installation of sensors to "listen" for wire breaks in post-tensioning.
d. Monitor and assess temperature distribution and history of different bridge elements both during construction and during service. Temperature gradient is significant and often a governing load for bridges of this type. The temperature gradient data collected is important as the dimensions of the subject box girder are outside the range of most of the bridges where data has been collected.
e. Collect supplementary information for assessment including concrete material data, ambient temperature and relative humidity in and around the box girder.

4.0 How to Monitor - Instrumentation and Data Collection

After establishing what needs to be monitored for a particular structure, the details of how to collect the information need to be developed. Several illustrations from the new Benicia Martinez Bridge are attached to describe the health monitoring system planned for this bridge. Figure 2 indicates the instrumentation locations for most of the health monitoring with the exception of the modal analysis and seismic sensors. Figure 3 indicates the locations of the different instruments and sensors with respect to the superstructure depth. Table 1 indicates the total number of each type of sensor at each of these locations. Figure 4 indicates the complete layout of the modal analysis sensors. Figure 5 denotes a typical seismic monitoring layout of a frame.

4.1 Deflection

Long-term deflections in Span 7 will be measured using a base-line system attached to the underside of the deck as close as possible to the longitudinal centerline of the box girder. The system consists of a No. 8 stainless steel piano wire as a reference line, two end brackets

at the live and dead ends, base plates, and a caliper. The live end and dead end brackets are anchored to the underside of the deck with expansion anchor bolts as close as possible to the diaphragms at Piers 7 and 8. The piano wire is anchored to the bracket at the dead end and passes over a pulley at the live end. The wire is stressed to approximately 80 percent of its breaking strength using dead weights at the live end. Deflections are measured manually at midspan and at one fifth point. At each deflection location, a true horizontal reference steel plate is attached to the concrete using expansion anchor bolts. The distance between each base plate and the piano wire is measured using a digital caliper with a magnetic base. The base-line system will be installed immediately after the midspan closure of Span 7 is complete. In order to relate the base-line deflection readings to a prior survey performed during construction, a tie-in optical survey will be performed simultaneously with at least one set of base-line system readings. This simple system set up inside the bridge is safe and could be monitored by untrained personnel.

As an alternate to the piano wire system requiring manual readings, a system of interconnected liquid levels, monitored with precision vibrating wire level sensors, and capable of automatically reporting accurate differential deflections to the automatic data acquisition system (ADAS) may eventually be used.

4.2 Change in Length

Longitudinal length changes in Spans 7 and 8 will be measured using extensometers. Each extensometer consists of a 6-mm diameter graphite rod with a low coefficient of thermal expansion inserted into an 18-mm diameter PVC pipe that is attached to the underside of the top slab. The graphite rod is fixed to the concrete deck close to one diaphragm. The other end is attached to a linear variable displacement transducer (LVDT) attached to the concrete deck near the other diaphragm. The system will be installed along the longitudinal centerline of the box girder immediately after the midspan closures are complete. The LVDT's are connected to the ADAS.

4.3 Strain

Strains are measured using vibrating wire strain gages (VWSG). Vibrating wire strain gages will be equipped with thermisters for measurement of temperature at the gage location. VWSG's are supported prior to concrete placement such that they are held in position during concrete placement but not restrained from any longitudinal length change. Gages will be connected to the ADAS prior to concrete placement.

4.4 Rotation

Rotations are measured using tiltmeters. Two tiltmeters are installed, one in a horizontal and one in a vertical position on the sloping walls of the box girder. Tiltmeters at Locations B and D (see Fig. 2) will be installed and connected to the ADAS prior to completion of closure pour in Span 7. The tiltmeter at Location E will be installed immediately after the footing is cast and connected to the ADAS prior to completion of closure pour in span 7.

4.5 Concrete Temperature

Concrete temperatures are measured using Copper-Constantan Type 'T' thermocouples with a temperature range of -46°C to 121°C. Thermocouples are installed and connected to the ADAS prior to concrete placement and will be held rigidly in place during concrete placement to prevent movement from their intended locations. Heat of hydration due to mass concrete at deep bent cap and footing locations are a major concern on this bridge.

4.6 Ambient Temperature

Air temperatures are measured using Copper-Constantan Type 'T' thermocouples with a temperature range of -46°C to 121°C. Thermocouples are installed and connected to the ADAS prior to concrete placement and will be held rigidly in place during concrete placement to prevent movement from their intended locations.

4.7 Relative Humidity

Relative humidity is measured at two locations. One meter is located inside the box girder of Span 7 and the other meter is placed outside the box girder near Pier 7 to measure external humidity. They will be protected from the direct influence of the sun and rain by their location in the permanent shadow of the box girder. The humidity meters will be installed and connected to the ADAS immediately after construction of the pier segment at Pier 7.

4.8 Prestressing Force

Forces in two span-tendons of the seventh span are to be measured with center hole load cells having a capacity of 3000 KN. The load cells are installed around the strand prior to post-tensioning and are located between the anchor plates for the wedges and the concrete build-out for the anchor plate bearing. Load cells with a maximum non-linearity of one percent over their load range are connected to the ADAS prior to stressing the instrumented tendons. Tendons with the load cells are not grouted.

4.9 Hinge Force

Load Cells for the measurement of hinge forces are incorporated in the Hinge C and D bearings. At Hinge D in Span 8, four bearings per pair of steel box beams, for a total of 8 cells will be connected to the data collection system.

4.10 Wire Break Detection

Condition of the post-tensioning tendons is continuously monitored to detect and record failures of individual wires. Wire breaks are detected using surface mounted broad band accelerometers. A total of 90 sensors will be mounted on the underside of the deck span after removal of the formwork. Sensors will be connected to the SoundPrint® data acquisition system provided by Pure Technologies Ltd.

4.11 Corrosion, Epoxy Coated Reinforcement

The potential for corrosion of reinforcement is measured using rebar probe assemblies with reference electrodes. Eight probes with reference electrodes are placed at Piers 7 and 8 for a total of 16 pairs. At each pier, four pairs are placed in the footing at mean sea level and four pairs in the pier shaft not more than 1 m above the top of the footing. Sensors are attached to the layer of reinforcement closest to the surface.

4.12 Corrosion, Steel Pile Casings

The potential for corrosion of the steel pile casings is measured using immersion reference electrodes. Four sensors are placed on four different steel pile casings at each of Piers 7 and 8 for a total of eight sensors. The sensors are installed on the outside of the casing within 1 m of the underside of the footing, then connected to the ADAS.

4.13 Survey Monuments

Three permanent corrosion resistant monuments are to be installed on top of each footing for assessment of horizontal and vertical movements and rotations. The monuments will be installed with their elevations and positions determined before construction of the pier shafts.

4.14 Seismic sensors

The California Department of Transportation in association with the California Department of Mines and Geology is instrumenting the complete length of this bridge with

extensive free field and down hole sensors. Numerous seismic recording accelerometers will be placed at strategic locations on and off the bridge including a) pier tables, b) along the height of columns, c) footings, d) along the depth of the piles, e) at different depths in the soil. Displacement sensors will also be placed at several locations on the bridge to monitor the displacement history during a seismic event. Displacement and acceleration characteristics of the bridge during a seismic event will be recorded using data recorders and accessible from remote locations. Battery backup power will allow for readings through power outages.

4.15 Modal Analysis

Sensors will be installed in the longest frame at quarter span locations along the span and at quarter points along the column height. A baseline modal system will be established using prescribed dynamic testing prior to subjecting the bridge to live loading. Modal parameters such as the resonant frequencies and mode shapes will be constantly measured and compared to the baseline parameters. Established damage detection methodologies will then be used to identify damage areas in the structure and establish the severity of damage. The results from the analysis could subsequently be used to determine load capacity, rating and useful life.

5.0 Data Acquisition System and Installation Schedule

A data acquisition system capable of collecting all the above data will be used on the Benicia Martinez Bridge. The data collected using an automatic data acquisition system will be used to monitor and assess the performance of the structure and to enhance current design practices. Table 2 indicates the installation schedule for the different sensors outlined in Section 4. A joint effort involving Caltrans, a University of California research team, the California Department of Mines and Geology, the design team, and the contractor will ensure proper installation, data collection and interpretation.

6.0 Material testing

In addition to the material testing for quality control, the tests indicated in Table 3 will be performed on the materials used in Regions A through D. The data collected from these tests will be used to validate the design parameters.

7.0 Cost of Health Monitoring System for the Benicia Martinez Bridge

The cost for the instrumentation of health and seismic monitoring of the new Benicia Martinez Bridge is approximately $ 2,000,000. The California Department of Mines and

Geology will furnish the seismic monitoring equipment valued at approximately $375,000. In addition to the instrumentation, the State of California anticipates spending about $600,000 for data collection and monitoring over the next five years. The monitoring cost is expected to significantly drop thereafter. The cost to health monitor this structure is a fraction of the total construction cost in exchange for valuable data on complex structure behavior.

8.0 Conclusions

New technologies and advances in data acquisition systems have helped make assessing very specific aspects of bridge performance possible. But what can be assessed comes at a price and is not appropriate for all structures. When newly designed important bridges include what could be considered "extra-ordinary" design features, sophisticated analyses, unusual construction methods, and/or high performance materials, health monitoring systems can be economically effective at verifying assumptions and detecting and assessing unexpected behavior. Any health monitoring program must be planned in detail and include clear understanding of how collected data will be processed, analyzed and acted upon. When completed, the health monitoring system installed in the new Benicia Martinez structure will allow for the measurement and collection of a vast amount of data to help assess the short and long-term performance of that structure. This data will help maintain the structure to provide a safe and efficient bay crossing for the traveling public. It will also serve as a useful database of performance information for bridge design engineers around the world. This proactive approach to improving the quality of structure design is a well-justified step in responsible engineering.

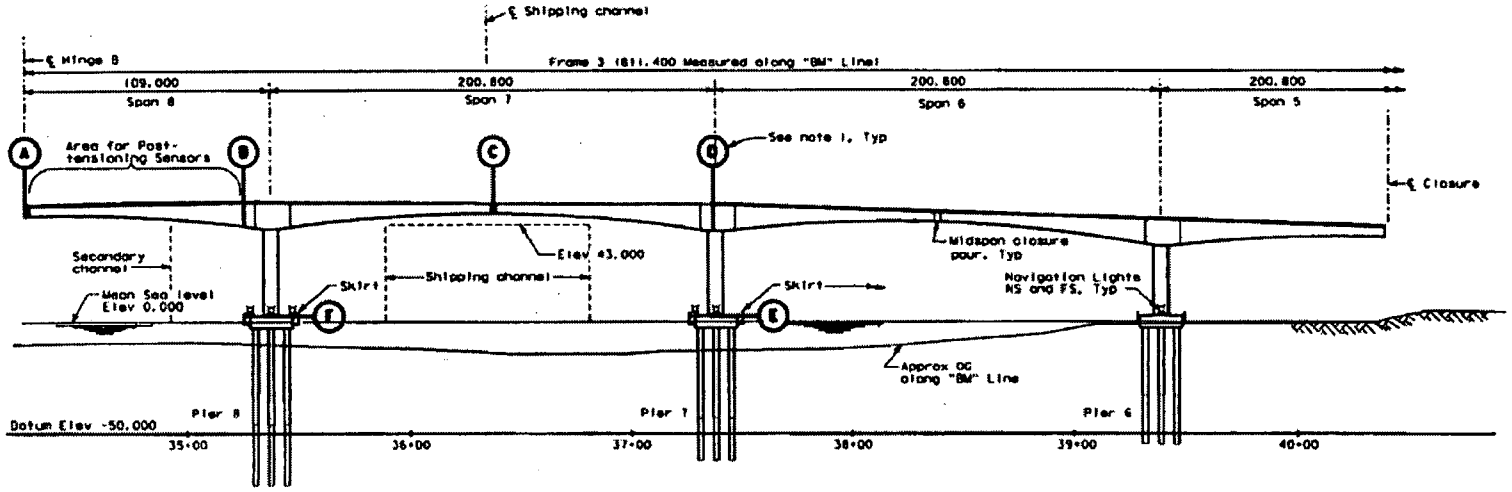


Fig. 2 Instrumentation Locations.

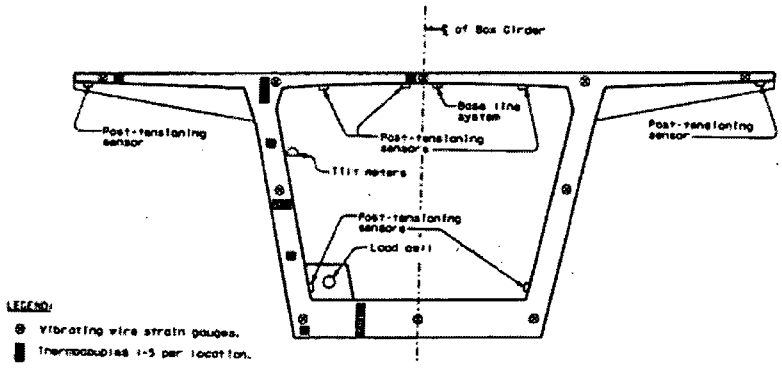


Fig. 3 Location of instruments in a cross section

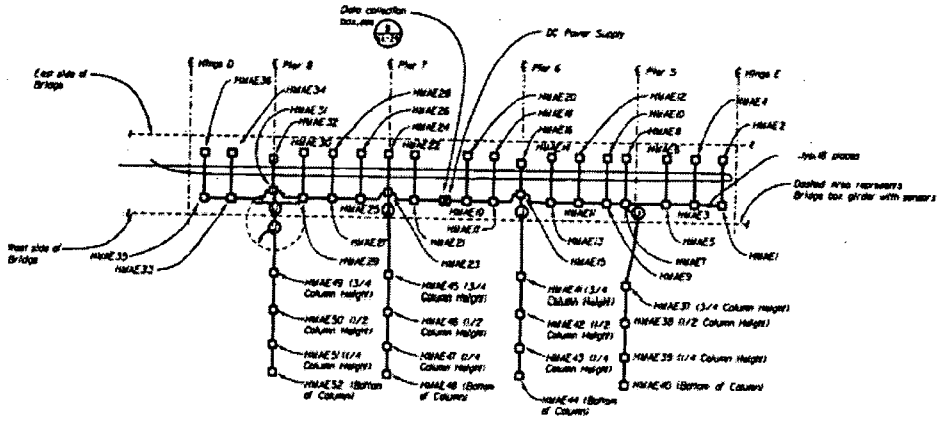


Fig. 4 Layout of Modal analysis sensors

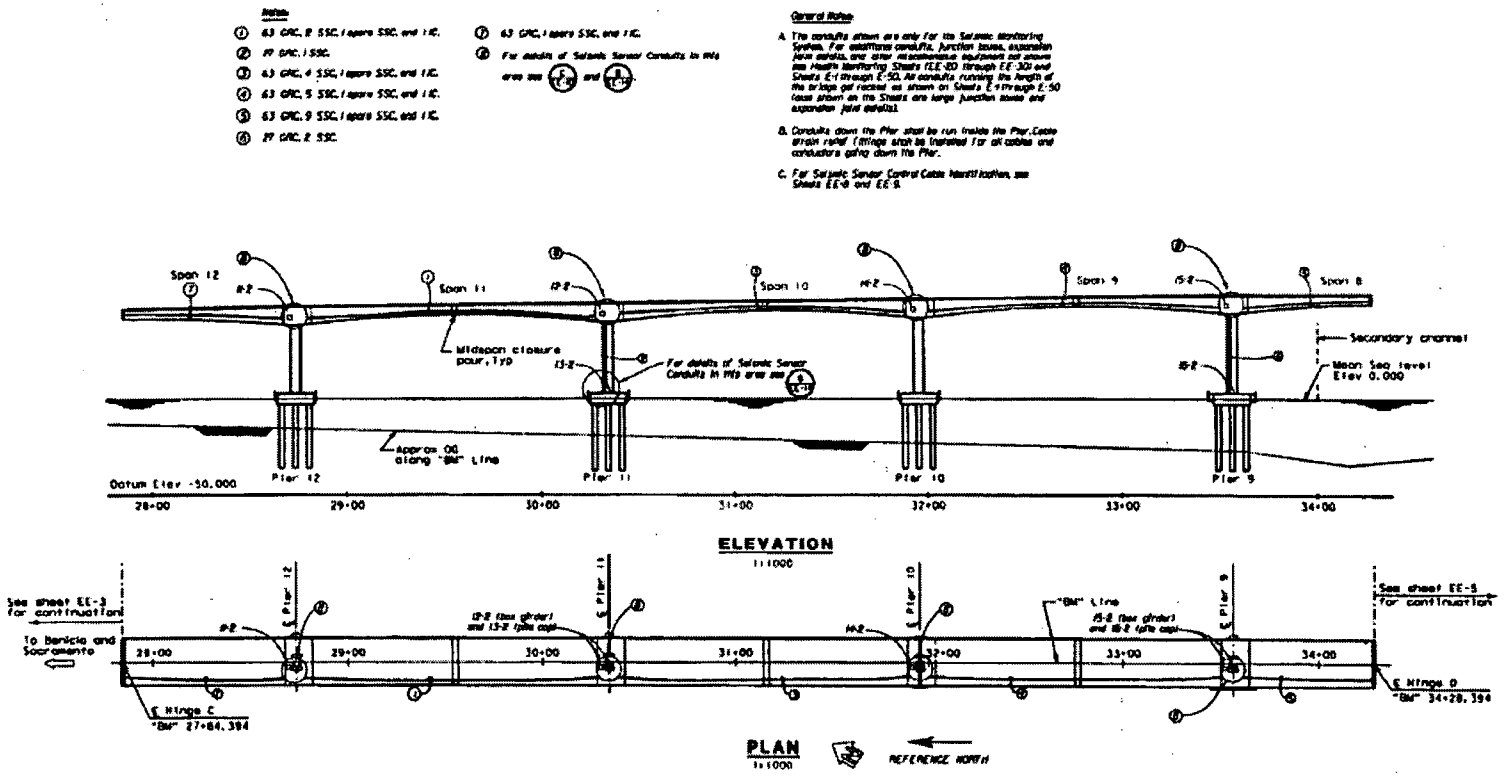


Fig. 5 Typical Seismic Monitoring layout.

Type of Measurement		Deflection	Length Change	Strain	Rotation	Temper-ature	Humidity	Prestress Force	Hinge Force	Wire Break	Corrosion
Sensor Type		Base-line System	Extenso-meters	Vibrating Wire Strain Gages	Tilt-meters	Thermo couples	Relative Humidity Meters	Load Cells	Load Cells		Reference Cells
Location	Key										
Near Hinge, Span 8	A		1 (Span 8)	10					8	90	
Near Pier 8, Span 8 (sand lightweight concrete)	B	1 (Span 7)		10	1						
Midspan, Span 7	C		1 (Span 7)	10		20		2			
Pier Table Span 7 Pier 7	D			10	1	20	2				
Footing, Pier 7	E				1	10					12
Footing Pier 8	F										12
Total		1	2	40	3	50	2	2	8	90	24

NOTES:

1. Not all instrument are installed at each location.

Table 1 General location of the Health Monitoring Instrumentation.

Measurement Type	Sensor	Installation
Deflection	Base-line system	After midspan closure of Span 7
Length Change	LVDT	After midspan closures of Span 7 and Span 8
Strain	VWSG	Before concrete placement
Rotation at Locations B and D	Tiltmeter	Before midspan closure of Span 7
Rotation at Location E	Tiltmeter	After footing concrete is placed
Concrete Temperature	Thermocouple	Before concrete placement
Air Temperature	Thermocouple	Before concrete placement
Relative Humidity	Humidity meters	After casting pier segment at Pier 7
Prestressing Force	Load Cell	During tendon installation
Hinge Force	Load Cell	During hinge installation
Wire Break Detection	Broadband accelerometers	After midspan closure of Span 7
Corrosion - Reinforcement	Reference cells	Before concrete placement
Corrosion - Steel Pile Casings	Reference cells	After footing concrete is placed
Survey Monuments	N/A	After footing concrete is placed

Table 2 Installation Schedule

Material Property	Number of tests at Each Age, Days						Total Specimens
	3	7	28	56	91	180	
Compressive Strength 18 cylinders from each of 4 locations	12	12	12	12	12	12	72
Modulus of Elasticity 18 cylinders from each of 4 locations	12	12	12	12	12	12	72(NOTE 1)
Coefficient of Thermal Expansion 3 cylinders from each of 4 locations	12	N/A	12	N/A	N/A	12	12
Creep and Shrinkage 12 cylinders from each of 4 locations							
Creep	8	N/A	8	N/A	N/A	8	24
Shrinkage	8	N/A	8	N/A	N/A	8	24

NOTES:
1. Same specimens as compressive strength.
2. Total number of cylinders is 33 per instrumentation locations. Locations are A, B, C, and D as identified in Fig. 2.

Table 3 Concrete Materials Testing Program

Acknowledgements

The authors acknowledge the efforts of Mr. Scott Hunter with TY Lin International for proposing portions of the health monitoring system across the shipping channel, Mr. Pat Hipley with the California Department of Transportation (Caltrans) and the California Department of Mines and Geology for architecture of the seismic monitoring, Mr. Charles Sikorsky with Caltrans for devising the modal analysis instrumentation, Mr. James Lacy with Caltrans for devising the electrical connectivity of this complex system, and Mr. Ron Bromenschenkel with Caltrans for his efforts during the development of this program.

References

1. Caltrans, contract plans and specifications for the New Benicia Martinez Bridge, Bridge Number 23-0153R.

2. Arnouti, C., Sangakkara, S. R., "Creep and shrinkage in lightweight concrete", Magazine of concrete research, vol. 36, no. 128, Sep. 1984.

3. "Prediction of creep, shrinkage and temperature effects in concrete structures", Designing for creep and shrinkage in concrete structures, ACI publication, SP 76-10, 1982.

4. Murugesh, G., Reddy, D.V., Sinha, V., Arockiasamy, M, "Ultimate load, creep, shrinkage and reliability studies of a single cell segmental bridge with external post-tensioning", ACI fall convention, Dallas, TX, Nov 10-15, 1991.

5. Sikorsky, C., "Development of a health monitoring system for civil structures using a level IV non destructive damage evaluation method", Proceeding, 2nd International workshop on structural health monitoring, Stanford university, Stanford, Ca Sep. 8-10, 1999.

6. Several internal memorandum and communications with agencies involved.

Experimental Studies on Retrofit by Partially Encased Concrete to the Steel I-Girder subjected to Buckling Deformation

Kenji HAYASHI[1], Shoji ONO[2] and Shun-ichi NAKAMURA[3]

Abstract: The authors have proposed a new type of steel-concrete composite bridge using the partially encased composite girder, reinforcing bars are welded to the flanges and concrete is filled into the areas surrounded by the flanges and web, and already proved through experiments and analyses that the encased composite girder had extremely high ultimate bending and shear strength as compared with the conventional steel I-girder. In this paper, the retrofit or rehabilitation method of partially encasing with concrete is suggested, to the steel I-girder deformed by buckling or subjected to damage. In order to confirm the effects of retrofit by the method and having the ultimate strength enough of the partially encased composite girder, bending tests and combined tests subjected to bending and shear simultaneously of the steel I-girder and the encased composite girder retrofitted by the above method are carried out. Consequently, the validity of this retrofit method is verified.

Key words: partially encased concrete, composite structure, steel I-girder, retrofit, maintenance, bending strength, buckling deformation, confined effect

1. Introduction

The continuous steel I-girder is one of the most common forms of bridge structures. At the intermediate supports, large bending moments and shear forces exist and the web is stiffened by vertical and horizontal stiffeners. Furthermore, the concrete slab is in tension due to hogging bending moments and does not contribute to bending strength. The lower flanges and lower parts of webs are in compression and are vulnerable to flexural-torsional and shear buckling. The flange size at intermediate supports is usually the maximum in the whole span. On the other hand, at the span center, bending moments are large but shear forces are small. The concrete slab is in compression due to sagging bending moments and contributes to bending strength. The upper flange is in compression but the lateral displacement is restrained after the concrete slab is erected. Therefore, the girder area around the intermediate supports is the critical part of the continuous girder.

A new structural form has been proposed to increase bending and shear strength of steel I-girders around the intermediate supports of continuous girders [1-3]; concrete is filled into areas surrounded by the upper flange, lower flange and web, as shown in Fig.1. The encased concrete is expected to prevent buckling of web and flange plates in compression and the concrete itself also contributes to the bending and shear strength. The use of encased girders can eliminate most of the stiffeners as the

[1]Manager, Engineering Department of Steel Structure Division, TOPY Industries Ltd.
[2]Chief, Engineering Department of Steel Structure Division, TOPY Industries Ltd.
[3]Professor, Department of Civil Engineering, Tokai University

web is stiffened by the encased concrete. It also prevents flexural-torsional and shear buckling of the plate girder and consequently the number of cross beams is reduced. In this bridge system with the encased composite girder, concrete is filled only around the intermediate supports and the weight of the encased concrete does not increase the design bending moment of girders very much.

However, measures must be taken so that the encased concrete would not fall off, if it should be crushed or damaged. There are certain ways to prevent this: studs are welded on the web, or reinforcing bars are welded to the web [4-7]. In this study, reinforcing bars are placed vertically and welded to the upper and lower flanges. This type of encased composite members has been proposed for the beams and columns of buildings [4-6], but they have used the rolled steel H-section with a width-to-height ratio (the flange width divided by the web height) of about 1.0. But, the bridge girders have a larger web height with a width-to-height ratio of under 0.3 and the research for the building members cannot be fully applied to the bridge girders.

From the above point of view, bending and shear tests have been already performed to study the bending and shear strength of the encased composite girders[3]. It has been proved that the encased composite girder had extremely high ultimate bending and shear strength as compared with the conventional steel I-girder. Next, the analytical methods have been also suggested and it has been verified that these methods were valid as the estimation method compared with the test results[3]. In this paper, it is the main purpose of establishing the new retrofit method to the steel I-girder bridge subjected to damage(buckling deformation, corrosion and fatigue crack, for example). Thereupon, as the application of the above-mentioned new type of steel-concrete composite bridge using the partially encased composite girder, the new retrofit or rehabilitation method of partially encasing with concrete is proposed to strengthen the steel I-girder deformed by buckling or subjected to damage. Previously, the bending test and combined (subjected to bending and shear simultaneously) test of the steel I-girder are performed to bring ultimate strength to occur local buckling. Next, for the partially encased composite I-girder strengthened by the new retrofit method, the bending and combined test are also carried out, and it is confirmed the encased girders have much strength capacity and the retrofit method is valid. This paper summarizes above results.

2. Partially encased composite I-girder

2.1 Outline of the encased I-girder

As above mentioned, although the continuous steel I-girder bridge is one of the most common bridge, large bending moment and shear force occur around the intermediate support and the lower flange is on compression side by negative bending moment. For that reason, an improvement is needed to prevent local buckling. Generally, the way that the thickness of upper/lower flange and web are large or many stiffeners are allocated around the intermediate support is adopted. But, the complicated work is needed at that way.

As a solution of this problem, the authors have proposed the new type of steel-concrete composite bridge using partially encased I-girder which reinforcing bars are welded to the flanges and concrete is filled into the areas surrounded by the flanges and web, and by the flanges and vertical stiffeners (Fig.1). By encased concrete, not only concrete contributes itself to increase the cross-sectional

stiffness, but also the deformation of flanges and web is constrained by the encased concrete so that it is expected to increase the strength against the flexural-torsional buckling of compression flange and the shear buckling of the web.

2.2 Structural characteristics of the encased I-girder

First of all, the bending tests were carried out to grasp the structural characteristics of the partially encased composite I-girder and the conventional steel I-girder[3]. In the encased I-girder, the concrete restrained the local buckling of flange and web at the same time the concrete showed confined effect. As a result, the ultimate bending strength of the encased I-girder was 2.08 times than that of the steel I-girder.

Secondly, the shear tests of the encased I-girder and conventional steel I-girder were carried out. It was also cleared that the ultimate shear strength of the encased I-girder was 2.89 times than that of the steel I-girder. It was presumed that this improvement upon the ultimate shear strength of the encased I-girder would be due to the effect based on the truss theory, which consist of compression strut by concrete and tension strut by steel web.

3.Proposal of the retrofit by partially encased concrete

3.1 Damage of the steel I-girder and the retrofit

The corrosion (rust) of the steel plate, the fatigue crack from the weld part (as shown in Fig.2), the flexural-torsional buckling of the compression flange and the shear buckling of the web have been regarded as the damage of the steel I-girder. Usually, strengthening with cover plate and bolt (as shown in Fig.2) is carried out about corrosion or fatigue crack, however, it is often dealt with as a temporary strengthening method and has not been established as a permanent strengthening method.

Heating reform is taken as a retrofit method for the shear buckling of the web when deformation is small, but it is disadvantageous from a viewpoint that it must be done carefully in the site. In case of large deformation, a troublesome treatment, which is the method of exchanging and renewing object members, is needed. In addition, there are few examples for the flexural-torsional buckling of the compression flange.

3.2 Retrofit by partially encased concrete

In case that web or flange of the steel I-girder is taken large buckling deformation by the excessive load or crash of heavy equipments, there are hardly any proper strengthening method and the standardized method hasn't been proposed so far. On these backgrounds, as a new attempt, the authors have proposed that these damaged steel I-girders should be strengthened by partially encasing with concrete into the damaged panel as shown in Fig.3.

4.Verification of the Retrofit Effect

4.1 Outline of the tests

Two specimens of the steel I-girder with shape and dimension shown as Fig.4 and Fig.5 were fabricated and the bending test and combined test about these specimens were carried out. Flange

and web were excessively deformed by torsion and shear force respectively. Their specimens were encased with the concrete after the test, and above loading tests were carried out again.

For convenience, the bending test is simply expressed as M, and combined test as H, and the steel I-girder as S, the encased I-girder as C. For example, the steel I-girder in bending test is expressed as MS.

Rolled steel for welded structure(symbol SM490Y) was used for steel plate, and steel bar for concrete reinforcement(symbol SD345) and nominal diameter D10 was used for the steel bar. The high-early-strength portland cement was used for the concrete, and the nominal maximum size of coarse aggregate was set to 15mm[8]. Mechanical properties of the steel plates used are shown in Table 1. And requirements for mixture and compressive strength(28-day strength) of the concrete used are shown in Table 2.

The panel between two loading points was noticed about MC. Four vertical steel bars were welded between upper and lower flange at one side, and three horizontal steel bars were set (not welded) between two vertical stiffeners. The panels adjacent to the center loading point were noticed about HC.

The loading was held by load control using the oil pressure jack. The measurement subjects were load and displacement of the lower flange in the center of the span and the others, the detail of the measurement was omitted since they were the same as that of reference 3.

4.2 Experimental results and consideration

The tests of MS and HS were held previously. The final form of MS and HS after buckling deformation is shown as Fig.6 and Fig.7. In MS, after flexural-torsional deformation and buckling in the upper flange, the upper side of the web was deformed to the out-of-plane direction. In HS, flexural-torsional deformation and buckling was found in the upper flange of the left-side panel, simultaneously, diagonal tension struts were appeared in the panel. The edge of the upper flange was deformed 30mm to the vertical direction, and the web was deformed 15mm to the out-of-plane direction. HS was also deformed like that. MC and HC consist of these deformed steel I-girders and the encased concrete with the steel bars.

Fig.8 shows the relation between load and displacement of MS and MC in bending test. Fig.9 shows the relation between load and displacement of HS and HC in combined test. As a result, it became clear that the ultimate strength increased remarkably by encasing with the concrete and were 1.47 times and 1.59 times than that of the steel I-girder, respectively, and that they had enough deformation capacity.

5.Conclusions

In this paper, the application of the new type of steel-concrete composite bridge using the partially encased composite girder, the new retrofit method of partially encasing with concrete was proposed to strengthen the steel I-girder deformed by buckling or subjected to damage. And it was proved that the new structure, mentioned so far, was so valuable to retrofit the steel I-girder even if it was deformed excessively. Hereafter, it is important to investigate the effectiveness and availability for

retrofitting fatigue crack and corrosion, and in the future, to establish the method of the retrofit using this new structure. In addition, the part of this research was done in Japanese Society of Steel Construction (Committee for High Performance Steel Bridge using Composite Structure, chairman: Professor Nakamura, Tokai Univ.)

References

[1] Nakamura S.: New structural forms for steel/concrete composite bridges, *Structural Engineering international*, IABSE, Vol.10, No.1, 45-50, 2000.

[2] Nakamura S.: New technologies of steel/concrete composite bridges, *J. Constructional Steel Research*, Vol.18, No.1, 90-121, 2002.

[3] Nakamura S., Narita N. and Hayashi K.: An experimental study on partially encased composite steel I-girder, *Steel Construction Engineering*, JSSC, Vol.9, No.36, 79-92, 2002(in Japanese).

[4] Elnashai A.S., Takanashi K., Elghaouli A.Y. and Dowling P.J.: Experimental behaviour of partially encased composite beam-columns under cyclic and dynamic loads", *Proc. Institution Civil Engineering*, Part 2, Vol.91, 259-272, 1991.

[5] Elnashai A.S. and Elghazouli A.Y.: Performance of composite steel/concrete members under earthquake loading, Part I. Analytical model", *Earthquake Engineering and Structural Dynamics*, Vol.22, 315-345, 1993.

[6] Elnashai A.S. and Broderick B.M.: Seismic resistance of composite beam-columns in multi-storey structures", *J. Constructional Steel Research*, Vol.30, 201-229, 1994.

[7] Kindmann R. and Bergmann R.: Effect of reinforced concrete between the flanges of steel profile of partially encased composite beams", *J. Constructional Steel Research*, Vol.27, 107-122, 1993.

[8] JSCE: Standard specification for concrete, design, 1996.

Table 1 Mechanical property

Test Specimen		Material	Yield point	Tensile Strength	Total elongation
			MPa	MPa	%
MS,MC	Flange(t=12mm)	SM490YA	372	511	30
	Web(t=6mm)		349	513	30
HS,HC	Flange(t=12mm)	SM490YA	400	513	33
	Web(t=6mm)		385	531	33

Table 2 Requirements of mixture

Test specimen	Slump	Entrained Air	Nominal Strength	Compressive Strength
	cm	%	N/mm^2	N/mm^2
MC	8.5	4.2	40	46.8
HC	11.5	4.4	40	58.3

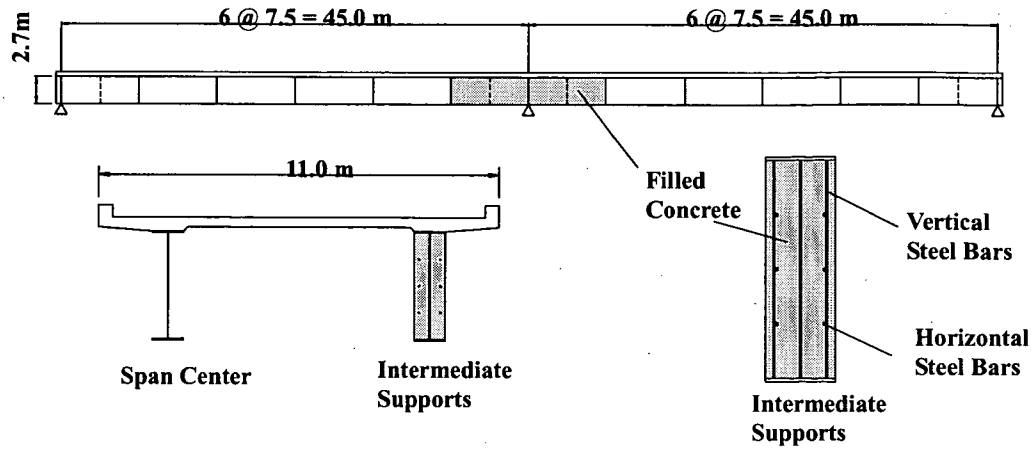


Fig.1 Partially concrete-filled steel I-girder Bridge.

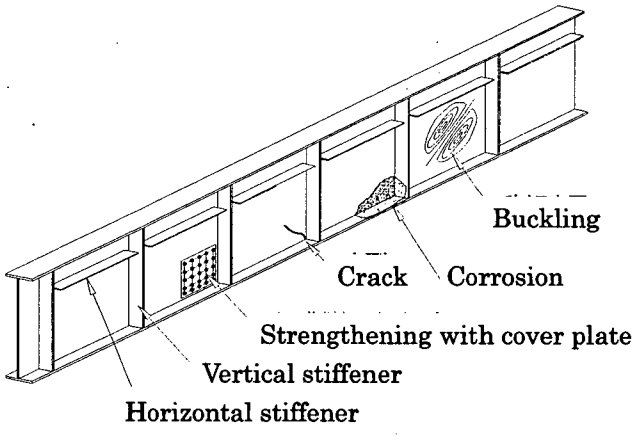


Fig.2 Damage of the steel I-girder bridge and the Strengthening(Repair).

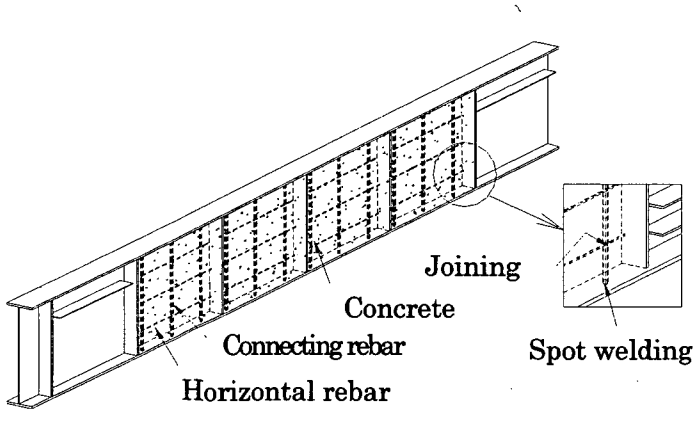


Fig.3 A new retrofit method.

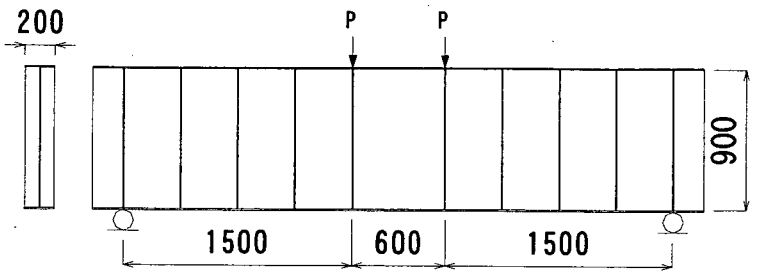


Fig.4 Bending Test.

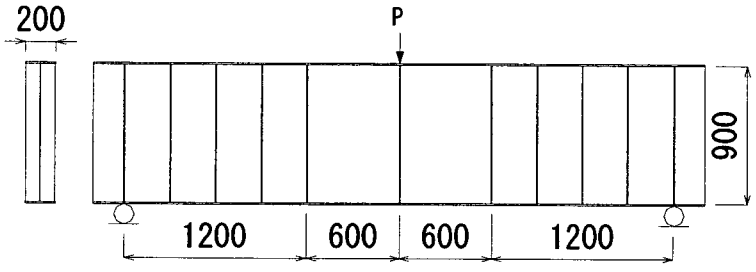
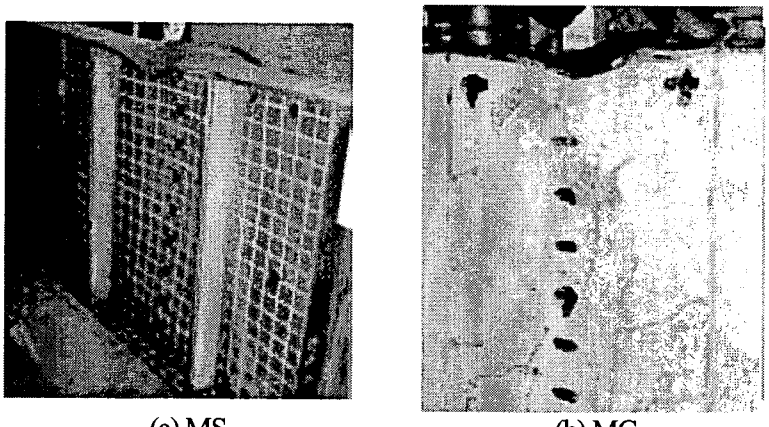
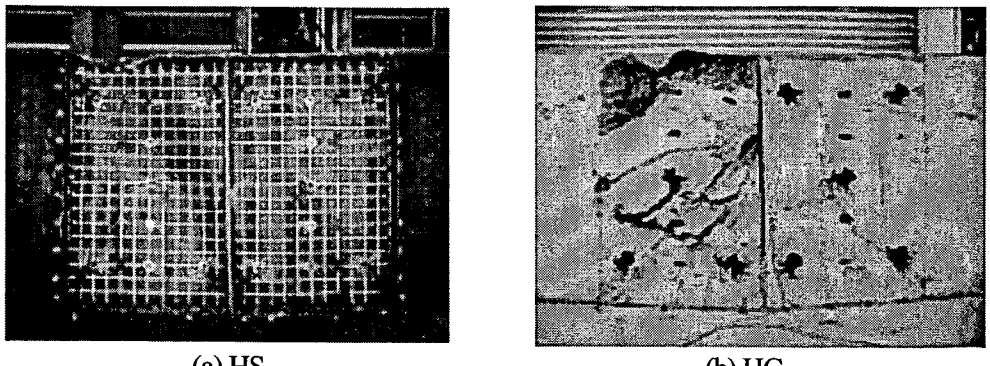


Fig.5 Bending and shear test.



(a) MS (b) MC

Fig.6 Final deformation in bending test.



(a) HS (b) HC

Fig.7 Final deformation in bending and shear test.

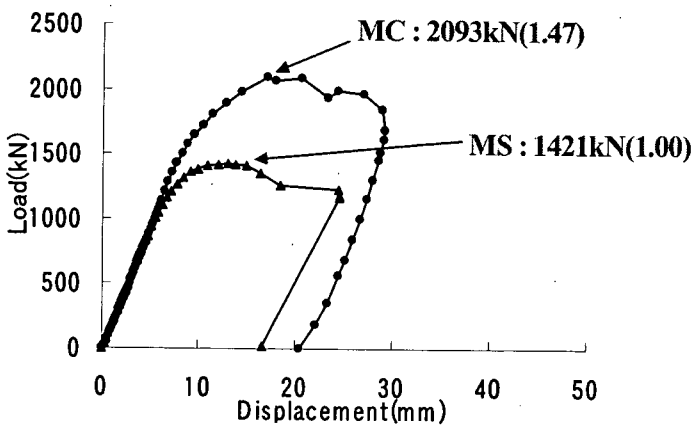


Fig.8 Load and Displacement in bending test.

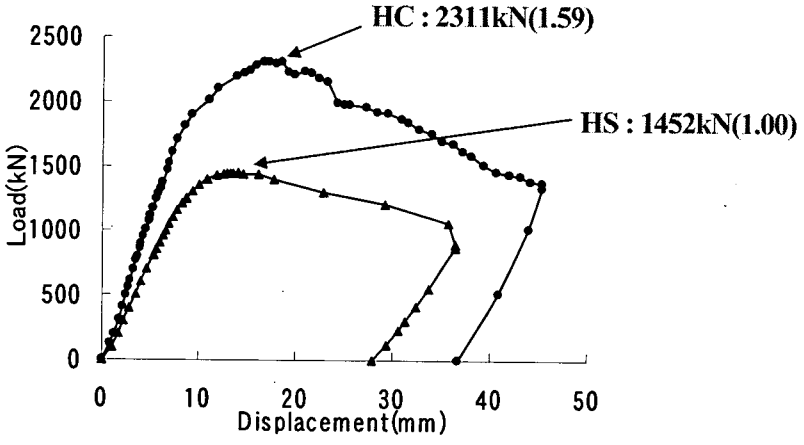


Fig.9 Load and Displacement in bending and shear test.

U.S.A.'s EXPERIENCE USING FIBER REINFORCED POLYMER (FRP) COMPOSITE BRIDGE DECKS TO EXTEND BRIDGE SERVICE LIFE

Jerome S. O'CONNOR[1], and John M. HOOKS[2]

Abstract

Though fiber reinforced polymer (FRP) composites have been used in other industries for years, their use for highway bridge decks is relatively new. Over the past six years, however, approximately 50 bridges have been built or rehabilitated with FRP decks. Since all of these were designed and constructed without the benefit of nationally accepted standards, there are varied lessons to be garnered from these projects. This paper summarizes the experience of state agencies, presents some case studies, and, based on this information, suggests when the use of FRP decks is most appropriate.

BACKGROUND

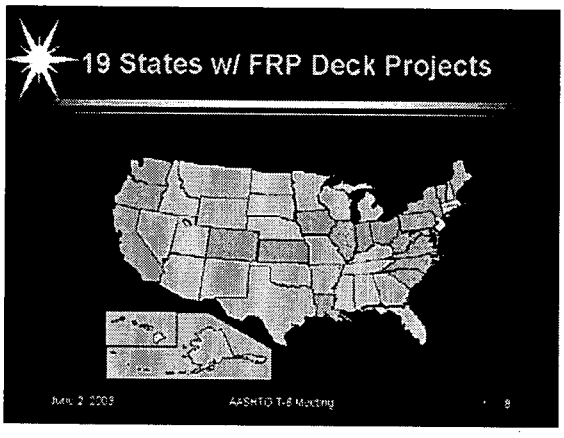


Figure 1. States that have installed FRP decks.

Fiber reinforced polymer composite decks & superstructures have been used in lieu of conventional construction material on approximately 50 bridges in the USA. The purpose of this paper is to summarize experience with these bridge elements and suggest when their use should be considered. Implementation of composite technology has been fostered through a special funding program authorized under the Transportation Equity Act for the 21st Century and administered by the Federal Highway Administration (FHWA). This Innovative Bridge Research and Construction (IBRC) Program is part of a recent emphasis better construction practices and materials that will improve the performance of our nation's bridges.

[1] Multidisciplinary Center for Earthquake Engineering Research, Buffalo, NY ; FHWA's FRP Virtual Team

[2] Federal Highway Administration, McLean, VA; FHWA's FRP Virtual Team

The FHWA has defined a vision for a "bridge of the future" by listing general performance requirements. Composite materials have characteristics that can help meet these objectives. This ideal bridge will have characteristics that will allow the objectives listed below to be met.

- Life cycle cost is a fraction of the current expectation.
- Construction time is a fraction of the current time.
- Material degradation is no longer an issue.
- It is immune to attack from floods and earthquakes.
- A total systems approach is used in their design
- Adaptable to new demands

In addition to advocating moving toward the "bridge of the future", the FHWA is promoting stewardship and management of the existing bridge infrastructure. Some strategies being promoted include: using cost-effective and innovative repair and rehabilitation techniques (in lieu of replacement); use of accelerated construction techniques for rehabilitation of bridges; and use of prefabricated or modular components and systems. Fiber reinforced polymer composite decks & superstructures are ideal systems for use in these strategies and, in some cases, can be effectively used in cases of deteriorated decks, load posted bridges and narrow bridges.

MATERIALS and MANUFACTURE

FRP bridge decks and superstructures are typically made with vinyl ester or polyester resin reinforced with E-glass fiber. They are pre-fabricated in a shop, then assembled and installed at a bridge site where a wearing surface is added. FRP's are engineered materials with their strength dependent on several factors such as fiber type, orientation and percent volume, resin type, manufacturing method, and the bonding materials used in the final assembly.

In the U.S. there are more than six competitive suppliers of these systems. Each uses one of three basic manufacturing methods:

- *pultrusion* (e.g. Martin Marietta Composites),
- *vacuum-assisted-resin-transfer-molding* (VARTM) (e.g. Hardcore Composites)
- *open mold hand lay-up* (e.g. Kansas Structural Composites)

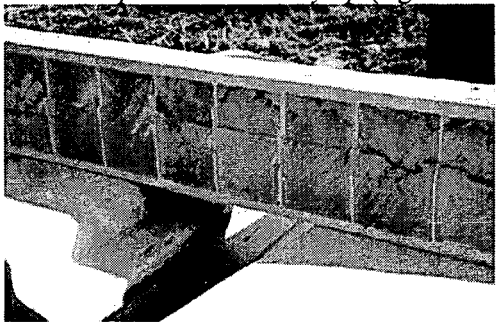


Figure 2. X-section of a VARTM deck.

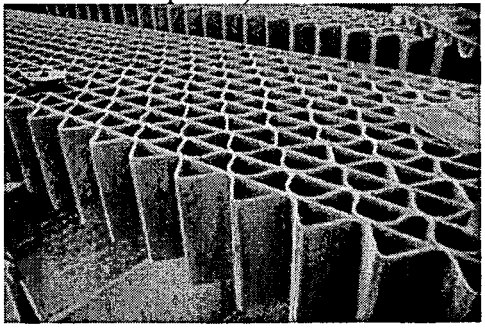


Figure 3. Core of an open mold deck.

Figures 2 and 3 illustrate two "sandwich" systems where a core is bonded between a top and bottom face sheet. Table 1 is offered as a qualitative comparison of the manufacturing methods. Each method has its own merits.

Figures 4 and 5 illustrate the pultrusion manufacturing process. A complex array of glass fiber is pulled through a resin bath and heated as it passes through a die to produce sections that are bonded together to form deck panels.

Manufacturing method	**Ability to customize**	**Adherence to dimensional tolerance**	**Attractive cost**	**Ability to incorporate special features (e.g. scuppers)**	**Overall quality**
1. Pultrusion	L	H	L	L	H
2. VARTM	H	L	H	H	M
3. Open mold	H	M	H	M	M

Table 1. Qualitative comparison of manufacturing methods.
Relative benefit: H = high, M = Medium, L = Low

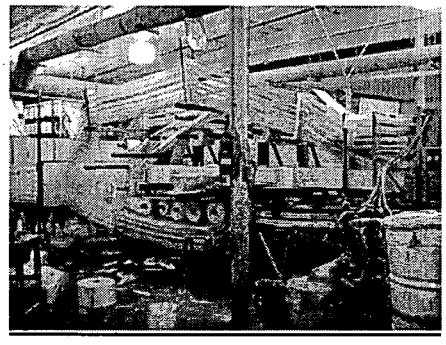


Figure 4. Pultrusion of glass fiber and resin.

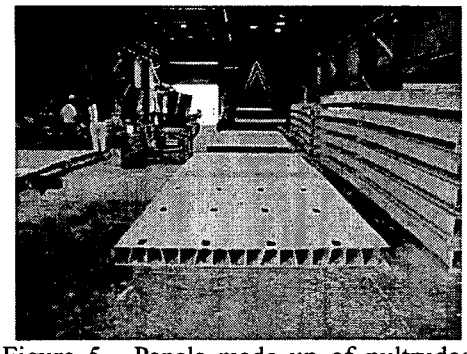


Figure 5. Panels made up of pultruded sections.

A list of known suppliers and completed projects can be found at the following internet web site: http://www.fhwa.dot.gov/bridge/frp/frppract.htm

BENEFITS

Currently, bridge decks made of composite materials cost more than conventional concrete decks. However, comparing costs on a unit area basis does not always give a true indication of value. The unique properties that FRP materials give certain advantages that can still make FRP a prudent choice for bridge decks and superstructures.

One important benefit is derived from the *prefabricated* nature of FRP decks. These benefits are shared with pre-cast concrete construction and are well known for their ability to *speed construction* and *minimize traffic delays*. An environmentally controlled factory environment also lends itself to an improvement in *quality*. The Federal Highway Administration is encouraging modular construction as a means of meeting tax payers' demands for *less environmental and economic impact* resulting from construction projects (e.g. less delay, wasted fuel, noise, and pollution). Additionally, because of the short time needed to fabricate a bridge and the possibility of stockpiling standard sizes, a project's initiation and planning phase can be dramatically decreased. This can be a big benefit in emergency situations. Establishing standard bridges for mass production could also simplify the purchase of these modular units to allow installation by smaller agencies with small work forces and light equipment.

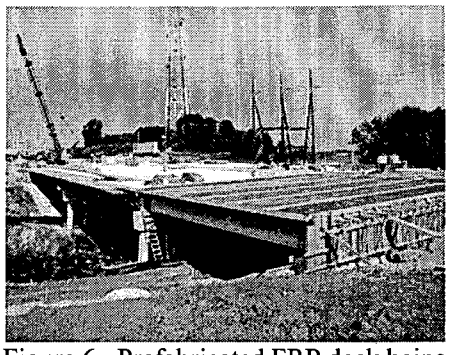


Figure 6. Prefabricated FRP deck being installed on prefabricated prestressed concrete beams. Bettendorf, Iowa.

Another spectrum of benefits stems from the *light-weight* nature of FRP. Weight savings over concrete can allow the conversion of dead load to live load carrying capacity. Instead of 581 kg/m^2 (120 psf) for a typical concrete deck, a bridge can be designed for 122 kg/m^2 (25 psf) or less. On a rehabilitation project, the weight savings can result in an improvement in load ratings, possible removal of weight restrictions and restoration of full service even after factoring in the reduced capacity of a steel superstructure due to section loss. Use of a light deck can also allow widening to accommodate an additional lane or shoulder without requiring major improvements to the substructure.

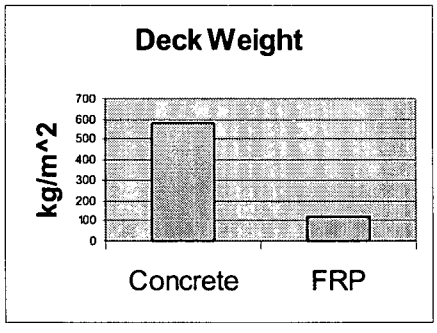


Figure 7. Weight per Unit Area

On new construction, the weight savings might *lower foundation requirements* (e.g. fewer or smaller piles). The reduced mass also provides a substantial *reduction in earthquake induced displacements*. This is particularly helpful on elevated structures or those in proximity to a fault.

Composite decks also offer the potential for *long service life*. Though they have yet to undergo the test of time, the fact that they do not crack like concrete nor corrode like steel suggest that they will last for many years with little maintenance. Concrete decks are typically predicted to last 25 years before requiring replacement. Today, design life

of FRP decks is comfortably set at 75 years (i.e. the life of the bridge). De-icing salt is not a problem for a properly detailed FRP system. Noticeably, over half of FRP deck projects in the USA have been in the states of West Virginia, Ohio, and New York where the use of de-icing salts has led to the premature deterioration of many existing concrete bridge decks and steel bridge superstructures.

The properties of composite bridge elements can be *tailored to meet the requirements* of the job by changing the fiber architecture. By varying the fiber type, density within the matrix, number of layers, and orientation, the strength of a deck can be customized in each direction. By engineering the material, most efficient use can be made of each constituent, thereby optimizing the overall system and improving cost effectiveness. Although this may not be worthwhile on a project by project basis, a manufacturer's deck design can easily be tailored to certain classes of bridges to match required load and deflection criteria.

The benefits of prefabrication, weight and *corrosion resistance* make composite materials a good material for certain types of bridges.

Project cost savings can be realized when FRP materials are prudently utilized. For instance, if it is possible to rehabilitate an old steel truss bridge using composite material, a complete bridge replacement can be avoided, resulting in substantial savings. This "fixes the problem" and frees up funds for use on other deficient bridges.

Certain bridge types are well suited to FRP decks. *Historic bridges* particularly benefit from light-weight decks. These older structures were often designed to accommodate a light (e.g. timber) decking material and need a product of similar weight when rehabilitated. Using a high tech material like FRP offers advantages unavailable when replacing in-kind. The FRP system is most often *water-tight* and provides protection to the flooring system below. In contrast, timber decking is prone to leakage that can lead to premature corrosion of lightly designed steel members. The composite system also can accept a thin, light, skid resistant wearing surface that can further improve live load capacity.

Movable bridges are a particularly good application for FRP decks. Whether for rehabilitation or new construction, the lower weight can decrease *lift requirements*, resulting in lower capital, operating and maintenance expenses while at the same time reducing the potential for excessive displacements during earthquake induced ground motion.

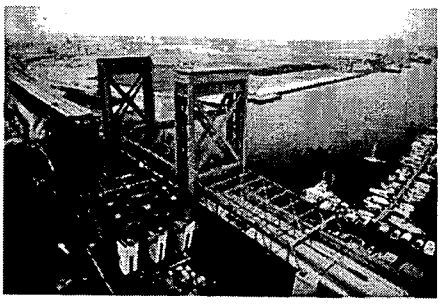


Figure 8. Schuyler Heim lift bridge Long Beach, CA

CASE STUDIES

Case Study #1

Location: Route 367 over Bentley Creek, Chemung County, New York State

A 126' truss, built in 1941, was posted with a 14 Ton weight restriction due to section loss in the steel superstructure and flooring system. There was also excessive dead load from numerous courses of asphalt wearing that had been added over the years. Using VARTM-FRP technology, the service life of the bridge was extended from 60 years to 90 or more.



Figure 9. NY 367 over Bentley Creek, a typical truss application.

Relieving the bridge of 265 Tons of dead load allowed it to be restored to full service, thereby avoiding a complete bridge replacement. Replacing the deck in-kind with concrete would not have alleviated the posting problem.

Because so many bridges are in need of replacement, competition for funds and a place on the capital program would have meant making the public wait five years or more for a solution. The rehabilitation with FRP was started immediately upon discovery of the problem instead of waiting. By custom designing the composite material and using a depth of 14", the deck could be designed to span from transverse floor beam to floor beam. This meant that deteriorated longitudinal steel stringers would become non-supporting and could be left in place without repair. Computed load ratings for the bridge were verified through load testing and were shown to be even higher than the bridge's original design. The total project cost was $1 million less than the next most feasible alternative.

Case Study #2

Location: MD Route 24 over Deer Creek, Harford County, Maryland

This was also a truss rehabilitation, but the structure is on a severe skew (34°). The state DOT formed a committee of state and federal engineers, a university professor and contractors to assist with selection of the decking supplier. Since costs on the proposals received contained approximately the same unit price, the primary consideration was constructability. The group chose to use pultruded panels placed transversely and secured to the steel stringers with grouted pockets encasing stud shear connectors. It was supported along the skewed edge with a concrete diaphragm. The project successfully demonstrated how quickly an FRP deck system could be installed.

The bridge, originally built in 1934, was redecked in just weeks. Upon completion, and prior to opening to traffic, a load test was conducted to demonstrate that the conditions of the deck specification were met, and to establish a baseline for future testing. The testing also verified that the chosen connection detail provided composite action between the deck and steel. Continuous monitoring is being performed with network of strain gages and a wireless communication system.

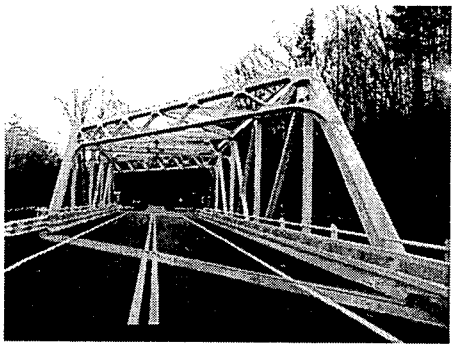


Figure 10. MD Route 24 over Deer Creek Note the high skew angle.

Case Study #3

Location: NY Route 248 over Bennetts Creek, Steuben County, New York State

In this case, a severely deteriorated concrete slab bridge, which was posted at 10 Tons, was removed and replaced with an all composite superstructure. The project was easily accomplished by a bridge maintenance crew which was not accustomed to doing this type of work. The installation of the superstructure took just a few hours. The replacement bridge arrived at the site on a truck in two pieces, then was placed on reconstructed abutments. The final wearing surface came pre-installed, as did composite stay-in-place forms for a concrete barrier.

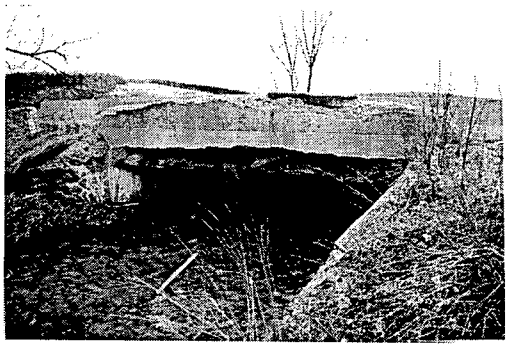


Figure 11. Original concrete slab built in 1926.

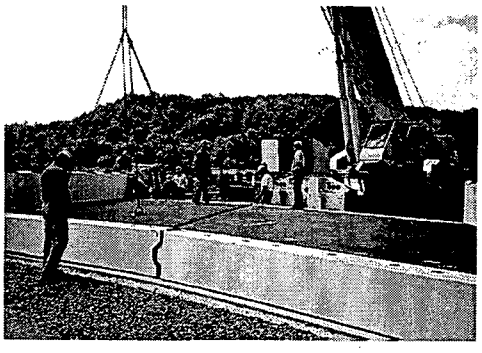


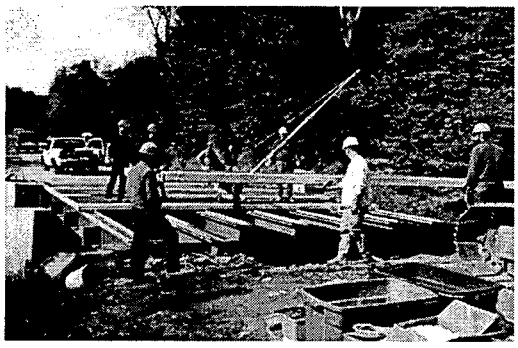
Figure 12. FRP slab bridge built in 1998.

The objective of the project was to replace a deteriorated 1926 bridge with a FRP superstructure and do it on a compressed time schedule using in-house DOT maintenance forces. The 24 inch deep FRP superstructure consists of two skewed panels. The panels are joined along the centerline of the road with a shear key and adhesive grout providing load transfer between them. A crown was provided by sloping the bridge seat. The bridge railing is a cast-in-place concrete parapet with double steel box beam tubing mounted on the face. The parapet is anchored to the

superstructure by epoxy coated rebar cast into the FRP deck at the time of fabrication. A 3/8-inch epoxy/basalt polymer concrete wearing surface (Transpo T-48) was applied in the shop. The project was opened to traffic in October 1998, nine months ahead of schedule.

Case Study #4

Location: County Route 46 over East Branch Salmon River, Lewis County, New York



The goal of this project was to replace the existing open steel grating at an economical cost. Five deck panels, each 5-inches thick, were installed transversely on the existing supporting steel. The panels were all placed within two and a half hours. The panels were of high quality and the fit of the panels was precise. Initial load test confirmed that the structure meets HS20 Loading.

Figure 13. CR46 over East Branch Salmon River

SUMMARY

There are about 50 bridges in the United States that are carrying public traffic on fiber reinforced polymer composite decks. Experience with this technology has been generally favorable and further deployment of the technology is anticipated. This section summarizes the benefits of FRP, some of the limitations, issues that need to be studied further, and facets that affect the economics of their use. Observation of the installed decks while in service will provide a great deal of additional insight.

Value Added

Economic value

Since these decks cost more than conventional materials when compared on a unit area basis, applications need to be selected on some criterion other than first cost. Situations where their value might be recognized include when:

1) Life cycle cost is considered in the economic analysis. The expected service life of the composite deck exceeds 75 years with little or no maintenance. This is about three times the expected life of a concrete bridge deck.
2) Their light weight provides a direct benefit by allowing the load capacity ratings of

a bridge to be increased or maintained, such as when:

a) A bridge was originally designed for a light weight deck. FRP will allows the bridge to carry the same live loads without continuing problems associated with open grate decks.
b) Additional dead load has been added over the years. The dead load from the original deck and overlays can be "traded in" for live load capacity.
c) There is reduced capacity in the steel superstructure due to section loss. Using a light deck can allow the same loads to be carried without having to strengthen members weakened by loss of cross section.
d) Weight savings can lead to decreased operating expense, e.g. movable bridges.
e) Switching from a heavy deck to a light weight deck can increase load capacity to compensate for loading that was not anticipated during design.

3) The deck can be used to protect the flooring system from water and salt
4) Speedy construction results in
   a) Shorter need for maintenance and protection of traffic schemes
   b) Decreased user cost (e.g. fuel costs, value of time)

Less tangible benefits

Additional value can be obtained with the use of FRP decks, although they are not so easily identified and quantified by an economic analysis. Further reasons to consider their use are:

a) FRP can make the salvage and restoration of a historic structure possible.
b) Quick and easy installation means less disruption to the environment (e.g. air and noise pollution).
c) Speedy construction results in decreased inconvenience to the user.
d) There is less maintenance required due to resistance to chemical attack.
e) Alternative procurement methods become available because of their pre-manufactured nature. A bridge deck can be purchased and installed instead of built on site. This type of product delivery can result in less administrative cost while accelerating implementation of a solution to the problem at hand.
f) They can lessen a structure's vulnerability to dynamic loads such as earthquakes.
g) Several manufacturers are willing to provide a product warranty which is not typical for the construction industry. A department of transportation (DOT) agency frequently discovers defects in construction projects within a few years of completion, but since it is well beyond formal project acceptance, they are forced to accept the consequences. Using warranteed manufactured projects can eliminate some of the problems intrinsic to with field construction.

At his point in time, the technology is most suitable for trusses, historic structures, bridges originally designed for light loads, bridges to be widened, bridges where the superstructure is in good condition but the deck is poor, bridges that can be rehabilitated with a complete FRP superstructure and the abutments are salvageable, bridges where a low dead load is desirable, movable bridges, emergency bridges and temporary, rapidly deployed bridges.

Disadvantages

There are certain disadvantages associated with using FRP at the present time. Initial cost is probably the largest barrier to widespread use of these materials. Even when there is a valid case for their use, it is not always obvious that FRP provides a cheaper alternative. For instance, consideration of user costs and life cycle costs is not always a practice of a transportation agency that is trying to allocate resources based on a limited amount of construction funding. A careful assessment of the circumstances is necessary to assure a prudent use of limited resources; extra time and money can be consumed convincing key decision makers that the risk of using an unfamiliar material is reasonable and acceptable.

Also, FRP has a low modulus of elasticity when compared to steel and concrete (~3,000 ksi vs. 29,000 ksi). This has a direct affect on the stiffness of an FRP structure or deck panel. In order to meet serviceability requirements for deflection, FRP systems are inevitably over designed from a strength perspective. New shapes, manufacturing methods, and hybridization with other materials may lead to a more optimal design, but for now we accept a high factor of safety that is counter to economy of cost. Similarly, uncertainty over material properties gives rise to conservatism and subsequently higher cost. Until manufacturing methods become adopted that assure consistency in material properties that are verifiable with standard testing methods, specification writers will necessarily need to write a tight specification to insure the finished product will be safe and reliable.

Also, manufacturers have not demonstrated a desire to produce a shared standard design. Because of their complexity, a new deck design typically requires a finite element analysis. Furthermore, engineers have ethical responsibilities that prevent them from accepting a "black box" design without fully understanding its behabior. Manufacturers' proprietary interests inhibit acceptance by the practicing engineer and create unnecessary difficulty and confusion. Most bridge designers are not experts in composite materials and prefer to stay with well understood materials rather than venture into the world of new materials and fiber architecture. Since they also need to be considerate of the cost of their services to the bridge owner, it is reasonable for them to take this approach. This also protects them from a perceived increased liability stemming from the use of a non-standard, relatively unknown commodity.

Further Research

Further evaluation of installed decks and laboratory specimens will result in a better understanding of the performance of materials and systems. This will aid the development of better specifications. Some issues needing further investigation are listed in Table 2.

1. Thermal properties (both global and local) 2. Composite behavior 3. Connections to the superstructure 4. Design optimization 5. Deflection control 6. Selection, grading and durability of resins and adhesives 7. Local deformation under wheel loads 8. Wearing surface selection and installation 9. Field joints between prefabricated panels 10. Bridge railing and attachment to the deck 11. Fatigue and long term performance 12. Methods of inspecting and monitoring 13. Repair, strengthening, and stiffening 14. Creep and the potential for sudden failure due to rupture 15. Changes in a bridge's global response to dynamic loading after relieving dead load 16. Ability to reuse or recycle materials

Table 2. Further investigation needed.

Lessons learned

1. Since FRP material is not commonly understood by engineers designing infrastructure projects, FRP suppliers should be held to a performance based specification. Using performance standards also has additional benefits of encouraging innovation and allowing the refinement of new technology.
2. Anticipated strains should be kept under 20% of minimum guaranteed ultimate strength to avoid the risk of creep rupture.
3. Imposed deflection limits should be given careful consideration because of the effect on the cost of the system. The limit selected is a function of rider comfort, but also the ability of the wearing surface to endure local flexure.
4. Consideration should be given to the fact that composite material properties may deteriorate with time. Manufacturers' certified values for material properties may need to be "knocked down" to account for this.
5. An owner should insure that a manufacturer can credibly certify consistency of quality and then should provide its own quality assurance checks. Because most agencies do not have in house expertise in composite materials (and the manufacturer will often be in another state), it will not be feasible to deploy full time plant inspectors to oversee fabrication of FRP decks. Bridge owners will need to rely on a third party certification procedure (e.g. ISO 9001 certification).
6. DOT agencies should ask for a manufacturer's product warranty. Though not offering as much safeguard as a performance bond, it provides a certain level of protection to offset increased risk.

In addition to technical hurdles, increased use of advanced materials for bridge decks

will depend on such factors as

a) Training among engineers who are currently practicing and those passing through the academic institutions now.
b) Standard specifications for design, construction and materials testing.
c) Comfort level and understanding. It's new and unfamiliar to the industry. In contrast, properties of reinforced concrete are well known.
d) Risk and fear of the unknown.
e) FRP industry's lack of understanding of standard construction practices and the importance of project schedules. DOT's have a very direct interaction with their client, the tax-paying, traveling public and manufacturers may not be sensitive to the associated responsibilities.

Conclusion

Currently, FHWA encourages the use of innovative construction materials and techniques by providing earmarked funding. The Innovative Bridge Research and Construction Program has provided engineers with the opportunity to exploit the unique properties of these materials even though they might not otherwise be competitive. While the program successfully created an incubation period for engineers to try out the materials, the true measure of success will come when FRP decks are able to compete on their own without supplemental financial support. The above case studies and discussion should offer some insight as to when they can be cost effectively used today.

Acknowledgments

Funding for many of the projects studied was provided by the U.S. DOT Federal Highway Administration (FHWA) under its Innovative Bridge Research and Construction (IBRC) program. The authors thank all contributors of project photographs and Martin Marietta Composites for providing photographs of the manufacturing process.

Disclaimer

Content is the sole responsibility of the authors and does not necessarily reflect policy of Federal Highway Administration, MCEER, or any other agencies cited. Mention of any material, manufacturer, or supplier does not constitute endorsement by the authors or agencies involved.

Fatigue Life Extension of Damaged RC Slabs by Strengthening with Carbon Fiber Sheets Attaching Method

Nobuhiro Hisabe[1], Masasumi Okada[2], Daisuke Miyama[2], Shigeyuki Matsui[3], Hiroshi Onishi[3], Akira Kobayashi[1], Hideaki Fukagawa[1], and Yousuke Mimoto[1]

Abstract

A series of wheel trucking fatigue tests were conducted on the intentionally damaged reinforced concrete slabs of highway bridges strengthened with carbon fiber sheets attached by the grid bonding method. As a result of this experiment, it was found that grid-bonding method where carbon fiber sheets were bonded with intervals on the bottom surface of concrete decks was roughly 10 times higher than that of a non-strengthened RC slab, and there was no problem in adhesiveness in grid bonding parts.

1. Introduction[1)2)3)]

Recently, the deterioration of infrastructures becomes a very important social problem in Japan. Especially, the deterioration of bridges that are ones of structural factors for transportation network is recognized as the most important problem. The decks of road bridges are key members in bridges because many damage cases are found out in these members. The serious damages in decks lead to the loss of performance of bridges and it often becomes the cause of replacement of bridges.

To keep the performance of bridges, it is the one of most important propositions to keep the soundness of decks. In the situation as mentioned above, many methods of repair of decks are developed.

The carbon fiber sheets (hereafter called CFS) attaching method is the one of the remarkable repairing methods. Because it is able to apply to the bridge decks without any influence on the traffic and the application of this method is easier than other methods. However, it is often pointed out that there are following problems.

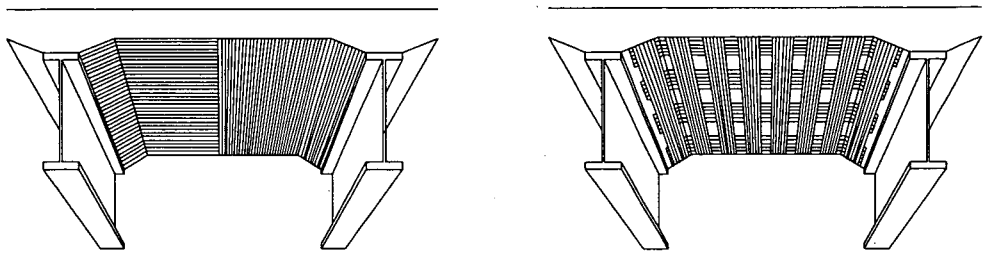
1. There is not any accurate checking method of the state of decks after application of the CFS attaching method.
2. In the decks applied with CFS attaching method, it is difficult to drain off the rainwater supplied from upside because of the lack of the performance on the draining water.

To solve these problems, the authors picked up the new attaching method. As shown in **figure 1**, the strips of CFS are attached in the grid style in this method. And the opening areas between CFS are used as the drainage for water and the windows for observation to check the situation of decks. In this method, the problems mentioned above will be solved.

But it is necessary to check the influence of the discrete arrangement of CFS because it is not clear whether the CFS in discrete arrangement is effective or not. Then the authors

[1] Carbon Fiber Repair and Reinforcement Research Association (CFRRA), Japan
[2] Tokyo Metropolitan Expressway Public Corporation, Japan
[3] Civil Engineering Graduate School Osaka University, Japan

prepared the deck specimens applied the CFS attaching method in two arrangements and carried out the wheel load running test with these specimens to investigate the influences of arrangement of CFS.



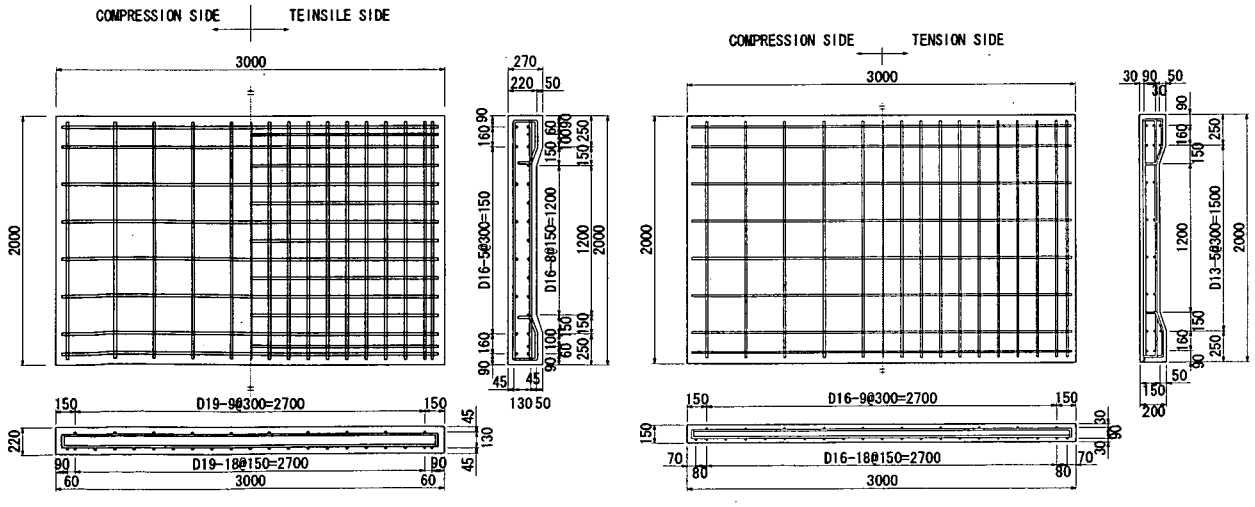
(a) Continuous arrangement (b) Grid arrangement

Figure 1 Arrangements of CFS

2. Structure of experiment

2-1 Test specimen

To investigate the influence of attaching styles, 6 specimens of decks were prepared. These specimens were divided into 3 groups (type A, B and C) by its structure. As an example, the structure of the specimens of type A and B used in this study is shown in **figure 2**. The dimensions of the specimens are 3,000mm long and 2,000mm wide. The thicknesses of specimens are 220mm (type A), 150mm (type B) and 180mm (type C). The span of the specimens is 1800mm long. The specimen of type A is designed with Japanese specifications for highway bridges in 1996. And the specimens of type B are also designed with Japanese specifications for highway bridges in 1964. The arrangements of reinforcements are shown in **table 1**.



(a) Type A (b) Type B

Figure 2 Structure of specimens

In this study, the authors picked up the two types of the arrangements of CFS to confirm the strengthening effect of new grid form arrangement. The tested arrangement is shown in **figure 3**. The width of CFS is 250mm and the spacing between CFS is set as 100mm or 150mm width as shown in figure 3. The elastic modulus of CFS used in this test is 440GPa. The attached values of CFS are set at 400g/m^2 (0.220mm) or 470g/m^2 (0.259mm) to check the influence of the attached value of carbon fiber. The combinations of the structure, types of carbon sheet and spacing between carbons sheets are shown in **table 2**.Properties of CFS are shown in **table 3**.

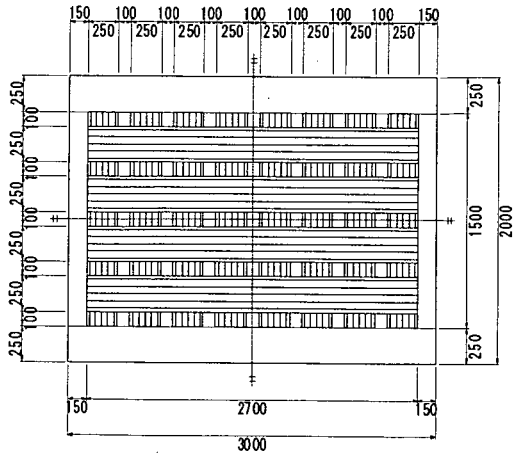
Table 1 Arrangements of reinforcements

Thickness of specimens	Main bar		Distribution bar	
	Diameter (mm)	Spacing (mm)	Diameter (mm)	Spacing (mm)
220 mm	16	150 (300)	13	300
150 mm	16	150 (300)	13	140 (280)
180 mm	19	150 (300)	16	150 (300)

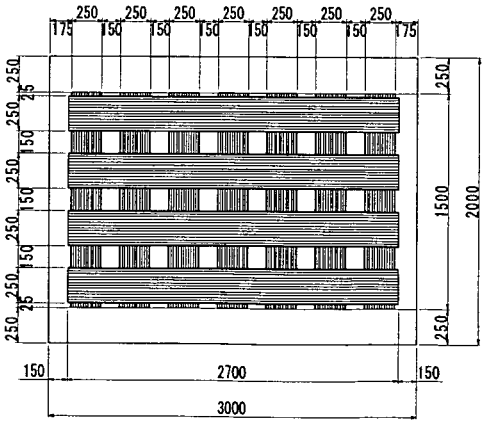
Notice) Parenthetical reference is the spacing in compression side

Table 2 Combination of parameters on tested specimens

Specimen No.	Thickness of Slab (mm)	CFS(g/m^2)	Spacing (mm)	Remarks
1	220	-	-	Without strengthening
2	150	-	-	Without strengthening
3	150	470	100	
4	150	400	100	
5	180	470	150	
6	180	400	150	



(a) Spacing: 100mm



(a) Spacing: 150mm

Figure 3 Attachment styles of CFS

Table 3 Properties of CFS (standard value)

Fiber mass per unit area (g/m^2)	400	470
Tensile strength (N/mm^2)	2400	2400
Tensile elastic modulus (N/mm^2)	$4.40 \pm 0.44 \times 10^5$	$4.40 \pm 0.44 \times 10^5$
Design thickness (mm)	0.217	0.255

2-2 Loading method

(1) Wheel trucking machine

The testing device is for simulating a wheel trucking machine acting directly on a deck slab. **Fig. 4** shows the outline of the testing machine. The testing machine is composed of the chassis running by applying load on the test specimen and the railway on which the chassis is reciprocated by motor rotation. **Table 4** shows the features of the testing machine.

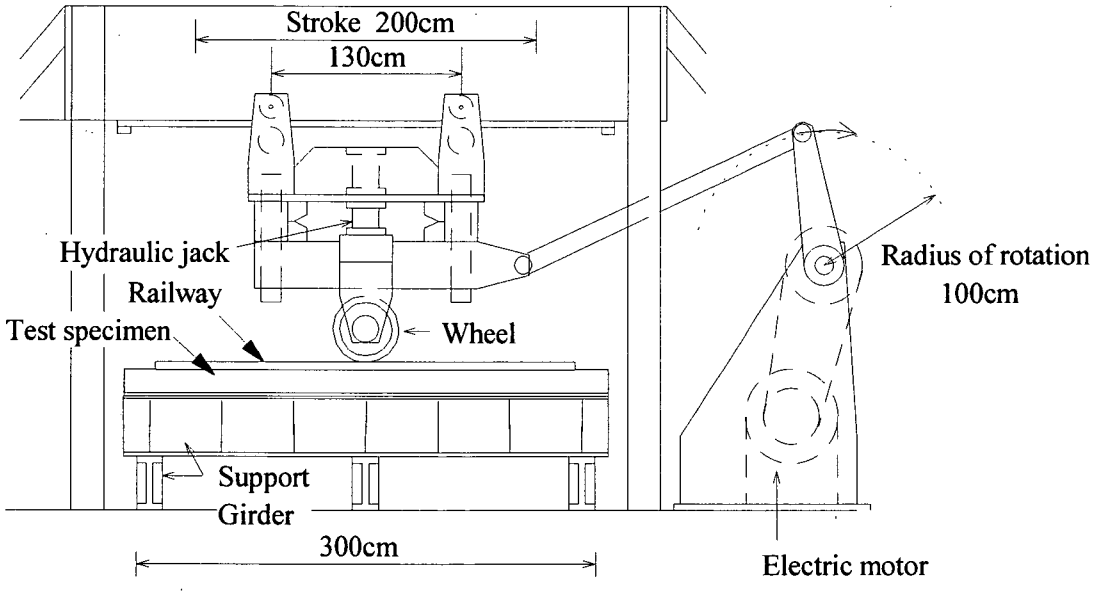


Fig. 4 Outline of testing machine

Table 4 Features of testing machine

Loading capacity	100 ～ 300 kN
Range of load trucking	±100cm from the center of deck slab
Trucking speed	112 m/min. (28 reciprocations / min.)
Diameter and width of wheel	50cm and 30cm

(2) Method of supporting test specimen

The test specimen is supported so that two longer sides are supported simply and two other sides are supported elastically by transverse girders. Furthermore rising prevention device is mounted at four corners of deck slab to prevent the deck slab from rising on account of the wheel load-trucking test.

(3) Track

The track as shown in **Fig. 6** was adopted to realize the area load due to an actual tire running, because an iron wheel was used as the wheel of testing machine. To shift the load by ensuring a constant loading area, many blocks of same size were arranged on the top of deck slab and the traveling load was given to the deck slab through the blocks. The block size was of 12*30*5cm reduced to 60% of each side of the wheel loading area (50*20cm) required by the Road Bridge Regulation. Nineteen (19) blocks were arranged to get a caterpillar form having the clearance of 5mm among blocks. An iron plate of 10mm thick was placed on these blocks to keep the smoothness of wheel traveling surface and in addition, plywood was placed between deck slab and block, and between block and steel plate, respectively to relieve an impact and to prevent friction on the top of deck slab.

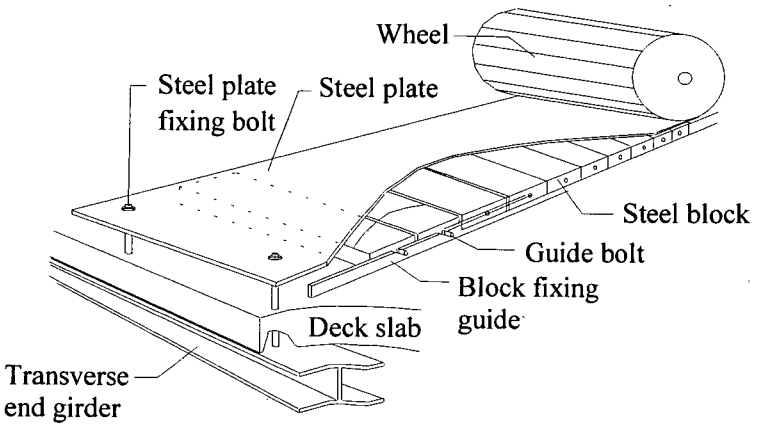


Fig. 6 Outline of track

2-3 Loading procedures

The specimens were pre-loaded by the wheel-trucking machine as the non-reinforcement condition, and after introducing crack damage, the specimens were reinforced with CFS. For No.3 - No.6 after pre-loading, CFS were bonded, and after reinforcing, these were set again to the wheel-trucking machine for the main loading test.

Generally, the fatigue durability (life of slab from the start of loading to failure) of non-strengthened RC slab is indicated uniformly by the relationship of applied load and number of cycles obtained by the existing studies (S-N curve). However, since the S-N curve for CFS strengthened RC slab has not been clarified yet, the fatigue durability shall be evaluated by relative comparison with non-strengthened specimens. Thus, in this test, as an evaluation of the reinforcing effect by CFS, the fatigue durability is evaluated by the relative comparison of the number of loading cycles until failure between non-strengthened and strengthened slabs.

In the experiments, the loads were increased stepwise. For the specimens No. 1, 5, and 6, loading program was started at 150kN and increased to 180kN and then to 210kN. For the specimens No.2-No.4 whose slab thickness are 15cm, loading program was started at

100kN and increased to 120kN, and then to 150kN, since 15cm thick slabs are much weaker than the slabs whose thickness is more than 18cm and damage proceeds rapidly and makes measurement difficult with the 150kN load **(see Figure 6)**.

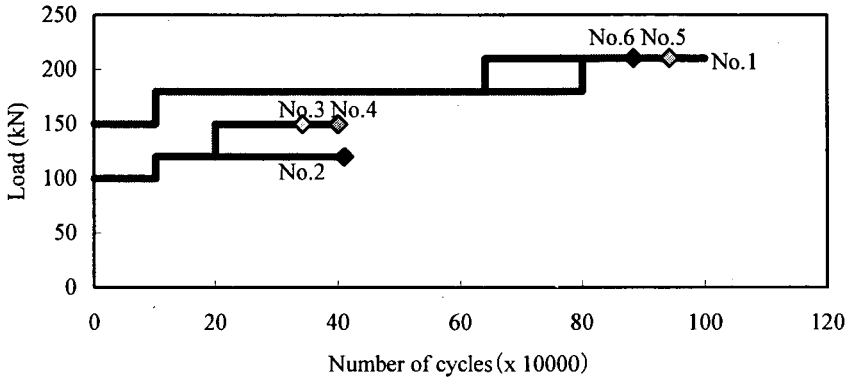


Figure 6 Loading procedures

2-4 Calculation method of converted failure number of cycles

As the applied loading programs are different among specimens, it is difficult to compare the fatigue durability directly with the number of cycles until failure. Thus, to examine the fatigue durability of specimens by comparison, the converted the number of cycles until failure at a constant loading with the reference load P_0=15tf was calculated using the S-N relationship Equation (1) of the WRM at Osaka University and the Miner's rule[4]. Here, for the shear strength of slab P_{sx} [6], the value of the concrete slab without carbon fiber sheet was used.

$$Log\left(\frac{P_0}{P_{sx}}\right) = -0.7835Log(N) + Log(C) \quad (1)$$

Where, P_0: Reference load

P_{sx}: Punching shear strength of the effective cross section perpendicular to the main bars of the slab

N: Number of cycles until failure

C: Constant C= 1.52 when dried, C=1.24 when wet

Here, it is assumed that Miner's rule is applicable to the repeated loading under a random load condition. From Equations (1) and Miner's rule, for the RC slab subjected to random loading, the accumulated equivalent number of cycles n_{eq} to the reference load P_o is shown by Equation (2).

$$n_{eq} = \sum_{i=1,j}\left(n_i \cdot \left(\frac{P_i}{P_0} \right)^{\frac{1}{0.07835}} \right) = \sum_{i=1,j}\left(n_i \cdot \left(\frac{P_i}{P_0} \right)^{12.76} \right) \quad (2)$$

Where, n_{eq}: Equivalent number of cycles with reference load P_o
n_i : Number of cycles with actual load P_i in actual loading condition
P_i : Actual load
P_0: Reference load

3. Experimental result and consideration

3-1 Converted number of cycles until failure

That cracks occurred in two directions was observed on the bottom surface, however, the specimen No.1 did not reach failure until the specified number of loading cycles. Then the test was finished after loading 1million cycles. Specimens No.2-No.6 failed with punching shear failure, which is the same failure mode of non-strengthened specimens. The relationship of the equivalent number of cycles until failure given by equation (2) and the non-dimensional index P_o/P_{sx} is shown in **Table 5** and **Figure 7**. The S-N formula of the slab without CFS is shown with a solid line in Figure 7. The results of the fatigue test given by the wheel-trucking machine at Osaka University [7] were also plotted.

Table 5 Converted the number of cycles until failure

Specimen name	Punching shear capacity of slab P_{sx}(kN)	Reference load P_0(kN)	P_0/P_{sx}	Experiment converted failure number of cycles N_{eq} (cycles)	Remarks
No.1;t22-S96-Without strengthening	41.0	15.0	0.366	21,911,657	Finished before failure
No.2; t15-S64-Without strengthening	21.6	15.0	0.693	18,546	Punching shear failure
No.3;t15-S64-grid bonding EA80	21.5	15.0	0.699	148,366	Punching shear failure
No.4;t15-S64-grid bonding EA68	21.3	15.0	0.706	242,366	Punching shear failure
Calculation;t18-S68 -Without strengthening	28.2	15.0	0.532	654,168	Calculation result
No.5;t18-S68-grid bonding EA70	28.2	15.0	0.532	17,635,963	Punching shear failure
No.6;t15-S68-grid bonding EA60	28.0	15.0	0.537	17,197,202	Punching shear failure

*t15-S64-grid bonding EA80:15cm thick slab, Designed by 1964 Specification for Steel Highway Bridges, Grid-bonding, reinforced with carbon fiber sheet which rigidity (EA) is 80 kN

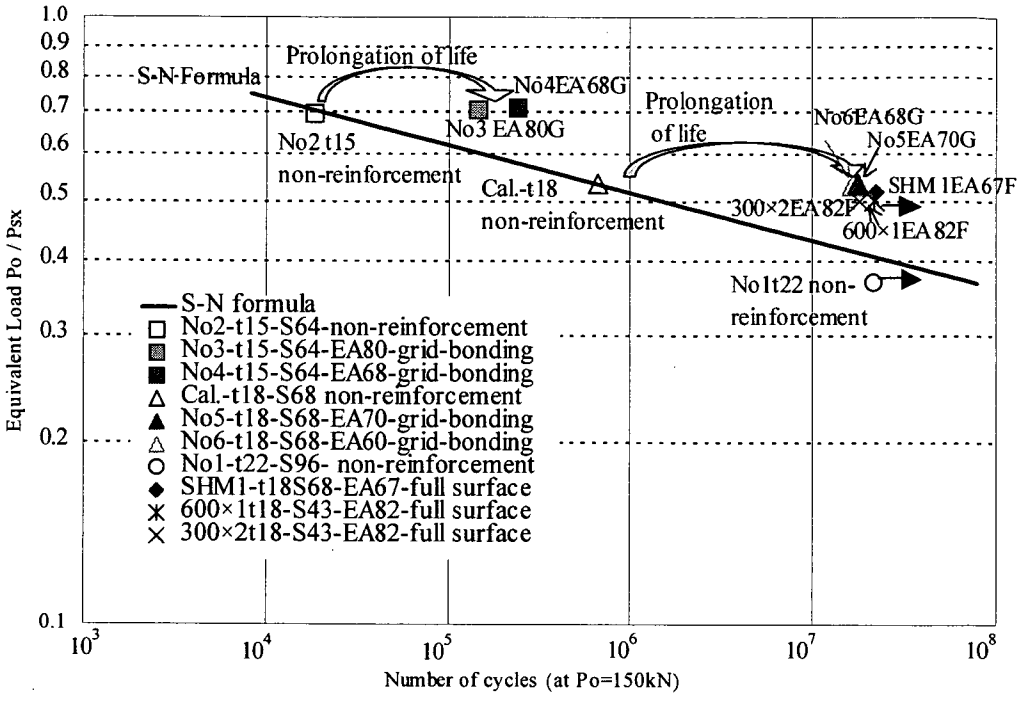
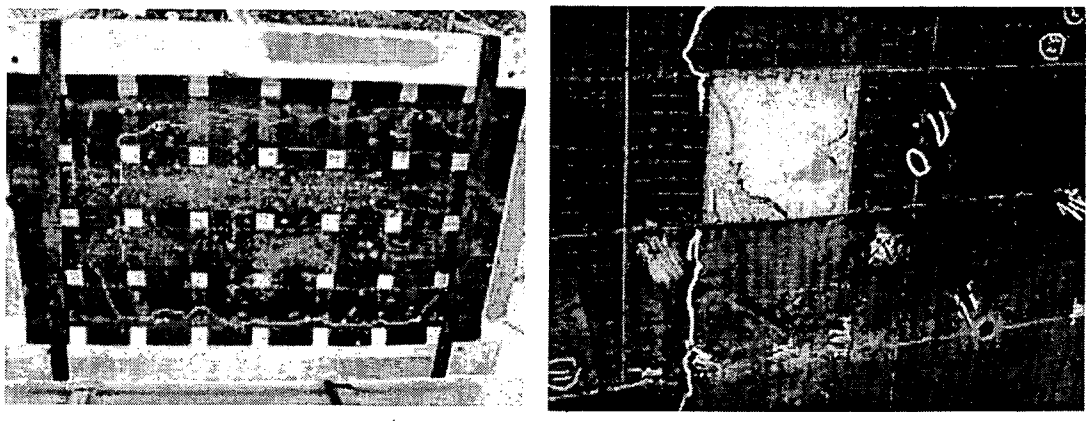


Figure 7 The relationship between number of cycles until failure and load P_o/P_{sx}

3-2 Conditions of grid-bonded part and sheet overlap splices part

During loading, there was no separation of CFS at crossing part (stepped parts) of the main bar and distribution bar directions. Grid bonding did not influence the shape of punching shear failure of slab concrete.

Moreover, even after the failure, there was no separation of the carbon fiber sheet observed in the main bar and distribution bar directions. There were neither new cracking and concrete separation along the edge of CFS, nor the damage of carbon fiber sheet at the grid step parts. In the overlap splice part (10cm), separation and damage of CFS did not occur. As the results, there was no problem in adhesiveness as well as in workability to the grid bonding (**see Photo 1**).



(a) Overview (b) Enlargement of the grid part

Photo 1 Failure status of No.3

3-3 Considerations

With the objective of the more reliable maintenance for RC decks, a strengthening method using carbon fiber sheets was experimentally evaluated. The results of a series of wheel load running tests of the slabs strengthened by the grid bonding are summarized below:

(1) When 15cm thick RC slabs were strengthened with grid bonding carbon fiber sheets (No.3, No.4), fatigue durability was roughly 10 times higher than that of a non-strengthening RC slab (No.2) and came to have sufficient fatigue durability for practical use.

(2) When the 15cm thick slabs were strengthened with grid bonding with 2 types of intermediate modulus of elasticity CFS (No.3 with fiber mass per unit area of 400g/m^2, No.4 with Fiber mass per unit area of 470g/m^2), there was no significant difference in fatigue durability between the 2 types, and strengthening with even 400g/m^2 CFS has significant fatigue durability. In this case, the tensile rigidity of CFS is 68kN/mm, which is about 17% less than the current 82kN/mm.

(3) When 18cm thick slabs (No.5, No.6) strengthened with grid bonding CFS, the slabs came to have sufficient fatigue durability, about 20 times compared to the calculation value obtained by the S-N relationship of non-strengthened RC slabs.

(4) When the 18cm thick slabs were strengthened with grid bonding with 2types of intermediate modulus of elasticity CFS (No.5 with fiber mass per unit area of 400g/m^2, No.6 with fiber mass per unit area of 470g/m^2), there was no significant difference in fatigue durability between the 2 types, and strengthening with even 400g/m^2 CFS has significant fatigue durability. In this case, the tensile rigidity of CFS is 60kN/mm, which is about 25% less than the current 82kN/mm.

(5) When the test result (No.5, No.6) of grid-bond strengthened 18cm thick slabs in this experiment were compared with the previous result (SHM1) of full-surface bonding of CFS, there was no significant difference. Therefore, the grid bonding method had equivalent strengthening effect to the full-surface bonding.
When the amount of strengthening was about the same, grid bonding and full-surface bonding were shown to obtain equivalent reinforcement effects.

(6) For economy, grid bonding reduces the amount of strengthening members as well as bonding areas. In terms of direct work cost, including material costs and construction costs (surface treatment, level adjustment, bonding, and finishing), a reduction of about 15% (in case of 15-17cm thick slabs) or about 20% (in case of 18-20cm thick slabs) is possible compared to the current full-surface bonding of intermediate modulus of elasticity CFS (EA=82kN/mm).

4. Conclusion

Conclusions obtained in this study are as follows:

1. RC slabs were strengthened with grid bonding CFS came to have sufficient fatigue durability for practical use.

2. Grid bonding specimens were observed in the shape of punching shear failure of slab concrete as well as the full-surface bonding.

Acknowledgement

The authors express their thanks to the members of the graduate school of OSAKA UNIVERSITY for their cooperation in this study.

References

[1] Onishi, Matsui, Okada, Fukagawa, "Fatigue Life Extension of Damaged RC Slabs by Strengthening with Carbon Sheet Attaching Method" Proceedings of 5th Japanese-German Joint Symposium on Steel and Composite Bridges, September9-12, 2003, pp307-316

[2] Okada, Onishi, Matsui, Kobayashi, "Stiffening effect with CFRP sheets arranged in grid pattern on RC decks", Proceeding of 3rd Symposium on Decks of Highway Bridges, pp.175-180, 2003.6 (Japanese)

[3] Public Research Institute of Ministry of Construction: Technical report of the collaboration research work on repair and strengthening of concrete members – part 3: Guideline for design and construction of repair and reinforcement of concrete members of road bridge with carbon fiber sheet bonding method, draft, No. 235, 1999.3. (In Japanese)

[4] Hanshin Expressway Public Corporation: The cracking damage and durability of RC slabs of road bridge, 1991.12

[5] Matsui and Maeda, "A rational evaluation method for deterioration of highway bridge decks", Journal of structural mechanics and earthquake engineering, No. 374/ I-6, 1986.10

[6] Maeda and Matsui, "Punching shear load equation of reinforced concrete slabs", Journal of materials concrete structures and pavements, No. 348/V-1, 1984.8

[7] Hoshijima, Otaguro, Sakai and Matsui, "Experimental sturdy on effect of strengthening to the damaged road bridge deck slabs by carbon fiber sheets", Bridge and foundation, 1998.9

PRESERVATION OF EXISTING BRIDGES IN KENTUCKY USING ADVANCED COMPOSITES

Issam HARIK[1], Tong ZHAO[2], and Ching Chiaw CHOO[3]

Abstract

Three bridge retrofitting projects involving the use of advanced composites – Fiber Reinforced Polymer (FRP) – will be briefly discussed in this paper. These applications of FRP composites include the following areas: repairing and strengthening of RC beams due to shear deficiency; flexural strengthening of RC beams due to increased loads; and repairing of PC beams due to the shrinkage. The success and effectiveness of FRP composites illustrated in the aforementioned projects, due to their tremendous advantages over conventional techniques, will definitely elevate their use in many other structural applications in the near future in Kentucky.

Keywords: Fiber reinforced polymer (FRP) composites, reinforced/prestressed concrete, bridge, retrofit

Introduction

According to the National Bridge Inventory Database (FHWA 2003), there are reportedly 591,220 numbers of bridge structures in the United States. Of this number 81,437 are classified as "*structurally deficient*" and 81,573 are "*functionally obsolete*". This indicates that an estimated 28 percents of the nation bridges are in need of repair or replacement. The same database also reveals that 3,997 of 13,461 bridge structures in Kentucky are in either category.

The use of advanced Fiber Reinforced Polymer (FRP) composites for repair and rehabilitation is rapidly gaining acceptance worldwide due to their resistance to corrosion, high strength-to-weight ratio, flexibility, etc. Some of the common applications involving FRP composites are: strengthening and repairing of RC and PC beams; repairing of seismic deficient RC columns and piers; and retrofitting of walls and slabs (Avramidou et. al. 1999, Hamilton et. al. 1999, Holloway and Leeming 1999, Hutchinson and Rizkalla 1999, Karbhari et. al. 1999, Norris et. al. 1997, Sonobe et. al. 1999, Tan 1997, Yamakawa et. al. 1999, and Zhao et. al. 2002). This paper intends to showcase some of the bridge preservation projects using FRP composites in the state of Kentucky. Three such projects will be discussed in this paper. These projects include the following areas of FRP applications: shear strengthening of precast prestressed concrete box beams; flexural strengthening of cast-in-place reinforced concrete beams due to increased live loads; and

[1] Professor and Chair, Department of Civil Engineering, University of Kentucky, Lexington, KY 40506-0281. E-mail: iharik@engr.uky.edu
[2] Visiting Research Professor, Kentucky Transportation Center and Dept. of Civil Engineering, University of Kentucky, Lexington, KY 40506-0281
[3] Ph.D. candidate, Department of Civil Engineering, University of Kentucky, Lexington, KY 40506-0281

crack repairs of precast prestressed I-girders due to plastic shrinkage cracking. Conclusions and insights drawn from working with FRP composites will also be included.

Applications on Repair & Retrofit of Existing Bridges Using Carbon Fiber Reinforced Polymer (CFRP) Composites

The Carter County Bridge on KY-3297, Carter County, KY

The retrofitting project of the Carter County Bridge was funded by the Innovative Bridge Research & Construction (IBRC) Program – one of the Federal Highway Administration's (FHWA) Discretionary Programs intended to develop and promote the use of new materials and construction techniques for the repair, rehabilitation, replacement, or new construction of bridges and other structures, and it was also the first full-scale repair project using FRP composites undertaken by the Kentucky Transportation Cabinet, KY. A brief description of the bridge, the problem and the associated retrofitting technique will be discussed in the following sections.

The three-span [68'-98'-42' (21-30-13 m)] composite precast prestressed concrete box-beam bridge is situated on route KY-3297 crossing the Little Sandy River in Carter County, KY. This bridge was designed based on the Load Factor Design method using HS25 as design live load (i.e. an increase of 25-percent over the existing standard of HS20-44 truck and lane loads) of AASHTO specifications. The bridge plans were completed and approved in February of 1992, and all work was completed in April of 1993.

A first and routine inspection conducted in April 1996 found significant diagonal shear cracks that were as wide as 3.2 mm, and 1.8 to 2.4 m long (see Fig. 1) had formed in all four precast prestressed box beams at both ends of Span 2. Following that an in-depth inspection was scheduled and an investigation to re-evaluate the bridge was launched. Subsequent inspections revealed that the shear cracks in Span 1 were propagating at an alarming rate, and new shear cracks were also beginning to develop in Spans 1 and 3. In addition, the re-evaluation confirmed that the box beams were indeed under-reinforced in shear.

The retrofitting process for the Carter County Bridge began in September, and completed in October of 2001. The process was performed in two phases: (1) crack repairs; and (2) application of CFRP fabric. The goal of crack repairs was to partially restore the capacity of the beams, and the application of CFRP fabric was to strengthen and compensate for shear deficiency. Fig. 2 depicts the retrofitting process: (a) mounting of injection ports in cracks; (b) sealing cracks using epoxy through injection ports; (c) applying two-part resin; and (d) attaching CFRP fabric to concrete. Note that the CFRP fabric is attached to both sides of the concrete beams with a 45-degree angle (see Fig. 2d).

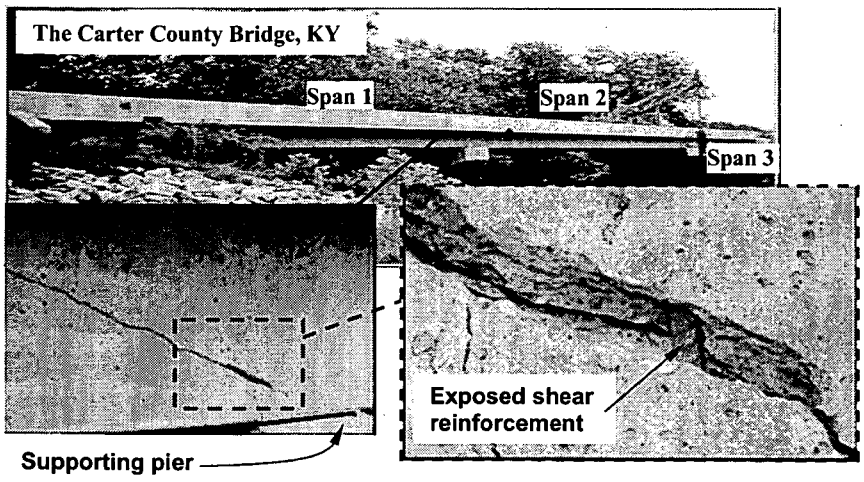


Fig.1 – Diagonal shear crack in span 2 of the Carter County Bridge.

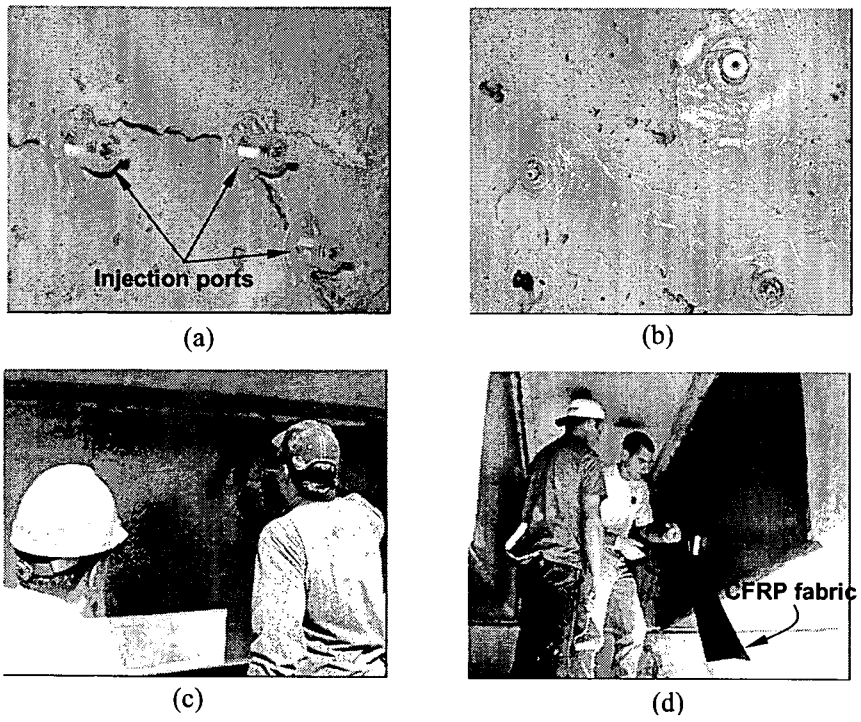
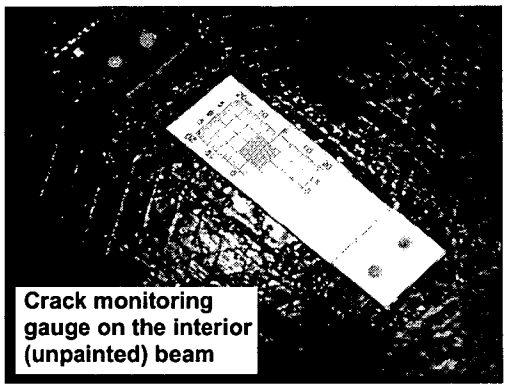
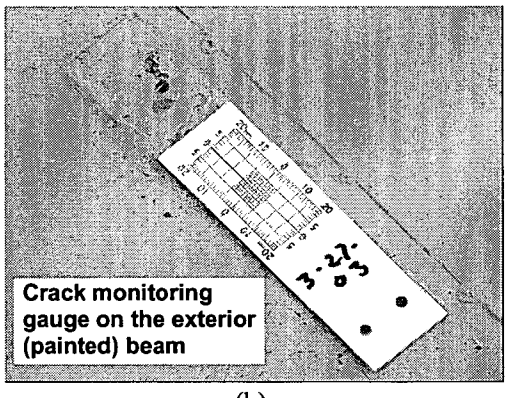


Fig. 2 – Retrofitting of concrete box-beams: (a) mounting of injection ports in cracks; (b) sealing cracks using epoxy; (c) applying two-part resin; and (d) attaching CFRP fabric to concrete.

During the retrofitting process, crack monitoring gauges were mounted directly onto the beams over the repaired cracks (see Fig. 3). As of April 2003, the repaired beams have shown no indication of distress as zero movement has been registered on these monitoring gauges.



(a)



(b)

Fig. 3 – Crack monitoring gauges mounted on repaired beams.

The overall success of the project demonstrated that the use of advanced composites can be an effective retrofitting alternative. Additionally, the Kentucky Transportation Cabinet had reportedly saved approximately $300,000.00 to repair the bridge than to replace the entire superstructure as initially planned.

Louisa-Fort Gay Bridge, Lawrence County, KY

The Louisa-Fort Gay Bridge is located in a small mining community of Lawrence County, Eastern Kentucky. The multi-span bridge has both steel plate girders and concrete RC girders supporting the concrete bridge deck in the end and middle spans, respectively. A schematic plan view of the middle RC spans (Spans 4-5-6-7) is shown in Fig. 4.

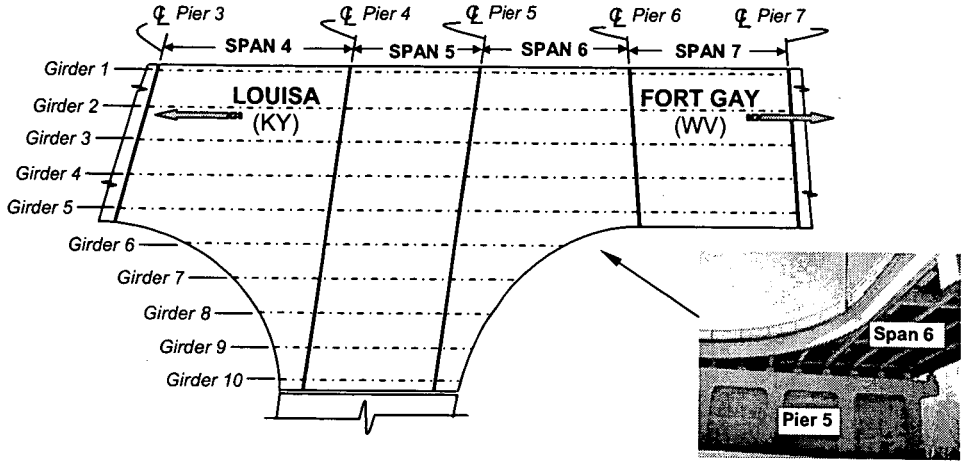


Fig. 4 – The reinforced concrete spans of the Louisa-Fort Gay Bridge.

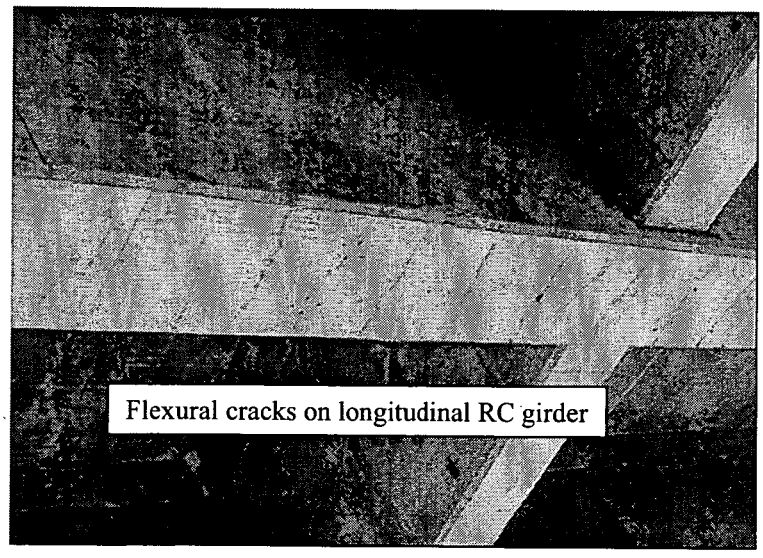


Fig. 5 – Flexural cracks on longitudinal reinforced concrete girders.

Bridge inspection indicated that flexural cracks had developed in the RC girders in Spans 4, 6, and 7 due to heavy truck loads – coal trucks (Type 9) as heavy as 225,000 lbs (1,000 kN) had been recorded [Note: AASHTO HS20-44 Truck is 72,000 lbs (320 kN)]. For illustrative purposes, moment-curvature analysis, as shown in Fig. 6, reveals how much Girder 4 in Span 4 is being overloaded. Strengthened Girder 4 in Span 4 using CFRP laminates is also included in Fig. 6b. The retrofitting process is similar to the one

previously described for the Carter County Bridge, except that CFRP laminates will only be mounted to the bottom of the RC girders (see Fig. 7).

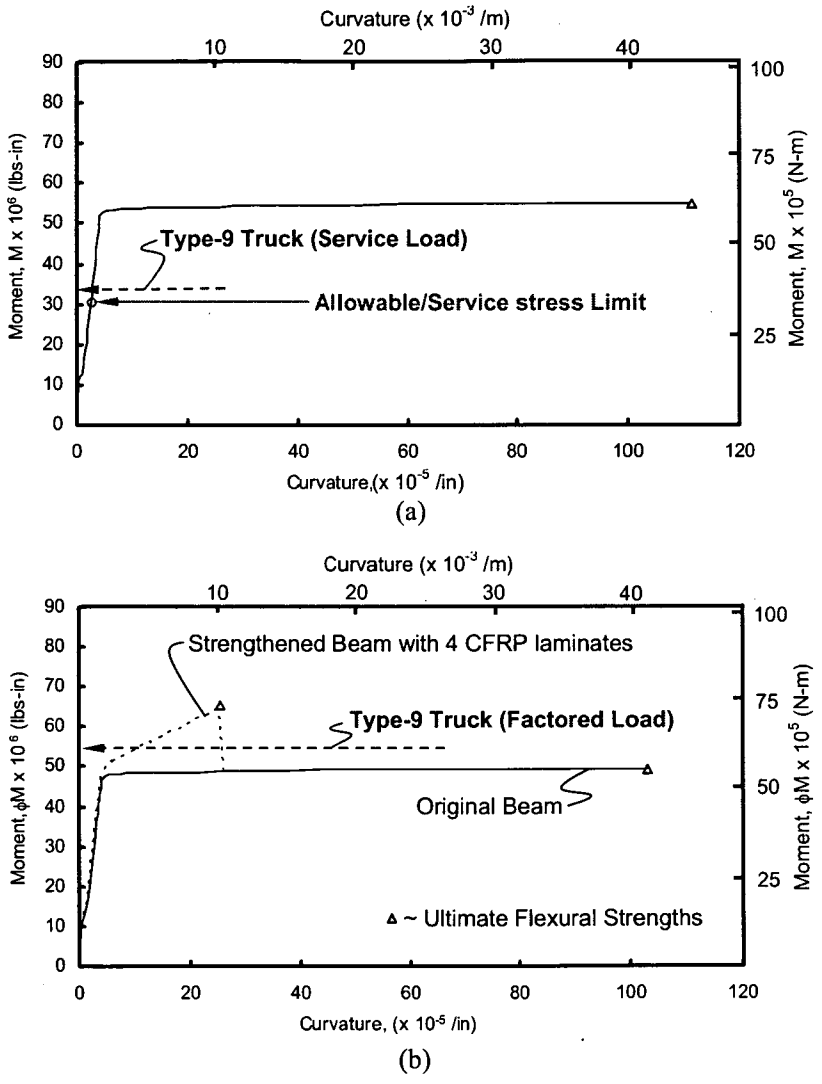


Fig. 6 – Moment-curvature analyses of girder 4 in span 4.

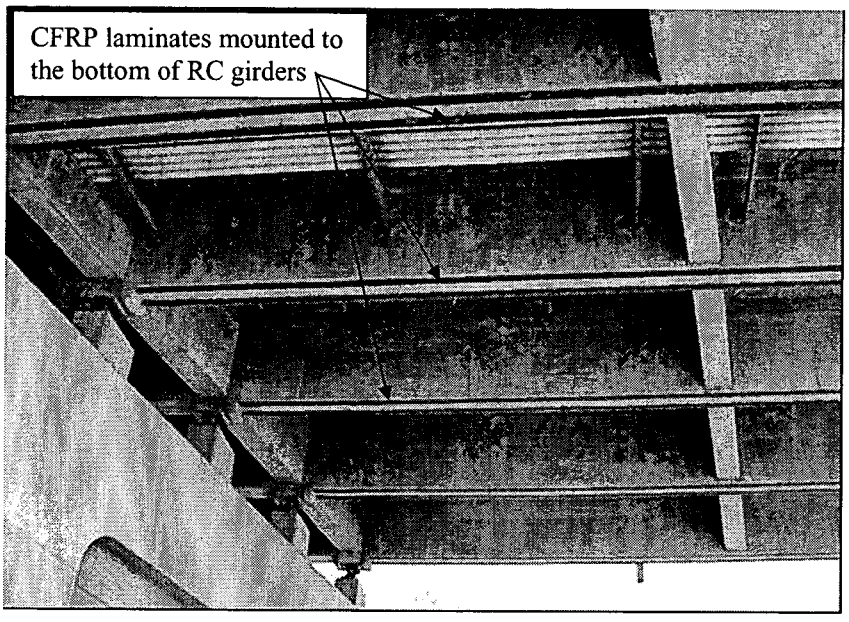


Fig. 7 – Girders in Span 6 strengthened with CFRP laminates.

I-65 Elevated Highway Bridges in Louisville, Jefferson County, KY

This interstate 65 elevated highway bridges in Louisville span across a number of streets in the heart of Louisville, Jefferson County, KY. The bridges were completed in 1979, and a number of cracks had developed on many of the prestressed concrete girders over the years. As indicated in Fig. 8, the cracks are vertical cracks and are located near or at the supporting piers. Preliminary investigations indicated that these cracks may have developed due to shrinkage. The cracks are especially apparent at piers with fixed restraints where the axial shortening of girders is prevented. In some cases, severe corrosion of steel reinforcements has been detected at the locations of cracks (Fig. 9). As noted in the ACI 224 report (2001), cracking due shrinkage is inevitable in concrete structures, and cracking in these structures must be controlled or otherwise more severe serviceability problems may arise.

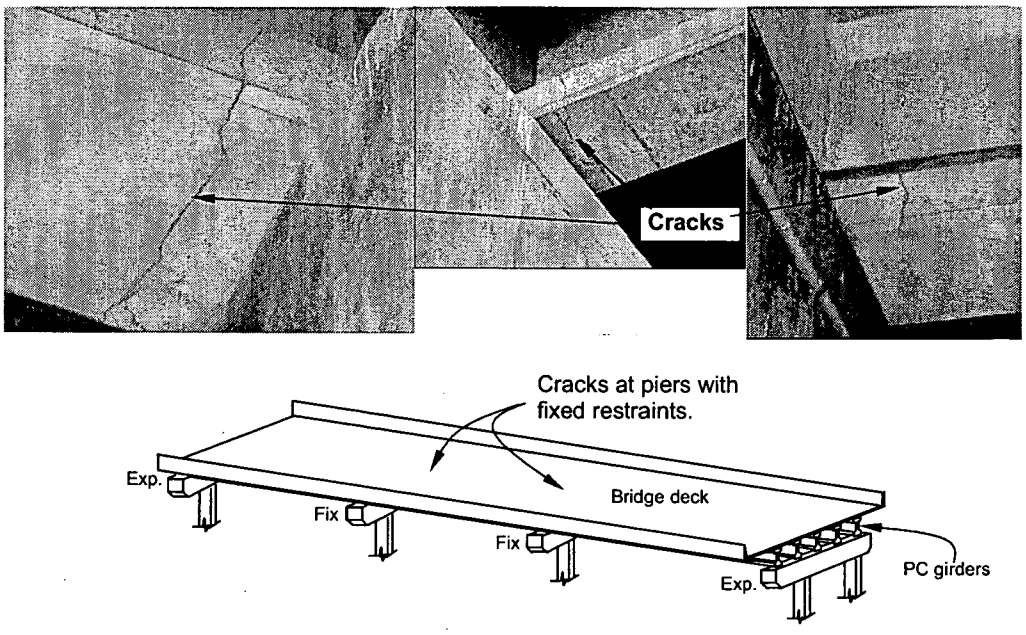


Fig. 8 – Cracks on prestressed concrete I-girders on the elevated portion of I-65 Highway Bridges.

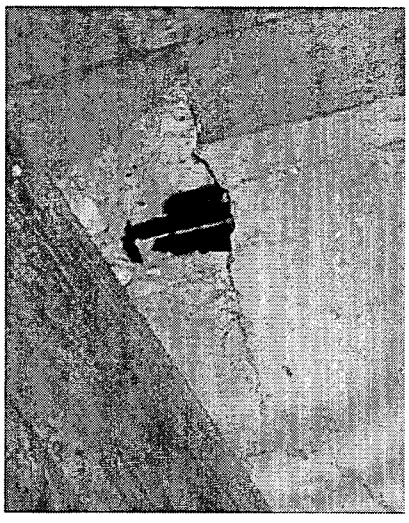


Fig. 9 – Corroded strands at crack location.

Detailed analyses to estimate the restraining tensile forces due to volume change of PC girders had been performed. The primary goal of these analyses is to estimate the amount of FRP composites required for the restoration or strengthening process. In this

particular case, FRP composites have been selected as the primary retrofitting material because of their tremendous flexibility and conformity, in addition to their excellent tensile strength. As shown in Figs. 7 and 8, cracks on PC AASHTO I-girders are generally located at hard-to-reach-areas near or at the supporting piers. The retrofit will initiate in Fall 2003 and is expected to be completed in Spring 2004.

Summary and Conclusions

Three bridge retrofitting projects involving the use of FRP composites in Kentucky are briefly discussed in this paper. These projects address three different areas of strengthening or repairing: (1) repairing and strengthening of RC beams due to deficiency in shear; (2) flexural strengthening of RC beams; and (3) repairs of PC beams due to shrinkage.

Based on the above experiences, the following advantages offered by FRP composites in the preservation of existing bridges can be observed:

1. It can eliminate or minimize traffic disruption during the retrofitting process.
2. It can eliminate or minimize the use of heavy equipments. Only hand tools and minimal man-power are often required.
3. It offers greater flexibility and conformity. Repairing in areas where other means of repair are difficult to perform
4. It offers a cost-effective alternative.

The success and effectiveness of advanced composites in retrofitting would certainly elevate their use in many areas of applications in Kentucky in the future to come.

References

ACI Committee 224, "Control of Cracking in Concrete Structures," American Concrete Institute (ACI 224R-01), May 16, 2001.

Avramidou, N., Drdacky, M.F., and Prochazka, P.P., "Strengthening Against Damage of Brick Walls by Yarn Composites," Proceeding of the 6th International Conference on Inspection, Appraisal, Repairs & Maintenance of Buildings & Structures, Melbourne, Australia. 1999.

FHWA, "National Bridge Inventory," Bridge Technology – Infrastructure, United State Department of Transportation, Federal Highway Administration. February 2003.

Federal Highway Administration (FHWA, IBRC, 2001). Innovative Bridge Research & Construction Program, USA

Hamilton, H.R., Holberg. A., Caspersen, J., and Dolan. C.W., "Strengthening Concrete Masonry with Fiber Reinforced Polymers," Fourth International Symposium – Fiber Reinforced Polymer Reinforcement for Reinforced Concrete Structures, ACI International SP-188, Farmington Hill, Michigan. 1999.

Holloway, L.C., and Leeming, M.B., "Strengthening of Reinforced Concrete Structures using Externally-Bonded FRP Composites in Structural and Civil Engineering," 1st Ed., Cambridge: Woodhead Publishing Limited. 1999.

Hutchinson R.L. and Rizkalla, S.H., "Shear Strengthening of AASHTO Bridge Girders Using Carbon Fiber Reinforced Plastic Sheets," Fourth International Symposium – Fiber Reinforced Polymer Reinforcement for Reinforced Concrete Structures, ACI International SP-188, Farmington Hill, Michigan. 1999.

Karbhari, V.M., Seible, F., Seim, W., and Vasquez, A., "Post-Strengthening of Concrete Slabs," Fourth International Symposium – Fiber Reinforced Polymer Reinforcement for Reinforced Concrete Structures, ACI International SP-188, Farmington Hill, Michigan. 1999.

Norris, T., Saadatmanesh, H., and Ehsani, M., "Shear and Flexural Strengthening of R/C Beams with Carbon Fiber Sheets," Journal of Structural Engineering, New York, ASCE, v.123, n. 7. July 1997.

Sonobe, Y., Matsuzaki, Y., Nakamura, H., Iso, M. and Watanabe, M., "Experimental Study on Reinforced Concrete Columns having Wing Walls Retrofitted with Continuous Fiber Sheets," Fourth International Symposium – Fiber Reinforced Polymer Reinforcement for Reinforced Concrete Structures, ACI International SP-188, Farmington Hill, Michigan. 1999.

Tan, K.H., "State-of-the-Art Report on Retrofitting and Strengthening By Continuous Fibers – Southeast Asian Perspective – Status, Prospects and Research Needs," Non-Metallic (FRP) Reinforcement for Concrete Structures – Proceedings of the Third International Symposium, Vol. 1, 1997.

Yamakawa, T., Satoh, H., and Zhong, P., "Seismic Performance of Hybrid Reinforced Concrete Circular Columns Confined in Aramid Fiber Reinforced Polymer Tube," Fourth International Symposium – Fiber Reinforced Polymer Reinforcement for Reinforced Concrete Structures, ACI International SP-188, Farmington Hill, Michigan. 1999.

Zhao, T., Zhang, C.J., and Xie, J., "Study and Application on Strengthening the Cracked Brick Walls with Continuous Carbon Fibre Sheet," Advanced Polymer Composites for Structural Applications in Construction, Proceedings of the 1st International Conference, University of Southamption, UK. 2002.

19th US-Japan Bridge Engineering Workshop

Seismic 1

co-Chairs:
S. Unjoh & J. Cooper

Enforcing Methods of Existing Old Bridges on Soft Ground For a Very Large Earthquake (In-Cap Method)
Y. Shioi

Comparative Design of a Bridge in New Jersey using the NCHRP 472 Comprehensive Specification for the Seismic Design of Bridges and the 1998 LRFD
H.A. Capers Jr.

Experimental Study on Liquefaction-induced Earth Pressure on Bridge Abutment
M. Kondoh

Static and Dynamic Behavior of Flared-Column Bents
D. Sanders

Structural Response Characteristics in Consideration of Directional Uncertainty of Earthquake Ground Motion
H. Nishida

Enforcing methods of existing old bridges on soft ground for a very large Earthquake (In-Cap Method)

Shioi Yukitake [1] , Aoyagi Mamoru [2], Ooya Tsutomu [3] ,
Kato Koji [4] , Fukada Hisashi [4],

ABSTRACT

About the aseismicity of foundation structures to the level 2 earthquake motion in existing old bridges, the insufficient aseismicity of existing bridges cannot be denied. So we propose "the anti-seismic reinforcement method of the existing foundations on soft ground ". This construction method expects increase of the horizontal and vertical resistance, by driving underground walls around the existing foundation and consolidating the inside.

We executed several analyses such as frame analysis and FEM and showed that both the maximum moment and the horizontal displacement generated to a pile, can be decreased also. We are planning the static experiment by centrifugal model equipment, and want to examine a consolidation between the results of experiment and this analysis technique.

1.Introduction

About the aseismicity of foundation structures to the level 2 earthquake motion in existing old bridges, when the earthquake motion taken into consideration by revision of an design code is improved, or their functions are expanded, the insufficient aseismicity of the existing bridges cannot be denied.

As the foundation reinforcement work generally requires the great construction cost and the time because of several conditions such as narrow space under superstructures, and tends to become comparatively large-scale, these works are not so many compared with past other reinforcement works.

However, on the other hand, a generation of the Kanto,the Tokai, the Tonannkai, or the Nankai earthquake is anxious in the first half of this century. Since presently the countermeasures to prevent disaster for various kinds of civil structures are reexamined, development of the efficient anti-seismic enforcing method for existing foundations is inevitable. Then, we decided to propose "the anti-seismic reinforcement method of construction of the existing foundations on soft ground " which can attain reduction of cost and time necessary for completion to the foundation and also can be easily applied in a narrow space.

This method of construction expects increase of the horizontal and vertical resistance, by driving underground walls around the existing foundation and consolidating the inside. By this process we aim that the improved area with the surrounding underground walls performs as a

---

1) : Hachinohe Institute of Technology
2) : Shiraishi Corporation
3) : Nittoc Construction Co. ,Ltd
4) : Fudo Construction Co. ,Ltd

foundation.

This paper describes the results of two-dimensional static frame analysis, two-dimensional dynamic FEM and three-dimensional static FEM analysis prior to three-dimensional dynamic analysis in order to examine the effects of the proposed method.

2. The outline of proposed method

The process of this reinforcing method is composed of driving steel sheet piles up to the given depth to surround the existing foundation on soft ground, and consolidating the inside of sheet pile wall using soil improvement method. The outline is shown in Fig.-1.

By this process increase of the horizontal and vertical resistance are expected. The outline of the mechanism of a resistance is shown in Fig. -2 and Table -1 .

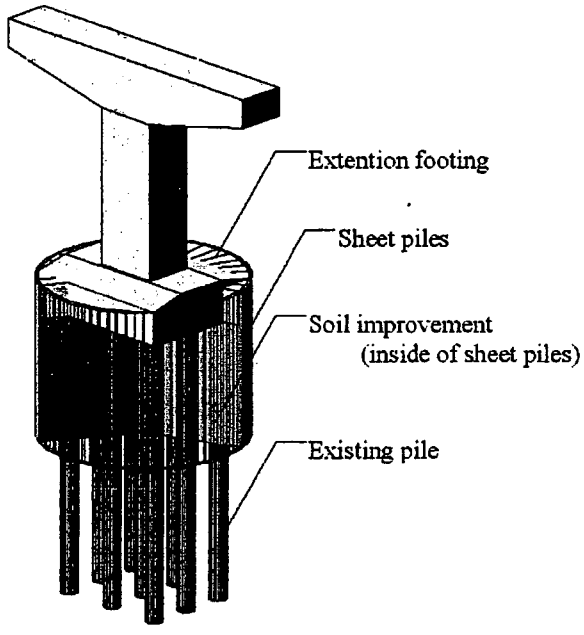


Fig-1 The outline of this method

Table-1 Resistance elements of this method

		effect	mechanizm of reinforcement
horizontal resistance	increase of resistance area	○	originated in improved soil and sheet pile
	strength increase of resistance element	×	
vertical resistance	increase of resistance area	○	originated in friction of sheet pile
	strength increase of resistance element	○	originated in friction between improved soil and pile
rigid increase in base body		×	

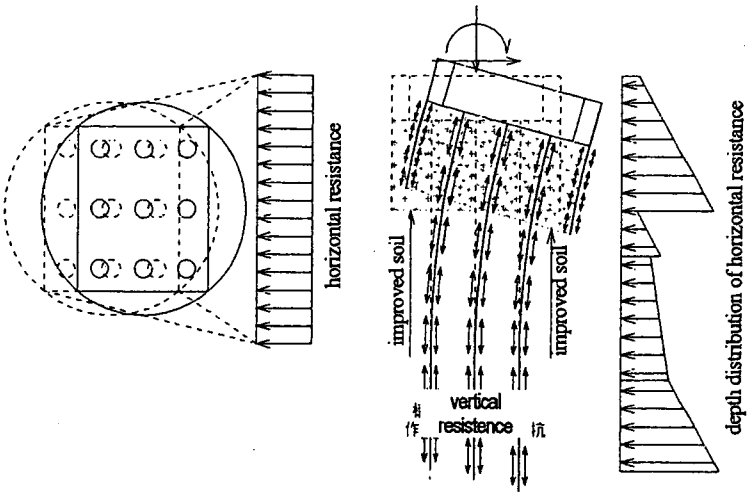


Fig-2 The mechanism of a resistance element

3. Two-dimensional static frame analysis

In this paper, the target of existing structure is a pile foundation structure currently mentioned to "Reference-Data of Japan Highway Association about Reinforcement of the Existing Highway Bridge Foundation" as an example of a design, and it reinforces the bridge pier of which the seismic performance was judged insufficient by the revision of Design Codes of Japan Highway Bridge. The figures of a structure are shown in Fig. -3.

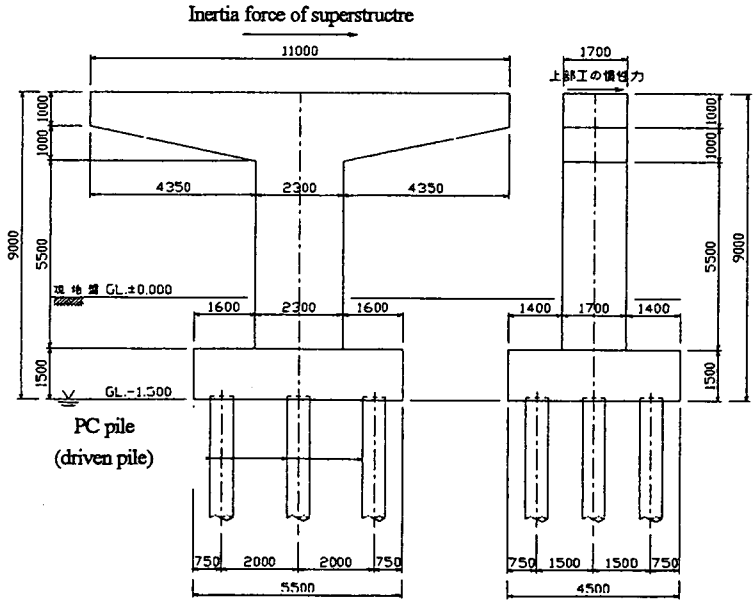


Fig-3 The target existing structure

The design strength of the foundation computed from the resistance of the bridge pier after reinforcement in case of the level 2 earthquake, are Pu=3734 kN and Mu=31345 kNm.

The properties of soil surrounding by this pile foundation are shown in Table -2. When a pile was calculated as a beam on the elastic soil using the constant of Table-2 , the characteristic values $1/\beta$ which show the performance of deformation of a pile is 2.924 m. On this model, moreover, the 1st layer of a surface ground is judged as perfectly liquefying in case of the level 2 earthquake. The properties of improved soil are derived from the "Jet Grout Method, Japan Grout Association." Each resistance element of the ground and the improvement block in the analysis is modeled according to "Design Codes of Japan Highway Bridge, Vol. IV, Foundation, 2002, Japan Highway Association ".

In this analysis, three cases of the improvement range from $1/\beta$ to $\pi/2\beta$ are analyzed in the both cases of which liquefaction is disregarded and considered respectively. The analyzed results in each case are shown in Table -3.

Table-2 Soil Properties surrounding pile foundation

		Thickness of a layer	N value	density	cohesion	friction angle	E modulus
		m		kN/m3	kN/m2	deg.	kN/m2
*	improved soil			18	500	23	400000
lay 1	sand	10	5	18	0	23	14000
lay 2	clay	4.8	5	17	30	0	14000
lay 3	sand	2.9	15	18	0	30	42000
lay 4	sand	1.2	50	19	0	40	140000

Table-3 Analized Results

		existing	case-1	case-2	case-3
imploved area	L(m)	0.0	3.0	4.5	7.5
β -imploved area ratio	β L	0.000	1.026	1.539	2.565
design strength	P(kN)	2384	4916	5618	7213
required design strength ratio	P/P0	0.638	1.317	1.505	1.932
plasticity rate	μ	21.625	5.781	3.153	-

When the liquefaction is disregarded, the improved effect is able to find in the case 1 which enforces 3.0m ($1/\beta$) which is the characteristic value of the existing foundation. When the liquefaction is taken into consideration, the improvement range is needed beyond the characteristic value but it confirmed that it is less than the allowable ductility of 4.0 in the case of which the improved range is 4.5m ($\pi/2\beta$). The results are shown in Fig.-4.

In addition, in this analysis, a nonlinear two-dimensional static FEM analysis is also carried out for the existing foundation and the reinforcement case 1 in the case of which the liquefaction is disregarded, and the same result with frame analysis is obtained. The results are shown in Fig.-5.

However, the above-mentioned effect is considered affected by the physical-properties values of the improvement block incorporated into modeling of a resistance element. Furthermore, since the behavior of the improvement block in this reinforcement method is not clear, the models were made under some assumptions. As mentioned above, the component experiments to the characteristic of each resistance element etc. are due to be conducted in near future.

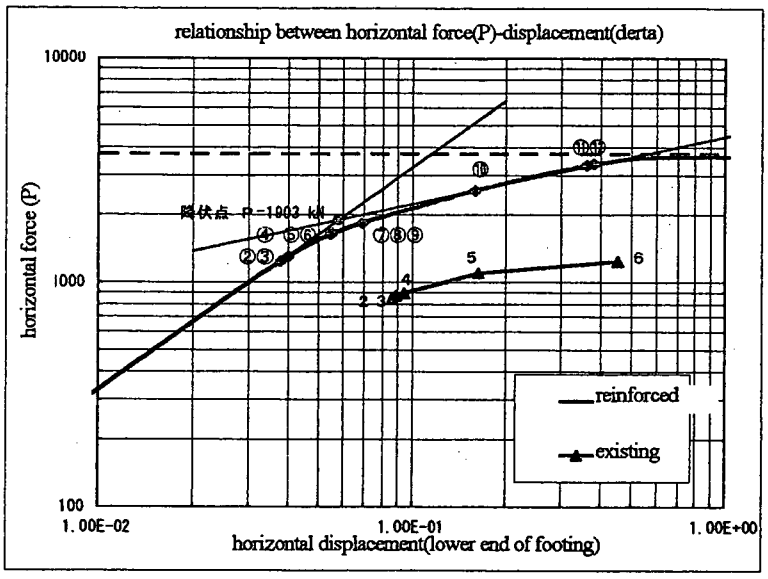


Fig-4 The relationship between horizontal force and displacement

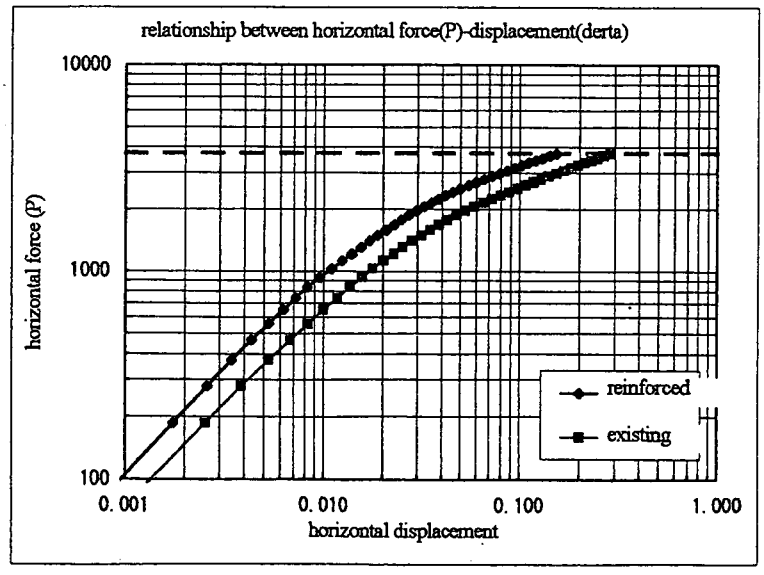


Fig-5 The relationship between horizontal force and displacement in FEM analysis

4. Two-dimensional dynamic analysis

The equivalent linear analysis code FLUSH by FEM was used for the two-dimension dynamic analysis. The physical-property values used for analysis are shown in Table-4. The input motion of earthquake is the adjusted wave of Max250gal of the wave observed at Hachinohe in 1968, and inputted into the base rock (G. L.-26.9m). The analyzed cases are two. Case-1 is made for the existing foundation, and Case-2 is made for the state of existing foundation where steel sheet piles are installed and improvement are given to $1/\beta$. The structure is modeled with the beam elements and the concentrated load is added to the pier head. An analysis model (Case-2) is shown in Fig. -6.

The distribution of shear strain in each case is shown in Fig. -7, and the distribution of bending moment of pile is shown in Fig. -8. Fig. -7 shows that the shear strains at the improved area near the pile head become very small caused on steel sheet pile installation and soil improvement. Moreover, the shear strains of the area between piles are also suppressed.

Fig. -8 shows that the maximum bending moment of the pile occurred at the lower part of improved area in the depth of the bottom of steel sheet pile installed. This is considered to be the effect of soil improvement. The value of bending moment is about a half compared with the case without improvement, and it can be evaluated as an effect of this measure.

Table-4 Soil properties for dynamic analysis

	density γ (kN/m^3)	poisson's ratio μ	shear modulus G (kN/m^2)	modulus E_0 (kN/m^2)
imploved soil (clay)	17.0	0.40	35,700	98,000
imploved soil (sand)	18.0	0.40	107,100	300,000
sand3	18.0	0.38	5,100	14,000
sand2	18.0	0.38	5,100	14,000
clay	17.0	0.48	4,700	14,000
sand1	18.0	0.33	15,800	42,000
base sand	19.0	0.26	55,600	140,000

	density γ (kN/m^3)	shear modulus G (kN/m^2)	moment of inertia I (kN/m^2)	area A (m^2)	damping ratio h
pile	24.5	13,192,000	0.003180	0.1410	0.01
footing	24.5	13,192,000	0.035160	1.5000	0.01
sheet pile	77.0	79,154,000	0.000174	0.0191	0.01

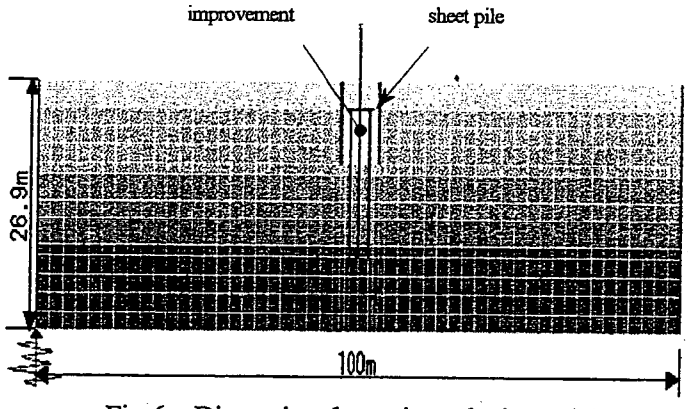


Fig-6 Dimension dynamic analysis model

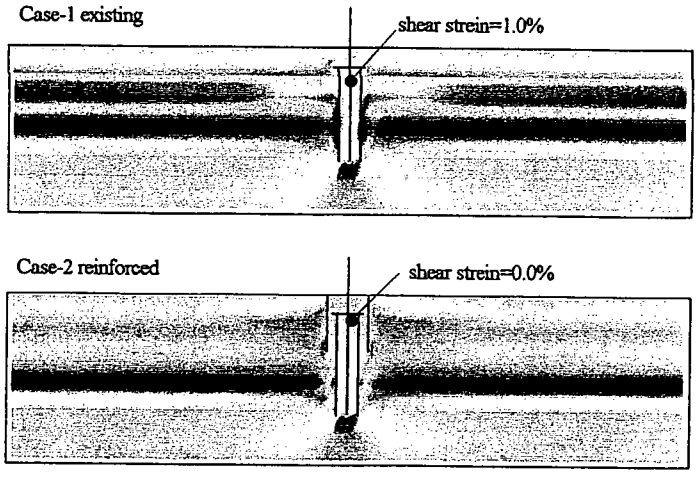
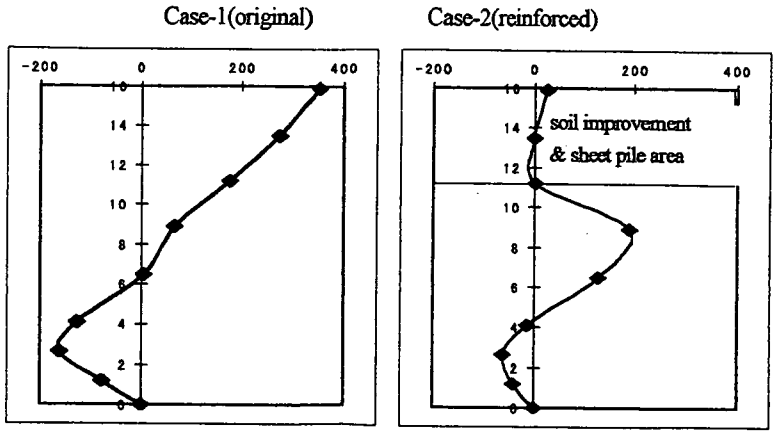


Fig-7 contour of shear strain



Fig－8 The distribution of bending moment (pile)

5. Three-dimensional static analysis

The three-dimensional static analysis is a preliminary step for the three-dimensional dynamic analysis, and finally we will use more actual model, such as incorporating various kinds of boundary elements, to know a dynamic behavior. In this analysis, the superstructure is disregarded and a bridge pier and footing is modeled as a lamped mass, and piles are used the elastic material elements. Moreover, the soil is also modeled into an elastic material.

Many physical-property values are the same with the two-dimensional dynamic analysis fundamentally. The analysis model of a reinforced structure portion is shown in Fig. -9, the ground surrounding by the structure is taken into account up to the radius of 50m.

Horizontal load P_h=2384kN is applied on a pier head within the limit of the yield load of the pile foundation for the reinforced pier. The rigidity of piles is the rigidity in the yield state without axial force, and is modeled as an elastic material. Since the surface sand layer at the front of footing is yielded, in the condition of the yielded pile in two nonlinear-dimensional FEM analyses, the strength of the soil element as a linear material gradually from zero to an original rigid value, from the surface toward the lowest part of the layer as shown in Fig. -10.

The cases of analysis are shown in Table-5. The distribution of bending moment and the horizontal displacement of the pile on pushing side compared in two cases is shown in Fig. -11. The first is the case of the existing structure only and the second is the basic case with sheet piles and soil improvement in the length of $1/\beta$.

From this result, the change point of a bending moment is seen at the lowest of steel sheet pile and the improvement block. The maximum moment of a pile is reduced to about 25%, and the horizontal displacement decreases to about 40%. So the effect of anti-seismic reinforcement is recognized in this structure.

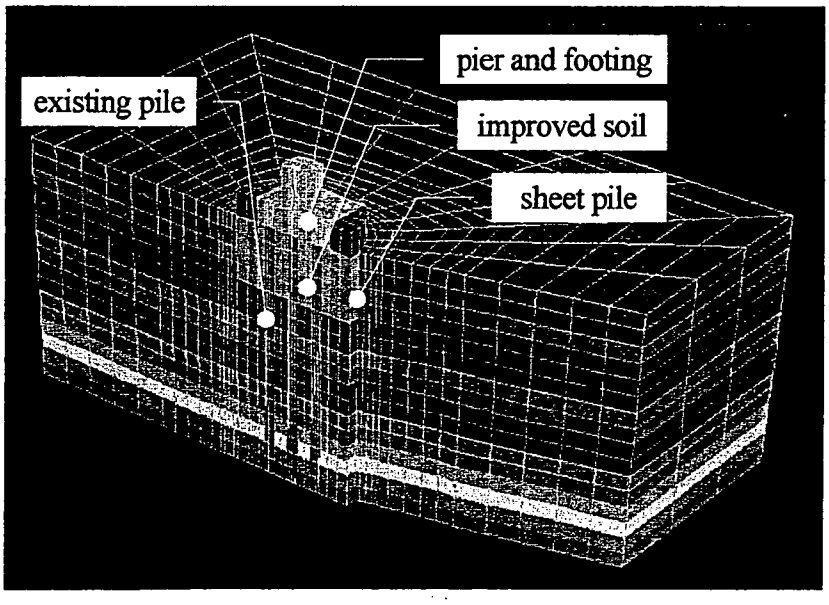


Fig-9 The model in three dimensional FEM analysis

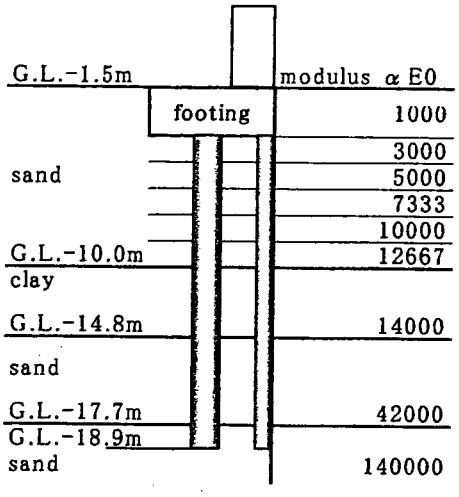


Fig-10 3dimension FEM analysis set

Table-5 Case of the three-dimensional static analysis

	sheet pile length depth of lower end G.L.-(m)	implovement depth depth of lower end G.L.-(m)	
Case-1	0.0	0.0	existing case
Case-2	6.0	6.0	reinforced case

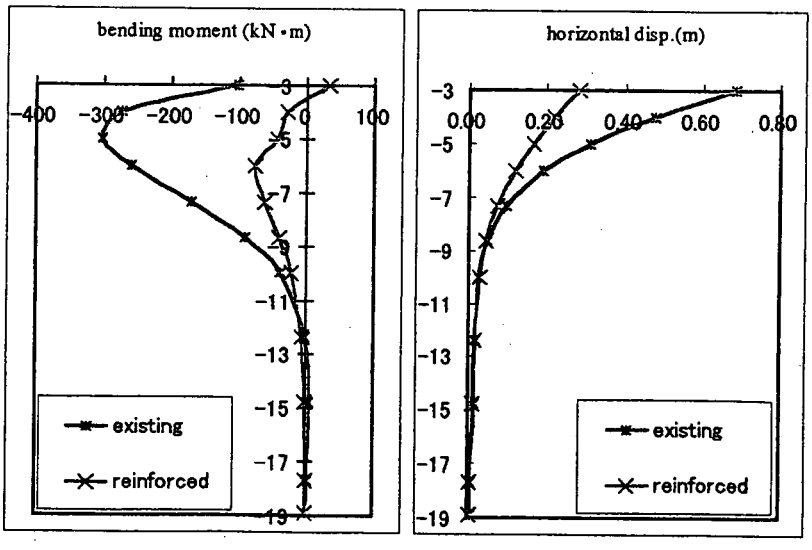


Fig-11 The distribution of bending moment and horizontal displacement

6. Conclusion

Based on these analyses, the component experiment to examine the detailed performances are progressing after this report. We are planning the static experiment of 1 / 50 model by a centrifugal equipment, and want to report anew the results concerning to the real behavior by a full-scaled model.

We want to examine correlations between an experiment and this analysis technique, and investigate boundary conditions such as steel sheet piles and an improvement block, piles and an improvement block, and steel sheet piles and the ground. So, we intent to examine optimal combination about the steel sheet pile length, the volume to be improved, and the strength of improved soil, to establish the design system based on these studies.

This paper is a part of the joint research cooperated with the foundation and basic 21 study group (Nittoc Construction Co., Ltd. Fudo Construction Co., Ltd. and Shiraishi Corporation), and the authors express a great gratitude to the related persons for their cooperation and benefitable advices.

References

1) Nunomura, A., (2002): "The subject of disaster measures and view to Tokai, the Tonankai , and the Nankai earthquake," Japan Society of Civil Engineers, Conference research debate in the 2002.

2) Japan Highway Association(2000), : "Reference data about reinforcement of the existing Highway Bridge Foundation"

3) Design Codes of Japan Highway Bridge, Vol. IV, Foundation, Chapter 12 , Pile Foundation, 2002, Japan Highway Association .

COMPARATIVE DESIGN OF A BRIDGE IN NEW JERSEY USING THE NCHRP 472 COMPREHENSIVE SPECIFICATION FOR THE SEISMIC DESIGN OF BRIDGES AND THE 1998 LRFD

Harry A. Capers Jr., P.E.[1]

Abstract

With the completion of a National Cooperative Highway Research Program (NCHRP) project known as NCHRP Project 12-49 "Comprehensive Specifications for the Seismic Design of Bridges", NCHRP Report 472, with the same name, was recently issued. Along with the report, a proposed new seismic design specification was issued. The new seismic design specification was to be considered by the American Association of State Highway and Transportation Officials (AASHTO) as a replacement for its existing aged seismic design provisions. While not adopted in the form presented, the new specifications are available for consideration by jurisdictions to use them in their bridge designs. New Jersey saw some value in utilizing the new specifications.

This paper discusses New Jersey's findings in performing two trial designs in support of the NCHRP project as well as current activities occurring in the State of New Jersey in tailoring the new specifications for use in its bridge designs.

[1] Harry A. Capers Jr., NJ State Bridge Engineer, New Jersey Department of Transportation

Background

In the fall of 1998, a project was initiated by NCHRP to develop new comprehensive seismic design specifications for highway bridges. The proposed specifications were intended to replace the existing specifications developed for the AASHTO Standard Specifications For Highway Bridges in 1983 and commonly referred to as Division 1-A of that publication. The new specifications were to be compatible with the new Load and Resistance Factor (LRFD) design philosophy of the latest design specification issued by AASHTO's Subcommittee on Bridges and Structures. It was to reflect the latest knowledge and design approaches and was to produce designs with a high level of seismic performance.

NCHRP Project 12-49, *Comprehensive Specification for the Seismic Design of Bridges* was began in August, 1998 and concluded in November, 2001 with the issuance of NCHRP Report 472, *Comprehensive Specifications for the Seismic Design of Bridges.* The research was performed by a joint venture of the Applied Technology Council and the Multidisciplinary Center for Earthquake Engineering (ATC/MCEER).

To assist the Subcommittee on Bridges and Structures' evaluation of the specification, the ATC/MCEER team provided leadership with a group of states in performing trial designs of a sampling of bridges in various parts of the country. Trial designs were performed by the states of Alaska, New Jersey, Missouri, Washington, Arkansas, California, Oregon, South Carolina, Tennessee, Illinois, Nevada, Georgia, New York and the Federal Highway Administration's (FHWA) Central Federal Lands Highway Division. In all, 19 trial designs were performed. As can be seen from the list of States, the sample designs covered a variety of areas with differing seismicity. As such, an impact to a variety of bridge owners was demonstrated.

In support of this effort, New Jersey designers performed two trial designs. The bridges selected were bridges that had already been designed using the provisions of Division 1-A of the AASHTO Standard Specifications. This permitted a comparison between the two specifications. Consultants who had performed the original work for the on the selected bridges performed both trial designs. The following is a discussion of their findings:

The Doremus Avenue Bridge

The first structure for which a trial design was performed was the replacement of the Doremus Avenue Bridge over the Conrail Oak Island Railyard in the City of Newark, New Jersey. The existing Doremus Avenue Bridge was built in 1918 and was in poor condition with severe settlement throughout. The current bridge evaluation revealed that it should be classified as structurally deficient and functionally obsolete. Traffic estimates indicated that about 15,000 trucks per day or 1.4 million truck containers annually would cross the new bridge. This bridge is part of a very significant system of roadways in the Port Newark area. Doremus Avenue serves as a major truck route into and out of the port. This will help to very actual large vehicle configurations that are used in New Jersey. From this identification a permit vehicle configuration will be established for State.

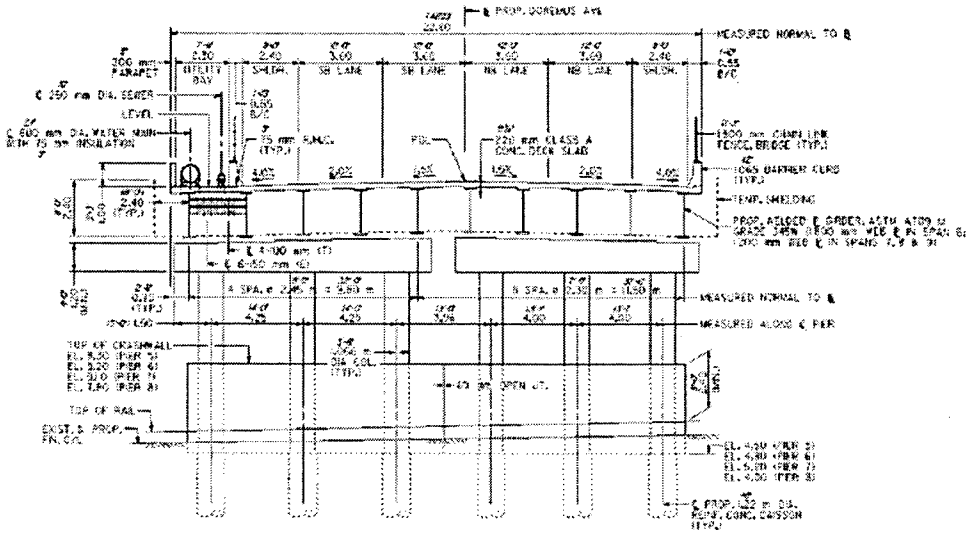


Figure 1 – Section of Doremus Avenue Bridge over the Conrail Oak Island Railyard

The new bridge is approximately 400 meters long and consists of three (3)- 3 span continuous units for a total of nine (9) spans. It will consist of variable depth steel plate girders (AASHTO M270M, Grade 345W) with a 220 millimeter (8.7 in) steel reinforced concrete deck. The foundations consist of drilled shafts embedded into bedrock. A cross section of the bridge is shown as Figure 1. Figure 2 provides an Arial view of the project site. The new bridge was designed by Parsons-Brinkerhoff-FG, Princeton, New Jersey.



Figure 2 - Ariel view Doremus Avenue bridge over the Conrail Oak Island Railyard

The following is provided for those who are interested in the specific assumptions made by the designer in performing the comparative designs.

A) The Doremus Avenue Bridge was originally analyzed for seismic loads according to AASHTO Division 1-A requirements using the following parameters:

Acceleration Coefficient, A=0.18
Seismic Performance category, SPC = B
Soil Profile Type III
Site Coefficient, S=1.5
Elastic Response Spectrum as per AASHTO
Damping Coefficient = 0.05
Response Modification Factor, R=3.0 per AAHSTO Table 3.10.7.1-1 for non-critical bridges.
The Extreme Event –1, LRFD loading Combination was used in combination with the Orthogonal Seismic Load Combination – 100/30 Rule.

Extreme Event 1 = 1.0 DL + γ_{eq}LL +1.0EQ
Where EQ can be obtained from LC1 = 100% Longitudinal + 30% Transverse
LC2 = 30% Longitudinal + 100% Transverse

γ_{eq} = 0.5

B) The trial design using the NCHRP Guidelines utilized the following key parameters:

Spectral acceleration parameters Ss of 0.421g and S1 0f 0.094g were used.
Seismic Design and Analysis Procedure (SDAP) D Elastic Response Spectrum Method was used with Seismic Detailing Requirements of 4
Site class of E was selected based on geotechnical conditions of the site.
Vertical Acceleration effects were ignored

An Elastic Response Spectrum Analysis using Multi-mode Dynamic Analysis was performed. The structure was modeled as a single line of frame elements using equivalent stiffness of the members. The multimode analysis used gross section properties of members and elements rather than cracked section properties. Cracked section properties usually result in smaller seismic forces and larger deformations.

The performance level selected for the bridge was life safety.
The use of Earthquake Resisting systems was permitted.
The seismic Hazard Level was IV.
R factor used was R=4.0
No Transverse displacements were assumed at abutments due to foundations being built on piles.

The Extreme Event –1, LRFD loading Combination was used in combination with the Orthogonal Seismic Load Combination – 100/40 Rule.

Extreme Event 1 = 1.0 DL + γ_{eq}LL +1.0EQ

Where EQ can be obtained from LC1 = 100% Longitudinal + 40% Transverse

LC2 = 40% Longitudinal + 100% Transverse

$\gamma_{eq} = 0.5$

Forces on the substructure obtained from performing the two designs are summarized in the following table:

Pier Number	AASHTO Division I-A			NCHRP Guidelines	
	F_x (kN)	F_y (kN)	Governing Load Comb.	F_x (kN)	F_y (kN)
Pier 1	110*	144	Strength I	110*	140
Pier 2	458	315	Extreme Event I	294	288
Pier 3	82.3*	628	Extreme Event I	82.3*	665
Pier 4	454	415	Extreme Event I	313	380
Pier 5	142*	278	Strength I	142*	255
Pier 6	376	487	Strength I	260	510
Pier 7	80*	226	Extreme Event I	80*	209
Pier 8	91*	87	Strength I	91*	83

Figure 3 Resulting Design Loads

In the above table, the listed forces are per girder, forces marked with * are forces from friction between the pier cap and the bearing. In general, NCHRP Guidelines resulted in smaller loads than the AASHTO Division I-A requirements except at Pier 6 in the y direction.. Pier 6 design was governed by Strength load combination originally, and it appears that the "square-root of the sum of the squares" combined seismic load would not govern the design if the NCHRP Guidelines were used.

Seismic loads for Pier 4 using the NCHRP Guidelines were tabulated and compared with the same loads obtained by using the AASHTO Division I-A guidelines. The load combination for the Extreme Event-1 was calculated using the proposed NCHRP 12-49 Guidelines Subsection 3.5 and Table 3.5-1, and modified with the Response Modification Reduction Factor of 4.0 as per Subsection 4.7. It should be noted that the largest moment for the extreme event load combination obtained using AASHTO Division I-A was 2673 kN-m, which governed the design of the columns. The largest moment for the extreme event load combination obtained following the NCHRP 12-49 code was 1212 kN-m, which is less than the moment obtained by the other strength limit states. This value would not govern the design.

For this particular structure, NCHRP Guidelines resulted in a more moderate design requirement when compared to the AASHTO Division I-A Seismic Design requirements. For

the piers, where seismic loads governed the design using Division I-A, the design loads remained practically unchanged. Therefore, no significant change in substructure cost would result.

For the original design of the Doremus Avenue Bridge, the seismic analysis was performed in accordance with Division I-A using Multimode Spectral Analysis Method - Procedure 3. SEISAB analysis software by Imbsen Software Systems was used. For this exercise, the One-Step Procedure suggested in the NCHRP Report was used. Except for a possible learning curve it was felt that there was no significant difference in the design effort required by either method.

The Scotch Road Bridge over Route Interstate 295

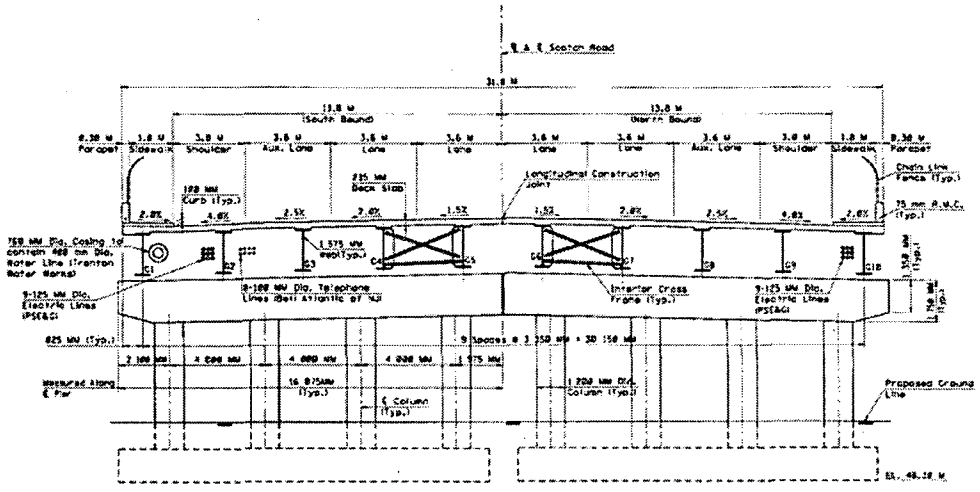


Figure 4 – Section of Scotch Road over Interstate Route 95

The second trial design was performed for the Scotch Road Bridge over Interstate Route – 95 in Ewing Township, New Jersey. The new bridge is a 90.9-meter long two span continuous structure. The span lengths are 45.45m with a web depth of 1.58m. The tangent alignment of the existing Scotch Road was maintained on the new bridge. The new bridge carries two 3.6m lanes, one 3.6 auxiliary lane, one 3.0m shoulder, and a 1.8m sidewalk in both the northbound and southbound directions. There is a 1.9m high, curved top chain link fence mounted on a 0.815m high parapet along each side of the bridge. The superstructure out-to-out dimension will be 31.8 m. Arora and Associates, P.C of Lawrenceville, New Jersey

provided design services for this bridge. A cross section of the bridge is shown as Figure 3 and Figure 4 provides an aerial view of the project site.



Figure 5 – Ariel view of Scotch Road over Interstate Route 95

Specific notes on the sample design experience by the consultant were as follows:

The dynamic shear modulus was not measured at this site. The soil is comprised mainly of decomposed fractured shale. The shear wave velocity has been estimated to be between 760 meters per second and 1500 meters per second. Therefore, a classification of Site Class B was utilized. The ground surface shaking parameter was taken as
FaSs = 0.36. According to Table 3.10.3-1, the Seismic Hazard Level is equal to III. The structure meets the criteria for analysis under the SDAP D: Elastic Response Spectrum Method. Since this structure was evaluated with an Operational Performance Level, according to Table 3.10.3-2, the Seismic Detailing Requirement (SDR) is 5.

The seismic analysis of the structure was performed using SEISAB analysis software by Imbsen Software Systems. The model loading used in the analysis was the Arbitrary Curve Data. The response spectrum curve generated for this analysis is based upon the local ground

motion values and Figure 3.10.2.1-3: Design Response Spectrum, Construction Using the Two-Point Method. A three second period was used for this analysis.

The original analysis was based upon the 1998 AASHTO LRFD Bridge Design Specifications 2nd Edition with current interims and as modified by the NJDOT LRFD Bridges and Structures Design Manual – 4th Draft Edition. Subsection 3.10.3 of the NJDOT LRFD Bridges and Structures Design Manual – 4th Draft Edition modifies the AASHTO LRFD Specifications by directing the design engineer to assume the bridge to have an Importance Category of "critical". Therefore, according to AASHTO, the response modification factors used were equal to 1.5 (the foundation R- Factor is 1.0). The bridge foundation was originally designed to be elastic under the design seismic loading.

No mechanisms developed in the pier by using the NCHRP provisions. This is because the effective seismic loading using the NCHRP provisions reduced the effective seismic loading on the pier by approximately 30 to 40 percent. In addition, the R-Factors used in the NCHRP provisions are also 1.5. No mechanisms developed in either the cap, columns or footing. The abutments are integral for this structure. Therefore, no mechanisms formed in the abutment.

Earthquake Resisting Systems (ERS) used at the pier include guided sliding bearings. A portion of the transverse seismic loadings are resisted by the bearings and transferred to the supporting pier. The longitudinal seismic loads are dissipated into the soil through the use of integral abutments.

The footing sizes are 15.500m x 6.000m footings. They support 4 - 1.200m diameter columns at each bent. There are two adjacent bents for this structure. The columns support a 1.400m wide x 1.500m deep cap beam. The abutments are integral with the superstructure. The majority of the seismic loading at the abutment is transferred to the soil. The transverse seismic loading at the abutment is resisted in part by the soil and also by the integral abutment pile system.

The structure was designed elastically. Since an Importance Category classification was designated for this structure, and also since the seismic forces were appreciably lower than the current AASHTO provisions, the pier components, as designed, will behave elastically.

The overall structure construction costs, using the NCHRP provisions, would be lower than the AASHTO LRFD provisions. The column capacity is significantly increased when the NCHRP provisions are checked against the AASHTO LRFD specifications. Either less reinforcement can be utilized or perhaps a smaller column diameter could be used. The footing size could also be reduced. However, the cost savings are not very significant. The seismic eccentricity requirements for spread footings did not significantly reduce the footing dimensions at this location.

The overall design effort for this example was not as significant as it would have been had a reduced Importance Category been designated. The higher performance level classification at this location made an elastic design the appropriate design method for this bridge. Design time using an elastic approach was less than what would have been required had a capacity approach been used. Reduced performance levels would make the capacity design method the appropriate design approach to use; thereby increasing the design time. Seismic detailing requirements would also increase. The designer felt that the provisions were clearly written and the learning curve was not significant.

Recommendations for revisions to the code:

The Designer of the Doremus Avenue Bridge made the following recommendations regarding the new code that was developed under NCHRP Project 12-49:

1. The NCHRP Guidelines require the analysis to be done using the cracked section. Cracked section properties in some textbooks are given as 50% of the gross section properties; however, it could also be assumed to be 70% or any other percentage. Clarification should be given whether this number should it be left to the designer or should it be the owner's decision.
2. The R factor depends on the T (bridge period). It is unclear how this is determined.
3. Guidance on developing site-specific data is needed.
4. Clarification is needed on decision making as to whether a bridge should be judged to have a critical or an essential Importance Category classification.
5. The NCHRP SDAP D, Elastic Response Spectrum Analysis Method has been used for this bridge structure. Regularity requirements, given in Subsection 5.4.2 for the uniform load method covers bridges up to 6 spans. The subject bridge has 9 spans that are composed of three 3-span continuous units. In addition, the South Abutment and Piers 1 through 4 have no skew while Piers 5 through 8 and the North Abutment have a skew of 15 degrees. The applicability of the multi-mode dynamic analysis method to cases similar to this should be addressed in future revisions.

The Designer for the Scotch Road Bridge suggested potential areas of refinement as follows:

1. The bridge performance level needs to be defined more clearly. Significant design parameters are highly dependant on this determination. This is typically done on a state-by-state basis.

2. It should be noted that the AASHTO LRFD designation of a "critical" structure is very similar to the NCHRP's "operational importance" SDAP D designation. The R-Factor values are similar to each other. The LRFD foundation R-Factor is equal to R/2 which cannot be less than 1.0. The NCHRP report says that "If the elastic foundation forces are less than the forces resulting from column hinging, they may be used for the foundation design. The foundation shall be designed using an R-Factor of 1.0". Therefore, effective foundation R-Factors can vary depending on the column hinging forces (NCHRP 15.8).

Further clarification of Subsection 15.8 and how it may impact Subsection 3.10.3.7 would be useful.

3. The transverse reinforcement for longitudinal reinforcement in the columns required prestressing steel. This was due to the stringent design requirements. It was assumed that this should only be used for structures with an a critical Importance Category classification and that typical bridges would not require this measure.

4. Although the pier in this example did not include any pile foundations, NJDOT modifies the AASHTO LRFD Specifications and directs the engineer to design deep foundations using the 17th Edition of the AASHTO Standard Specifications. Therefore, unless the NCHRP guidelines address NJDOT's concerns regarding deep foundation designs, deep foundations will require a similar modification when using the NCHRP provisions.

5. The combination of seismic loads using the AASHTO LRFD Specifications is a (100% - 30%) combination. The NCHRP guidelines increase the seismic force effects to a (100% - 40%) combination. Whereas, a simple hand calculation can convert the LRFD seismic loads to the NCHRP load combination, seismic analysis software companies should gear their software to accept both the traditional method or the NCHRP method.

6. The major editorial suggested was to include a summary table of the major similarities between the two codes. This table can be shown in the commentary. For example, the load factor for DL changed from yp (1.25) to 1.0, or the combination of seismic force effects changed from (100% - 30%) to (100% - 40%)...

New Jersey Department of Transportation's Reaction.

Even though the AASHTO Subcommittee on Bridges and Structures did not approve the adoption of the NCHRP recommended specification as a Guide Specification in the form presented for consideration, based on New Jersey's experience in these two trial designs the Department directed that, NCHRP Report 472, "Comprehensive Specification for the Seismic Design of Bridges" may be used as an alternative to the use of the AASHTO LRFD Specifications Division 1-A. Designers may submit a request to the Manager, Bureau of Structural Engineering for the use of the NCHRP Report guidelines. A comparison of the effects on the design of a project between the two documents should be made to validate the request.

In conjunction with the issuance of this guidance NJDOT undertook a research project with Rutgers University's School of Civil and Environmental Engineering. Their initial findings include the following:

1. NCHRP 12-49 provisions do not necessarily result in higher seismic loads compared to existing AASHTO LRFD specifications. For example, longer span bridges on stiff soils will have lower seismic forces using the NCHRP 12-49 provisions compared to the AASHTO LRFD specifications.

2. The 2500-year return period for the MCE (rare) earthquake is very conservative compared to other extreme events such as vessel impact and floods. A return period of 1500 years is being considered; however, no USGS maps are available. An acceleration equal to 2/3 of that of the 2500-year event could similarly be used with the IBC provisions.

3. Also being considered is the 1000-year event for which USGS seismic maps are available; however, this event seems to have lower accelerations than current AASHTO LRFD specifications.

4. Soil amplification factors Fa and Fv are high for medium to soft soils and have a major impact on the design response spectra and the selection of the seismic hazard level. For locations with soft soils and high accelerations, site specific response spectra needs to be considered to lower the seismic demand. (See Figure 6)

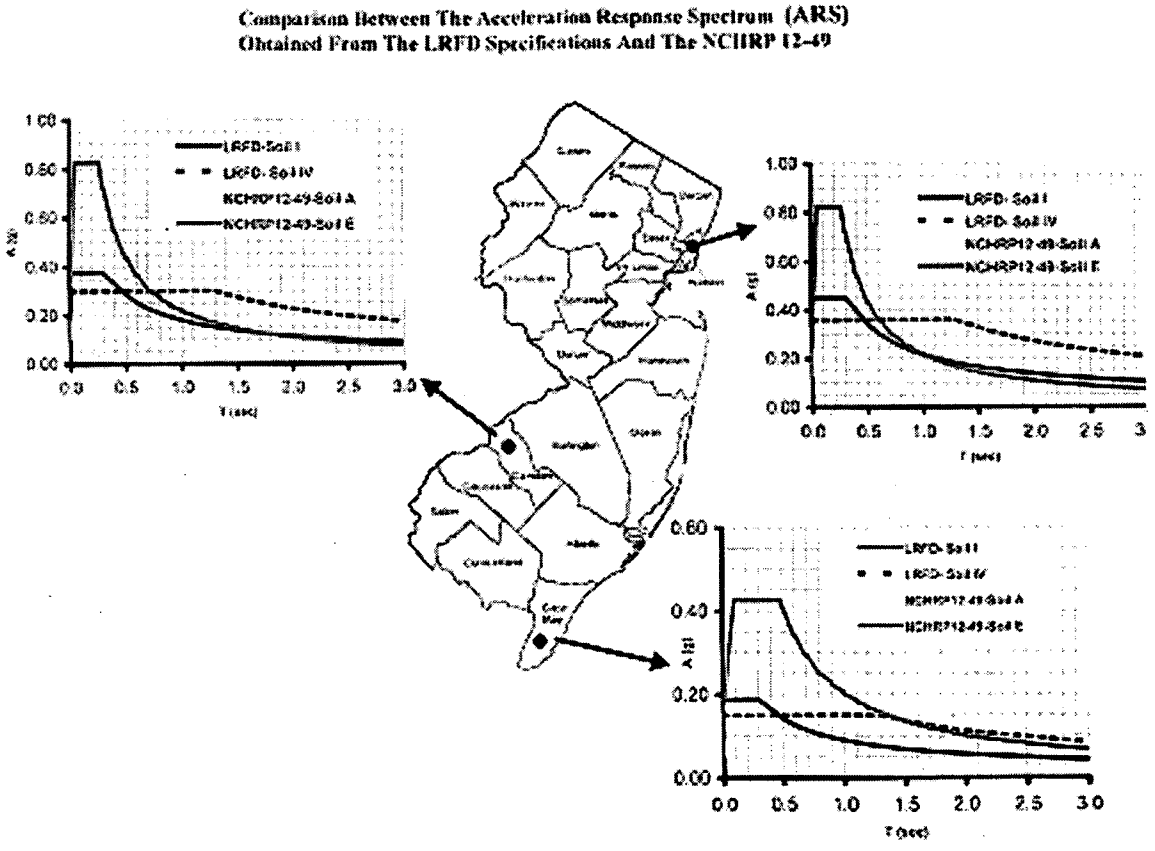


Figure 6

5. The new specification provides more information on the analysis of integral and seat abutments and on foundation stiffness.

6. The new specification provides more flexibility in the analysis and design procedures to be used. For example SDAP C, D, and E could be used in most cases for bridges in New Jersey.

7. Reduction factors of elastic seismic loads R are tabulated in more details for various cases. Pushover analysis is rewarded by allowing larger R-values when this analysis is used.

The researchers at Rutgers have suggested the following preliminary recommendations for consideration by the New Jersey Department of Transportation:

1. Extreme EQ event (MCE) based on 2/3 of the 2500 years spectral acceleration seems more realistic and will not be overly conservative compared to other extreme events in the AASHTO LRFD Specifications. For secondary bridges, a lesser return period may be used.

2. Maximize the number of bridges in New Jersey that can be classified as ordinary and for which detailed seismic analysis and design is not needed. This will depend on soil factors, return period and importance of bridge.

3. The NCHRP provisions include detailed procedures for analysis and design. Most of these will be followed and will be designated as design criteria. Provide specific guidelines and analysis models for the seismic design of abutments.

4. Provide detailed examples for the analysis and design of integral and seat abutments consistent with the NCHRP 12-49 provisions

5. Provide state-of-the-art information of the seismic analysis and design of retaining walls and buried structures

To date several requests have been made to use the NCHRP guidelines and several more projects are being examined relative to their potential use. While, mainly for the reasons outlined above, no designs have been produced using the new specifications, the outlook appears promising that we will be able to give more specific guidance in the near future that will address many of the barriers to our full deployment of this state of the art specification.

ACKNOWLEDGEMENT

A special thanks to Joseph J. Romano, P.E., Project Manager, Arora and Associates, P.C., New York City, NY and Mahir Sen and Sam Fauzy of Parsons Brinkerhoff-FG, Inc., Princeton, NJ for all of their assistance in conducting the comparison design studies. A special thanks to Jack Mansfield, PE Manager, Geotechnical Engineering, NJDOT, Rod

Lewis, Supervising Engineer, Jose Lopez, Project Engineer, and Sharon Harrison, Administrative Assistant, all of NJDOT's Bureau of Structural Engineering for their tremendous support in editing and formatting this paper.

REFERENCES

ATC/MCEER Joint Venture, 2002 "NCHRP Report 472 – Comprehensive Specification for the Seismic Design of Bridges", Transportation Research Board, National Research Council, 2101 Constitution Avenue, NW, Washington, DC 20418

AASHTO 2002, "Standard Specifications for Highway Bridges", Sixteenth Edition, American Association of State Highway and Transportation Officials, Inc., 444 North Capital Street, NW, Suite 249, Washington, DC, 20001

AASHTO 2002, "AASHTO LRFD Bridge Design Specifications", Second Edition, American Association of State Highway and Transportation Officials, Inc., 444 North Capital Street, NW, Suite 249, Washington, DC, 20001

NJDOT 1998, "Bridges and Structures Design Manual", Third Edition, New Jersey Department of Transportation, Bureau of Structural Engineering, PO Box 615, Trenton, NJ 08625-0615

NJDOT 2002, "Bridges and Structures Design Manual-LRFD", Fourth Edition, New Jersey Department of Transportation, Bureau of Structural Engineering, PO Box 615, Trenton, NJ 08625-0615

EXPERIMENTAL STUDY ON LIQUEFACTION-INDUCED EARTH PRESSURE ON BRIDGE ABUTMENT

Masuo KONDOH[1] and Keiichi TAMURA[2]

ABSTRACT

A bridge abutment, which is a type of retaining structures, needs designing against earth pressure from the backfilling. In addition to earth pressure from the backfilling during an earthquake, an abutment that is constructed on the liquefiable ground may be subjected to lateral movement of backfilling due to liquefaction. However, there remain many uncertaties regarding how earth pressure and earthquake behavior affect abutments through ground liquefaction-induced movement. Therefore, the authors conducted dynamic centrifuge tests for the purpose of studying how earth pressure affects bridge abutments. In this paper, we report the results of an experimental study, in which we focus on earth pressure on bridge abutments that occurs during an earthquake as well as earth pressure that occurs with ground movement.

INTRODUCTION

Liquefaction and the associated ground flow inflicted serious damage to various infrastructures including foundations of highway bridges in the 1995 Hyogo-ken Nanbu earthquake. At a bridge abutment on liquefied ground, the liquefaction of the ground causes the backfill to settle, causing earth pressure (liquefaction-induced earth pressure) to act on the bridge abutment. A bridge abutment is a type of retaining structures. While being subjected

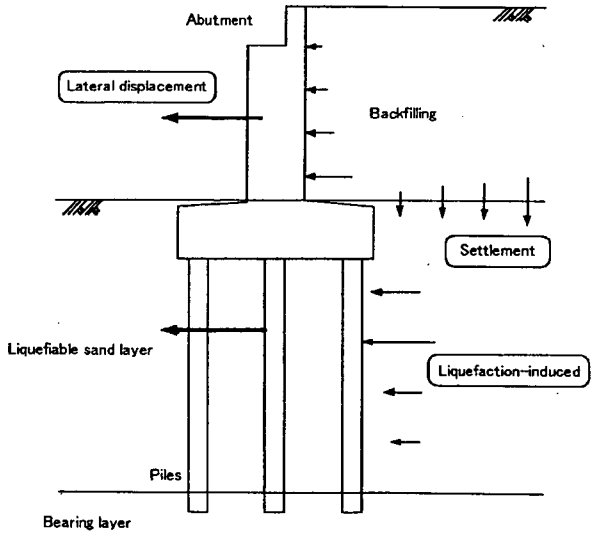


Figure 1. Schematic figure of piled bridge abutments on liquefiable sand layer

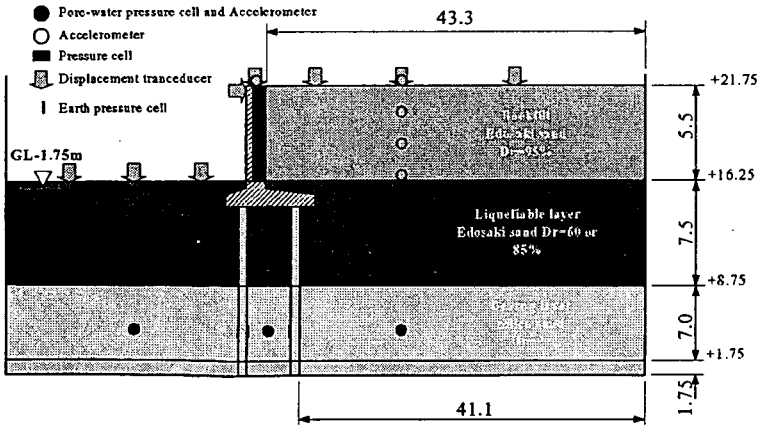
[1] *Senior Research Engineer, Earthquake Disaster Prevention Research Group, Public Works Research Institute*
[2] *Team Leader, Earthquake Disaster Prevention Research Group, Public Works Research Institute*

Table 1. Test conditions

Case	Foundation type	Top of the abutment	Thickness of liquefiable layer (mm)	Thickness of bearng layer (mm)	Relative density D (%)	
					Liquefiable layer	Bearng layer
1	Pile foundation	free	150	140	85	90
2	Pile foundation	free	150	140	60	90
3	Pile foundation	free	190	100	60	90
4	Spread foundation	free	150	140	85	90
5	Pile foundation	restrict	150	140	85	90
6	Pile foundation	restrict	150	140	85	90
7	Pile foundation	restrict	190	100	60	90
8	Pile foundation	restrict	150	140	60	90

to earth pressure from backfilling, it is required to stably maintain the load of the superstructure. Even after an earthquake, damaged bridge girders and piers can be repaired relatively easily, however, damaged bridge abutments are difficult to repair. Because of this, Japan's seismic design specifications for highway bridges[1] require that bridge abutments remain elastic, even during major earthquakes. There are many cases when the bridge abutments are constructed at the soft subsoil. Loose sandy soil may liquefy during earthquakes, and there is the possibility that earth pressure caused by lateral movements that are coincidental to subsidence of backfilling may come to bear on bridge abutments. There is a report of a case where, at a bridge abutment previously damaged by an earthquake, such liquefaction-induced lateral force caused another damage[2]. Many aspects of the mechanism that causes this liquefaction-induced lateral force have not been completely understood yet. There are many uncertaties regarding the mechanism that causes this lateral movement. Thus, it is necessary to understand the characteristics of seismic earth pressure that acts on the bridge abutment structure and to accurately evaluate these characteristics for rational seismic design of bridge abutments.

The authors conducted dynamic centrifuge tests using bridge abutment models on the liquefiable ground with pile foundations. This paper reports the relationship between earth pressure on the rear of the bridge abutment during earthquakes and ground liquefaction based on the experiment results. The paper also presents comparisons of these results with seismic earth pressure on the rear of bridge abutments as prescribed in the Japan's seismic design specifications for highway bridges.



Unit: m (converted for prototype model)

Figure 2. Cross section of model

Table 2. Soil properties of sand

Properties	Silica sand	Edosaki sand
G_s	2.65	2.68
D_{50} (mm)	0.17	0.17
U_c	1.68	4.2
F_c (%)	4.0	11.0
e_{max}	1.63	1.52
e_{min}	1.24	1.15
F_{dmax} (%)	-	1.57
w_{opt} (%)	-	14.3

EXPERIMENTAL MODELS

The dynamic centrifuge tests were carried out in a total of eight "cases", in which constraint conditions were altered by ground density, thickness of liquefaction layer, and upper structure. A large geotechnical dynamic centrifuge with a radius of 6.6 m has been development at PWRI in 1997. For the purpose of the geotechnical earthquake studies, a powerful electro-hydrauric shaking table designed to work in the centrifuge has also been developed. This shaking table provides 40G shaking acceleration observed durng the 1995 Hyogo-ken Nanbu Earthquake for a model at 50G centrifugal acceleration field. As shown in **Figure 2**, 1:50-scale models of an inverted T-type abutment were used. As is shown in **Table 1**, two types of ground density were used: one for which liquefaction occurs easily (relative density of 60%) and one for which liquefaction does not occur easily (relative density of 85%). The relative density of the backfilling and that of the supporting layer directly below the layer of liquefaction were the same in all cases. In preparing the ground model, a supporting layer was created by compacting dry silica sand to the prescribed relative density (approximately 90%), on top of which a liquefaction layer was created by compacting Edosaki sand with a water content of 18% to the prescribed relative density (approximately 60% or 80%). **Table 2** shows the properties of the sand used in the experiments. After compacting backfilling soil onto the prepared liquefaction level, the completed soil models were put into a vacuum chamber. They were then saturated by passing an aqueous solution of Metolose from the bottom of the soil layers (in the centrifuge experiments, the chamber temperature was kept at 10℃ and a Metolose aqueous solution having a density of 1.8% was used) that was adjusted to 50 times the viscosity of water in order to satisfy the similarity law for permeation. Stainless steel was used in preparing the bridge abutment model, with lead being added to some areas to adjust the model's weight and center of gravity. The pile model was made of acrylic resin and fixed to the bottom of the bridge abutment with screws. The bottom tip of the pile was made free. In terms of restraint conditions caused by the upper structure, experimental cases were established whereby deformation in the forward direction was confined through impact with the end of the girder, and cases where the bridge abutment could transform freely without constraint. As a result, top of the abutment can be move for the elastic deformation of the rubber (approximately 30 cm if converted to 1:1 scale), even in the cases where the bridge abutment was fixed.

EXPERIMENTAL RESULTS

The experiments took place at a 50 G centrifugal acceleration field using equipment for load testing of dynamic centrifugal force. Because the model was built at a scale of 1:50, it was possible to reproduce stress conditions found in the actual ground by conducting the experiments under 50G. In saturating the ground, the groundwater level was raised to the

ground surface. For this, water was extracted from the bottom soil layer when the centrifugal speed was brought up to 50 G. The groundwater level was brought to the prescribed position (1.75 meters below the surface of the front ground), and the dynamic loading experiments were begun. In the dynamic loading experiments, 20 cycles of sinusoidal shakings with a frequency of 100 Hz, and the input level at Step 1 was set at 12 G (approximately 250 gals when converted to 1:1 scale). In Step 2, the input level was set at 25 G (approximately 500 gals when converted to 1:1 scale). **Figure 3** shows the actual 1:1 conversion of the Step 1 pressure measured using load cells installed at the back of the bridge abutment. Also presented in **Figure 3** are calculations of active earth pressure during earthquakes by use of the Japan's seismic design specifications for highway bridges. Although there is amplification of earth pressure in the rear of the bridge abutment during earthquake in the Japan's seismic design specifications for highway bridges, there are many uncertainties concerning the characteristics of acceleration amplitude. Because, as is shown in **Figure 4**, seismic earth pressure was brought to bear on the wall of the bridge abutment using the same earthquake force. Earth pressure on the rear of the bridge abutment during earthquakes[1)] was calculated according to the following formula:

$$P_{EA} = \gamma \times x \times K_{EA} + q' \times K_{EA} \qquad (1)$$

Here,

P_{EA} : active seismic earth pressure (kN/m^2) at a depth of x (m)

K_{EA} : coefficient of active seismic earth pressure

When the backfilling consists of sand or gravel

$K_{EA} = 0.21 + 0.90\ k_h$

When the backfilling consists of sand or gravel

$K_{EA} = 0.24 + 1.08\ k_h$

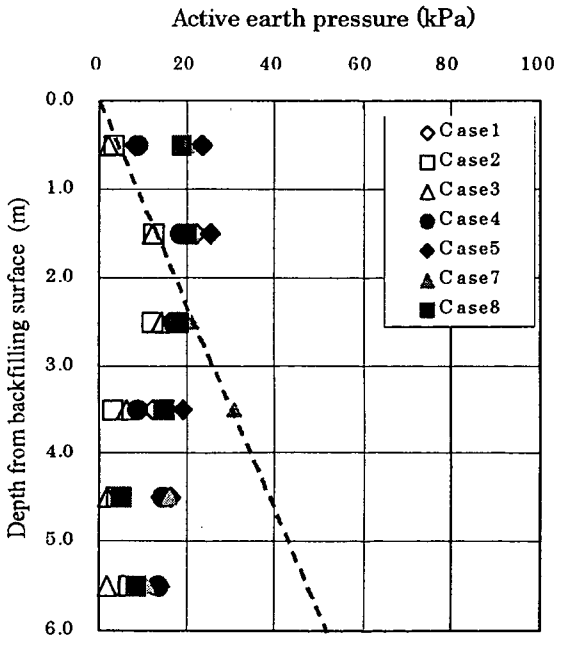


Figure 3. Active earth pressure (Step 1)

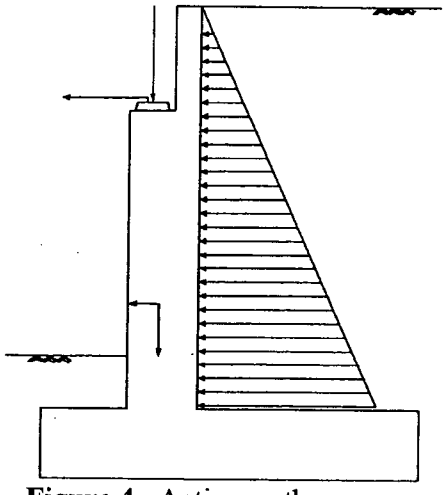
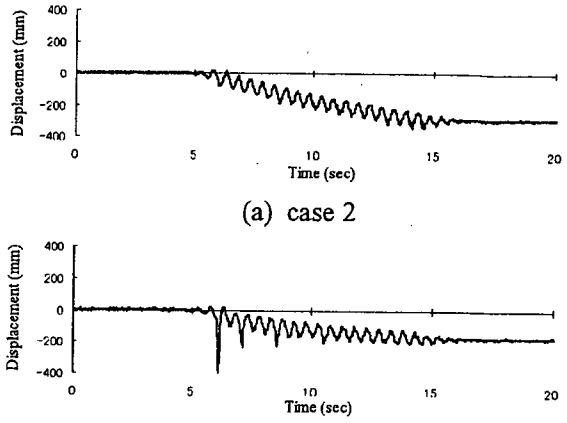


Figure 4. Active earth pressure



(a) case 2

(b) case 5

Figure 5. Displacement at top of the abutment (Step 1)

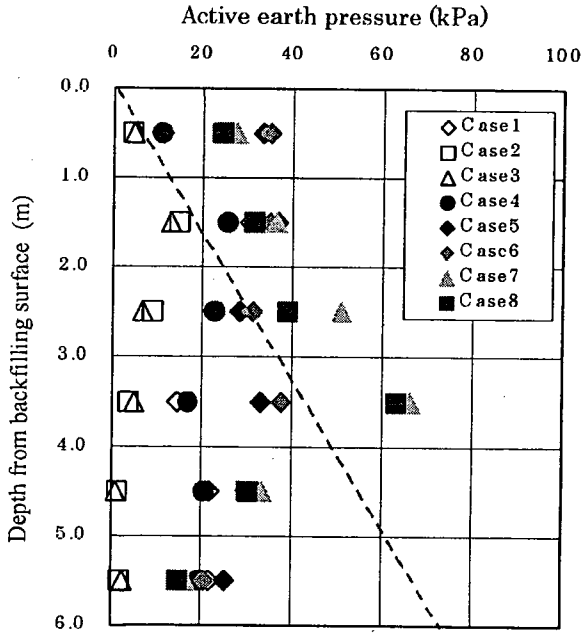


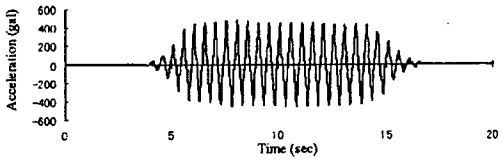
Figure 6. Active earth pressure (Step 2)

k_h : design horizontal seismic coefficient using calculation of earth pressure during an earthquake

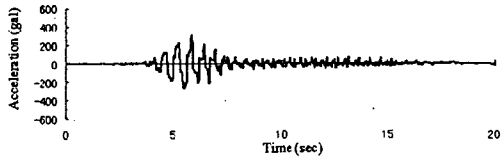
y : unit weight of earth (kN/m^3)

q' : acting load at the surface of backfilling (kN/m^2)

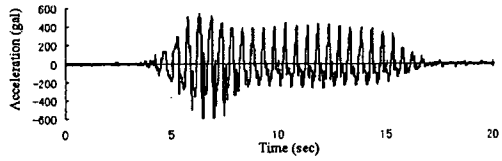
Comparing the cases 2, 3, 7, and 8, in which liquefaction occurred, and the cases 1, 4, and 5, in which liquefaction did not occur, a slightly greater amount of ground pressure was generated in the latter cases. Also, in the cases 5, 7, and 8, in which displacement of the top end of the bridge abutment was constrained, it was found that the calculated value of earth



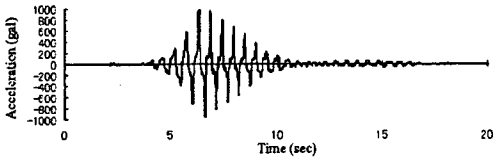
(a) bottom of container (case 2)



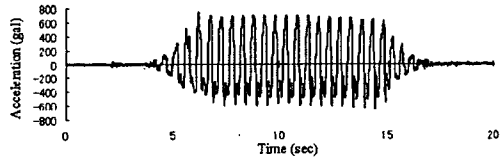
(b) surface of the front-side ground (case 2)



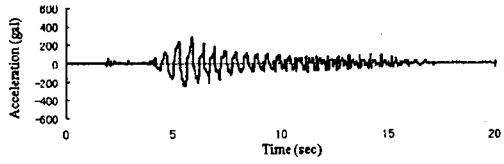
(c) surface of the backfilling-side ground (case 2)



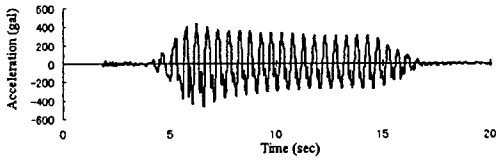
(d) surface of the front-side ground (case 5)



(e) surface of the backfilling-side ground (case 5)



(f) surface of the front-side ground (case 8)



(g) surface of the backfilling-side ground (case 8)

Figure 7. Response acceleration (Step 2)

pressure near the surface of the backfilling was higher. As is shown in **Figure 5**, this is attributed to a fact that displacement of the top end of the bridge abutment was confined through impact between the end of the girder and the abutment, and increased earth pressure on the rear side of the abutment. Accordingly, at the earth pressure increases where is low displacement confinement (Step 1, where input acceleration are low), this tendency was limited to a shallow range beneath the ground surface of the backfilling; however, it was recognized that ground pressure increased even at deeper levels when the displacement constraint becomes larger (Step 2, where input acceleration are high).

Next, **Figure 6** shows the results of Step 2, where the ground liquefied and the notable lateral movement in the backfilling occurred. In the same Figure, it can be seen that differences in displacement constraint conditions of the top end of the abutment had a larger influence than ground liquefaction. Looking at the cases 1, 2, 3 and 4, in which displacement of the top end of the abutment was not constrained, the calculation values were in general within the same range as those for Step 1. However, it was found that, in cases 5, 6, 7, and 8, in which displacement of the top end of the abutment was constrained, earth pressure far exceeded the calculation values. Although there was a reduction in transmission of acceleration due to liquefaction after the maximum acceleration of roughly 1,000 gals was reached on the front-side ground of the abutment (see **Figure 7**(d)) because the relative density of the layer of liquefaction was high in cases 1, 5, and 6, as is shown in **Figure 7**(e), it was not found that acceleration was reduced near the surface of the backfilling soil because of

differences in effective constraining pressure. Thus, it was understood that the backfilling side ground underwent incomplete liquefaction. On the other hand, as shown in **Figures 7** (c) and (g), even the ground on the backfilling of the abutment underwent liquefaction in cases 2, 3, 7 and 8, and response acceleration near the surface was reduced. Because the ground had the same degree of liquefaction in these cases, the difference in earth pressure acting on the abutment was displacement of the top of the abutment. Even when comparing case 7 and case 8, where the thickness of the level of liquefaction was altered, a notable difference in earth pressure on the rear side of the abutment was not found. Accordingly, there was impact between the abutment and the end of the girder when the abutment underwent horizontal movement toward the bridge axis and when the laying gap between the girder ends shrank. It is considered that the effect of impact between the abutment and the end of the girder appeared sensitively. As a result, seismic earth pressure exceeded design values at the abutment.

CONCLUSION

We measured active seismic earth pressure that affects the abutment by centrifuge test. The following points were identified during the course of research.

1) Acceleration within the backfilling ground increased from the deeper regions toward the surface. Nearly uniform earth pressure acted on the abutment from the backfilling.
2) Until a depth of some 4 meters from the surface, seismic earth pressure that affected the backfilling of an abutment did not exceed the results of the formula indicated in the specifications for highway bridges when the abutment was free to move. However, if deformation of the upper part of the abutment was constrained through impact with girder end, earth pressure at the time of earthquake exceed the results of the formula, regardless of whether ground liquefaction occurred or not.
3) If deformation of the upper part of the abutment was constrained by impact with girder end, the backfilling of the abutment subsided when ground liquefaction occurred, which led to forward movement. As a result, lateral earth pressure acted on the abutment with lateral movement of the backfilling.

REFERENCES

1) Japan Road Association (2002). Design Specifications for Highway Bridges Part V. Seismic Design
2) Fukui J., Miyamoto K., Someya K., Saeki M., Shirato S., Analysis of Cases of Earthquake Damage to Road Bridge Abutments and Foundations, Proceedings of the Fourth Civil Engineering Symposium on Progress in Earthquake and Natural Disaster Based Processes to Prevent Collapse of Structures, pp.247-252, 2003 (in Japanese)
3) Keiichi TAMURA and Takuo AZUMA (2003). "Development of Analytical Procedure for Estimating Effects of Liquefaction-Induced Ground Flow on Bridge Foundation." Proceedings of 2003 Pacific Conference on Earthquake Engineering, 2003

STATIC AND DYNAMIC BEHAVIOR OF FLARED-COLUMN BENTS

Suhas S. CHANDANE[1], David H. SANDERS[2], M. "Saiid "SAIIDI[3], Saad EL-AZAZY[4]

Abstract

Past earthquakes have shown poor performances of flared-column bents. During the earthquake the plastic hinge was shifted to the base of the flare, increasing the shear demand above the design level and causing shear failure. Caltrans is placing a gap at the top of the flare in order to seismically isolate the flare from the rest of the bent. An experimental and analytical study has been conducted in order to determine the behavior of this system. The project consisted of 4 specimens that were tested on the shake table with two of those specimens being retested statically. In this paper, one of the shake table test will be described that has a gap size that was two times what was used in previous tests. The paper will also describe the two static tests. They were conducted to study the post peak performance of the bents.

1. INTRODUCTION

Design of flared columns is complicated due to the varying cross section. In past earthquakes these columns have shown poor performances. Due to the increased capacity of the flared section, the plastic hinge shifted to the bottom of the flare. The columns behaved as if they were much shorter. Therefore, there was an increase in shear demand above the design level causing brittle shear failure. The brittle shear failure can lead to collapse of the structure before achieving sufficient inelastic deformation.

It was assumed in previous designs that flares with small amounts of transverse and longitudinal flare reinforcement would fail during the earthquake and the column core would resist the load. The experimental studies of flared columns show that even lightly reinforced flares contribute to the flexural capacity of the section (Sanchez and Priestley 1997). To solve this problem, Caltrans determined to separate the flares from contributing to the flexural capacity of the column. This was achieved by creating a gap between the flares and the bottom of the beam (Fig. 1). Caltrans came up with these recommendations based on slow-cyclic testing of single columns (Sanchez and Priestley 1997) and not on bents tests. To study the performance of the flares and the behavior of the beam-column connection, shake table tests on the bents were conducted at the University of Nevada Reno (Nada et al. 2002). Three specimens of 1/5 scale were tested, two of them had flexure dominated columns while one had shear dominated columns; this was achieved by using two different column heights. The columns were pinned at the base with two-way hinges. One tall specimen had the transverse flare reinforcement as per current Caltrans recommendations (Caltrans Seismic Design Criteria) (LFCD1) and the other had only minimum transverse reinforcement throughout the flare height (LFCD2). The short specimen had the minimum transverse reinforcement (SFCD2) throughout the flare. The gap at top of the flares was same in all specimens and was as per current specifications.

[1]Graduate Research Assistant, Dept. of Civil Engineering, University of Nevada Reno, NV-89557
[2]Associate Professor, Dept. of Civil Engineering, University of Nevada Reno, NV-89557
[3]Professor, Dept. of Civil Engineering, University of Nevada Reno, NV-89557
[4]Senior Design Engineer, California Department of Transportation, Sacramento, CA

The current Caltrans recommendations for flares are as follows:

- Minimum gap thickness 50 mm (2 in) or higher if analysis proved gap closure,
- Nominal longitudinal flare reinforcement, and
- Variable confinement steel ratios.

  $\rho_h = 0.45\% \pm 0.05$, top 1/3 of flare

  $\rho_h = 0.075\% \pm 0.025$, bottom 2/3 of flare

  $\rho_h = 2\ A_b / s\ D$

Where,

ρ_h = Confinement steel ratio,

A_b = Area of reinforcement bar,

s = Spacing of the reinforcement, and

D = Diameter of the section.

In the testing of Nada et al., none of the specimens completely failed due to the limits of the shake table. All the specimens showed gap closure at very low ductility and increase in strength after that. In order to fully test the specimens and observe post-peak behavior, it was decided to statically test two of the specimens. The static test on LFCD1 was called LFCD1S and SFCD2 was called SFCD2S. Another issue from the initial series was that the gap at the top of the flare in all specimens closed at a very low level of ductility. Therefore, it was decided to test a short specimen with increased gap width at the top of the flares. The new specimen with increased gap width at the top of the flare was designated as SFCD3.

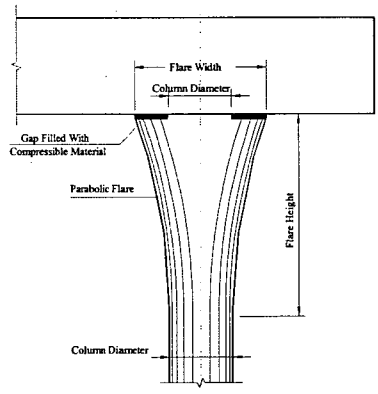
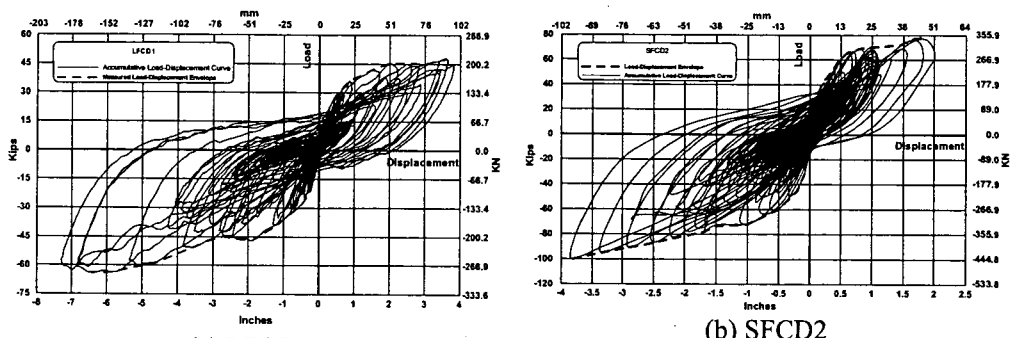


Figure 1 Layout of the proposed detail

2. PREVIOUS TEST RESULTS

The testing of LFCD1 and SFCD2 was stopped, after significant yielding and gap closure, due to the capacity of the shake table. The specimens did not fail. Figure 2 shows the load-displacement relationships for LFCD1 and SFCD2. Figure shows that the testing was stopped before observing the post-peak load performance of the specimens. Table 1 describes the basic experimental response of the specimens. As the specimens did not fail and their post-peak load performance was not observed, it was decided to test the specimens statically till failure.



(a) LFCD1 (b) SFCD2

Figure 2 Load-displacement relationships for LFCD1 and SFCD2

Table 1 Structural response of LFCD1 and SFCD2

	LFCD1	SFCD2
Effective Yield Displacement mm (in)	23.4 (0.92)	10.2 (0.40)
Effective Yield Force KN (Kips)	181.5 (40.8)	279.3 (62.8)
Minimum Displacement mm (in)	165.1 (6.5)	94 (3.7)
Maximum Measured Force KN (Kips)	284.6 (63.98)	433.2 (97.38)
Ductility Ratio	7.07	9.1
Displacement at Gap Closure mm (in)	67.3 (2.65)	42 (1.65)
Ductility Ratio at Gap Closure	2.88	4.0
Ductility Ratio without Base Hinge Disp.	6.12	8.5

3. MODEL DESIGN

Table 2 shows a summary of the characteristics of LFCD1S, SFCD2S and SFCD3. Figure 3 shows the reinforcement details for LFCD1 (LFCD1S). The models were 1/5th scale. The columns of LFCD1 (LFCD1S) were 1625 mm (64 in) tall and in SFCD2 (SFCD2S) and SFCD3 they were 991 mm (39 in). The major change in the new specimen of SFCD3 was the gap at the top of the flare was increased to 19 mm (0.75 in) in comparison to 9.5 mm (0.375 in) in (LFCD1) LFCD1S and SFCD2 (SFCD2S). The 9.5 mm (0.375 in) gap width stands for current Caltrans recommendations. In SFCD3 the confinement steel in the flare was minimum throughout the flare height as it was in LFCD2 and SFCD2 (SFCD2S), while it was as per Caltrans recommendations in LFCD1 (LFCD1S). The beam skin reinforcement in LFCD1 (LFCD1S), LFCD2 and SFCD2 (SFCD2S) had only one reinforcement bar while SFCD3 had distributed skin reinforcement to make it more representative of current specifications. In all specimens the area of the skin reinforcement was the same. Figure 4 shows the reinforcement differences in LFCD1S, SFCD2S and SFCD3. Table 3 gives the material properties for all the specimens.

Table 2 Flare details for LFCD1S, SFCD2S and SFCD3

Flare Detail	LFCD1	SFCD2	SFCD3
Transverse reinforcement at top 1/3 of flare height	4.87 mm Dia. @ 28mm (0.192" Dia. @ 1.1")	3.75 mm Dia. @ 97mm (0.148" Dia. @ 3.8")	3.75 mm Dia. @ 97mm (0.148" Dia. @ 3.8")
Transverse Ratio	0.44%	0.08%	0.08%
Transverse reinforcement at remaining 2/3 of flare height	3.75 mm Dia. @ 97mm (0.148" Dia. @ 3.8")	3.75 mm Dia. @ 97mm (0.148" Dia. @ 3.8")	3.75 mm Dia. @ 97mm (0.148" Dia. @ 3.8")
Transverse Ratio	0.08%	0.08%	0.08%
Vertical Flare Reinforcement	6 Wires - 3.75 mm (0.148") Dia.		
Gap width	9.5 mm (0.375")	9.5 mm (0.375")	19 mm (0.75")

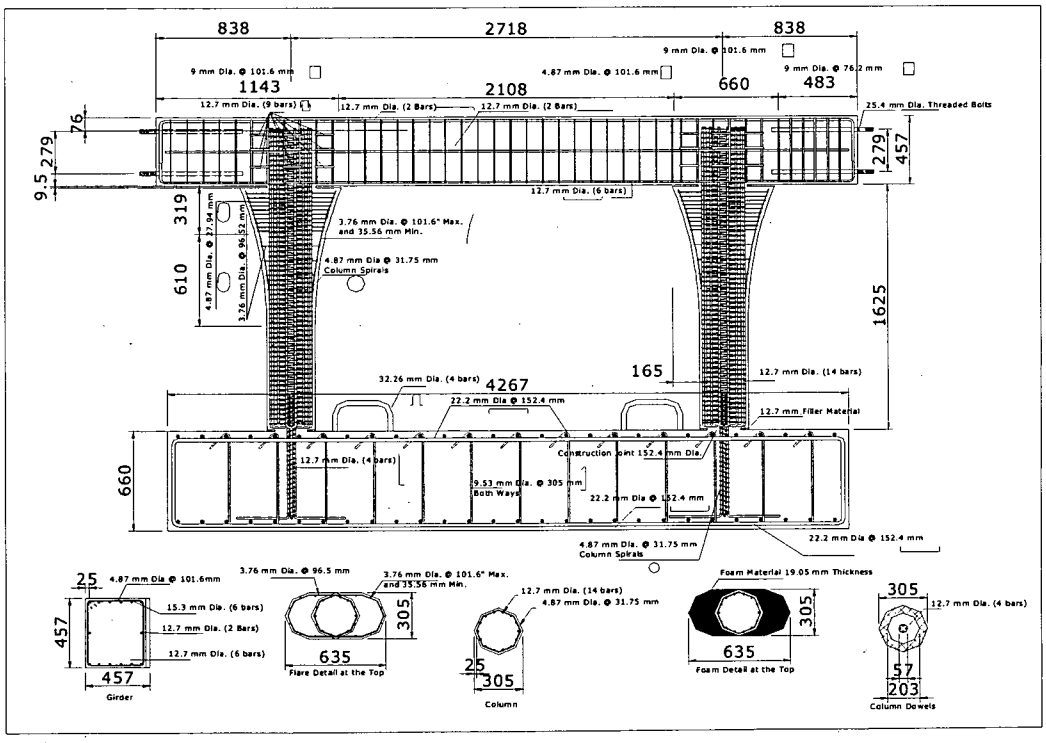


Figure 3 Reinforcement details for LFCD1S

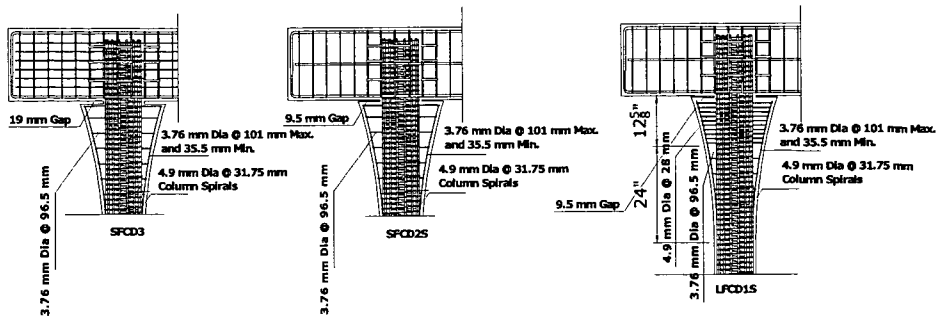


Figure 4 Reinforcement differences in LFCD1S, SFCD2S and SFCD3

Table 3 Material properties for LFCD1S, SFCD2S and SFCD3

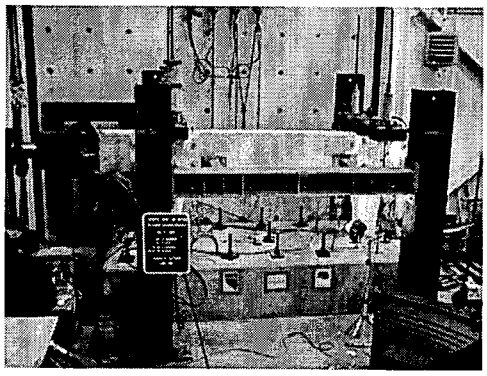
CONCRETE	FOOTING MPa (psi)	COLUMN MPa (psi)	BEAM MPa (psi)
LFCD1S	39(5647)	41(5992)	45(6523)
SFCD2S	42(6089)	45(6549)	43(6278)
SFCD3	41 (5980)	46 (6650)	43 (6180)

STEEL	16 mm (# 5) MPa (ksi)	13 mm (# 4) MPa (ksi)	4.87 mm Bar (0.192 in) MPa (ksi)	3.76 mm Bar (0.148 in) MPa (ksi)
YIELD STRENGTH	483(70)	428(62)	418(60)	492(71)

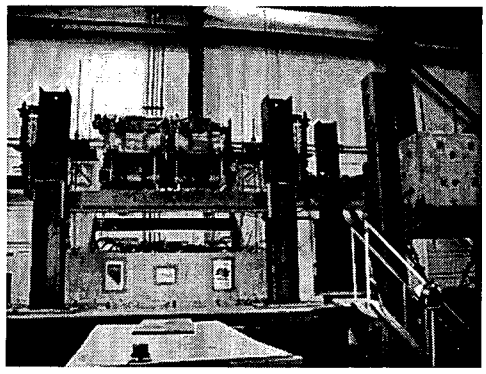
4. TEST SETUPS

The axial load was set as 0.1 x A_g x f'c; where A_g was the gross column cross section area and f'c was the concrete compressive strength. The axial load was equal to 400 KN (90 kips) for the system. In the shake table testing the axial load and the inertial loads were created by a combination of lead buckets mounted on the bent as well as hydraulic rams on top of the bent. The capacity of shake table restricted the weight of lead bucket, so some of the axial load was carried by the hydraulic rams. The axial load through the hydraulic rams was self equilibrating and applied directly onto the columns. The strains in the beam longitudinal reinforcement were very low at the beginning of the test indicating a small effect of gravity bending moment in the beam. While the distribution of weight did not exactly model the actual structure, the moments from the gravity load are much smaller than those experienced from the lateral load. The lead weights also apply inertial loads but the hydraulic rams do not, therefore the remaining inertial load equal to the load applied by the hydraulic rams must be applied by an outside source. The remaining inertia loading system is called a mass-rig. It consists of a structure with 4 pins that carries concrete blocks and these blocks are connected to the specimen through a rigid link so that the inertia load is transferred to the specimen. In static testing the total axial loading was applied through hydraulic rams only and an actuator

was used for the lateral load. Figure 5 shows the test setups for the shake table and static tests. The specimens were tied down to the reaction surface with post tensioning bars.



(a) Static test



(b) Shake table test

Figure 5 Test setups

For SFCD3 the instrumentation consisted of 154 strain gages, and 57 displacement transducers. Transducers were installed to measure the curvature along the height of the columns, shear displacement in the beam-column connections and the flare, and global displacement of the specimen along with the base-hinge displacement. Accelerometers were used to measure the acceleration of the specimen at different places.

For LFCD1S and SFCD2S, 33 displacement transducers were used. They were used to measure the curvature along the column height, shear deformation in the joint, and the global displacement of the specimens including any base slip of the specimen and global movements of the bent.

5. LOADING PROGRAM AND PRELIMINARY ANALYSIS

The loading procedure for the SFCD3 consisted of a series of earthquakes. The runs steps were chosen so that it would capture important points like cracking, yield and ultimate. The specimen was excited with scaled version of the Sylmar record from the 1994 Northridge Earthquake. The accelerations of original records were multiplied by factors. The intensities of earthquakes were 0.25, 0.5, 0.75, 1.0, 1.25, 1.5, 1.75, 2.0, 2.25, 2.5, 2.75, 3.0, 3.25 and 3.5 times Sylmar. This is the same loading program that was used in the study by Nada et al. The peak acceleration for 1.0 times Sylmar was 0.61g.

A preliminary analysis was done using a program called RC-Shake (Laplace 1999) developed at University of Nevada Reno. The program gives the response of the structure to the given earthquake excitation. The program models the specimen as a single degree of freedom system. The program requires a bilinear stiffness curve and mass of the system as well as an acceleration time history. The moment-curvature analysis program RCMC (Wehbe 1997), developed at University of Nevada Reno, was used to calculate effective yield and ultimate points for RC-Shake. Figure 6 shows the response of SFCD3 for intensities of earthquakes from 0.25 to 3.5 times Sylmar.

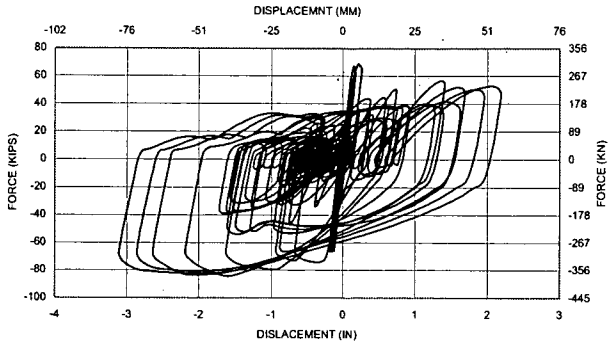


Figure 6 Load deflection diagram from RC-Shake for Sylmar runs of 0.25, 0.5, 0.75, 1.0, 1.5, 2.0, 2.5, 3.0, 3.25 and 3.5

LFCD1S and SFCD2S were pushed and pulled through the various points such as first yield, idealized yield, gap closure, and the maximum shake table displacement. The specimens were then pushed and pulled into new displacements until failure. Table 4 shows the loading history for both the specimens. SFCD2S was not pushed to idealized yield displacement. As the first yield displacement and idealized yield displacement were very close to each other, it was decided to push/pull the specimen to the first yield displacement only.

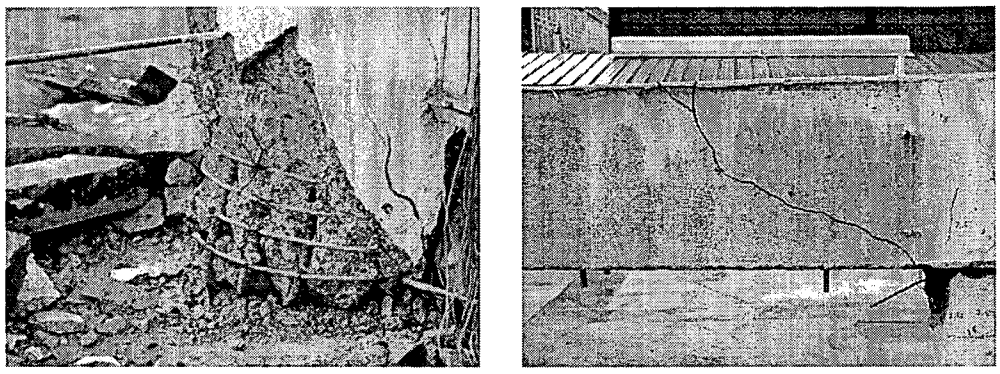
Table 4 Loading program for LFCD1S and SFCD2S

PUSH AND PULL	FIRST YIELD	IDEALIZED YIELD	GAP CLOSURE	MAX. SHAKE TABLE DISP.	FINAL PUSH
LFCD1S	17 mm (0.7")	23.4 mm (0.92")	67.3 mm (2.65")	165 mm (6.5")	388 mm (15.3")
SFCD2S	8.4 mm (0.33")	-	41.9 mm (1.65")	94.0 mm (3.70")	134 mm (5.28 ")

6. TEST OBSERVATIONS

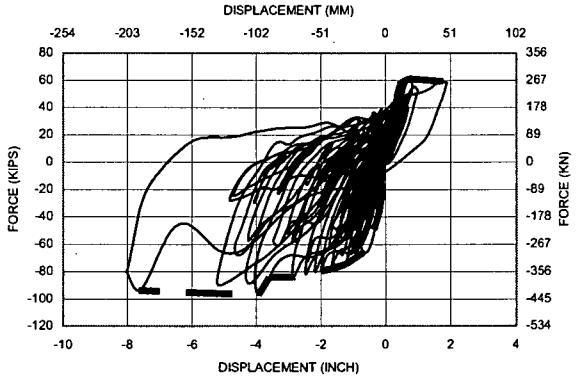
(1) SFCD3- The reinforcement in the base-hinge started to yield at 0.5 times Sylmar. The strain data shows that the column longitudinal reinforcement started to yield at 0.75 times Sylmar. Beam bottom longitudinal reinforcement started to yield at 0.75 times Sylmar. Specimen failed in the base-hinge at 3.5 times Sylmar (Figure 7a) with substantial cracking and center spalling at the top of the flare. Figure 8a shows the cumulative load-displacement curve for all runs for SFCD3. The diagram shows the increase in load carrying capacity after significant yielding. This was caused by gap closure. The top of flare came in contact with the beam bottom increasing the effective area of the section; this caused an increase in moment carrying capacity. Significant slippage in the base-hinge was also observed. Shear cracking was observed in the beam after bucket removal (Figure 7b). The increase in moment capacity created an increase in the shear demand in the beam. Table 5 summarizes the response of the structure. Curvature measured along the height of the specimen indicates that plastic hinges were formed at the top and the bottom of the column. Figure 8b compares the load-displacement envelope for SFCD2 and SFCD3. The curve shows gain in strength due to gap closure at higher level of ductility in SFCD3 compared to the SFCD2. The displacement

ductility for gap closure in SFCD2 was 4.0, and in SFCD3 it was 6.9. The minimum displacement ductility required by the current specifications is 5. As the gap closure was at a higher level of ductility than required, the gap width of 19 mm (0.75 in) performs well. Figure 9 shows the damaged flare section after the failure with spalling of the flare concrete and damage of the core.

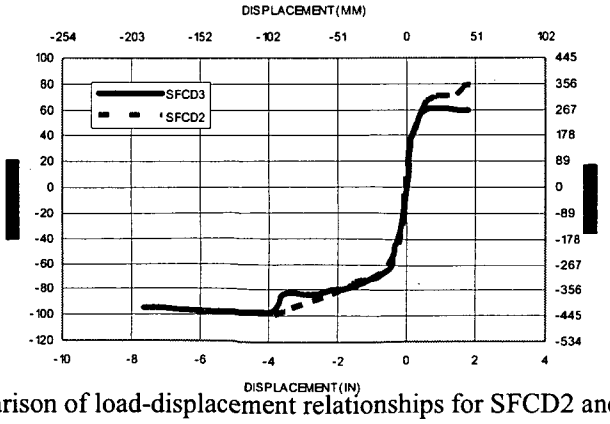


(a) Base-hinge failure (b) Shear cracking of beam

Figure 7 SFCD3 at failure



(a) Load-displacement relationship for SFCD3



(b) Comparison of load-displacement relationships for SFCD2 and SFCD3

Figure 8 Load-displacement for SFCD2

Table 5 Structural response of SFCD3

	Yield Disp.	Yield Force	Max. Disp.	Max. Force	Drift	Ductility
Ultimate	13.7 mm (0.54 in)	365 KN (82 K)	194 mm (7.64 in)	431 KN (97 K)	16	14.15
Gap Closure	-	-	91.7 mm (3.61 in)	374 KN (84 K)	7.5	6.69

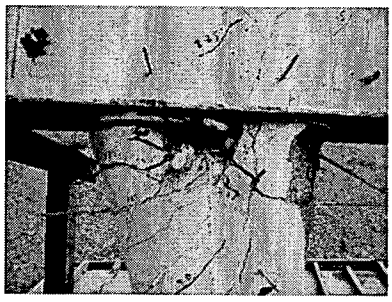
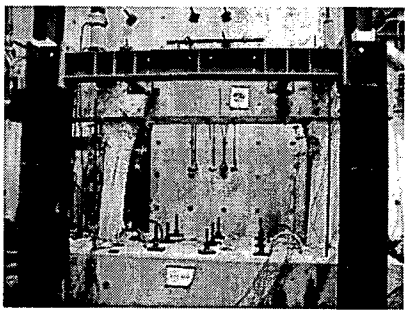
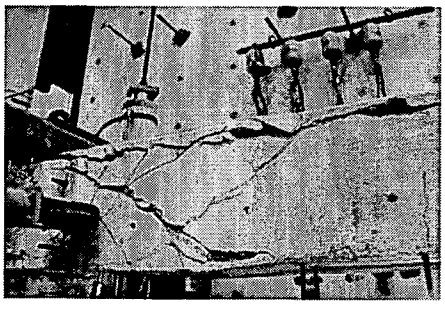


Figure 9 Damaged flare after the failure of SFCD3

(2) LFCD1S- Wide shear cracks were seen in the beam of LFCD1S but the beam did not fail (Figure 10 a). The test was stopped because of a slight drop in load-carrying capacity and excessive displacements. Figure 11a shows the cumulative load-displacement curve for all loading stages for runs for LFCD1S. Table 6 summarizes the structural response. It shows the maximum ductility of the specimen was 16, this high ductility is due to the fact that the yield point is dominated by the column core section while the final behavior includes the effects of the larger section. Figure 11b compares the load-displacement envelope for LFCD1 and LFCD1S. The LFCD1S is a continuation of LFCD1. Figure 12a shows damaged flare section after the testing.



(a) Large drift and displacement before stopping the testing of LFCD1S

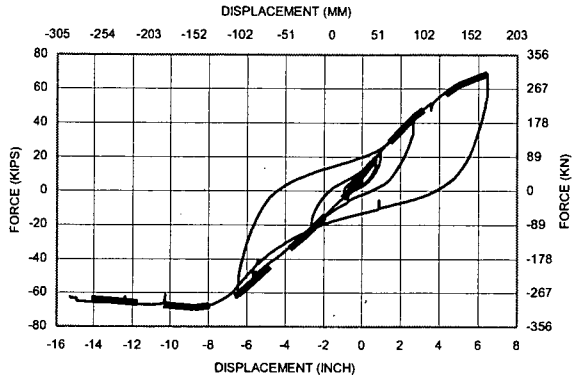


(b) Beam shear failure in SFCD2S

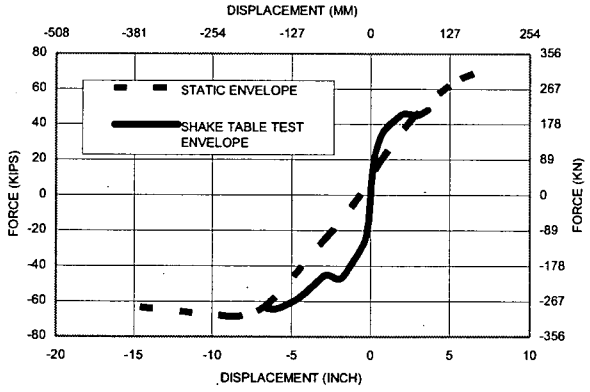
Figure 10 Behavior of static specimens

Table 6 Structural response of LFCD1S and SFCD2S

	MAX DISP	MAX FORCE	MAX. DRIFT	MAX DUCTILITY
LFCD1S	388 mm (15.3 in)	305 KN (68.6 K)	21 %	16
SFCD2S	134 mm (5.28 in)	482 KN (108.4 K)	11 %	13



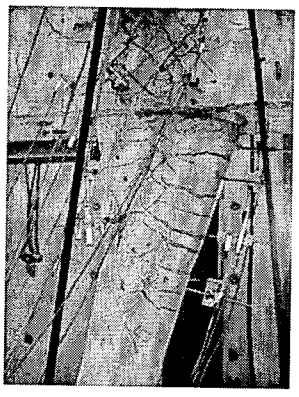
(a) Load-displacement relationship for LFCD2S



(b) Comparison of load-displacement relationships for LFCD1 and LFCD2S

Figure 11 Load-displacement for LFCD1

(3) SFCD2S- Extensive beam shear cracking was seen after gap closure. SFCD2S failed in beam shear (Figure 10b). Figure 13a shows the cumulative load-displacement curve for all loading stages for SFCD2S. Table 6 summarizes the performance of the specimen. The maximum displacement achieved was very high compared to the current specifications. Figure 13b compares the load-displacement envelope for SFCD2 and SFCD2S. The SFCD2S is almost continuing the SFCD2 curve. Figure 12b shows the damaged flare after failure. While the cracking is extensive, the flare is intact.

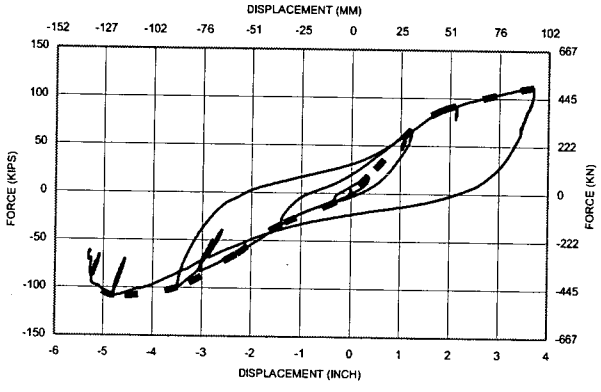


(a) Final condition of LFCD1S after the test

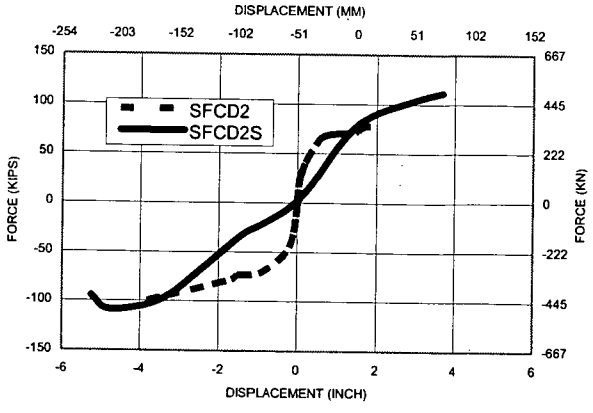


(b) Final condition of SFCD2S

Figure 12 Final Specimen Condition



(a) Load-displacement relationship for SFCD2S



(b) Comparison of load-displacement relationships for SFCD2 and SFCD2S

Figure 13 Load-displacement for SFCD2S

7. GAP WIDTH CALCULATIONS

(1) Caltrans Method - Current Caltrans procedure was used to estimate the gap closure status. The procedure is based on curvature analysis of the section. Using the effective yield curvature value and the ultimate curvature value, the yield rotation and plastic rotation at the top section of the flare can be calculated. The yield rotation, θ_y, can be calculated using the moment-area method by integrating the moment along the column height. For the plastic rotation, θ_p, equation 1 was used.

$$\theta_p = L_p (\phi_u - \phi_y) \quad (1)$$

Where,
L_p = Plastic hinge length,
ϕ_y = Effective yield curvature, and
ϕ_u = Ultimate yield curvature.

The value of the plastic hinge length is calculated using equation 2 provided by Caltrans.

$$L_p = G + 0.3 f_{ye} d_{bl} \quad (2)$$

Where,
G = Gap width,
f_{ye} = Expected yield stress for longitudinal reinforcement, and
d_{bl} = Bar diameter for longitudinal reinforcement

The total displacement of the flare edge can be calculated by multiplying the total rotation, which is the summation of θ_p and θ_y, by the distance from the neutral axis of the section at ultimate curvature to the edge of the flare. The gap will not close as long as the calculated deformation is less than the gap width.

For the current specimens, the needed gap width was calculated to be 9.4 mm (0.372 in). The gap width was set at 9.5 mm (0.375 in) for the initial specimens. In the case of SFCD3, the gap was increased to 19 mm (0.75 in) but it still closed. Finite element analysis done by Nada et al. shows that even the specimens with gap width 25 mm (1.0 in) gap closes at a displacement ductility of 10, which is much higher than required.

The procedure was also applied to two flared column specimens statically tested at University of California, San Diego by Sanchez et al: RDS-3 (gap width 25 mm (1.0 in)) and RDS-4 (gap width 50 mm (2.0 in)). The Caltrans Method indicated a require gap size of 18 mm (0.72 in). In RDS-3, the gap width was 25 mm (1.0 in). This specimen showed gap closure at high displacement ductility of 8.2 and drift of 4.7 %, while it failed at a displacement ductility of 13.6 and drift of 7.8 %. In RDS-4, the gap width was 50 mm (2.0 in) and the specimen failed without gap closure. The gap size in which failure in the column will occur at the same time as gap closure is somewhere in between 25 mm (1.0 in) and 50 mm (2.0 in). The Caltrans Method under predicts the needed gap size.

To determine a sufficient gap width to prevent gap closure, a factor of safety is required. The minimum factor of safety of 2 is needed based on the San Diego tests and 3 is needed based on the Reno tests. In order to be conservative, 3 was selected.

(2) NCHRP 12-49 Method – NCHRP recommends the minimum gap width of 0.05 times the distance from the center of the column to the extreme edge of the flare or 1.5 times the

calculated plastic hinge rotation from the push-over analysis times the distance from the center of the column to the extreme edge of the flare. NCHRP 12-49 provides an equation for plastic hinge rotation capacity of the section, which can be used to predict the minimum gap width. This minimum gap width is multiplied by 1.5 to determine the required gap width. The equations are 3 through 6.

$$\theta_p = 0.11\,(L_p/D')\,(N_f)^{-0.5} \quad (3)$$

$$N_f = 3.5\,(T_n)^{-1/3} \quad (4)$$

$$L_p = L_g + 8800\,\varepsilon_y\,d_b \quad (5)$$

$$L_{G\,required} = \theta_P\,L_{FLARE} \times 1.5 \quad (6)$$

Where,

θ_p = Plastic rotation capacity of the section (rad),

L_p = Plastic hinge length,

D' = The distance between the outer layers of the longitudinal reinforcement on opposite faces of the member,

N_f = number of cycles of loading expected at the maximum displacement amplitude,

T_n = natural period of vibration of the structure,

L_g = Gap width provided,

ε_y = Yield strain of the longitudinal reinforcement,

d_b = Diameter of member longitudinal bar,

L_{FLARE} = Distance from the center of the column to the extreme edge of the flare, and

$L_{G\,required}$ = Minimum gap width required for no gap closure.

For the specimens tested at Reno, 0.05 times the distance from the center of the column to the extreme edge requires a gap size of 16 mm (0.63 in). The plastic rotation procedure gives a minimum gap width of 13 mm (0.52 in) and a required value of 20 mm (0.78 in). As shown from the specimens, this gap would not be sufficient to prevent gap closure.

For the San Diego specimens, the plastic hinge method gives minimum gap width of 22 mm (0.86 in) and a required size of 33 mm (1.29"). The distance from the center to the edge of the flare is 760 mm (30 in.). Therefore, the 0.05 criterion requires a gap size of 38 mm (1.5 in). Therefore, the 0.05 limit is sufficient for the San Diego columns but the plastic hinge method predicts too small of a gap.

Based on a comparison between experimented specimens and the analysis for both the tests at San Diego and Reno, a factor of safety of 2 is needed instead of only 1.5 recommended by the NCHRP method to ensure no gap closure when using the plastic rotation method. An increase in the 0.05 limit is also necessary. Based on the limited test data, a value of 0.08 times the distance from the center of the column to the flare edge should be used.

(3) Drift Method - Another way to estimate minimum gap width is with demand drift. Calculating a demand drift and then multiply it with a factor of safety, say 1.5. A required plastic rotation can be calculated from the required demand drift using the equations 7 and 9. This is done assuming that all displacement of the system is handled by the rotation at the top of the column.

$$\Delta_{FDD} = \text{Drift}_{FDD}\,L_D \quad (7)$$

$$\theta_P = \Delta_{FDD} / H_C \quad (8)$$

$$L_G = \theta_P\,L_{FLARE} \quad (9)$$

Where,

Δ_{FDD} = Displacement at factored demand drift,
Drift $_{FDD}$ = Demand drift multiplied by the safety factor,
L_D = Height of structure considered for drift,
H_C = Height of column,
θ_P = Minimum required plastic hinge rotation for the required demand drift,
L_G = Minimum gap width required, and
L_{FLARE} = Distance from the center of the column to the extreme edge of the flare.

8. CONCLUSIONS

(1) All the specimens showed good displacement ductility but current prediction methods do not estimate gap size well

(2) If there is a chance that the gap will close, shear reinforcement must be added to the beam to handle the additional shear. The reinforcement should be designed based on the analysis of flared column section without gap. In the case of the column shear reinforcement, the size of the flare compensates for the increase in shear demand in the plastic hinge zone. As long as the non-flare portion of the column is not included in any plastic hinge, it should be sufficient.

(3) Longitudinal beam bottom reinforcement yields very earlier. Increase in its force demand should be considered in design. This is caused by the longitudinal bars not being developed to the top of the beam. This can be predicted by strut-and-tie model (Nada et al.). Hinge bars also yielded very early and further investigation is needed.

(4) Minimum gap width can be calculated by the Caltrans, NCHRP and Drift method but required a factor of safety.

9. ACKNOWLEDGEMENT

This research was funded by Caltrans. The authors appreciate Caltrans for this support. The authors are also thankful to staff in the laboratory. The opinions expressed in this report are those of authors and do not necessarily represent the opinions of the sponsor.

10. REFERENCES

(1) Caltrans Seismic Design Criteria, Version 1.1 (July 1999), Caltrans, Sacramento, CA.

(2) Anthony V. Sanchez, Frieder Seible, and M.J. Nigel Priestley (1997), Seismic Performance of Flared Bridge Columns, Report No. SSRP-97/06, University of California, San Diego.

(3) Hisham M. Nada, David H. Sanders, and M. "Saiid" Saiidi (2001), Seismic Performance of RC Bridge Frames with Architectural-flared Columns, University of Nevada Reno.

(4) Nadim I. Wehbe, M. Saiid Saiidi, "User's Manual for RCMC v 1.2", Report No. CCEER-97-4, University of Nevada, Reno.

STRUCTURAL RESPONSE CHARACTERISTICS IN CONSIDERATION OF DIRECTIONAL UNCERTAINTY OF EARTHQUAKE GROUND MOTION

Hideaki Nishida[1] and Shigeki Unjoh[2]

Abstract

This paper presents structural response characteristics in consideration of the directional uncertainty of earthquake ground motion. Bilateral Acceleration Response Spectrum (BARS) for SDOF system was compared with unilateral one (UARS) to evaluate the variation of ARS caused by the directional uncertainty. The results showed that BARS was 1.2-1.3 times larger than UARS which was calculated from the unilateral component for arbitrary direction. Furthermore, the method to estimate BARS that were based on the Square Root of Sum of Squares (SRSS) combination rule and Percentage combination rule was proposed. It was found that proposed methods estimated BARS well.

Introduction

Earthquake ground motion is consisted of three orthogonal components, i.e., two horizontal components and vertical component, the structure responds in three-dimensional behavior. However, the structure is generally designed so that the seismic loads are applied independently for the principal axes of the structure (for example, bridge axis and perpendicular bridge axis). Moreover, the impact of the input direction of ground motion cannot be known without carrying out trial and error analyses. Therefore, the structure might not satisfy the strength demand due to underestimation of the structural response even if the analytical model could simulate the structural response perfectly.

Several seismic design specifications prescribe the combination method to take this effect into consideration. ISO 3010[1)] prescribes that the total design seismic action E is obtained from seismic actions E_x and E_y for two orthogonal horizontal components of the structure as follow;

$$E = \sqrt{E_x^2 + 2\varepsilon E_x E_y + E_y^2} \tag{1}$$

where, ε: coefficient (from -1 to1, empirically taken as 0 to 0.3)

If ε=0 at Eq.(1), this corresponds to the Square Root of Sum of Squares (SRSS) combination rule method.

As the first order approximation of Eq.(1), Eq.(2a) and Eq.(2b) are obtained as;

$$E = E_x + \alpha E_y \tag{2a}$$

$$E = \alpha E_x + E_y \tag{2b}$$

---

[1] Researcher, Earthquake Engineering Research Team, Public Works Research Institute
[2] Team Leader, ditto

where, α: rate of premium (taken as 0.3 to 0.5)

This combination rule, generally called "Percentage combination rule", is specified in many specifications, though rate of premium α are different. For example, α is prescribed as 0.3 (30%) in AASHTO Standard Specifications[2] and Caltrans Seismic Design Criteria[3], 0.4 (40%) in ATC-32[4]. Eurocode 8[5] is also applied for either formula (α is taken as 0.3 for Eq.(2a), (2b)) including the vertical component which is usually not considered in many specifications.

Wilson et al. [6] recommended the SRSS combination rule because it could be easily obtained by multiplying an additional factor which gave greater result than the input spectra for arbitrary direction and it gave conservative results though the percentage combination rule didn't cause major errors.

Menun and Kiureghian [7] proposed the extension method of the CQC combination rule (called "CQC3" in Refernce 7)), which is commonly used to combine the modal responses resulting from the arbitral directional component of ground motion. They indicated that the CQC3 method should be adopted as a general rule because this method covered the current methods as one of the special cases and it can be easily calculated.

However, it is not clear which combination rule is appropriate to obtain the total response of the structure. The purpose of this study is to propose the method to estimate the maximum acceleration response of elastic structure in the horizontal plane based on the statistical analysis.

Definition of UARS and BARS

To focus on the effect of directional uncertainty of ground motion, the structure is simply modeled as SDOF system that has the isotropic elastic stiffness in the horizontal plane as a column with circular cross section. Natural periods are assumed as 0.1-5.0 second with every 0.1 second and damping ratio is assumed as 5%.

The acceleration waveforms of ground motion for arbitrary direction are calculated by two orthogonal horizontal components of earthquake ground motion records as shown in Figure1. They are obtained by rotating original waveforms every 15 degrees between 0 and 180 degree for coordinate axis (so, 12 waveforms are given by each original earthquake record) and unilateral acceleration response spectrum (UARS) are calculated for these waveforms.

It is assumed that the acceleration responses for two orthogonal components be independent in the elastic response because the effect of bilateral bending on the structural response is generally small. Hence, the bilateral acceleration response spectrum (BARS) is defined as maximum magnitude of vector sum of orthogonal unilateral acceleration responses as Eq.(3);

$$BARS(T) = max\sqrt{\left(UARS_x(T)\big|_t\right)^2 + \left(UARS_y(T)\big|_t\right)^2} \qquad (3)$$

where

T : Natural period of SDOF system (second)

$UARS|_t$: Unilateral acceleration response at time t

x,y : Coordinate axes

Accurate maximum value of SDOF system can be obtained for this equation directly, even if the direction at BARS is different from coordinate axes of the input ground motion.

Following 5 large earthquake ground motion records are used for this analysis; JMA Kobe, JR Takatori Station[8] and Higashi Kobe Bridge records during 1995 Hyogo-ken Nanbu Earthquake, JMA Kushiro record during 1993 Off Kushiro Earthquake and Sylmar record during 1994 Northridge Earthquake.

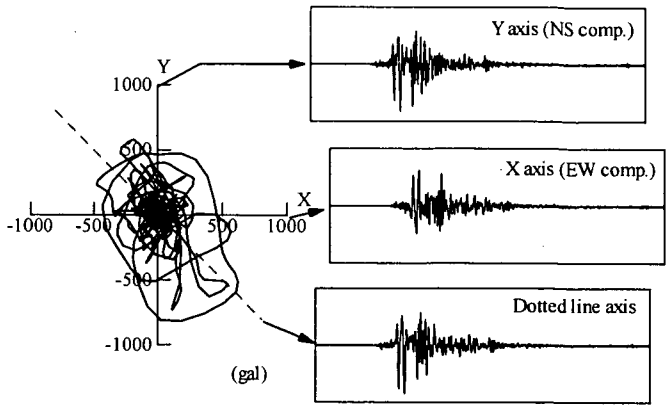


Fig. 1 Acceleration waveform for each principal axis (JMA Kobe at 1995 Hyogo-ken Nanbu earthquake)

Methodology of BARS estimation

Only one component waveform or the seismic load is commonly used for the structural design, it is necessary to estimate the value corresponding to BARS without using two orthogonal horizontal components of waveforms.

In this study, 2 cases are assumed; UARS is given only for arbitrary directional component (Case1), and is given for two orthogonal horizontal components (Case2).

In Case1, estimated BARS (EBARS1) is assumed using UARS with coefficient β as,

$$EBARS1(T) = \beta \cdot UARS(T) \tag{4}$$

In Case2, 2 methods referred to current estimation methods are assumed.

a) SRSS combination method

$$SRSS(T) = \sqrt{(UARS_1(T))^2 + (UARS_2(T))^2} \tag{5}$$

where, 1,2 (subindex): axis1 and axis2 (orthogonal axes)

b) Percentage combination method (PARS)

$$PARS1(T) = UARS_1(T) + \alpha \cdot UARS_2(T) \tag{6a}$$

$$PARS2(T) = \alpha \cdot UARS_1(T) + UARS_2(T) \tag{6b}$$

Where, rate of premium α is assumed as 0.3. PARS is defined as the maximum value of these equations for each natural period of SDOF system.

$$PARS(T) = \max(PARS1(T), PARS2(T)) \tag{6c}$$

Spectral ratio (SR), which is defined as Eq.(7), is used to remove bias caused by the difference of absolute value.

$$SR = EBARS(T)/BARS(T) \tag{7}$$

where, *EBARS*: estimated BARS by EBARS1(=UARS) or SRSS or PARS

Statistical analyses for the spectral ratios are carried out to evaluate the accuracy of estimated values for above 3 methods.

Assuming that the variation of EBARS and BARS depends on the normal distribution, the variation of SR depends on the lognormal distribution. The logarithmic mean λ and the logarithmic standard deviation ζ are obtained at each natural period for each case. Coefficient of variation (CV) is useful to evaluate the variation of the estimation methods. Hence, CV can be derived from Eq.(9) on the basis of the relation between the normal distribution parameters and the lognormal distribution parameters as Eq.(8a) and Eq.(8b),

$$\mu = \exp\left(\lambda + \zeta^2/2\right) \tag{8a}$$

$$\sigma = \mu\sqrt{\exp\left(\zeta^2\right)-1} \tag{8b}$$

$$CV = \sigma/\mu \tag{9}$$

where

μ : mean of the normal distribution

σ : standard deviation of the normal distribution

Based on the results of the statistical analysis, modification coefficients for 3 methods are proposed to obtain the maximum structural acceleration response value of elastic SDOF system.

Principal axis analysis of earthquake ground motion

To examine the relationship between the predominant shaking direction of ground motion and the maximum structural response direction, the eigen value analysis for ground motion by Penzien and Watabe technique[9] is carried out.

Eigen value is found by Eq.(10) for the matrix defined as Eq.(11).

$$E\boldsymbol{a} = \gamma^2\boldsymbol{a} \tag{10}$$

$$E = \sum_{i=1}^{n}\begin{bmatrix} x_i x_i & x_i y_i \\ y_i x_i & y_i y_i \end{bmatrix} \tag{11}$$

where,

γ : eigen value

$\boldsymbol{a}$: eigen vector

x_i, y_i: acceleration at i-th data for x component and y component

n : number of data for ground motion record

The eigen value and the eigen vector are obtained for 2 pairs, (γ_1, $\boldsymbol{a}_1$) and (γ_2, $\boldsymbol{a}_2$), where γ_1 is larger than γ_2. Therefore, strong axis is given by $\gamma_1 \times \boldsymbol{a}_1$ and weak axis is given by $\gamma_2 \times \boldsymbol{a}_2$.

Comparison between BARS and UARS

Figure 2 shows the comparison between BARS and UARS. The maximum response direction for each natural period and the principal axis of the earthquake ground motion are also shown in these figures. The values of UARS at the same natural period are varied widely by the input direction of the earthquake ground motion, especially in the vicinity of peak natural period of BARS. For example, the maximum UARS at the natural period of 0.8 second obtained from JMA Kobe record is about 3 times larger than the minimum one.

It is often that the correlation between maximum response directions and principal axis of earthquake ground motions is not good, especially long natural period range and Sylmar record case. This result means that BARS is unable to be estimated by only one UARS for arbitrary directional component.

Comparison between BARS and combination methods (SRSS, PARS)

Figure 3 shows the comparison between BARS and SRSS or PARS. SRSS and PARS, which are calculated from 6 orthogonal UARS pairs, are also shown in these figures.

Spectral shapes of SRSS or PARS are similar to those of BARS for all natural period range of SDOF system. Spectral variations of SRSS or PARS for 6 UARS combination pairs are smaller than that of UARS cases. Moreover, the absolute response values of SRSS or PARS are nearly equal to those of BARS in long natural period range. These results indicate that BARS can be estimated well using SRSS or PARS.

Statistic analysis of spectral ratios

Figure 4 shows the spectral ratios to BARS of UARS (UARS/BARS) or SRSS (SRSS/BARS) or PARS (PARS/BARS) for each record. Figure 5 shows the logarithmic mean λ and the logarithmic standard deviation ζ of spectral ratios.

Variation of UARS/BARS is large in comparison with the other types of spectral ratios. The margin of fluctuation of λ of UARS/BARS is from -0.4 to -0.1 and that of ζ is from 0.1 to 0.5 for each earthquake ground motion record. In SRSS/BARS and PARS/BARS, these values are from 0.0 to 0.3 for λ and from 0 to 0.1 for ζ.

The most characteristic thing is that the margin of fluctuation of ζ of UARS/BARS is obviously larger than that of SRSS/BARS and PARS/BARS. Moreover, ζs of SRSS/BARS and PARS/BARS are stable for all natural period range independently of the difference of earthquake ground motion records. The variation of λ and ζ caused by the difference of records are generally small except for the JMA Kobe record case. In this case, λ becomes small in proportion as natural period of the system becomes long.

λ and CV calculated for all records are shown in Figure 6. λ of SRSS/BARS and PARS/BARS are stable and the values are about 0.1 for all natural periods. This trend is also found UARS/BARS case (λ is approximately -0.3). CVs of SRSS/BARS and PARS/BARS are also stable and small (approximately 5-8%). On the contrary, CV of UARS/BARS tends to become large as natural period becomes long (approximately 15-40%).

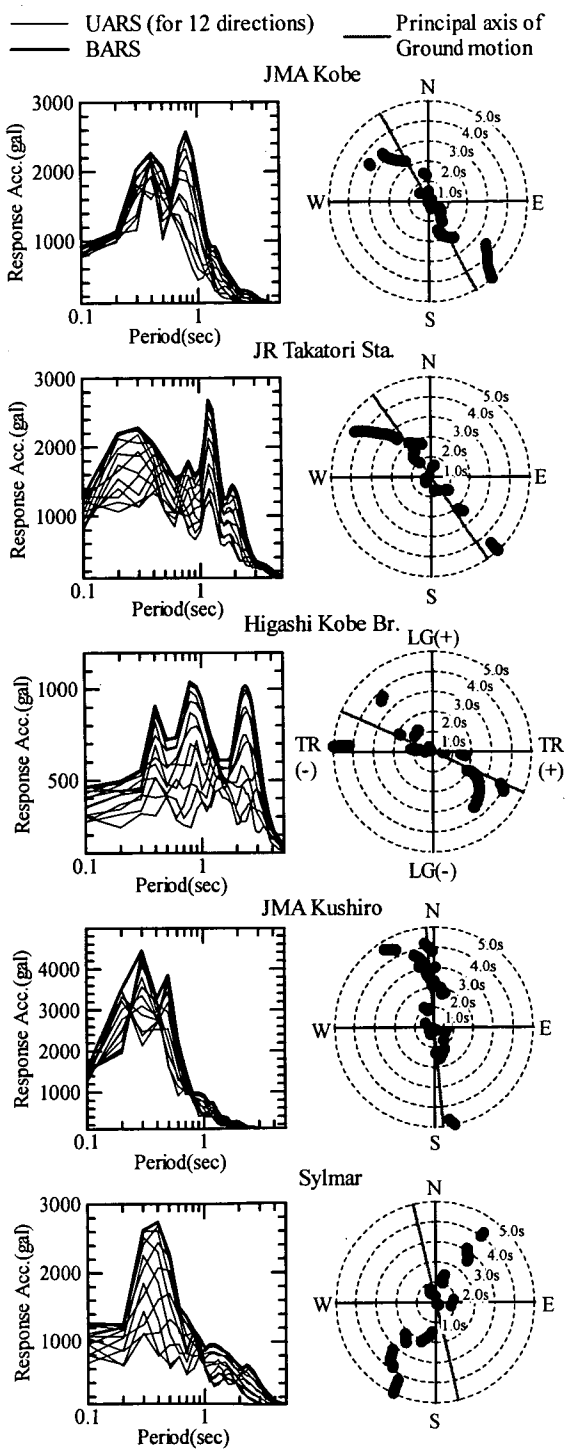


Fig. 2 Comparison between BARS and UARS (Left) & Maximum response direction of BARS (Right)

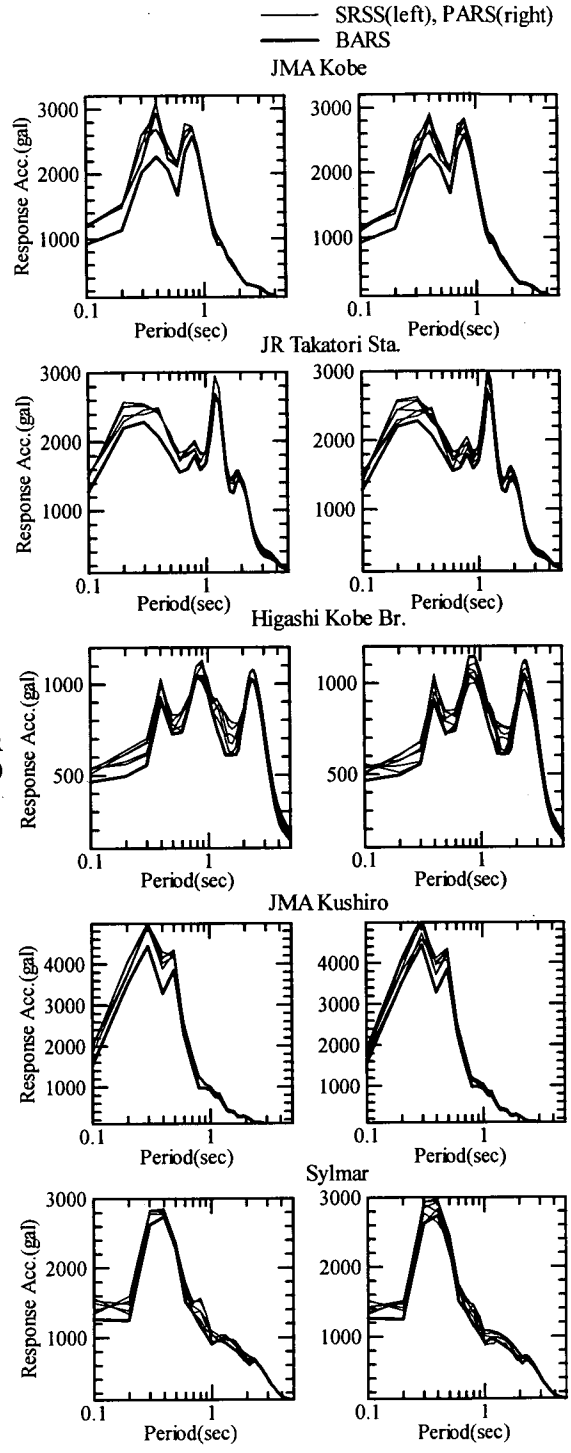


Fig. 3 Comparison of response spectra (Left: BARS and SRSS Right: BARS and PARS)

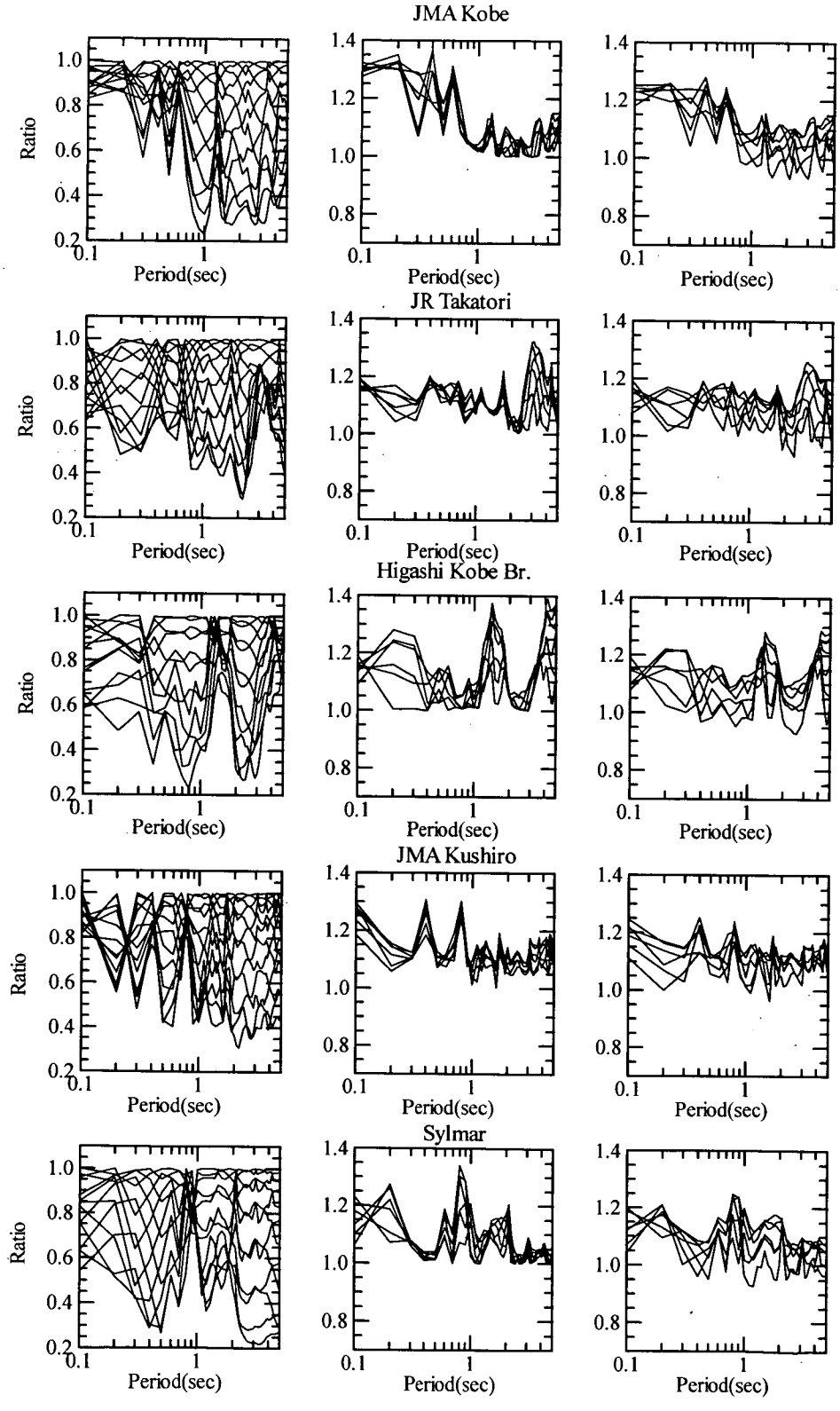


Fig. 4 Comparison of spectral ratios
(Left: UARS/BARS Center: SRSS/BARS Right: PARS /BARS)

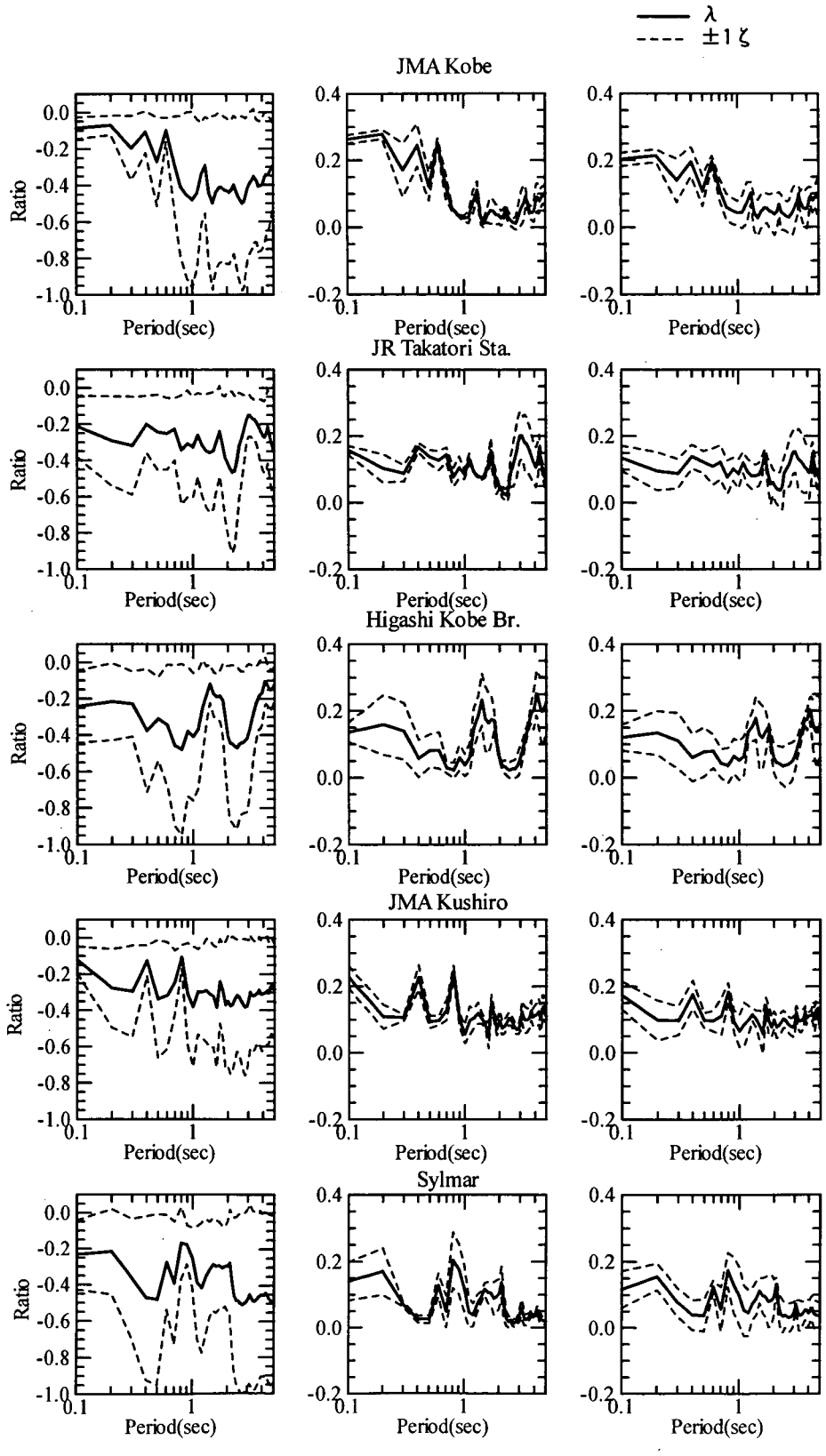


Fig. 5 Logarithmic average and standard deviation of spectral ratios
(Left: UARS/BARS Center: SRSS/BARS Right: PARS /BARS)

These results show that BARS can be estimated well based on the 3 methods though the accuracy of estimated values are different for the estimation methods.

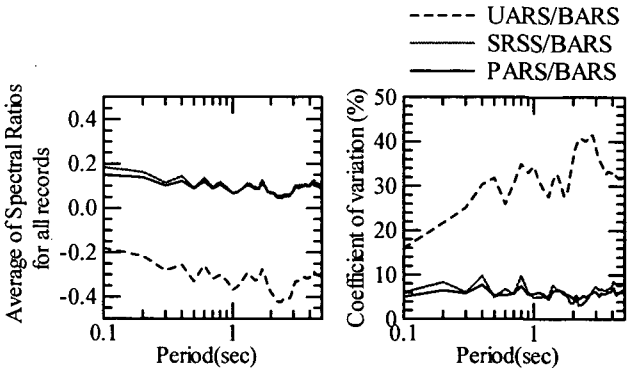


Fig. 6 Comparison of spectral ratios for 5 records (Left: Average Right :Coefficient of variation)

Modification of estimation methods

Since the logarithmic mean λ is stable for all natural periods, modification coefficient is proposed as fixed value for each method. Then, modification coefficient is given based on λ as follows; 0.75 for EBARS1 (λ=-0.3), 1.10 for SRSS and PARS (λ=0.1).

To compare EBARSs by the difference of the estimation methods simply, it is assumed that UARS for arbitrary direction is equal to that for perpendicular direction at natural period *T*. The estimation results are;

$$EBARS(T)\big|_{EBARS1} = \frac{UARS(T)}{0.75} = 1.33UARS(T) \qquad \text{(EBARS1)} \qquad (12)$$

$$EBARS(T)\big|_{SRSS} = \frac{\sqrt{2}UARS(T)}{1.10} = 1.29UARS(T) \qquad \text{(SRSS)} \qquad (13)$$

$$EBARS(T)\big|_{PARS} = \frac{1.3UARS(T)}{1.10} = 1.18UARS(T) \qquad \text{(PARS)} \qquad (14)$$

EBARS for each method is 1.2-1.3 times larger than UARS. However, accuracy of estimated values are different by the estimation methods that mentioned above, the reliability of estimated EBARSs by using two orthogonal unilateral acceleration responses (SRSS, PARS) is higher than that by using one unilateral acceleration response (EBARS1).

Conclusions

Due to directional uncertainty of ground motion, acceleration response for arbitrary direction is not always maximum one in the horizontal plane. To estimate maximum acceleration response in the horizontal plane, bilateral acceleration response spectrum for SDOF system (BARS) is calculated and the estimation methods are proposed based on statistical analysis.

The results of this study are concluded as;

(1) BARS can be estimated well by proposed 3 estimation methods; EBARS1 method,

Square Root of Sum of Squares (SRSS) rule method and Percentage rule method (PARS).

(2) Estimated values of BARS for each method (EBARS) are 1.2-1.3 times larger than UARS. However, accuracy of estimated values are different for the estimation methods, the reliability of estimated EBARSs by using two orthogonal unilateral acceleration responses (SRSS, PARS) is higher than that by using one unilateral acceleration response (EBARS1).

References

1) ISO/CD 3010[1999], "Bases for design of structures – seismic actions on structure"
2) AASHTO [1996], Standard Specifications for Highway Bridges, 16th Edition
3) Caltrans [1999], Seismic Design Criteria Version 1.1
4) ATC-32 [1996], Improved Seismic Design Criteria for California Bridges: Provisional Recommendations.
5) European Committee for Standardization (CEN) [1996], Eurocode8
6) E.L. Wilson, I. Suharwardy and A.Harbibullah [1995], "Clarification of the Orthogonal Effects in a Three-Dimensional Seismic Analysis", pp.659-666, Earthquake Spectra, Vol.11, No.4.
7) C. Menun and A. D. Kiureghian [1998], "A Replacement for the 30%, 40%, and SRSS Rules or Multicomponent Seismic Analysis", pp.153-163, Earthquake Spectra, Vol.14, No.1.
8) Y. Nakamura [1995], "Waveform and its Analysis of the 1995 Hyogo-Ken-Nanbu Earthquake", JR Earthquake Information No.23c, RTRI
9) Penzien, J. and M. Watabe [1975], " Characteristics of 3-dimentional earthquake ground motion, pp.365-374, Earthquake Engineering and Structural Dynamics, Vol.3

19th US-Japan Bridge Engineering Workshop

Seismic 2

co-Chairs:
H. Kanaji & R. Land

The Effect of Abutments as Displacement Limiting Measure on Seismic Performance of Bridges
T. Mikami

Blue Ribbon Panel Recommendations for Bridge and Tunnel Security
J. D. Cooper

Ultimate Shear Strength of Pile Caps
M. Shirato

A Sloping Surface Roller Bearing and its lateral Stiffness Measurement
G. C. Lee

Design and Construction Highway Piers with Interlocking Hoops in Japan
K. Osada

THE EFFECT OF ABUTMENTS AS DISPLACEMENT LIMITING MEASURE ON SEISMIC PERFORMANCE OF BRIDGES

Taku MIKAMI[1], Shigeki UNJOH[2], Masuo KONDOH[3]

ABSTRACT

The objective of this research is to make the structure of the girder end of bridges more rational and to adopt the high seismic performance bridges. With numerical simulation of inelastic seismic response considering the collision between bridge girder and abutment, the effect of abutments as displacement limiting measure on seismic performance of bridges are presented.

INTRODUCTION

In the recent seismic design of highway bridges, the girder end often incorporate sufficient laying gap to prevent the girder and abutment or neighboring girders from colliding with each other during a major earthquake. Many aspects of the mechanism that the dynamic behavior of collision between the girder end and the abutment have not been completely understood yet. In reality, as a bridge using rubber bearings generally has relatively large displacement at the bearing during intensive earthquake, the large enough laying gap at the girder is necessary to avoid a collision. In these cases, although the expansion joints with large displacement stroke are required, the expansion joint with large displacement stroke is not effective because of the economical reasons.

Where a major earthquake occurs, the relative displacement at the girder end becomes large and the collision between the girder end and the abutment or neighboring girder may be occurred. In the past earthquakes, there were cases that the collision between the neighboring girders increased the displacement of one girder and caused the deformation and damage of the girder end and the parapet wall of abutment. Conversely, it was surmised from the damage experiences that absorbing the energy and limiting the girder displacement by the collision between the girder and the abutment or neighboring girders reduced the damage of other structural members such as bridge columns.

From the results of author's analysis, when the collision between girder and abutment having appropriate stiffness occurred, it was found that earthquake response of bridges could be reduced [Unjoh 2002]. It is important to understand the effect of the collision between girder and abutment during the major earthquake on seismic performance of bridges, and to make the structure of the girder end of bridges more

[1] Researcher, Earthquake Engineering Research Team, Public Works Research Institute
[2] Leader, Earthquake Engineering Research Team, Public Works Research Institute
[3] Senior Researcher, Ground Vibration Research Team, Public Works Research Institute

rational and to adopt the high seismic performance bridges.

This paper presents earthquake response characteristics considering the collision between girder and abutment during the major earthquake. The earthquake response characteristics for highway bridge with abutments at each end of the bridge are analyzed. The effect of abutments as a displacement limiting measure on seismic performance of bridges is examined to study the possibility to increase the seismic performance.

EARTHQUAKE RESPONSE ANALYSIS

Analytical Model of Bridge

In this study, this frame model shown in Figure 1 is employed as analytical model of inelastic response analysis considering the collision phenomenon. The superstructure is modeled as two-dimensional beam and the piers and abutments are modeled as frame member supported by ground spring. Plastic hinge spring is assumed at the base of piers. The bearings are rubber bearings modeled as a linear spring. The model of abutment is

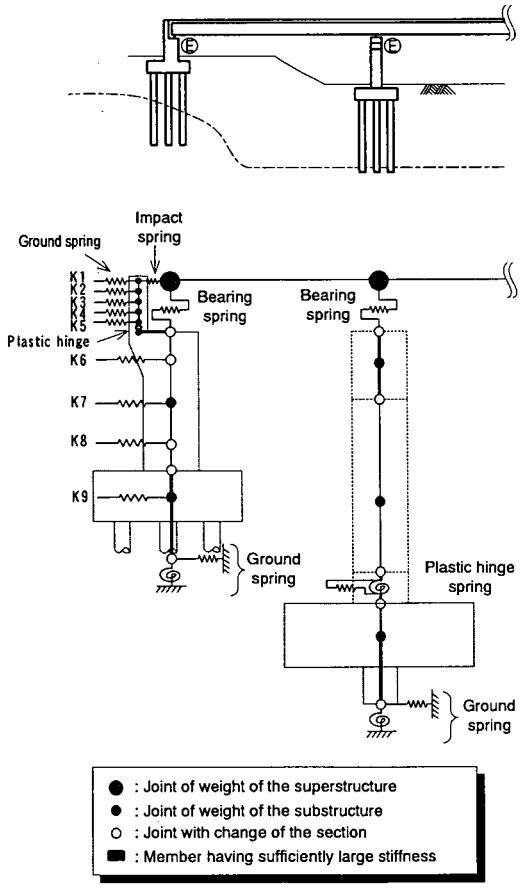


Figure 1. Analytical Model considering the Collision between Girder and Abutment

beam member considering inelastic response characteristics, and foundation is modeled as a linear spring. The backfill soil is modeled as discrete inelastic springs.

Analytical Model of Impact Spring

The collision phenomenon between the bridge girder end and the parapet wall of abutment is modeled as an impact spring with inelastic hysteretic characteristics. When the superstructure moves across the laying gap and approaches the parapet wall of abutment during an earthquake, it is assumed that the reaction force is developed at the impact spring with stiffness K.

As the collision phenomenon is the impact phenomenon in a very shot time, it is important that the impact spring constant, integral time step and damping factor are set to appropriately reproduce the behavior of bridges during a major earthquake in inelastic analysis. In this paper, the impact spring constant K is employed by equation (1) [Kawashima 1999].

$$K = \gamma EA/L \tag{1}$$

Where;

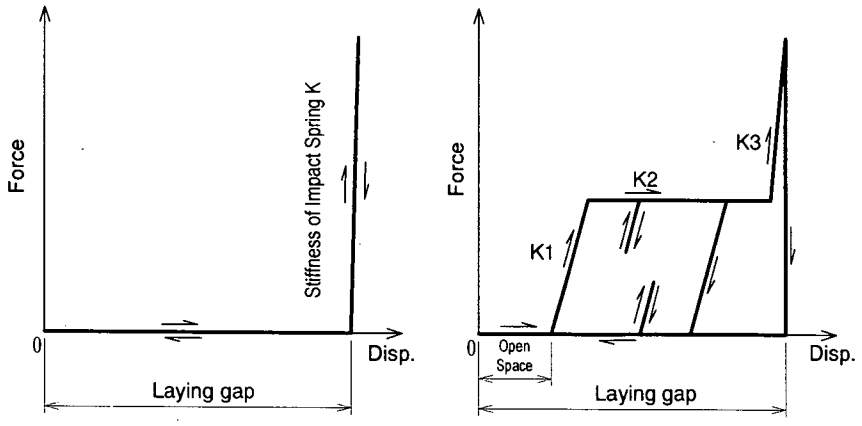
EA : Stiffness of Axial Cross Section of Superstructure

L : Length of the Member of Superstructure

γ : Ratio of Impact Spring Stiffness to Stiffness of Superstructure

In this analysis, the γ value is assumed as 20 from the study to check the relationship between the spring constant of impact spring and the integral time distance [Unjoh 2003].

Figure 2 shows the analytical models of the impact spring. These models are assumed for the case of free end (Figure 2(a)) and the case with shock absorbing device (Figure 2(b)).



(a) Free End

(b) Yielding Type (with shock absorbing device)

Figure 2. Model of Impact Spring

Numerical Analysis

Three earthquake waves for class II ground in the Level 2 (type II) standard acceleration waves are used as an input earthquake motion. Reyleigh type of damping matrix is assumed as damping factor considering the first mode (h=3.7%) as the horizontal behavior of the superstructure and the second mode (h=12.2%) as the behavior of the pier. The integral time step is 1/1000 second for stability of numerical analysis.

BRIDGE ANALYZED AND ANALYTICAL PARAMETER

Bridges Analyzed

The bridge analyzed is 5 span continuous bridge with rubber bearings to distribute the lateral force during an earthquake shown in Figure 3 [Road Association of Japan 1997]. It is assumed that the collision at the girder end occurs between the girder and right-and-left both abutments. The design parameters of the bridge analyzed are shown in Table 1.

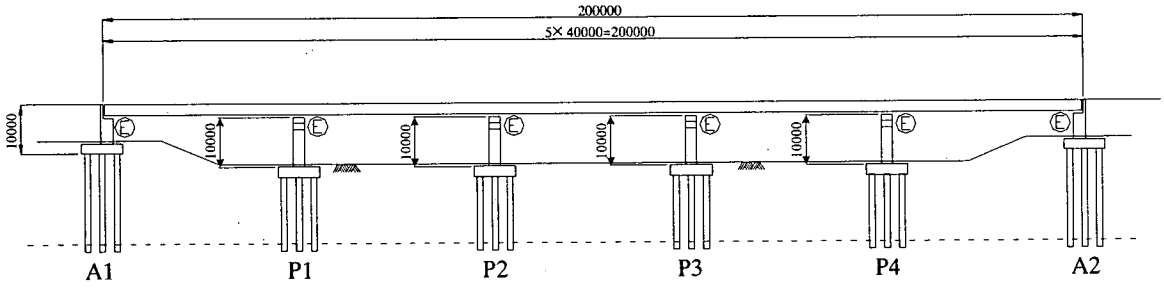


Figure 3. Analytical model of Bridges

Table 1 Design Parameters of Bridge Analyzed

Superstructure styles	5 span continuous steel plate girder bridge
Bridge length and span	200m (5@40m)
Abutment styles	Cantilever
Pier styles and Height	Single column pier, Height = 10m
Foundation styles	Piled foundation
Bearing styles	Rubber bearing
Ground types	Class II

Analytical Parameter (Ground Spring Model of Backfill)

The relation between bearing capacity and deformation of backfill soil shown in Figure 1 is modeled as a spring model yielding in compression side and no resistance in tension side (Figure 4). The accurate behavior of backfill in case of with the collision at the girder end since the experimental and analytical study is inadequate. In this study, the ground spring of backfill is assumed as 3 kind of model, as follows. Table 2 shows the stiffness and upper limit for bearing capacity of backfill soil.

a) No considering (Case 1)
b) Stiffness and upper limit for bearing capacity based on the study for the caisson foundations (Case 2) [Road Association of Japan 2002b]
c) Upper limit based on the passive earth pressure (Case 3) [Road Association of Japan 2002a]
d) Stiffness and upper limit based on the design code of Caltrans (Case 4) [Caltrans 1992]

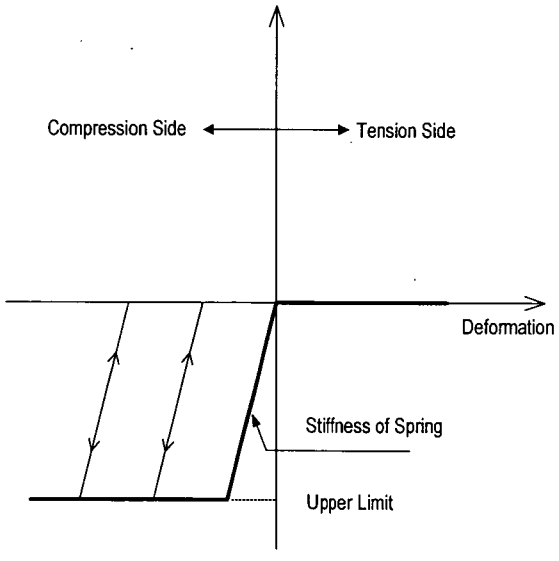


Figure 4 Spring Model of Backfill

Table 2 Spring Constant and Upper Limit for Bearing Capacity of Backfill Soil

Number	The name of model		K1	K2	K3	K4	K5	K6	K7	K8	K9
Case 2	Based on the caisson foundation	spring constant	110871	73914	73914	73914	110871	246873	246873	246873	295656
		upper limit	569	776	1190	1620	3101	11154	17057	23591	37695
Case 3	Based on the caisson foundation and the passive earth pressure	spring constant	110871	73914	73914	73914	110871	246873	246873	246873	295656
		upper limit	427	582	894	1212	2328	8369	12788	17676	28235
Case 4	Suggested by Caltrans	spring constant	0	0	1692000	0	0	0	2820000	0	1128000
		upper limit	–	–	3567	–	–	–	25526	–	18842

Analytical Parameter (Model of Abutment)

When the collision between the girder and the abutment occurs, the parapet wall of abutment may be damaged. The damage of the parapet wall causes the increase of the displacement of the superstructure and the extent of damage at the pier. Even if the collision between the girder and the abutment occurs, it might be desirable not to receive damage for the parapet wall of abutment. Therefore, the parapet wall of abutment is modeled as 2 types;

a) Thickness of the parapet wall of 0.5m
   The parapet wall of abutment is modeled as inelastic member and has the plastic hinge at the base.
b) The thickness of parapet wall of 2.0m
   The parapet wall is modeled as an elastic member.

NUMERICAL RESULTS OF INELASTIC RESPONSE ANALYSIS

Effect of Model for the Parapet Wall of Abutment

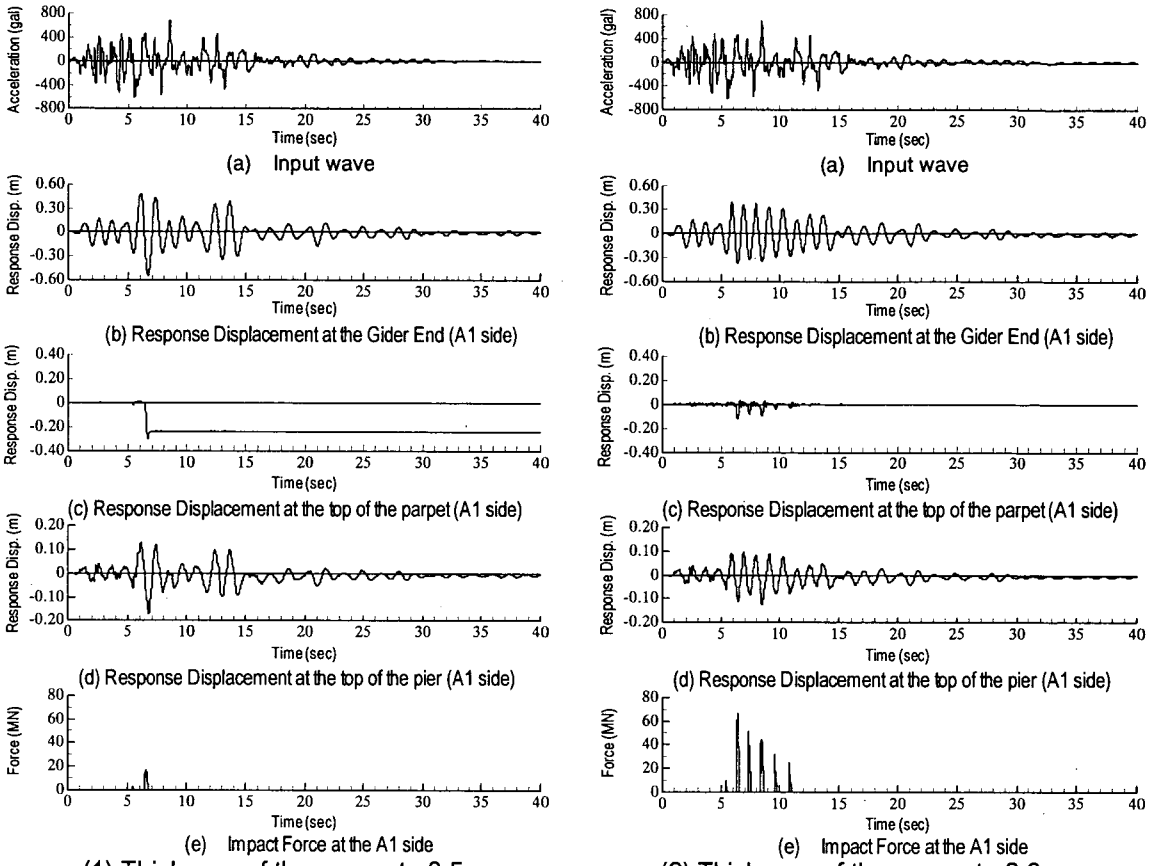
Figure 5 shows the effect of the model for the parapet wall of abutment on earthquake response considering the collision between the girder end and abutment. In these figures, the laying gap is assumed as 25cm, the ground spring model for backfill is the model based on the caisson foundation and the thickness of the parapet wall is 0.5m (in the left figures) and 2.0m (in the right figures).

In Figure 5(1), the parapet of the abutment behaves in a plastic range by the collision between the girder end and abutment at the time of around 6 second, and residual displacement of the parapet is developed. By the plastic deformation of the parapet, the displacement of girder end becomes peak at around 7 second. The behavior at the top of the pier is almost the same as the behavior at the girder end. In Figure 5(2), the parapet of the abutment behaves elastically. The impact force is less than 1/4 force for the case of plastic parapet compared to elastic parapet. However, the response displacement at the top of the pier with the elastic (strong) parapet is significantly reduced than that one with the plastic (weak) parapet.

Effect of the Ground Spring Model for the Backfill

Figure 6 shows the effect of the ground spring model for the backfill on earthquake response considering the collision between the girder end and abutment. In these figures, the laying gap is assumed as 25cm, the parapet model with the thickness of 0.5m is assumed.

From Figure 6, plastic hinge rotation at the base of pier changes somewhat with the ground spring model for the backfill to be used. However, even if which model is assumed, the analysis results is hardly different.



(1) Thickness of the parapet : 0.5m (2) Thickness of the parapet : 2.0m

Figure 5 Effect of Parapet Model on Earthquake Response

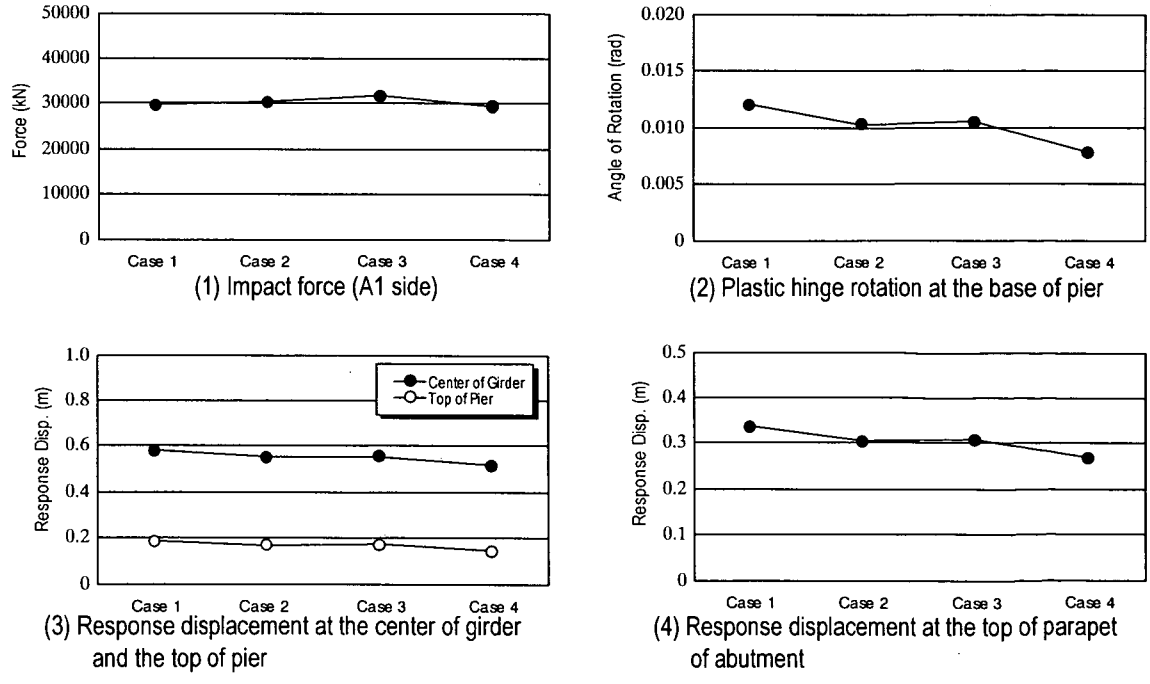


Figure 6 Effect of Ground Spring Model for Backfill on Earthquake Response

CONCLUSIONS

The followings are the major findings on the effect of abutments as displacement limiting measure on seismic performance of bridges;

1. The response displacement at the top of the parapet of abutment and the pier is limited by the collision between the girder end and the parapet wall of abutment.
2. The effect of the ground spring model for backfill on the response of bridges is not significant for the analyzed bridge model.

Reference

Caltrans (1992): "Seismic Design References," California Department of Transportation, Sacramento, Calif., 1992.

Kawashima, K. and Shoji, G. (1991): "Effectiveness of Rubber Type Restrainer to Mitigate Pounding Effect between Adjacent Decks during an Strong Earthquake", *Journals of the Japan Society of Civil Engineers*, No.612/I-46, pp.129-142, 1991.1. (in Japanese)

Road Association of Japan (1997): "Literature for Seismic Design of Highway Bridges," 1997.3. (in Japanese)

Road Association of Japan (2002a): "Design Specifications of Highway Bridges, Part V. Seismic Design," 2002.3. (in Japanese)

Road Association of Japan (2002b): "Design Specifications of Highway Bridges, Part IV. Substructures," 2002.3. (in Japanese)

Unjoh, S., Kondoh, M. and Mikami, T. (2002): "Earthquake Response Characteristics considering the Collision between Bridge Girder and Abutment," *Civil Engineering Journal*, Vol.44, No.2, Public Works Research Center, pp.20-25, 2002.2. (in Japanese)

Unjoh, S., Kondoh, M. and Mikami, T. (2003): "Collision Analysis between Bridge Deck and Abutments during Earthquakes," *Civil Engineering Journal*, Vol.45, No.4, Public Works Research Center, pp.64-69, 2003.4. (in Japanese)

BLUE RIBBON PANEL RECOMMENDATIONS FOR BRIDGE AND TUNNEL SECURITY

James D. Cooper[1], Michael C. Smith[2], and Steven L. Ernst[3]

Abstract

The September 11, 2001 attacks on the World Trade Center and the Pentagon issued in a new era of challenges for infrastructure owners and bridge and highway engineers not only in the United States, but also around the world. Although the September 11th attacks targeted buildings, threats against bridges and tunnels and other highway infrastructure in various parts of the U. S. and undoubtedly elsewhere have heightened awareness and concern. Bridge and highway engineers are being asked to assess the vulnerability of structures and to identify means for reducing this vulnerability.

This paper, taken from a report (1) by a special Blue Ribbon Panel (BRP) that was appointed by the Federal Highway Administrator at the request of the American Association of State and Highway Transportation Officials (AASHTO) summarizes their work to develop short and long term strategies for improving the safety and security of the nation's bridges and tunnels, and provide guidance to highway infrastructure owners and operators. A PDF version of the Panel's full report is available on the Federal Highway Administration (FHWA) website at: http://www.fhwa.dot.gov/bridge/security/brpcover.htm

I. Introduction

A Blue Ribbon Panel (BRP) of bridge and tunnel experts from professional practice, academic, federal and state agencies, and toll authorities convened to examine bridge and tunnel security and to develop strategies and practices for deterring, disrupting, and mitigating potential attacks. The BRP, sponsored jointly by the Federal Highway Administration (FHWA) and the American Association of State Highway and Transportation Officials (AASHTO), acknowledges that the nation's bridges and tunnels are vulnerable to terrorist attacks.

The success and safety of the transportation system, combined with the perceived existing number of parallel routes can lead to the conclusion that the transportation system is so robust that it is not susceptible to significant disruption by terrorist attack. In the opinion of the Blue Ribbon Panel members, this conclusion is incorrect. In many parts of the country the transportation system is straining to keep up with the current demands of society and the economy. The actions of terrorists can impose critical damage to some bridges, and, with explosive forces, exert loads, which exceed those for which components are currently being designed. Worse yet, in some cases the loads can be in the opposite direction of the conventional design loads. Among the approximately

[1]P.E., Bridge Technology Consultant, Purcellville, VA.

[2]Ph.D., Senior Scientist/Ass't Vice President, Science Applications International Corporation, Charlottesville, VA.

[3]P.E., Structural Engineer, Federal Highway Administration, Washington, D.C.

600,000 bridges in the United States, preliminary studies indicate that there are approximately 1000 where substantial casualties, economic disruption and other societal ramifications would result from isolated attacks. *The system has vulnerabilities, which must be addressed. This is important enough to be a matter of national security policy for the United States.*

With prospects of losses and related significant replacement and user costs looming in the aftermath of a successful terrorist attack, the U.S. Congress recognized that terrorism presents risks unlike risks typically encountered by those who own and/or operate assets that are important to the nations' well being. Typically, bridge owners manage risks associated with natural hazards using well developed risk assessment methods based on mature occurrence models that allow them to make informed trade-off decisions among mitigation alternatives. Unlike the case of natural hazards, owners are in the dawn of an era in which they feel overwhelmed by uncertainties about the occurrence and potential costs of terrorist attacks and about their legal responsibilities to protect the users of their structures. It is therefore imperative to identify critical transportation infrastructure, particularly bridges and tunnels, and to provide strategic guidance for investing in countermeasures and risk mitigation strategies. In the case of bridges and tunnels of regional or national significance, the federal government is the funding source of last resort for recovery operations and to restore capability in the event of terrorist attacks. Significant investment to prevent or reduce the consequences of such attacks may well be justified as an alternative to the high cost of response and recovery and subsequent socioeconomic damage.

The Blue Ribbon Panel made seven overarching recommendations to accomplish the overall goal of reducing the vulnerability of bridges and tunnels to terrorist attacks that fall into three areas related to institutional, technical, and fiscal responsibilities. The recommendations included the need for interagency coordination including the development of outreach and communication strategies, new funding sources for bridge and tunnel security and technical recommendations.

This paper focuses on the Panel's strategy and recommendations for planning, design and engineering approaches to improve bridge and tunnel security. Included are suggested countermeasure options and operational security practices.

II. Panel Strategy for Developing Bridge and Tunnel Security

Bridge and tunnel security, like security for any infrastructure asset, includes a broad range of issues that must be addressed to ensure that adequate measures are taken to protect the asset and the people and goods that utilize the asset. Table 1 shows the bridge and tunnel security issues considered by the panel organized into topical areas. Several of the topics and related issues are of general interest and apply to all transportation infrastructure; others relate more directly to bridges and tunnels. For example, the "management and operational practices" issues apply to most infrastructure assets (transportation and otherwise), as do "information security," "mobilization and response," and "recovery" issues. However, issues that fall within the "planning, design, and engineering" area may be unique to bridges and tunnels and require special solutions that

go beyond what might be needed to reduce the vulnerability and improve the security of other infrastructure assets.

Table 1. Bridge and Tunnel Security Issues

Key Topics in Infrastructure Security	Specific Issues
Foundations for Policy	• Criteria establishing Investment Priorities
Planning, Design, and Engineering	• Institutional Continuity • Design Review for Secure Structures • Research and Development Needed to Support "Design for Security • Design Criteria • Design Specifications
Management and Operational Practices	•Best Practices •Practice Review • Institutional Relationships • Preparedness • Personnel and Vehicle Security • Communications/Outreach
Information Security	• Procurement Practices • Information Security
Mobilization ("Notice") and Response ("Trans-event")	• Threat Warning • Early Response • Initial Response
Recovery ("Post-event")	• Damage Assessment • Functional Continuity

The panel's special expertise was in the area of bridge and tunnel planning, design, and engineering, the primary focus of recommendations contained in the report addresses near- and long-term design and engineering solutions to bridge and tunnel vulnerabilities.

III. Overarching Panel Recommendations For Planning, Research and Development, and Design and Engineering

Because of its heterogeneity in size and operations and the multitude of owners and operators nationwide, the transportation infrastructure network in the United States is highly resilient, flexible, and responsive (2). Unfortunately, the sector is fractionated and regulated by multiple jurisdictions at state, federal, and sometimes local levels. The size and pervasive nature of the U.S. transportation infrastructure poses significant protection challenges (3). However, these protection challenges can be mitigated through technical collaboration and coordination.

Planning

A planning or review and prioritization process is necessary for prioritizing all bridges and tunnels with respect to their vulnerability in terms of their criticality of the ability to deter, deny, detect, delay, and defend against terrorist attacks. In addition, a risk assessment model must be developed as a framework for evaluating alternatives for thwarting attack. Several agencies have developed methods for identifying and prioritizing critical transportation assets, and these methods share many commonalities. The prioritization procedure outlined in the AASHTO's methodology uses a set of critical asset factors to identify assets that are important to achieving an agency's mission. Next, the AASHTO methodology assesses the vulnerability of these critical assets to terrorist attack based on target attractiveness (potential casualties and symbolic value); accessibility (access controls and physical security); and expected damage (including environmental hazards), (2). The TSA approach determines relative risk as a function of relative target attractiveness (an assessment of the target's importance and consequences); relative likelihood of occurrence (an assessment by TSA Intelligence of the likelihood of occurrence, as compared to the other scenarios); and vulnerability (a measure of how likely the terrorist is to achieve the threatening act given that an attempt is made). Relative risk is re-calculated based upon the implementation of a suite of countermeasures, including the implementation of people, procedures, and/or technology to reduce vulnerability (4).

Because national prioritization of funding will be required, the process of evaluating proposals to enhance bridge and tunnel security must be a joint effort by federal and state agencies and other owners and operators. The large number of bridges (600,000) and tunnels (500) lends itself to a two-tier approach: prioritization and risk assessment. The first tier, prioritization, is typically most efficiently done in two steps. The first step is a data-driven approach, such as that used by the Texas Department of Transportation (TxDOT), for ranking bridges using common criteria (5). The National Bridge Inventory (NBI) provides much of the data needed for this step. In the second step of prioritization, additional data comes from owners and operators familiar with specific characteristics of the facilities and the services they provide. In this first tier ranking, prioritization of bridges and tunnels should be based on characteristics such as the following:

- Potential for mass casualty based on Average Daily Traffic (ADT) and associated peak occupancies
- Criticality to emergency evacuation and response to emergencies
- Military or defense mobilization
- Alternative routes with adequate available capacity
- Potential for extensive media exposure and public reaction; symbolic value (to what extent does the facility represent ideals and values that are important to the American public, also visual symbolism, e.g., "signature bridges")
- Mixed-use bridges and tunnels where highway and rail are co-located
- Potential for collateral damage (land, marine, rail), including collateral property and utilities
- Maximum single span length as it relates to the time required to replace the facility
- Commercial vehicle vs. passenger vehicle mix and volume as a surrogate for

economic impact
- Bridge or tunnel dimensions (as a surrogate for replacement time/cost)
- Significance of revenue streams (e.g., tolls, fares) associated with the facility
- Bridges and tunnels at international border crossings

The second tier is a risk assessment of high priority bridges taken from the first tier (prioritization) to determine vulnerabilities and evaluate countermeasures to deter attack and/or mitigate damages. The risk, **R**, to the facility is determined following an approach similar to that developed for seismic retrofit and can be expressed as follows:

$$\mathbf{R = O \times V \times I}$$

where,

O = Occurrence: In the general form of the risk equation, this factor is hazard oriented and will change with the nature of the hazard. In the context of this report, the occurrence factor approximates the likelihood that terrorists will attack the asset. It includes target attractiveness (from the perspective of the threat), level of security, access to the site, publicity if attacked, and the number of prior threats. Input into this factor typically comes from the law enforcement and intelligence communities familiar with threat and operational security measures.

V = Vulnerability: In the general form of the risk equation, vulnerability is an indication of how much the facility or population would be damaged or destroyed based on the structural response to a particular hazard. In the context of this report, vulnerability is the likely damage resulting from various terrorist threats (weapon type and location). It is a measure of expected damage, outcome of the event, expected casualties, and loss of use, all features of the facility itself. Input into this factor typically comes from engineering analysis and expertise.

I = Importance: Importance is a characteristic of the facility, not the hazard. In principle, importance is the same for any hazard. Importance is an indication of consequences to the region or nation in the event the facility is destroyed or unavailable. Is the facility on an evacuation or military mobilization route; is it likely to be used by first responders to emergencies; what is its historic and associated significance; what is its peak occupancy? Input into this factor typically comes from owners, operators, users, and beneficiaries of the facilities, often governmental sources, and will use factors similar to those used in the first tier prioritization.

This formula properly expresses the interaction among the three factors. Dominant factors magnify risk; negligible factors diminish it. Other formulas, such as models that add the factors, fail to account for their interactive effects. For example, in the absence of a threat ('O' = 0), the risk should be zero as this model provides; additive models would have a residual risk. In the multiplicative model, eliminating anyone factor to zero (or near zero) reduces the risk to near zero (e.g., low importance leads to low risk regardless of other factors).

The countermeasures that reduce the risk associated with an asset may be designed to reduce the occurrence factor (e.g., make the asset less accessible); the vulnerability factor (e.g., harden the facility to reduce damage); or the importance factor (e.g., add redundant facilities to reduce dependence on the asset).

The panel made near-term (3-6 months), mid-term (6-12 months) and long-term (12-18 month) recommendations for state identification and prioritization of bridges and tunnels, followed by a federal re-prioritization for federal funding based on the following:

Near-term (3-6 months):

(1) FHWA determines and promulgates a methodology for reviewing bridges and tunnels with respect to their risk and vulnerability in terms of their ability to detect, deny, delay, and defend against terrorist attacks. Methodologies that may be considered should be developed and include the AASHTO Guide for Highway Vulnerability Assessment, the Texas DOT methodology, and others.

(2) Using methodology promulgated by the FHWA similar to that described above, states should prioritize their bridges and tunnels and submit prioritized lists of their most critical bridges and tunnels to FHWA.

(3) FHWA/AASHTO should oversee the development of an immediate, near-, and mid-term cost-benefit methodology based on probabilistic risk assessment for implementing countermeasures. Within the framework of probabilistic risk assessment of the kind that has been adopted for seismic retrofit programs, consideration should be given to existing methodologies.

Mid-term (6-12 months):

(1) FHWA takes states' priority lists of critical bridges and tunnels and develops a national list of critical bridges and tunnels.

(2) States use the risk assessment methodology to develop a countermeasures plan using a cost-benefit ratio as a metric and provide costs for implementing countermeasures for each of their critical bridges and tunnels to FHWA.

Long-term (12-18 months):

(1) FHWA, in collaboration with DHS/TSA and other agencies, seeks new appropriations from Congress to implement a national bridge and tunnel countermeasure program. FHWA begins allocating funds to the highest priority bridges and tunnels as identified by the states and other owners/operators in accordance with accepted risk assessment methodologies.

(2) Non-state DOT bridge and tunnel owners begin implementing countermeasures consistent with federal security standards using appropriate funding sources, including federal sources where applicable.

(3) FHWA in coordination with AASHTO develops and implements modifications to existing bridge and tunnel inspection programs to evaluate conformance to federal security standards.

(4) States implement countermeasures with funding as available. One source recommends an initial sum of at least $1.5 billion to address near-term security measures (6).

Research and Development

The Panel supported the need for a strong Research and Development program to advance design practice and engineering. Areas in need of R&D are described next. The analysis of current structural components and their behavior to blast loads is recognized by the panel as key to understanding the proper and most efficient ways to mitigate terrorist attacks through structural design and retrofit. Table 2 lists key structural bridge components that the panel considered.

Table 2. Critical Bridge Components

Suspension and Cable Stayed Bridges	Truss Bridges	Arch Bridges	Multi-girder/Freeway Overpass Bridges
• Suspender ropes, stay cables • Tower leg • Main cable • Orthotropic steel deck • Reinforced and pre-stressed bridge decks • Cable saddle • Approach structures • Connections • Anchorage • Piers	• Suspended span hangers • Continuous and cantilever hold-down anchorages • Compression chords or diagonals • Connections • Decks • Piers	• Tension-tie • Connections • Decks • Piers	• Decks • Connections • Piers

The goal of the R&D initiatives recommended by the Panel is to create empirically validated computational tools, design methods, and hardening technologies to assist in "designing for the terrorist attack." The recommendations have one or more short-term and long-term elements and all are directed to the FHWA, AASHTO, and other government-sponsored research organizations, including universities and federal laboratories. Additionally, these five recommendations are interrelated and interdependent and should be pursued simultaneously. They include:

(1) Assess performance of critical elements under credible loads (including load reversals)

Short-term (within the next year):

- Synthesize current state of knowledge for component properties and modeling

Long-term (more than one year):

- Establish the load structure and load interaction

- Start component experiments; recommend large-scale testing using real materials, components, and connections under comparable strain rates
- Conduct comparative parameter studies of typical components and materials

(2) Validate and calibrate computational methods and modeling with experiments to better understand structural behavior from blast loads

Short-term (within the next year):

- Pull together and examine studies and research that have already been conducted on bridge and tunnel elements and components
- Investigate transferability of seismic design

Long-term (more than one year):

- Develop a predictive round robin analysis of actual blast experiments on bridge and tunnel components
- Test critical components, such as suspender ropes, stay cables, concrete and steel decks, side loads on towers, and box sections, for testing and blast performance

(3) Validate and calibrate computational methods and modeling with experiments to better understand structural behavior from thermal loads

Short-term:

- Pull together and examine studies and research that have already been conducted on bridge and tunnel elements and components

Long-term:

- Evaluate various mitigation fire effects in tunnels, double deck bridges, and overpass bridges

(4) Determine the residual functionality of bridge and tunnel systems and their tolerance for extreme damage

Short-term:

- Examine bridges and tunnels compromised in wars and after demolition attempts

Long-term:

- Determine progressive collapse potential of various bridge and tunnel systems

(5) Develop mitigation measures and hardening technologies

Short-term:

- Assess existing hardening technologies and the applicability to bridges and tunnels

Long-term:

- Develop new materials and new design methodologies

In addition to these R&D recommendations, the BRP suggests AASHTO work with university engineering institutions to develop R&D programs for students and bridge professionals to address security concerns. The panel recommends that DHS work jointly with industry and state and local governments to explore and identify potential technology solutions and standards that will support analysis and afford better and more cost-effective protection against terrorism.

Design and Engineering

The acceptability of a threat is the criterion for determining how to design for the threat. Performance level design is based stating assumptions and setting expectations and goals. These factors could include threats, casualties, damage, and recovery. To set a performance level design criteria, the design process must first be described, taking into account the potential threats to the existing or planned bridge or tunnel. The panel recommends that bridge and tunnel owners and operators use the following six-step process:

(1) Use previously determined "R," the risk for each bridge or tunnel, whether existing or planned, determined using the R = OVI model.
    (a) Determine Threats. There are several potential threats that exist. The first and most serious is a precision demolition attack. If carried out, this attack will destroy or seriously damage the bridge or tunnel. Therefore, this threat must be mitigated so that it will not be allowed to happen. Other threats to consider are conventional explosives, collision, and fire.
    (b) Determine the Consequence. Based on the potential threats to the bridge or tunnel, the owner must decide the potential consequences if carried out.
(2) Determine the acceptability of consequences. If the consequences are acceptable, then the owner may decide to do nothing.
(3) If the consequences are unacceptable, then one of two options exists:
    (a) Mitigate the Threat. Generally, these actions can be taken in the short term (3-6 month range). Owners should take measures to lessen the attractiveness or deny access through technology, operational procedures, and physical measures.
    (b) Mitigate the Consequence. These actions fall into the mid- to long-term time frame. Reduce the damage and resulting loss of life, property, functionality, and economic viability through design, engineering, and operational strategies. (This step in the process requires detailed engineering analysis, vulnerability assessments, and statistical analysis of specific facilities and postulated threats to those facilities.)
(4) Estimate the cost of mitigating the threat or consequence.
(5) Recalculate the R=OVI based on the recommended mitigation approach to determine the risk reduction achieved.
    (a) Assets that receive a high R score should be categorized as a "high priority" structure. Steps should be taken to mitigate the largest possible threat in this situation. Designs should be performed so that in the event of this threat there would be no irreparable damage and the structure could return to operable condition in 30 days. Higher probability threats should be designed so that in event of threat there is not loss of service.
    (b) Assets that receive a low R score should be categorized as a "low priority" structure. The criteria for these structures in the event of the largest possible threat is that total loss be acceptable. The destruction of these low priority assets will not be devastating to the region because of alternative routes, size, economic implications, and socio-political messages. Higher probability

threats should be designed so that in the event of threat there is minimal loss of service.

(6) Compare the costs and benefits (risk reduction) of varying mitigation combinations and strategies under designated analysis scenarios. In determining the cost and benefits associated with various mitigation strategies and countermeasures, the analysis should include cost related to increased user cost and potential environmental/energy cost effects if the facility were destroyed or seriously damaged.

As an alternative possibility for acceptability criteria guidance, the bridge owner may consider what sort of time frame it can handle for loss of service. For example, if the time frame is 13 days, then the bridge owner can determine what sort of threat type (from car, boat, etc., or size of explosives) could potentially do this damage, and mitigate for this threat.

The recommendations for design criteria are based on various mitigating strategies. Owners have the choice to mitigate the threat (preventing terrorists facility access), mitigate the consequence effect (lessening the effect from an attack), or apply both options.

The following are examples of approaches to **mitigate threats**:

- Establishing a secure perimeter using physical barriers
- Inspection surveillance, detection and enforcement, closed circuit television (CCTV)
- Visible security presence
- Minimize time on target

The following are examples of approaches to **mitigate consequences**:

- Create Standoff Distance. The first level of mitigating terrorist attacks should be to incorporate sufficient standoff distances from primary structural components. Providing standoff distance is highly recommended. There are three basic approaches to blast resistant design: increasing standoff distances; structural hardening of members; or higher acceptable levels of risk. Often, utilizing a percentage of each strategy is optimal.
- Add Design Redundancy. Structural systems that provide great redundancy among structural components will help limit collapse in the event of severe structural damage from unpredictable terrorist acts.
- Hardening/Strengthening the Elements of the Structure. Structural retrofitting and hardening priority should be assigned to critical elements that are essential to mitigating the extent of collapse. Secondary structural elements should be dealt with to minimize injury and damage.
- Develop an Accelerated Response and Recovery Plan. Alternative routes and evacuation plans should be known and established.

The Panel recommends that the FHWA, in collaboration with AASHTO and TSA, should use the countermeasures development and evaluation methods described in this section to assess countermeasure effectiveness. Typical countermeasures to be considered are

described in the next section. Countermeasures should be ranked and implemented based on a technically sound cost-benefit analysis such as described in the full report.

IV. Countermeasure Options (7)

The countermeasures listed below are available to bridge and tunnel owners and operators for their use in planning and implementing more effective security practices. The list is provided in the interest of sharing information that may prove helpful to individuals and agencies, but the panel does not recommend specific countermeasures or their application to specific facilities.

Planning and coordination measures
Update the emergency operations plan/crisis management plan to include response and recovery to a terrorist threat involving a bridge. Based on the Federal Emergency Management Agency (FEMA) guidelines, the plan should include the following:

- Concept of operations
- Coordinated response, responsibilities, and liaisons among different departments and agencies
- Sequence of events that should occur for an effective response
- List of potential areas of vulnerability
- Procedures for notification and activation of crisis management teams
- Establishment of a mobile command center with essential communications equipment
- Designated radio frequencies for emergency communications
- Procedures for dealing with bomb threats and suspicious objects
- Evacuation and shutdown procedures
- Identification of emergency evacuation routes and staging areas for response teams
- Measures ensuring safety and security after an incident
- Procedures for restoring service and establishing alternate routes
- Removal plan for damaged equipment and structural elements
- Procedures for issuing information and reassuring the public
- Procedures for dealing with victims and notification of relatives
- Regular updates based on events that identify vulnerabilities in the plan
- Communication and coordination with local, state, and federal law enforcement agencies to obtain terrorism intelligence, training, and technical support
- Regular drills, tabletop exercises, no-notice responses, and full-scale simulations aimed at specific objectives to identify problem areas and test response procedures, communication, and coordination
- Plans for rapid debris removal and repairs
- Development of a training plan for maintenance personnel (observant of surroundings and knowing how to deal with suspicious objects)
- Establishment of a security policy

Information control measures

- Review and sanitize websites for potential information that may be beneficial to terrorists. However, removal of data from websites must be balanced with the need for information sharing. For example, information about a specific bridge can be very useful for identifying weaknesses and planning an attack, but general design guidelines and "standard" plans generally provide information that is not directly beneficial to terrorists.
- Establish a common classification system for sensitive information. Implement procedures for the control of sensitive information, including document classification, disposal of sensitive materials, and tracking the distribution of design information to contract tenderers.
- Establish "need-to-know basis" procedures for the release of vulnerabilities, security measures, emergency response plans, or structural details for specific bridges.

Site layout measures

- Improved lighting with emergency backup (combined with elimination of hiding spaces below)
- Clearing overgrown vegetation to improve lines of sight to critical areas
- Creative landscaping with regular maintenance to increase standoff distance to critical areas
- Elimination of access to critical areas (beneath deck, maintenance rooms with access to cables, etc.)
- Elimination of parking spaces beneath bridges
- Providing pass-through gates in concrete median barriers to enable rerouting of traffic and access for emergency vehicles
- Review of locations of trashcans or other storage areas that could be used to conceal an explosive device, ensure they are not near critical areas

Access control/deterrent measures

- Police patrol and surveillance
- Guards
- Enhanced visibility
- Signs issuing warnings that property is secured and being monitored
- Marked vehicles
- Keyless entry systems
- Exterior and interior intrusion detection systems
- Boundary penetration sensors (below bridge)
- Volumetric motion sensors (for towers, maintenance buildings, inside box girders, etc.)
- Point sensors (critical connections)
- CCTV placed where it cannot be easily damaged or avoided while providing coverage of critical areas (to monitor activity, detect suspicious actions, and identify suspects)

- Incorporation of a higher level of identification procedures and credentials for maintenance personnel, security personnel, and external contractors
- Denied/limited access to critical structural elements (i.e., providing fencing around cable anchors, restricting access to box girders and cable towers, etc.)
- Denied/limited access to inspection platforms
- Physical barriers to protect piers
- Physical barriers to control access to the deck during credible threats to a specific bridge (used in conjunction with random vehicle searches)
- Rapid removal of abandoned vehicles
- No fly zones around critical bridges
- Emergency telephones to report incidents or suspicious activity
- Use of an advanced warning system, including warning signs, lights, horns, and pop-up barricades to restrict access after span failure (manually activated or activated by span failure detectors)

Retrofit Options

- Reinforcing welds and bolted connections to ensure that members reach their full plastic capacity (designed for 120% of connected member capacity to account for strength increases during high-rate straining)
- Using energy absorbing bolts to strengthen connections and reduce deformations
- Adding stiffeners and strengthening lateral bracing on steel members to prevent local buckling before they reach their full plastic capacity
- Designing portions of the deck to "blowout" and create a vent to reduce pressures on the support structure (possibly near the abutments where large pressures build up from confinement effects)
- Adding Carbon Fiber Reinforced Polymer (CFRP) hoop wraps on concrete columns, which can be reinforced with longitudinal wraps, to enhance concrete confinement, increase bending resistance and ductility, and add protection against spalling (can also be used on bents and beams)
- Strengthening the lower portions (or full height) of columns against impacts and localized blast damage by encircling them with a steel casing (connected with high strength bolts and epoxy or a layer of grout)
- Adding lateral bracing to columns to allow them to develop plastic hinges while preventing buckling
- Adding 360-degree pier protection for impacts and standoff distance – possible alternatives include concrete barriers, stationary fender systems, dolphins, rotational bumper systems, or elastomeric energy absorbers
- Restraining sections of the bridge with steel cables to reduce the chance of deck collapse at the supports, including cable supports to keep the deck from separating at the joints and hinge restrainers to hold the deck to the columns (can also be accomplished with high-strength threaded rod restrainers and pipe seat extenders)
- Increasing the size of abutment seats and adding hinge seat extensions under expansion joints to reduce the chance of deck collapse at the supports

- Increasing footing size (possibly combined with adding additional pilings in the ground or using steel tie-down rods to better anchor the footings to the ground) to improve resistance to cratering and large column deformations
- Wrapping the lower portions of cables on cable-stayed bridges and suspension bridges with CFRP or other types of protective armor to protect against damage from blast and fragmentation
- Increasing standoff distance and reducing access to critical elements with structural modifications (extending cable guide pipe length, moving guard rails, etc.)
- Including reinforcing steel on top and bottom faces of girders to increase resistance to uplift forces from blasts that are in the opposite direction from those due to gravity and live loads
- Providing system redundancy to ensure alternate load paths exist (through continuity, strengthening of connections, redundancy in cables and girders, etc.) should a critical structural element fail or become heavily damaged as a result of a terrorist attack
- Strengthening the deck on curved steel trapezoidal girder bridges to ensure that sufficient torsional strength is provided should a portion of the deck be compromised

V. Operational Security Practices

This list of Operational Security Practices was developed during the AASHTO/FHWA BRP initial meeting to ensure that the panel considered the full range of security strategies. Following the initial meeting, the panel focused more narrowly on the design and engineering considerations contained in the body of this report.

Management and Operational Practices

- Best Practices. Current and timely exchange of practical information among owners and operators concerning the potential for and counters to terrorist attacks and related matters
- Practice Review. Process for reviewing overall security management practices, including personnel policies, training, procedures, and use of technology
- Institutional Relationships. Clarification and/or establishment of roles and responsibilities among federal, state, and local entities and effective partnerships for preventing, defeating, and responding to terrorists' attacks
- Preparedness. Guidance to owners/ operators regarding preparations for responding to terrorists' attacks, including coordination with other federal, state, and local agencies, communication protocols, and equipment interoperability
- Personnel and Vehicle Security. Guidance to operators for ensuring that employees, contractors, vendors, visitors, and the vehicles they operate are authorized, verified, and authenticated, as appropriate
- Communication/Outreach. Communication strategies for community outreach and coordination of sensitive information (e.g., with other agencies, media, private sector entities)

Information Security

- Procurement Practices. Means for procuring security-sensitive technologies without public disclosure and for soliciting construction bids without disclosing security-sensitive design features
- Information Security. Means for controlling public access to "as built" drawings and related information

Mobilization ("notice") and Response ("trans-event")

- Threat Warning. Means (protocols) for timely notification of owners/operators concerning imminent threats to specific assets
- Early Response. Policies and processes for interdicting identified threats, informing/instructing travelers, and evacuating facilities
- Initial Response. Policies, process, and technologies needed to execute the preparedness plan in response to terrorists' attacks

Recovery (Post-event)

- Damage Assessment. Procedures and technologies that assist in initial assessment of structural damage to the asset to determine the effect of the attack on functionality (e.g., closure, restricted use)
- Functional Continuity. Contingency plans for reestablishing asset functionality (including use of available alternatives, emergency repairs)

VI. Summary

Terrorism against American citizens and assets is real and growing. The number and intensity of domestic and international terrorist events, along with the September 11, 2001, attacks, change the way Americans think and live. Terrorists attack targets where human casualties and economic consequences are likely to be substantial. Transportation and related assets are attractive terrorist targets because of their accessibility and potential impact on human lives and economic activity. There is no question that terrorists are interested in bridges and tunnels as attractive targets of opportunity to disrupt societal function.

A Blue Ribbon Panel (BRP) of bridge and tunnel experts from professional practice, academia, federal and state agencies, and toll authorities convened to examine bridge and tunnel security and to develop strategies and practices for deterring, disrupting, and mitigating potential attacks. The BRP, sponsored jointly by the Federal Highway Administration and the American Association of State Highway and Transportation Officials acknowledges that the nation's bridges and tunnels are vulnerable to terrorist attacks. The intent of this paper was to summarize BRP recommended policies and actions to reduce the probability of catastrophic structural damage that could result in substantial human casualties, economic losses, and socio-political damage.

Appendix

Blue Ribbon Panel Members

- Mr. James E. Roberts, BRP Chair, Consulting Bridge Engineer, Imbsen and Associates, Inc.
- Dr. John M. Kulicki, BRP Vice Chair, President/CEO and Chief Engineer, Modjeski and Masters
- Mr. Dwight Beranek, Deputy Director of Military Programs, U.S. Army Corps of Engineers
- Mr. Joseph M. Englot, Assistant Chief Engineer/Design, Port Authority of New York and New Jersey
- Dr. John W. Fisher, Professor Emeritus, Lehigh University
- Mr. Henry Hungerbeeler, Director, Missouri Department of Transportation, and Chair, AASHTO Transportation Security Task Force
- Dr. Jeremy Isenberg, President and CEO, Weidlinger Associates, Inc.
- Dr. Frieder Seible, Dean, Jacobs School of Engineering, University of California at San Diego
- Mr. Kenneth E. Stinson, Chairman and CEO, Peter Kiewit Sons, Inc.
- Dr. Man Chung Tang, Chairman of the Board and Technical Director, T. Y. Lin International
- Mr. Kary Witt, Bridge Manager and Deputy General Manager, Golden Gate Bridge, Highway and Transportation District

References

(1) Recommendations For Bridge and Tunnel Security, Blue Ribbon Panel on Bridge and Tunnel Security, Washington D.C., September 2003. (Also, FHWA Website at: http://www.fhwa.dot.gov/bridge/security/brpcover.htm

(2) A Guide to Highway Vulnerability Assessment for Critical Asset Identification and Protection, prepared for AASHTO by Science Applications International Corporation, Vienna, VA, under NCHRP Project 20-7/Task 151B, SAIC, May, 2002.

(3) The National Strategy for the Physical Protection of Critical Infrastructures and Key Assets, The Office of the United States White House, Washington D.C., 2003.

(4) Briefing to the FHWA/AASHTO Blue Ribbon Panel on Bridge and Tunnel Security, Tom Reilly, Transportation Security Administration, Department of Homeland Security, March 27, 2003.

(5) Briefing, "Transportation Security Update," Tom Rummel, P.E., Project Development Section, Bridge Division, Texas Department of Transportation, February 2003.

(6) National Needs Assessment for Ensuring Transportation Infrastructure Security, prepared by Douglas B. Ham and Stephen Lockwood, Parsons Brinckerhoff, for the American Association of State Highway and Transportation Officials (AASHTO) Transportation Security Task Force under NCHRP Project 20-59/Task 5, October 2002.

(7) Design of Bridges for Security, presentation by Capt. David Winget, University of Texas Department of Civil Engineering at NCHRP Bridge Infrastructure Vulnerability Assessment Workshop, February 10, 2003.

Acknowledgement

The authors are indebted to the Blue Ribbon Panel Members, a group of renowned engineering experts who generously contributed their time, without compensation, to guide government leaders, infrastructure owners, and the engineering community on how to improve the security of bridges and tunnels. The panel's initiative and collective wisdom reflected in their report will help America and perhaps other countries meet future challenges to strengthen the transportation infrastructure network.

The authors also acknowledge the contributions of numerous others whose contributions throughout Blue Ribbon Panel deliberations formed the basis for portions of the full report. Specific recognition is given to: Mr. Dan Hartman, Transportation Security Administration, Department of Homeland Security; Dr. Anthony Kane, Director of Engineering, American Association of State and Highway Transportation Officials (AASHTO); Mr. Richard Land, State Bridge Engineer, California DOT (CALTRANS); Mr. Paul Liles, State Bridge Engineer, Georgia DOT; Mr. Stephan Parker, Senior Program Manager, National Cooperative Highway Research Program; Ms. Mary Lou Ralls, State Bridge Engineer, Texas DOT; Mr. James Ray, Research Engineer, ERDC, Corps of Engineers; Mr. Tom Reilly, Transportation Security Administration, Department of Homeland Security; and Capt. David Winget, Graduate Student, University of Texas, Austin.

Ultimate shear strength of pile caps

Masahiro SHIRATO[1], Jiro FUKUI[2], Naoki MASUI[3], Kenji KOSA[4]

Abstract

This paper proposes a design methodology for ultimate shear strength of pile caps subject to various stresses, based on experiments and numerical analyses. First, we determine an evaluation equation for shear strength of pile caps with compressive piles. Second, we clarify the shear resistance mechanism of pile caps with pull-out piles, and confirm to be able to apply the determined evaluation equation to those with pull-out piles by modifying the setting of shear span. The proposed methodology was introduced into the current version of the Japanese Specifications for Highway Bridges (March 2002).

1 INTRODUCTION

Due to the disastrous consequences of earthquakes in past decades, the need for an approach that would unify and simplify design procedures for bridge foundation has been recognized. In the 1995 Hyogo-ken Nanbu Earthquake there was a clear demand from structural engineers for an appraisal of consistent design methodologies that could provide a realistic description of the behavior of pile caps. This paper describes two investigations on the behavior of pile caps.

The first one introduces a newly established design method for ultimate shear strength of pile caps supported by compression piles. Typical pile caps are in the category of deep beams or two-way slabs. This paper reviews extensive research activities on pile caps and establishes a design method to enhance the structural performance of pile caps consisting of deep beams.

The second investigation focuses on damage to pile caps due to the pull-out of piles subjected to a heavily inclined-eccentric load during an earthquake. In former design specifications of bridges in Japan, the structural design method of pile caps with pull-out piles was not well documented. In addition, there have been few studies on the structural evaluation of pile caps with pull-out piles because the occurrence is not common in moderate earthquakes. The Public Works Research Institute (PWRI) therefore conducted experimental studies to investigate the shear-resisting mechanism

[1] Research Engineer, Foundation Engineering Research Team, Public Works Research Institute
[2] Team Leader, ditto.
[3] Deputy General Manager, Design Department, Obayashi Corporation
[4] Associate Professor, Department of Civil Engineering, Kyushu Institute of Technology

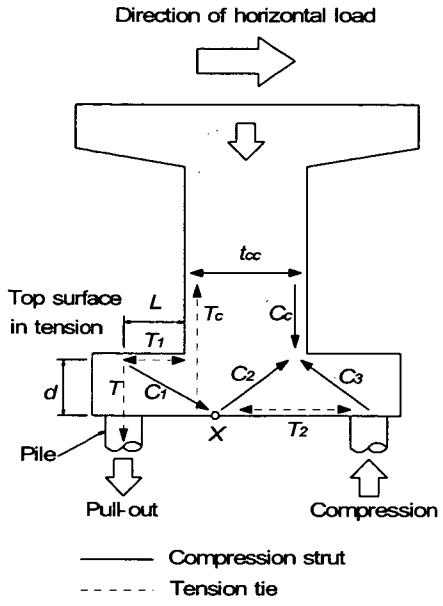


Figure 1 Struts and ties in a pile cap

of pile caps. The experiment included several specimens consisting of columns and pile caps using the parameters of shear span to depth ratio. Load-deformation relationship, strain development, crack pattern and so on were observed in the experiment. In addition, numerical analysis demonstrated the validity of these observations for establishing a design system.

This paper proposes a design methodology for ultimate shear strength of pile caps subject to various stresses, which leads to a more accurate, economical and rational approach for these structural units. The proposed methodology was introduced into the current version of Japanese Specifications for Highway Bridges (March 2002). PWRI has also proposed a design method for the slab effect (punching shear) based on relevant experimental investigations. The detailed discussion is given elsewhere [1, 2].

2 IDENTIFICATION OF LOAD PATHS IN PILE CAPS USING STRUT-AND-TIE MODELS

For deep beams, walls and discontinuous regions of structures, design methods based on strut-and-tie models are frequently utilized to describe load effect and resistance [3]. This relies on the assumption that the design expects convenient load paths to form within structural concrete members that are considered to form struts and ties or various types of truss models.

Figure 1 illustrates the load (stress) paths in a pile cap where solid lines and dotted lines represent compression struts and tension ties, respectively. The right-hand

side of Figure 1 explains that the pile reaction is supported by forming a "force triangle" consisting of C_3 (compression) and T_2 (tension).

Many experimental studies have confirmed the applicability of strut-and-tie models for pile caps with compression piles. On the other hand, the force equilibrium is different in the pile cap due to the pull-out pile. It seems that conventional compression strut is not available in this case, which means that point X has to be determined by a complicated and sophisticated load pass. This is the main difference in the design of pile caps in the case of compression and pull-out piles.

3 REVIEW AND RE-EVALUATION OF THE SHEAR DESIGN OF PILE CAPS

3. 1 Existing shear design of pile caps

The design procedure for pile caps documented in the Specifications for Highway Bridges IV; Substructures, Japan [4, 9] includes 1) shear span a to effective depth d ratio, 2) shear strength of concrete contribution and 3) shear resistance due to transverse reinforcement. The shear span to effective depth ratio a/d in pile caps is an important parameter in shear design. The shear strength of a pile cap is the sum of the concrete contribution and resistance of shear reinforcement.

$$S_d = S_{dc} + S_{ds} = c_{dc}S_c + c_{ds}S_s \tag{1}$$

$$S_{dc} = c_{dc}S_c, \quad S_{ds} = c_{ds}S_s \tag{2}$$

where S_d is shear strength as deep beams, S_{dc} is shear resistance carried by concrete in deep beams and S_{ds} is shear resistance carried by transverse reinforcement in deep beams. S_c is shear resistance carried by concrete in ordinary (slender) beams, S_s is shear resistance carried by transverse reinforcement derived from truss analogy, c_{dc} is the modification coefficient of S_c and c_{ds} is the modification coefficient of S_s, both being dependent upon a/d.

In 1996, the design specification introduced a design formula for evaluating shear strength of pile caps. The coefficients c_{dc} and c_{ds} were provided as follows:

$$c_{dc} = \frac{6.3}{1.3 + 0.8(a/d)^2} \tag{3}$$

$$c_{ds} = \frac{a}{2.5d} \tag{4}$$

Both coefficients are valid for beams of a/d less than 2.5. However, these seem to be overly conservative, particularly with respect to Eq. (3). Although the coefficients c_{dc} was determined from the results of numerous experiments on various deep beams, the

coefficient was set considerably lower than the average value because of the large scatter in the load test results. The coefficient c_{ds} was given by conservative judgment because only minimal data was available.

Accordingly, the small shear strength of concrete using Eq. (3) requires a considerable amount of transverse shear reinforcement in some cases, so there is a demand to review and modify Eqs. (3) and (4).

3.2 Review of load test results [5, 6]

Existing experimental data on the shear strength of deep beams without shear reinforcement was collected and summarized in Figure 2, in which the parameters are shear span to depth ratio and the ratio of shear strength to ordinary beams, where S_e is the observed shear strength. The figure shows considerable scatter in the data and no explicit increase in shear strength with decrease of a/d. In Figure 2, the dotted line derived from Eq. (3) seems to cover the lower bounds of the shear strength. The most probable shear strength of deep beams was obtained by applying the least mean squares method for data of a/d from 0.4 to 3.0. The result is Eq. (5) shown in Figure 2.

$$c_{dc} = \frac{12.2}{1+(a/d)^2} \tag{5}$$

The large variation in experimental data is probably due to something other than a/d. Through a review of load test results, as shown in Figure 3, it was found that there is a clear difference in the shear strength of concrete between $b/d = 0.2$ and 0.4, where b is the width and S_{dc} is calculated by Eqs. (2) and (5). Since the width of the pile caps should be larger than their depth, i.e., wide beams or slabs, we can omit the experimental results of the specimens in which b/d is less than 0.4. Figure 4 illustrates that the relation between S_e/S_c and a/d derived from previous load tests in which the results of specimens with small b/d ($b/d < 0.4$) are eliminated gives the best fit coefficient in Eq. (6), as shown by the solid line.

$$c_{dc} = \frac{14.0}{1+(a/d)^2} \tag{6}$$

As the variation in data could be minimized by eliminating the results of the thin specimens, Eq. (6) exhibits high reliability for shear design of deep beams. A reliability analysis was introduced to re-evaluate the modification coefficient c_{dc} employed in the design provisions. Because design practice requires a safety margin in the shear strength, a reliability index, so called β, was set to 2.0, into which only 2.3% of the data may fall. Eq. (7) is also shown in Figure 4 by the broken line.

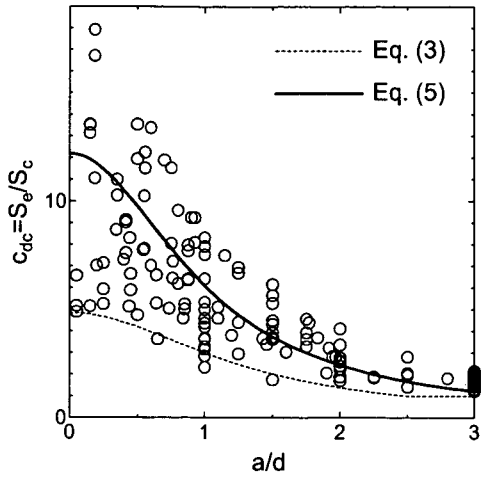


Figure 2 Effect of shear span to depth ratio on shear strength of concrete

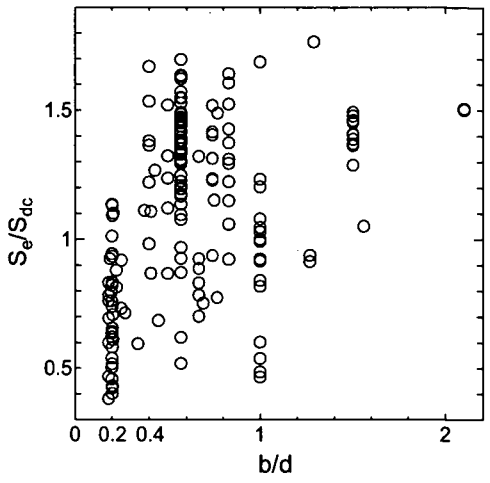


Figure 3 Effect of beam width to depth ratio on shear strength in deep beams

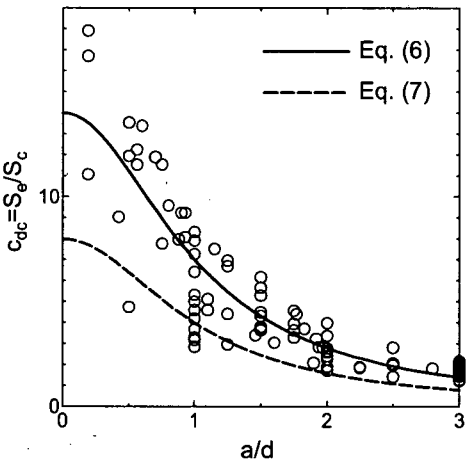


Figure 4 Effect of shear span to depth ratio on shear strength of concrete in the case of $b/d \geq 0.4$

$$c_{dc} = \frac{7.98}{1+(a/d)^2} \tag{7}$$

where c_{dc} derived from Eq. (7) is 30–50% larger than that derived from Eq. (3).

3.3 Effect of transverse reinforcement

In slender beams, transverse reinforcement is effective for increasing both the resistance against diagonal tension after cracking and the strength of concrete compression strut by confinement. In deep beams, however, the angle of compression strut and diagonal cracking increases with the decrease of a/d; in other words, the

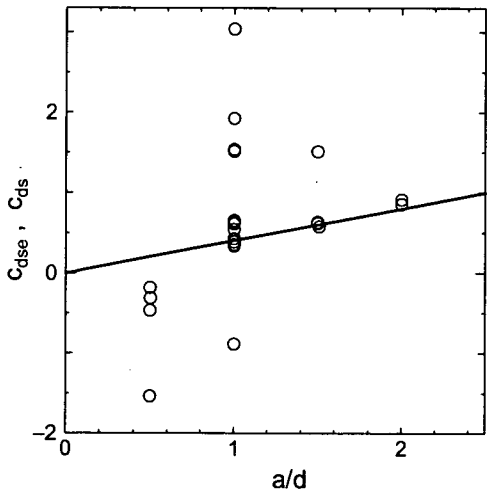


Figure 5 Effect of shear reinforcement on deep beams in the case of $a/d \leq 2.5$

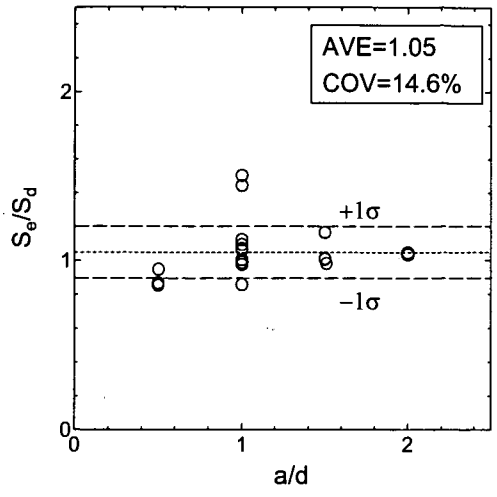


Figure 6 Comparison of observed shear strength S_e and calculated S_d

effect of transverse reinforcement becomes smaller. Although the contribution of transverse reinforcement of deep beam to shear strength was recognized through the experiments, quantitative evaluation on shear reinforcement has not yet been established in the design provisions.

As shown in Figure 5, the shear strength carried by transverse reinforcement depends upon a/d, where all data has b/d of not less than 0.4. In this figure, c_{dse} is derived from the following equation.

$$c_{dse} = \frac{S_e - S_{dc}}{S_s} \tag{8}$$

where c_{dse} is a modification coefficient of the effect of transverse reinforcement on shear strength estimated from experimental results, S_e is observed shear strength, S_{dc} is concrete shear strength calculated by Eqs. (2) and (6) and S_s is calculated shear strength carried by reinforcement by truss analogy. According to Figure 5, the solid line derived from Eq. (4) passes the mean shear strength. In Figure 6, the shear strength S_d calculated by Eqs. (1), (2), (4) and (6) is close to the observed data S_e. These figures clearly demonstrate that Eqs. (4) and (6) give an accurate estimation of the shear strength of deep beams. In comparison with the variation in Figure 5, the variation in Figure 6 is small. The reason is considered to be the small variation of material strength in the reinforcements and the variation of shear strength depends on that of the shear strength carried by concrete. In consideration of the concept of consistent shear capacity of pile caps with and without transverse reinforcement, the current design provision adopts Eqs. (1), (2), (7) and (4).

4 RESEARCH ON THE SHEAR OF PILE CAPS WITH PULL-OUT PILES

4.1 Experimental study [7]

The experimental program, which consists of three test series, involves the investigation of the mechanism and the development of a design method for the shear of pile caps subject to pull-out load.

The parameters in Series A and B tests, which employed two-dimensional models, are shear span to depth ratio. Test Series C adopted complete three-dimensional scale models of a pile cap with a column. The details of the three test series are described below. None of the specimens included shear reinforcement. In these load tests L represents the distance between the face of the pier and the center of the pull-out pile and is commonly used as the shear span in compression piles. On the other hand, in pull-out piles the shear span can be expected to be a little larger than L.

(1) Series A

The scale model involves a column and one half of a pile cap, as shown in Figure 7. The table in the same figure describes the parameters of shear span to depth ratio. The observed behavior is illustrated in Figure 8, where the initiation and propagation of cracks and final diagonal cracking are marked.

(2) Series B

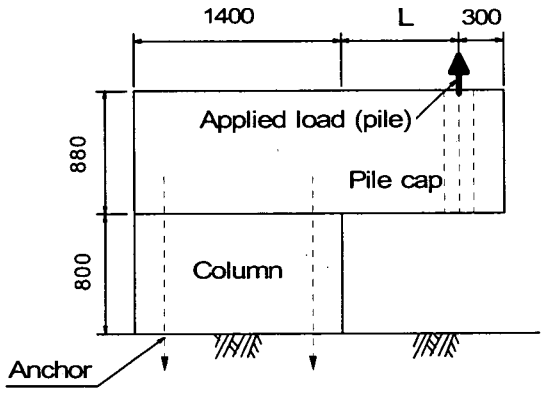
Similar test series, as shown in Figure 9, were conducted to evaluate the effect of shear span to depth ratio on the shear strength of concrete. The cracking behavior up to the point of diagonal shear failure was similar to that in Series A, as shown in Figure 10.

(3) Series C

Different from Series A and B, the Series C test has complete three-dimensional models of a pile cap with a column. The dimensions of the scale models used in this series are shown in Figure 11. The main parameter in Series C is also shear span to depth ratio. The cracks at failure are shown in Figure 12.

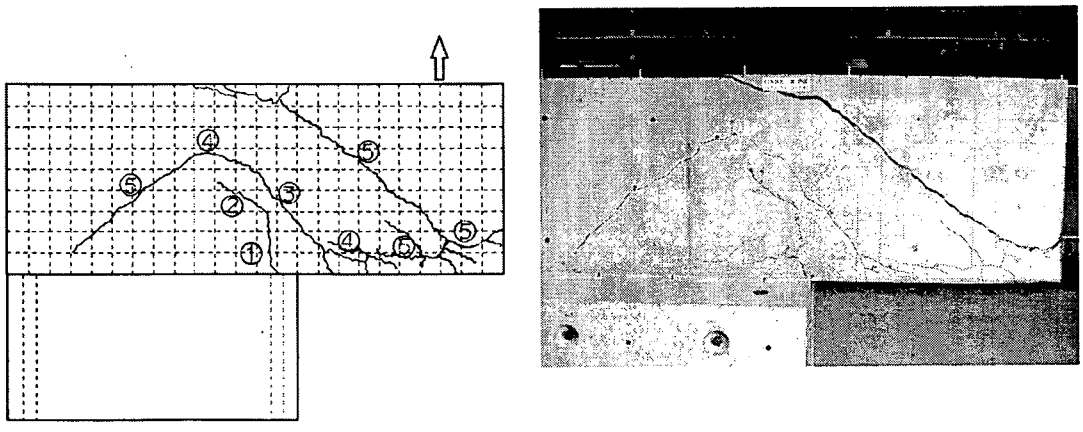
(4) Summary of experimental results

The observed shear capacity is useful data for proposing a design formula for pile caps with pull-out piles (loads). As introduced in Eq. (1), it seems that the modification coefficient c_{dc} for deep beams is applicable in this case by increasing the shear span length to some extent. The increase in shear span is recognized by the load path illustrated on the left-hand side of Figure 1. Figure 1 shows that the length of shear span may be determined by the load path, which depends upon the geometrical condition consisting of effective depth of pile cap d and depth of column t_{cc}. Figure 13 shows that the coefficient of shear strength c_{dc} calculated by Eq. (6) is closely related to a/d where three types of shear span a are compared. The effective depth of the pile caps and the half depth of the columns are not very different (10–20%) in Series A, B and C. Figure 13 gives similar results on the relation between a/d and c_{dc}.



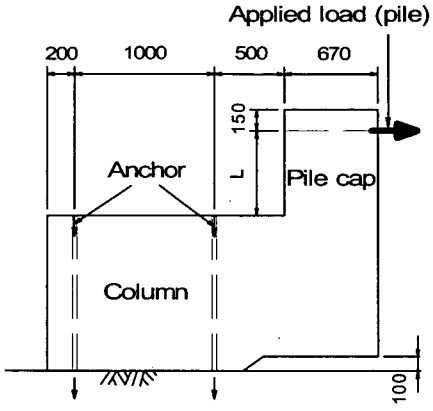
Specimen	A-1	A-2	A-3
Span to depth ratio L/d	0.5	1.0	1.5
Span L (mm)	400	800	1,200
Width b (mm)	600	600	600
Longitudinal rebar	0.83%, f_{sy} =365 N/mm^2		
Concrete strength (N/mm^2)	23.4	24.7	22.6
Maximum load (kN)	1276	737	660

Figure 7 Test specimens and maximum loads in Series A



Crack 1. Initial crack
Crack 2. Change in direction of crack
Cracks 3 and 4. Propagation of crack to column base
Crack 5. Initiation and propagation of second diagonal crack (failure)

Figure 8 Crack pattern in A-1



Specimen	B-1	B-2	B-3	B-4
Span to depth ratio L/d	1.0	0.5	2.0	2.5
Span L (mm)	600	300	1,200	1,500
Width b (mm)	500	500	500	500
Longitudinal rebar	0.84%, f_{sy} =361 N/mm^2			
Concrete strength (N/mm^2)	23.5	26.0	27.3	27.1
Maximum load (kN)	380	514	249	239

Figure 9 Test specimens and maximum loads in Series B

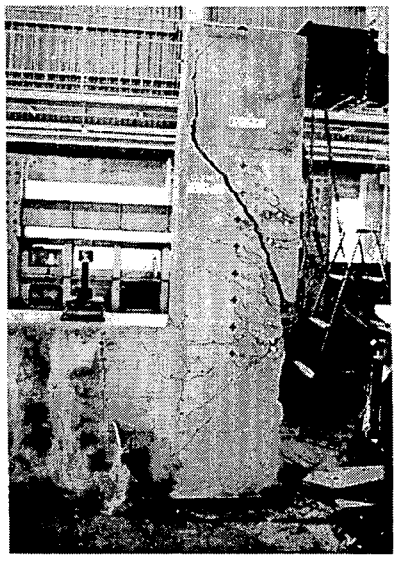
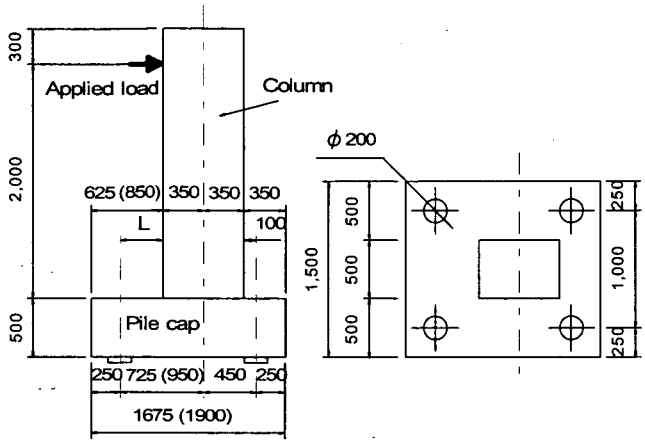


Figure 10 View of load test in Series B



Specimen	C-1	C-2
Span to depth ratio L/d	0.833	1.33
Span L (mm)	375	600
Width b (mm)	1500	1500
Longitudinal rebar	1.62%, f_{sy} = 375 N/mm^2	
Foundation type	Four piles	
Concrete strength (N/mm^2)	26.2	29.4
Maximum load (kN)	681	575

Figure 11 Test specimens and maximum loads in Series C



Figure 12 View of load test in Series C

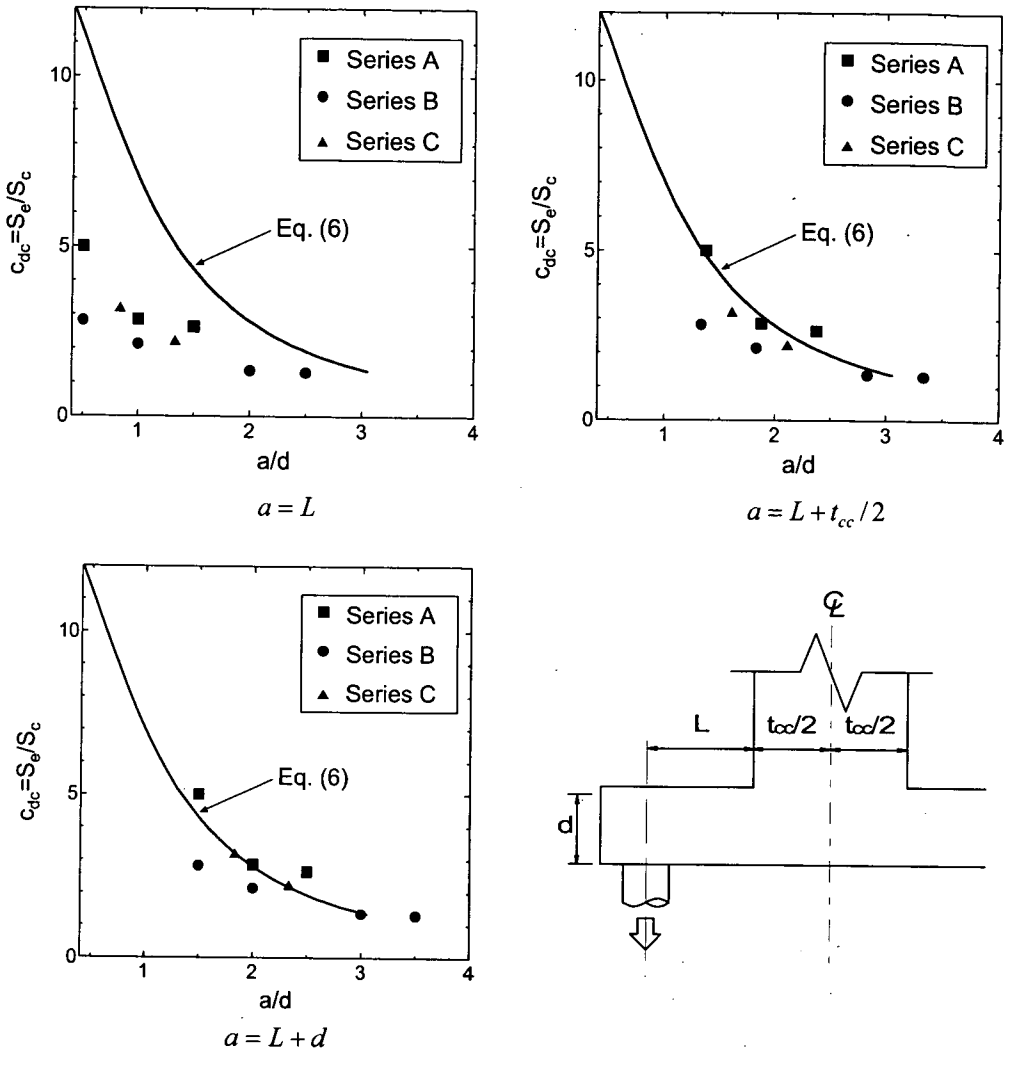


Figure 13 Relation between c_{dc} and a/d for three types of shear span

4.2 Numerical analysis observations [8]

The two-dimensional finite element (FE) models described herein represent the specimens of the experiment. A nonlinear FE analysis was performed for the test specimens of A-2 and C-2.

The load-displacement curves at the loading points are shown in Figure 14. The observed and calculated load-displacement curves are quite similar, indicating that the analysis is capable of describing the load transfer mechanism of the test specimens.

Principal compression stress distributions are shown in Figure 15. On the basis of these figures the compression stress derived from the analysis satisfactorily supports the assumption that the compression strut runs from the pull-out pile to the inside of the column in the case of pull-out piles.

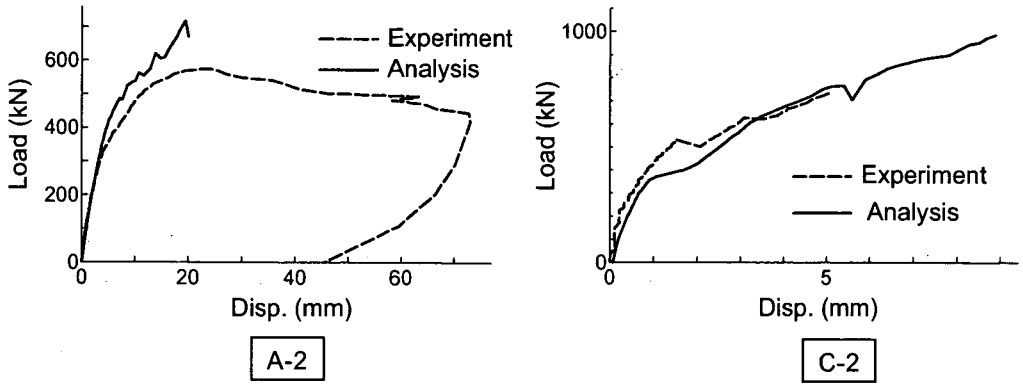


Figure 14 Comparison of measured and calculated load-deformation curves at the loading point

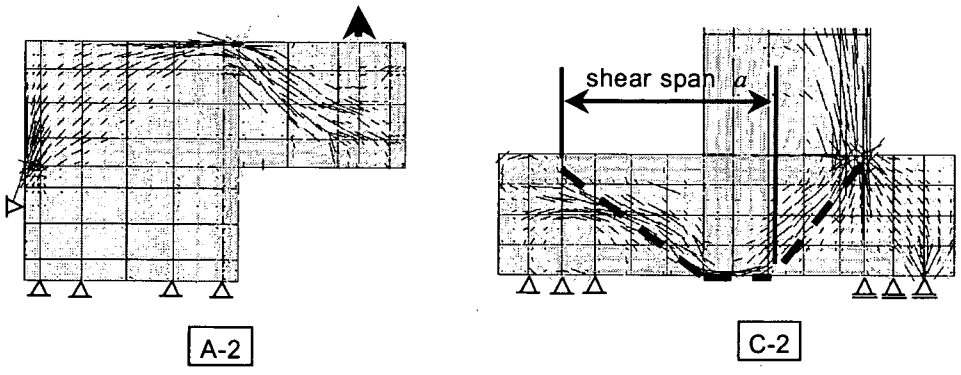


Figure 15 Principal compression stress distribution from FEM

In addition to the above experiments, numerical analysis was conducted for a number of pile caps subject to lateral load on the top of the column in order to evaluate the stress flow and to find an appropriate shear span. The analysis parameters are:

- width of columns,
- effective depth of pile caps, and
- number of rows of piles.

The analysis shows the principal stress in the pile caps in the manner denoted by the thick broken line in Figure 15. As the assumed shear span in Figure 15, a conservative assumption has been made that point X from which the compression strut changes direction as defined in Figure 1 is regarded as the farther point from a couple of the points at which the direction of the stress flow changes near the bottom in the pile cap such that the estimated shear span becomes longer. Consequently Eq. (9) gives the shear span of a pile cap with pull-out piles.

$$a = \min(L + t_{cc}/2,\ L + d) \tag{9}$$

5 CONCLUDING REMARKS

The following extensive investigation shows that a rational design approach has been established for pile caps.

- Re-evaluation of concrete shear strength in deep beams
- Effect of shear reinforcement

Based on the experiments and numerical analyses, the following hypotheses were found to be valid and applicable in the design of pile caps with pull-out piles.

- In the case of pull-out piles, a tied arch appears in the pile cap. However, the flow of compression stress forming the arch has a slightly different angle and runs into the column.
- The above stress flow means that the shear span in the pull-out pile is larger than that in the compression pile.
- The formula for the shear strength of pile caps with compression piles is applicable in cases of pull-out piles by modifying the shear span.

These conclusions were introduced into the current version of the Specifications for Highway Bridges in Japan (March 2002) [9].

ACKNOWLEDGMENTS

This research work was conducted for revision of the Specifications for Highway Bridges in Japan. Comments and support from the Working Group for Pile Cap Design (Chairman Prof. Kenji Kosa) established in the Committee of Substructure in the Japan Road Association are gratefully acknowledged.

REFERENCES

[1] Fukui, J., Nanazawa, T., Katou, H. and Minamizawa, S.: Experimental study on shear strength of pile caps and deep slab in bridge foundation. Technical Memorandum of PWRI, No. 3483, 1997. (in Japanese)

[2] Fukui, J., Nanazawa, T., Katou, H., Ohkoshi, M., Minamizawa, S. and Watanabe, A.: Experimental study on structural design and retrofit of pile cap. Technical Memorandum of PWRI, No. 3550, 1998. (in Japanese)

[3] Niwa, J.: Shear strength mechanism of reinforced concrete with deep beams. Doctoral Dissertation, the University of Tokyo, 1983. (in Japanese)

[4] Japan Road Association: Specifications for Highway Bridges IV; Substructures, Maruzen, Tokyo, 1996. (in Japanese)

[5] Shirato, M., Fukui, J., Kosa, K. and Umebara, T.: A study on shear capacity of deep beams and bridge footings. J. of Struct. Eng., JSCE, Vol. 47A, pp. 1315-1325, 2001.

(in Japanese)

[6] Fukui, J., Shirato, M. and Umebara, T.: Study on shear capacity of deep beams and footing. Technical Memorandum of PWRI, No. 3841, 2001. (in Japanese)

[7] Shirato, M., Furusho, S., Fukui, J. and Katou, H.: An experimental study for the critical state of footings subjected to movement and shear by tension. J. of Struct. Eng., JSCE, Vol. 47A, pp. 1327-1338, 2001. (in Japanese)

[8] Shirato, M., Kawamoto, A., Fukui, J. and Kosa, K.: A design equation of shear capacity of a pile cap at the top of which is tension. J. of Struct. Eng., JSCE, Vol. 48A, 2002. (in Japanese)

[9] Japan Road Association: Specifications for Highway Bridges IV; Substructures, Maruzen, Tokyo, 2002. (in Japanese)

A Sloping Surface Roller Bearing and its lateral Stiffness Measurement

George C. Lee[1] and Zach Liang[2]

Abstract

In this paper the laboratory performance and advantages of a new roller-type seismic isolation bearing for highway-bridge are briefly presented. The new bearing, with steel cylinders rolling on sloping surfaces in two directions, has the feature of keeping the acceleration of the superstructure at a relatively low and constant level while tolerating a relatively large bearing displacement.

In order to develop design guidelines for the roller bearings, it is necessary to first consider how to evaluate its seismic performances. One of the most important parameters in seismic isolation design is the lateral stiffness which directly affects the working period and damping coefficient. The current standard procedure using "effective stiffness" is shown not to be a suitable measure for the evaluation of the seismic performance of the roller bearings and that a different evaluation procedure has to be developed. A major objective of this paper is to present this problem to the participants of the workshop and to seek advice on how to best develop the evaluation procedure.

The Sloping Surface Roller Bearing (SSRB)

Vibration isolation bearings have been discussed by Den Hartog (1956) for mechanical engineering applications and by Naeim and Kelly (1999) in earthquake engineering applications. The sloping surface roller bearing (SSRB) reported herewith is recently developed for seismic isolation.

The conceptual drawing of a single roller type of SSRB is shown in Fig. 1, with its working mechanism shown in Fig. 2(a) and its capability of tolerance of large displacement shown in Fig. 2(b). Fig. 2(b) shows that the displacement of the superstructure, H_D, can be twice as much as the roller displacement, H_B. That is, the bearing can tolerate very large displacement with relatively smaller dimension. A prototype bearing with single roller is shown in Fig. 3(a).

In Figs. 1 and 2, a single layer bearing is shown. For two directional ground motion, two layers, one in each mutually perpendicular direction, can be used. A two-layer assembly is shown in Fig. 3(b). The total height of the bearing will depend upon the vertical load. For example, for 1000 Ton (2000 Kips) vertical load the bearing will have about 30-33 cm (12 – 13″) in the vertical direction.

[1] Samuel P. Capen Professor of Engineering, Multidisciplinary Center for Earthquake Engineering Research, Department of Civil, Structural and Environmental Engineering, University at Buffalo, Buffalo, NY 14261, USA.
[2] Research Associate Professor, Multidisciplinary Center for Earthquake Engineering Research, Department of Civil, Structural and Environmental Engineering, University at Buffalo, Buffalo, NY 14261, USA.

The horizontal acceleration is mainly determined by the angle of the sloping surface(See Fig. 2(a)). That is, despite the magnitude of the ground acceleration, the acceleration of the superstructure, A, can be written as

$$A = \alpha g \qquad (1)$$

Since the angle of the slope is quite small, around 1.5^0 to 2.5^0, the acceleration contributed by the bearing can be as small as 0.03 -0.05 g, even with an overdamped design, say the damping force is around 0.05-0.10g, the total lateral acceleration can still be kept at less than 0.15g.

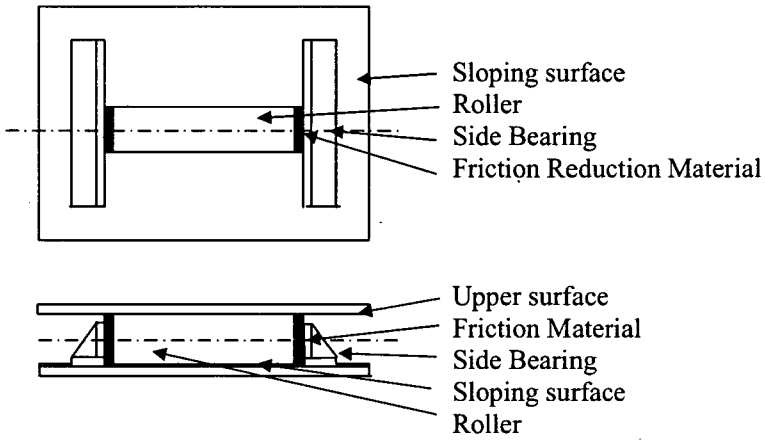


Figure 1. Assembly of a single layer bearing.

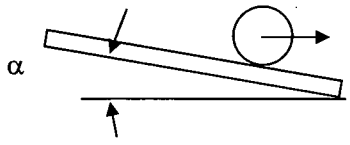


Figure 2(a). Horizontal acceleration of bearing

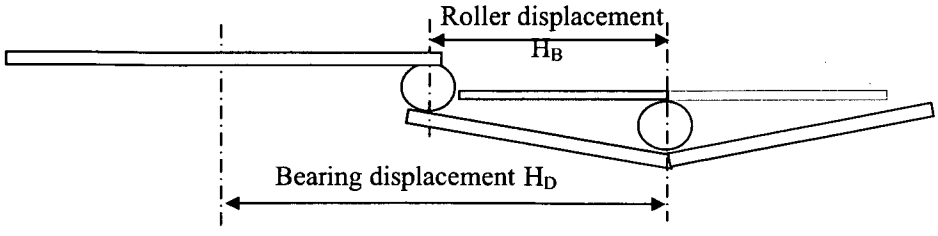


Figure 2(b). Displacement of Roller Bearing

The bearing displacement is also an important design parameter. To reduce the displacement is a challenging task in isolation design. When the ground motion has a large displacement, no matter it is pulse-like or otherwise the bearing displacement can be quite large. In the working range, where the period of the isolation system is longer than that of the major earthquake components, using large damping seems to be the only approach to regulate the displacement. However, large damping will increase the level of the acceleration at the same time. In typical bearing design, compromise is usually made between the acceleration and the displacement.



Figure 3(a). Photos of a single layer bearing assembly

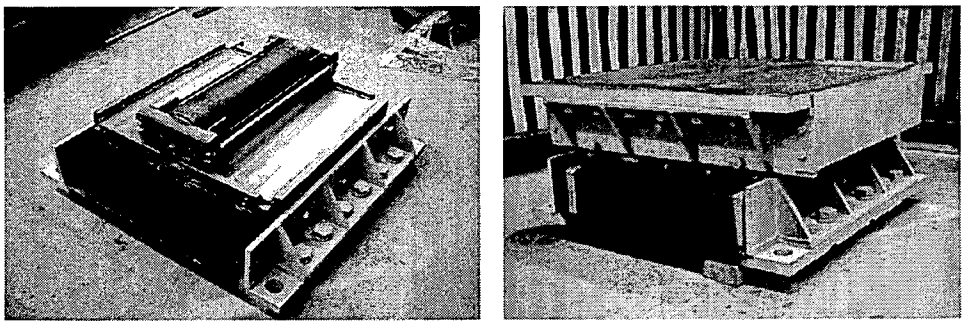


Figure 3(b). Photos of a double layer bearing assembly

For the roller bearing, the acceleration amplitude is almost a constant. The designer should not be concerned with excessive acceleration of the superstructure. Since the acceleration level is relatively small, they can rely on damping to further reduce the bearing displacement. This is an important advantage of the SSRB.

Shaking Table performance of SSRB

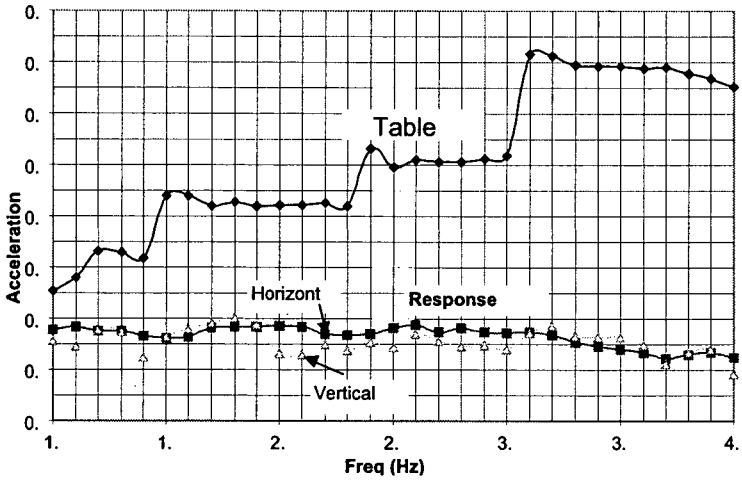


Figure 4. Acceleration level under sweep sine test

Fig. 4 shows results of shaking table test of the first generation prototype bearing, where the slope angle is 4.5^0. These results show that the bearing acceleration response is relatively constant under different input table motions. For the second generation prototype bearing, the angle used is less than 2^0. Fig. 5 shows measured results of the acceleration and base shear from the experiments of the second generation prototype bearing conducted at the University of Nevada at Reno. It is seen that, the acceleration level is almost fixed, despite of the levels of the amplitude of ground motion and the frequencies.

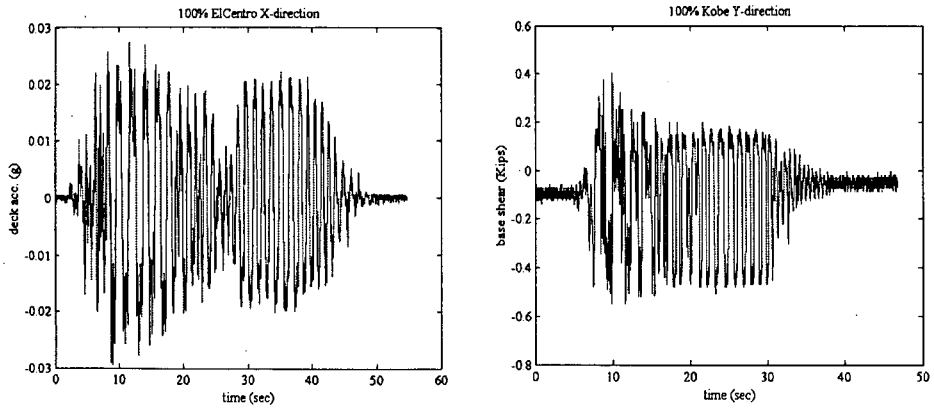


Figure 5. Acceleration and base shear levels under earthquake excitation

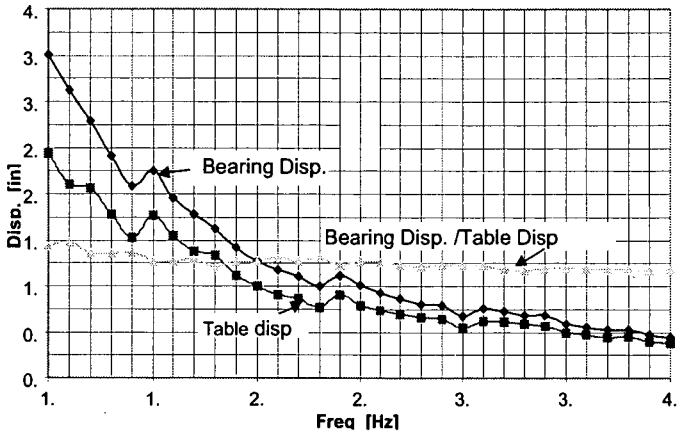


Figure 6. Bearing displacement under sweep sine excitation

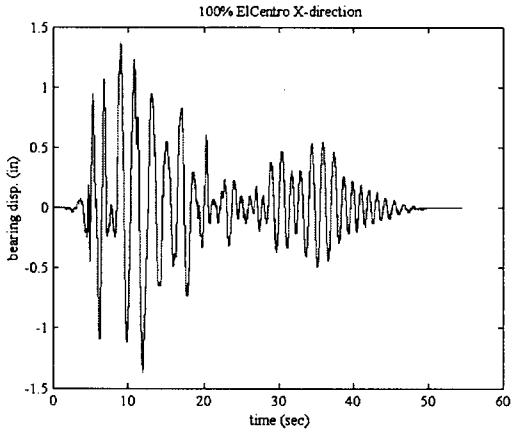


Figure 7. Bearing displacement under earthquake excitation

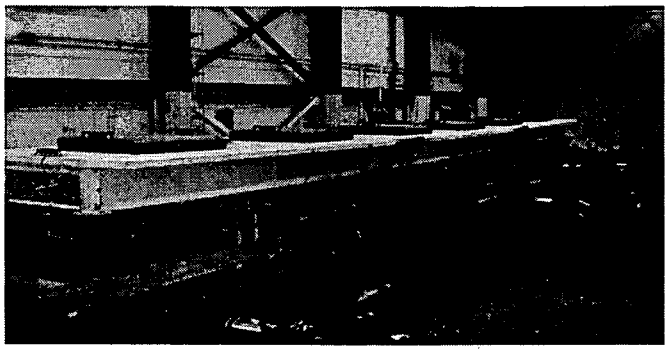


Figure 8. Overview of the deck of the model bridge

Fig. 6, shows the bearing displacement of the first generation bearing (4.5° angle) under sweep sine excitation. It is seen that the ratio of the bearing displacement vs. the table's movement is also nearly constant. In Fig. 7, we show the typical bearing displacement of the second generation of roller bearing under El Centro earthquake excitation conducted at the University of Nevada at Reno. Because the bridge model is 2/5 down scaled, the real displacement for a full scaled bridge should be 2.5 times larger, which is 3.5 inches. It is a reasonably small value. Fig. 8 shows the test setup at Reno, where the bridge superstructure is supported by two separate shaking tables at its ends.

The AASHTO Approach of Bearing Evaluation

While the roller bearing has certain distinct advantages, its performance evaluation cannot be readily carried out using current method. One of the problems is the value of lateral stiffness. In the following the concept of stiffness in seismic isolation design is firstly reviewed, followed by an explanation of the problem area of evaluating the roller bearing.

Seismic isolation design by means of the design response spectrum uses mainly two parameters, the period and the damping coefficient, which directly relate to the lateral stiffness of isolation bearings. Denote **M** and **K** as the mass of the superstructure and the lateral stiffness respectively, the period of the isolation system, T, is given by

$$T = 2\pi\sqrt{\frac{\mathbf{M}}{\mathbf{K}}} \tag{2}$$

Denote the energy dissipated by the bearing system in one sinusoidal cycle as E_d and the maximum bearing displacement as D_A respectively. The damping ratio, ξ, is defined as

$$\xi = \frac{E_d}{4\pi(\frac{\mathbf{K}D_A^2}{2})} = \frac{E_d}{2\pi\mathbf{K}D_A^2} \tag{3}$$

In seismic isolation design the damping coefficient is solely determined by the damping ratio.

Equations (2) and (3) show that the stiffness is an important factor in isolation design. Generally, a stiffness of a system is defined as the capability of a structure or system to resist deformation under applied loading. Or,

$$\mathbf{K} = \frac{F}{D} \tag{4}$$

Equation (4) is a measure of the applied force per unit deformation. It is also a measure of the capability of a system that can restore the potential energy of the deformed structure. In Equation (3), the term $\frac{\mathbf{K}D_A^2}{2}$ is actually the restored potential energy of the isolation

system when the maximum displacement D_A is reached. In an isolation system, this potential energy can be transformed into kinetic energy, $\frac{\mathbf{M}V^2}{2}$, in which V denotes the velocity. Thus, with an approximate sinusoidal vibration in resonant status,

$$\frac{\mathbf{K}D_A^2}{2} = \frac{\mathbf{M}V_A^2}{2} \tag{5}$$

Where V_A is the maximum velocity when the system damping is ignored. This gives,

$$V_A = \frac{2\pi}{T} D_A. \tag{6}$$

From the above one can obtain the definition of the period, as given by Equation (2).

Equation (4) is the standard definition of stiffness in structural engineering. It is for a linear system under sinusoidal vibration. For systems that do not have a pure sinusoidal vibration, the response can be analyzed by multiple sinusoidal forms with the help of the Fourier Transform. When the component with fundamental period dominates, the concept of period can still be used. In isolation design, most bearings are nonlinear. In order to utilize the above concept an effective stiffness, K_{eff}, has been defined and used, referred to as the AASHTO approach.

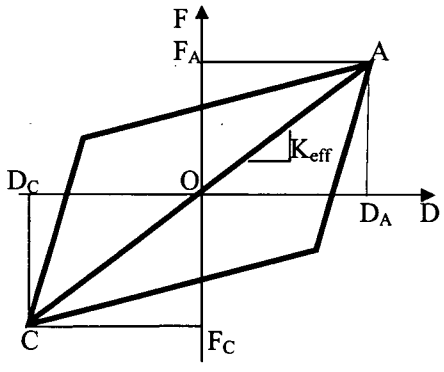


Figure 9. Bi-linear relationship of force vs. displacement

As shown in Fig. 9, the effective stiffness is defined by the slope of line AOC, or

$$K_{eff} = (F_A - F_C)/(D_A - D_C) \tag{7}$$

Where, D_A and D_C are the zero velocity displacements, and F_A and F_C are the resistant forces at the zero velocity displacements. With the effective stiffness, the percentage of critical damping can be measured by Equation (3), by replacing K with K_{eff} and D_A with design displacement D_0. where,

$$D_0 = (D_A - D_C)/2 \tag{8}$$

It has been shown that this approach is reasonably reliable for evaluation of systems having velocity-dependent characteristics. Typically the system has a definite structural period and the percentage of critical damping measured by equation (3) is less than 30%(AASHTO).

Challenges of Roller Bearing Evaluation

It is inappropriate to evaluate the roller bearing by using the AASHTO approach. The basic reason may be explained as follows: The roller bearing separates the superstructure from the ground or piers with a constant restoring force when the superstructure is on either sloping sides (see Fig. 2(b)). The system does not have a structural period as can be observed from the results of the sweep sine experiment, shown in Figs. 4 and 6. Thus, it is displacement-dependent rather than velocity-dependant.

The difference between the displacement-dependent isolation device and the velocity-dependent device can be seen by comparing the force-displacement loop of the roller bearing with that of the bi-linear model in Fig. 9.

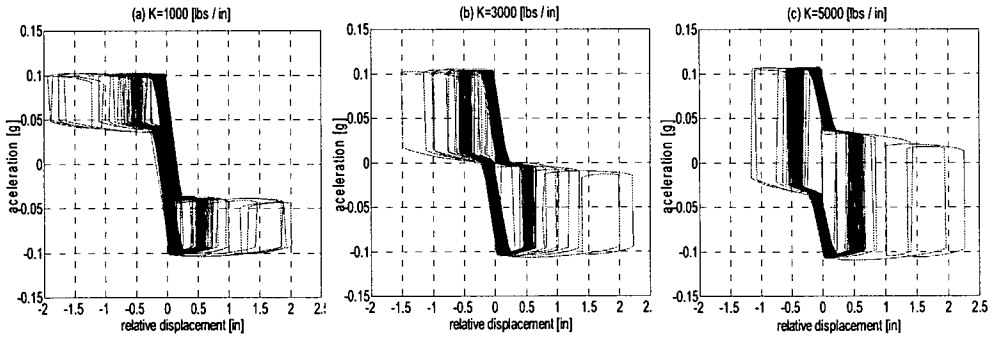


Figure 10. Experimental acceleration displacement loops of different spring stiffness for input sinusoidal wave 0.6 g 3.5Hz (1st generation roller bearing)

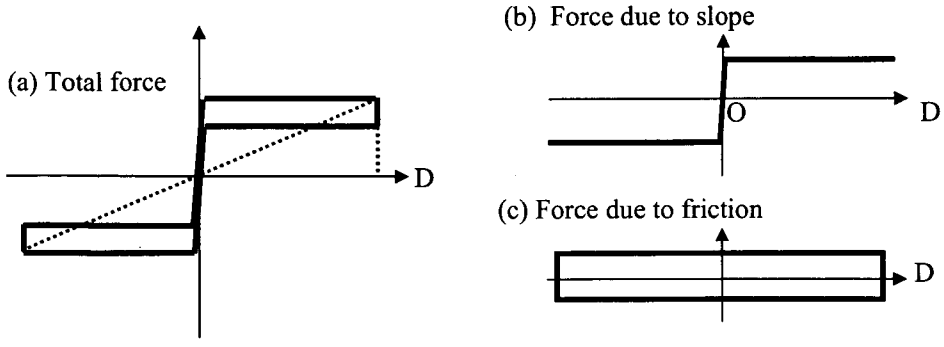


Figure 11. Force vs. displacement of the roller bearing

In Fig. 10, several measured acceleration-displacement loops of a prototype roller bearing (first generation) are shown, where the symbol K is the stiffness of an "internal absorber" and it is not the lateral stiffness. Further, the driving frequency is form 0.2 Hz (period = 5 sec) up to 5Hz (period =0.2 sec). In those experiments, the results shown are for 3.5 Hz driving frequency. (The rest of the tests have similar results.) Based on the experimental results such as those shown in Fig. 10, we approximate the force-displacement loop of roller bearings by decomposing it into two idealized parts, one each due to slope and friction, as shown in Fig. 11.

Figure 9 and Fig. 11 show that, the isolation system having velocity-dependent characteristics will restore much energy transmitted from the ground as the displacement increases. Part of energy will be dissipated by damping and part of it will be transformed into kinetic energy. For the isolation system having displacement-dependent characteristics such as the roller bearings, not too much energy is stored and can be transformed into kinetic energy later and that the period of the roller system can not be defined.

The experimental results of the roller bearing have shown that the isolation system with displacement-dependent characteristics has certain distinct advantages, such as: small acceleration, small base shear and large displacement tolerance. To apply this type of isolation system to engineering structures, certain evaluation procedure based on principles of structural dynamics will have to be established. The current method established from the principles of statics is more suitable for the type of bearings with strong velocity-dependent characteristics.

Summary

The following may be briefly summarized:

Roller bearings have the advantage of fixed and very low superstructure acceleration because its lateral stiffness is nearly a constant and it has no "period effect" to the superstructure. With this property, the designer can focus more on how to reduce the relative displacement of the structure. For this purpose, adding damping plays an important role.

The current evaluation method is not suitable for roller bearings due to their strong displacement-dependent characteristics. A new evaluation approach considering dynamic properties of the bearings is necessary. This is the current research effort of the authors.

Acknowledgements

This study is supported by a research contract from the US Federal Highway Administration. (Contract No. ETFH61-98-C-00094)

References

Constantinou, M.C, Soong T. T. and Dargush G. F. , "Passive Energy Dissipation Systems for Structural Design and Retrofit" lecture notes, short course presented by National Center for Earthquake Engineering Research, Seattle, Washington, 1996.

Clough. R. W. and Penzien J. , *Dynamics of Structures* 2nd ed. McGraw-Hill Book Co. 1993.

Den Hartog, J. P., *Mechanical Vibrations* 4th Ed. McGraw-Hill, NewYork, 1956.

Naeim, F. and Kelly, J. M., Design of Seismic Isolated Structures from Theory to Practice Jon Wiley & Sons, Inc., New York, 1999.

Highway Innovative Technology Evaluation Center (HITEC), "Technical evaluation report: Evaluation Findings for FIP-Energy Absorption Systems, L.L.C. Slider Bearings" September 1998, Product 9.

Liang, Z. and Lee, G.C., "Damping of Structures: Part 1 - Theory of Complex Damping", Technical Report NCEER-91-0004. NCEER, State University of New York at Buffalo, 1991.

Liang, Z. Song, J. Wang, J. and Lee, G.C. (2003), "A Sloping Surface Roller Bearing System for Seismic Isolation of Highway Bridges," Technical Report, MCEER, State University of New York at Buffalo. (in preparation)

Liang, Z. Song J. and Lee, G.C. (2003), "On Evaluation of Stiffness of Isolation Bearings," Technical Report, MCEER, State University of New York at Buffalo. (in preparation)

AASHTO 1999, "RFD Bridge Design Specifications".

Weaver, W. Jr., Timoshenko, S. P., and Young, D. H. *Vibration Problems in Engineering* / 5th Ed. Wiley, New York, 1990

Design and Construction Highway Piers with Interlocking Hoops in Japan

Kazuyuki Mizuguchi[1)]
Norimasa Higashida[2)]
Koji Osada[3)]
Gaku Ohashi[3)]

1. Introduction

The Hyogo-ken Nanbu Earthquake of 1995 caused severe damages on various infrastructures, including highway bridges. From these experiences, Specifications for Highway Bridges now mandates in its structural detailed items section that bridge piers with a rectangular cross section should have an arrangement of intermediate hoop reinforcement at one-meter or less intervals in order to improve the deformation performance of the piers after they suffer plastic deformation. In addition, the end of hoop ties should be attached with hooks and secured to inside a bridge pier.

As Photo-1 shows, it results in such dense an arrangement that operatives cannot enter the concrete casting area, creating a problem in concrete quality management.

Bridge piers with interlocking hoops offer high restraining effects and help reduce the volume of reinforcing steel as well as enhance constructability. Starting around the mid-1970's, bridge piers having interlocking hoops appeared in California, USA, and the interlocking hoop reinforcement system was adopted by AASHTO in its standards in 1977 and by CALTRANS in 1990.

In Japan, a study on interlocking-hoop bridge piers began around 1997. In 1997, bridge piers with two interlocking hoops were built for the first time in Japan for the Trans Chubu Expressway constructed by the Japan Highway Public Corporation(JH). In 2001, reinforcement using four interlocking hoops was applied to wall bridge piers at the third work section in expressway construction. With the demand for lower cost and higher concrete quality getting greater, more use of interlocking hoops in bridge piers is expected.

This paper presents a summary of experimental results carried out by JH and others, and analyzes the applicability of bridge piers with interlocking hoops to typical expressways in Japan in terms of cost performance, constructability, and application range. Lastly, the construction of interlocking four hoops is introduced.

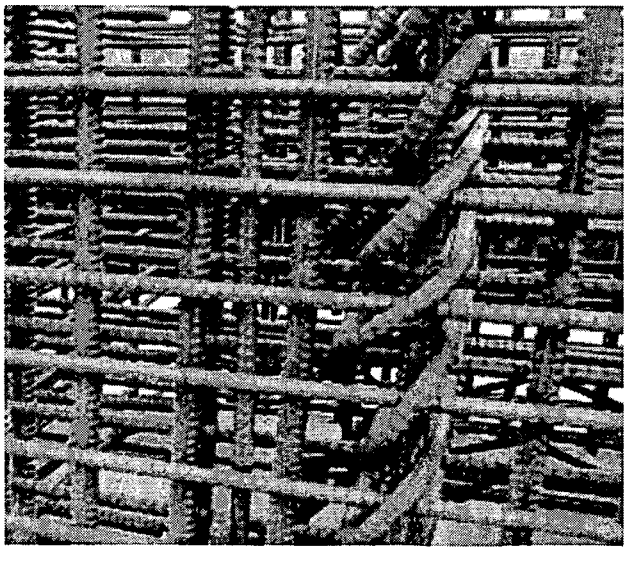


Photo-1 Example of arrangement of reinforcing bar

1) Japan Highway Public Corporation Engineering Department Bridge and Structural Engineering Division

2) Japan Highway Public Corporation Hokkaido Branch

3) Japan Highway Public Corporation Expressway Research Institute Bridge Division

2. Study of the application of interlocking-hoop piers to road bridges on Japanese expressways

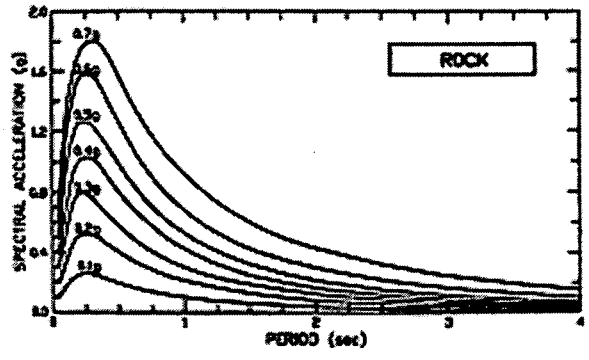
(1) Background behind common use of wall bridge piers in Japan

In both the U.S. and Japan, bridge piers with a circular cross section are considered to have greater deformation performance because they have greater restraining effects than those with a rectangular section. Reflecting this view, circular-section bridge piers are widely used in the U.S., while in Japan, the prevalence of wall bridge piers is still seen today even after introduction of the design method considering restraining effects. One of the circumstances behind this would be shown as follows:

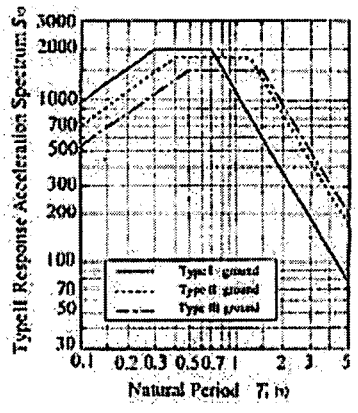
The values of seismic waves used for design calculations vary with countries since different countries assume different seismic motions and ground conditions. Figure-1 is a comparison example of response spectrum to seismic waves used in design process between the U.S. and Japan. As it shows, the U.S. data displays more conspicuous decline of response acceleration in the long-period range in the case of good soil. With rock, the peak acceleration occurs when the natural period is 0.1 second, and the longer the vibration period is, the smaller the response acceleration becomes. In Japan, even with the ground categorized as Class 1, the best ground condition, the acceleration stays at its peak, 2000 gal, with an increase in natural periods up to 0.7 seconds.

Thus, there is not much benefit for Japan to pursue a longer natural period in the direction perpendicular bridge axis as there is in the U.S. Due to this, in Japan, wall-type piers have been adopted more often than the multiple independent piers as a result of considering the foundation cost and the formwork cost for cross sectional areas of piers to obtain required bending strength.

Further, due to its difference from the U.S. in design approach to the allowable degree of damage to connections between super- and substructures of a bridge, Japan has seen a wider adoption of bridge construction method of separating the upper and lower works by installing rubber bearing. Moreover, wall bridge piers have a greater advantage in terms of the need to obtain a broader cross sectional area for bearing. This also has encouraged the use of wall bridge piers in Japan.



Response Acceleration Spectral Curves from ATC-32 (ATC, 1996), USA



Response Acceleration Spectral Curves from Specifications for Highway Bridges, Japan

Fig.1 Comparison example of Response Acceleration Spectral Curves between USA(ATC-32) and Japan(Specifications for Highway Bridges)

(2) Test results on expressway road bridges

Table-1 is a summary of the tests for interlocking-hoop/spiral bridge piers conducted by JH and others. Loading was performed in the direction perpendicular to the bridge axis as well as in the bridge axis direction. The subjected cross sectional areas range from 600 x 900 mm to 500 x 1300 mm. Tests with regard to interlocking hoop reinforcement were conducted also on wall bridge piers. The range of the shear span ratios, a/d, is between 1.9 and 5.0.

Table-1 Tests for interlocking hoop bridge piers conducted in Japan

Unit	Type of hoop	Section w*d (mm)	Shear span ratio a/d	Loading direction	Volume ratio of lateral restraining reinforcement (%)	Ultimate Ductility factor	Organization	Year	Legend in fig.2
1	2 hoops	900*600	5	bridge axis	0.19	7.2	JH	1998	●
2	2 hoops	900*600	5	bridge axis	0.29	8.4		1999	
3	2 hoops	900*600	5	bridge axis	0.52	7.1		1999	
4	2 hoops	1000*600	5	bridge axis	0.32	6	PWRI[1]	2000*	▬
5	2 hoops	850*600	1.9	perpendicular	0.46	11.9	JH	1997	■
6	2 hoops	850*600	1.9	perpendicular	0.23	8		1997	
7	2 hoops	850*600	1.9	perpendicular	0.12	8		1997	
8	2 hoops	600*400	3	perpendicular	1.04	9.9	Tanaka and R.Park[2]	1993*	◆
9	2 hoops	600*400	3	perpendicular	0.83	10		1993*	
10	2 hoops	600*400	3	perpendicular	1.11	12		1993*	
11	2 hoops	500*300	3	perpendicular	0.49	8.3	Yanagishita,Tanaka and R.Park[3]	2000*	
12	2 hoops	538*300	3	perpendicular	0.49	9.7		2000*	
13	2 hoops	500*300	4.8	perpendicular	0.49	8		2000*	
14	4 hoops	1300*500	6.4	bridge axis	0.31	9.8	JH	2002	▲
15	4 hoops	1300*500	6.4	bridge axis	0.51	10		2002	
16	4 hoops	1300*500	6.4	bridge axis	0.75	7.9		2002	

1) Public Work Research Institute Ministry of Construction : Study of simplified reinforcement, Pulic Work Reserch Institute Ministry of Construction

2) H.Tanaka, R.Park : Seismic Design and Behavior of Reinforced Concrete Columns with Interlocking Spirals, ACI Structual Journal, 1993.3-4

3) F.Yagishita, H.Tanaka, R.Park : Cyclic Behavior of Reinforced Concrete Columns with Spirals, Journal of Concrete Structures, 2000.11

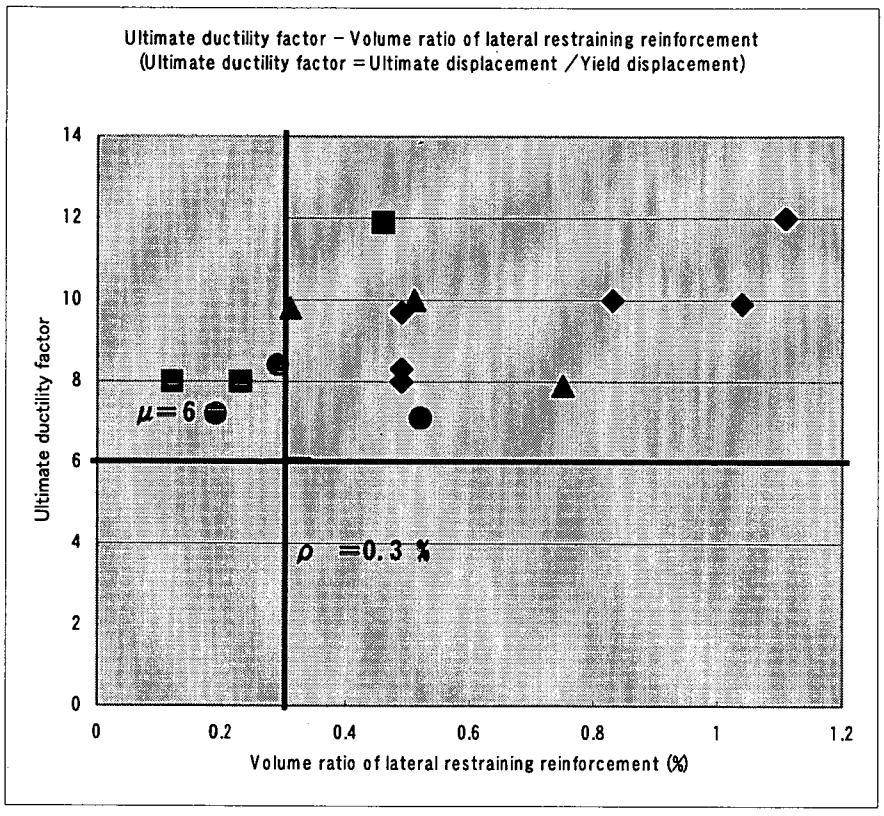


Fig.-2 Graph of the relation between hoop reinforcement ratio and ductility factor

Fig.-2 plots the relation between the hoop volume ratio and its ductility factor.

As can be seen from Table-1 and Fig.-2, the ductility factor of 6 or greater can be obtained when the center to center pitch of the hoops is less than 0.75 times the diameter of pier and the hoop volume ratio is 0.3% or greater.

From the result above, as far as interlocking-hoop bridge piers falling within the extent of the test above are concerned, we consider it acceptable to develop design on the assumption that the ultimate ductility factor, can be obtained as 6 at the minimum, if the center to center hoop pitch is up to 0.75 times the pier diameter and if the design satisfies the design details for improving ductility of RC piers of Design Specifications of Highway Bridges with the exception of the omission of intermediate restraining reinforcement.

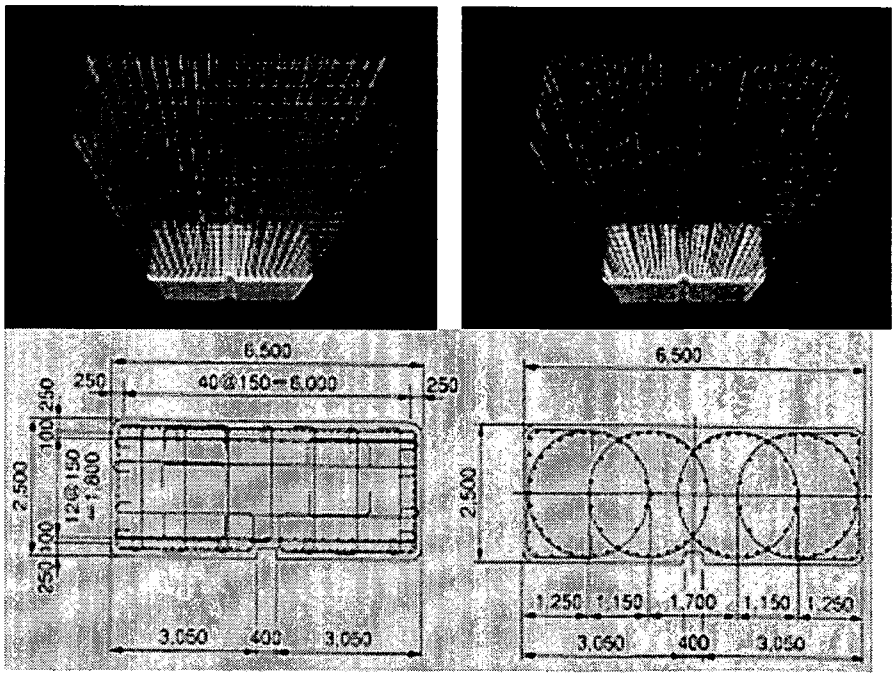
Furthermore, if it is mandated that the design should be based on the Standards mentioned above except for the calculation of the ultimate ductility factor, it will then necessitate designing the residual deformation volume as within 1/100 of the pier height in the light of ensuring their quick restoration performance when they are damaged. And as a result of this, check will be made in actual design tasks in order to ensure that excessive displacement will not be caused.

3. Economic effects of the application of the interlocking hoops to wall bridge piers

Table-2 compares the economic impacts when bridge piers with normal bar arrangement were changed to those with interlocking hoops. In this case, since the design details of the superstructure had been completed, we determined the volume of reinforcing steel in the axis direction in a manner that would produce the same ultimate strength before and after this change, in order to minimize the adverse effect on the foundation and superstructure of the alteration to the bar arrangement. Accordingly, we consider it possible to achieve a further cut in steel volume in the axis direction if the ductility improvement gained from adopting interlocking hoops can be reflected in the seismic design. Even though the ultimate bending strength of the steel is designed to be the same, it is possible to reduce the volume of hoops to about 60% of the steel for normal pier by omitting intermediate hoops and other means. Thus, the total work cost can be reduced by 10%. In the future, based on the result, we will study the range that will achieve cost reduction with the use of interlocking hoop reinforcement, and for bridge piers from which cost reduction can be expected, we think we will proactively work to change normal re-bar arrangement to interlocking spirals or hoops.

Table-2 Economic comparison when normal re-bar arrangement was changed to interlocking hoops

	Bridge pier with normal bar arrangement	Bridge pier with interlocking hoops	Interlocking /Normal
Sectional shape	6,500 x 2,500	6,500 x 2,500	-
Formwork (m^2)	306	306	0
The volume of longitudinal re-bar (t)	42.05	43.13	103%
The volume of lateral re-bar (t)	49.52	30.01	59%
Concrete volume (m^3)	276.25	276.25	100%
	¥17,100,000	¥15,400,000	90%



Normal bar arrangement Interlocking bar arrangement

Fig.-3 Example of changing the normal to interlocking bridge pier

4. Application range of bridge piers with interlocking hoops

1) Pier height

In many cases, bridge piers over 30 m in height are designed as a hollow pier in order to reduce the dead load. If the application of interlocking hoops is limited to piers with a hollow section, then if they are applied to piers exceeding 30 m, it may possibly require a larger-scale foundation due to the dead load. Consequently, it seems that the application range of interlocking hoops is limited to piers shorter than about 30 m.

For piers with less height, interlocking hoop reinforcement offers an advantage of obtaining high ductility. It cannot be said that this advantage is displayed, when bridge piers are too small in a/d. The lower limit of a/d in the past tests is about 2, and it seems appropriate that the application range of interlocking hoops should be 2 or greater in a/d.

Based on the above, we consider that the application range of interlocking hoop reinforcement in terms of pier height is generally between 5 m and 30 m.

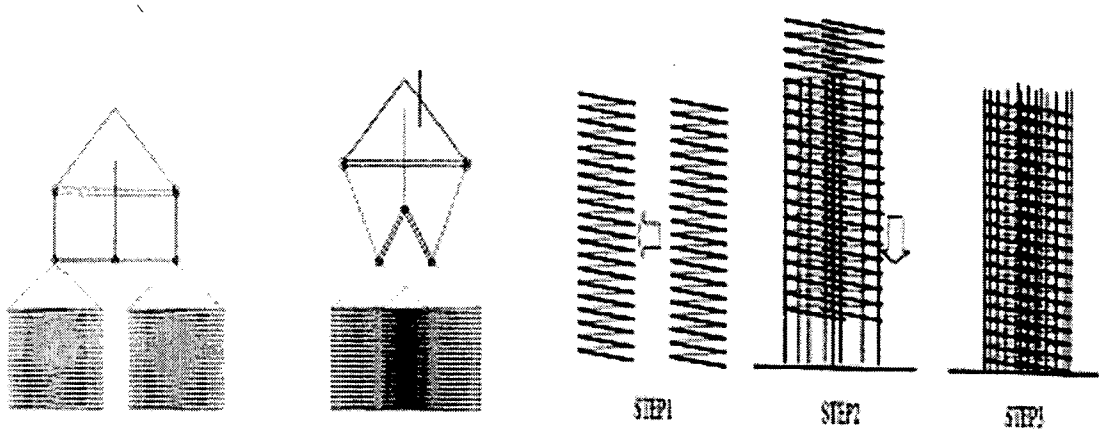
2) Sectional shape of pier

Although it is possible to attempt rationalization of re-bar arranging work by using spirals instead of hoops, it is difficult to fabricate spirals at the site, and when considering their transportation from the factory, the diameter is limited to 3.25 m or smaller. As described below, the maximum number of interlocking spirals in the direction perpendicular bridge axis, when they are used, is four for construction reasons, and if taking the center-to-center distance of the hoops as 75% of the pier diameter, the maximum interval in the direction perpendicular to the bridge axis becomes 10.56 m. Given the concrete cover over the re-bar, the maximum sectional area of the pier possible to be constructed using spirals is calculated as 3.5 m x 11 m. When exceeding this limit, the hoops need to be placed in two separate parts, considerably reducing the constructability.

In the case of a three-lane cross section and a PC single-cell box girder superstructure, the width of the lower floor slab is about 10 m. Even for bridge piers without overhang, it is possible to design them by using interlocking hoops.

5. Construction of bridge piers with interlocking hoops

Fig.-4 is a work flow diagram of placement status of spiral or hoops. As can be seen, hoops are put together while being suspended and then, keeping their position, are placed into the longitudinal reinforcing bars. Photo-2,3 shows the construction status of bridge pier with four interlocking spiral hoops. As can be seen, it was demonstrated through field application that rational construction of bridge piers with interlocking spiral hoops is possible when four or fewer hoops are used.



(1) Pattern diagram of adjusting center-to-center pitch of spirals

(2) Pattern diagram of placing spirals or hoops into the longitudinal reinforcing bars

Fig.-4 Pattern diagram of placement status of spirals or hoops

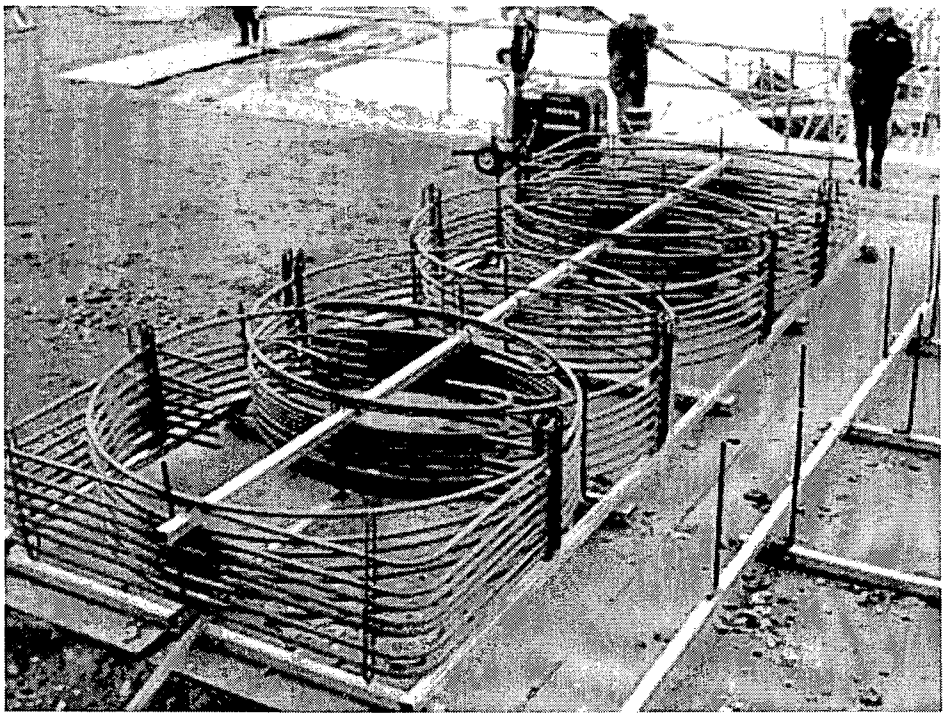
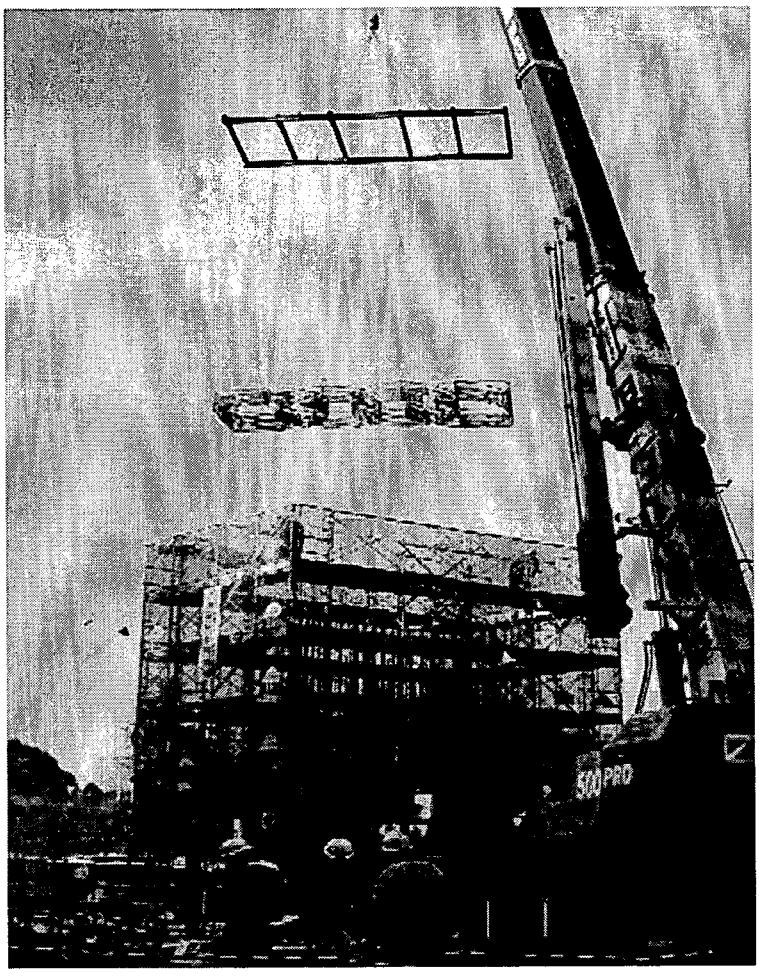
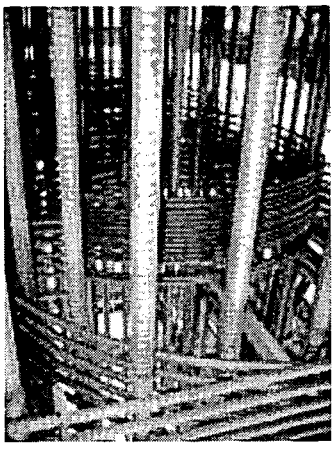


Photo-2 Construction status (1)





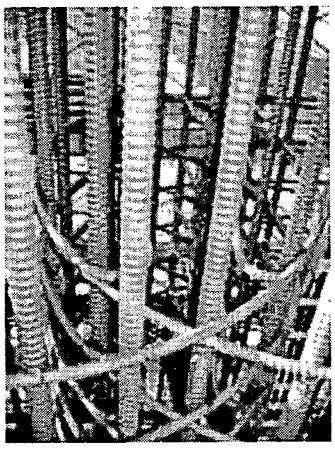


Photo-3 Construction status (2)

19th US-Japan Bridge Engineering Workshop

Seismic 3

co-Chairs:
M. Ishida & G. Lee

A Study on Site-Specific Strong Ground Motion for Seismic Retrofit Design of the Hanshin Expressway Long-span Bridges in Osaka Bay Area
T. Nishioka

Seismic Retrofit of the Poplar Street Bridge
M. R. Capron

Seismic Verification of Long-span Bridge of Honshu-Shikoku Bridges
C. Kawatoh

Seismic Design and Retrofit of Bridges on Missouri's Earthquake Priority Routes
S. Gupta

A STUDY ON SITE-SPECIFIC STRONG GROUND MOTION FOR SEISMIC RETROFIT DESIGN OF THE HANSHIN EXPRESSWAY LONG-SPAN BRIDGES IN OSAKA BAY AREA

Tsutomu NISHIOKA*, Toshihiko NAGANUMA*, Hidesada KANAJI* and Takao KAGAWA**

ABSTRACT

The site-specific strong ground motion in Osaka Bay Area is studied in order to estimate the seismic load for the seismic retrofit of the Hanshin Expressway long-span bridges. We consider the crustal earthquake and the plate boundary earthquake as the maximum credible earthquake deterministically. The empirical Green's function method and the stochastic semi-empirical Green's function method are used to predict the site-specific ground motion. The study shows that there are some differences in the acceleration response spectra between the predicted strong ground motion and the standard ground motion in the Japanese specifications for highway bridges.

1. INTRODUCTION

Many bridges suffered heavy damage from the Hyogoken-nanbu earthquake that struck the Kobe city in Japan on Jan. 17, 1995. The seismic retrofit program for the existing bridges made a full-fledged start slightly behind the restoration of the damaged structures in the wake of the disaster in Hanshin Expressway Public Corporation. Until today, we have already strengthened most of the middle- or small-scale brides seismically. But the long-span bridges, mainly located in Bay Route of the Hanshin Expressway network, have not retrofitted yet due to the financial problems.

Although most of the highway bridges are retrofitted seismically according to the standard seismic loads in the current Japanese specifications for highway bridges [JRA(2002)], it is desirable in view of earthquake engineering that the input ground motion for the seismic design of a structure is estimated in consideration of source, path and local site effects, shown in Figure 1. In this paper, the site specific strong ground motion for seismic retrofit design of the Hanshin Expressway long-span bridges are estimated and compared with the Japanese specifications for highway bridges in terms of the acceleration response spectra.

2. THE LONG-SPAN BRIDGES IN HANSHIN EXPRESSWAY NETWORK

The 18 sites of the Hanshin Expressway long-span bridges, mainly located along the coastline of Osaka Bay, are the objective sites to predict the strong ground motion. Table 1 is the list of the 18 long-span bridges, indicating regions, bridge names, bridge types, abbreviations of each bridge and longer natural periods between the longitudinal and transverse direction. The locations of the 18 bridges are shown in Figure 2.

* Hanshin Expressway Public Corporation

** Geo-Research Institute

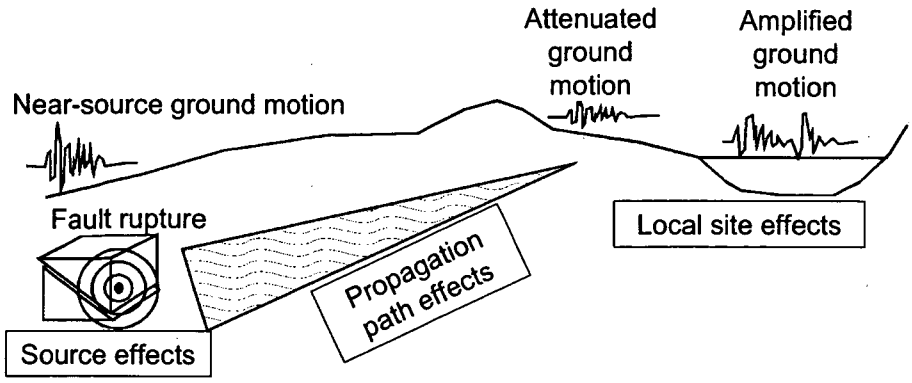


Figure 1 Schematic diagram of source, path and local site effects

Table 1 List of the 18 Hanshin Expressway long-span bridges

Region	Bridge	Type	Abbrev.	Period (s)
Kobe	Rokko Island	Lohse arch	rar	2.5
	Higashikobe	Cable stayed	hkb	4.9
	Shinashiyagawa	Girder	sas	2.5
	Nishinomiyako	Nielsen arch	nmk	2.0
North Osaka	Amagasakiko	Girder	amk	1.8
	Nakajimagawa	Nielsen arch	njk	1.2
	Kanzakigawa	Nielsen arch	kzk	1.2
	Shorenji	Girder	srj	1.8
Central Osaka	Umemachi	V-shape rigid frame	uto	1.6
	Tempozan	Cable stayed	tbz	3.8
	Minato	Gerber truss	mnt	4.6
	Nankosuiro	Lohse arch	msr	1.4
South Osaka	Hirabayashi	Girder	hrb	2.6
	Yamatogawa1	Cable stayed	ymt	3.1
	Yamatogawa2	PC Box Girder	yms	2.5
	Shinhamadera	Nielsen arch	sht	1.9
Far South Osaka	Harukigawa	Girder	hkk	2.5
	Kisiwada	Nielsen arch	kwt	2.9

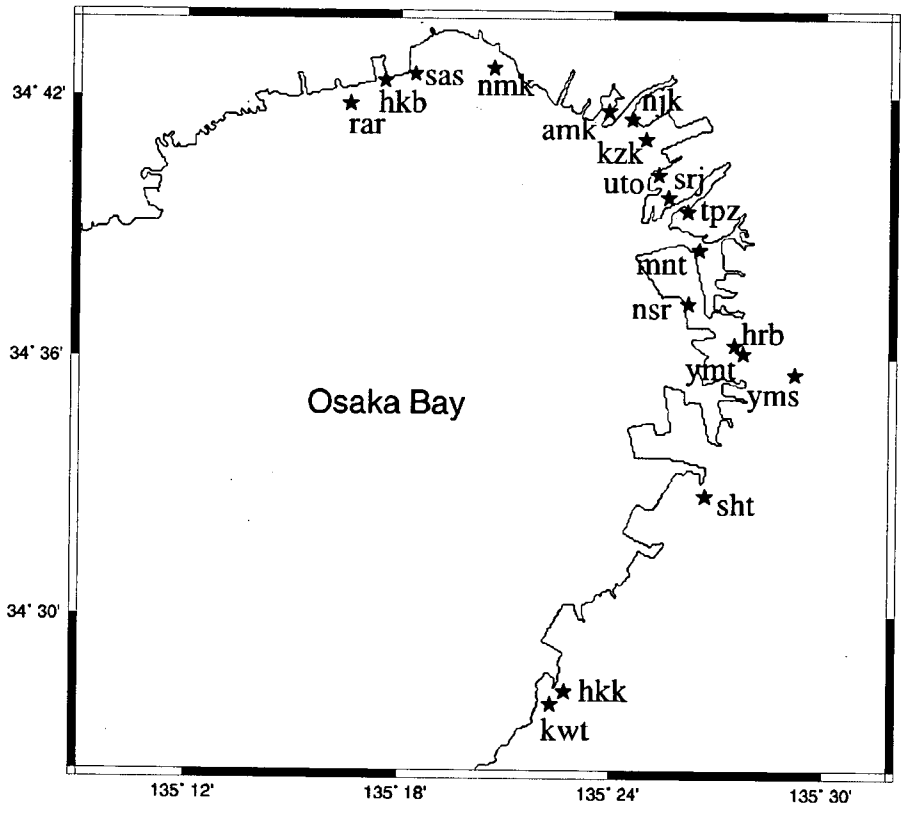


Figure 2 Locations of the 18 Hanshin Expressway long-span bridges

3. ACTIVE FAULTS IN OSAKA BAY AREA AND PLATE BOUNDARY FAULTS

There are 6 active faults recognized in Osaka Bay area, shown in Figure 3. As Rokko-Awaji faults triggered the 1995 Hogoken-nanbu earthquake only 8 years ago, they are neglected in this study. Out of the other 5 faults, Uemachi faults and Osaka Bay faults are selected on the basis of the peak ground acceleration (PGA) attenuation study.

In addition to the active faults in Osaka Bay Area, we consider the plate boundary faults located off the southwestern coast of Japan Islands. We adopt the fault model studied by the central government to predict the strong ground motion of the plate boundary earthquake. The fault model is shown in Figure 4.

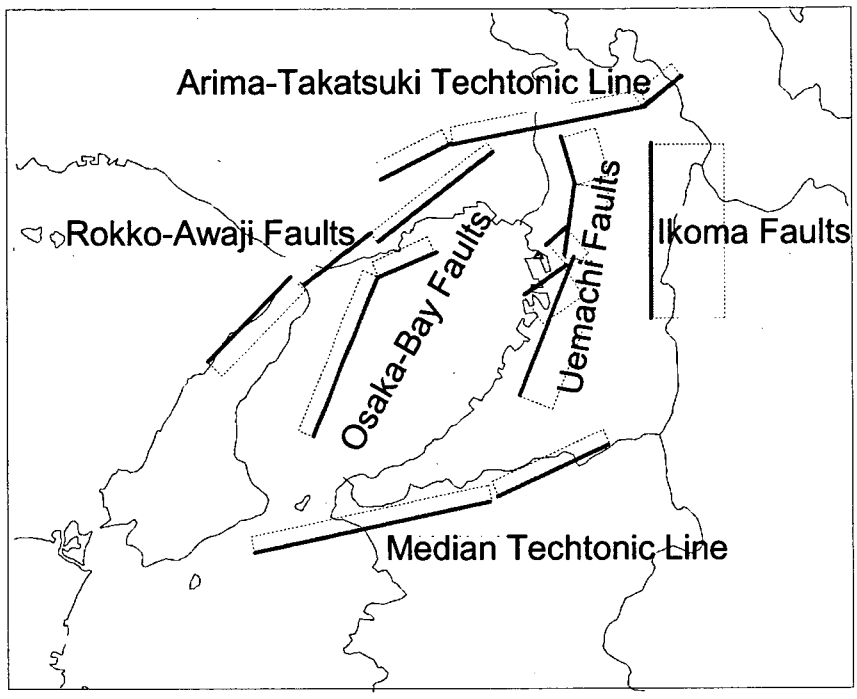


Figure 3 Active faults recognized in Osaka Bay Area

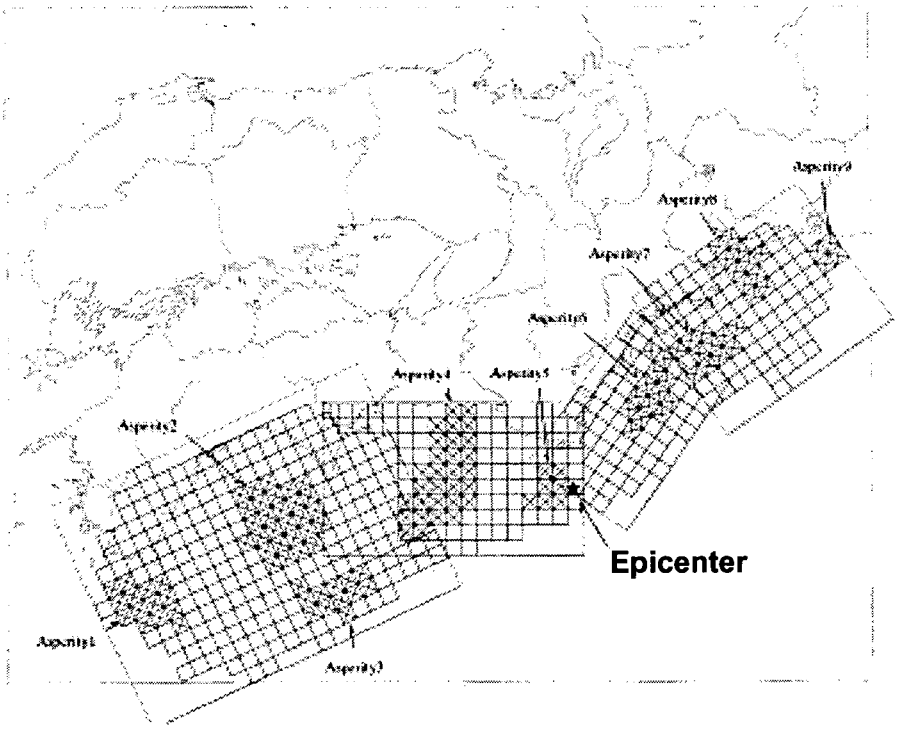


Figure 4 Fault model of the plate boundary earthquake

4. SYNTHESIS PROCEDURE OF STRONG GROUND MOTIONS

The strong ground motions are estimated for the crustal earthquake and the plate boundary earthquake respectively. We suppose that the active faults should cause the crustal earthquake and that the plate boundary faults should bring about the earthquake due to the continental plate movement. Two methods are used for simulating strong ground motion at a specific site resulted from a large earthquake. One is the empirical Green's function method [Irikura(1986)] and the other is the stochastic semi-empirical Green's function method [Boore(1983), Kamae and Irikura(1992)].

The empirical Green's function method is one of the most effective techniques for predicting strong ground motion for the purpose of seismic design of a structure. This method synthesizes ground motion at a site from observed records as empirical Green's function. A large earthquake is constructed by a superposition of many small earthquakes based on the regional scaling relation of source parameters. Figure 5 shows the schematic source model for synthesis. Since the method considers propagation path effects, local site effects, rupture propagation effects on the fault plane and geometrical relation effects between source and site, it is very powerful for predicting the strong ground motion by a future large earthquake. But appropriate records in the objective site are not always available as the empirical Green's function.

The stochastic semi-empirical Green's function method is a revised simulation method when no suitable observation data are available as empirical Green's function. This method uses the stochastically simulated small-event motion based on seismological spectral model as semi-empirical Green's function, instead of the actual observed records.

Since appropriate observation records don't exist as empirical Green's functions for the crustal earthquakes generated by Uemachi faults and Osaka Bay faults, we use the stochastic semi-empirical Green's function method to predict the ground motion of the crustal earthquake. On the other hand, we obtained suitable records in the objective region for the plate boundary earthquake. We use the empirical Green's function method to predict the ground motion of the plate boundary earthquake.

For the crustal earthquake, we consider 3-D topography of deep geologic structure in Osaka Bay Area and calculate the ground motion by the 3-D elastic finite-difference model [Graves(1996), Pitarka(1999)]. Figure 6 shows the 3-D topography of deep geologic structure in Osaka Bay Area. We simulate the ground motion of the crustal earthquake in use of the hybrid method. That is to combine the short period range (0.1-2.0sec.) by the stochastic semi-empirical Green's function method and the long period range (1.0-10.0sec.) by the 3-D elastic finite-difference model. This hybrid method takes the advantages of the two methods.

The prediction procedure in this study is shown in Figure 7.

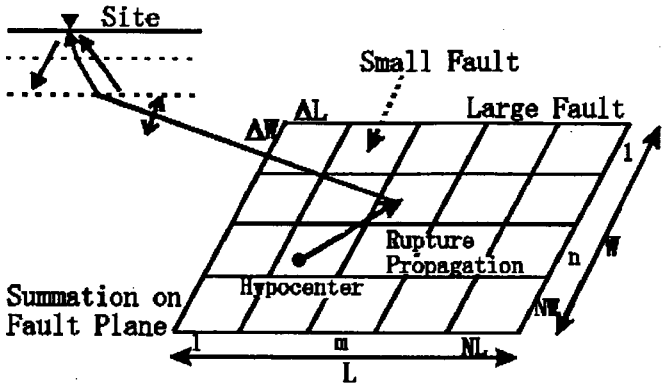


Figure 5 Schematic source model for synthesis

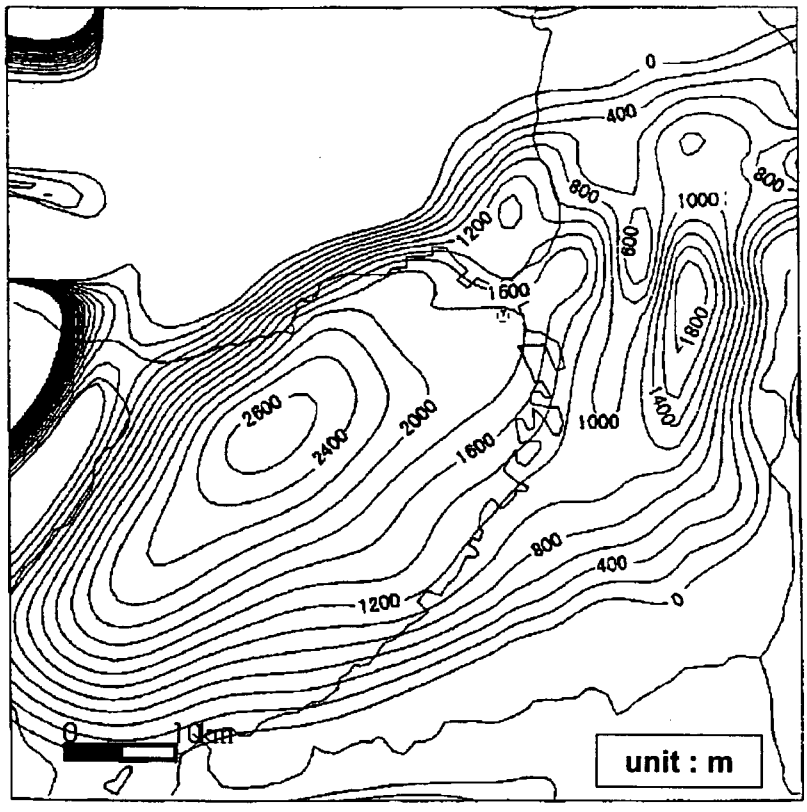


Figure 6 3-D topography of deep geologic structure in Osaka Bay Area

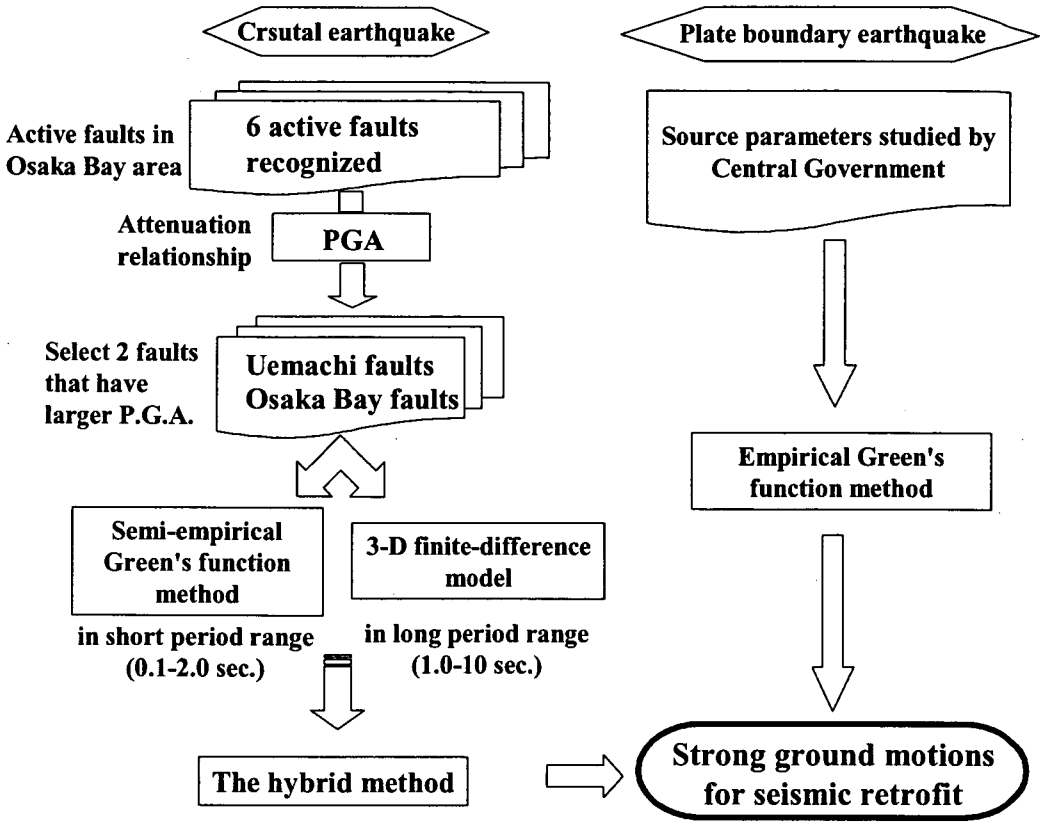


Figure 7 Prediction procedure

5. STRONG GROUND MOTIONS OF THE CRUSTAL EARTHQUAKE

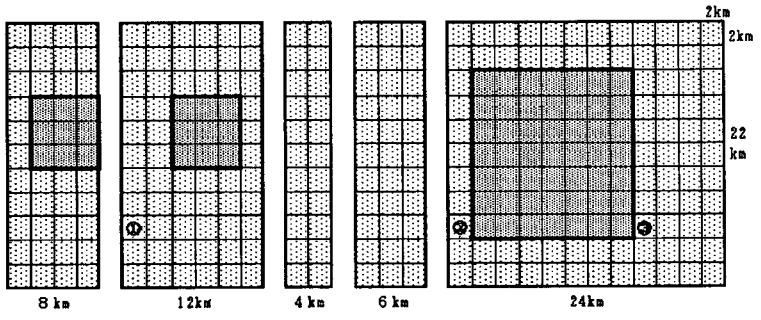
The source parameters of Uemachi faults and Osaka Bay faults are shown in Table 2. Uemachi faults consist of 5 segments. The moment magnitude of the maximum credible earthquake (MCE) by Uemachi faults is assumed to be M_w=6.9. Osaka Bay faults are made up of 2 segments and the moment magnitude of MCE is M_w=6.7. For synthesizing the strong ground motion, we assume 5 fault rupture scenarios to Uemachi faults and Osaka Bay faults. The 5 types of the asperities are shown in Figure 8. These assumptions are based on Irikura(2002)'s research.

The acceleration response spectra S_A of the synthesized ground motion are calculated in the 5 regions (Kobe, North Osaka, Central Osaka, South Osaka and Far south Osaka). The non-linearity of the seismic response of the surface ground is taken into account by the SHAKE program. Figures 9-13 are the S_A of the simulated ground motion. The spectrum of the Japanese specifications for highway bridges, drawn with broken line in Figures 9-13, is the one of the strong ground motion of the maximum credible crustal earthquake in the soil classification 3 [JRA(2002)]. The comparison shows that most of the S_A of the site-specific ground motion in the short period range are smaller than those of the

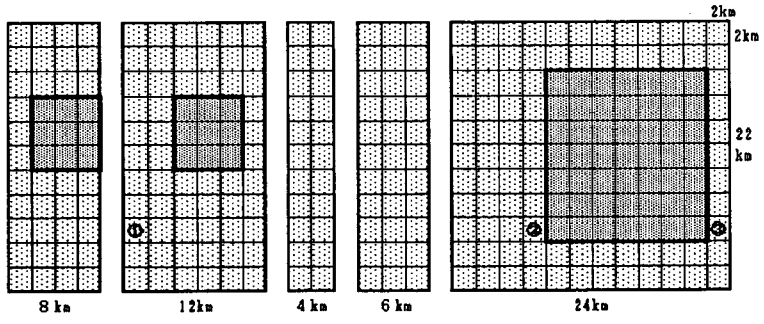
specification. However, in some longer periods, the S_A of the site-specific ground motion go beyond those of the specification. Since the long-span bridges have long natural periods, we should pay much attention to the S_A of the site-specific ground motion in the long period range when we conduct the seismic retrofit design of those structures.

Table 2 Source parameters of Uemachi faults and Osaka Bay faults

	Uemachi faults					Osaka Bay faults	
	Part A	Part B	Part C	Part D	Part E	Part A	Part B
Length (km)	8	12	4	6	24	26	10
Width (km)	22					16	
Strike (deg.)	-16.2	7.4	48.4	55.8	21.4	-158	-114
Dip (deg.)	60					80	
Moment magnitude M_w	6.9					6.7	
Seismic moment (10^{19} N·m)	0.38	0.58	1.29	0.32	0.19	1.03	0.39

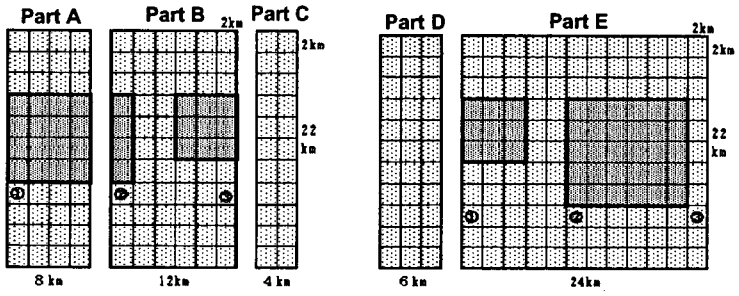


(a) Uemachi faults, Type 1

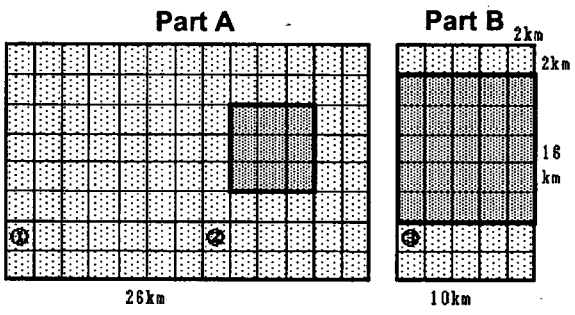


(b) Uemachi faults, Type2

Figure 8 Assumed asperities in Uemachi faults and Osaka Bay faults

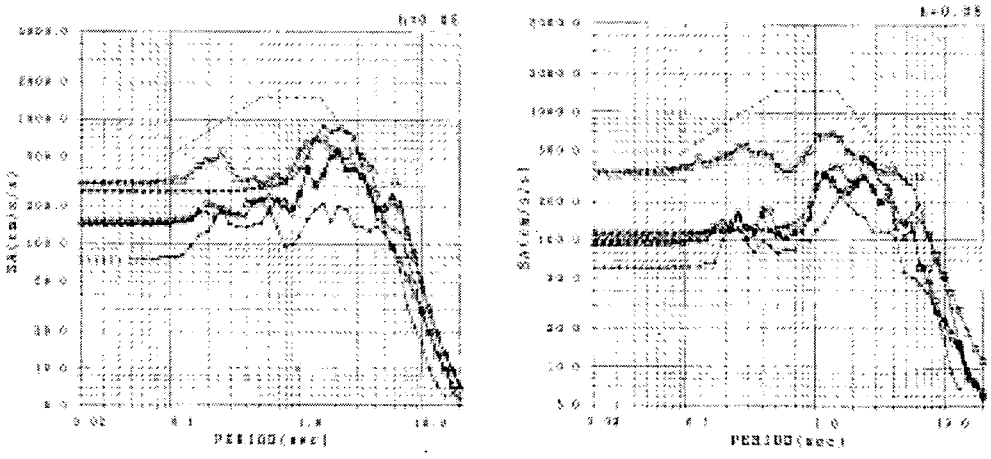


(c) Uemachi faults, Type 3 (d) Uemachi faults, Type 4



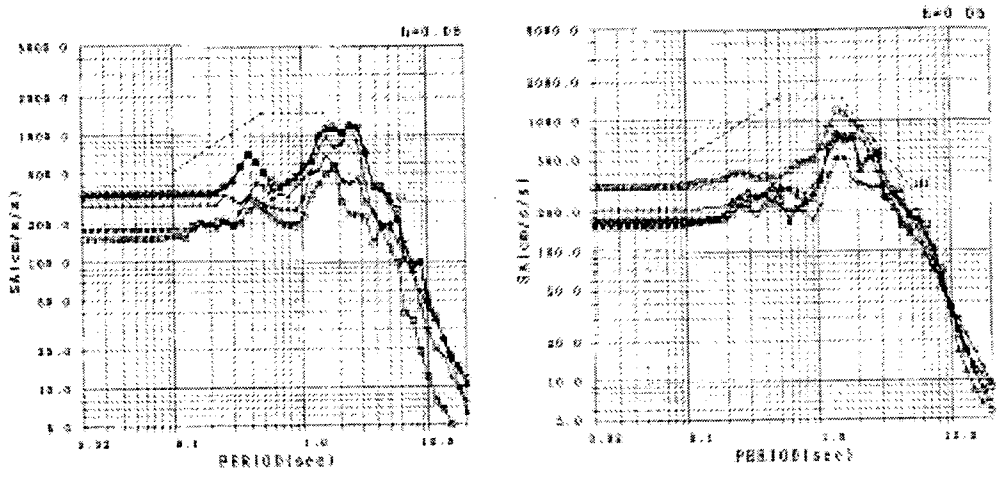
(e) Osaka Bay faults, Type5

Figure 8 Assumed asperities in Uemachi faults and Osaka Bay faults



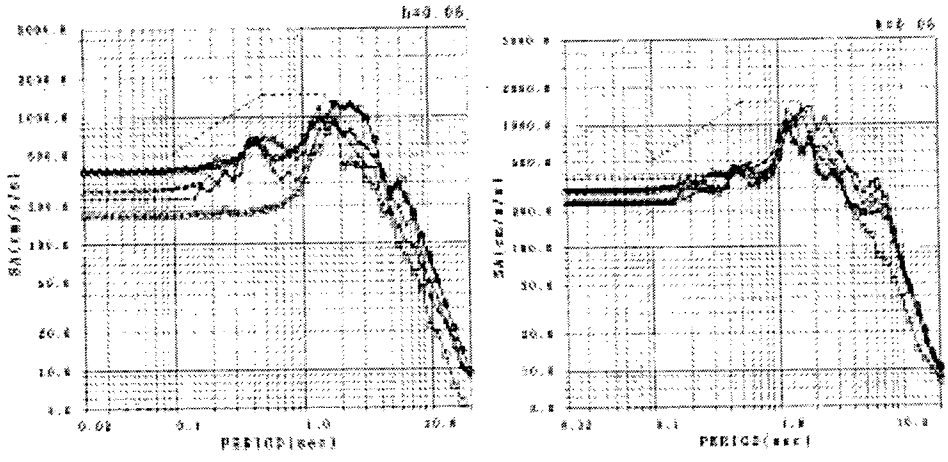
(a) EW component (b) NS component

Figure 9 Acceleration response spectra S_A of the ground motion in Kobe Region



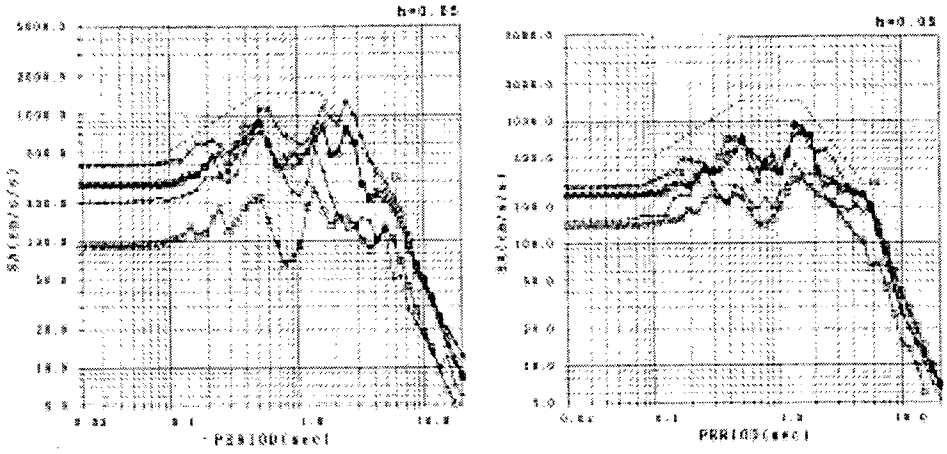
(a) EW component (b) NS component

Figure 10 Acceleration response spectra S_A of the ground motion in North Osaka Region



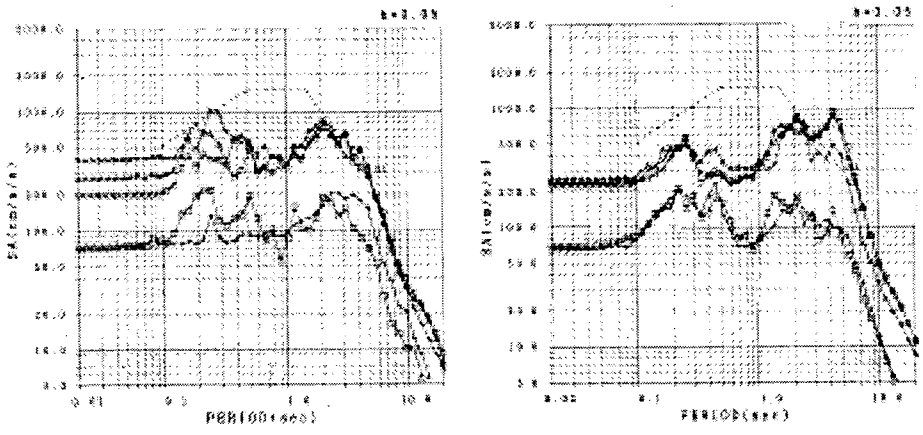
(a) EW component (b) NS component

Figure 11 Acceleration response spectra S_A of the ground motion in Central Osaka Region



(a) EW component (b) NS component

Figure 12 Acceleration response spectra S_A of the ground motion in South Osaka Region



(a) EW component (b) NS component

Figure 13 Acceleration response spectra S_A of the ground motion in Far South Osaka Region

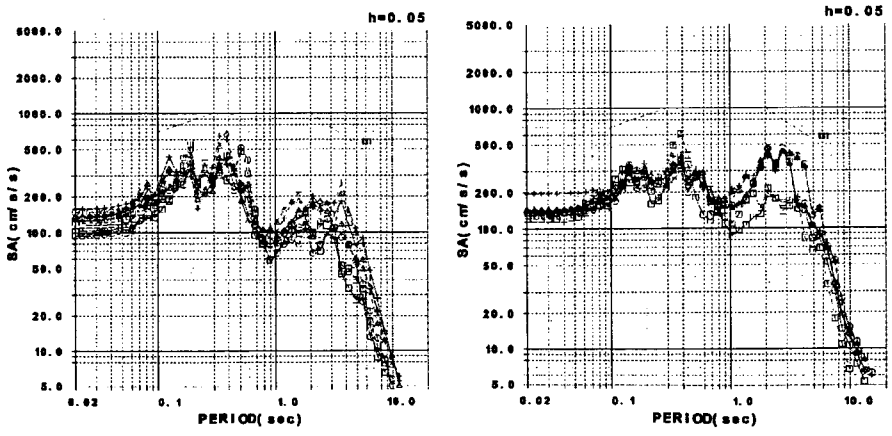
6. STRONG GROUND MOTIONS OF THE PLATE BOUNDARY EARTHQUAKE

The source parameters of the plate boundary faults are shown in Table 3. The fault model, shown in Figure 4, is based on the study of the central government. There are Nankai faults and East Nankai faults off the southwestern coast of Japan Islands. The moment magnitude of MCE is assumed to be M_w=8.6 when Nankai faults and East Nankai faults are ruptured at the same time.

The S_A of the synthesized ground motion in the 5 regions are shown in Figure 14. The broken line is the S_A of the Japanese specifications for highway bridges with the maximum credible plate boundary earthquake in the soil classification 3 [JRA(2002)]. The S_A of the site-specific ground motion are found to be below the S_A of the specifications in most period range.

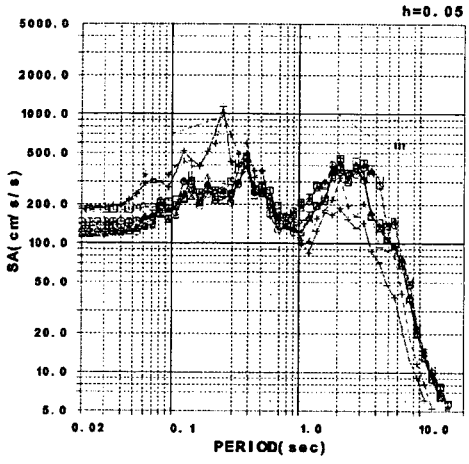
Table 3 Source parameters of the plate boundary faults

	Nankai faults		East Nankai faults	
	Part A (West)	Part B (East)	Part A (West)	Part B (East)
Length (km)	220	170	120	130
Width (km)	160	100	80	110
Strike (deg.)	245	270	215	235
Dip (deg.)	7	14	14	10
Moment magnitude M_w	8.6			
Seismic moment (10^{22} N·m)	1.08			

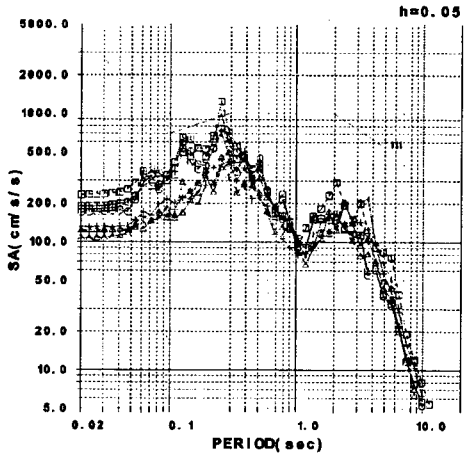


(a) Kobe Region (b) North Osaka Region

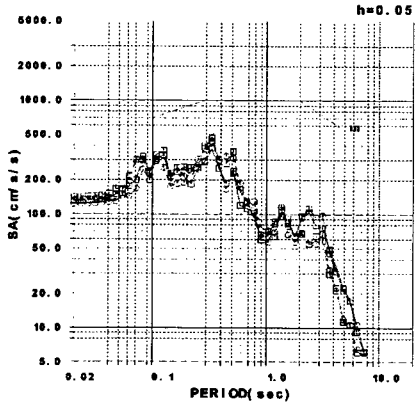
Figure 14 Acceleration response spectra S_A of the ground motion of the plate boundary faults



(c) Central Osaka Region



(d) South Osaka Region



(e) Far South Osaka Region

Figure 14 Acceleration response spectra S_A of the ground motion of the plate boundary faults

7. CONCLUSION

The site-specific strong ground motion in Osaka Bay Area is studied in order to estimate the seismic load for the seismic retrofit of the Hanshin Expressway long-span bridges. The study shows that there are some differences in the acceleration response spectra between the predicted strong ground motion and the standard ground motion in the Japanese specifications for highway bridges. Since it is desirable to consider source, path and local site effects for the seismic design of a structure, the site-specific ground motion should be taken into consideration, especially for the important structures such as the long-span bridges.

ACKNOWLEDGEMENT

We have precious advice from Prof. Tadanobu Sato and Prof. Sumio Sawada, Kyoto University in this study. We would like to express our appreciation to them.

REFERENCES

Boore, D. M.(1983): Stochastic simulation of high-frequency ground motions based on seismological models of the radiation spectra, *Bulletin of the Seismological Society of America*, 73, 1865-1894.

Graves, R. W.(1996) : Simulating Seismic Wave Propagation in 3D Elastic Media Using Staggered-Grid Finite Differences, *Bulletin of the Seismological Society of America*, 86, 1091-1106.

Irikura, K.(1986): Prediction of strong acceleration motion using empirical Green's function, 7th Japan Earthquake Engineering Symposium, 151-156.

Irikura, K. et al.(2002): The revised recipe and its verification sot the prediction of the strong ground motion, 11th Japan Earthquake Engineering Symposium, 567-572. (in Japanese)

Japan Road Association (2002): Specifications for highway bridges, Part V seismic design, Maruzen Inc.

Kamae, K. and K. Irikura (1992): Prediction of site specific strong ground motion using semi-empirical methods, 10th World conference of Earthquake Engineering, 801-806.

Pitarka, A.(1999): 3D elastic finite-difference modeling of seismic motion using staggered-grid with non-uniform spacing, *Bulletin of the Seismological Society of America*, 89, 54-68.

Seismic Retrofit of the Poplar Street Bridge

Mark R. Capron[1]

Abstract

This paper summarizes the seismic evaluation, retrofit strategy, design, and construction of the seismic retrofit for the Poplar Street Bridge over the Mississippi River at St. Louis. The 660 meter (2,165 foot) structure consists of two parallel five span continuous roadways with orthotropic steel deck and steel box girders. The seismic evaluation considered three levels of design earthquakes and identified deficiencies in the bearings, reinforcement splices in the columns and piers, and one foundation. The retrofit included adding longitudinal shock transmission units, transverse shear blocks, column splice confinement, shear walls, and rock anchors.

Introduction

Jacobs Civil Inc. (formerly Sverdrup Civil) has supported the Missouri Department of Transportation (MoDOT) in evaluating and designing retrofits for several major bridges and bridge complexes throughout the state. Evaluation of these structures using current guidelines (FHWA 1983, 1995) has identified significant seismic deficiencies in critical bearing, column, and foundation elements, in spite of design acceleration coefficients as low as 0.12g. This paper presents the application of the seismic retrofitting guidelines to the Poplar Street Bridge over the Mississippi River at St. Louis. Design of seismic retrofits for this structure was developed in two phases: Phase 1, consisted of seismic evaluation and development of a retrofit strategy, and Phase 2, consisted of additional studies to refine the strategy and final design of selected alternatives. Construction of the seismic retrofit was completed in late 2002 at a cost of 6.2 million dollars. The following paragraphs present a description of the bridge, the approaches and results of the seismic evaluation, the retrofit strategy, construction issues, and conclusions from this project.

Description of the Bridge

The Poplar Street Bridge carries more than 130,000 vehicles per day across the Mississippi River at St. Louis, Missouri via U.S. 40/I-64 and I-55/70, see Figure 1. The 660 meter (2,165 foot) structure consists of two parallel five span continuous roadways, each providing four lanes of traffic. Span lengths from west to east are 91, 152, 183, 152, and 81 meters (300, 500, 600, 500, and 265 feet). Two variable depth steel box girders support each roadway. The deck is of orthotropic steel plate construction consisting of a deck plate, trapezoidal longitudinal ribs and transverse floor beams. The deck plate acts as the top flange of the transverse floor beams, the trapezoidal ribs, and the main longitudinal box girders. The reinforced concrete substructure from west to east consists of a hollow shear wall type structure at Pier 1, solid shafts with rectangular columns and continuous cap beams at Piers 2, 3, 4, and 5, and a hollow shear wall structure at Pier 6. The

[1] P.E., Jacobs Civil Fellow, Project Manager, Jacobs Civil, Inc.

substructure is founded on 1.8 meter (6 foot) diameter caissons to rock at Piers 1, 3, 4, 5, and 6, and a spread footing on rock at Pier 2. The superstructure is supported on the substructure by expansion bearings that allow rotation using spherical bearings and longitudinal translation through guided rollers at Piers 1, 2, 4, 5, and 6, and fixed bearings that allow only rotation with spherical bearings at Pier 3. Sverdrup and Parcel and Associates originally designed the bridge in 1963. The pier reinforcing steel is spliced near the base of the columns with lap splices of 24 bar diameters in length and confined with #5 ties spaced at 30 cm (12 inches), as typical of bridges designed in this timeframe. There are also similar splices in the reinforcing steel where the base of the pier shafts connects to the footings.

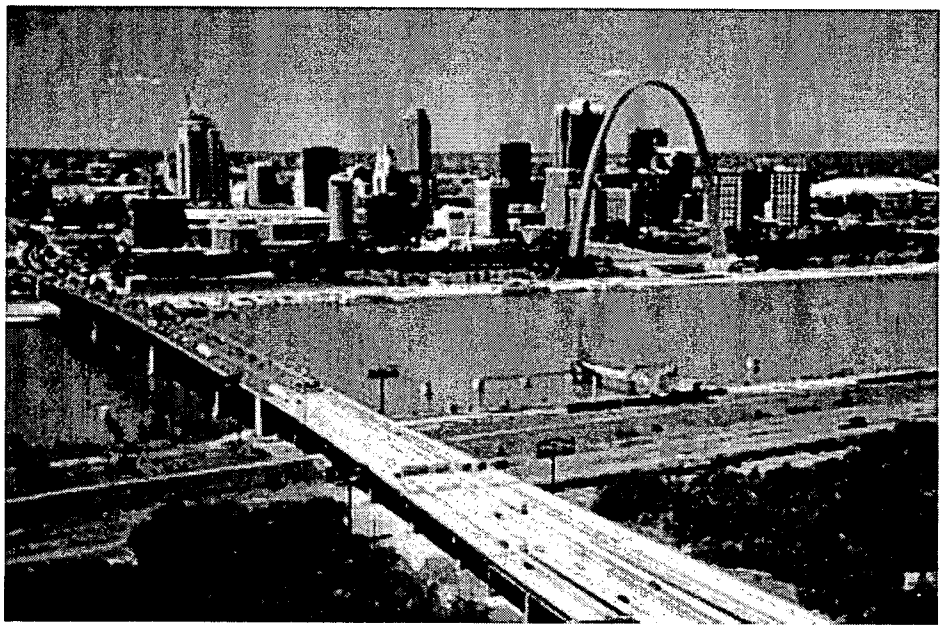


Figure 1. Poplar Street Bridge in St. Louis, Missouri

Seismic Evaluation

The analytical model used in the seismic evaluation consisted of over 15,000 degrees of freedom and included representation of the deck, box girders, and Piers 1 and 6 with shell elements, while the bearings, cross frames, and Piers 2, 3, 4, and 5 were modeled with beam elements. Linear spring elements were included in the model to represent the stiffness of the soil/foundation system, and mass was applied to account for unmodeled components such as parapets, major sign structures, and one lane of traffic live load per roadway.

Dynamic analysis was performed using the linear elastic response spectrum method and spectra based on the parameters and return periods shown in Table 1. In addition to the three design spectra, the analysis considered cases with completely rigid soil springs, with linear soil springs, with existing bearings, and with expansion bearings supplemented by "rigid" longitudinal restrainers.

Table 1. Design Response Spectra Parameters

Acceleration Coef. (A)	Soil Type	Return Period (yr.)	Reference
0.12	2	475	(AASHTO 1996)
0.23	S_2	2,500	(FEMA 1991)
0.50	2	---	Maximum Credible Earthquake (MCE) - estimated from unpublished literature review

The results of the dynamic analyses were evaluated using the Capacity /Demand (C/D) ratio method presented in the guidelines (FHWA 1983, 1995). In the context of the guidelines, C/D ratios approximate the percentage of the design earthquake at which a particular component can be expected to fail; therefore, ratios less than 1.0 indicate insufficient capacity. The significance of individual C/D ratios
depends on the consequences of failure of each particular component, or groups of components. Table 2 summarizes the C/D ratios computed for the existing structure at the various design levels.

Table 2. C/D Ratios for Existing Structure

	C/D Ratios			
	Design Level			
Component	AASHTO 475 yr.	FEMA 2500 yr.	MCE	Remarks
Bearing Displacement	8.9	5.2	1.7	Unrestrained bearings at Piers 1 and 6, Method 2, Method 1 0.59 all levels
Bearing Force (longitudinal)	0.3	0.3	0.1	Pier 3 only point of longitudinal seismic resistance
Bearing Force (transverse)	0.8	0.5	0.2	All Piers similar
Cap Beam Yielding	0.5 - 0.7	0.4 – 1.2	*	No collapse mechanisms at AASHTO Pier 3 near collapse mechanism at FEMA * Collapse mechanisms Piers 3, 4, and 5 at MCE
Splice Details at base of Columns	0.2 – 0.6	0.1 – 0.4	*	
Splice Details at base of Piers	0.2 – 0.9	---	---	Longitudinal collapse mechanism at AASHTO, ratios not computed for FEMA 2500 or MCE, results < AASHTO
Foundation Rotation	0.9 - 10.8	0.7 – 8.8	---	Ratios not computed for MCE
Cross Frames	1.2 – 3.7	0.6 – 2.0	0.3 – 0.9	

The C/D ratios for the existing structure identified significant deficiencies in the bearings, the lap splices at the base of the columns, the lap splices at the base of the Piers at the AASHTO design level. Evaluation of the structure with engaged restrainers at expansion Piers 1, 2, 4, and 6 showed notable improvement in the critical C/D ratios of Pier 3 at the AASHTO design level, but indicated the need to increase the overturning capacity of Pier 1. Comparison of the AASHTO 475 year and FEMA 2500 year design levels showed similar types of retrofits would be required for both levels, while the MCE design level would require major changes in the structural response, which could conceptually be provided by isolation bearings, and/or major increases in capacity.

Seismic Retrofit Strategy

Based on the findings and recommendations of the evaluation, MoDOT selected the AASHTO 475 year spectrum as the design level for the seismic retrofit, and a retrofit strategy that involved adding shock transmission unit type longitudinal restrainers to expansion Piers 1, 2, 4, 5, and 6; increased transverse force capacity of the bearings at Piers 1, 4, 5, and 6 using reinforced concrete shear blocks and steel bumpers; strengthening the longitudinal and transverse capacity of the Pier 3 bearings; adding rock anchors to the Pier 1 foundations; confinement of the lap splices in the reinforcement at the base of the columns; and reinforcement of the lap splices at the base of Piers 2, 3, 4, and 5. The construction cost of these retrofits was estimated to be on the order of 7.2 million dollars.

In the context of this retrofit, shock transmission units refer to devices that are designed to allow slow thermal expansion movements of the existing bearings and to lock-up and resist relatively fast movements, such as caused by earthquake loading. These devices are also referred to as force transmitters or lock-up devices. Also, the concept of adding shock transmission units to the existing expansion piers was adopted over replacing the bearings with seismic isolation bearings to minimize disruption of traffic on the bridge, to maintain the functionality of the existing bearing system, and to avoid the construction issues and costs associated with changing bearings on this major structure.

During Phase 2, the retrofit strategy was further refined by evaluating damper versus shock transmission unit longitudinal restrainers at all piers; investigation of using longitudinal restrainers at Piers 2, 4, and 5 with bearing seat extensions at Piers 1 and 6; investigation of the longitudinal shear capacity of Piers 1 and 6; investigation of alternatives for confining the lap splices in the column reinforcement; and investigation of alternatives for reinforcing the lap splices at the base of the piers.

The study of retrofitting with dampers, which are designed to dissipate significant amounts of energy as the structure moves longitudinally under earthquake loading, included time history dynamic analysis of the structure. These analyses used were based on AASHTO spectra compatible synthetic ground motions and damper characteristics developed from recommendations from damper manufacturers. Based on the results of this study, shock transmission units were selected for the retrofit, primarily because obtaining force reductions with the dampers was dependent upon the ability of the existing bearings to displace through multiple cycles under seismic loading. Because the actual displacement characteristics of the existing bearings could not be readily quantified, the shock transmission units, which did not require significant bearing displacement, were believed to provide a more reliable alternative to dampers for this project.

The analysis of retrofitting with longitudinal shock transmission units at all piers versus only the interior piers, showed that the former alternative provided greater longitudinal displacement control, and greater capacity for resisting seismic loading, as expected. The final longitudinal restrainer configuration provided four 1.56 mega-Newton (350 kip) shock transmission units at each of the expansion bearings at Piers 2, 4, and 5,

and two 2.59 mega-Newton (500 kip) shock transmission units at each of the expansion bearings at Piers 1 and 6.

Evaluation of the longitudinal shear capacity of Piers 1 and 6 showed that these piers did not have sufficient longitudinal capacity to resist the design level restrainer forces. Consequently, the retrofit design included addition of reinforced concrete shear walls inside of Piers 1 and 6 to provide the required capacity. Also, because the depth to rock at Pier 1 was less than 8 meters (26 feet), the retrofit included adding rock anchors through the grade beams at the base of the pier, to increase overturning resistance.

Confinement of the lap splices near the base of the 4 meter (13 foot) by 3.7 meter (12 foot) rectangular columns with conventional grout filled elliptical steel jackets was considered undesirable for this project because the jackets would be exposed to stream flow during flood stages, and ice flow during the winter. Investigation of composite wrap alternatives showed that this approach would not provide the required confinement near the centers of the faces of these large columns. Because of the limitations of these alternatives, confinement of the lap splice regions by steel plates with closely spaced post-tensioned steel rods was selected for the retrofit design. This approach provided minimal horizontal exposure to stream and ice forces, and tension in the rods, which were extended into the core of the column, provided the desired confining pressure.

While the lap splices near the connection of the base of the pier shafts and the footings are poorly confined, like the columns, the location below the mud line and about 15 meters (50 feet) below the surface of the river, made retrofit of these details difficult. Retrofit alternatives that were investigated included drilling vertically through the pier walls and adding grouted post-tensioned steel rods that were continuous through the splice region and anchored into the footings, and external confinement that would be installed inside dewatered coffer dams, or installing precast concrete segments without dewatering. Based on evaluation of the cost of these alternatives, and the associated construction risks, along with evaluation of the ductility demands and potential failure modes associated with the existing details, a strategy of no retrofit was selected at the base of the piers.

Construction Issues

The following points summarize the major construction issues that were addressed on the project.

- Because the bridge is a major transportation link for the region, minimizing disruption of traffic on the bridge during construction was a major project objective. To address this issue, the Contractor elected to perform all construction activities from below the bridge, using barges for work in the river, and working from the ground, when possible during low water. This approach required coordination with barge operators on the river, but was accomplished with minimal disruption of construction work, and no disruption of the traffic on the bridge.

- Construction of the steel plate confinement retrofit for the column splices required installation of over 6,600 tensioned rods. To minimize conflicts between the rods and

the existing column reinforcement, ground-penetrating radar was used to locate the reinforcing steel, and the rod layout was planned for each location, prior to fabrication of the plates or drilling the holes for the rods.

- Installation of the brackets for the shock transmission units required core drilling through the pier cap beams, which were approximately 3 meters (10 feet) thick, and installing high strength steel rods. In addition to control of the accuracy of the drilling operations, this modification required selection of a grouting material and installation method that would that would provide sufficient strength and durability, and allow sufficient construction time with sufficient flow characteristics under the temperature conditions that were expected at the time of construction.

- Installation of the shear walls inside Piers 1 and 6 required consideration of how the formwork, reinforcement, and concrete would be placed, and the formwork removed within the confined space of the piers. Construction access to these areas was gained by cutting 2.4 meter (8 foot) by 2.7 meter (9 foot) openings in the pier walls. These openings also were used to provide access for the necessary construction equipment for installing the rock anchors through the grade beams inside of Pier 1. These temporary openings were closed with reinforced concrete, after work inside the piers was completed.

- Construction of the various retrofit measures required field verification of dimensions to sufficient tolerance for fabrication of retrofit components. In some cases, templates were developed for existing bolt patterns to facilitate fit-up of fabricated steel components.

- Fabrication, testing, and delivery of the shock transmission units required a majority of the 17-month duration of the project, and were major scheduling considerations.

Conclusion

Seismic evaluation of this structure using current guidelines identified deficiencies in the bearings, piers, and foundations, in spite of a design acceleration of only 0.12g. A retrofit strategy was developed and implemented for the selected design level that involved adding shock transmission units to the existing bearings, and strengthening critical substructure components. Figures 2 and 3 show the completed retrofits of Pier 2 and the shock transmission units and transverse shear blocks at Pier 1. Construction of the retrofit was completed at a cost of 6.2 million dollars in late 2002.

Acknowledgment

The Author wishes to express appreciation to the Missouri Department of Transportation and the Federal Highway Administration for their support in the development of this project. The Author also wishes to acknowledge the Massman Construction Co. for constructing the project, and Taylor Devices, Inc. for supplying the shock transmission units for the project.

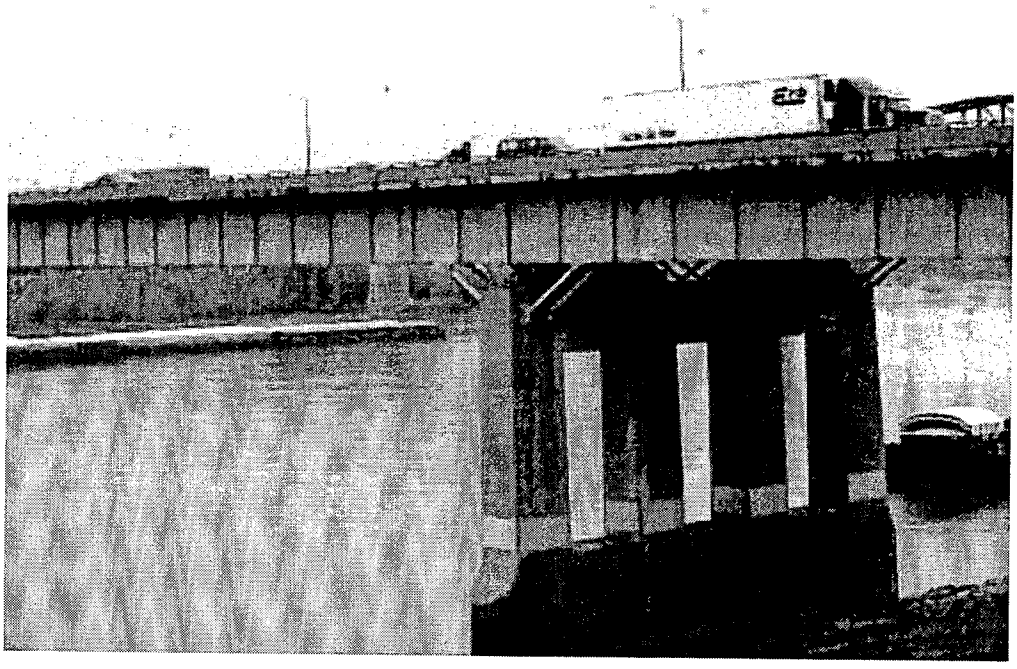


Figure 2. Pier 2 with retrofit installed

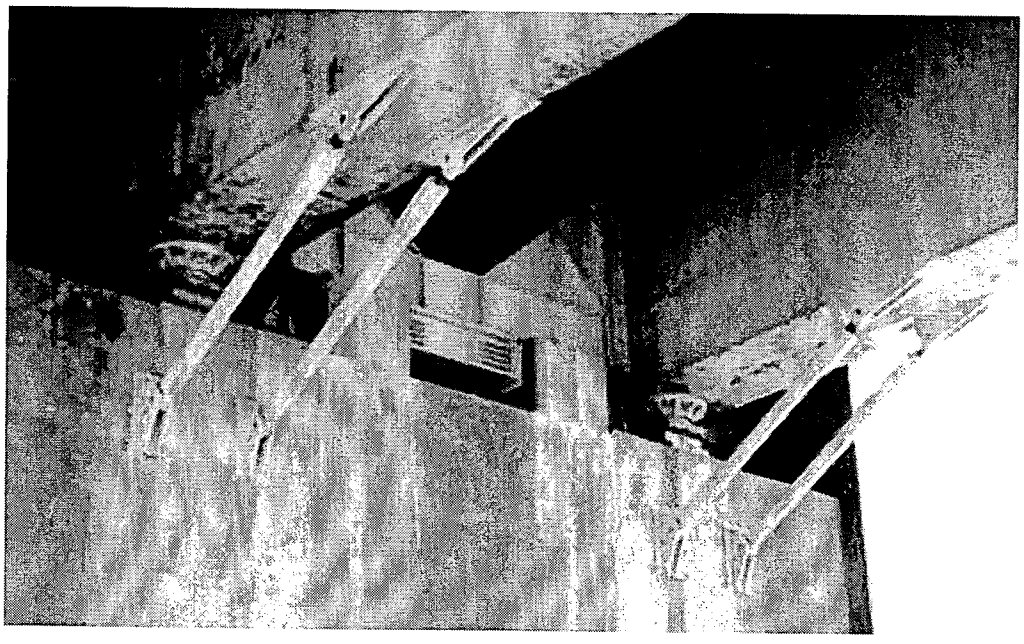


Figure 3. Pier 1 retrofits

References

American Association of State Highway Transportation Officials (AASHTO). 1996. "Standard Specifications for Highway Bridges." Sixteenth Edition. Washington, D.C.

Federal Emergency Management Agency (FEMA). (1991). "NEHRP Recommended Provisions for Seismic Regulations for New Buildings." No. 222. Washington, D.C.

Federal Highway Administration (FHWA). (1983). "Seismic Retrofitting Guidelines for Highway Bridges." Report No. FHWA/RD-83/007, McLean, VA.

FHWA. (1995). "Seismic Retrofitting Manual for Highway Bridges." Publication No. FHWA-RD-052, McLean, VA.

SEICMIC VERIFICATION OF LONG-SPAN BRIDGE OF HONSHU-SHIKOKU BRIDGES

Chihiro kawatoh[1], Koji Kawaguchi[2]

Abstract

Honshu-Shikoku Bridge Authority (HSBA) has carried out seismic verification for the very strong ground motion (level2 earthquake) to Long-span bridges which HSBA managed after Hyogoken-Nambu earthquake. This paper presents a policy of the seismic verification including the examples of Akashi-Kaikyo Bridge and Ohnaruto Bridge and indicates principle for seismic retrofit of Honshu-Shikoku Bridges.

1. Introduction

The Hyogoken-Nambu Earthquake, which struck Japan on January 17, 1995, had an epicenter very close to the Akashi-Kaikyo Bridge. A number of investigations into the effects of the earthquake on the bridge were carried out immediately after the event. These checks led to some remedial steps, such as a change in stiffening girder length, but almost no damage to the main structure was found. The bridge was completed successfully with safety and its function was ensured.

On the other hand, long-span bridges over the straits and its approach bridges of Honshu-Shikoku Bridge Authority (HSBA) were designed using seismic design standards of HSBA and seismic design specifications for Highway bridges of 1990 version or specifications before that and were not being taken into consideration as for the strong motion such as a Hyogoken-Nanbu earthquake. HSBA decided that it was necessary to grasp that seismic performance of existing bridges in order to maintain appropriately. Then HSBA selected the target bridges for and have continued out the seismic analysis and verification.

This paper describes the evaluation of the seismic performance of the long-span bridges over the strait, the policy of the seismic retrofit and examples of seismic verification of the Akashi-Kaikyo Bridge and multi-columns foundation of Ohnaruto Bridge.

2. Outline of Honshu-Shikoku Bridges

The Honshu-Shikoku Bridges (HSB), consisting of three routes, connected Honshu-and Shikoku-island across the Seto Inland Sea as follows (from eastern side);
Kobe-Naruto (Kobe-Awaji- Naruto Expressway)
Kojima-Sakaide (Seto-Chuo Expressway & JR Seto Ohhashi Line, often called the Seto Ohashi Bridge)

1. Engineering Information Division, Long-span Bridge Engineering Center, Honshu-Shikoku Bridge Authority
2. Manager, ditto

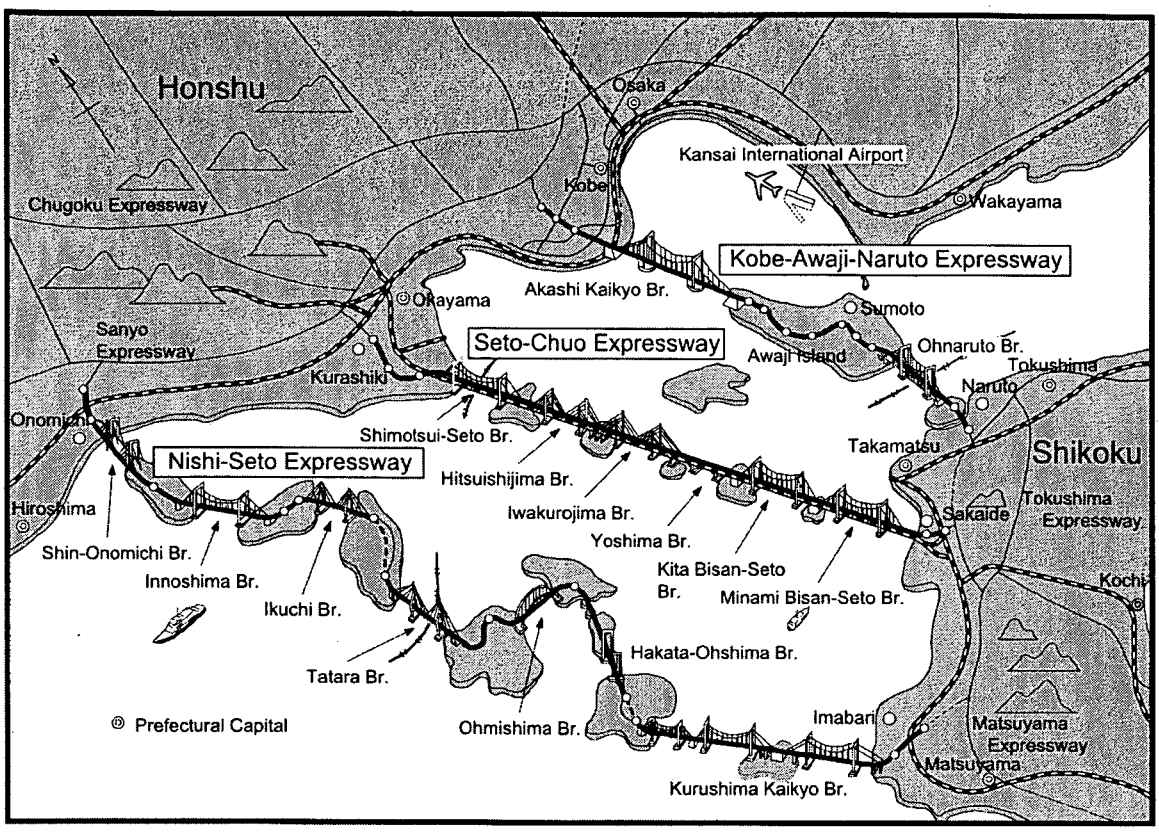


Figure1 Three routes of Honshu-Shikoku Bridges

Onomichi-Imabari (Nishi-Seto Expressway, often called Setouchi-Shimanami Kaido)

The construction of the three routes was finished except about 13 kilometers, two sections located in both Ikuchi and Ohshima islands, on Onomichi-Imabari route. Figure1 shows the three routes of Honshu-Shikoku Bridges.

3. Seismic verification

3.1 Seismic standard and codes for Honshu-Shikoku Bridges

Table-1 shows the seismic standard and codes for HSB [1] [2] [3]. These standards were made for long-span bridges with over 200m-center span. Seismic coeds for Akashi-Kaikyo Bridge and Kurushima-Kaikyou Bridge were special ones, and contained the latest seismic information at that time. But these standards do not reflect the influence of an inland near-field type earthquake (level2 type II earthquake, Seismic Specification for Highway Bridges, Japan Road Association, 1996,[4] here in after JRA). Therefore HSBA decided to verify the seismic performance of bridges for leve2 type II earthquake.

3.2 Target bridges for seismic verification

HSBA selected bridges over the strait and its approach bridges for seismic verification. The bridges over the straits and its approach bridges should have the same seismic

Table-1 Seismic Standard and Codes for Honshu-Shikoku Bridges

Design Standard		HSBA Seismic Design Standard		Akashi kaikyo Bridge Seismic Design Code		Kurushima Kaikyo Bridge Seismic Design Code	
		Input Earthquake Ground Motion	Seismic Performance Level	Input Earthquake Ground Motion	Seismic Performance Level	Input Earthquake Ground Motion	Seismic Performance Level
Level 1 Earthquake Ground Motion (Highly probable during the bridge service life)		The earthquake of about M=8 that an occurrence is expected 1-2 times in 100years at far out at sea of Kii peninsula or Shikoku island	Not exceeding allowable stress	○ Calculated by statistical theory from historically recorded earthquakes. The acceleration response spectrum has a return period of 150 years. ACC=0.8G	Not exceeding allowable stress	○ Calculated by statistical theory from historically recorded earthquakes. The acceleration response spectrum has a return period of 150 years. ACC=0.75G	Not exceeding allowable stress
Level 2 Earthquake Ground Motion	Type I Earthquake Ground Motion (an interplate earthquake)	Type I is taken into consideration on small earthquake level		○ Its magnitude and epicenter distance is assumed to be 8.5 in Richter scale and 150km ACC=0.8G	Not exceeding allowable stress	○ Its magnitude and epicenter distance is assumed to be 8.5 in Richter scale and 200km, and another is 8.0 in Richter scale and 150km ACC=0.75G	Not exceeding allowable stress
	Type II Earthquake Ground Motion (an inland near-field earthquake)	× Type II is not being taken into consideration		Type II is taken into consideration on Level 1 earthquake in probability calculation		The same as the left	

performance for the strong ground motion, because there is no alternative route in the over-strait portion.

The number of seismic verification bridges is 44. The total number of seismic verification bridge is 51 which were added the shed structure. Seismic verification of 24 bridges were finished in 51 bridges in substructure and 22 bridges were finished in 53 bridges in superstructure (2 bridges are added on account of superstructure type).

4. Earthquake ground motion

4.1 Level 2 type I ground motion

Because HSB are located on the ground with better condition (Vs=600m/s) than type I ground(more than Vs=300m/s), earthquake ground motion of site will be different from the characteristic of ground motion defined with Specifications for Highway Bridges.

Based on seismograms recorded at the Kobe Meteorological Observatory of the Japan Meteorological Agency (JMA Kobe), the earthquake wave at the top of the granite bedrock, which was adopted as the seismic bedrock in the seismic design of the bridge, was calculated and used as the input wave for analysis. And for the purpose of the verifying the suitability of this input wave, HSBA calculated the input wave by fault model using the active faults parameters. The strength of acceleration spectrum estimated by fault model was less than the JMA Kobe wave acceleration spectrum. Therefore, HSBA decided JMA Kobe wave as seismic verification wave for the level2 type II earthquake.

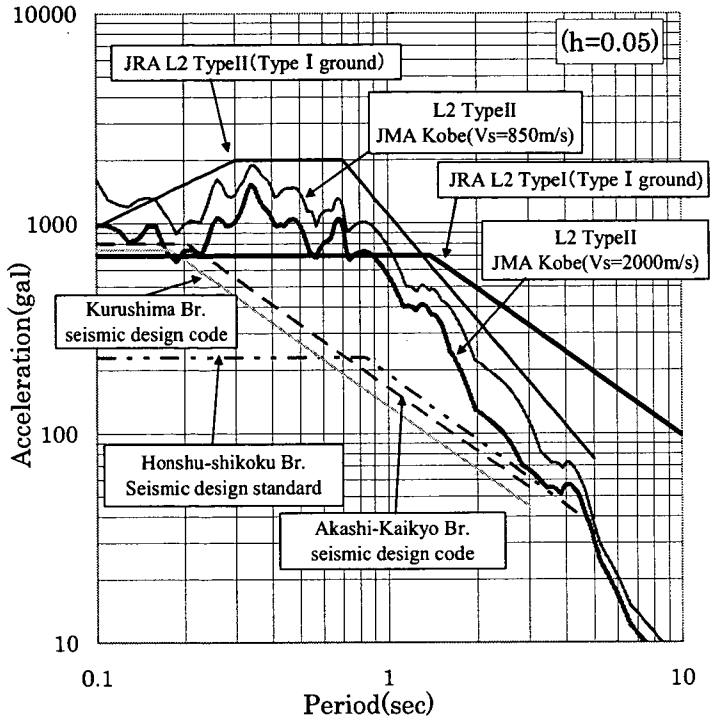


Figure2 Comparison of acceleration of each standard

4.2 Level2 type I ground motion

Earthquake ground motion was calculated by fault model using the Nankai earthquake fault parameters. The calculated acceleration spectrum of the Nankai earthquake was included in the JMA Kobe wave acceleration spectrum. On the other hand, table-1 shows that the level2 type I earthquake is taken into consideration in the seismic design codes of Akashi-Kaikyo Bridge and Kurushima-Kaikyo Bridge as the design earthquake ground motion.

5. Example of seismic verification

5.1 Akashi-Kaikyo Bridge

(1)Outline

The Hyogoken-Nambu Earthquake caused seabed ground movements in the vicinity of the Akashi-Kaikyo Bridge, shown in Fig-3, which was under construction at that time.

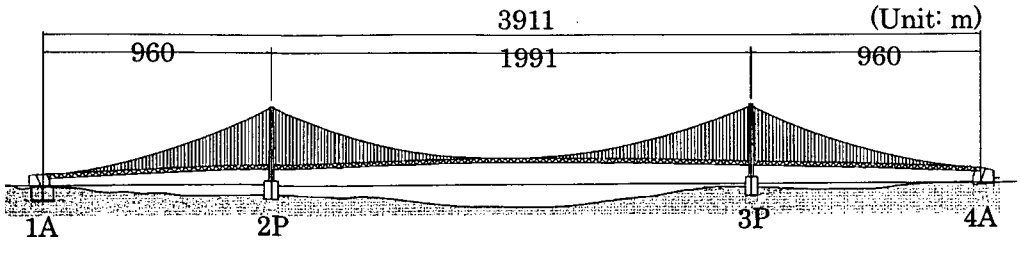


Figure3 General View of Akashi-Kaikyo Bridge after Earthquake

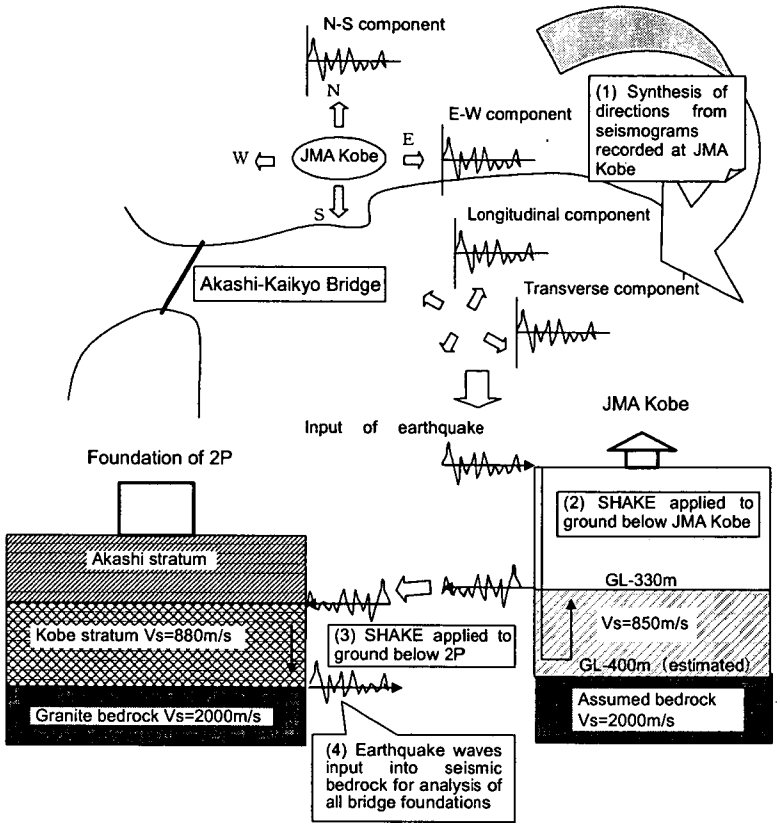


Figure4 Calculation of Earthquake Wave Input into Seismic Bedrock

Since this earthquake occurred directly beneath the bridge, and such an occurrence had not been considered in the original seismic design of this bridge, the HSBA decided to check the bridge in its completed state for resistance to same scale earthquake as the Hyogoken-Nambu Earthquake.

Based on the JMA Kobe earthquake wave, the earthquake wave at the top of the granite bedrock, which was adopted as the seismic bedrock in the seismic verification of the bridge, was calculated and used as the input wave for analysis. Figure 4 shows an outline of this calculation.

(2)Analytical condition

To evaluate that the foundation of the complete bridge are able to withstand earthquake motions on the same scale as those experienced in the Hyogoken-Nambu Earthquake, a time-history response analysis was performed by using the earthquake waves obtained in section 4 and 5.1. Since the bridge foundations would respond nonlinearly to ground motions set up by large earthquake such as the Hyogoken-Nambu Earthquake, a nonlinear time-history analysis of the tower-foundation system using FEM model was performed. Strain dependency of ground and uplift characteristic of foundation were taken into account.

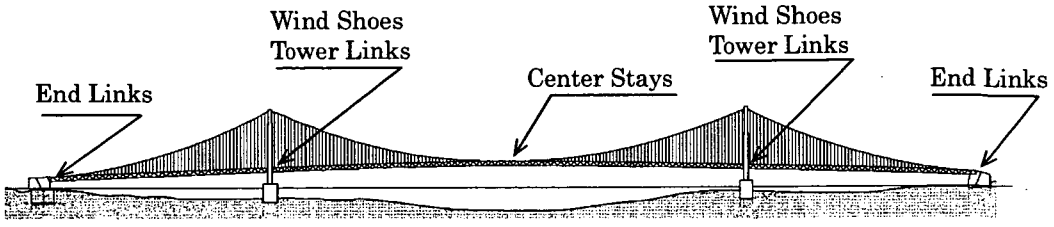


Figure5 Location of Links, Wind Shoes and Center Stays

As same as the foundation, a time-history response analysis was carried out to verify resistance of the superstructure of the complete bridge by using effective earthquake motion. A three-dimensional frame model of the bridge including its foundations was used for the analysis. For damping factor of the superstructure, nonlinear characteristic were not taken into account because it was assumed its response would remain the elastic range. The damping factor of the towers and cables were assumed to be 1%. Further, the damping factors of the girder were assumed to be 2%.

(3)Results of analysis

1) Superstructure

The maximum stresses developed in the tower shaft corner were calculated. These calculations showed that the maximum stresses in 2P and 3P tower would be 434 and 430MPa, respectively, which are below the yield stress value of 451MPa.The axial forces acting on the towers were calculated. Even at minimum, a compressive force of 133MN acted on the base of the east shaft of 2P tower, and there was no tensile force. The maximum axial forces developed in the tower links and end links were within the allowable limit, respectively.

Of the reactions at the wind shoes, the maximum reaction was 22,952kN in the case of the shoe on the central span side of the 2P main tower. Although this value exceeds the limit value of 17,640kN, it seemed to have no effect on the overall stability of the suspension bridge system. The tension induced in hangers and center stays were below the limit values of the original design standards. The relative displacement of the girder ends at the anchorages and towers were found to be within the movable range of the expansion

Table-2 Stability of foundations

	Safety factor for bearing capacity	Safety factor for sliding	Direction of calculation
1A	3.33	4.43	Longitudinal direction
2P	1.67	2.01	Transverse direction
3P	2.27	2.58	Transverse direction
4A	4.39	1.58	Longitudinal direction
Allowable Limit Value	2.00	1.20	-

joints at each point. Figure5 shows the location of links, wind shoes and center stays.

2) Foundations

Based on the forces acting on the base of the foundations, which were obtained from nonlinear time-history analysis of the tower-foundation system using the FEM model, the foundations were checked for stability. As can be seen in table-2, the design safety factors are satisfactory, except at the case of the 2P foundation. Although the safety factor for bearing capacity at 2P foundation is less than the allowable value of the original design code, the 2P foundation is considered to be secured, because the result was obtained by a non-linear FEM time-history analysis method which was considered to be more realistic than the linear FEM time history analysis method used in the original design.

(4)Conclusions

Nonlinear time-history analysis by the FEM model has been applied to a tower-foundation system and the foundations are verified to be stable when exposed to earthquake motion of the same scale as the Hyogoken-Nambu Earthquake. Three-dimensional model considering nonlinearity of dynamic restoring forces is applied to a response analysis of the superstructure and the superstructure of the bridge in its completed state is also verified to be stable.

5.2 Multi-column foundations of Ohnaruto Bridge

(1)Outline

The Ohnaruto Bridge is a 3-span 2-hinged stiffening-truss suspension bridge. Figure6 shows the general view. The piers for towers adopted a multi-column foundation system, in which the tidal current flows between columns, to minimize both the force of tidal current acting on the piers and disturbance of the tidal flow, which creates whirlpools, a well known sightseeing stuff. Photo1 shows the multi-column foundation of 3P tower.

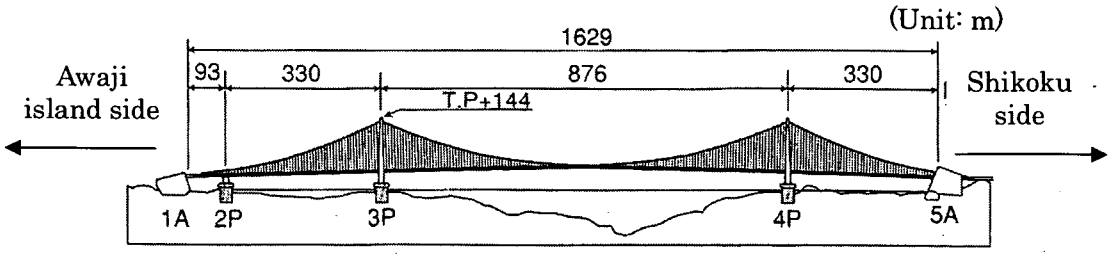


Figure6 General View of Ohnaruto Bridge

The pier was composed of columns and footing. Double sets of 8 columns of a 4m diameter each are aligned in a rectangle with two 7m diameter columns at each center, and the footing caps atop the sets of columns. These columns and footing are RC structure. These columns were composed of RC piers and steel-pipes, which were not strength members, but they were designed as RC piers protection members from outer damage. Since the earthquake motion for seismic verification is stronger than the original design earthquake motion, the steel pipe was regarded as strength member in the seismic analysis. Figure7 shows the outline of structure of the multi-column foundation.

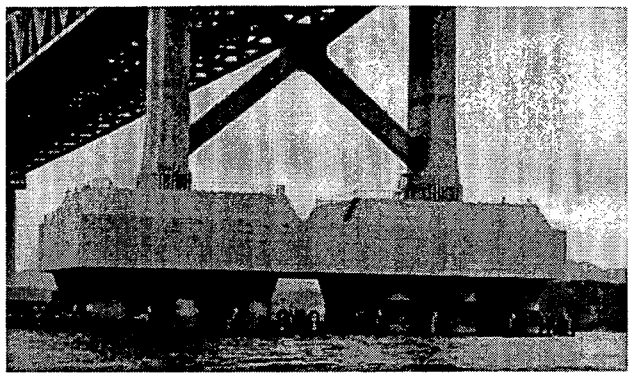


Photo1 Multi-column foundation

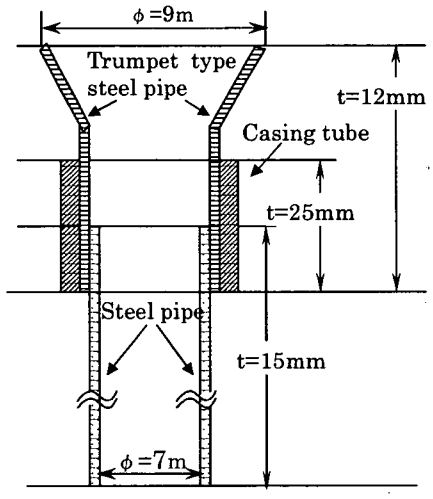


Figure7 Structure of 9m diameter column of multi-column foundation

(2)Analytical condition

A three-dimensional frame model of bridge including multi-column foundations was used for time-history analysis. JMA Kobe earthquake wave calculated in section 4 was used as the input wave for analysis. The influences of ground for multi-column foundation were taken into account by using the Penzien model. The relationship between bending moment and curvature of multi-column was modeled to tri-linear model, and Takeda model was used for a hysteretic model. The damping factor of the superstructure was assumed to be 2%, and Rayleigh damping was adapted.

(3)Results of analysis

The distribution of the bending moment and shear force of the 7m diameter column at 3P tower are shown in Fig-8, 9. Figure8 shows that bending moment is smaller than yield bending moment with all length of column. Although bending moment at some columns exceeds the yield bending moment slightly, bending moment of rests of column were within the yield bending moment. Therefore, multi-column foundations have enough strength for bending moment. It can be seen that shear force exceeds the strength of shear

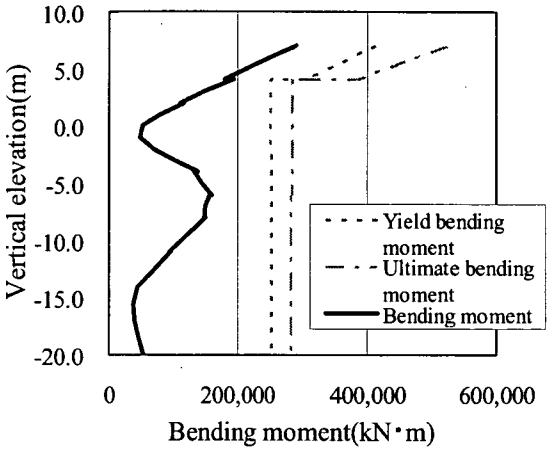


Figure 8 Distribution of Bending moment

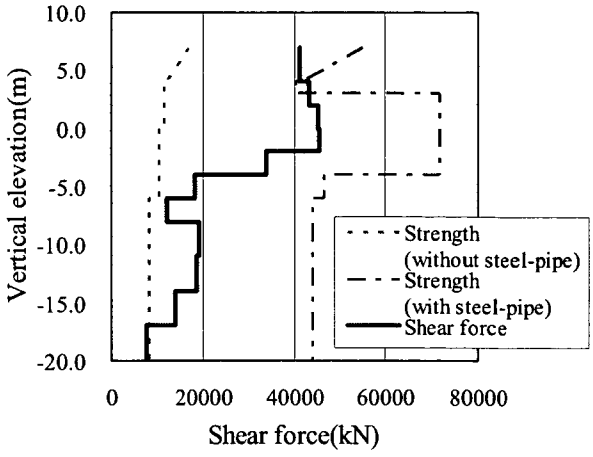


Figure9 Distribution of Shear force

force at small part in transverse direction case in Fig-9. This part over the shear strength is between casing tube and trumpet type steel-pipe and its length is about 2m and thickness of plate is 12mm.

HSBA has judged that there is no possibility of the failure from the following facts; ratio that shear force exceeds the shear strength is small, generally the material strength being used for the steel pipe and etc is higher than nominal value., the section which lacks the shear strength is short in comparison with the diameter of the steel-pipe, if shear failure occurs, direction of the shear failure occurs in the oblique direction. The shear forces of all columns of 4m diameter were within the shear strength in consideration of the steel pipe.

(4)Conclusion

It can be judged that the multi-column foundations as a whole have enough seismic performance against the level2 earthquake, when the steel pipes are regarded as the strength member, though some excess over allowable shear strength appears in small portion

6. The policy of future seismic verification and seismic retrofit

The seismic verification already conducted revealed that the fatal damage will not occur in the long-span suspension bridges and cable stayed bridges, though a few excess over allowable value in some parts of the bridges. However, there are some approach bridges where the piers lack of shearing strength and the shoes lack of ultimate strength.

The seismic retrofit work in those approach bridges will start in accordance with the priority one after another.

All bridges should be evaluated for their seismic performance in consideration of the

priority of seismic retrofit. However, the seismic response analysis shall not be conducted for the bridges in case that their seismic performance can be evaluated by analogy with other bridges because of the similarity of structural type, ground condition, etc.

The priority of the seismic retrofit is decided synthetically in consideration of the following conditions.

1) The section of the IC which contains bridges over strait
2) Applied standard (For example, Specification for Highway bridges of 1971, 1980 applicable bridges)
3) Seto-Ohhashi (Highway-railway combined bridges)
4) Occurrence probability of future earthquake (Nankai earthquake)

The fatal damage to the user and the public owing to the bridge collapse must not be caused, and the road should keep a function as an emergency transportation route. Therefore, the unseating prevention system etc should be set up in parallel with the reinforcement of the substructure.

7. Conclusions

The outline about seismic verification of the long-span bridges over the strait of HSB was mentioned in this report.

1) Seismic design standards of HSBA do not consider the influence of an inland near-field type earthquake. Therefore HSBA decided to verify the seismic performance of bridges for Leve2 type II earthquake.
2) HSBA decided that the JMA Kobe wave in the Hyogo-ken Nambu Earthquake should be used for the seismic verification wave.
3) The seismic verification already conducted revealed that the fatal damage will not occur in the Akashi-Kaikyo Bridge and the Ohnaruto Bridge, though some excess over limit value appears in some parts of the bridges. The verification results for other bridges are the same as these two bridges.
4) HSBA will continue to execute the seismic verification of the bridges taking the priority of the seismic retrofit into consideration.

References

[1] Honshu-Shikoku Bridge Authority, Seismic Design Standard for Honshu-Shikoku Bridges, 1977.3(in Japanese)
[2] Honshu-Shikoku Bridge Authority, Seismic Design Code for Akashi-Kaikyo Bridge, 1988.3(in Japanese)
[3] Honshu-Shikoku Bridge Authority, Seismic Design Code for Rigid body foundation of Kurushima-Kaikyo Bridge, 1990.3(in Japanese)
[4] Japan Roadway Association, Specification for Highway Bridges: Seismic Design, 1996.12(in Japanese)

SEISMIC DESIGN AND RETROFIT OF BRIDGES ON MISSOURI'S EARTHQUAKE PRIORITY ROUTES

Shyam Gupta,[1] P.E., Bryan A. Hartnagel,[2] Ph.D., P.E.

Abstract

The heart of the New Madrid Seismic Zone lies in the southeast corner of Missouri. This was the site of a series of very powerful earthquakes that took place during the winter of 1811-1812. The New Madrid Seismic Zone affects approximately 1,900 of the Missouri Department of Transportation's 10,000 bridges. This paper will briefly describe the seismic classification of the structures, details of a typical retrofit on a routine structure and the cost required to bring a small subset of the bridges up to the current seismic design provisions.

Introduction

New Madrid, Missouri is the location of a violent series of earthquakes that took place during the winter of 1811-1812. During this period, five major earthquakes with estimated magnitudes (Ms) greater than 7.7 and over 200 events with Ms greater than 4.3 took place. Otto Nuttli estimated that approximately 2000 total events with Ms greater than 3.0 occurred *(1)*. The New Madrid Seismic Zone (NMSZ) is located in the central United States and encompasses portions of Missouri, Illinois, Indiana, Kentucky, Tennessee, Mississippi and Arkansas.

The heart of the New Madrid Seismic Zone lies in the southeast corner of the State of Missouri. Soil conditions in this area, commonly referred to as the "Boot Heel," are primarily loose to dense sands that range from meters to a couple of kilometers thick. As one travels north along the Mississippi River the layers of sand gradually thin with competent limestone rock very near the surface in some areas. Parts of southeast Missouri underwent widespread liquefaction during the earthquakes of 1811-1812 as evidenced by numerous sand boils still visible in the area.

The potential for future large earthquakes in the NMSZ exists and potential damage to the State of Missouri's transportation infrastructure is high. Missouri began designing bridges for seismically induced forces in 1990. This paper will briefly describe: the provisions used to design bridges for seismic forces, a typical retrofit on a routine bridge and the Missouri

[1] State Bridge Engineer, Missouri Department of Transportation, Bridge Engineering Unit, P.O. Box 270, Jefferson City, Missouri, 65102
[2] Structural Special Assignments Engineer, Missouri Department of Transportation, Bridge Engineering Unit, P.O. Box 270, Jefferson City, Missouri, 65102

Department of Transportation's (MoDOT) Earthquake Response Plan development.

Seismic Design in Missouri

Missouri currently (2003) uses the provisions of Division IA found in the 17th Edition of the AASHTO *Standard Specifications for Highway Bridges (2)*. The seismic hazard presented in the Division IA provision is based on the 1988 U.S. Geological Survey (USGS) map with a 90 percent probability of not being exceeded in 50 years. This is equivalent to a 10 percent probability of exceedance (PE) in 50 years and is approximately equivalent to a return period of 500 years. A map of Missouri showing the current acceleration coefficients is presented in Figure 1. Missouri's ten districts are also shown on the figure. The Division IA provisions divide the seismic design of structures into four seismic performance categories (SPC). Categories are labeled A, B, C and D. The seismic performance category is based on the horizontal acceleration shown on the USGS map at the bridge location and the importance classification (IC) of the structure. An importance classification is only assigned for bridges with acceleration coefficients greater than 0.29 g. Essential bridges are given the importance classification I, any other bridge is given the importance classification II. Classification of the structure is based on security/defense and social/survival requirements. Table 1, taken from the AASHTO Division IA provisions *(2)*, describes the basis for the selection of the seismic performance category.

Missouri has approximately 10,000 bridges in the state bridge inventory and approximately 13,000 additional structures under county, city or local jurisdiction. Of the 10,000 bridges in the state bridge inventory, approximately 1,900 are in seismic performance categories B, C and D. Bridges in these categories (~1,250 in B, ~520 in C and ~130 in D) require additional effort and expense to design and construct to resist the seismic hazard. The Missouri Department of Transportation (MoDOT) began designing bridges to resist seismic hazards in 1990. However, many of the structures listed above in SPC B, C and D were not designed to resist seismic induced forces. Several structures in St. Louis that were designed and constructed before 1990 have been retrofitted to resist seismic induced forces. The retrofit of a typical bridge on an earthquake priority route will be described in the next section.

Typical Seismic Retrofit of a Routine Bridge

In the past 12 years MoDOT has retrofitted a number of routine structures to resist seismic forces. Most of the structures that were retrofitted were in SPC B. Typical retrofit details on the routine structures include replacing high profile steel pin and rocker bearings with neoprene elastomeric pads, adding restrainer cables to girder expansion joints, placing steel jackets around columns and strengthening footings.

This section will describe the retrofit of a typical interstate overpass. Bridge A32073 in St. Louis County, Missouri is located on Interstate 70 and crosses the Earth City Expressway. The structure is a four span (31'-55'-55'-31', 9.45 m-16.8 m-16.8 m-9.45 m) continuous composite wide flange steel beam bridge. Total length of the structure is 175' (53.3 m) and the width is 177.5' (54.1 m). Figure 2 shows the general elevation of the structure. The retrofits to the bridge will be described beginning at the deck level and working down. Figure 3 shows the elevation of the structure and notes where seismic retrofits were applied. The contract bid cost of the retrofit was $327,673. The estimated cost to replace this structure would have been approximately $1,500,000 to $1,800,000.

High profile steel bearings at each of the intermediate bents were replaced with neoprene elastomeric pads. Intermediate bent number 3 was the fixed pin of the bridge in the original configuration. Intermediate bents number 2 and 4 both had rocker bearings, as did the end bents number 1 and 5. Figure 4 shows the front and side view of the replacement elastomeric bearing pad detail. During earthquake shaking the high profile steel rocker bearings had the potential to become unstable and tip over. The rocker bearings at end bents number 1 and 5 were left in place but bearing blocks were added to restrain lateral motion of the end of the girder and catch the beam if the rocker bearing was on the verge of tipping over. See Figure 5.

All columns of the intermediate bents received a 5/16-inch (8 mm) thick steel jacket on the top and bottom of the column. The steel jackets were intended to restrain the plastic hinge joint locations on the columns. The length of the steel jacket on the top and bottom of all interior columns was 3 feet (0.91 m) and 4.25 feet (1.30 m) on the top and bottom of the exterior columns of each intermediate bent. See Figure 6. The inside diameter of the steel jacket was 1.5 inches (38 mm) greater than the diameter of the existing column. This void was filled with grout after the steel jacket was installed on the column.

The existing footings did not have any reinforcing steel in the top of the footing. This makes the footings susceptible to cracking on the top surface as the bridge rocks back and forth during an earthquake. To prevent this cracking, an additional 12" (305 mm) of concrete and two layers of reinforcing steel were added to the top of each footing. The additional concrete and reinforcing was attached to the existing concrete with a series of "L" shaped bars that were resin anchored to the existing footing. Figure 7 shows the typical detail for adding reinforcing steel to the top of the footing and the resin anchor detail.

MoDOT Earthquake Response Plan

In 1999, the Missouri Department of Transportation in collaboration with the State

Emergency Management Agency created an Earthquake Response Plan as a manual for operations after a major earthquake in the New Madrid Seismic Zone. The plan serves as a guide of action to ensure and restore the operational capabilities of the transportation system in the areas affected by an earthquake in the NMSZ. A Bridge Engineering Unit plan was also created as a part of the larger Department response plan. Earthquake Priority Routes were selected as part of the development of the plan. The primary purpose of the priority routes is to have roads identified for personnel, equipment and materials to travel from the MoDOT Headquarters located in Jefferson City to the District 10 Headquarters in Sikeston and the District 6 Headquarters in St. Louis after a large earthquake event. The majority (~1,850) of the bridges in SPC B, C and D are located in Districts 6 and 10.

Two main criteria were used to select the priority routes: avoid major river crossings (if possible) and follow the ridges of the topography. These two criteria were selected to limit the number of structures on the priority routes. Both the route to District 6 and District 10 had to cross the Osage River (a large river crossing) outside of Jefferson City. However, both of the structures on Route 50/63 over the Osage River are newly constructed (one is currently under construction) and designed to resist seismic forces. The structures are also located in SPC A so it is anticipated that the structures will suffer little, if any, damage. Once the routes were selected, the Bridge Engineering Unit and the Maintenance Unit visited each bridge site to take photographs and notes. Information on availability of detours and seismically sensitive details such as girder hinges, short columns and beam seat width were noted. This field information was summarized into a report for each priority route.

The first priority routes from Jefferson City (GHQ) to District 6 (D6) and Jefferson City (GHQ) to District 10 (D10) were further studied to determine the cost to retrofit or replace the deficient bridges on the routes. Additional lower priority routes were also selected for travel between GHQ and D6 and GHQ and D10. However, on these lower priority routes costs and deficiencies were not estimated. A map of the first and second priority routes from GHQ to D6 and GHQ to D10 is shown in Figure 8.

On the route from Jefferson City to St. Louis, GHQ to D6, there are a total of 35 bridges, 29 in SPC A and 6 in SPC B. An estimate was calculated to retrofit and replace all the deficient bridges on the first priority route. Nine of the structures on the route were recently constructed to current seismic design standards. For the remaining 26 structures it was estimated to cost $5,000,000 to retrofit and $29,000,000 to replace the structures. Further screening removed an additional 10 bridges that were deemed to have an "easy" detour. This would include using exit ramps to bypass a damaged or collapsed overpass or using pipes and rock to cross small streams. The estimates to retrofit or replace the remaining 16 bridges were $3,000,000 and $20,000,000 respectively.

The route from Jefferson City to Sikeston, GHQ to D10, is significantly longer than the route from GHQ to D6. There are a total of 93 bridges on this first priority route. Nine structures on this route were also recently constructed to current seismic design standards and therefore require no additional upgrades. The initial estimate to retrofit and replace the remaining 84 structures was $13,000,000 and $64,000,000 respectively. As before the list of structures was reduced by eliminating bridges with "easy" detours or adjacent seismically designed twin structures. A total of 38 bridges remained which did not have a readily available bypass. Estimates to retrofit and replace the remaining 38 structures was $8,000,000 and $35,000,000 respectively.

In summary, there are a total of 128 bridges on the two seismic priority routes that will enable personnel, equipment and materials to travel from the MoDOT General Headquarters to the District offices in the two Districts that will be most affected by a major earthquake. It was estimated (in year 2001 dollars) to cost $18,000,000 to retrofit all the seismically substandard structures on the two routes and $93,000,000 to replace all substandard bridges. These estimates only include bridge related costs and do not include costs of roadway modifications or right-of-way acquisition. One will note that it is substantially less expensive to retrofit the seismically substandard bridges than it is to replace the structures. However, retrofitting many of the structures will only remove the seismic deficiencies while still leaving an inadequate roadway width or load carrying capacity by today's standards. Even with the higher cost of replacement, it was deemed prudent to recommend replacement of many of the structures to address the other deficiencies.

Current funds for replacement of structures are limited and many other priorities exist. Discussions on how to fund the needs to replace deficient structures on the earthquake priority routes took place. It was suggested that a modification in the current funding prioritization method be made to place a higher emphasis for bridges on the earthquake priority routes. However, since the earthquake priority routes only include 67 bridges of the approximately 1,900 bridges in the SPC B, C and D it was thought that the structures would probably not move up much in the funding priority list when all other factors are taken into account.

Bridge Retrofit and Replacement Cost Estimates

Retrofit and replacement cost estimates were based on square feet of existing bridge deck, structure type, and seismic performance category. Deck area of the existing structure was increased by 15 percent when calculating the replacement cost to account for substandard roadway widths and hydraulic conditions. Dollar amounts per square foot of deck area

were estimated for five different structure types and the four different seismic performance categories (SPC). The structure types were: plate girders, prestressed concrete beams, deck girders (reinforced concrete tee-beams), slabs and trusses. The estimated costs per square foot of deck area to retrofit and replace are presented in Table 2.

The cost estimates presented in Table 2 are based on actual retrofit costs on structures that were let for bid in the previous years. As mentioned above, the costs were estimated for five types of bridge structures and the four seismic performance categories. Costs were adjusted to account for inflation and reflect year 2001 dollars.

For bridges in SPC B the primary retrofit method for plate girders and prestressed I-girders consisted of applying a steel jacket on single column bents and placing steel restrainer rods across expansion gaps. On steel plate girders, high profile steel bearings were also replaced with elastomeric bearings. On prestressed I-girders the bearings were modified to include dowels to anchor the bearings to the beam cap. Slab and deck girder bridges were also retrofitted with dowel bars to restrain motion at selected supports. Truss structures required modifications to the bearings and anchorage to piers.

Bridges located in SPC C required more extensive retrofit than SPC B. Plate girder retrofit costs were calculated based on a 6-inch concrete jacket on all columns, and lead-rubber isolation bearings. Prestressed I-girders, slab structures and deck girders also required a 6-inch concrete jacket on all columns in addition to the retrofits necessary for SPC B. Since a limited number of retrofits were completed and none of the retrofits were in SPC D the costs estimates for SPC D were obtained by increasing the cost of retrofit for SPC C by 25 percent.

Since adequate funds are not available to upgrade all structures located in zones that may experience seismic hazard, MoDOT is currently creating a policy to further prioritize which structures will be seismically upgraded. Factors influencing which structures are seismically upgraded include: average daily traffic (ADT), is an adjacent twin structure designed with seismic resistance, is the structure on a priority route and can the structure be easily bypassed. For routine structures, seismic upgrade will generally only be considered when the structure is scheduled for rehabilitation due to poor condition of the bridge.

Summary

The Missouri Department of Transportation currently has about 1,900 (out of a total of approximately 10,000) structures that are located in seismically active zones. Many of the structures were built before 1990 when MoDOT began designing structures to resist seismic forces. Therefore, a large percentage of the structures are vulnerable to the seismic hazard

that is inherent to their location in the New Madrid Seismic Zone. Several structures have been retrofitted to resist seismic forces. Typical details used on one structure are presented in this paper. MoDOT developed an Earthquake Response Plan that includes the identification of Seismic Priority Routes to enable manpower, equipment and materials to travel from the MoDOT General Headquarters to District Offices that will be most affected by an earthquake in Missouri. Lists of bridges on the priority routes were studied for seismic deficiencies and a cost was estimated to retrofit or replace the deficient structures. Inadequate funds are available to bring all deficient structures up to current seismic design standards so MoDOT is currently devising a method to prioritize which structures will be upgraded with the very limited funds available.

References

1. United States Geological Survey. "Large Earthquakes in the United States: New Madrid 1811-1812." http://neic.usgs.gov/neis/eqlists/USA/1811-1812.html. Accessed September 10, 2003.
2. AASHTO. *Standard Specifications for Highway Bridges*, 17th ed., 2002. American Association of State Highway and Transportation Officials, Washington, D.C.

Table 1 Seismic Performance Category (SPC)

Acceleration Coefficient	Importance Classification (IC)	
A (% of g)	I	II
$A \leq 0.09$	A	A
$0.09 < A \leq 0.19$	B	B
$0.19 < A \leq 0.29$	C	C
$0.29 < A$	D	C

Taken from AASHTO (2002) Division IA – Seismic Design *(2)*

Table 2 Retrofit and Replacement Costs Per Square Foot of Deck Area (based on year 2001 dollars)

Cost for retrofit ($/ft^2)	SPC			
	A	B	C	D
Plate Girder	$12.70	$25.39	$25.96	$32.45
Prestressed Concrete Girder	$9.87	$19.74	$23.49	$29.36
Slab Structure	$1.89	$1.89	$21.86	$27.32
Deck Girder	$10.56	$21.11	$37.10	$46.35
Truss Structure	$9.45	$18.89	$78.43	$98.04

Cost for replacement ($/ft^2)	SPC			
	A	B	C	D
Plate Girder	$76.00	$80.00	$95.00	$112.00
Prestressed Concrete Girder	$57.00	$60.00	$72.00	$84.00
Slab Structure	$80.75	$85.00	$102.00	$119.00
Deck Girder	$76.00	$80.00	$95.00	$112.00
Truss Structure	$166.25	$175.00	$210.00	$245.00

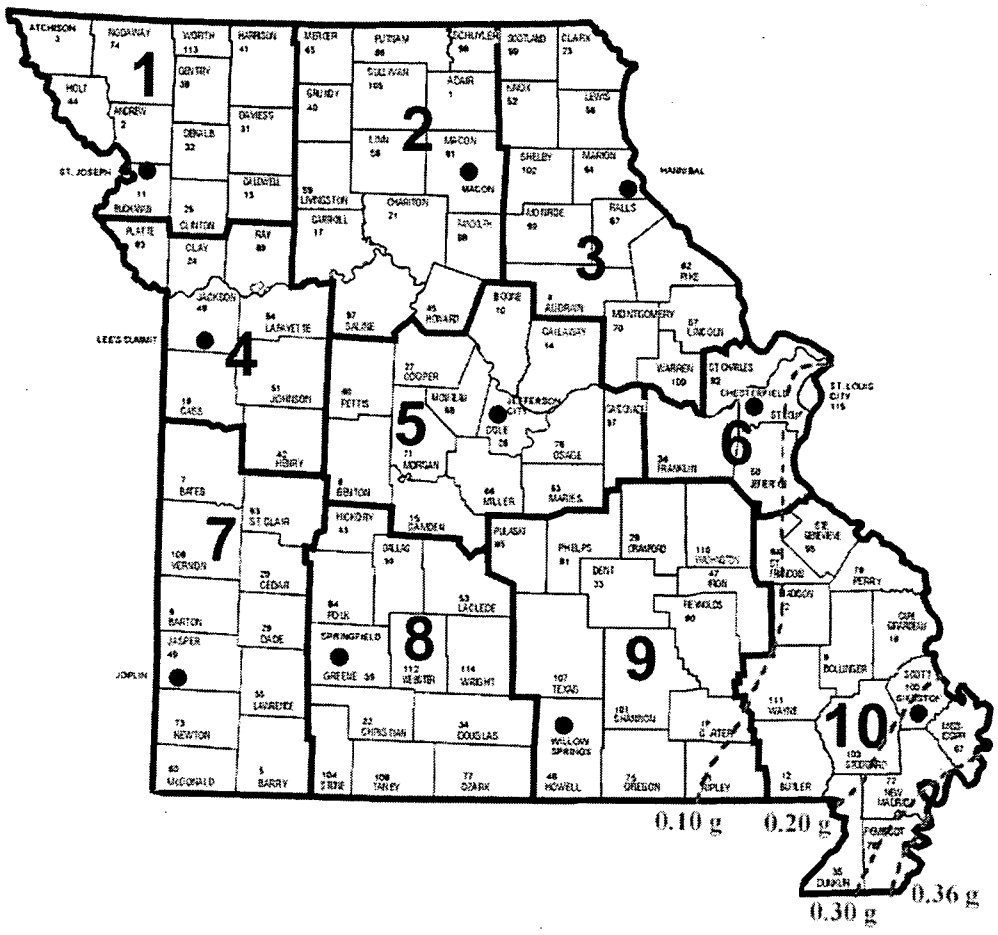


Figure 1 Current AASHTO Division IA seismic acceleration coefficients with a 10% probability of exceedance in 50 years

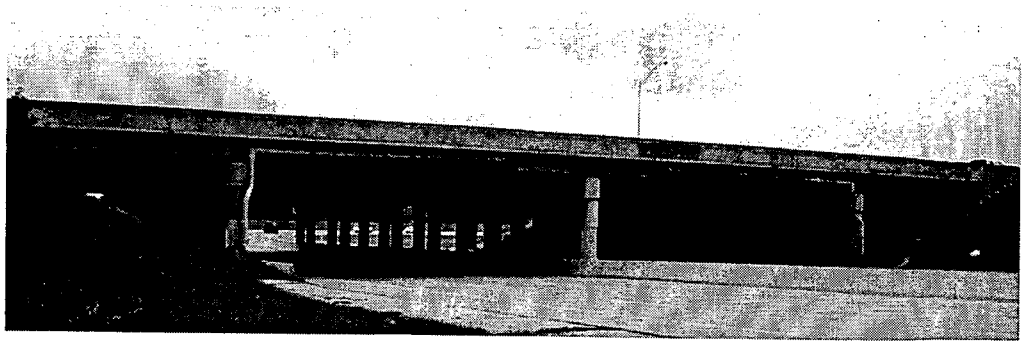


Figure 2 Elevation of Bridge A32073

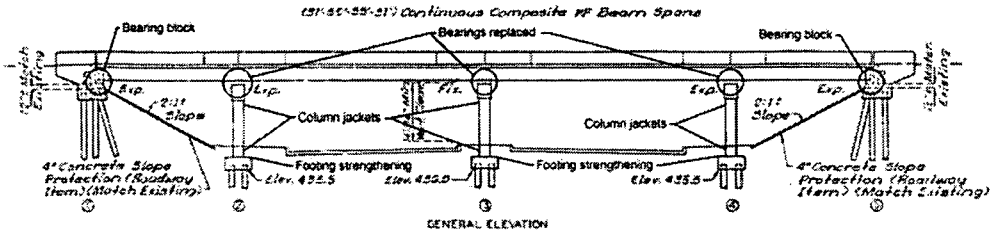


Figure 3 Elevation of Bridge A32073 detailing locations of seismic retrofits

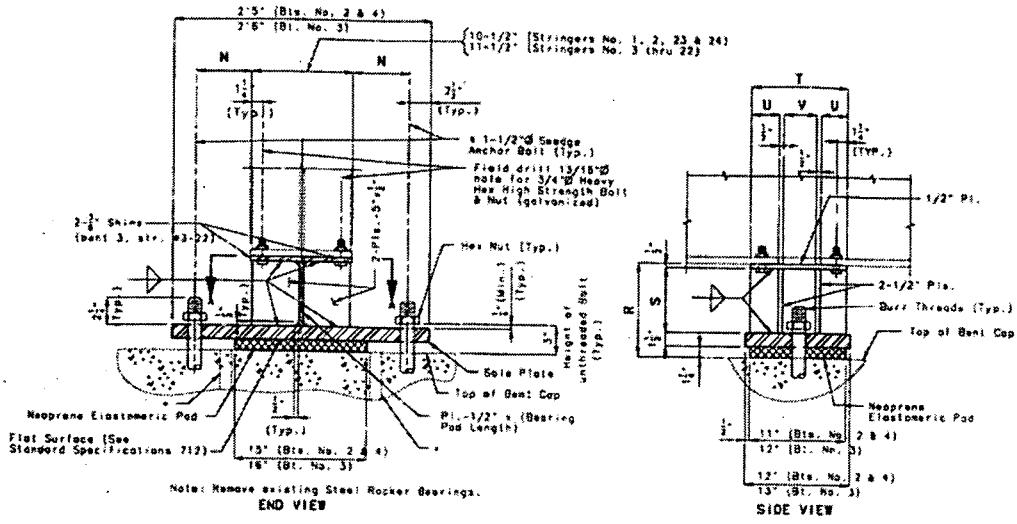


Figure 4 Typical detail of neoprene elastomeric pad used as a replacement for steel bearings at intermediate supports

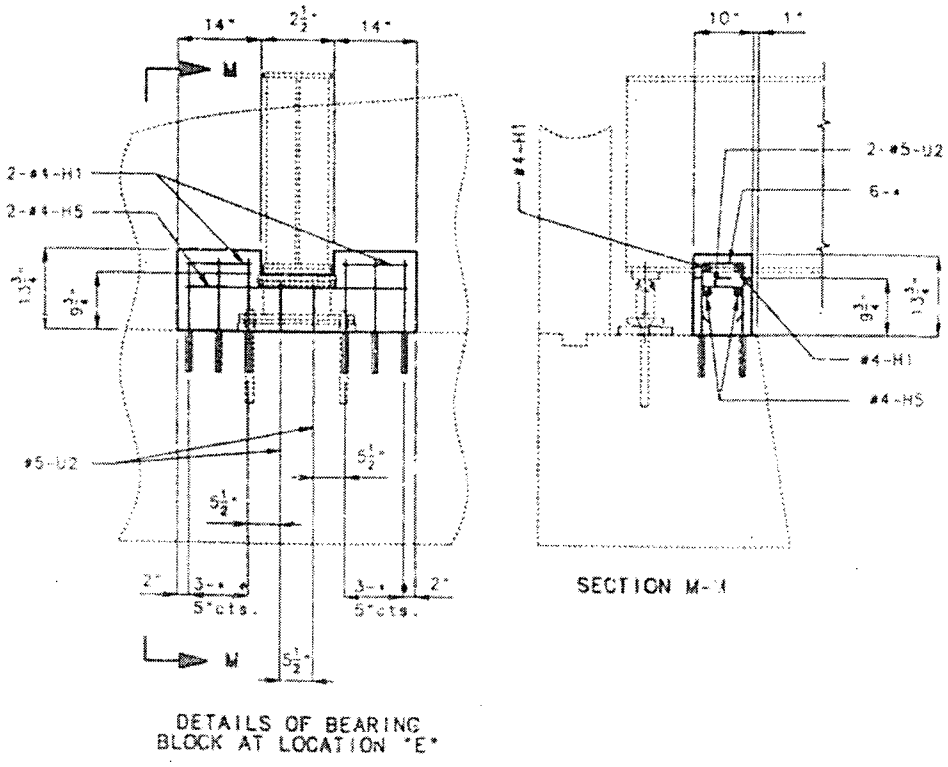


Figure 5 Typical detail of bearing block used at end bents

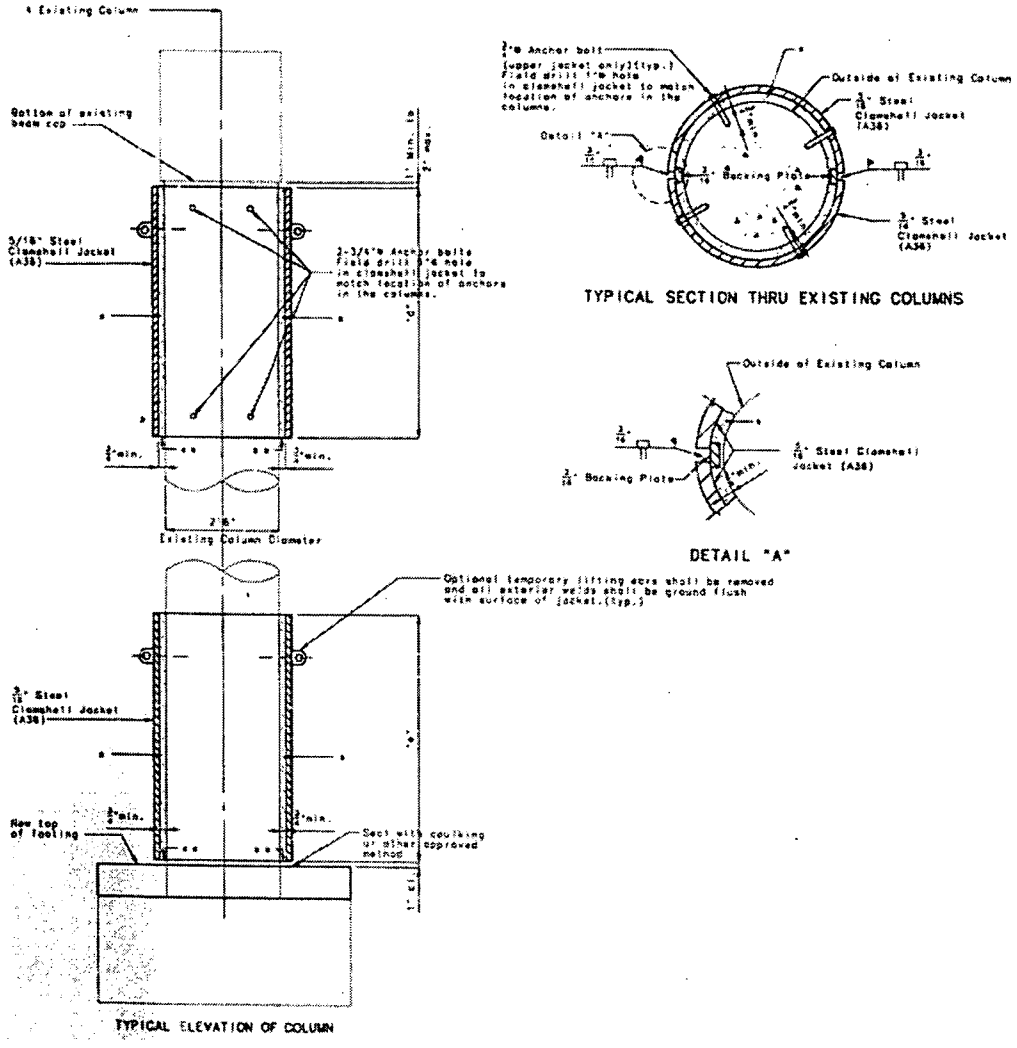


Figure 6 Steel jacket used at top and bottom of all columns on the intermediate bents

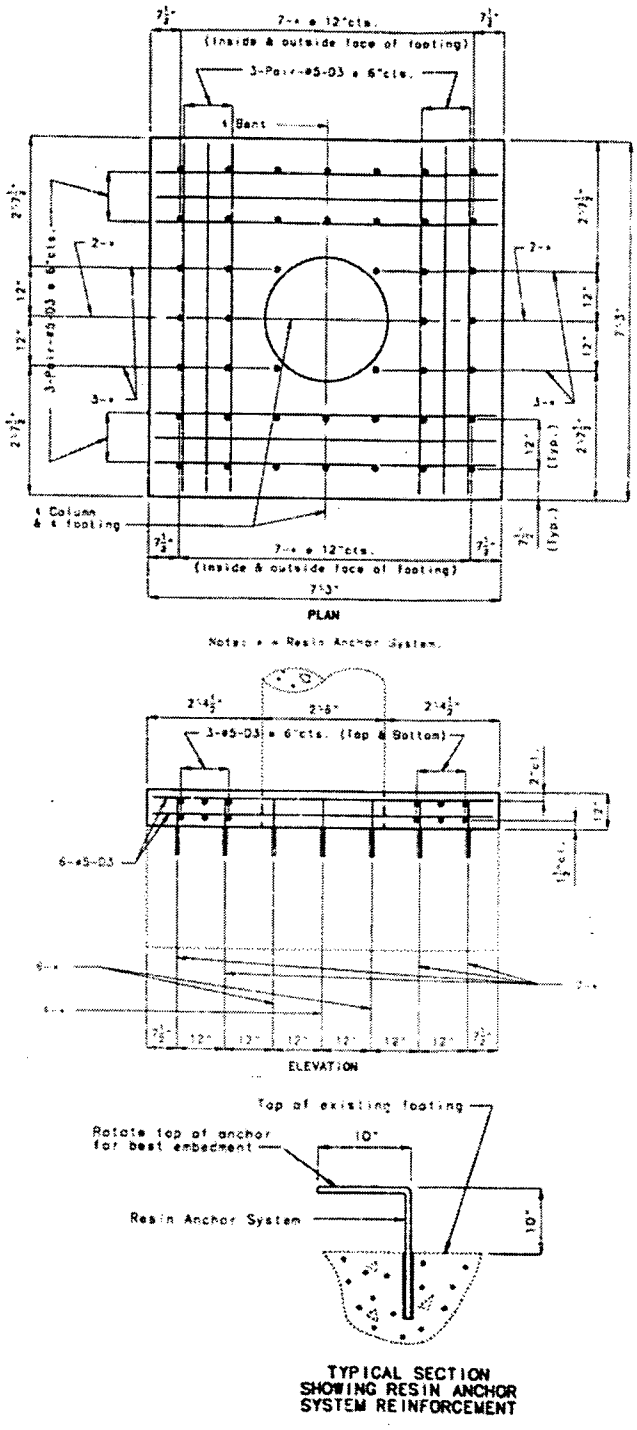


Figure 7 Typical footing retrofit to add reinforcing steel to top of footing

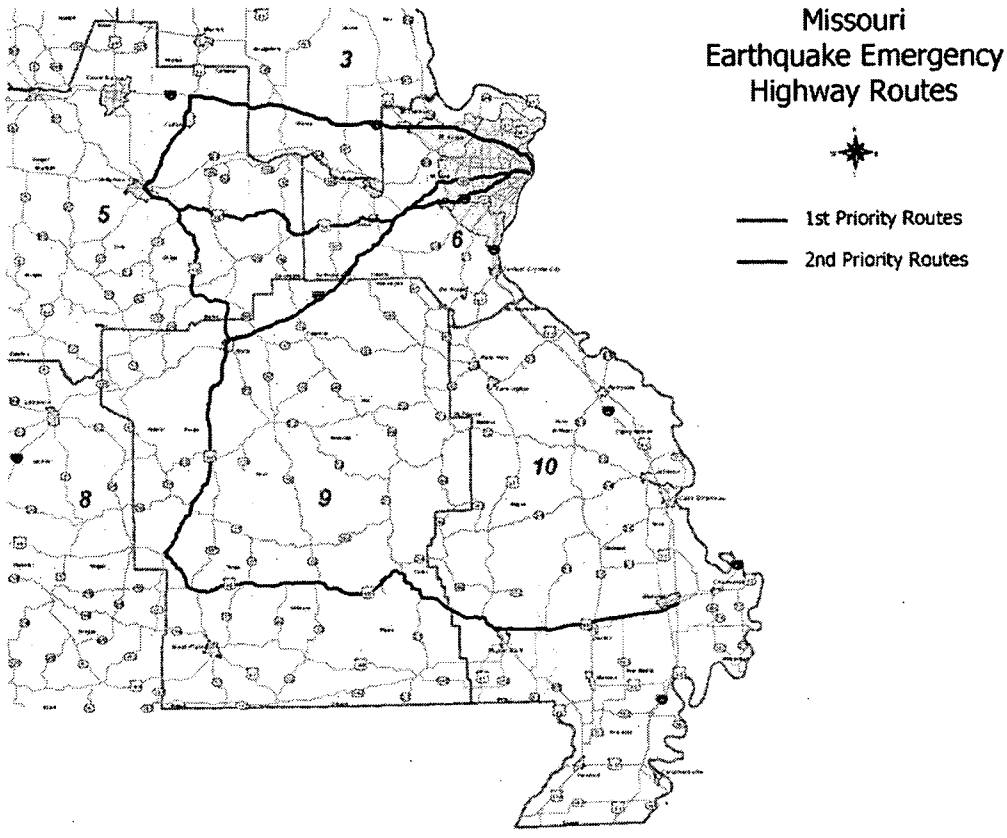


Figure 8 Earthquake priority routes from Jefferson City to St. Louis and Sikeston

19th US-Japan Bridge Engineering Workshop

Seismic 4

co-Chairs:
C. Kawatoh & S. Gupta

Seismic Retrofit Strategy using Damage Control Design Concept and the Response Reduction Effect for a Long-span Truss Bridge
H. Kanaji

Research Opportunities using the U.S. George E. Brown, Jr. Network for Earthquake Engineering Simulation (NEES)
J. M. Pauschke

Experimental Study on the Repair Effect of RC Piers Damaged by Earthquakes
K. Watanabe

Seismic Retrofit Strategy using Damage Control Design Concept and the Response Reduction Effect for a Long-span Truss Bridge

Hidesada KANAJI[1], Masahiko KITAZAWA[2], and Naoto SUZUKI[3]

Abstract

A 980m-long-span cantilever truss bridge located in the Port of Osaka on the Hanshin Expressway, known as Minato Bridge is considered herein to evaluate a rational seismic retrofit strategy which considers the damage control design concept and the response reduction effect. Seismic vulnerability of this bridge is caused by severe damage to several truss main members when subjected to a *Level 2 Earthquake* considered in the earthquake safety evaluation of bridges. The damage control design concept differentiates the main members, which support vertical load, from sub members such as lateral bracings designed to resist lateral forces such as seismic force or wind force. According to the concept, main members should be designed to be elastic and sub members are allowed to behave under plastic deformation in order to provide adequate damping to the entire bridge. In this paper, floor seismic isolation system and hysteretic damper bracing are proposed based on the damage control design concept. Their effects of response reduction from a series of dynamic analyses are also described.

Introduction

The Hyogo-ken Nanbu earthquake hit Kobe, Japan at the dawn of January 17, 1995 and caused severe damage to the structures on the Kobe route and Wangan route of the Hanshin Expressway. After this devastating earthquake, seismic retrofit projects have been accelerated in Japan. The first step carried out was to increase shear strength and ductility of columns by using steel jacketing, as well as reinforced concrete jacketing or carbon fiber sheets jacketing. The second retrofitting step is targeted for superstructures, and considers retrofitting countermeasures such as installation of cable restrainers instead of existing steel plate restrainers, replacement of vulnerable bearing supports, extension of cap-beams against girder dropping, and reinforcement of end diaphragms. However, the retrofit for long span bridges is lagging behind that for ordinary bridges in Japan. To our knowledge, the seismic retrofit project for the Minato Bridge is the first extensive

1. *P.E., Assistant Manager, Design Division, Osaka Bureau, Hanshin Expressway Public Corp.*
2. *Dr., P.E., Executive Director for Engineering, Hanshin Expressway Public Corp.*
3. *P.E., Manager, Second Engineering Dept, Osaka Branch, CTI Engineering Co., Ltd.*

challenge to retrofit a long span bridge in Japan.

The Minato Bridge was completed in 1974 and is the third longest truss bridge in the world. In the assessment of the seismic safety of this bridge, design seismic load was reviewed considering extremely large earthquakes whose return period exceeds 1000 years. Using these earthquake motions, a large number of dynamic analyses has been performed and it is found that a lot of truss members can't remain in elastic condition. To deal with this fact, there are two retrofitting alternatives such as reinforcement of members or seismic response modification for these members. We selected the latter method and employed the control design concept which keeps main members elastic and expects hysteretic damping of sub members such as lateral bracings, because reinforcement of a large number of members is uneconomical. The use of the seismic response modification method is also suitable to control the residual displacement of the entire bridge which should be very little in order to open the traffic immediately after an earthquake. This implies that the restoration cost and the economic loss will be dramatically reduced.

Minato Bridge Description

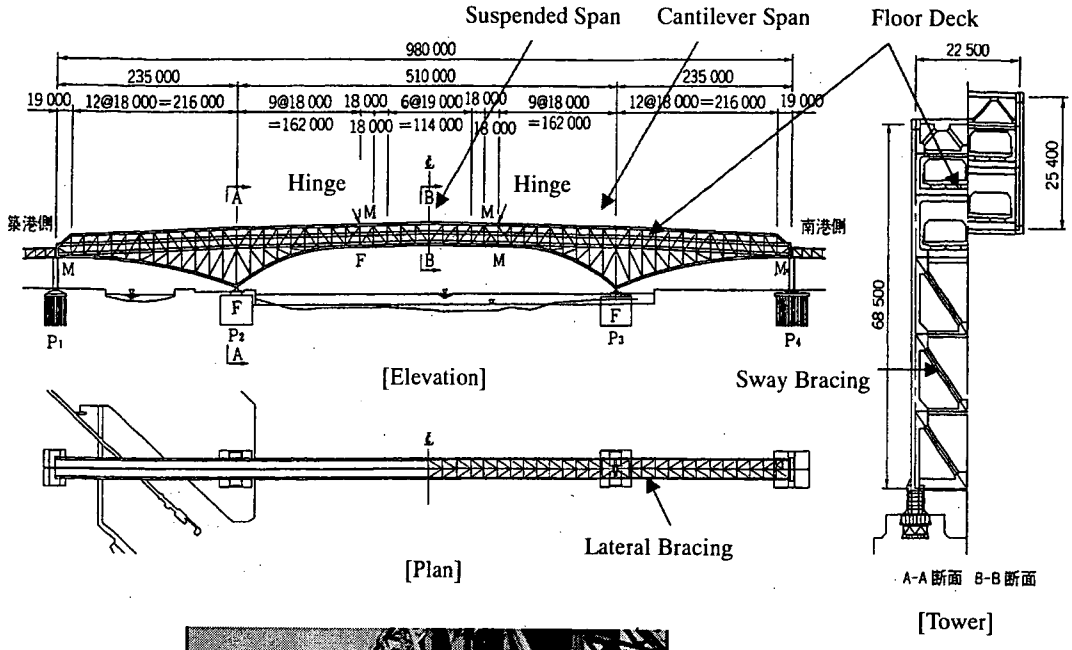
The 980m-long-span Minato Bridge is located in Osaka City on the Wangan route of the Hanshin Expressway. This cantilever truss bridge consists of two 235m side-spans and a 510m main-span and is composed by two-layer floor system with four lanes each (**Figure-1**). The floor system in one-layer is assembled by 14 floor structure portions arranged consecutively. The bearings of intermediate-portions are fixed against horizontal movements and their design capacity is 131.4MN for dead and live loads. The type of intermediate foundation of the bridge is caisson and that of edge foundation at both ends is steel piles.

The seismic design of the *as-built* structure was carried out by using the modified seismic coefficient design method and by taking into account the dynamic characteristics based on dynamic analysis with the original design acceleration response of 250 gals.

Assessment of the As-built Structure

Analysis Model

A 3-D global model, as shown in **Figure-2** is used to analyze the seismic performance of both the as-built structure and the retrofitted structure. The main members of the superstructure are elastic with a damping ratio assumed to be 2%. Ground springs at intermediate supports P-2 and P-3 consist of non-linear horizontal springs and rotation springs and those at edge-piers P-1 and P-4 are elastic springs. The non-linear springs for the caisson-ground interactive model are developed by using static pushover analysis and the Hardin-Drnevich model is applied for restoring characteristics of the caisson.



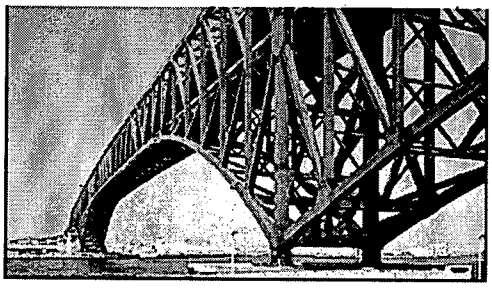


Figure-1 Structural characteristics of the Minato Bridge

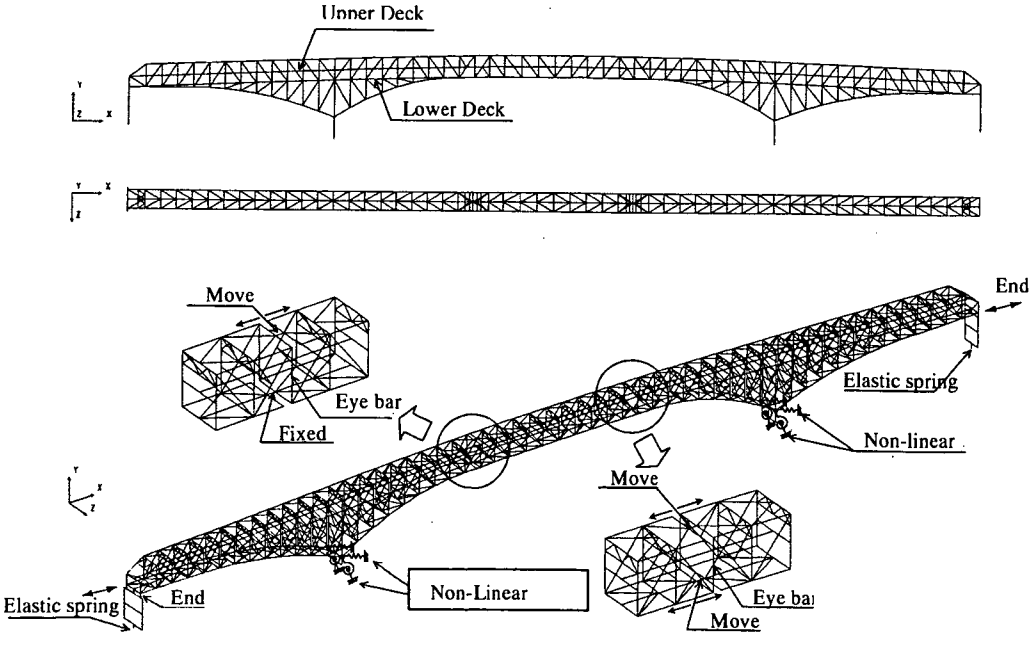


Figure-2 Analytical Model

Modal Analysis

Modal analyses considering the global 3D model of the as-built structure were conducted to evaluate its vibration characteristics. **Figure-3** provides the dominant modes for the longitudinal and transverse directions. The first mode for the longitudinal direction shows jackknife-shape at hinges and the natural period is 2.8s. The second mode with 1.4s natural period shows that the suspended span goes up and down. On the other hand, the first mode for the transverse direction also shows that that suspended span sways from side to side with 4.4s period. The second mode with 1.9s period shows that only side span bends.

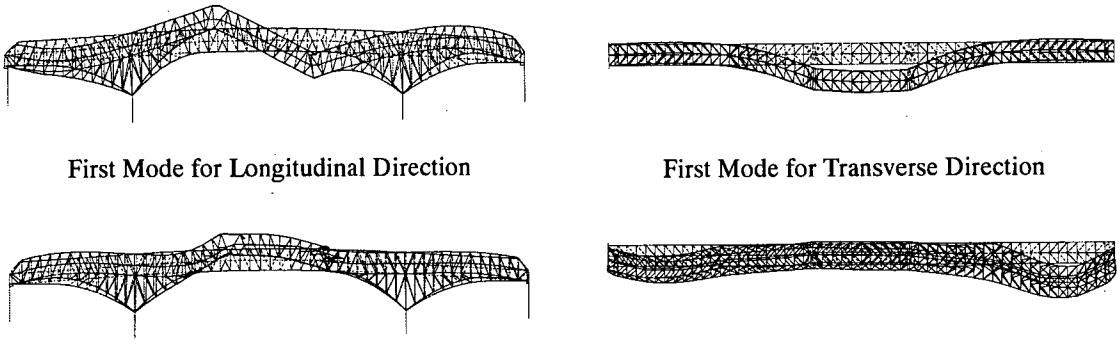
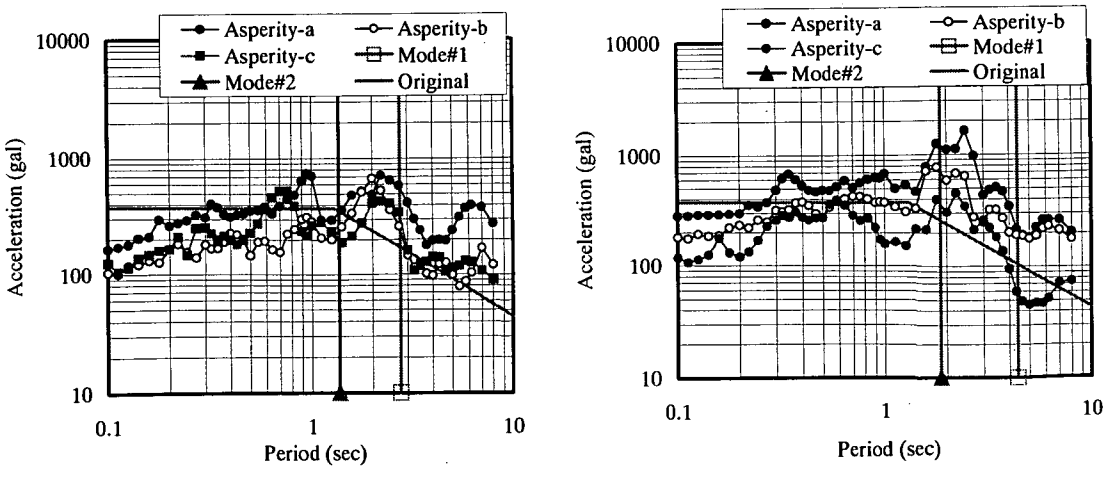


Figure-3 Vibration Mode

The relationship between design acceleration response spectra for this bridge and their natural periods are shown in **Figure-4**. Only the acceleration of the first mode for the transverse direction is relatively low. However all other accelerations are very large: the acceleration for the longitudinal is around 0.8g and that for the transverse is over 1g.



a) Longitudinal Direction. b) Transverse Direction

Figure-4 Acceleration Response Spectra

Current Seismic Performance

Response spectrum analysis and time history analysis using the site-specific earthquake motions are performed in order to evaluate the current seismic performance of this bridge.

According to response spectrum analysis, the effect of each vibration mode to the force response of members or structural components can be clarified. The response spectrum analysis shows that, the first mode for the longitudinal direction affects the lower chord members in the side spans, the upper chord members in the center span near the tower, and main bearings at towers. On the other hand, the first mode for the transverse direction accounts for the force of almost all upper chord and lower chord members in the center span. The second mode for the transverse direction makes up the great portion of member forces in the side spans. The time history analysis reveals the member stress for the ground motions considering the site-specific characteristics. Giving that the stress ratio should be the quotient of maximum stress and the allowable stress, the inelastic members can be expressed by the stress ratio over 1.0. Longitudinal motion caused inelastic behavior in chord members located near the edges of the bridge and hinges between the cantilever portion and the suspended span.

On the other hand, the transverse motions affects chord members located near the edges of the bridge as well as diagonal members, vertical members and lower chord members around towers. This implies that the first mode for the longitudinal direction and the second mode for the transverse direction are crucial in the seismic response of the bridge.

Retrofit Strategy

Damage Control Design

The retrofit strategy applied herein considers the damage control design concept in which damage is allowed only in sub members which support lateral forces. These sub-members are expected to behave in elasto-plastic condition and generate adequate hysteretic damping. The main members which support vertical forces such as dead load and live load should remain almost elastic. This concept has been already employed in the field of high-rise buildings in Japan. Using this concept, the structure would have only small residual deformation which permit the open traffic even after an extreme large earthquake. Moreover, restoration cost after a large earthquake can be significantly reduced, because the main members remain almost elastic.

Seismic Response Modification

Specific devices play a key-role for damage control design. These can be seismic isolation devices and energy absorption devices as seismic response modification devices. These devices, which are mounted in sub members, are very useful to reduce the seismic response because of their stable elasto-plastic behavior and damping.

By the way, the first mode for the longitudinal direction with 2.8s period and the second

mode for the transverse direction with 1.9s are selected as critical modes judging from their overstress ratios. The acceleration response spectrum provides important fodder for making a decision in applying devices. It is found that period elongation is very useful for the former mode, although it will make increase the acceleration for the latter mode if looked from the design spectra. Thus, it can be stated that isolation technique can be used to control the seismic response in the longitudinal direction and damping devices can be used for the transverse direction.

Seismic Response Modification Devices for the Longitudinal Direction

Floor Deck Isolation

The Minato Bridge has two-layer floor decks with 6 plate girders placed on the cross beams of the main truss. The weight of the floor systems amounts to approximately 200MN, which accounts for 40% of the total weight of the superstructure which in turn is supported by conventional steel bearings. According to the Dynamic analysis, these existing bearings, which suffered damages due to even the Hyogoken-Nanbu earthquake whose epicenter occurred approximately 40km away from the bridge site, will be severely damaged. Under these circumstances, isolation bearings are adopted as retrofitting countermeasure for the existing bearings in order to reduce the seismic response and avoid severe damage.

It is known that, there are several types of isolation bearings such as lead-cored rubber bearings, high-damping rubber bearings, sliding bearings, among others more. A sliding isolation system which consists of sliding bearings and lateral rubber springs was selected for the Minato Bridge as illustrated in **Figure-5**. Lead-cored rubber bearings and high-damping rubber bearings which must provide a long natural period around 3 s were not selected because they require high-shaped bearings which can't be installed in actual space at the site.

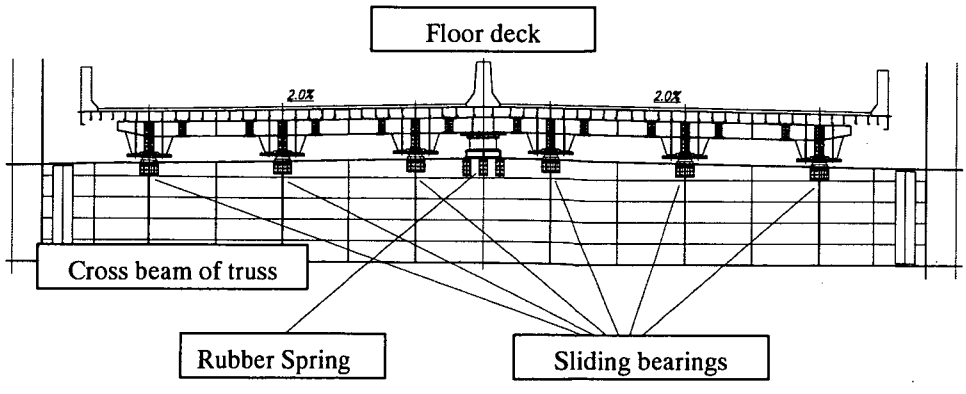


Figure-5 Floor Deck Isolation System

Response

Seismic isolation is based on period elongation, consequently the natural period of rubber springs is crucial for the force reduction of main truss members and displacement increase of floor decks. Moreover, the friction coefficient of sliding bearings also affects these responses. In order to calculate optimal design values the time-history analyses considering several rubber stiffness and friction coefficients of sliding bearings are conducted.

Figure-6 in which natural periods of rubber springs and friction coefficients of sliding bearings are the parameters to be varied, shows the relationship between the bearing displacement and the reduction ratio of chord member force. It was found that long periods such as T=3.0 and 3.5 s longer than the natural period of the first mode for the longitudinal direction reduce the member force and enlarge the bearing displacement with a decrease in the friction coefficient. On the other hand, a decrease in the friction coefficient for shorter natural periods than T=2.75 s increases both member force and bearing displacement. The displacement demand for the clearance at the edge of girders is approximately 50 cm. This design condition provides the optimal value which is the combination of T=3.0 s and μ=0.05, this provides the allowable member forces.

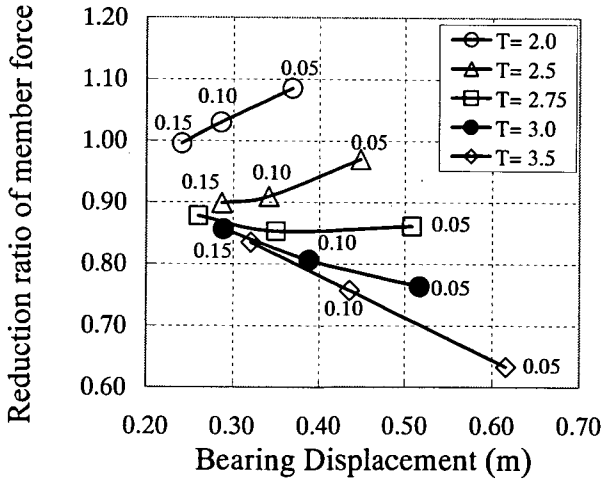


Figure-6 Responses by floor deck isolation

(T=natural period of rubber, μ=friction coefficient)

Seismic Response Modification Devices for the Transverse Direction

Hysteretic Damper Bracing

A steel hysteretic damper is composed of low-yield point core steel member (LYP225) and a restraint hollow against the bucking of core steel. Under normal conditions, buckling strength of a steel bracing should be lower than its yield strength so, hysteretic damping due to cyclic loading can't be expected. On the other hand, hysteretic damper bracings provide quite large damping without buckling.

The sway bracings of towers as well as lateral bracings on the lower side near towers will buckle under the compression force due to an extreme large earthquake in the transverse direction. In order to give adequate damping to the entire bridge and avoid the buckling or yield of main truss members, the design method in which these existing bracings are replaced with hysteretic damper bracings is selected (**Figure-7**).

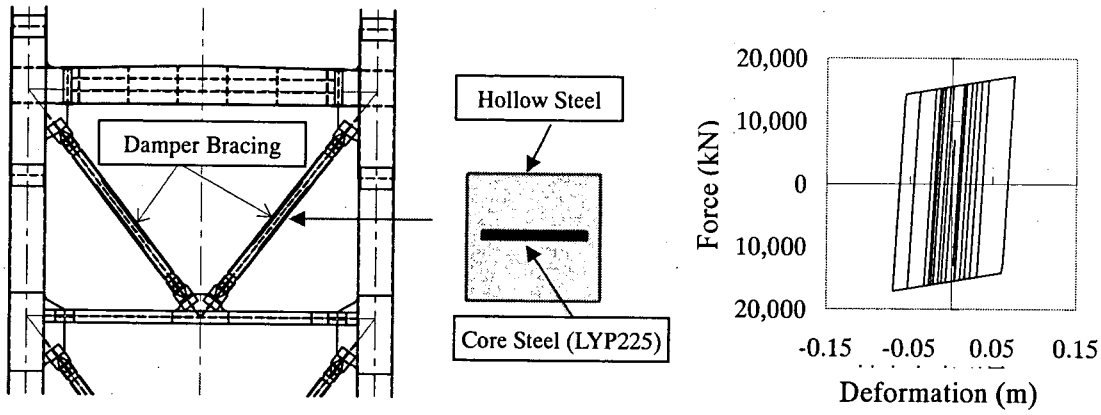


Figure-7 Steel Damper bracing and hysteretic loops

Layout of Hysteretic Damper Bracings

The damping of bracings is required against the second mode for the transverse direction which is the critical vibration mode as mentioned above. According to the mode analysis, strain energy for each member can be obtained and the members which have large strain energy are selected from the viewpoint of mode damping.

Under these aspects, the sway bracings of the tower and the lower lateral bracings near towers are determined to be replaced with hysteretic damper bracings as shown in **Figure-8**.

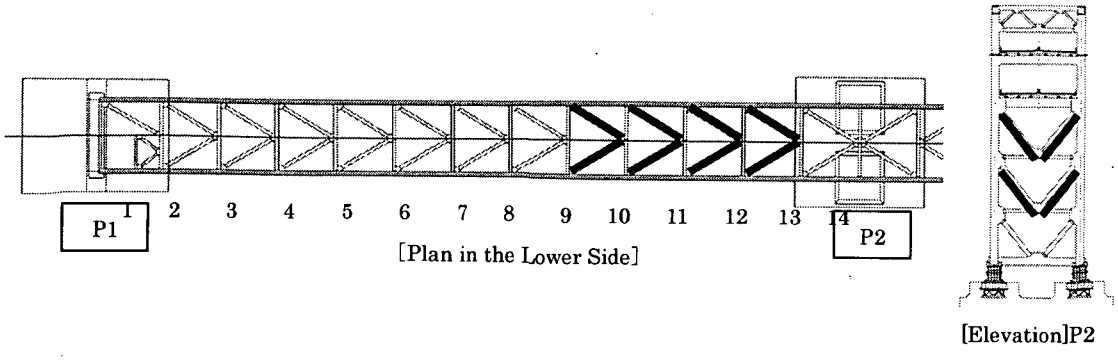


Figure-8 Optimal Layout of damper bracings

Response

Figures 9 and 10 show the change in strain energy of the upper and lower chord members by the effects of lower lateral damper bracings and sway damper bracings of towers for the *as-built* and *retrofit* cases respectively.

It was found that lower lateral damper bracings are extremely effective to reduce the strain energy of lower chord members near towers (Index of Member Position=#14), but their effect in the upper chord members is almost negligible.

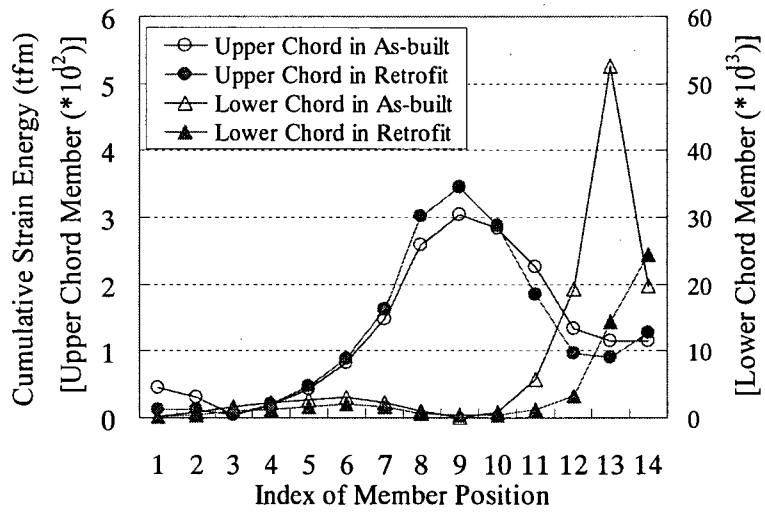


Figure-9 Effect of Lower Lateral Damper Bracings

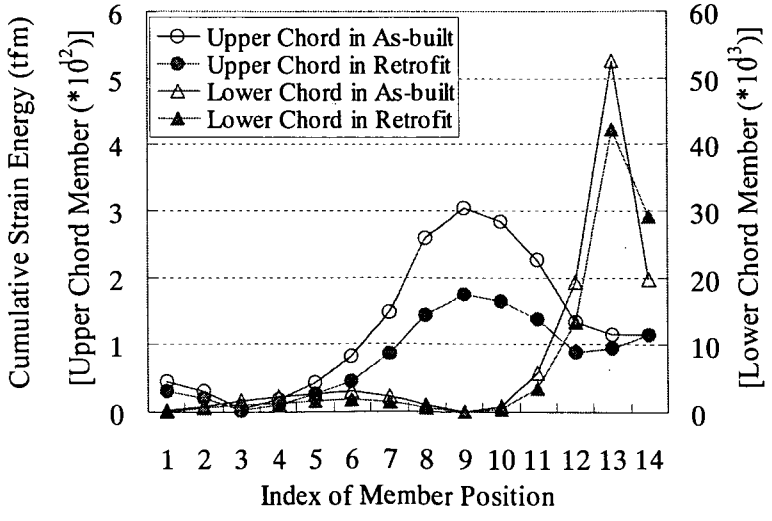


Figure-10 Effect of Sway Damper Bracings of the Tower

On the other hand, the sway damper bracings can reduce the strain energy of the upper chords in the center portion of the side span. **Figure-11** shows the change in the forces of the upper and the lower chord members using both sway and lateral damper bracings. The maximum reduction ratios for the upper and the lower chord members are 85% and 42% respectively.

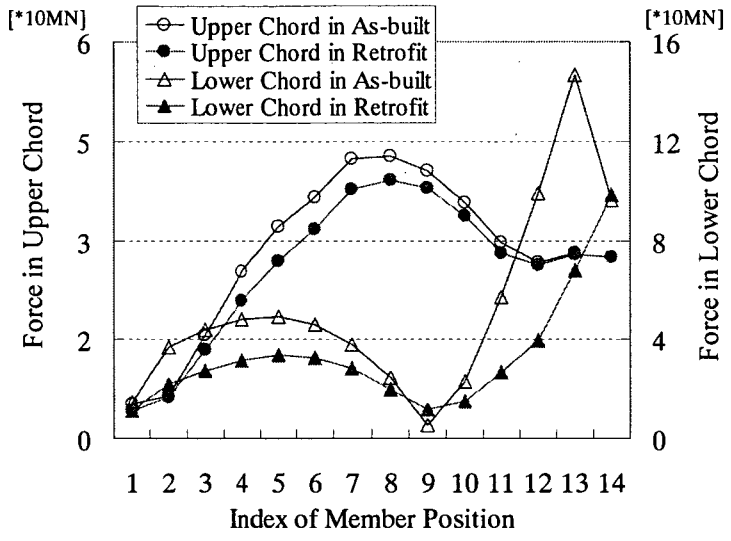


Figure-11 Effect of the Combined Damper Bracings

Effect of Retrofit Strategy

The retrofit strategy using seismic isolation devices and hysteretic damper bracings is being putting in practice for the Minato bridge by considering the overstress ratio R defined as following,

$$R_i = \sigma_{\max_i} / \sigma_{a_i}$$

where,

$\sigma_{\max_i}$ = Maximum stress obtained by dynamic analysis (i = 1,2,...)

σ_{a_i} = Allowable stress (i = 1,2,...)

The retrofit effect can be observed in **Figure-12.** It was found that the number of inelastic members is dramatically reduced in both the longitudinal and transverse directions by using this retrofit strategy. However some members remain inelastic and have to be replaced or strengthened in the final stage.

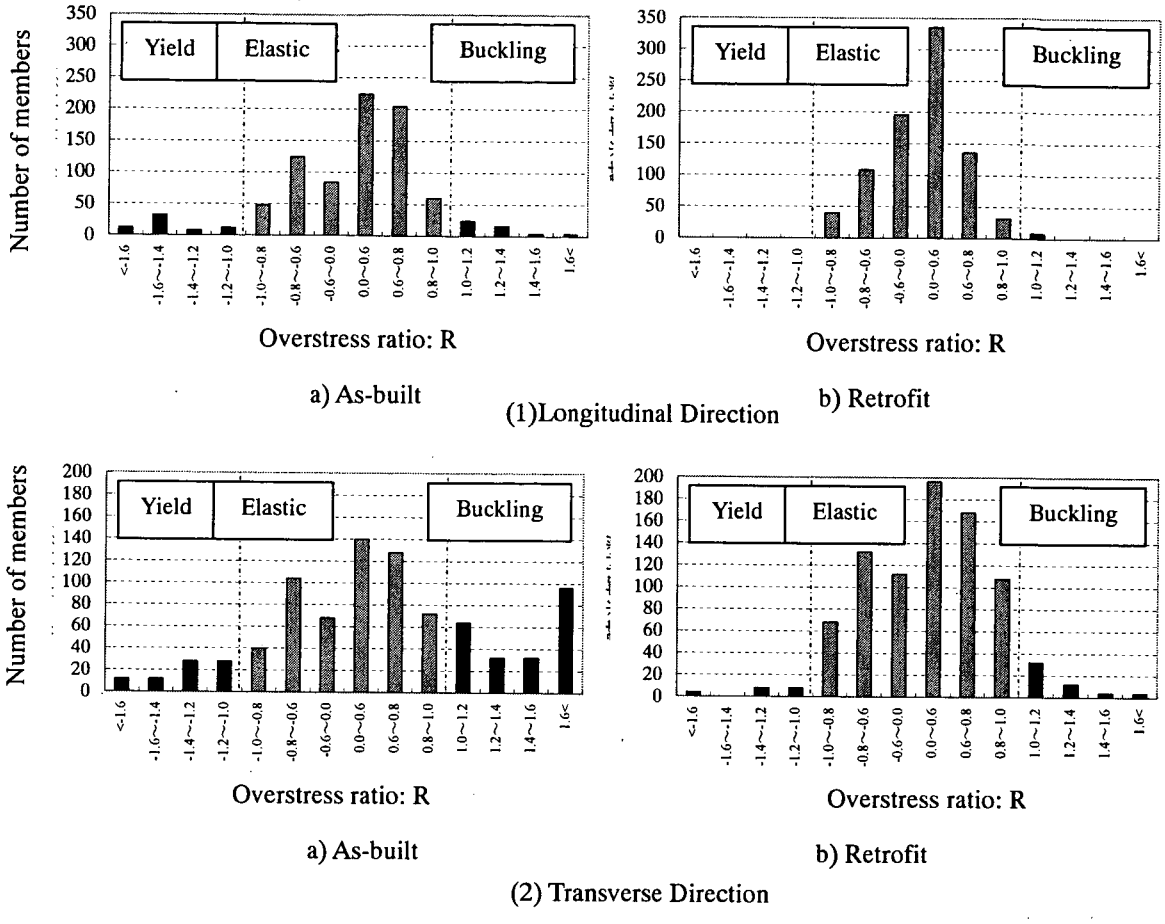


Figure-12 Effects of retrofit strategy in overstress ratio R

Concluding Remarks

The following concluding remarks were derived from the results of this study.

- The damage control design concept for the seismic retrofit of a long span bridge is very attractive because it makes possible to open traffic just after a large earthquake and also it dramatically reduces the restoration cost and then economic loss.
- Seismic isolation devices and hysteretic damper bracings are very powerful tools for the damage control design. However it is necessary to examine earthquake motions along with their response spectrums, in order to judge the applicability of these devices in the range of relatively long periods.
- It was found that rubber-spring periods such as T=3.0 and 3.5 s longer than the period of first mode for the longitudinal direction reduce the member forces and enlarge the bearing displacement along with a decrease in the friction coefficient in this sliding isolation system. The optimal combination of the natural period of a rubber spring and a friction coefficient founded in this study is T=3.0 s and μ=0.05.

- Hysteretic damper bracings installed in the lower lateral bracings are extremely effective to reduce the strain energy of lower chord members near the tower, but the effect for the upper chord is almost negligible. On the other hand, sway damper bracings of towers can reduce the strain energy of the upper chord in the center portion of the side span.

Acknowledgements

We are grateful to the committees and sub-committee on steel structure (Chairman: Prof. Eiichi Watanabe of Kyoto University) as well as the committee on seismic design (Chairman: Prof. Shiro Takada of Kobe University) of the Hanshin Expressway Public Corporation.

References

1. H.Kanaji, M.Kitazawa and N.Suzuki, "Dynamic Analysis and the Damage Control Design for the Seismic retrofit of the Long-Span Truss Bridge", Proceedings of the Symposium for the Seismic Retrofit of Existing Structures, Japan Society of Civil Engineering, *JSCE*, Nov. 2002.
2. H.Kanaji, N.Suzuki and T.Mino, "Optimal Structure and Layout of Hysteretic Steel Dampers for a Long-Span Truss Bridge Applying the Damage Control Design", Proceedings of the 6th Symposium for the Ductility Design for Bridges, Japan Society of Civil Engineering, *JSCE*, Jan.2003.
3. *Project Report on the Minato Bridge*, Hanshin Expressway Public Corporation, March 1978.

RESEARCH OPPORTUNITIES USING THE U.S. GEORGE E. BROWN, JR. NETWORK FOR EARTHQUAKE ENGINEERING SIMULATION (NEES)

Joy M. PAUSCHKE[1]

Abstract

The U.S. George E. Brown, Jr. Network for Earthquake Engineering Simulation (NEES) will be a shared network of 15 earthquake engineering experimental equipment sites, a national centralized data repository, an archive of earthquake engineering simulation software, and collaborative tools, all linked together by ultra-high-speed Internet connections and protocols. NEES is under construction during FY 2000 – FY 2004. NEES will be operated from October 1, 2004, through September 30, 2014, by the nonprofit NEES Consortium, Inc. The NEES Consortium will provide the national leadership and focal point for NEES through operation of the NEES infrastructure; maintenance of the data and simulation tools repositories; allocation of research time at the equipment sites; training, education, and outreach activities; and ties with U.S. and international partners.

Background on NEES

As a result of over a decade of planning by the U.S. earthquake engineering research community, the National Science Foundation (NSF) Directorate for Engineering initiated in fiscal year (FY) 2000 the five-year construction period for the George E. Brown, Jr. Network for Earthquake Engineering Simulation (NEES) to significantly improve our understanding of earthquakes and their effects. (Note: The U.S. federal government fiscal year begins on October 1 of the previous year; e.g., FY 2004 started on October 1, 2003.) The $81.8 million NEES project was named in honor of the late George E. Brown, Jr., former chairman of the House Science Committee and a champion of engineering and science in Congress for more than 30 years. Representative Brown authored the legislation creating the interagency National Earthquake Hazards Reduction Program in 1977, which, in turn, led to the creation of NEES.

NEES will network 15 geographically-distributed, shared use experimental earthquake engineering research equipment sites, with teleobservation and teleoperation capabilities, with a community curated data repository, collaboration tools, and unprecedented access to leading edge compute resources and open source simulation tools. NEES will transform the environment for earthquake engineering research and education through collaborative and integrated experimentation, computation, theory, databases, and model-based simulation across the NEES network to develop new fundamental knowledge in earthquake engineering, seismic design methodologies and mitigation technologies, and computational tools. Ultimately, the goal of NEES is to reduce earthquake losses in the U.S. through improved seismic design and performance of civil and mechanical

[1] Ph.D., Civil Engineering, NEES Program Director, Division of Civil and Mechanical Systems, National Science Foundation, Arlington, VA 22230 USA

infrastructure systems made possible through discoveries and new technologies enabled by NEES. A NEES web presence will facilitate remote participation in experiments by faculty and students at institutions that do not have experimental facilities of their own. A portion of the web presence will also provide educational information and outreach to the public. Figure 1 shows the concept for the shared NEES infrastructure.

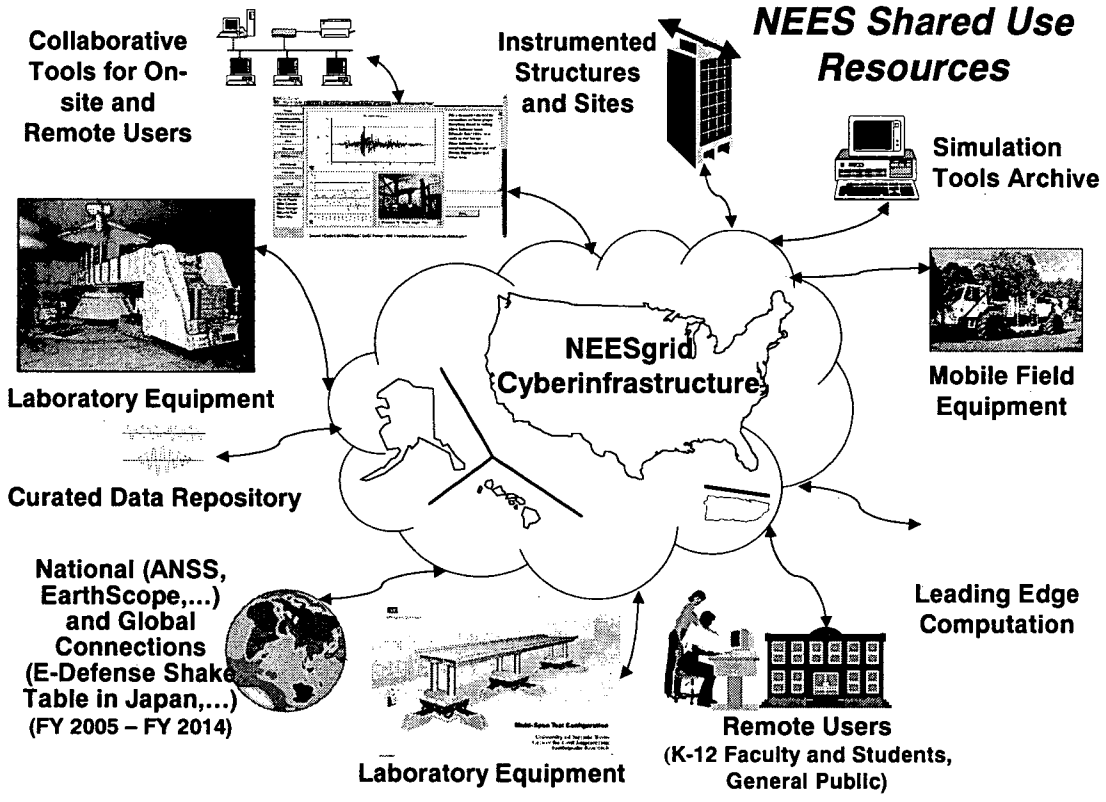


Figure 1. Concept for the NEES Infrastructure

The NEES infrastructure is being constructed during FY 2000 – FY 2004 through 18 awards (cooperative agreements) to 16 university and nonprofit organizations. Table 1 lists all the NEES construction awards. These awards are the outcomes of four competitive NSF program solicitations. The three main components of the NEES infrastructure are the following: (1) 15 equipment sites; (2) a national NEESgrid cyberinfrastructure to link together the 15 equipment sites (and enable teleparticipation), a national data repository, collaborative tools, and a simulation tools archive; and (3) the NEES Consortium, Inc., to operate the NEES infrastructure. NSF envisions that other major earthquake engineering equipment sites that bring unique experimental capabilities to NEES, both within the U.S. and abroad, will participate in NEES.

Table 1. Awards Made for NEES Construction

Award Number	Principal Investigator	Awardee Institution	Project Title
0086612	Bruneau, Michel	SUNY Buffalo	Versatile High Performance Shake Tables Facility towards Real-Time Hybrid Seismic Testing
0086624	Buckle, Ian	University of Nevada, Reno	Development of a Biaxial Multiple Shake Table Research Facility
0217293	Restrepo, Jose	University of California, San Diego	Large High Performance (LHP) Outdoor Shake Table
0086555	Dobry, Ricardo	Rensselaer Polytechnic Institute	Upgrading, Development and Integration of Next Generation Earthquake Engineering Experimental Capability at Rensselaer's 100 g-ton Geotechnical Centrifuge
0086566	Kutter, Bruce	University of California, Davis	A NEES Geotechnical Centrifuge Facility
0086571	Yim, Solomon	Oregon State University	Upgrading Oregon State's Multidirectional Wave Basin for Remote Tsunami Research
0086611	Bruneau, Michel	SUNY Buffalo	Large-Scale High Performance Testing Facility towards Real-Time Hybrid Seismic Testing
0086602	French, Catherine	University of Minnesota	A System for Multi-Axial Subassemblage Testing (MAST)
0086621	Moehle, Jack	University of California at Berkeley	Reconfigurable Reaction Wall-Based Earthquake Simulator Facility
0086592	Shing, P. Benson	University of Colorado, Boulder	Fast Hybrid Test Platform for the Seismic Performance Evaluation of Structural Systems
0217366	Stewart, Harry	Cornell University	Large Displacement Soil-Structure Interaction Facility for Lifeline Systems
0217393	Ricles, James	Lehigh University	Real-Time Multi-Directional Testing Facility for Seismic Performance Simulation of Large-Scale Structural Systems
0217325	Elnashai, Amr	University of Illinois at Urbana-Champaign	Multi-Axial Full-Scale Sub-Structuring Testing and Simulation Facility
0086605	Stokoe II, Kenneth	The University of Texas at Austin	Large-Scale Mobile Shakers and Associated Instrumentation for Dynamic Field Studies of Geotechnical and Structural Systems
0086596	Wallace, John W.	University of California, Los Angeles	Field Testing and Monitoring of Structural Performance
0217421	Youd, Leslie	Brigham Young University	Permanently Instrumented Field Sites for Study of Soil-Foundation-Structure Interaction
0117853	Spencer, Bill	University of Illinois at Urbana-Champaign	NEESgrid: A Distributed Virtual Laboratory for Advanced Earthquake Experimentation and Simulation
0126366	Reitherman, Robert	Consortium of Universities for Research in Earthquake Engineering	NEES Consortium Development Project

(1) Shared Experimental Equipment Sites

With NSF support, as well as institutional and other agency contributions, 15 universities in the U.S. are creating, expanding, or upgrading the specialized experimental equipment sites to be used in earthquake engineering research and education. These equipment sites include shake tables [one large uniaxial shake table with a high velocity input pulse, two relocatable 6 DOF shake tables, and three relocatable 2 DOF shake tables], reaction wall and strong floor laboratories, facilities for testing soil-foundation-structure interaction, lifelines/pipeline testing facility, geotechnical centrifuges that include biaxial shakers and robots for in-flight testing, a tsunami wave basin, and mobile and permanently installed structural and geotechnical field testing equipment. These facilities will overcome many of the past limitations on testing the seismic performance of geomaterials, foundations, structures, and systems. Each equipment site will be available as a shared use equipment site for researchers, educators, and practitioners around the U.S. These facilities may be used on-site or remotely through teleobservation and teleoperation. Several of the NEES equipment sites already have operational equipment (e.g., Oregon State University; University of California, Los Angeles; University of Colorado, Boulder; University of Nevada, Reno; University of Texas, Austin). The remaining sites will have operational equipment by September 30, 2004.

(2) NEESgrid Cyberinfrastructure

NEES will link the 15 experimental equipment sites, experimental and simulation data, and other shared tools through the NEESgrid cyberinfrastructure. NEESgrid builds upon the existing U.S. Internet network, grid framework, Globus toolkit, and the CompreHensive collaborativE Framework (CHEF) [CHEF is being developed by the University of Michigan http://www.chefproject.org/index.htm]. The result will be a layered, modular architecture, shown in Figure 2, which allows the NEESgrid system to be adapted during the 10-year operation of NEES to accommodate new applications, services, and experimental equipment. When fully linked, these resources will form a seamless, integrated laboratory. NEESgrid is being developed by the University of Illinois at Urbana-Champaign (UIUC), in partnership with Argonne National Laboratory, University of Michigan, University of Oklahoma, and University of Southern California.

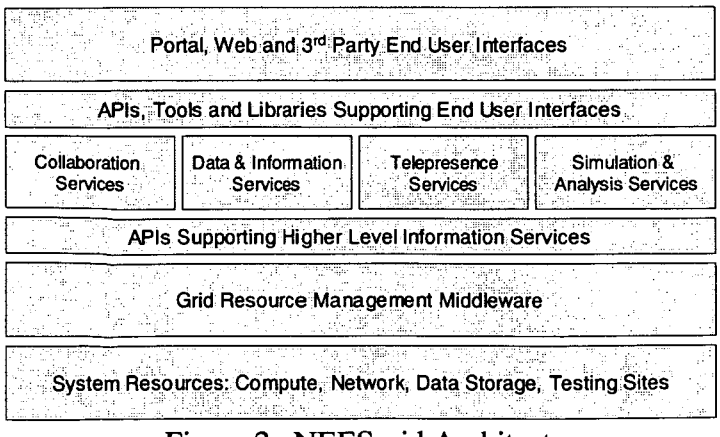


Figure 2. NEESgrid Architecture

NEES is designed to promote the integration of physical testing with simulation and visualization. NEESgrid will enable researchers to develop more comprehensive computational tools for modeling the response of the built environment to earthquakes by providing Internet-based resources that include the following:

- *Telepresence technologies.* Researchers, engineers, and students without direct access to specialized equipment sites can remotely observe (teleobserve) and teleoperate experiments.
- *Centralized data.* Experimental data and protocols, analytical results, models, and other information will be stored in a curated central repository. Standard formatting and information exchange protocols will facilitate data integration and access. An e-Notebook format will be available for capturing and archiving experimental information.
- *Simulation tools and computing power.* The software codes required for simulations of earthquake-related problems, along with grid support, will be available to investigators through an online library. Access to high-performance computing capabilities will speed the processing, analysis, and sharing of data and results.
- *Collaboration and visualization tools.* CHEF will enable students and researchers worldwide to collaborate in designing and conducting experiments.
- *Grid services.* Services such as user authentication and authorization, security, and monitoring of NEESgrid resources will enable users to conduct most network transactions and security checks in a single sign-on.
- *Support nodes.* Help desks and online databases will offer tutorials and other information on NEESgrid resources and how to employ them.

A prototype of NEESgrid capabilities was demonstrated on July 30, 2003, through the Multi-site Online Simulation Test (MOST) that brought together the UIUC NEESgrid team, the NEES Multi-Axial Full-Scale Sub-structuring Testing and Simulation (MUST-SIM) equipment site at UIUC, and the NEES Fast Hybrid testing equipment site at the University of Colorado (CU), Boulder. Along with the computational power at the UIUC National Center for Supercomputing Applications (NCSA), the UIUC MUST-SIM and CU equipment sites used a simple one-story, two-bay frame subjected to seismic input to demonstrate the NEESgrid features. During this pseudodynamic test, the response remained in the elastic range so that the results would be known and the demonstration could focus on the performance of the NEESgrid software and multi-site testing protocols. One column of the frame was tested at UIUC; a second column was tested at CU; and the remaining structure was simulated using computational resources at NCSA. During the experiment, force data was input to the computational model at NCSA; the correct displacements were calculated and transmitted to the UIUC and CU equipment sites; displacements were applied to the physical columns at these sites; and the forces for the next iteration were measured and sent to the computational model at NCSA. This cycle was repeated about 1,500 times during the MOST experiment, which lasted for about five hours.

The NEESgrid computational infrastructure plans to incorporate the open-source, object-oriented software framework *OpenSees* (Open System for Earthquake Engineering

Simulation), currently being developed by the NSF-funded Pacific Earthquake Engineering Research (PEER) center headed by the University of California, Berkeley, and Matlab. More information about OpenSees is available at http://opensees.berkeley.edu/. OpenSees includes a set of modules for developing models and simulations for structural and geotechnical systems using nonlinear elements (e.g., beam-column, connection, plate, and continuum elements) and materials (uniaxial and multi-axial for structural materials and soils) as well as providing analysis and solution methods and interfaces for databases and visualization modules. A computational finite element analysis framework is being developed at Berkeley using Matlab that can then dovetail into more advanced simulation using OpenSees.

As NEESgrid capabilities are being developed, the software, APIs, and technical reports about services and protocols are being released on the NEESgrid web site and workshops are being scheduled for system administrators and users. NEESgrid software version 2.0 was released in October 2003. Subsequent versions will be refined using experiment-based deployment at the 15 equipment sites. Version 2.1 is scheduled to be released in December 2003 and version 3.0 will be released in June 2004. Information about NEESgrid software capabilities and release dates, NEESgrid project schedule and workshops, technical reports, and the MOST experiment is available at http://www.neesgrid.org./

(3) NEES Consortium, Inc.

NEES will be operated from October 1, 2004, through September 30, 2014, by the NEES Consortium, Inc. The NEES Consortium was formally incorporated as a public benefit, nonprofit organization in January 2003. The Consortium will be the funding mechanism through which NSF provides support for NEES shared resources, including the 15 NEES equipment sites and the NEESgrid cyberinfrastructure. In its leadership role in the U.S. for NEES, the NEES Consortium will also allocate research time at the equipment sites; facilitate research planning by potential proposers to funding agencies; lead training, education, and outreach activities; and develop connections with U.S. and international partners. A critical role of the Consortium is to develop and implement policies governing open access and use of NEES research facilities and data. It is also expected to foster broad participation in NEES by all sectors of the earthquake engineering community, including researchers, teachers, students, and practitioners.

The Consortium of Universities for Research in Earthquake Engineering (CUREE), under an NSF NEES construction award, led the project to establish the NEES Consortium, Inc. The Civil Engineering Research Foundation (the research arm of the American Society of Civil Engineers), the Earthquake Engineering Research Institute (EERI), faculty members from academic institutions across the U.S., and practicing engineers were partners in the Consortium's development

During FY 2005 – FY 2014, the NEES Consortium, Inc., will:

- Manage NEES resources, including shared use operations at the NEES equipment sites and all other components of the Network.

- Establish policies and procedures for issues such as shared use access, user fees, and reimbursement of operating costs for the NEES equipment sites, as well as data policies and protocols for the curated repository.
- Work to enhance the integration of NEES resources to form a linked system of experimentation, computation, theory, databases, and model-based simulation.
- Plan, conduct, and coordinate outreach and training activities for the NEES equipment sites to encourage broad participation in NEES within the earthquake engineering community.
- Develop relationships with other U.S. and international experimentation, computational, grid, and visualization programs that could bring unique capabilities to NEES.
- Explore technological advances that could enhance the capabilities of the NEES experimental facilities and cyberinfrastructure.
- Interact with NSF and earthquake hazard reduction programs at other Federal agencies.

The Consortium is run by an elected and appointed Board of Directors. Those involved in the organization's planning, leadership, and management broadly represent the earthquake engineering community and provide expertise in areas such as organizational planning, earthquake engineering research, information technology, simulation, and assessment. Both individuals and institutions are eligible to join the NEES Consortium. During FY 2004, the Consortium will ramp-up operations and hire an Executive Director who will handle day-to-day operations. In addition, the Consortium has six committees to develop and oversee policies and procedures for the use of the NEES infrastructure and to facilitate its own operations:

- Site Operations
- Information Technology
- Data Sharing and Data Archiving
- Education, Outreach, and Training
- Nominations
- Finance

Further information about the NEES Consortium, Inc., is available at http://www.nees.org/.

Research, Education, and Outreach

(1) New Research Capabilities through the NEES Network

NEES unique experimental and cyberinfastructure capabilities will facilitate a variety of innovative experimental approaches, which, in turn, will lead to a better understanding of how the built environment responds during an earthquake. For example, various components representing parts of a large structural system might be tested in different laboratories. Hybrid methods based on real-time dynamic testing are being developed at several NEES equipment sites and could lead to more efficient ways of testing critical

components. This approach entails testing the seismic performance of a critical substructure component while simulating the response of the rest of the structure by computer. As another example, soil and rock, in both natural deposits and engineered fills, are the least investigated, most variable, and least controlled of all materials, but they significantly affect the performance of the built environment during earthquakes. NEES field equipment will enable researchers to advance our fundamental understanding of how natural and engineered geologic materials; earth structures such as dams, levees, and retaining walls; and soil-foundation-structure systems respond to earthquakes.

NEES will provide unique opportunities to pursue high-priority research, to demonstrate the validity of design concepts and guidelines, to speed the transfer of research into seismic design guidelines and specifications, and to develop well-informed preparedness and recovery strategies. To help guide NEES through the next decade, a panel organized by the National Research Council of the National Academies has developed a long-term research agenda for the earthquake engineering research community – *Preventing Earthquake Disasters: The Grand Challenge in Earthquake Engineering (A Research Agenda for the Network for Earthquake Engineering Simulation)* (August 2003) available at http://www.eng.nsf.gov/nees. In addition, the EERI published a research plan in 2002 for earthquake engineering field entitled *Securing Society Against Catastrophic Earthquake Losses.*

NEES research will provide the foundation for the development of new technologies in critical areas such as

- High-performance materials used to strengthen buildings, bridges, soils, and critical lifelines;
- Performance-based engineering involving codes and decisions related to seismic risk, new design, and retrofitting;
- Structural controls to protect buildings, bridges, and other structures;
- Monitoring tools and sensors to conduct rapid post-earthquake condition assessment of the built environment;
- Advanced warning systems to protect coastal regions from earthquake-generated tsunamis;
- In situ site evaluation and remediation to improve and stabilize soil response during earthquakes;
- Improved techniques to protect critical lifelines such as above- and below-ground fuel, water, and sewer pipelines and electrical, communication, and transit systems during earthquakes;
- Improved simulation tools for analyzing more complete and comprehensive models of seismic performance; and
- Methods to improve decision making with regard to planning and evacuation, emergency response, and post-earthquake recovery.

(2) NSF NEES Research Funding

In August 2003, NSF initiated the first year of the planned ten-year competitive George E. Brown, Jr. Network for Earthquake Engineering Simulation Research (NEESR) Program

Solicitation http://www.nsf.gov/pubsys/ods/getpub.cfm?nsf03589. Projects funded under this solicitation must make use of one or more of the 15 NEES equipment sites. Research will be funded under this solicitation as follows:

- Individual Investigator (II) awards will be made to individuals and small research teams to address a significant problem in earthquake engineering.
- Small Group (SG) awards will be made to cross-disciplinary, and preferably multi-organizational, teams of researchers to address a significant problem in earthquake engineering requiring extensive use of the NEES equipment sites.
- Grand Challenge (GC) awards will support geographically distributed, cross-disciplinary, and multi-organizational teams that take a comprehensive systems approach to address a significant problem in earthquake engineering requiring extensive use of the NEES equipment sites.

The GC and SG NEESR projects offer a unique opportunity for researchers outside the project team to utilize the project's test set-up to accommodate a considerably smaller experimental investigation of a "payload" component, referred to as a "payload project." The payload concept is modeled after the payload projects aboard the NASA space shuttle flights. A NEES payload component is not necessarily part of the main structural, geotechnical, or infrastructure system, e.g., the payload may be a mechanical, control, sensing, or nonstructural component that may detect or support operation of the overall system, but is not part of the load carrying system. Payload projects also may concern the load carrying structural system or its components. The GC or SG project's test set-up would provide the vehicle for testing the payload component(s). GC and SG projects may identify and include potential payload projects as part of the base proposal submission to this program solicitation. Alternatively, after a GC or SG award is made, NSF may fund payload projects separately, either to the project team or to researchers outside the project team, through the Small Grants for Exploratory Research (SGER) program.

For NSF-funded NEESR projects, access to and scheduling and announcing of experiments at the NEES equipment sites will be coordinated by NEES Consortium, Inc. As it becomes available, information about the use of NEES resources, i.e., the evolving policies on the shared use of the NEES equipment sites, sharing of data, and the evolving formats for data, metadata, and E-Notebooks, can be found at http://www.nees.org/ and http://www.neesgrid.org. Because these policies and formats are currently being developed by NEES Consortium, Inc., and the NEESgrid system integration project in conjunction with the earthquake engineering community, NSF expects researchers funded under this program solicitation to comply with these policies and formats, when established, for equipment facilities usage and documenting and sharing of NEESR experimental and analytical results. An important component of all NSF NEESR funded research is that all experimental data generated must be submitted electronically to the central NEES data repository. Data includes all measurements, calibrations, observations, analyses, images, commentary, reports, logs, notes and/or electronic notebook entries which relate directly to the conducted experiments. Any data (as described above), which is recorded in hardcopy of any form, must be losslessly transcribed/converted into an appropriate searchable format on to electronic media. In addition, this information

must be properly characterized with appropriate metadata descriptors and then subsequently stored into one of the NEES accepted digital formats to facilitate archiving in accordance with the data, metadata, and formats and policies established by the earthquake engineering community through NEES Consortium, Inc. (http://www.nees.org) and the NEES system integration project (http://www.neesgrid.org).

NEES construction is not funding the development of advanced simulation and visualization tools for earthquake engineering. Rather, researchers are encouraged to pursue other sources of funding within and outside of NSF for such development. NSF funded the NEES Consortium, Inc., in September 2003 to hold a community workshop at the University of Kansas, Lawrence, on December 1-2, 2003, to develop concepts for a computational simulation and visualization environment for NEES (https://www.fastlane.nsf.gov/servlet/showaward?award=0337807).

(3) Promoting Integration of Education and Research and Broader Participation

NEES will lead to a new era of collaboration in earthquake engineering research and education. Teams of experts in the U.S. and around the world will have unprecedented opportunities to jointly plan, conduct, and analyze the results of experiments and models. Easy access to NEES resources will facilitate broad participation—both informally and through official partnerships—by many communities of users, including researchers, educators and students, engineers, government agencies, professional organizations, industry, and disaster preparedness and response teams. The NEES Consortium, Inc., will facilitate the development of formal partnerships within the U.S. and internationally to expand the capabilities of NEES.

As a program of NSF, NEES fosters the integration of research and education and broadens opportunities, encouraging the participation of early career faculty, women, underrepresented minorities, and persons with disabilities. Widespread public interest in earthquake engineering and disaster preparedness makes highly visible national science and engineering initiatives such as NEES a natural vehicle for enhancing earthquake engineering knowledge. NEES enables many avenues for increasing public understanding and awareness of earthquakes through educational programs, such as museum exhibits, community forums, field trips or onsite demonstrations, and Internet-based activities.

NEES provides national resources for developing, coordinating, and sharing new educational programs and curricular materials to train the next generation of the earthquake engineering workforce. The NEES infrastructure has been designed to make it easy for researchers to share their expertise with educators and students, other scientists and engineers, professionals, and the public, often while experiments are being conducted. NEES can also enrich lessons for K-12 students and teachers by making them "virtual partners" in the process of experimental discovery and analysis. Learning about earthquake engineering research will make students aware of the importance of such research to society and may inspire some of them to become researchers and engineers. To facilitate the use of NEES for integrating research and education, in September 2003

NSF funded the NEES Consortium, Inc., to develop an educational strategic plan for NEES (https://www.fastlane.nsf.gov/servlet/showaward?award=0337808). This project will hold three workshops during FY 2004 to develop the educational strategy. More information about the workshops will be available at http://www.nees.org.

To Learn More About NEES

NEES inaugurates a new generation of earthquake engineering research capabilities in the U.S. and provides a pathway to engage broad participation in research and education by the earthquake engineering community. Partnerships with international facilities and resources will complement and expand the capabilities in the U.S. Ultimately, enhanced understanding of earthquakes and seismic performance made possible by the use of the NEES infrastructure for research and education will lead to innovative, cost-effective measures for better protecting the vast civil and mechanical infrastructure of facilities and services on which we all depend.

Further information about NEES resources and opportunities is available as follows:

- George E. Brown, Jr. Network for Earthquake Engineering Simulation
  http://www.eng.nsf.gov/nees
- NSF Directorate for Engineering, Division of Civil and Mechanical Systems
  http://www.eng.nsf.gov/cms
- NEES Research Solicitation
  http://www.nsf.gov/pubsys/ods/getpub.cfm?nsf03589
- NEES Consortium, Inc.
  http://www.nees.org/
- NEESgrid Network System Integration
  http://www.neesgrid.org/
- NEES Equipment Sites
  - Brigham Young University
    http://nees.crustal.ucsb.edu/
  - Cornell University
    http://nees.cornell.edu/
  - Lehigh University
    http://nees.atlss.lehigh.edu/
  - Oregon State University
    http://nees.orst.edu/
  - Rensselaer Polytechnic Institute
    http://nees.rpi.edu/
  - State University of New York, University at Buffalo
    http://nees.buffalo.edu/
  - University of California, Berkeley
    http://nees.berkeley.edu/
  - University of California, Davis
    http://nees.ucdavis.edu/
  - University of California, Los Angeles

http://www.cee.ucla.edu/nees

- University of California, San Diego
  http://www.structures.ucsd.edu/NEES/
- University of Colorado, Boulder
  http://ceae.colorado.edu/NEES
- University of Illinois, Urbana-Champaign
  http://www.cee.uiuc.edu/research/nees
- University of Minnesota, Twin Cities
  http://nees.umn.edu/
- University of Nevada, Reno
  http://nees.unr.edu/
- University of Texas, Austin
  http://www.geo.utexas.edu/nees

Experimental study on the repair effect of RC piers damaged by earthquakes

Kazunori Watanabe[*1], Akira Hatayama[*2]
Norimitsu Kishi[*3], Tadashi Hasegawa[*4]

Abstract: Cyclic loading tests using specimens approximately one-fourth the size of an actual structure was conducted for quantitative measurement of the repair effect depending on the degree of damage in the case of repair of an RC pier damaged by an earthquake. In the loading tests, specimens to which a certain amount of damage was inflicted through preliminary loading were repaired by the injection of epoxy resin or section restoration using non-shrink mortar, and load was then applied once again. The experiment revealed that tenacity and energy absorption could be improved in the repaired specimens and that their seismic performance could be equivalent to or higher than the specimens that had not been repaired, although the rigidity decreased up until the first yield displacement.

Keywords : RC pier, repair, cyclic loading, resin injection, sectional restoration

1. Introduction

Many RC piers were severely damaged by the Hyogo-ken Nambu Earthquake (Great Hanshin-Awaji Earthquake) that occurred in 1995. Many of the damaged piers had been designed many years before and had little hoop reinforcement. Under these circumstances, the importance of plastic deformation performance after member yielding was pointed out, and aseismic design based on the new criteria with emphasis on plastic deformation performance was introduced in Japan, in addition to the conventional aseismic design employing the seismic intensity method[1]. Introduction of this design method has since then dramatically improved the earthquake performance of RC piers.

Allowance of damage in the plastic range, however, means that it is necessary to conduct repair for restoration of functions in order to put the structure back into service after the earthquake.

Also, the repair effect of damaged RC piers has not been measured quantitatively although experimental studies[2) 3)] are currently being conducted concerning the repair of such piers. The authors determined that quantitative measurement of the seismic performance and repair effect of RC piers after being damaged could lead to the realization of rational and economical repair methods, and therefore conducted evaluation and examination of repair and recovery by producing wall-type RC pier specimens approximately one-fourth the size of an actual structure, inflicting a certain amount of damage to these specimens by preliminary loading and conducting cyclic loading tests.

*1 Researcher, Structures Section, Civil Engineering Research Institute of Hokkaido
*2 Hokkaido Regional Development Bureau
*3 Professor, Department of Civil Engineering and Architecture, Muroran Institute of Technology
*4 Department of Technology, Chodai Co., Ltd., Sapporo Branch

2. Outline of the experiment

2.1 Experimental method

The wall-type RC pier, which is commonly seen in road bridges, was chosen to be the subject of this study. To reproduce conditions as close as possible to those of an actual structure, cyclic loading tests were conducted while the vertical axial force of 150 kN, which was equivalent to the dead weight of the superstructure, was maintained using a vertical loading jack. Photo 1 shows a view of the experimental equipment. In cyclic loading, the yield strain of the axial reinforcement was first set at 1890 μ, which was obtained through material testing. Load was then applied by strain control until the strain of the tension-side reinforcement at the base of the pier reached yield strain.

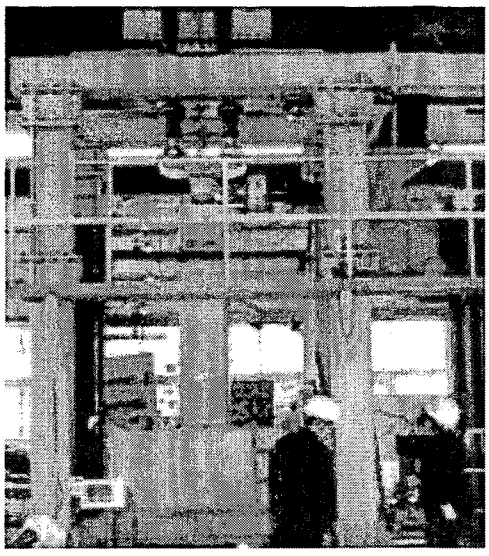


Photo 1 View of the experimental equipment

The loading point displacement at this point was defined as yield displacement δ_y and the horizontal load was defined as yield load P_y. In the subsequent loading, displacement was controlled by gradually increasing the single amplitude by an integral multiple of the yield displacement ($2\delta_y$, $3\delta_y$) and the loading was repeated three times for each displacement amplitude.

The ultimate displacement was defined as the loading point displacement of the stage where either positive or negative load became smaller than the yield load P_y at the first loading of each displacement amplitude.

In the case of the repaired specimens, a certain amount of damage was inflicted through cyclic loading as preliminary loading before the repair was made, the cracked parts were repaired by epoxy resin injection or section restoration using non-shrink mortar while maintaining the zero displacement and cyclic loading tests were conducted once again.

Because the strain gauge of the main reinforcement became unusable during the preliminary loading stage in the case of the repaired specimens, yield displacement δ_y of the standard specimen without repair was used as the standard displacement for cyclic loading.

2.2 Outline of specimens and repair

The specimens were constructed to simulate the wall-type RC pier, which is commonly seen in road bridges, and their size was approximately one-fourth that of an actual pier. Figure 2 shows a schematic diagram of the reinforcement arrangement of the specimens.

The specimens had rectangular sections (aspect ratio of side length 1:3) with a height of 2.0 m and section size of 0.38×1.14 m. The tensile reinforcement ratio was P_t = 0.45 % and the volume ratio of the hoop reinforcement was δ_s = 0.2 %.

Specimens to be repaired were supposed to be in the following three stages of damage before repair:

1) The stage with only horizontal cracking, 2) the stage before concrete cover began to swell and

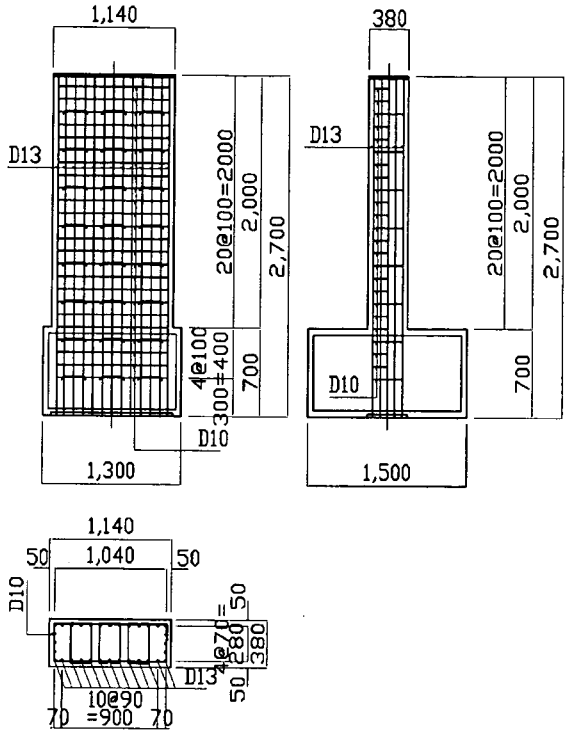


Table 1 Specimen list

Specimen	preliminary loading	Repair method
2.0-N	–	–
2.0-R-3	3δy	Epoxy resin injection
2.0-R-5	5δy	Epoxy resin injection
2.0-M-5	5δy	Non-shrink mortar sectional restoration
2.0-M-7	7δy	Non-shrink mortar sectional restoration

Table 2 List of physical properties for repair materials

Material	Compressive strength (N/mm2)	Tensile strength (N/mm2)
Epoxy resin	60.0 or higher	30.0 or higher
Non-shrink mortal	32.6 (Material age:3 days)	

Fig.2 Reinforcement arrangement of the specimens

3) the level at which the concrete cover had exfoliated and the reinforcement was buckled.
Based on the damage conditions in load testing of the standard specimen, a preliminary load of up to $3\delta_y$, $5\delta_y$ and $7\delta_y$ was applied, respectively. After that, repair was conducted under the condition in which the displacement was forcibly returned to zero, and the main load was applied.

Table 1 lists the specimens used. In the table, the first part of the name of each specimen shows the height of the specimen, the second part indicates the repair condition (N: no repair, R: resin injection, M: sectional restoration) and the third part represents the maximum displacement amplitude at the preliminary loading stage. Five specimens were used for the experiment: 2.0-R-3 and 2.0-R-5 for which epoxy resin was injected into cracks after applying a preliminary load of 3 δ_y and 5 δ_y, respectively; 2.0-M-5 and 2.0-M-7 for which the concrete cover was removed after applying a preliminary load of 5 δ_y and 7 δ_y, respectively, and section restoration was conducted using non-shrink mortar; and 2.0-N, which was employed as the standard specimen.

The repair area was only the part where cracking could be clearly observed. This area was in the range of 300 mm from the base for specimens with a preliminary load of 3 δ_y and 5 δ_y, and 500 mm from the base for specimens with a preliminary load of 7 δ_y. The size of the section was not increased for any of the specimens.

Also, Table 2 shows the physical properties of the materials used for repair. The mean compressive strength of concrete at the material age at the time of experiment was f'_c = 31.5 Mpa, the mean elastic modulus was 3.18 Gpa, reinforcement was SD345 type and the mean yield point strength according to the tension test was 389 Mpa.

3. Experimental results and consideration

3.1 Damage conditions of specimens

(1) 2.0-N specimen

Damage to the 2.0-N specimen, which was the standard specimen, occurred in the form of horizontal cracking over the range of 1,200 mm from the base, at intervals of approximately 100 mm, in the height direction and at the time of $1\delta_y$ to $3\delta_y$ loading. During and after the $3\delta_y$ loading stage, damage was concentrated within the range of 300 mm from the base, and almost no progress of damage was observed in the section above that. During the $5\delta_y$ loading stage, the exfoliation of the concrete cover due to the loss of adhesion of the axial reinforcement was found using the hammer tap tone, although swelling of the concrete cover was not observed near the base.

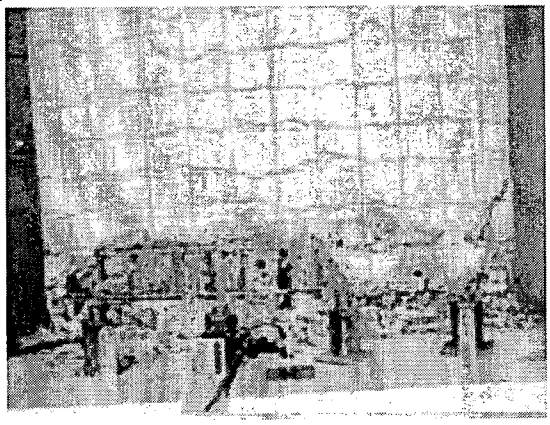


Photo2 Damage condition of the 2.0-N specimen

After that, the concrete cover began to swell during the $6\delta_y$ loading stage and exfoliated over a wide area at $7\delta_y$. The load decreased at $8\delta_y$ as the main reinforcement was broken and the ultimate stage was reached. The exfoliation of concrete cover occurred within the range of 300 mm from the base. Photo 2 shows the damage condition of the 2.0-N specimen at the ultimate stage.

(2) 2.0-R-3 specimen

Damage observed at the end of preliminary loading $(3\delta_y)$ was horizontal cracking at intervals of 100 mm in the height direction.

At the time of loading after repair, exfoliation or other damage of concrete cover was not confirmed until the $8\delta_y$ loading stage when the 2.0-N specimen reached the ultimate stage. After that, concrete cover exfoliated over a wide area during the $9\sim10\delta_y$ loading stage, and the ultimate stage was reached at $11\delta_y$ when the load dramatically decreased due to the breakage of multiple main reinforcement bars during loading.

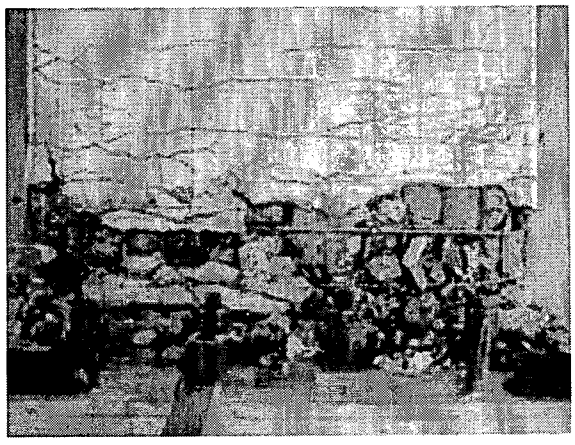


Photo3 Damage condition of the 2.0-R-3 specimen

The exfoliation of concrete cover occurred within the range of approximately 300 mm from the base. Photo 3 shows the damage condition of the 2.0-R-3 specimen at the ultimate stage.

(3) 2.0-R-5 specimen

Damage observed at the end of preliminary loading $(5\delta_y)$ was the exfoliation of concrete cover within the range of approximately 300 mm from the base.

At the time of loading after repair, exfoliation of or other damage to concrete cover was not confirmed until the $8\delta_y$ loading stage in the same manner as the case of the 2.0-R-3 specimen.

Although the swelling of concrete cover was observed during the $9\delta_y$ loading stage, injected epoxy resin prevented exfoliation of concrete cover, and resulted in a peculiar form of damage in which the exfoliation of concrete cover did not occur even when swelling became significant at $10\delta_y$. Concrete cover exfoliated during the $11\delta_y$ loading stage and the ultimate stage was reached at 12 and 13 δy when multiple main reinforcement bars were broken.



Photo4 Damage condition of the 2.0-R-5 specimen

The extent of the exfoliation of concrete cover was greater compared with the 2.0-N and 2.0-R-3 specimens, and within the range of approximately 500 mm from the base. Photo 4 shows the damage condition of the 2.0-R-5 specimen at the ultimate stage.

(4) 2.0-M-5 specimen

Damage observed at the end of preliminary loading $(5\delta_y)$ was the exfoliation of concrete cover within the range of approximately 300 mm from the base, in the same manner as the 2.0-R-5 specimen.

At the time of loading after repair, the expansion of the width of cracks was observed at the boundary between the non-shrink mortar part and the existing part during the $6\delta_y$ loading stage. Swelling of non-shrink mortar occurred during the $8\delta_y$ loading stage and the mortar exfoliated over a wide area during the $9\delta_y$ loading stage. The load gradually decreased through subsequent loading, and the ultimate stage was reached at $11\delta_y$.

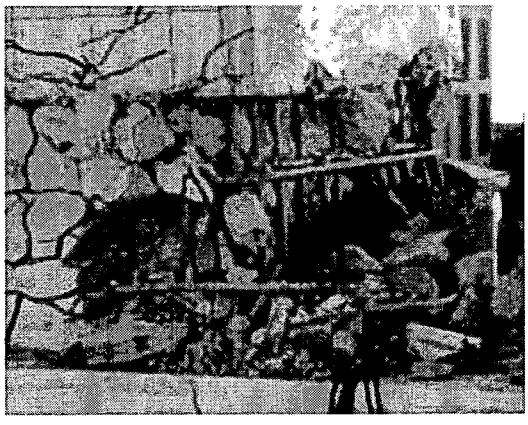


Photo5 Damage condition of the 2.0-M-5 specimen

The exfoliation of concrete cover occurred only within the range of 300 mm from the base where the section was restored , and the boundary between exfoliated and existing parts was clear. Photo 5 shows the damage condition of the 2.0-M-5 specimen at the ultimate stage.

(5) 2.0-M-7 specimen

Damage observed at the end of preliminary loading $(7\delta_y)$ was the exfoliation of concrete cover within the range of 300 mm from the base. The main reinforcement was already buckled and the exfoliation of concrete cover was observed within the range of 500 mm from the base.

At the time of loading after repair, partial

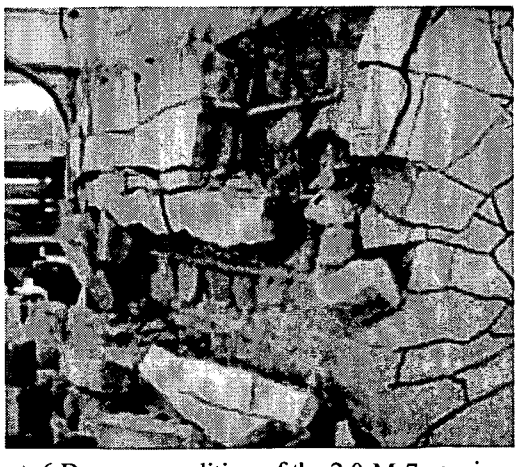


Photo6 Damage condition of the 2.0-M-7 specimen

exfoliation occurred in the non-shrink mortar of the repaired part after the 5 δ_y loading stage. After that, the range of exfoliation gradually expanded with the increase in displacement amplitude. Non-shrink mortar exfoliated over a wide area, the load decreased during the 9 δ_y loading stage and the ultimate stage was reached at 11 δ_y.

The exfoliation of concrete cover only occurred within the range of 500 mm from the base where the section was restored, and the boundary between the exfoliated and existing parts was clear. Photo 6 shows the damage condition of the 2.0-M-7 specimen at the ultimate stage.

3.2 Load-displacement relationship

Table 3 shows the list of experimental results and Fig. 3 shows the envelope of the load-displacement relationship (first stage of repeat loading, mean push-pull values). In the table, δ_y and P_y represent the horizontal displacement at the loading point and the load at the time of yield of the main reinforcement, respectively; P_a is the maximum load (mean push-pull values) and δ_u is the horizontal displacement at the ultimate stage.

Table 3 List of experimental results

Specimen	Displacement (mm)		Load (kN)		Ultimate Plasticity
	δ y	δ u	Py	Pa	
2.0-N	12.2	97.6	94	126	8
2.0-R-3	12.2	134.2	76	131	11
2.0-R-5	12.2	158.6	74	132	13
2.0-M-5	12.2	134.2	76	135	11
2.0-M-7	12.2	134.2	72	133	11

The table and figure show that, for all of the specimens after repair, the load P_y during the 1 δ_y loading stage was as small as 76 to 80% of that of the 2.0-N specimen, indicating that the initial rigidity was decreasing. This is probably because repair was only conducted for visible cracks and where resin injection was possible, and hair cracks and other fine cracks were not repaired. In addition, in the case of mortar repair, only the section restoration part was repaired.

During the 2 δ_y loading stage, the load of repaired specimens was larger than that of 2.0-N and the maximum load P_a also increased by 5 to 7%.

It can also be seen that the load on the 2.0-M-7 specimen gradually decreased after 5 δ_y when the exfoliation of non-shrink mortar occurred. On the other hand, the load did not decrease for the 2.0-R-3, 2.0-R-5 and 2.0-M-5 specimens even during the 8 δ_y loading stage when the 2.0-N specimen reached the ultimate stage.

The ultimate plasticity, which is evaluated by dividing ultimate displacement δ_u by yield displacement δ_y, was 11 for 2.0-R-3, 2.0-M-5 and 2.0-M-7 and 13 for 2.0-R-5, while it was 8 for the 2.0-N specimen, thereby indicating that tenacity increased dramatically compared with that before repair.

Figure 4 presents the load-displacement relationship from the beginning of loading to 1 δ_y. The figure shows that, in the 2.0-N specimen, there was a clear difference in rigidity before (displacement: 0 – 3 mm) and after the occurrence of

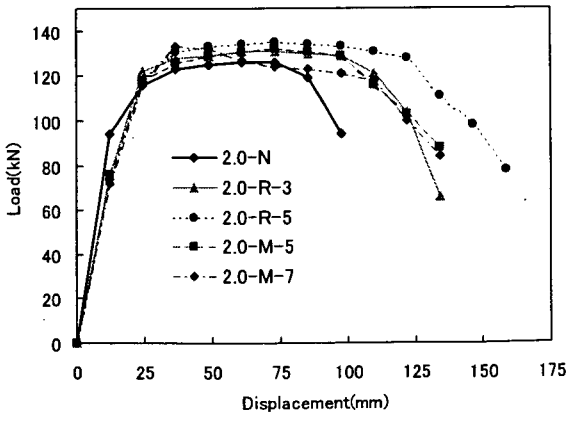


Fig.3 Load-displacement relation envelope

cracking (displacement: 3 – 12 mm). It can also be seen that the rigidity of repaired specimens from the beginning of loading was almost equivalent to that after the occurrence of cracking in 2.0-N. In the same way as mentioned above, it was probably because hair cracks and other fine cracks, for which resin injection was impossible, remained due to unloading after preliminary loading in 2.0-R-3 and 2.0-R-5, and because cracks outside the section restoration part were not repaired in the 2.0-M-5 and 2.0-M-7 specimens.

The starting points of loading differ in the figure because of the effect of the initial input caused by repair conducted while the displacement was maintained at zero.

3.3 Hysteresis absorbed energy

Figure 5 shows the relationship between the accumulated amount of hysteresis absorbed energy and displacement amplitude (δ / δ_y) up to the ultimate displacement of each specimen.

While the accumulated amount of hysteresis absorbed energy at the ultimate stage was 200.2 kNmm ($8\,\delta_y$) for the 2.0-N specimen, it was 366.6 kNmm ($11\,\delta_y$) for 2.0-R-3, 531.8 kNmm ($13\,\delta_y$) for 2.0-R-5, 371.7 kNmm ($11\,\delta_y$) for 2.0-M-5 and 274.9 kNmm ($11\,\delta_y$) for 2.0-M-7. These values were 1.4 to 2.6 times as large as that of the standard specimen.

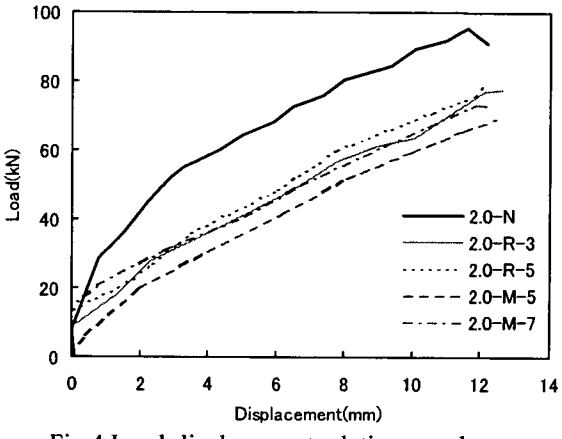


Fig.4 Load-displacement relation envelope (up to $1\,\delta_y$)

Focusing on the $8\,\delta_y$ loading stage when the 2.0-N specimen reached the ultimate stage, however, the hysteresis absorbed energy was low after $5\,\delta_y$ when the exfoliation of concrete cover occurred in 2.0-M-7 and the accumulated value was approximately 80% of that of 2.0-N, while the values for 2.0-R-3, 2.0-R-5 and 2.0-M-5 were 1.1 to 1.2 times as high as that of 2.0-N.

It was thus revealed that, at $8\,\delta_y$ loading in which the standard specimen 2.0-N reached the ultimate stage, the amount of hysteresis absorbed energy was higher if the degree of damage before repair was low and that hysteresis absorbed energy equivalent to or higher than that before repair was observed in specimens for which repair was conducted at a stage before swelling of the concrete cover began.

3.4 Equivalent viscous damping constant

Figure 6 shows the equivalent viscous damping constant that can be calculated from the hysteresis curve of each displacement amplitude.

The equivalent viscous damping constant h_{eq} of 2.0-N, which was the standard specimen, increased gradually from 11% during the $1\,\delta_y$ loading stage to the maximum of 26%.

While the value of 2.0-R-3 was smaller than that of 2.0-N until the $6\,\delta_y$ loading stage, the value became larger than that of

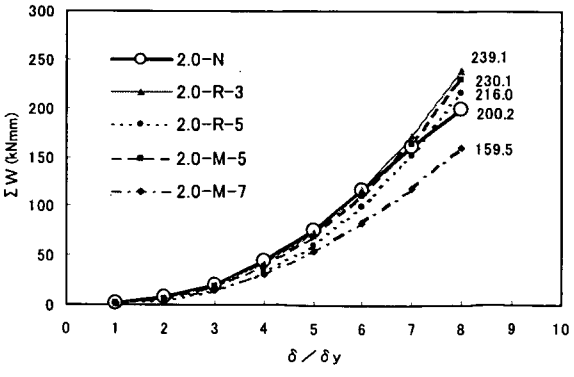


Fig.5 Hysteresis absorbed energy (in the terminal stage)

2.0-N during and after the 7 δ_y loading stage, and the maximum value was 29%.

While the value of 2.0-R-5 was smaller than that of 2.0-N until the 7 δ_y loading stage, the value became larger than that of 2.0-N during and after the 8 δ_y loading stage. After exhibiting the maximum value of 31% during the 10 δ_y loading stage, the value began to decrease and reached as low as 22% at the ultimate stage of 13 δ_y.

For 2.0-M-5, the value was smaller than that of 2.0-N until the 6 δ_y loading stage, and became larger than that of 2.0-N during and after the 7 δ_y loading stage. The maximum value was 28%.

Comparing the 2.0-R-5 and 2.0-M-5 specimens, it can be seen that the value of mortar repair was larger up to 9 δ_y and that of resin injection became larger after that.

The values for 2.0-M-7 tended to be smaller compared with other specimens, and it can be seen that the increase became smaller after the 5 δ_y loading stage, and h_{eq} was 10 to 21%. This is probably due to the occurrence of buckling in the main reinforcement during the preliminary loading stage and the exfoliation of non-shrink mortar after the 5 δ_y loading stage.

4. Conclusion

A loading experiment was conducted using RC pier specimens, which were repaired after preliminary loading, to establish rational and economical repair technology for damaged RC piers. The results obtained through this study can be summarized as follows:

1) Repair by injection of epoxy resin and sectional restoration using non-shrink mortar can recover the deformation performance to a higher level than before making the repair. The value of horizontal load also exceeded that before the repair during and after the 2 δy loading stage.
2) The value of load at the time of yield displacement decreased to 76 – 80% of that before the repair because fine cracks remained.
3) In the case in which exfoliation of concrete cover occurred at the preliminary loading stage, energy absorption and damping performance did not recover to the level before the repair, although ultimate plasticity was improved.

References

1) Japanese Specifications for Highway Bridges and manuals, V-aseismic design, 1996 edition, Dec. 1996.
2) Umihara et al.: Test results concerning the repair effect of high-toughness RC columns damaged by cyclic loading in the large deformation zone, 2nd Symposium on Earthquake-Proof Strengthening and Repair Technology and Earthquake-Proof Diagnosis Technology, pp. 71 - 78, July 1998.
3) Suzuki and Hirasawa: A basic experiment on the repair effect of RC square-section columns, summary of the 51st Annual Academic Lecture of the Japan Society of Civil Engineers, pp. 1128 - 1129, Sept. 1996.

Proceedings of the 19th US-Japan Bridge Engineering Workshop

UJNR Panel on Wind and Seismic Effects

APPENDIX1:
JAPAN PARTICIPANTS

(Public Works Research Institute)
Address: 1-6 Minamihara,Tsukuba-shi,Ibaraki-ken 305-8516
TEL: +81-298-79-6700
Fax: +81-298-79-6741

Tadahiko Sakamoto
Position: Chief Executive

Michio Okahara
Position: Deputy Chief Executive

Kazuhiro Nishikawa
Position: Director, Planning and Research Administration Department

Kenichi Tokida
Position: Director, Earthquake Disaster Prevention Research Group

Hiroshi Sato
Position: Director, Structures Research Group

Keiichi Tamura
Position: Team Leader, Ground Vibration Research Team

Masuo Kondoh
Position: Senior Research Engineer, Ground Vibration Research Team

Shigeki Unjoh
Position: Team Leader, Earthquake Engineering Research Team

Kazuo Endoh
Position: Senior Research Engineer, Earthquake Engineering Research Team

Hideaki Nishida
Position: Research Engineer, Earthquake Engineering Research Team

Taku Mikami
Position: Research Engineer, Earthquake Engineering Research Team

Jun Murakoshi
Position: Team Leader, Bridge Structure Research Team

Koichiro Fumoto
Position: Senior Research Engineer, Bridge Structure Research Team

Jiro Fukui
Position: Team Leader, Foundation Engineering Research Team

Masahiro Ishida
Position: Senior Research Engineer, Foundation Engineering Research Team

Masahiro Shirato
Position: Research Engineer, Foundation Engineering Research Team

Kenji IKEDA
Position: Director, Structures Div.,Structures Dept.
Civil Engineering Research Institute of Hokkaido(CERI)
Address: Hiragishi 1-3, Toyohira-ku, Sapporo, 062-8602 Japan
Phone: +81-11-841-1115
Fax: +81-11-820-2714
E-mail: ikedak@ceri.go.jp

Kenji FUJITANI
Position: Staff of Bridge Department, Public Works Division,
Public Works Bureau of Osaka City Government
Address: WTC-building 12F, 1-14-16 Nankokita Suminoe-ku,
Osaka City, 559-0034, Japan
Phone: +81-6-6615-6818
Fax: +81-6-6615-6583
E-mail: la0027@ii.city.osaka.jp

Hideaki FUKAGAWA

Position: Carbon Fiber Repair & Reinforcement
Research Association (CFRRA)
Senior Engineer
Functional Materials & Products Development Center
Toray Industries, Inc.

Address: 2-1,Nihonbashi-Muromachi 2-chome, Chuo-ku, Tokyo 103-8666 Japan

Phone: +81-3-3245-5755

Fax: +81-3-3245-5042

E-mail: Hideaki_Fukagawa@nts.toray.co.jp

Hidesada KANAJI

Position: Assistant Manager
Design Division, Osaka Construction Bureau
Hanshin Expressway Public Corporation (HEPC)

Address: 1-14-16 Nanko-kita Suminoe, Osaka, 559-0034 Japan

Phone: +81-6-6615-7461

Fax: +81-6-6615-7449

E-mail: kanaji@luck.ocn.ne.jp

Chihiro KAWATOH

Position: Engineering Information Division
Long-span Bridge Engineering Center
Honshu-Shikoku Bridge Authority

Address: 4-1-22, Onoedori, Chuo-ku, Kobe 651-0088 Japan

Phone: +81-78-291-1075

Fax: +81-78-291-1359

E-mail: kawatoh@hsba.go.jp

Yohei KOIKE
Position: Research Engineer
Research Laboratory Yokogawa Bridge Corp.
Address: No.27, Yamano-cho, Funabashi-shi, Chiba-ken
273-0026 Japan
Phone: +81-47-435-6161
Fax: +81-47-435-6160
E-mail: y.koike@yokogawa-bridge.co.jp

Kenji KOSA
Position: Professor of Civil Engineering
Kyushu Institute of Technology
(formerly a highway engineer)
Address: Sensui 1-1, Tobata, Kitakyushu 804-8550 Japan
Phone: +81-93-884-3123
Fax: +81-93-884-3123
E-mail: kosa@civil.kyutech.ac.jp

Tsutomu NISHIOKA
Position: Senior Engineer
Engineering Department
Hanshin Expressway Public Corporation (HEPC)
Address: 4-1-3, Kyutaro-machi, Chuo-ku, Osaka 541-0056 Japan
Phone: +81-6-6252-8121
Fax: +81-6-6252-4583
E-mail: tsutomu-nishioka@hepc.go.jp

Shinya OKADA
Position: Structures Division,
Structures Department,
Civil Engineering Research Institute of Hokkaido
Address: Hiragishi 1-3-1-34, Toyohira-ku, Sapporo 062-8602 Japan
Phone: +81-11-841-1698
Fax: +81-11-820-2714
E-mail: okada@ceri.go.jp

Ichiro OKURA
Position: Associate Professor
Department of Civil Engineering
Osaka University
Address: 2-1 Yamadaoka,Suita,Osaka 565-0871, Japan
Phone: +81-6-6879-7620
Fax: +81-6-6879-7621
E-mail: okura@civil.eng.osaka-u.ac.jp

Shoji ONO
Position: Engineering Department of Steel Structure Division
TOPY Industries, Limited
Address: 1,Akemi-cho, Toyohashi-shi, Aichi-ken 441-8510 Japan
Phone: +81-532-25-9551
Fax: +81-532-25-9557
E-mail: s-ono@topy.co.jp

Koji OSADA
Position: Deputy Director
Bridge Division
Road Research Department
Japan Highway Public Corporation
Address: 1-4-1, Tadao, Machida-city, Tokyo, 194-8508 Japan
Phone: +81-42-791-1621
Fax: +81-42-791-2380
E-mail: kouji.osada@jhnet.go.jp

Yukitake SHIOI
Position: Professor
Research Institute for Interdisciplinary Science
Hachinohe Institute of Technology
Address: 88-1,Ohbiraki,Myo,Hachinohe-shi,Aomori-ken 031-8501 Japan
Phone: +81-178-25-8081
Fax: +81-178-25-0722
E-mail: shioiyu@hi-tech.ac.jp

Takeshi SUGIMOTO

Position: Engineer
Bridge Maintenance Division Maintenance Department
Honshu-Shikoku Bridge Authority
Address: 4-1-22 Onoe-dori, Chuo-ku, Kobe, Hyogo 651-0088 Japan
Phone: +81-78-291-1093
Fax: +81-78-291-1359
E-mail: sugimoto@hsba.go.jp

Nobumasa SUZUKI

Position: Research Engineer
Civil Engineering and Research Department
P.S.Mitsubishi Construction Co., Ltd
Address: G-7 Bldg.,10F 7-16-12 Ginza, Chuo-ku, Tokyo 104-8215 Japan
Phone: +81-3-4562-3071
Fax: +81-3-4562-3075
E-mail: nobu-suzu@psmic.co.jp

Takeshi SUZUKI

Position: Assistant Manager
Survey and Design Division
Osaka Business and Maintenance Department
Hanshin Expressway Public Corporation(HEPC)
Address: 3-1-25,Ishida,Minato-ku,Osaka-shi,Osaka-fu 552-0006 Japan
Phone: +81-6-6576-3881
Fax: +81-6-6576-1918
E-mail: takeshi-suzuki@hepc.go.jp

Sentaro TAKAGI

Position: Deputy Director
Maintenance Section
Road and Street Administration Division
Bureau of Construction
Tokyo Metropolitan Government

Address: 2-8-1 Nishi-shinjuku Shinjuku-ku Tokyo, 163-8001 Japan

Phone: +81-3-5320-5294

Fax: +81-3-5388-1529

E-mail: Sentarou_Takagi@member.metro.tokyo.jp

Kazunori WATANABE

Position: Structures Division,
Structures Department,
Civil Engineering Research Institute of Hokkaido

Address: Hiragishi 1-3-1-34, Toyohira-ku, Sapporo 062-8602 Japan

Phone: +81-11-841-1698

Fax: +81-11-820-2714

E-mail: watanabe@ceri.go.jp

Proceedings of the 19th US-Japan Bridge Engineering Workshop

UJNR Panel on Wind and Seismic Effects

APPENDIX 2:
US PARTICIPANTS

Harry A. CAPERS, Jr.
Position: State Bridge Engineer
Bureau of Structural Engineering
New Jersey Department of Transportation
Address: 1035 Parkway Avenue PO Box 615 Trenton, NJ 08625-0615
Phone: (609)-530-2557
Fax: (609)-530-5777
E-mail: harry.capers@dot.state.nj.us

Mark R.Capron
Position: Jacobs Civil Fellow, Project Manager
Address: Jacobs Civil Inc.
501 North Broadway St. Louis, Missouri 63102 U.S.A.
Phone: (314)-335-4520
Fax: (314)-335-5120
E-mail: mark.capron@jacobs.com

Steven B. Chase,
Position: Technical Director for Bridges
Federal Highway Administration
Address: FHWA-TFHRC
6300 Georgetown Pike
McLean, VA 22101-2296
Phone: (202)-493-3038
Fax: (202)-493-3442
E-mail: steve.chase@fhwa.dor.gov

James D. Cooper
Position: Bridge Technology Consultant
Address: 19010 Black Oak Road Purcellville, VA 20132
Phone: (540)-338-1570
Fax: (540)-338-1570
E-mail: BridgeRDandT@aol.com

Ian FRIEDLAND
Position: Bridge Technology Engineer
Federal Highway Administration
U.S. Department of Transportation
Address: 400 7th Street, SW Room 3203, HIBT-30
Washington, DC 20007, USA
Phone: (202)-366-6712
Fax: (202)-366-3077
E-mail: ian.friedland@fhwa.dot.gov

Shyam Gupta
Position: State Bridge Engineer
Missouri Department of Transportation
Address: 105 W. Capitol Avenue P. O. Box 270
Jefferson City, MO 65102
Phone: (573)-751-4676
Fax: (573)-526-5488
E-mail: guptag@mail.modot.state.mo.us

Issam E. Harik
Position: Chair and Raymond-Blythe Professor of Civil Engineering, and
Head, Structures Section, Kentucky Transportation Center
University of Kentucky
Address: Department of Civil Engineering
161A Raymond Building
University of Kentucky
Lexington, KY 40506-0281
Phone: (859)-257-3116
Fax: (859)-257-1815
E-mail: iharik@engr.uky.edu

RICHARD D. LAND

Position: State Bridge Engineer Deputy Division Chief
Division of Engineering Services, Structure Design
California Department of Transportation

Address: P. O. Box 168041, MS 9-4/11G SACRAMENTO,CA 95816-8041

Phone: (916)-227-8807

Fax: (916)-227-8149

E-mail: Richard_Land@dot.ca.gov

Ivan R. Lasa

Position: Corrosion and Rehabilitation Technologist
State Materials Office Corrosion Research Laboratory
Florida Department of Transportation (FDOT)

Address: 5007 Northeast 39th Avenue Gainesville, Florida USA 32609

Phone: (352)-955-2901

E-mail: ivan.lasa@dot.state.fl.us

George C. LEE

Position: Samuel P. Capen Professor of Engineering
Multidisciplinary Center for
Earthquake Engineering Research
University at Buffalo, State University of New York

Address: 109 Red Jacket Quadrangle, Box 610025
Buffalo, NY 14261-0025

Phone: (716)-645-3391

Fax: (716)-645-3399

E-mail: gclee@buffalo.edu

Jerome S. O'CONNOR

Position: Senior Project Officer, Transportation Research
Multidisciplinary Center for Earthquake Engineering Research
University at Buffalo, State University of New York

Address: 102 Red Jacket Quadrangle Buffalo, NY 14261-0025

Phone: (716)-645-3391 Ext.107

Fax: (716)-645-3399

E-mail: jso7@buffalo.edu

Joy PAUSCHKE

Position: NEES Program Director
Division of Civil and Mechanical Systems
National Science Foundation

Address: 4201 Wilson Boulevard, Suite 545 Arlington, VA 22230 USA

Phone: (703)-292-7024

Fax: (703)-292-9053

E-mail: jpauschk@nsf.gov

David Howard Sanders

Position: Associate Professor of Civil Engineering, University of Nevada, Reno

Address: Dept. of Civil Engineering/258
University of Nevada; Reno, NV 89557

Phone: (775)-784-4288

Fax: (775)-784-1390

E-mail: sanders@unr.edu

Chia-Ming UANG

Position: Professor
Department of Structural Engineering
University of California, San Diego

Address: 409 University Center La Jolla, CA 92093-0085, USA

Phone: (858)-534-9880

Fax: (858)-534-6373

E-mail: cmu@ucsd.edu

James WACKER

Position: Professional Engineer
Forest Products Laboratory
Forest Service - Research Division
United States Department of Agriculture

Address: One Gifford Pinchot Drive Madison, Wisconsin, USA 53726-2398

Phone: (608)-231-9224

Fax: (608)-231-9303

E-mail: jwacker@fs.fed.us

W.Phillip Yen,

Position: Research Structural Engineer, Office of Infrastructure, R&D
Turner-FairBank Highway Research Center
Federal Highway Administration

Address: 6300 Georgetown, Pike McLean VA 22101

Phone: (202)-493-3056

Fax: (202)-493-3442

E-mail: wen-huei.yen@fhwa.dot.gov

Proceedings of the 19th US-Japan Bridge Engineering Workshop

UJNR Panel on Wind and Seismic Effects

APPENDIX 3:
STUDY TOUR GUIDES

Schedule

19th US-Japan Bridge Engineering Workshop

26 Oct. (Sun)

Arrive at Narita Airport (NRT)
Depart from Narita Airport by chartered bus to Tsukuba
Arrive at the hotel in Tsukuba
Stay at "Kenshu-kaikan" or "Hotel Okura"

27 Oct. (Mon)

Opening Session
Workshop at PWRI
18:00 Reception hosted by the Chief Executive of PWRI
Stay at "Kenshu-kaikan" or "Hotel Okura"

28 Oct. (Tue)

Workshop at PWRI
18:00 Reception hosted by the US side
Stay at "Kenshu-kaikan" or "Hotel Okura"

29 Oct. (Wed)

Workshop at PWRI
pm (Government members) FHWA/MLIT meeting at PWRI
(Other members) Study tour around Tsukuba
Stay at "Kenshu-kaikan" or "Hotel Okura"

Kenshu-kaikan
Phone: +81-29-864-2844

Hotel Okura
Phone: +81-29-852-1112

30 Oct. (Thu)

7:00 Leave "Kenshu-kaikan" by chartered bus
9:45 Arrive at Haneda Airport
10:45 Depart from Haneda Airport by Flight JAS323
12:20 Arrive at Kitakyushu Airport
13:30 Depart from Kitakyushu Airport by chartered bus
Study Tour of the bridge for New Kitakyushu Airport

Stay at Hotel New Tanaka (Yamaguchi City)
Phone: +81-839-23-1313
Fax: +81-839-25-6316

31 Oct (Fri)

8:30 Leave the hotel by chartered bus
Study tour of Wakato-Ohashi Bridge and Kanmon Bridge
Study tour of replacement site of Kintaikyo bridge (old timber bridge)

Stay at Onomichi Kokusai Hotel
Phone: +81-848-25-5931
Fax: +81-848-25-5930

1 Nov. (Sat)

8:00 Leave the hotel
Study tour of "Shimanami-Kaido"
(one of Honshu-Shikoku bridge routes)
13:30 Arrive at Matsuyama Airport
14:30 Depart from Matsuyama Airport by Flight NH592
15:45 Arrive at Haneda Airport (Tokyo)
16:15 Leave the airport by train
16:30 Arrive at the hotel
17:30 Study tour of bridges on Sumida River
18:45 Dinner at Asakusa
20:40 Arrive at the hotel

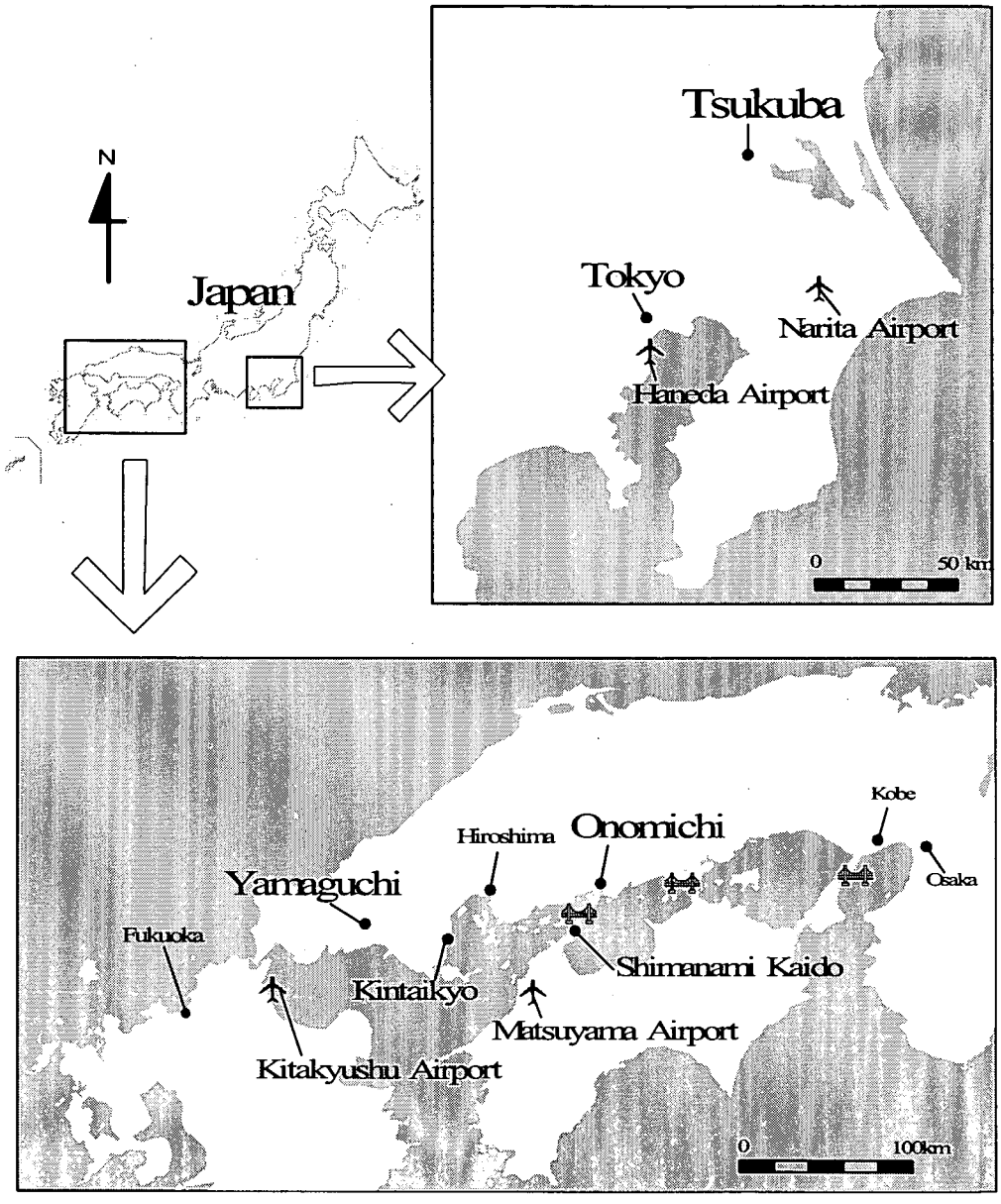
Stay at Shinagawa Prince Hotel
Phone: +81-3-3440-1111
Fax: +81-3-3441-7092
http://www.princehotels.co.jp/link/english/shinagawa.html

2 Nov. (Sun)

Leave the hotel to Narita Airport
Leave Japan

- Please see attached schedule of train or bus
- Two hours or earlier check in is recommended for international flights

MAP


N
Japan
Tsukuba
Tokyo
Narita Airport
Haneda Airport
0
50 km
Kobe
Hiroshima
Onomichi
Osaka
Yamaguchi
Fukuoka
Shimanami Kaido
Kintaikyo
Matsuyama Airport
Kitakyushu Airport
0
100km